

UCR LIBRARY

[Faint, illegible handwritten notes]



State of California
The Resources Agency

Department of
Water Resources

UNIVERSITY OF CALIFORNIA
DAVIS

MAY 1 1979

GOV'T. DOCS. - LIBRARY



The August 1, 1975 Oroville Earthquake Investigations

Bulletin 203-78
February 1979

U.C.D. LIBRARY



ON THE COVER:
Aerial View of Oroville Facilities

**Department of
Water Resources**

Bulletin 203-78

The August 1, 1975 Oroville Earthquake Investigations

February 1979

Huey D. Johnson
Secretary for Resources

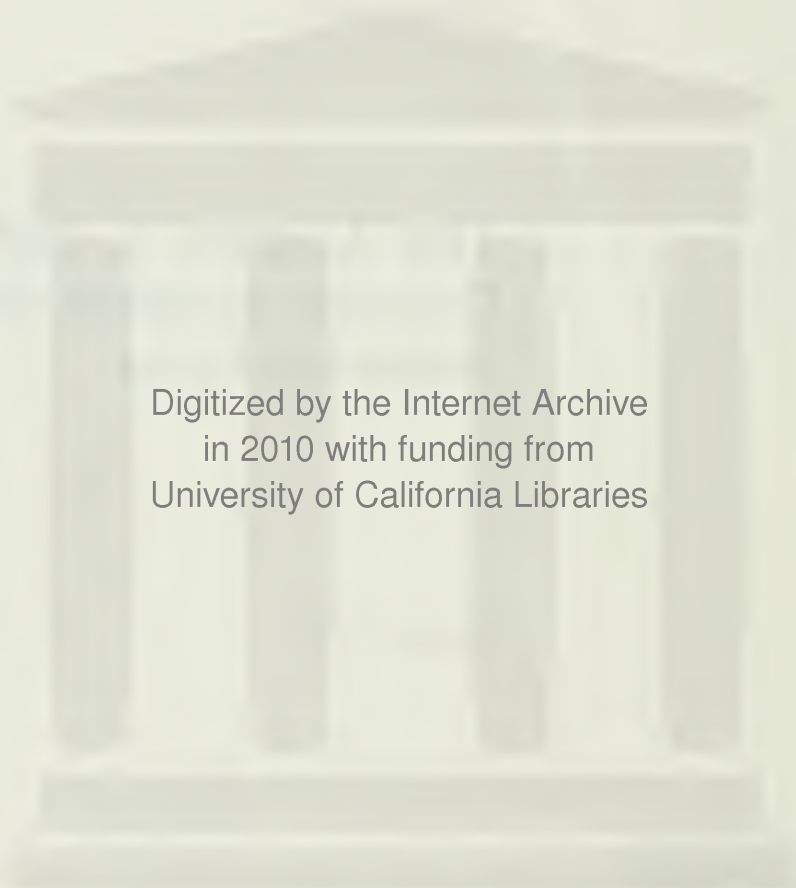
Edmund G. Brown Jr.
Governor

Ronald B. Robie
Director

**The Resources
Agency**

**State of
California**

**Department of
Water Resources**



Digitized by the Internet Archive
in 2010 with funding from
University of California Libraries

FOREWORD

The epicenter of the 1975 earthquake near Oroville, California was close to the Oroville-Thermalito features of the California State Water Project. Therefore, the Department of Water Resources initiated structural reanalyses of the Project facilities and seismological and geological investigations.

The performance of the Oroville-Thermalito facilities during the August 1975 earthquake sequence, reported in Bulletin 203 (April 1977), demonstrated their ability to withstand that seismic loading. No structural damage occurred. The only damage was to a few of the secondary facilities; this damage was only superficial.

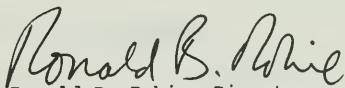
The Department conducted intensive investigations to determine:

1. Geologic and tectonic conditions
2. Fault mechanism and orientation
3. Crustal movements
4. Public safety as it relates to the Department's facilities.

The Department established a Special Consulting Board for the Oroville Earthquake, consisting of nine experts in the fields of seismology, geology, and dam design to review the Department's investigations and make recommendations.

Bulletin 203-78 presents a detailed reanalysis of the Department's facilities and results of the detailed seismological and geological investigations. On the basis of determinations from the investigations completed to date, the Department concludes that the Oroville facilities do not pose a threat to public safety.

The reanalyses of Thermalito Forebay, Afterbay and Power Plant Headworks, and the Bidwell Canyon Saddle Dam are still in progress, with publication planned by mid 1979.



Ronald B. Robie, Director
Department of Water Resources
The Resources Agency
State of California

State of California
Edmund G. Brown Jr., Governor
The Resources Agency
Huey D. Johnson, Secretary for Resources

DEPARTMENT OF WATER RESOURCES
Ronald B. Robie, Director

Charles R. Shoemaker
Acting Deputy Director

Gerald H. Meral
Deputy Director

Robert W. James
Deputy Director

Jack B. Johnston
Acting Assistant Director

Division of Operations and Maintenance

Howard H. Eastin Division Chief
Lawrence A. Mullnix Chief, Water Engineering Office
Clifford V. Lucas Chief, Civil Maintenance Branch
Philip F. Johns Chief, Oroville Field Division

Authors

Chapter I

John R. Campbell Project Surveillance Section

Chapter III

Paul W. Morrison, Jr. Earthquake Engineering

Chapter IV

John R. Campbell Project Surveillance Section

Chapter IX

J. P. Cedarholm Civil Maintenance Section

Division of Design and Construction

Gordon W. Dukleth Division Chief
Keith G. Barrett Chief, Design Office
Ernest C. James Chief, Civil Design Branch

Division of Design and Construction (Continued)

John W. Marlette Chief, Project Geology Branch
William M. Verigin Chief, Dams and Canals Section
Donald C. Steinwert Chief, Structures Section

Authors

Chapter II

John W. Marlette Chief, Project Geology Branch
Robert J. Akers Project Geology Branch
Kenneth A. Cole Project Geology Branch
Richard D. McJunkin Project Geology Branch

Chapter V

William D. Hammond Dams and Canals Section
Leslie F. Harder Dams and Canals Section

Chapter VI

Samuel J. Linn, Jr. Structural Section
Edgar R. Najera Structural Section

Chapter VII

Samuel J. Linn, Jr. Structural Section
Edgar R. Najera Structural Section

Chapter VIII

Arnold E. Eskel Structural Section
Samuel J. Linn, Jr. Structural Section

Edited by
Earl G. Bingham, Reports Administration

CONTENTS

	<u>Page</u>
Foreword	iii
Organization	iv

CHAPTER I. INTRODUCTION

Purpose	1
Description of the Oroville Facilities	1
The Investigating Organization	3
Reanalysis of Project Structures for Earthquake Safety	4
Summary of Conclusions and Recommendations	5
Geological Investigations (Chapter II)	5
Seismology (Chapter III)	6
Vertical and Horizontal Geodesy (Chapter IV)	6
Oroville Dam, Evaluation of Seismic Stability (Chapter V)	7
Oroville Dam, Flood Control Outlet Structure (Chapter VI)	7
Thermalito Diversion Dam (Chapter VII)	7
Reappraisal of Secondary Structures (Chapter VIII)	7
Fish Barrier Dam	7
Edward Hyatt Powerplant	7
Thermalito Powerplant	7
Miscellaneous Structures	8
Bridges	8
Switchyards	8
Contingency Plan for Seismic Emergencies (Chapter IX)	8
Department's Findings	8
Uncompleted Reports	8
Safety Review Requirements	8
Report of the Special Consulting Board for the Oroville Earthquake.	9
Review by the Division of Mines and Geology	13

CHAPTER II. GEOLOGIC INVESTIGATIONS

Purpose of Investigation.	15
Previous Work	15
Scope of Investigation.	17
Seismic History	19
The 1975 Earthquake Series.	21
Ground Cracking	23
Ground Elevation Changes.	26
Area Lineaments	27
Geologic Setting.	30
Geographic Location.	30
Geologic Framework	30
Descriptive Geology	33
Bedrock Series Rocks	33
Melange	34
Previous Investigations and Age.	34
Contact Relationships.	34
Lithologic Description	35

Arc Rocks	38
Previous Investigations and Age.	38
Contact Relationships.	38
Lithologic Description	38
Monte de Oro Formation.	40
Previous Investigations and Age.	40
Contact Relationships.	40
Lithologic Description	41
Smartville Ophiolite	41
Previous Investigations and Age.	41
Contact Relationships.	42
Lithologic Description	42
Intrusive Rocks	47
Previous Investigations and Age.	47
Contact Relationships.	47
Lithologic Description	48
Origin of Sierra Nevada Plutons.	49
Superjacent Series Rocks	50
Chico Formation	50
Previous Investigations and Age.	50
Contact Relationships.	50
Lithologic Description	50
Ione Formation.	51
Previous Investigations and Age.	51
Contact Relationships.	51
Lithologic Description - Ione Formation Undifferentiated . .	51
Lithologic Description - Auriferous Gravel	51
Lithologic Description - Oroville Tuff	52
Lovejoy Formation	53
Previous Investigations and Age.	53
Contact Relationships.	53
Lithologic Description	54
Tuscan Formation.	54
Previous Investigations and Age.	54
Contact Relationships.	55
Lithologic Description	55
Late Cenozoic Gravels	56
Previous Investigations.	56
Contact Relationships.	56
Lithologic Description	57
Quaternary Landslides.	57
Structural Geology.	61
Faults	61
Mesozoic Faults - Northern Foothills.	65
Mesozoic Faults - Project Area.	67
Swain Ravine, Paynes Peak and Prairie Creek	
Lineament/Fault Zones.	67
Oregon Gulch Fault	68
Monte de Oro Fault	69
Unnamed Faults	69
Glover Ridge Fault	69
Cenozoic Fault Movement	70
Swain Ravine Lineament Fault Zone.	71

Prairie Creek Lineament Fault Zone	74
Paynes Peak Lineament Fault Zone	74
Thermalito Powerplant Foundation Faults.	75
Chico Lineament	75
Soda Springs Lineament	77
Web Hollow Lineament	77
Paradise-Magalia Lineament	77
Summary.	79
Mesozoic Folds.	79
Cenozoic Folding.	79
Summary of Geologic History	80
Causes of the Oroville Earthquake	82
Reservoir-Induced Seismicity	83
Potential Hazards to State Water Facilities	86
Ground Shaking	86
Fault Displacement	86
Regional Changes in Ground Elevation	87
Potential Hazard to Specific Facilities.	87
Oroville Dam and Saddle Dams.	87
Thermalito Forebay and Afterbay	87
Thermalito Powerplant	88
Other Structures	88
Summary and Conclusions	88
References Cited	90
Addenda: Department of Water Resources Exploration Trench Logs	103

CHAPTER III. SEISMOLOGY

Introduction	123
Data	123
Results	124
Discussion	124
Conclusions	124
References Cited	139

CHAPTER IV. VERTICAL AND HORIZONTAL GEODESY

Vertical Crustal Movements	141
Introduction	141
Precise Survey Programs	141
September 1967	141
July-September 1968	142
October-November 1969	142
August-September 1975	142
January-April 1976	142
September-November 1976	142
September-November 1977	142
Precise Survey Adjustment	143
Free Adjustment	143
Spur Lines	144
Elevation Differential Isograms	146
General	146
September 1967-October 1969	146

October 1969-August 1975	146
September 1967-October 1977	146
August 1975-October 1976	146
October 1976-October 1977.	153
August 1975-October 1977	153
Elevation Differential Along Lines	153
General.	153
Avocado	153
Bald Rock	153
Bidwell	153
Bidwell Canyon Saddle Dam	157
Canyon Drive	157
Cleveland Hill	157
Dam	157
Dunstone	157
Feather Falls	157
Foothill	157
Miners Ranch	157
Mission Olive	157
Morris	167
Olive	167
Oro-Bangor	167
Oroville	167
Potter	167
Richvale	167
Thompson Flat	167
Wyn-Miners Ranch	167
103	167
Oroville Dam Crest Differential Settlement	167
General	167
Commentary	181
Conclusions	181
Horizontal Earth Movements	181
Introduction	181
Horizontal Geodetic Control and Triangulation Programs	181
September 1967	181
April 1968	183
August-September 1975	183
Computations and Analyses	183
Commentary	185
Conclusions	185

CHAPTER V. OROVILLE DAM: EVALUATION OF SEISMIC STABILITY

Acknowledgments	187
1. Introduction	188
Background.	189
Commentary.	190
Summary of Findings	190
Conclusions	191

2.	Description of Embankment Materials and Dynamic Instrumentation. . .	192
	Embankment Materials.	192
	Dynamic Instrumentation	194
	Original System.	194
	Upgraded System.	195
3.	Recorded Embankment Response to the 1975 Earthquakes	197
	General	197
	Recorded Events	197
	August 1, 1975	197
	August 5, 1975	199
	September 27, 1975	199
	Observed Natural Period	201
4.	Analysis of Static Stresses by Finite Element Method	203
	General	203
	Material Properties	204
	Static Stress Analysis.	205
	Seepage Forces	205
5.	Determination of Dynamic Shear Modulus and Damping Values for Embankment Shell Material.	208
	General	208
	Cyclic Triaxial Test.	209
	Analysis of Recorded Embankment Response During the 1975 Earthquakes	211
	General	211
	Natural Period for Two-Dimensional Analysis.	213
	Shear Strain for Two-Dimensional Analysis.	213
	Shear Modulus Reduction Factor	213
	K_{2max} vs. Natural Period	214
	Range of K_{2max}	214
	Comparison of Observed and Computed Crest Motions	214
	Embankment Response Model.	216
	August 1 Event.	216
	September 27 Event.	217
	Dynamic Properties Adopted for Gravel Shell.	217
6.	Reanalysis Earthquake.	221
7.	Analysis of Dynamic Stresses for the Reanalysis Earthquake	229
	Methods of Response Computation	229
	Acceleration Response of Dam to Design Earthquake	229
	Input Variables and Computed Shear Stresses	231
	Influence of Shear Modulus of Shell Material	232
	Influence of Shear Modulus of Core Material.	233
	Computer Programs LUSH and QUAD4	234
	Influence of Poisson's Ratio	237
	Influence of Embankment Section.	239
	Combined Influence of Variables	241
	Three-Dimensional Effect.	241

8. Cyclic Shear Strength.	244
Cyclic Strength Test Program.	244
Sample Gradations and Density	244
Modeling Embankment Shell Gradation.	244
Relationship of Test Sample Density to Field Density	244
Summary of Test Procedures.	249
30 cm Diameter Samples	249
7.1 cm Diameter Samples.	249
Results of Cyclic Triaxial Tests.	250
Investigation of Sample Behavior of Dense Sands in Static and	
Cyclic Triaxial Tests	251
Objective.	251
Program and Procedures	254
Static Tests on Monterey O Sand.	256
Cyclic Tests on Monterey O Sand.	260
Cyclic Tests on Oroville Sand.	262
Analysis of Test Results.	268
Extension Strain	268
Necking Behavior	268
Sample "Tension"	268
Cyclic Strength Interpretations Considered.	276
Strength Interpretation I.	276
Strength Interpretation II	276
9. Evaluation of Performance.	281
General Considerations.	281
Method of Evaluation.	281
Failure Planes	281
Equivalent Regular Stress Time History	282
Cases Analyzed and Assumptions.	282
Case a	284
Case b	284
Case c	284
Case d	285
Comparison of Cases.	285
Predicted Behavior - Best Judgment Case	285
Shell K_{\max}	285
Cyclic Shear Strength.	285
Three-Dimensional Effect	285
Drainage	285
Predicted Behavior	286
Estimated Displacements for Conservative Assumptions.	287
References	288

CHAPTER VI. SEISMIC ANALYSIS OF THE OROVILLE DAM FLOOD CONTROL OUTLET STRUCTURE

Commentary	291
Conclusion	294
Earthquake Analysis of the Oroville Dam Flood Control Outlet Structure, June 1977, by Edward L. Wilson, Frederick E. Peterson, and Ashraf Habibullah	299

CHAPTER VII. SEISMIC ANALYSIS OF THE THERMALITO DIVERSION DAM

Commentary	351
Earthquake Response Analysis of Thermalito Diversion Dam By Anil K. Chopra	355

CHAPTER VIII. REAPPRAISAL OF SECONDARY STRUCTURES

Introduction	389
Fish Barrier Dam	389
Description	389
Original Seismic Analysis	389
Recommendation for Seismic Reanalysis	395
Power and Pumping Plant Facilities	395
Edward Hyatt Powerplant	399
Conclusion	399
Thermalito Powerplant	399
Conclusion	395
Miscellaneous Structures	402
Oroville Operations and Maintenance Center	402
Oroville Dam	402
Thermalito Forebay and Afterbay	402
Feather River Fish Hatchery	402
Conclusion	403
Bridges	403
Conclusion	403
Switchyard Structures and Apparatus	403
Conclusion	404

CHAPTER IX. CONTINGENCY PLAN FOR SEISMIC EMERGENCIES

Organization and Responsibilities	405
Division Policy	405
Division Plan of Operation	405
Oroville Field Division Command Post	405
Operational Command Post	406
Operational Facilities	406
Operational Plan	406
Security Command Post	406
Security Plan	406
Procedures for Reacting to Seismic Events	406
Detection	406
Earthquake Magnitudes and Epicenters	406
Criteria for Notification	407
Response	407
Inspection of Project Facilities Following an Earthquake	408
Rapid Response Inspection Plan	408
Follow-up Inspection Plan	408
Returning Facilities and Equipment to Full Operational Status	408

Regulating Features	409
Nonregulating Features	409
List of Operating Criteria for Regulating Lake Oroville	414
Decision Making Criteria for Operating Features Which Can Be Regulated.	414
Palermo Outlet	414
Oroville Dam Spillway	414
River Outlet Valves	414
Edward Hyatt Intake	415
Edward Hyatt Powerplant	415
Critical Conditions for Features Which Cannot be Regulated	416
Oroville Dam	416
Bidwell Canyon Saddle Dam	416
Parish Camp Saddle Dam	417
Oroville Dam Spillway	417
Edward Hyatt Intake and Penstock	417
Palermo Intake and Outlet	417
River Outlet Valve Chamber	417
List of Operating Criteria for Regulating Thermalito Diversion Pool	417
Decision Making Criteria for Operating Regulating Features	417
Thermalito Diversion Dam.	417
Critical Conditions for Features Which Cannot Be Regulated	418
Thermalito Diversion Dam	418
Thermalito Power Canal Headworks	418
List of Operating Criteria for Regulating Thermalito Forebay Reservoir and Power Canal.	418
Decision-Making Criteria for Operating Regulating Features	418
Thermalito Intake Structure	418
Thermalito Powerplant	418
Critical Conditions for Features Which Cannot Be Regulated	419
Thermalito Forebay Dam	419
Thermalito Intake Structure	419
Thermalito Power Canal (Cut Section).	420
Thermalito Power Canal (Fill Section)	420
List of Operating Criteria for Regulating Thermalito Afterbay Reservoir	420
Decision-Making Criteria for Operating Regulating Features	420
Thermalito Afterbay River Outlet	420
Sutter-Butte Outlet	420
PG&E Outlet	420
Western Canal and Richvale Outlets	420
Thermalito Afterbay Dam Ground Water Pumping System	420
Critical Condition for Features Which Cannot Be Regulated	421
Thermalito Afterbay Dam	421
Thermalito Power House Structure	421
Thermalito Afterbay River Outlet	421
Sutter-Butte Outlets	421
PG&E Outlet	421
Western-Richvale Outlets	421
Commentary	421
Conclusion	421

TABLES

<u>No.</u>		<u>Page</u>
1	Exploration Trenches in Foothill Belt--Oroville to Auburn Area . . .	62
2	Summary of Geologic Events	80
3	Earthquake Epicenters, June 1975-December 1975	133
4	Earthquake Epicenters, January 1976-May 1978	137
5	Value of Stress-Strain Parameters for Analysis of Oroville Dam . . .	204
6	Static Stress Comparison	205

FIGURES

CHAPTER I

1	Oroville Dam	1
2	Location Map, Oroville Facilities	2
3	Thermalito Diversion Dam	3
4	Thermalito Forebay Dam	4
5	Thermalito Afterbay Dam	4

CHAPTER II

6	Location map of six quadrangle study area	16
7	Historic earthquakes within a 100 km (62 mi) radius of Oroville . .	18
8	Aftershock locations of the Oroville earthquake	20
9	Locations of the Cleveland Hill and Mission Olive crack zones and sites of Department of Water Resources exploration trenches . . .	22
10	Ground cracking that resulted from the August 1, 1975, Oroville earthquake	23
11	Close-up view of a ground crack on southwest slope of Cleveland Hill	23
12	Locations of ground cracking from the Oroville earthquake and major lineaments in the southern study area	24
13	Aerial view of northern limit of ground cracking	25

<u>Figure No.</u>		<u>Page</u>
14	Changes in ground elevations around Lake Oroville, August 1975 to October 1976	28
15	Changes in crest elevations of Bidwell Canyon Saddle Dam between November 1967 and October 1977	29
16	Lineaments and faults in the northwestern Sierran foothills	31
17	Natural geologic provinces of California with field area location .	32
18	Small-scale parasitic isoclinal fold within melange metasedimentary rock	35
19	Relict bedding cross cut by foliation in melange metasedimentary rock	35
20	Sheared volcanoclastic metaconglomerate in melange metasedimentary rock	36
21	Exotic marble block in melange	36
22	Sample of olistostromal marble-phyllite collected in melange	37
23	Relict bedding in arc metasedimentary rock	39
24	Arc complex metavolcanic tuff breccia	39
25	Arc complex relict pillow and flow lavas cut by fault	39
26	Relict bedding and cross-bedding in arc tuff breccia and tuffaceous metasedimentary rock	40
27	Igneous stratigraphy of Standard Oceanic Crust and Smartville ophiolite	43
28	Well developed metavolcanic Smartville pillows	43
29	Well developed metavolcanic Smartville pillows	44
30	Sheared metavolcanic Smartville pillows	44
31	Metavolcanic Smartville sheeted dikes	45
32	Gabbroic screen rock in Smartville metavolcanic sheeted dikes . . .	45
33	Granophyric screen rock in Smartville metavolcanic sheeted dikes . .	46
34	Mesozoic time scale with corresponding intrusive epochs in the Sierra Nevada region	47
35	Metavolcanic xenoliths within Swedes Flat plutonic rock	48
36	View of Bald Rock exhibiting surface exposure and exfoliation that is typical of the Sierra Nevada complex	49

<u>Figure No.</u>		<u>Page</u>
37	Ione Formation auriferous gravel with intercalated Oroville tuff (Mehrten Formation-?)	52
38	Lovejoy Formation basalt disconformably overlying Ione Formation . .	53
39	Lovejoy Formation basalt on North Table Mountain	54
40	Young erosional surface cut into Tuscan Formation that is adjacent to older and structurally higher erosional surface cut into mesozoic metamorphic rock	55
41	Tuscan Formation volcanic conglomerate, cross-bedded sand and lahatic mudflow breccia	56
42	Late Cenozoic gravel and cross-bedded sand (Red Bluff Formation-?) .	57
43	Late Cenozoic gravel (Red Bluff Formation-?) unconformably overlying Oroville tuff (Mehrten Formation-?) along the Feather River	58
44	Landslide in Ione Formation	59
45	Stringtown Mountain landslides	59
46	Prehistoric landslide north slope of Bloomer Hill	60
47	Major lineaments in the northwestern Sierran foothills showing exploration localities with faulting assessments for each site . .	61
48	Foothills Fault System of the western Sierra Nevada, California . .	66
49	Aerial view of Glover Ridge (klippe) and traced location of Glover Ridge Fault	70
50	Aerial northeast view of the Cleveland Hill Fault along the western side of Cleveland Hill	71
51	Aerial view of Chico monocline	75
52	Normal fault in Tuscan Formation	76
53	Normal fault in Tuscan Formation	76
54	Vertical aerial view of eastern fracture zone developed in Tuscan Formation	77
55	Map with cross section oriented perpendicular to suspected fault through Magalia Reservoir	78
56	Comparison of foreshock-aftershock patterns for the Oroville earthquake and Mogi's "Type II" (reservoir-induced earthquakes). .	84
57	Water level history of Lake Oroville from initial filling to September 1978	84

CHAPTER III

<u>Figure No.</u>		<u>Page</u>
58	DWR-USGS Oroville Sensitive Seismographic Network	125
59	Oroville Foreshocks, Mainshock, and Aftershocks; June 1, 1975- December 31, 1975	126
60	1975 Oroville Earthquake Hypocenters (North Vertical Cross Section)	127
61	1975 Oroville Earthquake Hypocenters (Middle Vertical Cross Section)	127
62	1975 Oroville Earthquake Hypocenters (South Vertical Cross Section)	128
63	Oroville Earthquake Epicenters (January 1, 1976-May 31, 1978) . . .	129
64	Oroville Earthquake Hypocenters, 1976-May 31, 1978 (North Vertical Cross Section)	130
65	Oroville Earthquake Hypocenters, 1976-May 31, 1978 (Middle Vertical Cross Section)	130
66	Oroville Earthquake Hypocenters, 1976-May 31, 1978 (South Vertical Cross Section)	131
67	Oroville Earthquake Hypocenters, August 2, 1975-December 31, 1975 (Middle Vertical Cross Section)	131
68	Oroville Sequence, Number of Aftershocks/Month, Water Surface Elevation (August 1975-June 1978)	132

CHAPTER IV

69	Lake Oroville Water Surface Elevation	142
70	Oroville Area Level Lines (1977)	143
71	Precise Level Net for Study of Lake Oroville - 1967.	144
72	Precise Level Net for Study of the Oroville Earthquake - 1977 . . .	145
73	Elevation Differential Isogram--September 1967-October 1969	147
74	Elevation Differential Isogram--October 1969-August 1975	148
75	Elevation Differential Isogram--September 1967-October 1977	149
76	Elevation Differential Isogram--August 1975-October 1976	150
77	Elevation Differential Isogram--October 1976-October 1977	151

<u>Figure No.</u>		<u>Page</u>
78	Elevation Differential Isogram--August 1975- October 1977	152
79	Avocado Elevation Differentials	154
80	Bald Rock Elevation Differentials	155
81	Bidwell Elevation Differentials	156
82	Bidwell Canyon Saddle Dam Elevation Differentials	158
83	Canyon Drive Elevation Differentials	159
84	Cleveland Hill Elevation Differentials	160
85	Dam Elevation Differentials	161
86	Dunstone Elevation Differentials	162
87	Feather Falls Elevation Differentials	163
88	Foothill Elevation Differentials	164
89	Miners Ranch Elevation Differentials	165
90	Mission Olive Elevation Differentials	166
91	Morris Elevation Differentials	168
92	Olive Elevation Differentials	169
93	Oro-Bangor Elevation Differentials	170
94	Oroville Elevation Differentials	171
95	Potter Elevation Differentials	172
96	Richvale Elevation Differentials (1 of 2)	173
97	Richvale Elevation Differentials (2 of 2)	174
98	Thompson Flat Elevation Differentials	175
99	Wyn-Miners Ranch Elevation Differentials	176
100	103 Elevation Differentials (1 of 3)	177
101	103 Elevation Differentials (2 of 3)	178
102	103 Elevation Differentials (3 of 3)	179
103	Oroville Dam Crest Differential Settlement (References to the Abutments)	180
104	Horizontal Geodetic Control and Triangulation Net (1967-1975) . . .	182

CHAPTER V

<u>Figure No.</u>		<u>Page</u>
105	Location Map	188
106	Oroville Maximum Section	192
107	Average Gradation Curves of Oroville Dam Materials	193
108	Oroville Dam Embankment, Original Dynamic Instrumentation	194
109	Oroville Dam Embankment, Present Dynamic Instrumentation (December, 1978)	196
110	Acceleration Records, Main Event of August 1, 1975	198
111	Acceleration Records with Corrected Time Scales, August 1, 1975	200
112	Acceleration Records, Event of August 5, 1975	201
113	Acceleration Records, Event of September 27, 1975	202
114	Acceleration Response Spectra for Crest Motions, Event of August 1, 1975	203
115	Finite Element Mesh, Maximum Section Oroville Dam	204
116	Contours of Effective Maximum Principal Stress in Oroville Dam, Full Reservoir	206
117	Contours of Effective Minimum Principal Stress in Oroville Dam, Full Reservoir	206
118	Contours of Maximum Shear Stress in Oroville Dam, Full Reservoir	207
119	Orientation of Principal Stresses	207
120	In-Situ Shear Moduli for Saturated Clays	208
121	Sample Gradation for Cyclic Triaxial Tests	209
122	Modulus Determinations for Gravelly Soils	210
123	Comparison of Damping Ratios for Gravelly Soils and Sands	211
124	Section on Long Chord of Dam Axis	212
125	Comparison of Natural Periods for Two-Dimensional and Three-Dimensional Embankment in Triangular Canyon	212
126	Shear Modulus Reduction Curve for Embankment Soils	213
127	Static Shear Strength Envelopes for Core Material	214

Figure No.		Page
128	K_{2max} vs. Natural Period	214
129	Maximum Accelerations Computed from 3D and Plane Strain Analyses Using Base Motions from Taft Record (after Makdisi)	215
130	Damping Ratios for Embankment Soils	217
131	Comparison of Acceleration Time Histories, August 1 Main Shock . . .	218
132	Comparison of Displacement Time Histories and Acceleration Response Spectra for Crest Motions, August 1 Main Shock	219
133	Comparison of Acceleration Time Histories and Response Spectra, September 27 Aftershocks	220
134	Lineaments, Faults and Recorded Epicenters Around Oroville	222
135	Location of Faults in Relation to Oroville Dam	223
136	Relationship of Oroville Dam to Assumed Northward Extension of Fault	224
137	Earthquake Ground Motion Characteristics	226
138	Reanalysis Earthquake	227
139	Response Spectra for the Reanalysis Earthquake	228
140	Acceleration Response to Reanalysis Earthquake	230
141	Influence of Shear Modulus of Shell Material on Computed Maximum Horizontal Dynamic Shear Stresses	232
142	Influence of Shear Modulus of Core on Computed Maximum Horizontal Dynamic Shear Stresses	234
143	Comparison of Horizontal Dynamic Shear Stress Time Histories from LUSH and QUAD4	235
144	Comparison of Horizontal Dynamic Shear Stress Time Histories from LUSH and QUAD4	236
145	Comparison of Computed Maximum Horizontal Dynamic Shear Stresses by Computer Programs LUSH and QUAD4	237
146	Model Embankment for Determining Influence of Poisson's Ratio on Dynamic Shear Stresses	238
147	Influence of Poisson's Ratio on Computed Dynamic Shear Stresses . .	239
148	Comparison of Computed Maximum Horizontal Dynamic Shear Stresses for Different Embankment Sections	240

<u>Figure No.</u>		<u>Page</u>
149	Comparison of Maximum Horizontal Shear Stresses Determined from 3D and Plane Strain Analyses Using Base Motions from Taft Record (after Makdisi)	242
150	Estimated Three-Dimensional Effect on Computed Maximum Horizontal Dynamic Shear Stresses	243
151	Field and Modeled Oroville Gravel Gradations	245
152	Final Statistical Analysis - Zone 3, Percent Compaction	246
153	Field Control Tests - Zone 3	247
154	Maximum Density Tests - Zone 3	248
155	Cyclic Triaxial Test Records for Modeled Oroville Gravel	252
156	Cyclic Triaxial Test Records for Modeled Oroville Gravel	253
157	Cyclic Triaxial Test Records for Modeled Oroville Gravel	254
158	Monterey "0" Sand and Oroville Sand Gradations	255
159	Typical Static Triaxial Compression Test Results for Monterey "0" Sand	257
160	Typical Static Triaxial Extension Test Results for Monterey "0" Sand	258
161	Summary of Static Triaxial Test Results for Dense Monterey "0" Sand	259
162	Cyclic Triaxial Strain Envelopes for Monterey "0" Sand	260
163	Static and Cyclic Triaxial Test Results for Dense Monterey "0" Sand .	261
164	Cyclic Triaxial Test Results for Monterey "0" Sand	262
165	Cyclic Triaxial Test Records for Monterey "0" Sand	263
166	Shear Plane Development during Final Stage of Necking for Monterey "0" Sand	264
167	Cyclic Triaxial Test Records for Monterey "0" Sand	265
168	Cyclic Triaxial Test Records for Oroville Sand	266
169	Cyclic Triaxial Test Records for Oroville Sand	267
170	Cyclic Triaxial Test Records for Modeled Oroville Gravel	269
171	Cyclic Traixial Test Records for Modeled Oroville Gravel	269
172	Cyclic Triaxial Test Records for Modeled Oroville Gravel	270

<u>Figure No.</u>		<u>Page</u>
173	Extension/Compression Cycle for Monterey "0" Sand Cyclic Triaxial Test	271
174	Compression/Extension Cycle for Monterey "0" Sand Cyclic Triaxial Test	273
175	Comparison of Shaking Table and Cyclic Triaxial Test Results for 5 Cycles	274
176	Comparison of Shaking Table and Cyclic Triaxial Test Results for 10 Cycles	275
177	Cyclic Strength Envelopes for Strength Interpretation I - Static and Cyclic Test Results	278
178	Typical Extrapolations of Isotropically-Consolidated Cyclic Triaxial Tests on Modeled Oroville Gravel	279
179	Cyclic Strength Envelopes for Strength Interpretation II - Extrapolated Cyclic Test Results	280
180	Representative Relationship Between τ/τ_{\max} and Number of Cycles Required to Cause Liquefaction (Seed et al, 1975)	283
181	Computed Compressive Strain Potentials in Upstream Shell - Percent	286

CHAPTER VI

182	Oroville Dam Flood Control Outlet Structure Plan and Elevation . . .	292
183	Elevation and Sections	293
184	Maximum Tensile Stresses at time 7.76 sec.	295
185	Maximum Tensile Stresses at time 8.46 sec.	296
186	Maximum Tensile Stresses at time 7.76 sec. in steel	297

CHAPTER VII

187	Plan and Elevation	352
188	Typical Sections	353

CHAPTER VIII

189	Location Map, Edward Hyatt Powerplant Facilities	390
190	Fish Barrier Dam	391
191	Fish Barrier Dam, Plan and Elevation	392

<u>Figure No.</u>		<u>Page</u>
192	Fish Barrier Dam, Section and Details	393
193	Location Map, Thermalito Powerplant, Forebay, and Afterbay	394
194	Transverse Section, Units Nos. 3, 4, 5 and 6	396
195	Generator Room, Plan - Elevation 252.0	397
196	Overall view of Edward Hyatt Powerplant Intake Structure	398
197	Transverse Section, Unit No. 1	400
198	Switchyard and General Floor	401
199	230-KV Power Circuit Breakers	404

CHAPTER IX

200	Schematic Diagram of Oroville Complex	410
201	Schematic Diagram of Oroville Dam and Vicinity	411
202	Schematic Diagram of Thermalito Forebay and Vicinity	412
203	Schematic Diagram of Thermalito Afterbay and Vicinity	413

APPENDIXES

A	Reports Prepared by the Special Consulting Board and Responses by by the Department of Water Resources	423
B	Acceleration Time Histories and Response Spectra for the August 1, 1975 and September 27, 1975 Recorded Motions on Dam Crest and Bedrock, in Upstream-Downstream Direction. (Figs. B-1 through B-8)	457
C	Static Stresses from Static Finite Element Analysis. Figs. C-1 through C-9)	467
D	Time Histories and Response Spectra for Reanalysis Earthquake. (Figs. D-1 through D-6)	483
E	Results of Dynamic Finite Element Analyses for Reanalysis Earthquake	489
	Maximum Section -- Shell $K_2 \text{ max}$ = 350, 200, 130	
	Element Stresses and Strains (Figs. E-1 through E-18) . .	490
	Shear Stress Time Histories (Figs. E-19 through E-39) . .	500
	Section 2 -- Shell $K_2 \text{ max}$ - 130 - LUSH and QUAD4	
	Element Shear Stresses and Strains (Figs. E-40 through E-45)	521

	Acceleration Time Histories (Fig. E-46)	525
	Section 3 -- Shell K_2 max = 130 - LUSH and QUAD4	
	Element Shear Stresses and Strains (Figs. E-47 through E-52)	526
	Acceleration Time Histories (Fig. E-53)	530
	Model Embankment -- Shell K_2 max = 130	
	Effect of Poisson's Ratio on Stresses (Figs. E-54 through E-55)	531
F	Embankment Response Model	533
G	Cyclic Triaxial Test Summaries of Modeled Oroville Gravel Tests. (Figs. G-1 through G-68)	541
H	Extrapolation of Isotropically-Consolidated Cyclic Triaxial Tests for Strength Interpretation II. (Figs. H-1 through H-25)	613
I	Cyclic Triaxial Test Results for Modeled Oroville Gravel Using Strength Interpretation II. (Figs. I-1 through I-10)	629
J	Procedure for Interpreting Cyclic Triaxial Test Data to Determine Cyclic Shear Stress on Potential Failure Plane	641
K	Cyclic Triaxial Test Results for Modeled Oroville Gravel Using Strength Interpretation I. (Figs. K-1 through K-10)	649
L	(Available on request later in 1979)	
M	Embankment Strain Potentials. (Figs. M-1 through M-4)	663

PLATES
(inside rear cover)

Plate 1. Geology of Lake Oroville Area, Butte County, California

Plate 2. Oroville Area Level Net Benchmark Locations

CONVERSION FACTORS

Metric to Customary System of Measurement

<u>Quantity</u>	<u>Metric Unit</u>	<u>Multiply by</u>	<u>To get customary equivalent</u>
Length	millimetres (mm)	0.03937	inches (in)
	centimetres (cm) for snow depth	0.3937	inches (in)
	metres (m)	3.2808	feet (ft)
	kilometres (km)	0.62139	miles (m)
Area	square millimetres (mm ²)	0.00155	square inches (in ²)
	square metres (m ²)	10.764	square feet (ft ²)
	hectares (ha)	2.4710	acres (ac)
	square kilometres (km ²)	0.3861	square miles (mi ²)
Volume	litres (l)	0.26417	gallons (gal)
	megalitres	0.26417	million gallons (10 ⁶ gal)
	cubic metres (m ³)	35.315	cubic feet (ft ³)
	cubic metres (m ³)	1.308	cubic yards (yd ³)
	cubic metres (m ³)	0.0008107	acre-feet (ac-ft)
	cubic dekametres (dam ³)	0.8107	acre-feet (ac-ft)
	cubic hectometres (hm ³)	0.8107	thousands of acre-feet
Flow	cubic kilometres (km ³)	0.8107	millions of acre-feet
	cubic metres per second (m ³ /s)	35.315	cubic feet per second (ft ³ /s)
	litres per minute (l/min)	0.26417	gallons per minute (gal/min)
	litres per day (l/day)	0.26417	gallons per day (gal/day)
	megalitres per day (Ml/day)	0.26417	million gallons per day (mgd)
	cubic metres per day (m ³ /day)	0.0008107	acre-feet per day
Mass	kilograms (kg)	2.2046	pounds (lb)
	tonne (t)	1.1023	tons (short, 2,000 lb)
Velocity	metres per second (m/s)	3.2808	feet per second (ft/s)
Power	kilowatts (kW)	1.3405	horsepower (hp)
Pressure	kilopascals (kPa)	0.145054	pounds per square inch (psi)
	kilopascals (kPa)	0.33456	feet head of water
Specific capacity	litres per minute per metre drawdown	0.08052	gallons per minute per foot drawdown
Concentration	milligrams per litre (mg/l)	1.0	parts per million
Electrical conductivity	microsiemens per centimetre (μS/cm)	1.0	micromho per centimetre
Temperature	degrees Celsius (°C)	(1.8 × °C) + 32	degree Fahrenheit (°F)

CHAPTER I INTRODUCTION

Oroville Dam (Figure 1) is situated in the foothills of the Sierra Nevada above the Sacramento Valley. The dam is 8 kilometres (5 miles) east of the City of Oroville and about 209 kilometres (130 miles) northeast of San Francisco.

On August 1, 1975, at 1320 hours (1:20 p.m.) PDT, an earthquake of Richter Scale magnitude 5.7 occurred about 12 kilometres (7.5 miles) southwest of Oroville Dam. During the main event and the many aftershocks that followed, the Oroville facilities continued operating without interruption except for about a 45 minute shutdown of power generation.

The Oroville earthquake sequence began with a number of foreshocks on June 28, 1975. Then, on August 1, twenty-nine foreshocks occurred within 5 hours of the main shock. The largest of these had a magnitude of 4.8. Many aftershocks, the largest of which had a magnitude of 5.1, occurred throughout August, and scattered shocks continued.

Purpose

Intensive investigations originating from the August 1, 1975, Oroville earthquake, were conducted to determine:

1. Geologic and tectonic conditions.
2. Fault mechanism and orientation.
3. Crustal movements.
4. Public safety as it relates to the Department's facilities.

The results of these investigations are presented in detail in the following chapters.

Description of the Oroville Facilities

Oroville Dam and its appurtenances, along with the Thermalito facilities (Figure 2), comprise a multiple purpose project, which includes water conservation, power generation, flood control, recreation,



Figure 1. Oroville Dam

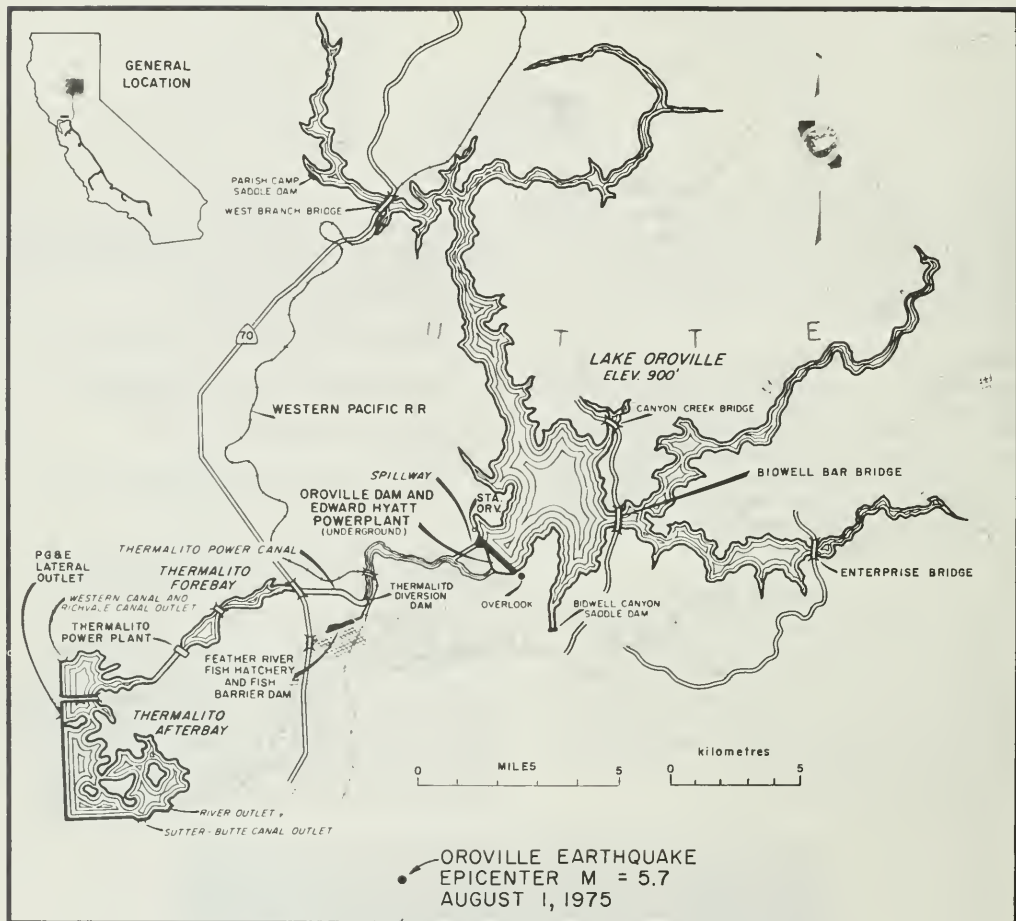


Figure 2. Location Map, Oroville Facilities

and fish and wildlife enhancement. The lake stores winter and spring runoff, which is released into the Feather River as necessary to supply project needs and commitments. The pumped-storage capability of the Oroville facilities permits maximum use of peaking capabilities and increases the value of power produced by the releases.

Water releases from Edward Hyatt Powerplant are largely diverted from the Feather River at the Thermalito Diversion

Dam (Figure 3), a concrete gravity structure with a radial gated crest section. These diversions pass through the Thermalito Power Canal and Thermalito Forebay (Figure 4), through Thermalito Powerplant, and into Thermalito Afterbay. The Thermalito Diversion Pool, Power Canal, and Forebay have a common water surface to accommodate flow reversals for the pumped-storage operation. Thermalito Afterbay (Figure 5) stores the plant discharges for the pumped-storage or conventional operation and reregulates flow for uni-

form return to the Feather River.

Migrating salmon and steelhead blocked by the Oroville Complex are diverted from the river into the Feather River Fish Hatchery at the Fish Barrier Dam, located 0.8 kilometre (0.5 mile) downstream from the Thermalito Diversion Dam.

The Investigating Organization

On August 8, 1975, the Department of Water Resources convened its Consulting Board for Earthquake Analysis to review the general post-earthquake situation and the preliminary data assembled. On September 11 and 12, 1975, a Special Consulting Board for the Oroville Earthquake, composed of the members of the Consulting Board for Earthquake Analysis and additional engineering consultants in the field of design and construction of dam and reservoir projects, was convened by the Department to review the Department's programs for data collection and evaluation of structural seismic safety.

The Special Consulting Board for the Oroville Earthquake consisted of the following members:

George W. Housner, Chairman
Clarence R. Allen
John A. Blume
Bruce A. Bolt
Wallace L. Chadwick
Thomas M. Leps
Alan L. O'Neill
Philip C. Rutledge
H. Bolton Seed

With recommendations from the Special Consulting Board, several earthquake-related investigations were undertaken by the Department. These include:

1. Geologic studies and mapping of the epicentral area and the causative fault.
2. Seismological studies dealing with the earthquake sequence and fault plane resolution.



Figure 3. Thermalito Diversion Dam



Figure 4. Thermalito Forebay Dam

3. Determination of the seismic safety of project structures under loading of the Reanalysis Earthquake selected for this area.
4. Surveys of the area.
5. Evaluation of the existing seismic instrumentation monitoring system.

The Special Consulting Board was reconvened on November 22 and 23, 1976, to

review the progress of the investigations and provide recommendations. On September 28 and 29, 1978, the Special Consulting Board was convened to review those completed reports on the investigations and reanalysis of the Oroville facilities prior to their being published in this bulletin. Progress of the uncompleted reports was also reviewed.

To meet regular State and Federal safety review requirements for the Oroville-Thermalito facilities, the Special Consulting Board was requested to be the Department's consultant for these requirements.

Reports prepared by the Special Consulting Boards and Department's responses are included in Appendix A.

Reanalysis of Project Structures for Earthquake Safety

The performance of State Water Project facilities during the August 1975 earthquake sequence demonstrated their ability to withstand this seismic loading. Only minor superficial damage was sustained by some of the secondary structures. The Department's Bulletin 203 (April 1977), Performance of the Oroville Dam and Related Facilities During the August 1, 1975 Earthquake, documents the performance of the Oroville complex



Figure 5. Thermalito Afterbay Dam

during the main event and succeeding aftershocks.

The Special Consulting Board reviewed the seismic environment of the Oroville facilities and recommended an earthquake motion be developed for reevaluation of the Oroville-Thermalito structures that has a magnitude of 6.5 producing a peak acceleration of 0.6g. Detailed development and characteristics of this Reanalysis Earthquake are described in Chapter V.

A program for dynamic structural analysis of critical structures was implemented in cooperation with Professors H. Bolton Seed, A. K. Chopra, and Edward L. Wilson of the University of California, Berkeley. The critical structures to be reanalyzed are: Oroville Dam, Oroville Dam Spillway (flood control outlet structure), Thermalito Diversion Dam, Thermalito Powerplant Headworks, Thermalito Forebay Dam, and Thermalito Afterbay Dam. Dynamic strengths of the material in Oroville Dam were determined by large-scale laboratory testing conducted by the University of California. Exploration and soils testing for the Thermalito Forebay and Afterbay Dams were conducted by the Department of Water Resources.

Summary of Conclusions and Recommendations

The following are conclusions and recommendations from the chapters in this Bulletin.

Geological Investigations (Chapter II)

1. The August 1, 1975, Oroville earthquake was accompanied by movement on the previously unrecognized Cleveland Hill Fault. A linear zone of discontinuous ground cracking developed along the fault about 7 kilometres (4.3 miles) east of the main shock epicenter.
2. Initial length of ground rupture on the Cleveland Hill Fault was about 1.6 kilometres (1.0 mile). Over a period of about 12 months

the ground cracking extended progressively to the north, reaching a total length of 8.5 kilometres (5.3 miles).

3. Offset along the fault was greatest in the southern segment, where the original cracking occurred. Offset increased with time; movement amounted to about 50 millimetres (2 inches) vertical displacement and 25 millimetres (1 inch) horizontal extension.
4. The Cleveland Hill Fault was not encountered by trenching or geophysical investigation north of Mt. Ida Road. Aftershock hypocenters projected up a calculated fault plane indicate the fault at the ground surface trends into Bidwell Canyon and that it may pass beneath Oroville Dam at depth.
5. Trenching across the Cleveland Hill Fault by Department of Water Resources and others provides evidence for multiple small fault displacements during the past 100,000 years. These displacements would likely have produced earthquakes similar to the 1975 Oroville event.
6. Three major lineament-fault zones, the Paynes Peak, Swain Ravine, and Prairie Creek, have been delineated in the area by geologic studies. These lineament-fault zones are complex bands of discontinuous, intertwined, steeply dipping faults which were formed during Mesozoic or earlier time under the influence of a different tectonic stress regime that exists today. The Cleveland Hill Fault is within the Swain Ravine Lineament fault zone.
7. Most Cenozoic fault movements in the Sierran foothill belt are caused by east-west extensional stresses reactivating pre-existing Paleozoic and Mesozoic faults such as those comprising the lineament-fault zone.

8. Historic (Cenozoic) faulting and historic earthquake records in the foothill region demonstrate that the current and long-range level of seismic activity is one of low- to moderate-magnitude earthquakes at relatively long recurrence intervals, occasionally resulting in minor ground rupture and offset.
9. Nothing was seen in this geologic study to indicate that earthquakes greater than Richter Magnitude 6.5 should be expected in the Oroville area.
10. Maximum offset that should be anticipated from another Oroville-type earthquake is estimated to be 50 millimetres (2 inches) of vertical displacement and 25 millimetre (1 inch) horizontal extension. For a somewhat larger event displacement might be several times larger than these values, along north-south trending faults.
11. The evidence available does not indicate a causal relationship between Lake Oroville and the earthquake, but the possibility cannot be eliminated conclusively at this time.

Seismology (Chapter III)

Since August 1, 1975, a correlation is not indicated between the Lake Oroville water surface variations and the rate of occurrence of Oroville aftershocks.

Within the boundary of the aftershock zone north of $39^{\circ}26'N$ latitude, vertical cross-sectional plots indicate that the Cleveland Hill Fault is a single, well defined break, dipping to the west at about 60° with the horizontal and with a near north-south strike. Vertical cross-sectional plots south of $39^{\circ}26'N$ indicate that the fault breaks along more than one plane.

Vertical and Horizontal Geodesy (Chapter IV)

Vertical Crustal Movements

The following conclusions are based on free adjustment holding the elevation of OM-27 fixed (1967 USC&GS adjustment) and therefore all elevations differentials are relative to OM-27.

1. Based on the preearthquake datum of 1967, the greatest elevation differential was only 63 millimetres (0.207 foot) on line Olive during the ten-year epoch (1967-1977).
2. The August 1, 1975, Oroville earthquake is associated with minor subsidence in the Oroville area, mainly south and southwest of Lake Oroville.
3. Most of the subsidence associated with the August 1, 1975, Oroville earthquake was measured between late August 1975 to October 1976.
4. The elevation differentials show movement of the fault zone that passes through the level lines Cleveland Hill and Mission Olive (ground cracking was evident before the lines were established). A fault zone may pass through the survey line Miners Ranch south of Lake Oroville; however, no ground cracking was found there.
5. Minor subsidence of less than 25 millimetres (0.082 foot) has been measured adjacent to Oroville Dam and Lake between 1967 to 1977 due to all causes.

Horizontal Crustal Movements

1. All computed horizontal movements are minor and in many cases within the accuracy of the existing surveys and computations.
2. The August 1, 1975, Oroville earthquake did not cause sufficiently large horizontal movements that could

be reliably measured and calculated within the Lake Oroville Monitoring Network.

Oroville Dam Evaluation of Seismic Stability (Chapter V)

1. The seismic stability of Oroville Dam was investigated for the Reanalysis Earthquake of Richter Magnitude 6.5, at a hypocentral distance of 5 kilometres (3 miles) from the dam, and producing the following ground motion characteristics at the base of the dam:

maximum acceleration	0.6g
predominant period	0.4 seconds
duration	20 seconds
acceleration time history	modified Pacoima plus modified Taft

It was concluded that this ground shaking was more severe than any future shaking likely to affect the dam.

2. Using "best judgment" choices for input soil properties and conditions, relatively small embankment deformations were estimated by the seismic evaluation procedures. It is concluded that Oroville Dam would perform satisfactorily if subjected to the Reanalysis Earthquake.

Oroville Dam Flood Control Outlet Structure (Chapter VI)

The investigations performed indicate that when the Oroville Flood Control Outlet Structure is subjected to the Reanalysis Earthquake ground motion it is stable, and that expected compressive and tensile stresses are within the allowable limits established for the structure.

Thermalito Diversion Dam (Chapter VII)

Conclusion by Dr. A. K. Chopra:

Based on results of dynamic analyses and available data for concrete strength, it is concluded that Thermalito Diversion Dam should be able to resist the stresses expected during the earthquake (Reanalysis Earthquake) ground motion specified by the State Department of Water Resources.

Reappraisal of Secondary Structures (Chapter VIII)

Fish Barrier Dam - A review of the original design of this dam indicated maximum compressive and tensile stresses of approximately 120 psi and 10 psi respectively. A check of stability using a pseudostatic analysis and seismic coefficients of 0.25 and 0.6 indicated a shear friction factor of safety in excess of 9. Based on this finding, no additional seismic analysis is recommended for the Fish Barrier Dam.

Edward Hyatt Powerplant - The powerhouse substructure has been reviewed using a comparative pseudostatic analysis of previously designed powerhouse substructures. Based on this comparison, it has been determined that this substructure would be capable of resisting the forces induced by a 0.25g peak ground acceleration; therefore, no modifications are required.

Modifications will be made to improve the seismic resistance of powerhouse superstructure components as necessary.

Thermalito Powerplant - The powerhouse substructure has been reviewed using a comparative pseudostatic analysis of previously designed powerhouse substructures. Based on this comparison, it has been determined that this substructure would be capable of resisting the forces induced by a 0.25g peak ground acceleration; therefore, no modifications are required.

Modifications will be made to improve the seismic resistance of powerhouse superstructure components as necessary.

Miscellaneous Structures - Damage that may occur to the miscellaneous structures are not considered to be a threat to public safety and property. For the purpose of the seismic reevaluation these structures are classified as noncritical.

Bridges - Bridge components that will not sustain the forces generated by a 0.25g peak ground acceleration will be modified to strengthen their seismic resistance.

Switchyards - Based on the consideration that failure of electrical equipment in the Edward Hyatt or Thermalito Powerplant switchyards does not pose a threat to public safety or property, the switchyards are classified as noncritical elements of the Oroville Complex.

Contingency Plan for Seismic Emergencies (Chapter IX)

The contingency plan is attentive to established Division Policy; it provides for detection, notification, and response to seismic events. The plan also includes a list of operational facilities and features along with criteria that must be met before returning to preearthquake operating status.

Department's Findings

Based on the preceding conclusions from the investigations completed to date, the Department concludes that these facil-

ities do not pose a threat to public safety.

Uncompleted Reports

The reanalysis of the Thermalito Powerplant Headworks and the Thermalito Forebay and Afterbay Dams has not been completed. Dr. A. K. Chopra (the Department's consultant) is currently reanalyzing the Thermalito Powerplant Headworks. The Department is continuing with the reanalysis of the Thermalito Forebay and Afterbay Dams. Investigations of the Bidwell Canyon Saddle Dam and the effect of fault movements with respect to the Oroville-Thermalito facilities will also be completed. These reports are planned for completion early in 1979 and publication by mid-1979.

Safety Review Requirements

The completion of the investigations and reanalysis of the Oroville facilities with concurrence by the Special Consulting Board fulfills the following two safety requirements:

1. The five-year Federal Energy Regulatory Commission's Part 12 Safety Inspection Report.
2. The five-year Department of Water Resources, Division of Safety of Dams' safety review under the regulations of the California Administrative Code, Title 23, Article 4, Sections 340-343.

Report of the Special Consulting Board

For the Oroville Earthquake

November 15, 1978

(see next page)

15 November 1978

Report of the Special Consulting Board for the Oroville Earthquake

Mr. Howard H. Eastin, Chief
Division of Operations and Maintenance
Department of Water Resources
P.O. Box 388
Sacramento, California, 95802

At meetings on September 28 and 29, 1978, of the Special Consulting Board for the Oroville Earthquake, staff members of the Department of Water Resources made presentations relative to the Department's draft of its report, "August 1, 1975, Oroville Earthquake Investigation - Bulletin 203-78." The Board has also reviewed chapters of the draft prior to the meeting. At the conclusion of the meetings, the Board was asked to respond to the following questions relating to the content of the Oroville Earthquake Investigation report. Our responses are presented below.

Question No. 1. Does the Board concur with the conclusions and the recommendations set forth in the Summary of Conclusions and Recommendations?

Response. The Board has reviewed the draft of the chapters of Bulletin 203-78 and has heard the presentations of the staff members, and has reviewed the "final Draft Chapter 1" which contains the Summary of Conclusions and Recommendations.

The Board concurs with the conclusions and the recommendations set forth in the Summary of Conclusions and Recommendations in the October 24, 1978, "final draft" of Chapter 1.

Question No. 2. Does the Board agree that the Oroville Division's critical structures (except Thermalito Forebay and Thermalito Afterbay Dams) would perform adequately with respect to public safety during the adopted earthquake ground motions?

Response. The Board agrees that the critical structures (except Thermalito Forebay and Afterbay Dams which have not yet been analyzed) would perform adequately with respect to public safety if subjected to the adopted earthquake ground motions.

Question No. 3. Does the Board have any comments on the studies completed to date for the seismic stability of Thermalito Forebay and Afterbay Dams?

Response. The Board does not have any comments except to urge completion of the studies at an early date.

Question No. 4. The Department intends to publish the results of the Thermalito Power Plant - Headworks, Seismic Evaluation, and Thermalito Forebay and Afterbay, Evaluation of Seismic Stability, reports next year, possibly as Bulletin No. 203-79. Does the Board consider another meeting necessary or could the Board's review, comments and report be handled by correspondence?

Response. The Board feels that another meeting would be desirable at which staff members would present the results of the analyses and respond to questions from the Board.

Question No. 5. Does the Board have any other comments or recommendations to make at this time?

Response.

a. The Board recommends that in Chapter 2-Contingency Plan for Seismic Emergencies^{1/} the criteria for notification given on page 5^{2/} be revised to read that 0.1g recorded at the ^{base}crest of Oroville Dam will replace the 3.0 Richter Scale criteria for notification, and 0.15g will replace the 4.0 Richter Scale criteria. It is also recommended that Annual Earthquake Drills be held so that personnel will be prepared to act in the event of an actual earthquake.

b. With reference to Chapter 5,^{3/} the Board recommends that DWR request NOAA to perform a precise level survey from a known, stable benchmark to benchmark OM 27, as this benchmark is a key element in the geodetic survey at Oroville Dam.

c. With reference to Chapter 5,^{3/} the Board recommends that resurveys be made at 5 year intervals, or after significant earthquakes, to monitor crustal movements that might have taken place.

The Board was favorably impressed by the investigations and analyses carried out by the Department, and commends the Department for the diligence and thoroughness of its work.

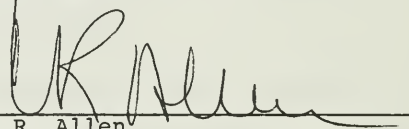
^{1/} Chapter IX in this bulletin.

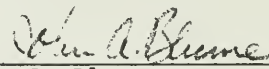
^{2/} See page 407 in this bulletin.

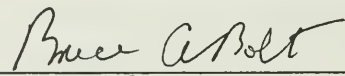
^{3/} Chapter IV in this bulletin.

Respectfully Submitted,


George W. Housner



C. R. Allen

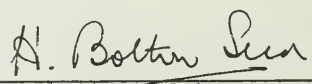

John A. Blume

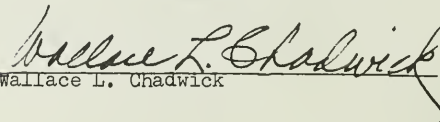

Bruce A. Bolt


T. M. Leps


Alan L. O'Neill


Philip C. Rutledge


H. Bolton Seed


Wallace L. Chadwick

REVIEW BY THE DIVISION OF MINES AND GEOLOGY

The Department requested the Department of Conservation, Division of Mines and Geology to review the final draft of Bulletin 203-78

The response from the Division of Mines and Geology on Bulletin 203-78 follows.

Memorandum

To : Clifford V. Lucas, Chief Civil Maintenance Branch Date: December 22, 1978
Division of Operations and Maintenance
Department of Water Resources
1416 9th Street
Sacramento, California 95814

From : **Department of Conservation**
Division of Mines and Geology
1416 - 9th Street, Sacramento 95814

Subject: Review of DWR Bulletin 203-78 Final Draft

This is our response to your request of December 11 that the Division of Mines and Geology provide review of final draft of DWR Bulletin 203-78. Our commentary is limited to one observation in Chapter IV, Seismology. 1/

The conclusion (page 5)^{2/} that there is no correlation between water levels and the rate of earthquakes does not consider the strengths of the earthquakes, but is based on a count of events regardless of magnitude. When the strengths of the earthquakes are considered, the resulting pattern of seismic strain released might be related to water levels. Most of the seismic strain appears to be released following episodes of filling, and very little strain release appears to occur during the actual filling.

We appreciate the opportunity to comment on this useful publication.


James F. Davis
State Geologist

cc: Priscilla C. Grew

1/ Chapter III in this bulletin.

2/ Page 124 in this bulletin.

CHAPTER II

GEOLOGIC INVESTIGATIONS

On August 1, 1975, a strong earthquake occurred near Oroville, California. The earthquake sequence began June 28, 1978, with the occurrence of several foreshocks; the largest of these foreshocks was magnitude 3.8. From July 8 through July 31, only five foreshocks occurred, giving the appearance that earthquake activity was ceasing. Then on August 1, twenty-nine foreshocks, the largest of which was magnitude 4.8, occurred within five hours prior to the magnitude 5.7 main shock at 1320 hours Pacific daylight time.

The hypocenter for the main shock of the Oroville earthquake series was approximately 1 km (0.6 mi) east-northeast of Palermo at a depth of 8.8 km (5.5 mi). Fault movement ruptured the ground approximately 7 km (4 mi) east of Palermo. This ground rupture is called the Cleveland Hill Fault.

Prior to the 1975 earthquake, seismic hazard was not regarded as being great in the Oroville area. It was recognized that earthquakes do occur in the surrounding region, and that the largest recorded earthquake was a magnitude 5.7 in 1940 north of what is now Lake Oroville. Fault movements were not considered likely to occur along faults in the area. Because fault movement occurred where no fault was suspected before the Oroville earthquake, it was obvious that existing geologic information did not identify potentially active faults in the Oroville area. Therefore, geologic investigations were started immediately.

PURPOSE OF THE INVESTIGATION

The purposes of geologic investigations were threefold: (1) to understand the geologic and tectonic conditions which caused the Oroville earthquake; (2) to

evaluate any potential hazards; and (3) try to determine if Oroville Reservoir caused the earthquake.

The original thrust of investigation was to determine if the Cleveland Hill Fault, movement along which caused the 1975 earthquake, was an old or new fault, and if it extended northward to endanger Department facilities in the Oroville area. The investigations later were expanded to cover the surrounding area.

PREVIOUS WORK

The area geology was first mapped in the late 1800's by Waldemar Lindgren and Harry Turner. Their work was published as the Bidwell Bar folio (Becker and others, 1898) and the Smartsville folio (Lindgren and Turner, 1895) of the U. S. Geological Survey Atlas of the United States series. These works include the Bangor, Oroville Dam, and Berry Creek quadrangles which comprise half of our study area (Figure 6).

The northern Sierra foothills were again the center of detailed mapping in the 1950's for studies of the Merrimac pluton (Hietanen, 1951) and the Bidwell Bar area (Compton, 1955). In 1955, Robert Creely completed a doctoral mapping thesis of the Oroville 15-minute quadrangle, which includes the Hamlin Canyon Cherokee, Shippee, and Oroville 7-1/2 minute quadrangles. Creely's work was published in 1965 as Bulletin 184 by the California Division of Mines and Geology.

Areas of the Oroville, Oroville Dam, Cherokee and Berry Creek quadrangles were mapped in detail during the late 1950's and early 1960's by geologists from the Department of Water Resources for studies associated with the construction of Oroville Dam and related

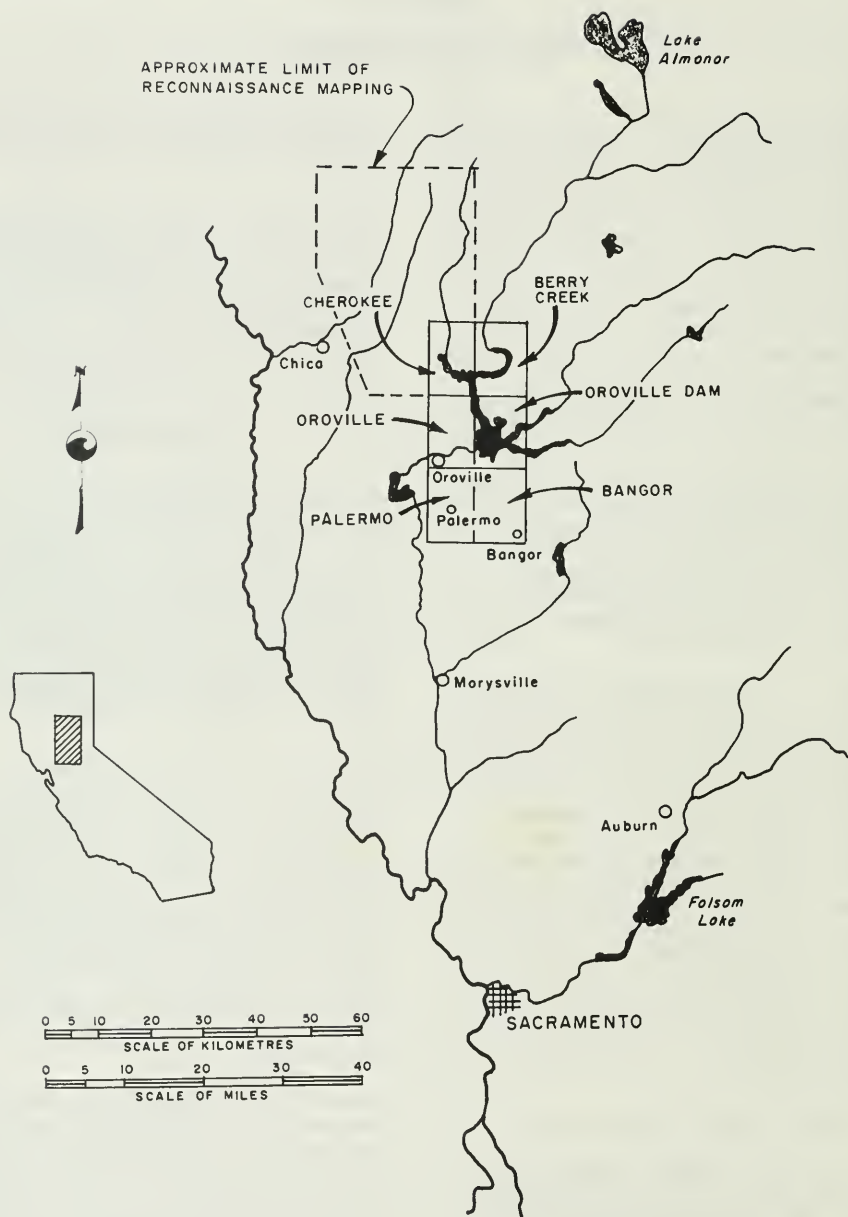


Figure 6. Location map of six-quadrangle study area.

facilities. Mapping to the south of the area by other individuals and agencies includes preliminary work in the Bangor quadrangle (Quintin Aune, unpub. data), graduate theses in the Smartville area (Buer, 1978; Costas Xenophontos, in progress), a regional study by the U. S. Army Corps of Engineers (1977) for the proposed Parks Bar Dam on the Yuba River, and fault studies made by Woodward-Clyde Consultants for both the U. S. Army Corps of Engineers and Pacific Gas and Electric Company. Additionally, Woodward-Clyde Consultants (1977) conducted a regional fault investigation in the northern foothill belt for the U. S. Bureau of Reclamation's Auburn Dam project on the American River.

Numerous other references contribute to a general understanding of structural and stratigraphic relationships in the Oroville area. Some of these include the Geologic Map of California, Westwood Sheet (Lydon and others, 1960), Geology of the Richardson Springs quadrangle (Burnett and others, 1969), and work by Hietanen (1973a, 1976, 1977). An understanding of the importance of faulting and some knowledge of its history and nature is provided in the works of Clark (1960, 1964, 1976), Cebull (1972), Duffield and Sharp (1975), and Schwieckert and Cowan (1975). Models and evidence for plate tectonic evolution of the area are adopted and modified after Hamilton (1969), Moores (1972), Schwieckert and Cowan (1975), and Schwieckert (1976).

SCOPE OF THE INVESTIGATION

Several types of imagery were used to find major structural trends and lineaments prior to field mapping. These included satellite imagery, high-altitude black-and-white and infrared photographs, radar imagery (SLAR), and low-altitude black-and-white and color photographs.

Satellite imagery was from the ERTS (now LANDSAT) program of the U. S.

Government (NASA). Radar imagery was obtained from Woodward-Clyde Consultants. High- and low-altitude photography is comprised of four sets flown for the Department of Water Resources, including a set of low-altitude low-sun-angle photographs, and one set from the U. S. Forest Service.

Detailed geologic mapping was done in the Palermo, Bangor, Oroville, Oroville Dam, Cherokee and Berry Creek 7-1/2 minute quadrangles (Figure 6). Reconnaissance geologic mapping was done in the remainder of the study area, extending northwest some 70 km (43 mi) from Oroville.

Detailed mapping was generally done on a 7-1/2 minute quadrangle base. Where more detail was desired, mapping was done on quadrangles enlarged to 1:12,000. Areas mapped in detail were covered on foot; samples of rock were collected, photographed or sketched where appropriate, and mapped. Most of the rock units were sampled and petrographic analyses were made by Costas Xenophontos of the University of California at Davis.

Reconnaissance mapping was done on 7-1/2 minute topographic base maps wherever possible. Much of the northern study area was mapped on preliminary topographic maps received from the U. S. Geological Survey. Areas along photo lineaments and faults indicated on the State geologic maps were checked in detail. In other areas we relied on previous works and field reconnaissance.

Mapping began in May 1976, and continued until May 1978. A total of 55 work months went into field work and report writing. The majority of mapping was done by Department of Water Resources geologists; three geology graduate students from the University of California at Davis assisted during July and August 1977.

Subsurface information was used whenever and wherever possible to map rock units and, especially, to aid in tracing faults

beyond surface exposures. Subsurface information was derived from exploratory trenches, road cuts, railroad cuts and utility trenches; existing tunnel logs, well logs, test boring logs, mining reports and Department of Water Resources design and construction reports were also reviewed. Geophysical methods were used to try to trace the Cleveland Hill Fault beyond the northernmost ground cracks.

Exploratory trenches in this study included 17 by the Department of Water Resources in the Oroville-Bangor area (trench logs, page 103 ff.) and several others by Pacific Gas and Electric Company, U. S. Army Corps of Engineers and the U. S. Bureau of Reclamation. The latter agencies were studying faulting in the Sierran foothills from Sonora to Oroville. Woodward-Clyde Consultants were involved as consultants to these three agencies.

Trenches by the Department of Water Resources and other agencies were primarily used to explore suspected faults. Many were cut across surface cracks shortly after the August 1, 1975, earthquake. Seismic and resistivity surveys were used by Department of Water Resources geologists, assisted by Elgar Stevens of the Department of Transportation, in attempts to trace faulting associated with surface cracking.

Tunnel logs reviewed include tunnels 1 through 5, Western Pacific Railroad relocation by the Department of Water Resources. Logs for Miners Ranch and Kelly Ridge tunnels by Bechtel Corporation for Oroville-Wyandotte Irrigation District were also reviewed.

The area around Oroville Reservoir and south to Wyandotte was surveyed immediately after the August 1, 1975, earthquake by teams from the Department of Water Resources and the U. S. Geological Survey. It was hoped that precise leveling surveys across the Cleveland Hill Fault would indicate the sense of movement on this structure.

The Department of Water Resources survey team ran additional first-order leveling surveys at regular intervals. Changes in elevation were contoured by computer and compared with geological and seismological data collected by the Department of Water Resources staff.

Most precise leveling surveys around Oroville post-date the August 1975, earthquake. A comparison of August 1975, first-order leveling data with third-order leveling data compiled in the 1940's would be the closest approximation of crustal movements from the Oroville earthquake.

SEISMIC HISTORY

Epicenters for earthquakes occurring in the Oroville area prior to 1934 are estimated from newspaper accounts and reports by local residents. After 1934, epicenters in the area have been instrumentally determined. Historic seismicity in the Oroville area from 1851 to 1975 is shown in Figure 7 with a few recent earthquakes, providing more reliable data, indicated by their date above the epicentral location.

Numerous low- to moderate-magnitude earthquakes have occurred in the northern Sierra Nevada in historic time (Townley and Allen, 1939; Wood and Heck, 1951). The most significant event affecting the Oroville area occurred near Virginia City, Nevada on December 27, 1869. Another earthquake shook the Oroville region on January 24, 1875, and is believed to have originated from movement of the Mohawk Valley Fault (Wolfe, 1967) located approximately 70 km (43 mi) to the northeast; reinterpretation of this earthquake suggests it was located southwest of Oroville (Paul Morrison, person. commun., 1978).

An earthquake on February 8, 1940, centered 54 km (34 mi) north of Oroville, is comparable in magnitude to the 1975 Oroville event. Seismic monitoring was

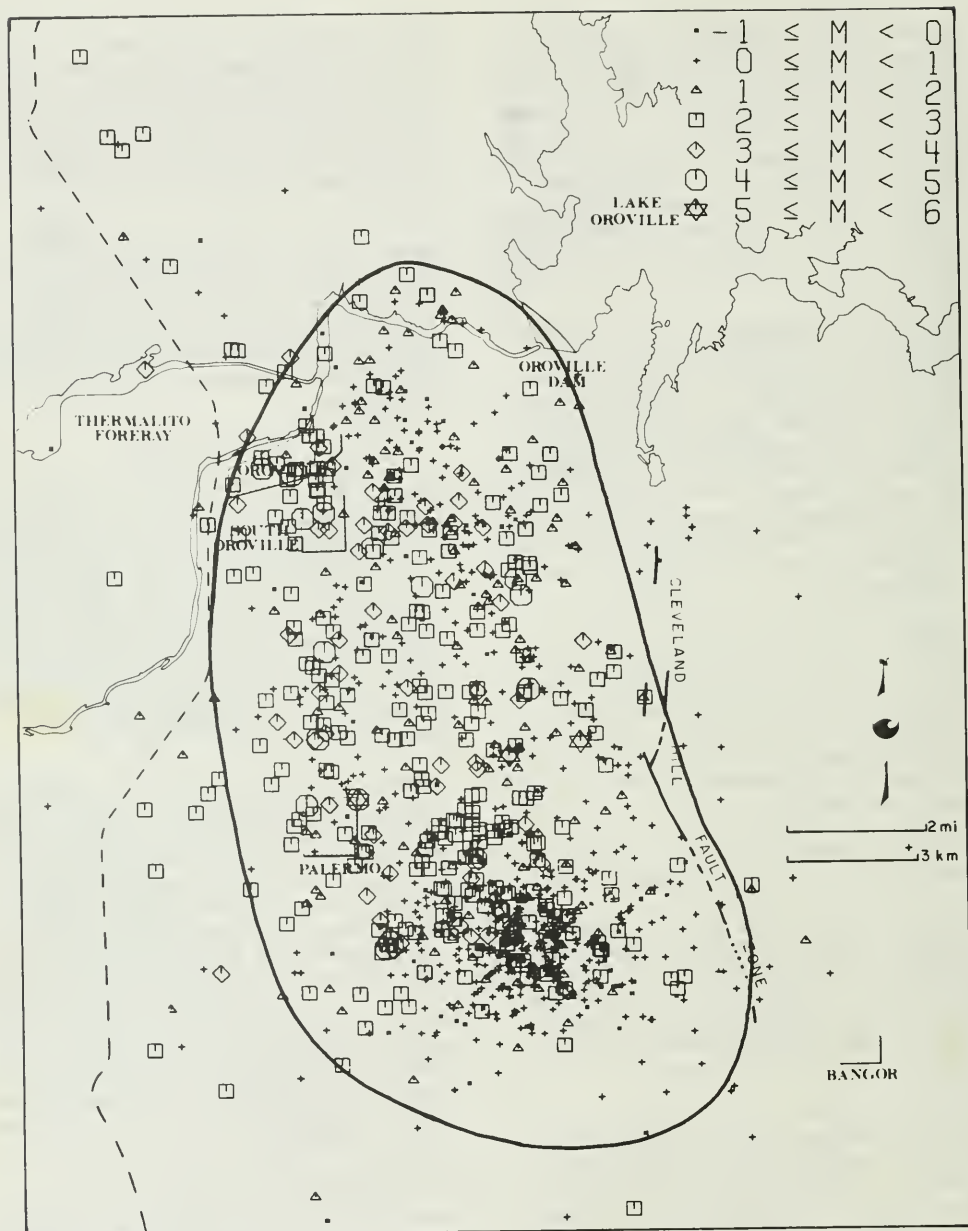


Figure 8. Aftershock locations of the Oroville earthquake. The envelope encloses 90 percent of the epicenters.

not good in 1940 and data on the earthquake are poor. A recent reassessment of these data shifted the epicentral location 40 km (25 mi) and changed the estimated magnitude from 6.0 to 5.7 (Morrison, 1974, p. 8). The epicenter does not fall on any known fault, and no fault plane solution is obtainable from the seismic data.

The May 24, 1966, "Chico" earthquake (Figure 7) is unique for this area because adequate data were obtained to calculate a fault plane solution. The timing of this earthquake coincided with a crustal determination experiment using a subsurface explosion off the Northern California coast. This magnitude 4.6 earthquake had a focal depth of 21 km (13 mi) and provided a fault plane solution for a N30W strike and a 65 degree northeast dip, with dominant right-lateral movement (Lomnitz and Bolt, 1967).

THE 1975 EARTHQUAKE SERIES

Foreshocks of the Oroville earthquake began June 28, 1975. Fourteen foreshocks with magnitudes from 2.1 to 4.7 occurred prior to the main shock at 1320 hours Pacific daylight time, on August 1, 1975.

The main shock had a Richter magnitude of 5.7 and was centered about 1 km (0.6 mi) northeast of Palermo and 12 km (7.5 mi) south of Oroville Dam. The focal depth was 8.8 km (5.5 mi).

Oroville earthquake aftershocks, including more than 5,600 recorded events, were still occurring in June 1978. Frequency of aftershocks has decreased steadily, from over 700 per day in early August 1975, to ten per month in June 1978.

The region of aftershocks increased in size for several months after the August 1, main shock (Lester and others, 1975); the most rapid increase was during the first week of this time period.

Surface area envelopes of aftershock epicenters are ellipsoidal with the elongated axis oriented north-south. This pattern matches the north-south trend of the Cleveland Hill Fault in the subsurface. Initially the aftershock zone expanded to the east, with the shocks occurring at shallower depths. Then the zone expanded both to the north and to the south, with the final expansion being to the north. An envelope containing the majority of aftershocks is shown in Figure 8. Aftershock epicenters have occurred as far north as Oroville Dam, and a few have occurred east of the Cleveland Hill Fault rupture.

Depths of aftershocks were 8 to 9 km (5 to 6 mi) on the west and became shallower toward the east. A fault plane solution shows the Cleveland Hill Fault strikes N25W to N5E (Beck, 1976; Clark and others, 1976; Morrison and others, 1976), dips 60 degrees west and passes 5 km (3 mi) beneath Oroville Dam (Lahr and others, 1976). First motion fault analyses indicate a dip-slip movement with the west side down; this movement indicates normal faulting and tensional deformation.

Property damage caused by the earthquake consisted of fallen plaster, toppled chimneys, broken windows, items thrown from shelves, etc. Major damage included homes shifted off their foundations and an older brick home that was damaged beyond repair. Damage to State facilities was very minor and consisted mostly of non-structural plaster cracks in buildings and some settlement and cracking of uncompacted fill embankments around Thermalito Afterbay.

Several changes in ground water occurred after the earthquake: (1) a few wells and springs went dry and others temporarily increased their flow, and (2) new springs appeared where none had been prior to the earthquake.

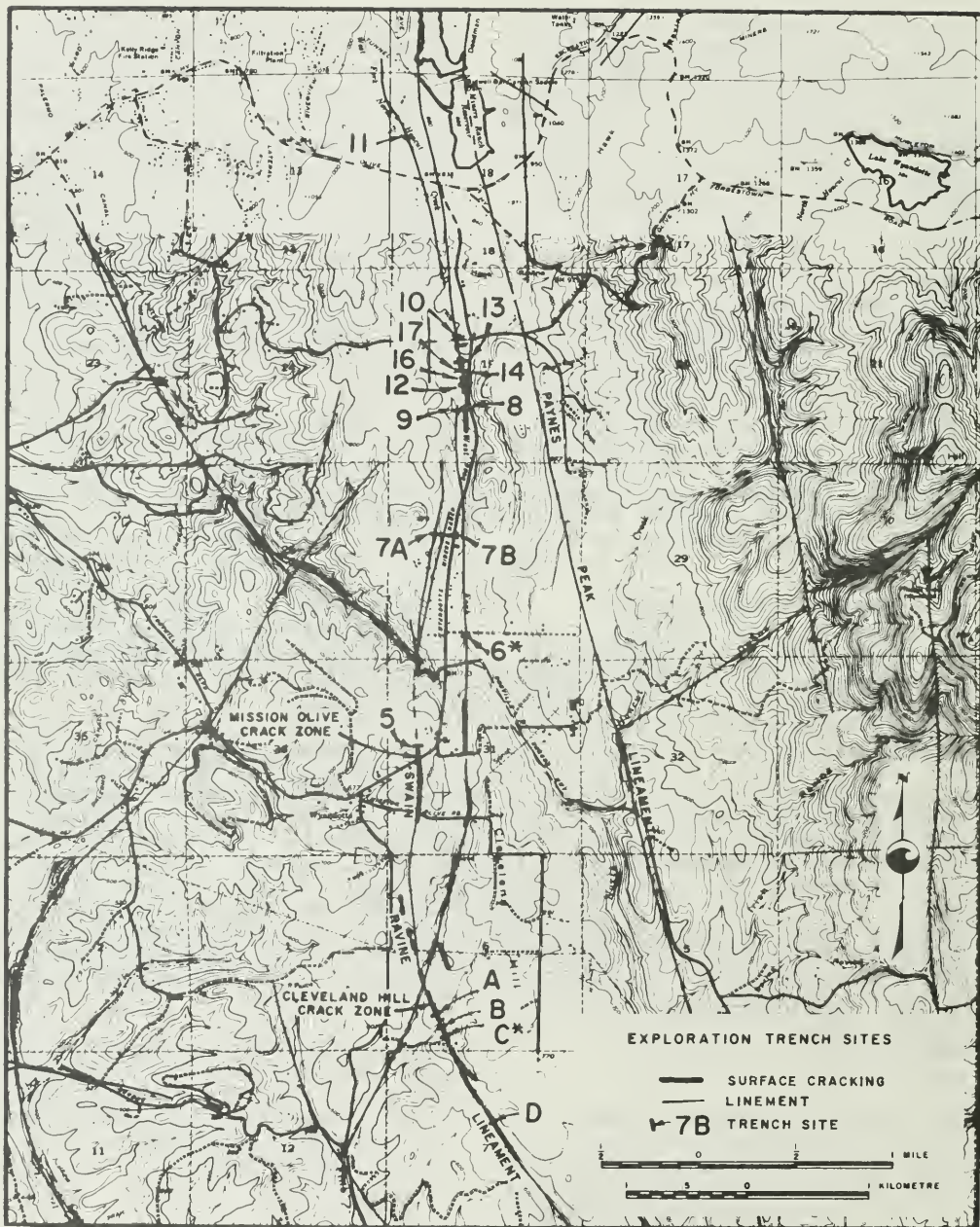


Figure 9. Locations of the Cleveland Hill and Mission Olive crack zones and sites of Department of Water Resources exploration trenches

GROUND CRACKING

Investigations were made of reported ground cracking during the first few days after the earthquake. Most cracks observed were lurch or settlement induced. Two areas of cracking did emerge as worthy of further investigation. These two zones are the "Palermo crack zone", trending northwest through the epicentral area, and cracking along Cleveland Hill Fault.

The "Palermo crack zone", the westernmost crack zone, consisted of discontinuous cracks at a number of locations. Collectively, the crack sites are aligned in a linear northwest trend. The crack zone lines up with the Prairie Creek Lineament to the southeast. The entire crack zone extended from 3 km (1.9 mi) south of Palermo to just south of Oroville for a total length of about 9 km (5.6 mi). Additional cracking, discovered later during the investigation, appeared to have occurred a considerable time after the main earthquake.

The linear trend of the Palermo crack zone gave rise to the suspicion that the

disturbance occurred along a fault zone. subsequent investigations did not reveal faulting but it is not really clear whether or not a subsurface fault extends northwest along the trend of the Prairie Creek Lineament.

Cracking near Cleveland Hill (Figure 9) was first detected on August 6, 1975. Cracking occurred in an en echelon pattern and formed a discontinuous zone 1 to 7 m (3 to 22 ft) wide and 1.6 km (1 mi) long. In 6 weeks some cracks widened to 40 mm (1.6 in) and showed up to 30 mm (1.2 in) of downdrop on the west side (Figures 10 and 11). The cracks became more pronounced with time and some were still visible 3 years after the main shock.

Early in October 1975, two approximately parallel crack zones were found north of Cleveland Hill. These cracks, named the Mission Olive crack zone (Figure 12), are 400 m (1,300 ft) apart and extend discontinuously for about 2 km (1.25 mi) to the north. The Mission Olive crack zone initially was seen in the asphalt paving on Mission Olive Road and Foothill Boulevard (Figure 9). The



Figure 10. Ground cracking that resulted from the August 1, 1975, Oroville earthquake.

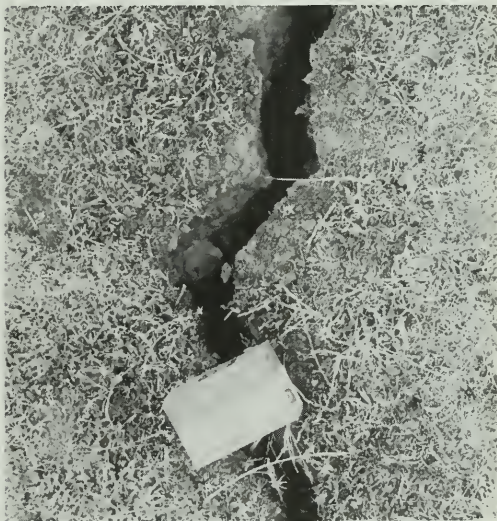


Figure 11. Close-up view of a ground crack on southwest slope of Cleveland Hill.

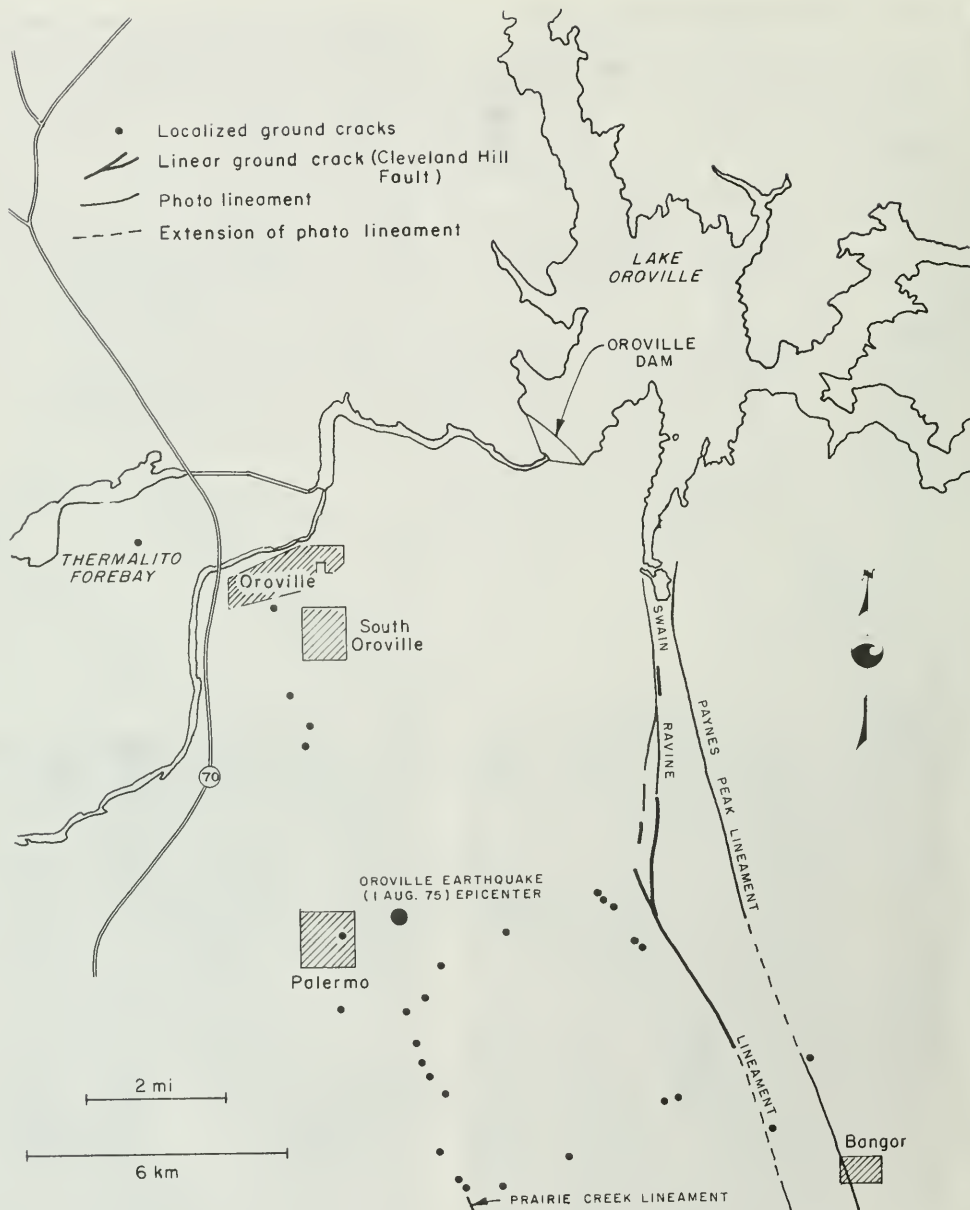


Figure 12. Locations of ground cracking from the Oroville earthquake and major photo lineaments in the southern study area

cracks definitely were not present in August 1975, when all paving between Cleveland Hill and the reservoir was inspected.

In February 1976, another 182 m (600 ft) of cracking was found in a pasture 3 km (1.9 mi) south of Bidwell Canyon Saddle Dam. This cracking was not present in October 1975, when the site was selected for an exploration trench on the Swain Ravine Lineament by Department of Water Resources geologists. In August 1976, another 116 m (380 ft) of cracking was found north of the pasture in an olive orchard. The crack zone now reached nearly to Mt. Ida Road which is 2.1 km (1.3 mi) south of Bidwell Canyon Saddle Dam (Figure 13).

In February 1977, an additional short segment of ground cracking was found along the Swain Ravine Lineament 1.8 km (1.1 mi) south of the southern end of the

Cleveland Hill cracks. This is the only instance of crack zone development progressing southward. Periodic field checks after discovery of the last crack zone have shown no new cracking to the north or south.

Initial cracking from the Oroville earthquake occurred only along the Swain Ravine Lineament west of Cleveland Hill. During the 12-month interval following the main shock, cracking propagated several kilometres northward. Timing of northward extensions of cracking is not precisely known and therefore cannot be related to specific aftershocks; extension of cracking is probably related to continuing readjustment on the fault. Overall extent of cracking is 8.5 km (5.3 mi) and the collective length of individual zones is 5.3 km (3.3 mi). Displacement on individual cracks was most pronounced in areas of initial cracking.



Figure 13. Aerial north view of northern limit of ground cracking (Cleveland Hill Fault) just west of Wyandotte Miners Ranch Road. These cracks project toward the Bidwell Canyon Saddle Dam.

In addition to the progressive increase in the areal extent of cracking with time, displacements along the cracking also increased as time passed. The increase in displacement was discernible by eye, particularly in the first few months following the earthquake. The most pronounced visual impact of displacement increase was near Cleveland Hill where ground cracking was first discovered. Here a noticeable vertical displacement (down to the west) developed with time and the cracks became wider.

The U. S. Geological Survey installed five arrays of survey monuments along the southern crack zone near Cleveland Hill to measure fault displacement. Initial surveys on some of these arrays were made as early as August 12, 1975, 11 days after the earthquake. Maximum displacements measured by April 1976, (Philip Harsh, person. commun., 1978) were 34.1 mm (1.3 in) extensional separation and 28.8 mm (1.1 in) vertical displacement for the August 12, 1975, to April 4, 1976, period, with a computed dip-slip component of 44.6 mm (1.8 in). Eight millimetres (0.3 in) of right lateral displacement also were measured. Displacement measured in April 1976, on the other four arrays were markedly smaller, ranging down to a minimum of 4.3 mm (0.2 in) vertical displacement and 0.6 mm (0.02 in) extensional separation for the October 1975, to April 1976, period.

The U. S. Geological Survey surveyed the arrays again in February 1978. Only dip-slip results from the 1978 survey have been reported to DWR, but the data does show movement continued. The 44.6 mm (1.8 in) component of dip-slip reported in 1976, increased to 57.6 mm (2.3 in).

An additional array of survey monuments was installed north of the U. S. Geological Survey array, by the Department of Water Resources, to measure changes in ground elevation across fault rupture discovered in October 1975. The DWR monuments were first leveled in

October 1975, and last measured in October 1977. Maximum change in elevation across the fault zone by October 1977, (See Figure 90, Chapter IV) was 50 mm (2 in), with the east side of the fault zone going up 10 mm (0.4 in), and the west side going down 40 mm (1.6 in).

Total fault displacement is not known, because the increment of movement between the time the earthquake occurred and the time the survey monuments were installed is not accounted for. However, comparing what was seen in the field with the survey data, gives the impression that the survey data probably accounts for most of the fault displacement.

The fault displacement cannot be evaluated precisely and, in fact, appears to vary from place to place. Maximum width of cracking measured over 40 mm (1.6 in), but this may be in part due to crumbling away of the crack edges. Most of the cracking was 25 mm (1 in), or less, in width. The collective data suggests vertical movements of about 50 mm (2 in) and horizontal extension of about 25 mm (1 in). It is expected another earthquake of similar magnitude would produce similar displacements.

GROUND ELEVATION CHANGES

Immediately after the August 1, 1975, earthquake, Department of Water Resources survey teams conducted first-order leveling traverses on the pre-existing Oroville project survey network. Points and lines were added to the network to provide additional elevations where needed. These lines were leveled at approximate six-month intervals through the next 26 months. For calculating elevation changes, a benchmark near the eastern edge of the project area was considered to be stable and all other points were adjusted accordingly.

Contours of elevation change for various time intervals following the earthquake were calculated and plotted by

computer. These plots were overlaid on geologic maps and analyzed for relationships to geologic structure and lithologic distribution. The plot for the period of August 1975, to October 1976, is shown in Figure 14. Since the intervals represented are all after August 1, 1975, the changes plotted do not include any changes which may have occurred concurrently with the main earthquake or early aftershocks.

In general, the settlement contour maps show an abrupt lowering of the ground surface west of a north-trending zone that coincides approximately with the Cleveland Hill Fault. Maximum total differential elevation change across this zone, for the period of August 1975, to October 1976, was 42 mm (1.7 in). The amount of settlement decreases to the north; survey control is lacking to determine how far this trend continues to the south. Elevation changes in the northern portion of the area are of lesser magnitude, generally less than 25 mm (1 in), and are not readily related to local geologic structure.

Repeated surveys show elevation changes, including increases, decreases and reversals in direction, continuing throughout the area -- but at a decreasing rate. The continuing elevation changes suggest that readjustment along the fault zone was occurring 26 months after the main shock.

Because initial studies indicated the northward progression of ground cracking was trending toward Bidwell Canyon Saddle Dam, periodic surveys were made along the crest of the dam to monitor changes in elevation. Results of these surveys are shown in Figure 15. The level line along the dam crest was surveyed four times since the earthquake. These surveys show the dam went down about 15 mm (0.6 in) more on the west than on the east. Most of the elevation change occurred at the west end in the vicinity of shearing in the foundation. The marked lowering of elevations in the vicinity of Monuments BB-2 and

BB-8 are mostly due to embankment settlement at places of maximum embankment height.

Although not conclusive, these data strongly suggest that the down-to-the-west pattern of crustal movements seen at Cleveland Hill continues, albeit somewhat diminished, northward to Bidwell Canyon Saddle Dam.

Four shears exposed in the foundation excavation for the saddle dam are shown on Figure 15. Most of the elevation change appears to be in the vicinity of the largest shear zone near the west end of the dam. This suggests the shearing at the west end of the dam is a zone along which the elevation changes are occurring. If so, the zone along which the Cleveland Hill Fault displacements occurred to the south, may pass through the west end of the Bidwell Canyon Saddle Dam.

AREA LINEAMENTS

A photo lineament is defined as, "Any line, on an aerial photograph, that is structurally controlled, including any alignment of separate photographic images such as stream beds, trees, or bushes that are so controlled. The term is widely applied to lines representing beds, lithologic horizons, mineral bandings, veins, faults, joints, unconformities, and rock boundaries" (Allum, 1966, p. 31). Because lineaments are often fault related, they are useful indicators of possible faults. Consequently, one of the early tasks for this project was to plot regional lineaments on topographic maps and then inspect them in the field.

The study of area lineaments began in May 1976, with a field reconnaissance of major photo lineaments north of Oroville Reservoir. A more comprehensive study, including detailed mapping and field observations, was done in September and October 1977. A similar study was conducted in 1976-77 by the U. S. Army Corps of Engineers as a part of their

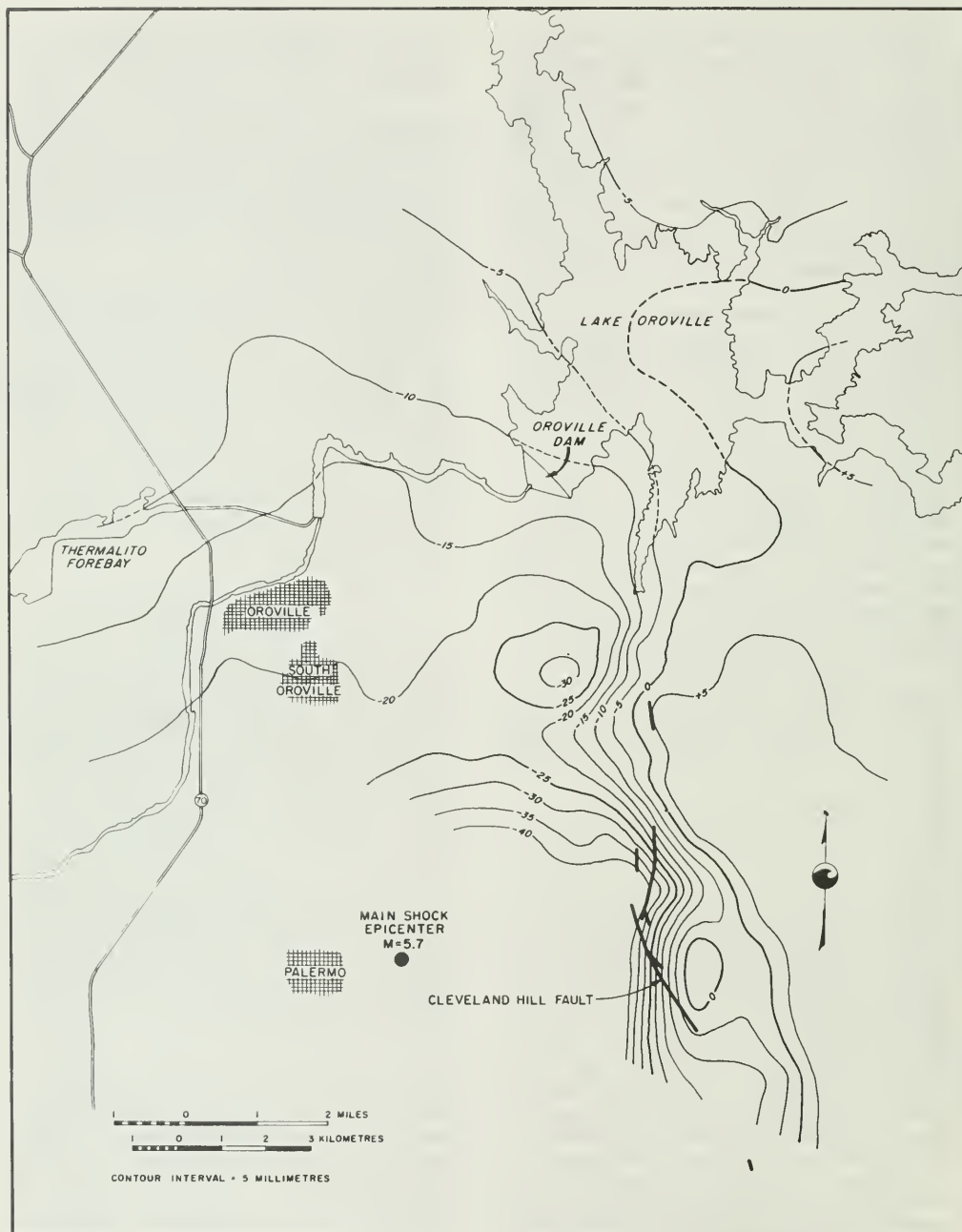


Figure 14. Changes in ground elevations around Lake Oroville, August 1975, to October 1976

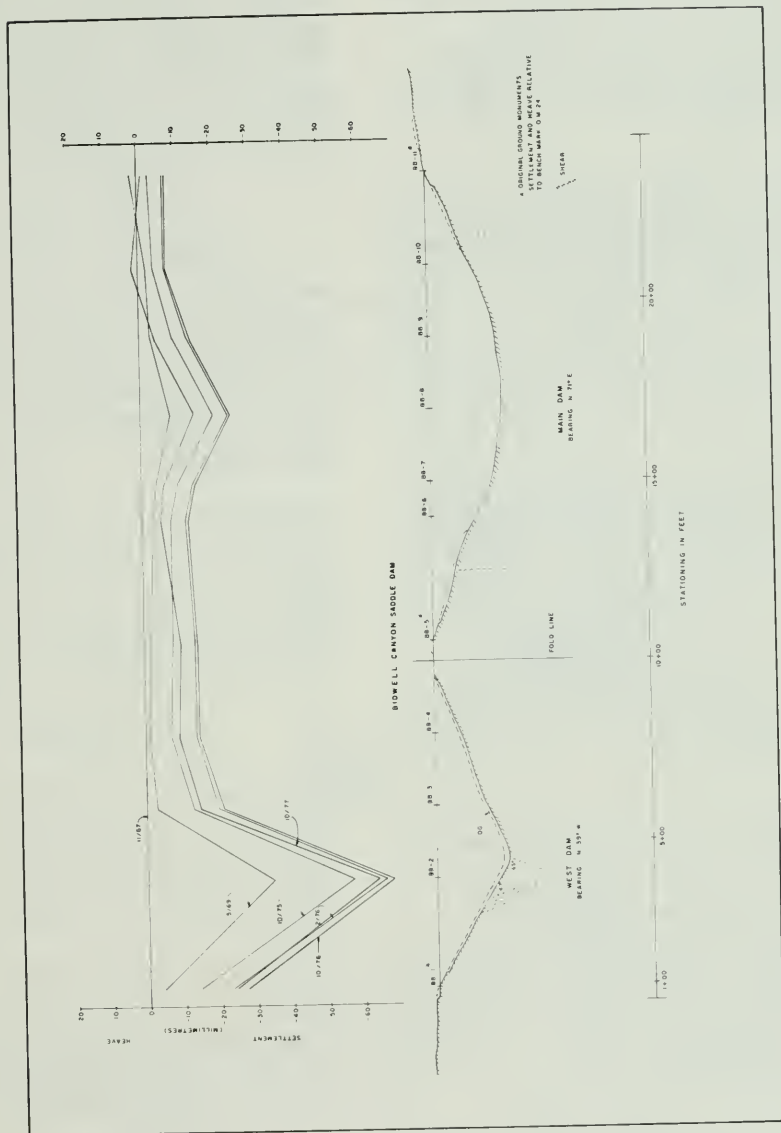


Figure 15. Changes in crest elevations of Bidwell Canyon Saddle Dam between November 1967, and October 1977

Marysville Lake project. Their work covered an area from Oroville to 9.6 km (6 mi) south of the Yuba River (U. S. Army Corps of Engineers, 1977). Woodward-Clyde Consultants also performed a major study of lineaments in the foothill belt as part of a seismic investigation for the Auburn Dam project.

The purpose of the lineament study was to determine which lineaments are faults. Methods of investigation included aerial reconnaissance, photo interpretation, field inspection and mapping; topography, springs, continuity of rock units, fault gouge or any other features which would suggest or refute faulting were investigated. Previous geologic maps were field checked and incorporated in the study.

Lineaments are categorized according to degree of certainty for a fault origin. Three categories are identified: (1) lineaments where field evidence contradicts a fault control and suggests origins are due to other causes (indicated as photo lineaments, dotted lines in Figure 16); (2) lineaments with no direct evidence of faulting, but are still thought to be faults (probable fault, dashed lines in Figure 16); and (3) lineaments which are faults (solid lines in Figure 16).

Three major photo lineaments are within the study area. These include the Paynes Peak, Swain Ravine and Prairie Creek Lineaments. Surface and subsurface data have been analyzed by California Department of Water Resources, Woodward-Clyde Consultants, Pacific Gas and Electric Company, U. S. Army Corps of Engineers, U. S. Bureau of Reclamation and U. S. Geological Survey in attempts to evaluate the past history of activity along these fault zones.

The major fault lineaments are in places defined by broad discontinuous linear valleys and aligned sections of sheared rock. The lineaments are not continuous but have gaps where nothing is evident

either on imagery or on the ground. The Cleveland Hill faulting started in one of these lineament gaps. The Swain Ravine Lineament merges with the Prairie Creek Lineament approximately 10 km (6 mi) north of the Bear River. In turn, the Prairie Creek Lineament extends southward and is truncated west of Auburn by the Rocklin pluton.

GEOLOGIC SETTING

Geographic Location

The Oroville study area is within the Sierra Nevada of California (Figure 17). The foothills of the Sierra Nevada separate the Sierran uplands from the relatively flat Sacramento and San Joaquin Valleys (the Great Valley). The study area comprises the northernmost part of these foothills.

Immediately north of, and included in the reconnaissance study, is the southernmost portion of the Cascade Range. Across the northern end of the Great Valley, northwest of the study area, are the Klamath Mountains which share many structural and lithologic characteristics with the Sierran foothills.

Geologic Framework

The Sierra Nevada province is an uplifted block of Mesozoic plutonic and metamorphic rock bounded by normal faults on the east and tilted to the west. The eastern side is very steep with pronounced fault topography, while the western side is of gentler relief.

The regional geologic fabric of Northern California is oriented north-northwest. Generally following this fabric is the Sierra Nevada crest, boundary faults, rock fabric, and foothills faults. The axis of the Great Valley, the crest of the Coast Ranges, and major faults in the Coast Ranges (e.g., San Andreas) also conform to this regional trend.

The foothills of the Sierra Nevada are underlain by Paleozoic to Mesozoic

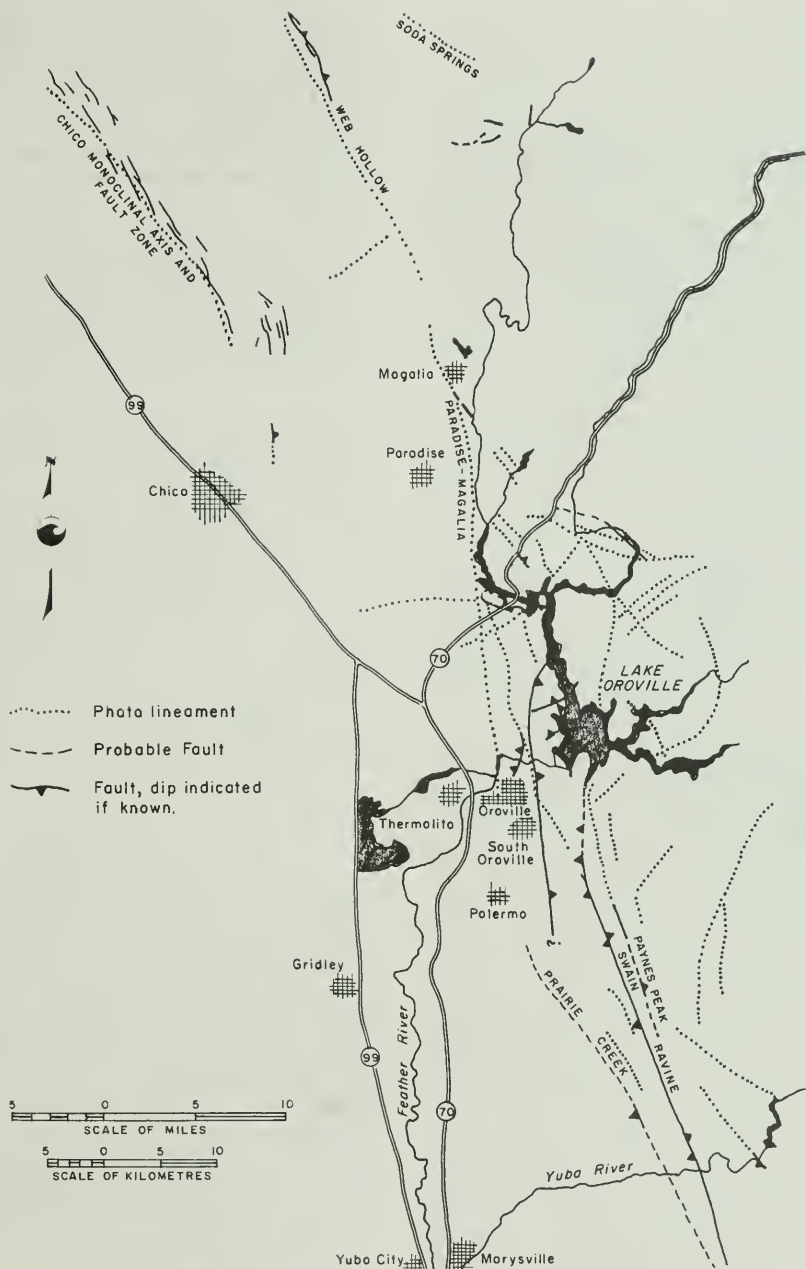


Figure 16. Lineaments and faults in the northwestern Sierran foothills

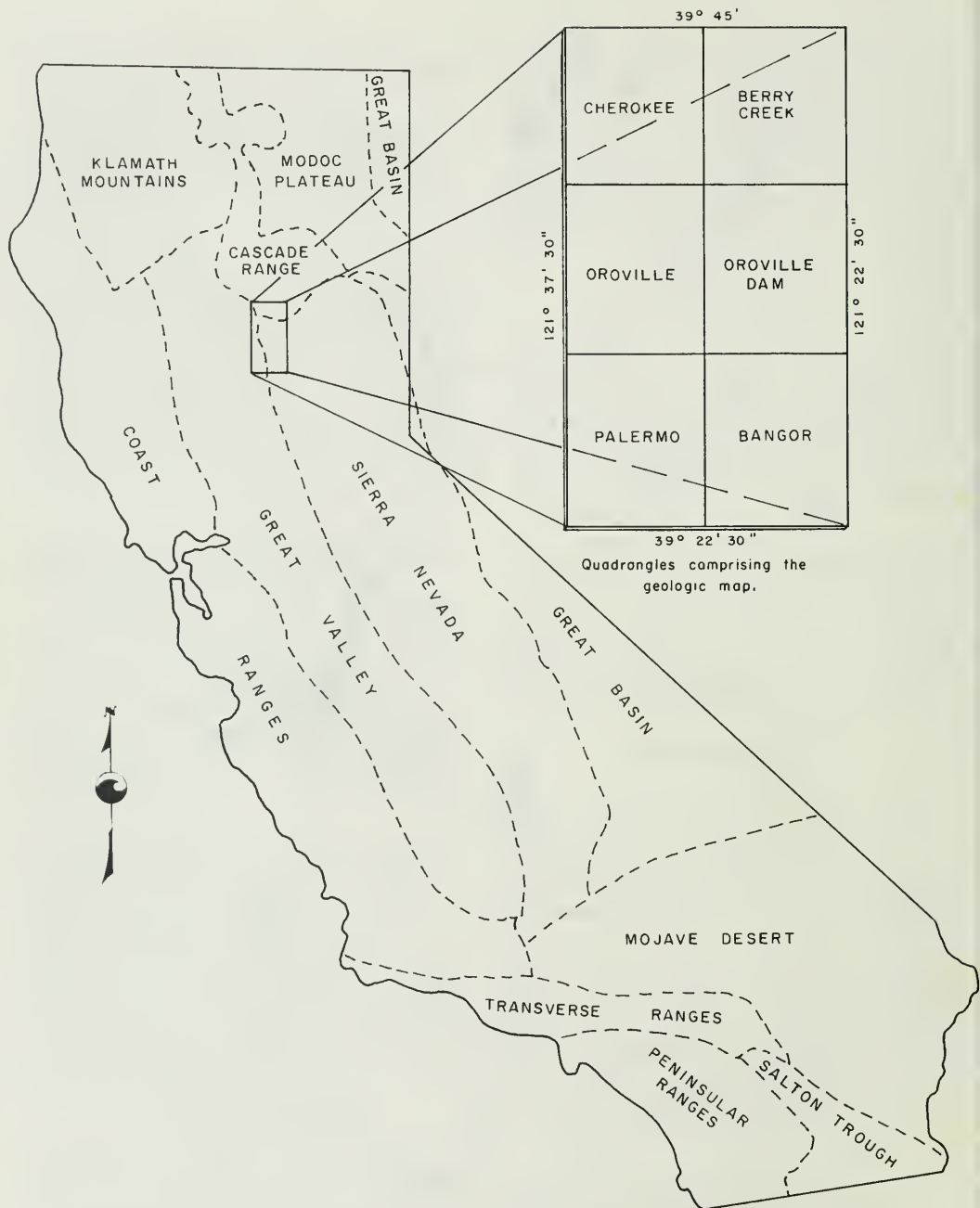


Figure 17. Natural geologic provinces of California with field area location

metamorphosed sedimentary and volcanic rocks, and plutons which are similar to, but generally smaller than, those forming the Sierra Nevada. The metamorphic fabric and trend of faults in the foothills are most commonly concordant with regional northwest trends; local variations occur about the intrusive bodies.

Overlying the metamorphic foothills bedrock is a thick sequence of unmetamorphosed upper Mesozoic and Cenozoic sedimentary and volcanic rocks (Superjacent Series rocks) and alluvium. These rocks are in most places undeformed and dip gently west.

The northern foothills have recently been interpreted as remnants of Mesozoic subduction complexes consisting of melange, arc rocks and ophiolite (Moore, 1972; Cady, 1975; Schweickert and Cowan, 1975; Buer, 1977, 1978; this study); this model also has been applied to the Klamath Mountains and Coast Ranges (Davis, 1969; Hamilton, 1969). The subduction zone is thought to have migrated westward during Late Jurassic time to form melanges of the Coast Ranges (Hamilton and Myers, 1966; Hamilton, 1969; Burchfiel and Davis, 1972, 1975).

DESCRIPTIVE GEOLOGY

Bedrock Series Rocks

Global applications of sea-floor spreading, as proposed by Hess (1959, 1962), have conceived new explanations and evolutionary interpretations for sea floor and continental rocks. Bedrock suites in this investigation are mapped and described assuming plate tectonic modes of origin and using evolutionary names, rather than formational names. Previous formational names are referenced in describing lithologic groupings. Geologic mapping of individual rock suites established the present structural configuration and provides explanations for plate tectonic development of the region; this includes the origin of lithologic suites and time-separated

episodes of faulting. Lithologic suites in the area include:

(1) Melange - This suite consists of chaotically mixed metasedimentary and metavolcanic rocks which include serpentine and exotic blocks of marble. Melange was formed at a convergent boundary that existed between late Mesozoic California (American plate) and Pacific sea floor (ancestral Farallon plate that is now subducted beneath American plate). These rocks formed by subduction underthrusting as an accretionary prism in the Benioff zone.

(2) Arc rocks - Rocks in this suite are volcanic and volcanoclastic derivatives that formed as an island arc complex in the ocean adjacent to Mesozoic California. Island arcs, common in many of today's oceans, develop relatively close to convergent plate boundaries where subducted lithosphere melts as it descends into the earth. The melted rock rises because of a lighter specific gravity, and volcanic mountains form if magmas reach the surface.

(3) Ophiolite - This lithologic suite is named Smartville ophiolite in the study area and includes metamorphosed mafic rocks (amphibolite) that have origins peculiar to the sea floor. Ophiolitic suites form at oceanic spreading centers (rifts) and require that several mafic and ultramafic rock types be present for a complete ophiolite sequence. These lithologies form layers of varying thickness in undisturbed ophiolite and include: (1) an overlying mantle (layer 1) of marine sediment and chert; (2) an intrusive-extrusive complex (layer 2) of submarine-extruded pillow lava that was fed by, and grades downward into intrusive sheeted dikes; (3) a quasi-stratiform intrusive complex (layer 3) of gabbro, cumulate gabbro and dunite; and (4) a tectonite basement (layer 4) consisting of harzburgite and minor dunite. Ophiolite exposed within continental margins necessitates special processes (obduction) for emplacement from oceanic source areas.

Melange

Previous Investigations and Age:

Melange rocks in the western Sierra Nevada were first mapped and named "Calaveras formation" by Turner (1893, p. 309) for prominent exposures in Calaveras County. The name "Calaveras formation" subsequently became a "...catchall for all Paleozoic rocks in the Sierra Nevada and hence has no stratigraphic significance..." (Taliaferro, 1943, p. 280); this excludes Silurian and Upper Carboniferous rocks in the Taylorsville region. Exposures of Calaveras rock have been studied in many investigations (Lindgren, 1900; Clark, 1964, 1976; Creely, 1965; Hietanen, 1973a, 1976, 1977), but no regional correlation of units has been achieved.

The first detailed study of melange in the immediate area was by Creely (1965). He subdivided and described the Pentz Sandstone and Hodapp Members from the Calaveras Formation; however, most occurrences of the formation were mapped as "undifferentiated Calaveras".

Melange terrane northeast of the study area is subdivided by Hietanen (1973a) into the Calaveras, Horseshoe Bend, Duffey Dome and Franklin Canyon Formations. In later works, Hietanen (1976, 1977) further mapped, subdivided and described the Horseshoe Bend Formation (Berry Creek quadrangle) and noted that these rocks are physically continuous with Creely's Calaveras Formation to the east. In Hietanen's works no mention of melange was used to describe these complex rock suites.

The first published description of melange in the Sierran foothills was by Moores (1972), who suggested that "remnants of subduction zones" may be present in foothill areas. Subsequent studies (Bateman and Clark, 1974; Duffield and Sharp, 1975; Schweickert and Wright, 1975; Schweickert and Cowan, 1975) have noted the widespread presence of melange in the Sierran foothills. Most recent

studies, recognizing the nature of these suites, have dropped the name "Calaveras Formation" and adopted the term "melange" to describe the rocks.

The age of melange in the foothill belt is misinterpreted as being late Paleozoic by most earlier researchers (Turner, 1893, 1894, 1896; Lindgren, 1900; Taliaferro, 1943, 1951; Clark, 1964, 1976). Early ages were established by using Tethyan fossils (Douglas, 1967) in limestone and marble bodies that crop out in melange matrix. These carbonate bodies are interpreted to be exotic blocks within melange.

Fossils collected from exotic blocks in melange do not represent the age of melange formation, but rather the age of the exotic block. In the Klamath Mountains late Paleozoic fossils are in bodies of limestone and marble (Irwin, 1972; Irwin and Galanis, 1976); cherts in melange-type rocks that include these carbonate bodies yield Late Jurassic radiolarians indicating the rock suites are much younger than fossils in marble and limestone bodies suggest (Irwin and others, 1977).

An Upper Jurassic fossil (a pelecypod, Buchia Concentrica as identified by, and in possession of Ralph Imlay, U. S. Geological Survey) was discovered in meta-sedimentary melange near Pentz, California (Bob Treet, person. commun., 1978); the fossil specifically dates from middle Oxfordian to upper Kimmeridgian time. The Buchia fossil locality is in the southeast quarter of section 13 (T21N, R3E) on the Cherokee quadrangle. It substantiates that melange (Calaveras Formation) in the northwestern Sierran foothills is much younger than previously suggested. The Upper Jurassic age of melange is the same as arc and ophiolitic rocks located to the south and indicates contemporaneous origins.

Contact Relationships: The southern margin of melange in the project area

is interpreted to be an obduction boundary with arc rocks in the Cherokee quadrangle. The contact with arc and ophiolite in the Berry Creek quadrangle is complex and not well exposed. The base of the melange is not exposed in the study area.

Melange in the study area is overthrust by obducted arc rocks. Allochthonous rocks underlie large portions of the northern study area and form more surface exposure than autochthonous melange. Uncertainty exists as to how much melange is overridden.

Lithologic Description: The melange complex in the study area includes meta-sedimentary rocks (argillites, schists, phyllites, meta-tuffaceous beds, relict pebble conglomerates, exotic marble blocks and chert), metavolcanic rocks (relict basalts, diabases and andesites) and serpentine. These rocks, mixed by tectonic and olistostromal processes, are isoclinally deformed into tight

folds that dip vertically or steeply to the east (Figure 18). Structural discontinuity and intercalation of melange lithologies suggests the sequence originated as an accretionary prism in a subduction zone; similar rocks and structural relationships are described at many active and ancient subduction zones (Hsu, 1971; Blake and Jones, 1974; Gansser, 1974; Karig, 1974; Scholl and Marlow, 1974; Karig and Sharman, 1975; Dickinson, 1975). Accretion, using several different models (Burk, 1965; Dewey and Bird, 1970; Gilluly, 1972; von Huene, 1972; Moore, 1973), is postulated as the process by which lower plate rocks become transferred (accreted) to the upper plate during subduction.

Relict basalt, diabase and andesite flows (?) and sills (?) are the most abundant metavolcanic rocks incorporated in melange. They are locally intercalated within metasedimentary sequences. Contacts between metavolcanic rocks and metasedimentary rocks are poorly exposed.



Figure 18. Small-scale parasitic isoclinal fold within melange metasedimentary rock, 1.5 km (1 mi) southwest of the West Branch Bridge.

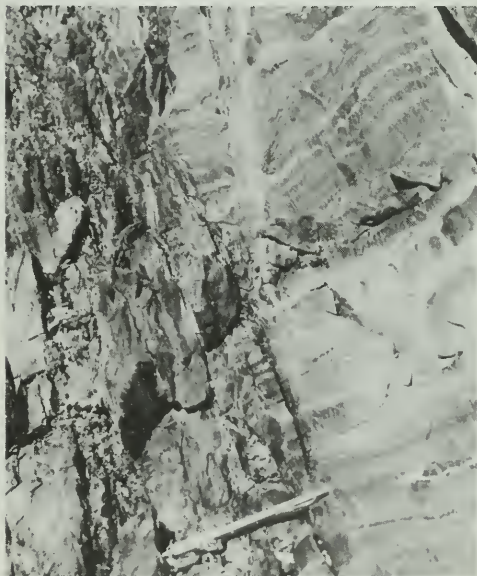


Figure 19. Relict bedding (parallel to pencil) cross cut by steeply east-dipping foliation in melange metasedimentary rock, 1.5 km (1 mi) southwest of the West Branch Bridge.

Meta-basalts and -diabases include uranitized amphibole and/or pyroxene, sodic plagioclase and secondary epidote. Accessory minerals are ilmenite or hematite, quartz and secondary chlorite.

Argillites and metagraywackes are dark when fresh and retain some of the original sedimentary features; shearing has locally transposed depositional structures into the plane of foliation (Figure 19). Sodic plagioclase, quartz, epidote, muscovite, chlorite and traces of metallic minerals comprise argillaceous rocks.

Pebble metaconglomerates of volcaniclastic origin are locally common within melange matrix (Figure 20). These are in places exposed against deep-water slates. Shearing has stretched clasts, however, the volcanic origin of both clasts and matrix remains visible.

Schistose and phyllitic rocks vary from dark- to light-green where fresh and

are various shades of buff if weathered. Syntectonic shearing has destroyed original textures.

Chert has limited exposure in melange terrane. Localized occurrences expose thin- to medium-bedded light-gray to white chert. Thin sections indicate chert is composed of 95 to 100 percent recrystallized quartz. Most chert in melange was clastically derived (Hietanen, 1977, p. 7).

Marble in melange (Figure 21) is white to bluish-gray. Most occurrences of marble are exotic and do not represent original in situ deposition. Samples collected along Nelson Bar Road (Cherokee quadrangle) exhibit marble and phyllite incorporated to form a rock with foliation discordantly cross-cutting the contact between the two lithologies (Figure 22). This indicates marble was incorporated into fine-grained sediments prior to metamorphism. An absence of shear at the marble-phyllite contact

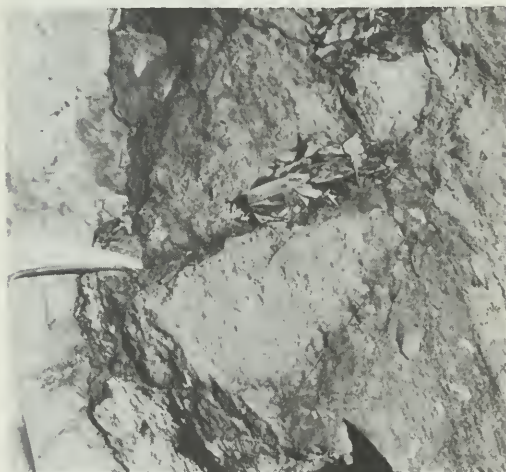


Figure 20. Sheared volcaniclastic metaconglomerate intercalated with black slates (not shown) in melange meta-sedimentary rock. Location is 1.5 km (1mi) southwest of the West Branch Bridge.

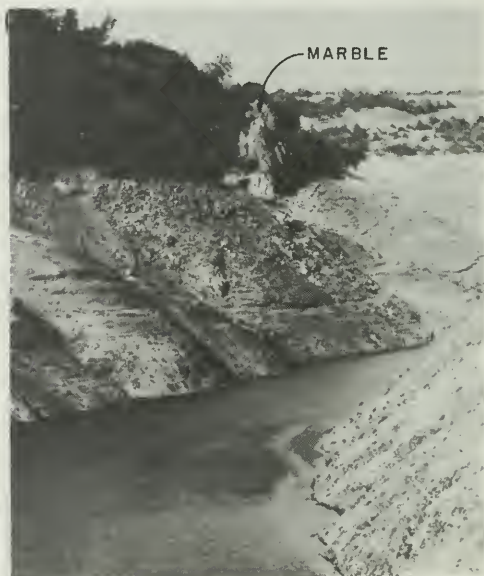


Figure 21. View north from the West Branch Bridge of exotic marble block in melange.

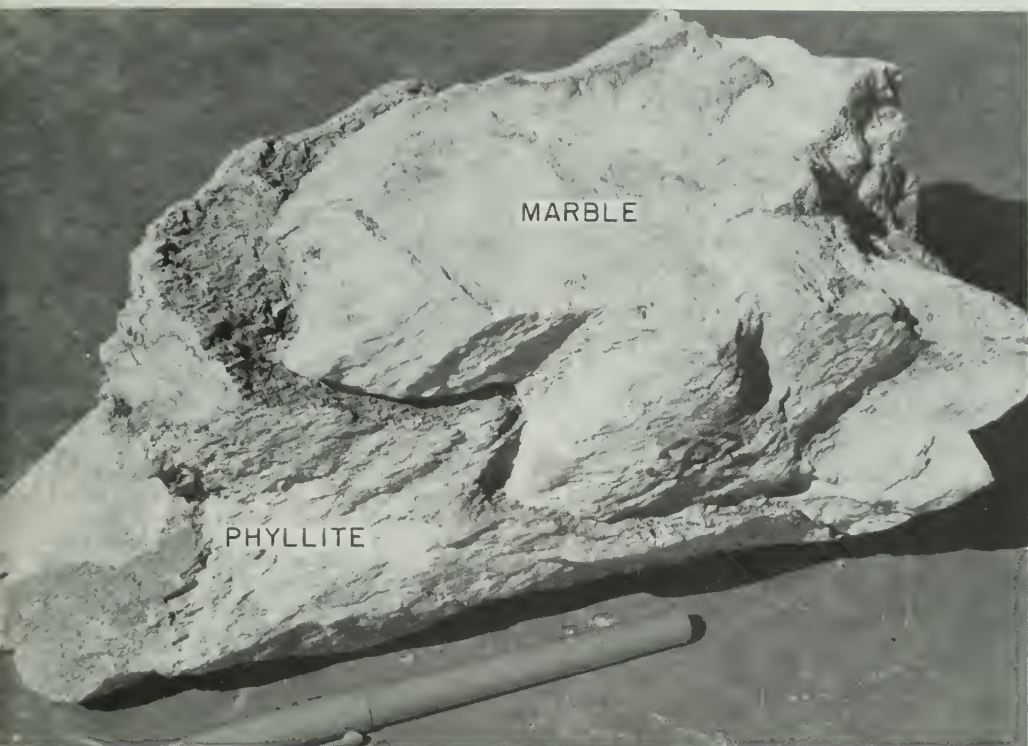


Figure 22. Sample of olistostromal marble-phyllite collected in melange along Nelson Bar Road just east of Oroville Reservoir (Cherokee quadrangle). Foliation in marble and phyllite is nearly perpendicular to the unsheared contact between the two rock types.

suggests gravity was the emplacement mechanism; therefore, this deposit is an olistostrome. Olistostromal deposits and tectonic knockers are common in many melange deposits (Hsu, 1966, 1968; Raymond, 1977).

The distribution of fossiliferous marble in the field area is restricted to a linear belt of exposures in West Branch Canyon. Marble exposures in other areas are scarce, non-fossiliferous and concordant with local bedding in meta-sedimentary melange.

Light- to dark-green serpentine, as highly-sheared to unsheared rocks, forms elongate discontinuous exposures that are concordant with the local foliation.

Contacts between serpentine and adjacent rocks are poorly exposed. Plate tectonic models associate serpentine with subduction (Benioff) zones at convergent boundaries (Hamilton, 1969; Bailey and others, 1970; Bateman and Clark, 1974; Lapham and McKague, 1964; Coleman, 1977). Lockwood (1971, 1972) has suggested that serpentine can be clastic or deposited as olistostromes. However, the sheared and truncated nature of serpentine in the study area suggests it was tectonically emplaced as opposed to a depositional origin. Elongate serpentine exposures in the area are interpreted as locations of ancient shear zones within the subduction complex.

Metavolcanic arc rocks are exposed in melange in the Cherokee and Berry Creek quadrangles. Contacts are not well exposed but most appear to be relatively flat-lying; these contacts conform to a model of arc rock overthrust on melange. It is possible that arc rocks were tectonically mixed into melange during subduction, however, it is also possible that the thrust plane has been folded and these exposures of arc rock are klippen.

Arc Rocks

Previous Investigations and Age: Basement Series greenstones in the Sierran foothill belt were first mapped and described by Becker and others (1898), and Lindgren and Turner (1895). Greenstone descriptions from these studies are refined in several later works (Creely, 1955, 1965; Bateman and Clark, 1974; Clark, 1976; Hietanen, 1977). Moores (1972) suggests part of the greenstone complex is an ancestral island arc. Subsequent investigations (Cady, 1975; Moores, 1975; Schweickert and Cowan, 1975; this study) have subdivided Sierran foothill greenstones into members whose origins are explained using a plate tectonic framework.

The most detailed academic study involving the westernmost suite of volcanic and volcanoclastic rocks in the greenstone belt is by Creely (1955, 1965). He applied the name "Oregon City Formation" to describe this metavolcanic sequence that is now recognized as an arc complex. These rocks are dated Late Jurassic (Oxfordian to Kimmeridgian) by an ammonite identified as Perisphinctes by Professor S. W. Muller, Stanford University (Creely, 1965).

Contact Relationships: A reverse fault forms the eastern contact of arc rocks with Smartville ophiolite in the Oroville area. Western margins of the arc complex are unconformably overlain by late Cenozoic Superjacent Series deposits and alluvium. Arc rocks are not exposed

in contact with other Basement Series rocks west of the foothills.

The arc complex ends abruptly in the southeastern Cherokee quadrangle. Field evidence at this location indicates arc rocks are thrust over melange by a late Mesozoic thrust fault. This fault is nearly flat-lying and probably represents an obduction suture.

Arc lithologies in the Oroville area are physically continuous to the south with Browns Valley Ridge volcanic rocks located in the foothills east of Marysville. Further south, they are time and structurally correlative with the Copper Hill and Gopher Ridge volcanic sequences located north of the Mokelumne River (Duffield and Sharp, 1975).

The base of the arc complex is not exposed in the study area. The thickest sequence is exposed in Morris Ravine on the west limb of the Monte de Oro syncline and includes approximately 400 m (1315 ft) of section.

Lithologic Description: Exposures of fresh arc rock are dark- to light-green and extremely well indurated. Foliation and relict flow structure are poorly developed.

Foliation is generally accentuated by weathering. It is not known if foliation and relict flow structure are concordant; metamorphism has transposed original structures in local metasedimentary rocks (Figure 23), and this characteristic probably exemplifies foliation in the arc sequence.

The arc complex is formed by several fine- to coarse-grained lithologies that are intermediate to basic in composition. Arc lithologies include andesitic tuff-breccia, lapilli tuff agglomerate, and epiclastic derivatives of these rocks; tuff-breccia and monolithologic agglomerates (Figure 24) are by far the most common. Relict flows, pillows (Figure 25), and sills (?) of meta-andesite and -basalt are present but not common.



Figure 23. Arc metasedimentary rock displaying relict bedding (dipping into photograph) that is nearly perpendicular to steeply east-dipping foliation (subparallel to pencil).

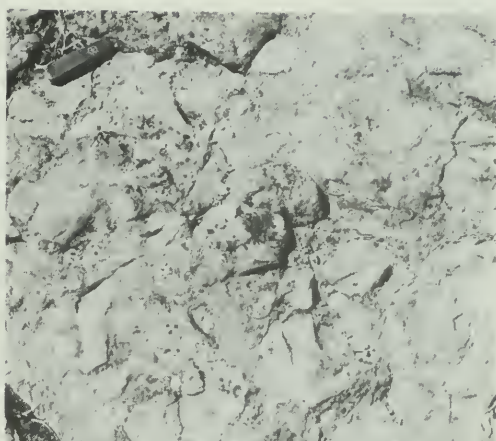


Figure 24. Arc complex metavolcanic tuff breccia at The High Rocks, approximately 1 km (0.6 mi) south-east of Oregon City. Note pocket knife for scale.



Figure 25. Arc complex relict pillow and flow lavas cut by fault, approximately 4 km (2.5 mi) northeast of Oregon City along the North Fork of Lake Oroville. Note pencil (center-left) for scale.

The fine-grained, metamorphosed nature of arc rocks makes field identification difficult; however, most of the present complex was probably water-lain.

Tuffaceous rocks include hornblende and/or augite, sodic plagioclase (saussuritized) and lithic fragments; these are set in a finer-grained tuff matrix which comprises the bulk of the formation. Vesiculated lithic fragments are commonly angular and of one rock type, suggesting derivation from local eruptive vents. Subrounded fragments of different rock types also are common and represent clastic water-lain sequences (Figure 26). Vesicles in clasts vary from 2 to 8 mm (0.08 to 0.3 in) in diameter and are filled with secondary quartz. Common minerals include epidote, clinozoisite, chlorite, and pyrite. Much of the groundmass observed in thin section is cryptocrystalline and comprises unidentifiable alteration pro-

ducts derived from secondary and metamorphic mineral reactions.

Monte de Oro Formation

Previous Investigations and Age: The Monte de Oro Formation was named and first described by Turner (1896). His work noted fossil debris throughout the formation which probably inspired some of the later studies. Subsequent investigations (Fontaine, 1900; Knowlton, 1910; Diller, 1908; Taliaferro, 1942; Creely, 1965) describe these rocks in great detail. Fossil flora, and to a lesser extent fauna, provided the earliest evidence that rocks in the Oroville area have Jurassic ages.

Contact Relationships: Monte de Oro Formation in the study area represents the tightly folded axis of a syncline overturned to the west. Approximately 375 m (1,230 ft) of Monte de Oro Formation is stratigraphically exposed.



Figure 26. Relict bedding and cross-bedding in arc tuff breccia and tuffaceous metasedimentary rock, 5 km (3 mi) southeast of Palermo. Darker area of outcrop (right-center) was wetted to accentuate structure.

The western contact of Monte de Oro Formation is depositionally conformable on arc rocks. Arc complex flows are intercalated with bedding in lower portions of Monte de Oro Formation and form a gradational contact between the two sequences; for this reason, Monte de Oro rocks are interpreted to be a sedimentary facies of the arc complex. The eastern margin of the formation is truncated against arc rocks by an east-dipping reverse fault.

Lithologic Description: Monte de Oro Formation in the Oroville area represents the only named exposures of these rocks in the Sierran foothills; however, similar metasedimentary rocks are exposed in the Bangor quadrangle to the south. These rocks are in structural alignment with Monte de Oro rocks near Oroville and may have been deposited in a common Upper Jurassic environment.

The Monte de Oro Formation is predominantly slightly-sheared, well-indurated, dark sandstone, siltstone, conglomerate and poorly-developed slate. Argillaceous siltstone and sandstone (metagraywacke) with poorly-developed interbedded slate constitute the bulk of the formation.

Exposures of metasiltstone are dark- to olive-gray where fresh and weather to light-olive-buff. Metasiltstone, commonly containing relict sandy and clayey sections, is moderately- to well-bedded and laterally continuous. Plant debris is locally abundant on metasiltstone bedding-plane cleavages.

Monte de Oro metasandstone is poorly-bedded and includes graywacke and arkose. Relict sandstone beds have lenticular shapes and are laterally discontinuous. The bulk of this material occurs in lower portions of the formation and is believed to have been reworked from underlying arc rocks.

Graywacke consists of subrounded, medium- to coarse-grained, poorly-sorted, feldspar, rock fragments and quartz or detrital chert. These constituents are

cemented by clay and silica (?) in an argillaceous matrix.

Arkose is fine-grained and consists predominantly of subrounded, moderately- to well-sorted feldspar. Clastic grains are set in a green chlorite (?) relict-silt matrix.

Monte de Oro metaconglomerate is formed of subangular to rounded, pebble- to cobble-sized clasts set in an argillaceous relict-sandstone matrix. These beds are lenticular and most abundant in relict sandstone sequences.

Predominant clast types in metaconglomerate are poorly sorted and include plagioclase- and quartz-rich porphyritic dacite (?), dark chert and black slate. Dark, fine-grained, indeterminate volcanic clasts are common but less abundant.

It is significant that many of the clasts in Monte de Oro metaconglomerate are not derived from the underlying arc complex. Exotic volcanic clasts, as well as accompanying chert and slate, were probably derived from pre-arc terrane; these sources may include melange.

Smartville Ophiolite

Previous Investigations and Age:

Studies by Lindgren and Turner (1895) and Becker and others (1898) provide early maps and descriptions of meta-volcanic greenstones in the northwestern Sierran foothills. The first detailed investigations of this greenstone suite were by Hietanen (1951), Compton (1955) and Creely (1955, 1965). More recent investigations (Moores, 1972, 1975; Cady, 1975; Schweickert and Cowan, 1975; Bond and others, 1977; Buer, 1977; Day, 1977; Hietanen, 1977) describe this greenstone sequence as dismembered ophiolite.

Cady (1975) proposed the name Smartville ophiolite in his study. This name is adopted in our investigation.

The age of Smartville ophiolite was

originally suggested to be late Paleozoic by Creely (1965) from a comparison with Oregon City Formation (arc complex) that was dated by fossils. In later works, Cady (1975) and Hietanen (1977) consider these rocks to be Jurassic in age.

The Smartville complex is interpreted to have formed by back-arc spreading (Schweickert and Cowan, 1975; Eldridge Moores, person. commun., 1977); similar spreading basins are active today in many areas of the Pacific Ocean (Hamilton, 1969; Karig, 1970, 1971a, 1971b, 1972; Moberly, 1972; Churkin, 1975; Karig and Sharman, 1975). Behind-the-arc spreading is suggested to have occurred in Callovian to Oxfordian time by Schweickert and Cowan (1975); however, their model has ophiolite originating prior to eruption of the Oxfordian age (Creely, 1965) Oregon City volcanic sequence. Smartville ophiolite is now interpreted to have formed in late Oxfordian to early Kimmeridgian time which is younger, but in part coeval with development of the arc complex.

A fault separates arc rocks and ophiolite in the study area, therefore, direct evidence is lacking to substantiate whether arc rocks are intruded by source magmas from a spreading interarc basin, or if the arc complex is built upon ophiolite. Field evidence is inconclusive and consists of: (1) Arc lithologies on Bloomer Hill, in the Berry Creek quadrangle, overlie ophiolite; however, poor contact exposures prevent a determination of whether the contact is depositional or fault controlled. (2) In the foothills east of Marysville, metabasaltic dikes similar to those in ophiolite appear to intrude arc lithologies of the Browns Valley Ridge volcanic sequence (Costas Xenophontos, person. commun., 1978). (3) A few hundred metres west of the California Highway 20 bridge over the Yuba River, Smartville pillow basalt is conformably overlain by argillite and arc-derived (Koll Buer, person. commun., 1978) tuff and pyroxene andesite tuff breccia.

Contact Relationships: The western margin of Smartville ophiolite in the study area is a near-vertical fault. The fault is not regional in extent; arc and ophiolite sequences are conformable along the Yuba River south of the area.

Sierran plutons truncate Smartville ophiolite on the east. Intrusive rocks entered ophiolite in directions subparallel to regional foliation.

The northern margin of the Smartville belt is poorly exposed; abundant meta-volcanic rock in melange further inhibits locating and interpreting the nature of the ophiolite-melange contact. The contact, although not mapped, is interpreted to be an obduction boundary.

Lithologic Description: Smartville terrane is a dismembered complex and does not contain all of the rock types and structural levels characteristic of ophiolite sequences as described by several researchers (Moores and Vine, 1971; Moores and Jackson, 1974; Coleman and Irwin, 1974; Williams and Stevens, 1974; Coleman, 1977). Common lithologies and structural layers that characterize the Smartville complex (Figure 27) include: (1) metasedimentary rock of layer 1 ophiolite; (2) layer 2 meta-basaltic and -diabasic pillows, pillow breccia, dikes and sills over a complex of metabasaltic and -diabasic dikes and sheeted dikes with felsic and gabbroic screen rocks; and (3) upper layer 3 gabbroic intrusions. Layer 2 pillows, dikes and sheeted dikes, with or without screen rocks, are the most common ophiolite members in the area. Layer 3 gabbroic intrusions, common in many ophiolites (Gass and Smewing, 1973; Jackson and others, 1975; Tysdal and others, 1977), are scarce in Smartville terrane.

Individual pillows (Figure 28) have subspheroidal to lobate shapes and are usually poorly preserved. Well-developed pillows of the Smartville complex are exposed south of the project area along the Yuba River (Figure 29).

OPHIOLITE STRATIGRAPHY

STANDARD OCEANIC CRUST

SMARTVILLE OPHIOLITE

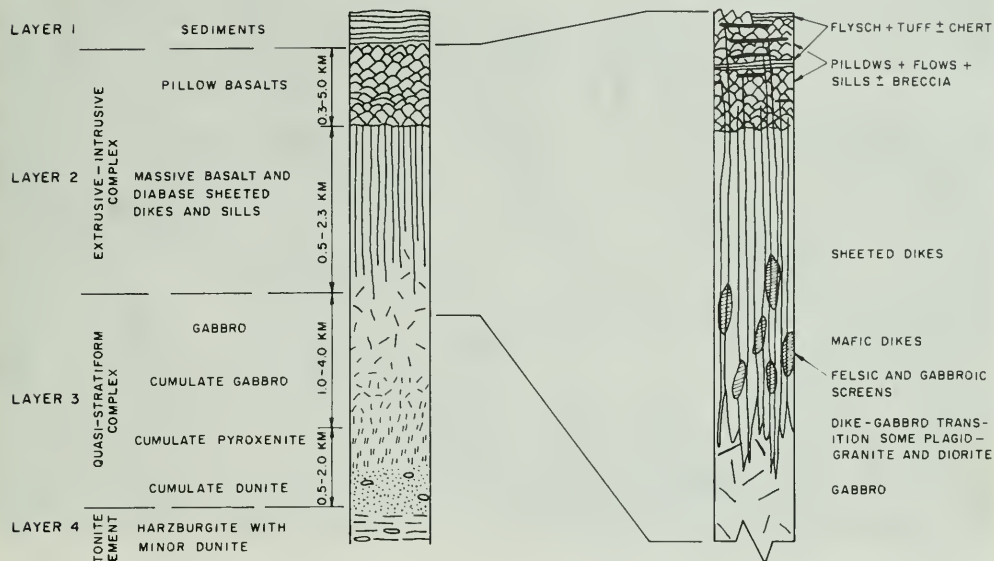


Figure 27. Igneous stratigraphy of Standard Oceanic Crust with member thicknesses (after Moores and Jackson, 1974) and Smartville ophiolite. Note that sections shown are unmetamorphosed. In most ophiolites, pillow basalts and the sheeted dike complex are metamorphosed to greenschist or amphibolite facies with almost total serpentinization of the cumulate and tectonized ultramafic rocks. An extensive shear zone commonly separates the cumulate and tectonized ultramafic rocks.

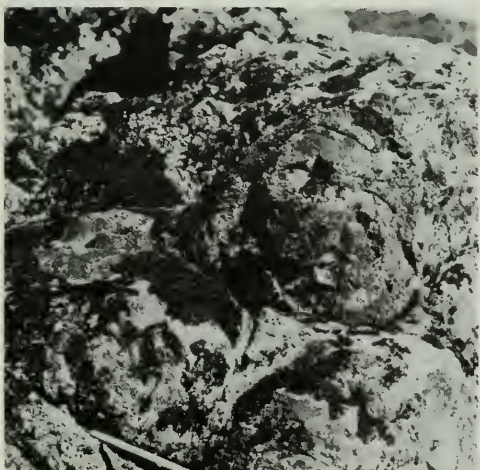


Figure 28. Well developed metavolcanic Smartville pillows 1.5 km (1 mi) south west of Bangor.

Synkinematically sheared pillows commonly yield phyllonitic rock (Figure 30). In shear zones all original rock structure is transposed and forms a cataclastic foliation.

Metabasalt forms most pillows and is dark-green to gray-green when fresh. Pyroxene, albite, epidote, and pyrite are the only minerals identifiable in hand specimen. Relict vesicles, filled with secondary quartz and epidote, are in places abundant. Quartz and epidote also fill discontinuous veinlets in these rocks and the cores of some pillows.

Sparse hyaloclastite or aquagene tuff forms selvages around individual pillows. Chert has been described as abundant in some pillow basalts (Bailey and others, 1964) but is not common in Smartville rocks.

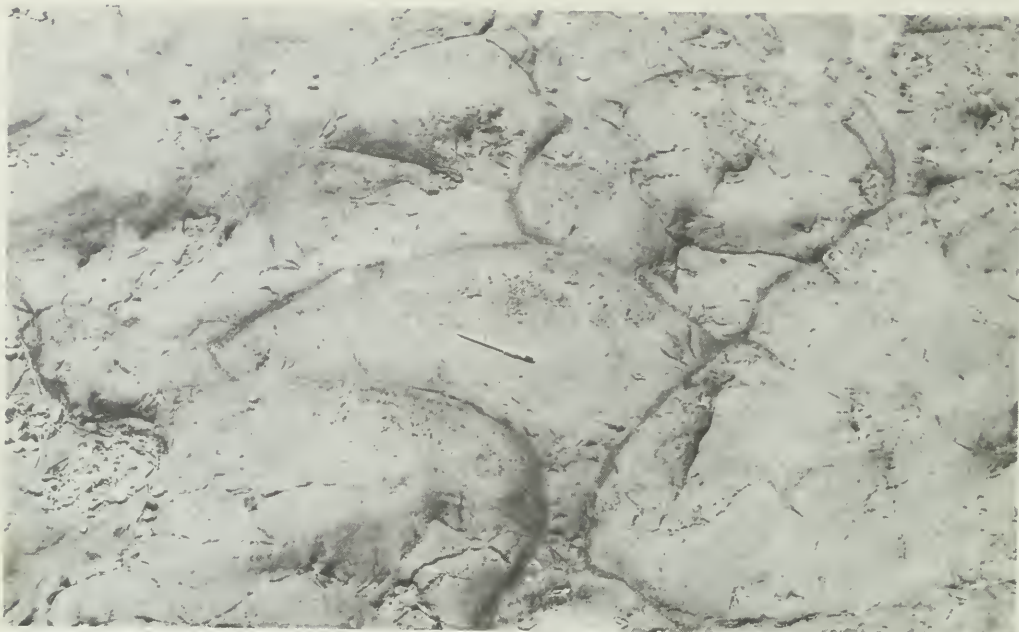


Figure 29. Well developed metavolcanic Smartville pillows at the south abutment of the California Highway 20 bridge crossing of the Yuba River. Tails on individual pillows indicate the section is right-side-up (to top of photograph) and dips steeply west.

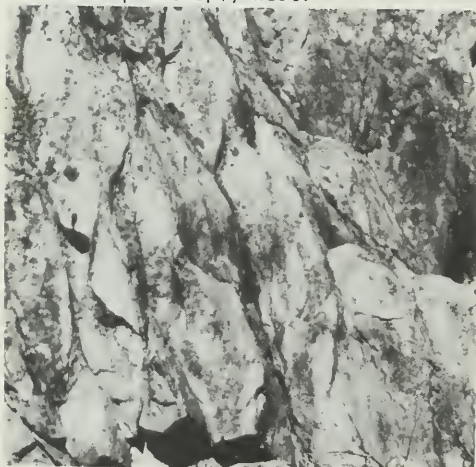


Figure 30. Sheared metavolcanic Smartville pillows in North Honcut Creek stream bed near bridge crossing of the Oro-Bangor Highway. Shearing renders the outcrop appearance of a phyllonite. Note pencil (center-right) for scale.

Pillowed basalt grades downward into meta-diabasic and -basaltic dikes and sheeted dikes (Figure 31). Dikes comprise the greatest volume of Smartville ophiolite in the study area. Models describing ophiolite (Moores and Vine, 1971; Moores and Jackson, 1974) identify lower layer 1 as a structural level where meta-basaltic and -diabasic dikes and/or sills intrude pillows. This relationship is rare in the project area.

Gabbroic and felsic screen rocks, indicating a deeper level of the ophiolite complex (Moores and Vine, 1971; Moores and Jackson, 1974), are locally abundant (Figures 32 and 33). Felsic screen rocks include quartz diorite, granophyric keratophre and trondhjemite, and represent differentiates from late-stage crystallization of sub-alkaline magmas (Coleman, 1971, 1977). Hyaloclastite screens are enclosed in dikes along California Highway 162 just south of Canyon Creek Bridge. These screens are phyllitic,



Figure 31. Steeply east-dipping metavolcanic Smartville sheeted dikes along Rocky Honcut Creek, approximately 1 km (0.6 mi) west of Oro-Bangor Highway bridge crossing.

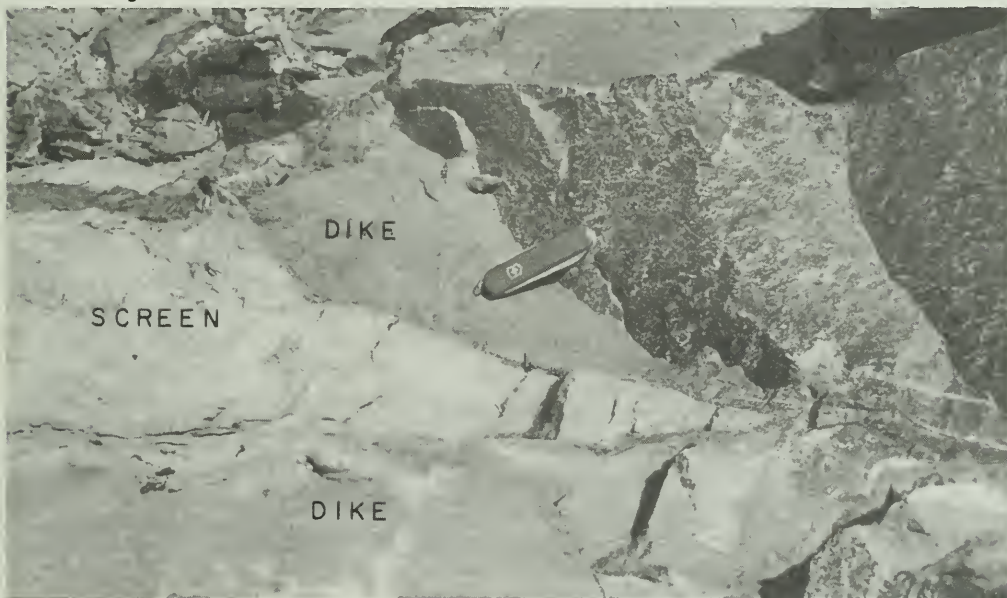


Figure 32. Grabbroic screen rock in Smartville metavolcanic sheeted dikes along Olive Highway just east of Quincy Place (Oroville quadrangle).



Figure 33. Granophyric screen rock in Smartville metavolcanic sheeted dikes along Rocky Honcut Creek, approximately 1 km (0.6 mi) west of Oro-Bangor Highway bridge crossing.

fine- to medium-grained and contrast greatly with the darker meta-diabasic dikes. Tuffaceous screens indicate dikes intruded to very shallow levels of the ophiolite, and probably fed pillows on the ancestral sea floor.

Dikes and sheeted dikes vary from 30 to 100 cm (12 to 39 in) in thickness and have continuous trends where exposed; discontinuous dikes do occur, but are rare. Foliation is concordant with contact margins. Average strikes are N5-25W and inclinations dip steeply east at angles greater than 65 degrees; west dips occur locally but are not considered representative for the dike complex.

Contacts between sheeted dikes and between dikes and screens are sharp and in places have chilled margins.

Major minerals in metavolcanic ophiolite are granoblastic clinopyroxene, albite, chlorite, epidote, clinozoisite, actinolite, tremolite and opaques (py-

rite and chalcopryrite). Unidentifiable cryptocrystalline metamorphic and hydrothermal alteration products form a groundmass for these minerals.

Gabbroic Smartville ophiolite in the study area is exposed as local dikes, plugs and stocks; gabbro is regionally limited in the complex. A gabbroic stock, with extremely complex intrusive contacts, is exposed west and northwest of Stringtown Mountain, in Woodman Ravine.

Gabbroic rock in Woodman Ravine is composed of coarse-grained plagioclase and cumulate pyroxene (uralitized). Dikes with well-developed chill margins cut gabbro in this area. Dikes contain gabbroic xenoliths which become less abundant to the south. Relationships of these mafic rocks are further complicated by intrusion of the Swedes Flat pluton.

Another gabbro (norite) intrusion underlies a small portion of the North Fork Feather River canyon west-southwest of Bloomer Hill. Lake Oroville inundates much of the gabbroic surface area.

Intrusive Rocks

Previous Investigations and Age:

Several previous investigators have mapped Sierran plutons in the study area (Becker and others, 1898; Hietanen, 1951, 1973b, 1976, 1977; Compton, 1955; Evernden and Kistler, 1970; Bateman and Clark, 1974; Clark, 1976). Plutonic terrane mapped for this project includes only western margins of these earlier regional studies.

Absolute ages of intrusive rocks in the study area are established by potassium-argon dating. Analyzed samples yield discordant hornblende and biotite ages and indicate that the dated plutons have experienced post-intrusive reheating with subsequent degassing of argon.

The Bald Rock pluton yields discordant ages of 131 and 126 million years on hornblende and biotite respectively (Evernden and Kistler, 1970). Two discordant age dates for the Merrimac pluton, using the same minerals respectively, are 129 and 131 million years (Gromme and others, 1967) and 132 and 129 million years (Evernden and Kistler, 1970). Dated locations of these plutons are not within project boundaries; however, granitic rocks are physically continuous from these locations into the study area.

Ages for the Bald Rock and Merrimac plutons indicate that emplacements were during Jura-Cretaceous time and synchronous with late stages of the Yosemite intrusive epoch (Figure 34). Late Jurassic to Early Cretaceous ages for the Sierra Nevada intrusive complex are suggested by several earlier researchers (Knoph, 1918, 1929; Erwin, 1934; Mayo, 1934, 1935) without the aid of radiometric dating.

Contact Relationships: The Bald Rock

and Swedes Flat plutons intrude Smartville ophiolite along the east-central and southeast margin of the metamorphic complex. In most places the plutons entered ophiolite subparallel to the pre-existing regional foliation. Xenoliths, from a few centimetres to several tens of metres in diameter, are in places locally abundant in plutonic

Age (m.y.)	Sys- tem	Se- ries	Intrusive epoch
70	CRETACEOUS	Upper	Cathedral Range
80			
90			
100		Lower	Huntington Lake
110			
120			
130	JURASSIC	Upper	Yosemite
140			
150			
160		Middle	Inyo Mountains
170		Lower	
180			
190	TRIASSIC	Upper	Lee Vining
200			
210		Middle	
220		Lower	
230			

(after Harland and others, 1964). Data modified after Evernden and Kistler (1970).

Figure 34. Mesozoic time scale with corresponding intrusive epochs in the Sierra Nevada region

rock near intrusive contacts (Figure 35); apophyses are locally present near intrusive margins.

The Merrimac pluton intrudes melange along the northeastern margin of the area. This pluton intruded subparallel with the regional foliation in melange country rock.

Thermal low-shear metamorphism forms aureoles in country rock surrounding Sierran plutons. Country rock around the Bald Rock and Swedes Flat plutons is thermally recrystallized by amphibolite facies metamorphism in a 1 to 3 km (0.6 to 1.8 mi) wide aureole (Compton, 1955). A contact aureole around the Merrimac pluton, also of amphibolite facies metamorphism and up to 4 km (2.5 mi) wide (Hietanen, 1977), is developed in melange.

Lithologic Description: Plutons in the area have textures, mineralogies and ages that are typical of the Sierran

intrusive complex. Rock types forming plutons include tonalite, granodiorite and quartz monzonite. Trondhjemite commonly forms the central portion of local plutons. Aplitic and pegmatitic dikes, representing late-stage intrusive rocks, are in places abundant near intrusive margins.

The Merrimac pluton is primarily medium- to coarse-grained granodiorite. Mineralogy of the pluton includes zoned and unzoned plagioclase (An_{30} to An_{40}), quartz, potassium feldspar and ferromagnesian minerals (biotite and hornblende). Accessory trace minerals include apatite, epidote, muscovite, sphene and zircon.

The Bald Rock pluton, a well-foliated compositionally-zoned intrusion, is a mixture of medium- to coarse-grained granodiorite, tonalite and trondhjemite. Tonalite and granodiorite are concentrated in outer margins of the pluton; trondhjemite forms the core of the complex. Stopping, assimilation and sub-



Figure 35. Metavolcanic xenoliths within Swedes Flat plutonic rock in Woodman Ravine, 6 km (3.5 mi) east of Oroville Dam.



Figure 36. View west-northwest of Bald Rock (foreground) 6 km (3.8 mi) east of Berry Creek. Rocks exhibit surface exposure and exfoliation that is typical of the Sierran batholithic complex.

sequent contamination is responsible for compositional layering in the Bald Rock pluton (Compton, 1955). Tonalite and granodiorite include quartz, plagioclase (An_{25} to An_{30}), microcline, hornblende, biotite, and accessory metallic minerals. Common minerals in trondhjemite are plagioclase (An_8 to An_{22}), quartz, potassium feldspar and muscovite; ferromagnesian minerals are rare.

Flow structure is well developed in the Bald Rock pluton. Flow banding dips steeply eastward and is defined by a planar parallelism of biotite, hornblende and, to a lesser extent, plagioclase. It is most strongly observable near intrusive margins where mafic minerals are concentrated. Flow layering toward the center of the pluton maintains an easterly dip and is more concentric than along its margins (Compton, 1955).

The Swedes Flat pluton is predominantly tonalite and granodiorite. Gabbro and diorite are present in subordinate amounts at the north and south ends of the pluton. Granophyric rock, as dikes and inclusion-charged masses, is abundant along the western margin of the pluton. Common minerals in Swedes Flat tonalite and granodiorite include saussuritized plagioclase (An_{20} to An_{35}), alkali feldspar, quartz, hornblende and biotite. Common accessory trace minerals are epidote, apatite and, in places, sphene.

Origin of Sierra Nevada Plutons: Tonalite and monzonite plutons in the study area (Figure 36) are similar in appearance, mineralogy and mode of origin to those comprising the Sierra Nevada batholith. Plate tectonic models developed during the late 1960's and early 1970's provide new interpretations for

the large-scale origin of plutonic complexes. In both oceanic and continental-margin settings, voluminous calc-alkaline magmas are formed above Benioff zones 150 to 500 km (93 to 124 mi) from the trench axis (Dickinson and Hatherton, 1967; Dickinson, 1968) and provide a tectonic model for Sierran plutonism.

An east-dipping Benioff zone was adjacent to the western coast of North America during much of Phanerozoic time (Hamilton, 1969; Burchfiel and Davis, 1972, 1975); inclination of the subduction zone is substantiated by potassium-silicon ratios in Mesozoic granitic rocks of California that increase eastward (Moore, 1959; Bateman and others, 1963; Dickinson, 1969) with a corresponding depth to the ancestral Benioff zone. Eastward subduction and partial melting of lithosphere at depth generated magmas (plutons) that rose to shallower structural levels beneath Mesozoic California. The calc-alkaline plutons were tensionally faulted, uplifted, and unroofed in Cenozoic time. These processes are currently active and have erosionally removed more than 8 km (5 mi) of roof rock (Bateman and Wahrhaftig, 1966) to expose the plutons.

Superjacent Series Rocks

Chico Formation

Previous Investigations and Age: Sandstone, shale and conglomerate of the Chico Formation were first described and named by Gabb (1869, p. 129). Diller and Stanton (1894) used the term "Chico group" in their study of these rocks; they considered all Cretaceous deposits in California part of the "Shasta-Chico series". Stanton (1896, p. 1,013) formally suggested the name "Chico group" to describe type-locality exposures along Chico Creek. Subsequent workers (Turner, 1896; Bryan, 1923; Brewer, 1930; Anderson, 1933; Taff and others, 1940; Popenoe, 1943; Creely, 1955, 1965) have described members and index fossils that characterize Chico Formation.

Fossils in the Chico Formation are abundant and provide accurate stratigraphic control. Fossils indicate that the age of the Chico Formation is Upper Cretaceous (Taff and others, 1940; Creely, 1965).

Contact Relationships: Basal contacts of Chico rocks are described as angularly unconformable in the Sierran foothills (Taff and others, 1940). The base of Chico Formation is not exposed in the study area, therefore, total thickness of the formation is uncertain. The thickest sequence in the study area includes 20 m (65 ft) of section.

Upper portions of Chico Formation in the project area are eroded and unconformably overlain by the Tertiary Ione and Tuscan Formations. West- and southwest-dipping strata in rocks above and below the erosional surface are slightly discordant and actually form a disconformity between Cretaceous and Tertiary rocks.

Lithologic Description: Cretaceous marine sedimentary rocks, representing arc-trench gap deposits (Dickenson, 1969), are regionally exposed at margins of the Central Valley of California and represent the base of Superjacent Series deposition. Chico Formation is the oldest Superjacent Series formation in the project area.

Chico Formation in the study area is predominantly a fine- to medium-grained, fossil-rich, friable sandstone (arkose); siltstone and pebble to cobble conglomeratic lenses occur locally. Fresh Chico Formation is light- to dark-buff to dark-gray; weathered exposures have orangish hues and are lighter in color than fresh rocks. Bedding, including abundant cross-beds, is thin to thick and well-defined.

Arkosic beds of the Chico Formation are moderately- to well-sorted and poorly cemented by calcite and clay. Individual clastic grains, forming arkosic

beds, are angular to subangular. Composition of grains includes quartz, feldspar (plagioclase and potassium feldspar) and rock fragments (primarily metamorphic clasts); accessory ferromagnesian minerals include biotite, hornblende, epidote, clinozoisite and muscovite.

Pebble- to cobble-sized clasts are well-rounded to sub-rounded and locally form interbeds in finer-grained sediments. These clasts include light to dark chert, quartzite, altered plutonic rocks and metavolcanic rocks. Conglomeratic beds, commonly containing an abundance of shell debris, are usually well-indurated by calcite cement.

Ione Formation

Previous Investigations and Age: The Ione Formation was named and first described by Lindgren (1894, p. 3) who assigned exposures near Ione, California as the type locality. Early investigations of Tertiary sandstone near Oroville were by Lindgren (1911) and Dickerson (1916). Subsequent detailed studies are by Allen (1929) and Creely (1965).

The age of Ione Formation is substantiated by fossil fauna and flora collected by many earlier researchers. These fossils indicate that Ione deposition occurred in Middle Eocene time.

Contact Relationships: The Ione Formation rests unconformably on the underlying formations. Ione deposits dip gently west and southwest and overlie arc, melange and the Chico Formation in the study area.

Upper sequences of the Ione Formation include auriferous gravel and tuffaceous sediment and are conformably overlain by Lovejoy basalt. Basalt extrusion was during late stages of Ione aggradation; therefore, the unconformity formed by basalt at the top of the Ione Formation is a matter of convention.

Auriferous gravel and Oroville tuff

(Mehrten Formation-?) are gradational in upper portions of the Ione Formation. Auriferous gravel and tuffaceous sediment, transported and deposited by Ione fluvial processes, are mapped as formational members in this study. Creely (1965) mapped quartz-rich sequences as "auriferous gravels" and tuffaceous rock as "Mehrten (?) Formation". Mehrten Formation in the Stanislaus drainage is dated by Dalrymple (1964) at 8.8 to 9.3 million years while tuffaceous deposits on South Table Mountain are pre-Lovejoy basalt (23 million years old) and older than Dalrymple's dated Mehrten Formation.

Tuffaceous beds are locally exposed through the Oroville area. These tuffs do not expose basal contacts and are overlain by late Cenozoic gravels. Such contact relationships provide no stratigraphic correlation with tuffs exposed on North and South Table Mountains which are topographically higher.

Lithologic Description - Ione Formation

Undifferentiated: White to yellowish-white, medium- to fine-grained, silty-clayey sandstone constitutes the greatest percentage of the Ione Formation in the study area; intercalated in sandstone are subordinate amounts of siltstone, shale, conglomerate and minor quantities of lignitic coal. Conglomeratic beds and pebble stringers are in most places composed of well-rounded quartz and chert pebbles. Bedding in sandstone is thick to thin and moderately- to poorly-defined; cross-bedding is common and best observed in cut slopes.

Most sandstone is friable, argillaceous and cemented by interstitial silt and clay. Individual sand grains are angular to subangular and composed of quartz, plagioclase, potassium feldspar and rock fragments. Trace amounts of heavy minerals include hematite, magnetite, epidote, zircon, hornblende, tourmaline and clinozoisite.

Lithologic Description - Auriferous

Gravel: Auriferous (gold bearing) gravel contains high percentages of white quartz-rich sand and gravel. In the Oroville area this gravel has a maximum thickness of 100 m (330 ft) and is exposed by numerous hydraulic mines cut into side slopes of North and South Table Mountains (Figure 37).

Sand in gravel is medium- to coarse-grained, sub- to well-rounded and exhibits fair sorting. Individual sandstone layers are thin- to thickly-bedded and manifested by slight variations in grain size, the presence of thin siltstone or pebble conglomerate lenses and thin mica-clay layers.

Conglomeratic sections are composed of subrounded to well-rounded quartz pebbles and cobbles. Clasts are loosely packed and set in a quartz-sand matrix. Individual conglomerate beds range from

thin pebble stringers in sandstone to layers more than 1 m (3 ft) thick.

Lithologic Description - Oroville Tuff (Mehrten Formation-?): Tuffaceous deposits include fine-grained clayey beds (relict ash); tuff clasts in coarse-grained, water-lain and cross-bedded deposits; white, fine-grained, sandy beds; and moderately- to well-cemented volcanic mudflow breccia. All of these rock types, including clay layers, which possibly represent an air-lain derivation, were eroded and transported from sources to the east and north.

Light colored and cross-bedded, sandy, tuffaceous sequences are locally exposed around Oroville and represent fluvial deposition. Whether separated tuffaceous outcrops represent rock- or time-



Figure 37. Lone Formation auriferous gravel with intercalated Oroville tuff (Mehrten Formation-?) in a hydraulic mining cut on the east side of South Table Mountain.

stratigraphic horizons is uncertain.

Mudflow volcanic breccia is formed by angular to sub-angular, vesiculated and amygdaloidal rhyodacite clasts set in a reddish-brown, sandy-silty matrix. Brecciated clasts are not locally derived. Source areas of the Ione Formation suggest the mudflow breccias were also derived from east and north of the area.

Lovejoy Formation

Previous Investigations and Age: The basalt on Oroville Table Mountain was first mapped and named "older basalt" by Turner (1894) to differentiate the unit from younger flows in the area. This basalt was correlated with the Lovejoy Formation by Durrell (1959b, 1966) which he considered, based on stratigraphic relationships, to be of Eocene age and derived from areas east

of the present Sierra Nevada crest. Dalrymple (1964) radiometrically dated rocks above and below Lovejoy Formation and determined the age of basalt to be Early Miocene; his oldest date, 23 million years, was obtained from a tuff bed below Lovejoy Formation on South Table Mountain and should be a maximum age for basalt in this area.

Contact Relationships: Lovejoy Formation in the study area disconformably overlies Ione Formation and Oroville tuff (Mehrtens Formation-?) (Figure 38); basalt rests unconformably on ophiolite and melange in two localized areas but this relationship is not common. Lower contacts of basalt are nearly planar and dip 2 to 3 degrees west-southwest. Upper and lower planar contacts indicate that the basalt has experienced little deformation during regional westward tilting and provide control for post-extrusive (late Cenozoic) faulting.



Figure 38. View south of Lovejoy Formation basalt disconformably overlying Ione Formation sedimentary rock in hydraulic cut face of the Cherokee Mine.



Figure 39. View east from upper reaches of Morris Ravine of Lovejoy Formation basalt on North Table Mountain. Basalt at this location has a minimum thickness of 75 m (246 ft) and rests disconformably on Lone Formation.

Lithologic Description: Lovejoy Formation forms the flat-topped mesas of North and South Table Mountains (Figure 39). Lovejoy basalt includes one or more sub-horizontal flows with a cumulative thickness in the Oroville area of less than 50 m (164 ft).

Lovejoy basalt is dark-brown to black and forms blocky outcrops. Poorly-developed columnar jointing is common in upper parts of the formation. Lower parts of the formation are generally fragmented and locally include a basal conglomerate. Vesiculated basalt is more abundant near the base of the formation. Basalt mineralogy includes plagioclase (An_{65} to An_{40}), olivine and traces of augite. Plagioclase microlites are abundant in some samples. A crystalline to glassy matrix comprises the

greatest volume of basalt.

Tuscan Formation

Previous Investigations and Age: Rocks of the Tuscan Formation were first described by Whitney (1865). Diller (1892, 1895) named the formation and described the type locality at Tuscan Springs in Tehama County.

Anderson (1933) published a comprehensive paper on the Tuscan Formation. This work includes many detailed rock descriptions and a discussion on the development of Tuscan breccia.

Recent studies of the Tuscan Formation are by Creely (1965) and Lydon (1968). Lydon's work is comprehensive and deals with the source areas for the rocks.

Tuscan Formation is Late Pliocene in age (Lydon, 1968). A potassium-argon age of 3.3 million years (Evernden and others, 1964) is determined for the Nomlaki Tuff member of the formation.

Contact Relationships: The Tuscan Formation unconformably overlies melange in the study area; locally Tuscan rocks rest disconformably on Chico and Ione Formations. Basal contacts of Tuscan Formation indicate the depositional surface is relatively flat and dips slightly to the southwest. This horizon trends below alluvium of the Sacramento Valley. Upper surfaces of Tuscan flows are relatively planar (Figure 40) and dip at low angles to the southwest. These flows are deeply incised by westerly flowing drainages.

Lithologic Description: The volcanic Tuscan Formation is composed of lahars, volcanic sand, conglomerate, tuff, tuff breccia, and intercalated andesite and basalt flows. These rocks when fresh are gray, purple, orange or brown. The maximum formational thickness in the study area is 180 m (590 ft).

Tuff breccia (lahar) forms about 75 percent of the formation. Clasts are basalt and andesite with basalt being predominant (Anderson, 1933). Flow breccias are unsorted and form irregular contacts with underlying rocks. The matrix of these rocks is well-indurated volcanic and tuffaceous sand. Intercalated flow rocks, a minor component of the Tuscan Formation, are predominantly olivine basalt and pyroxene andesite.

TUSCAN SURFACE

METAMORPHIC SURFACE



Figure 40. View north of lower and younger erosional surface on Upper Pliocene Tuscan Formation that is separated by the West Branch of the Feather River (not shown) from an older and structurally higher erosional surface cut into Mesozoic metamorphic rocks. Photograph taken from intersection of Highway 70 and Messilla Valley Road (Cherokee quadrangle).

Tuff, tuffaceous sandstone and volcanic sandstone are locally intercalated with the flows and breccias. These units are composed of angular crystal and lithic volcanic fragments with andesitic to basaltic compositions. Sequences are well-bedded, well-sorted, and commonly cross-bedded (Figure 41). Sediments are common at the western margins of the formation. Tuff breccia dominates the stratigraphically thicker eastern areas of Tuscan exposure.

Late Cenozoic Gravels

Previous Investigations: Late Cenozoic fluvial deposits of the Oroville area were first differentiated by Creely (1965). He assigned all older gravels in the area to the Pleistocene Red Bluff

Formation.

Recent mapping in the Bangor quadrangle (Quintin Aune, unpub. data) indicates there are several gravel units of varying ages and source areas. Mapping for this study confirms the presence of multiple gravels that probably are not time equivalent to the Red Bluff Formation. Therefore, they are named "late Cenozoic gravels" rather than Red Bluff Formation in this report.

Contact Relationships: Late Cenozoic gravels overlie both Basement Series rocks and Superjacent Series rocks in the project area. They are separated from basement rocks by an angular unconformity and from superjacent rocks by a disconformity.



Figure 41. Tuscan Formation volcanic conglomerate, cross-bedded sand and laharic mudflow breccia along Sycamore Creek 3 km (2 mi) northeast of Chico.



Figure 42. Late Cenozoic gravel and cross-bedded sand (Red Bluff Formation-?) exposed in a railroad cut 0.5 km (0.3 mi) south of intersection of Baggett Palermo and Baggett Marysville Roads (Palermo quadrangle).

Lithologic Description: Late Cenozoic gravels in the study area have a maximum thickness of 30 m (100 ft) and are composed of poorly-sorted, rounded to sub-rounded, pebble- to boulder-sized clasts. These are weakly to moderately cemented by varying amounts of clay, silt and orange amorphous silica; cementation is weak where sandy and moderate in clayey sections. Clast types, in descending order of abundance, are metavolcanic rock (including ophiolite, arc and younger dike rocks), intrusive rocks, and fine-grained porphyritic volcanic and siliceous clasts (including quartz, quartzite and red and black chert). Imbricate pebbles indicate source areas are to the north and east. Well-sorted and cross-bedded, weakly-cemented sand, and thin-bedded, moderately indurated silt and clay comprise the gravel matrix.

Sandy members of gravels are generally thinly- to moderately-bedded, lenticular and, in places, cross-bedded (Figure 42). Fine-grained sands and silty-clayey members, most common away from upland terranes, probably represent flood plain deposits of the ancestral Feather River and associated tributaries.

Clayey sections in gravel have minor occurrences in the study area. Clay in gravel sequences, probably reworked from underlying tuff units (Figure 43), represents low energy deposition.

Quaternary Landslides

Our investigation indicates that large-scale landsliding is more common in the project area than suggested by earlier detailed investigations. Failures com-

monly occur from slopes underlain by Ione Formation (Figure 44); this formation is the least competent of study area rock types.

North and South Table Mountains and the Campbell Hills are capped by Lovejoy basalt and have side-slopes underlain by gently west-dipping Ione Formation; south- and west-facing slopes in these areas daylight Ione bedding. Resistant cap rock overlying non-resistant Ione Formation provides ideal conditions for large-scale landsliding. In this situation, side-slopes are oversteepened by artificial support of the erosionally-resistant cap rock. A regional slope-stability study of the United States notes the western side-slopes of North and South Table Mountains at Oroville are highly susceptible to failure (Radbruch-Hall and others, 1976).

Landslides were not mapped in detail on Table Mountain or Campbell Hill side-slopes for this study. The time required for mapping gravity-induced structural complexities was not warranted for purposes of this investigation; therefore, landslides probably underlie more area than is indicated by our geologic map.

Numerous landslides occur along the Feather River and its major forks. Failures in this area are within arc and ophiolitic lithologies. The toe portions of these landslides occur near lower valley slopes and are now seasonally inundated by Lake Oroville. Landslide movements are mostly prehistoric, however, several failures indicate recent activity. The largest recent landslide is superimposed on an older failure that moved from the northwest side of Stringtown Mountain (Figure 45).



Figure 43. Late Cenozoic gravel (Red Bluff Formation-?) unconformably overlying Oroville tuff (Mehrten Formation-?) along the Feather River 1.0 km (0.6 mi) west-southwest of Oroville.



Figure 44. View west of landslide in Lone Formation. Note the vegetation stand in graben area of landslide. Location is in Campbell Hills just north of Thermalito Forebay by Highway 70 (center).



Figure 45. Aerial southeast view of Stringtown Mountain landslides. Note that the recent failure is superposed on a larger and older landslide.



Figure 46. Aerial east-southeast view of a prehistoric landslide that is part of a much larger failure involving the entire north slope of Bloomer Hill into the North Fork of the Feather River.

The largest landslide in the project area, underlying the north slope of Bloomer Hill, is a failure of arc rock into the North Fork of the Feather River (Figure 46). The landslide moved north as a large slump of several individual failures. This landslide could have temporarily dammed the river. Arcuate scars of disturbed arc rock define the landslide boundaries which are best observed using high-altitude aerial photographs.

STRUCTURAL GEOLOGY

Faults

Geologic evidence in the northern Sierran foothills suggests two periods of fault activity. The first episode of faulting was from compression before Late Jurassic time. This deformation occurred prior to the intrusion of local plutons (Nevadan orogeny-Yosemite intrusive epoch). The second period of faulting began in late Tertiary time and continues to the present. The late Tertiary to present tectonic regime is one of east-west extension which places older fault zones in tension. As a result, some recent movements have occurred along older Mesozoic faults. Other movements displace Tertiary rocks and have thus broken new ground, possibly from reactivation of underlying Mesozoic faults.

Data on foothills faulting between Oroville and Sonora is derived largely from exploration trenches by Department of Water Resources and other agencies. Locations of exploration trenches on major lineaments are shown in Figure 47 and findings are summarized in Table 1.

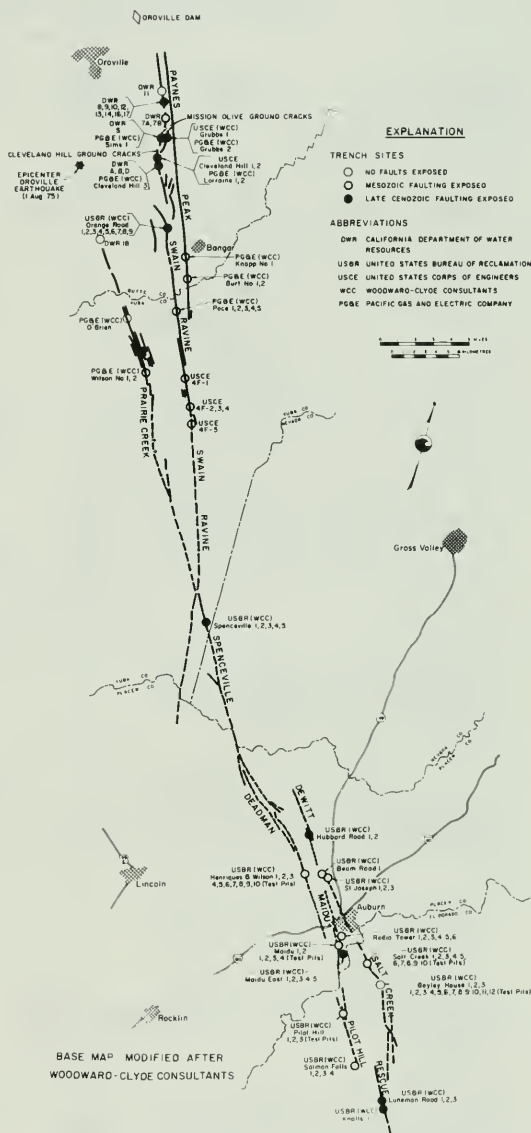


Figure 47. Major lineaments in the northwestern Sierran foothills showing exploration localities with faulting assessments for each site.

TABLE 1

EXPLORATION TRENCHES IN FOOTHILL BELT - OROVILLE TO AUBURN AREA

(Exploration sites listed from north to south on given lineaments)

<u>Lineament, Agency, and Trench Number</u>	<u>Faulting Exposed</u>	<u>Attitude</u>	<u>Cenozoic Movement</u>	<u>Comments</u>
<u>SWAIN RAVINE LINEAMENT</u>				
DWR				
11	No	--	--	--
10	No	--	--	--
13	Yes	N10-40W, 60-73SW	Yes	Trench located on crack; faulting does not offset soil-bedrock interface.
14	No	--	--	--
17	Yes	--	Yes	Fault does not offset bedrock-soil interface.
16	Yes	N12W, 65SW	Yes	Trench located on crack; faulting does not offset bedrock-soil interface.
12	Yes	N10W, 69SW	Yes	Trench located on crack; faulting does not offset bedrock-soil interface.
8	Yes	N20W, 70SW	Yes	Trench located on crack; faulting offsets gravel-soil contact 30 mm.
9	No	--	--	--
7A	Yes	N15W, 65SW	?	Faulting does not offset bedrock-soil contact.
7B	No	--	--	--
5	Yes	N9W, 54SW	Yes	Trench located on crack; faulting does not offset bedrock-soil interface.
USCE (WCC)				
Grubbs 1	Yes	--	Yes	Trench located on East Mission Olive crack zone.
PGandE (WCC)				
Grubbs 2	Yes	--	Yes	Trench located on East Mission Olive crack zone.
PGandE (WCC)				
Sims 1	Yes	--	Yes	Trench located on West Mission Olive crack zone.
USCE (WCC)				
Cleve. Hill 1 & 2	Yes	--	Yes	Trenches located on northern end of Cleveland Hill Fault; bedrock fault with at least 3 episodes of displacement described.
PGandE (WCC)				
Lorraine 1 & 2	Yes	--	Yes	Trenches located on eastern splay of Cleveland Hill Fault.
DWR				
A, B, D	Yes	--	Yes	Trenches located on Cleveland Hill Fault at southwest margin of Cleveland Hill.
PGandE (WCC)				
Cleve. Hill 3	Yes	--	Yes	Trench located on Cleveland Hill Fault at southwest margin of Cleveland Hill.
USBR (WCC)				
Orange Road 1-9	Yes	N11-21E, 55-59SE; N18-20W, 80NE	Yes	Faults located in trenches 2, 3, 4, 5, 6, 9
PGandE (WCC)				
Pace 1-5	Yes	--	No	Faulting does not offset bedrock-soil interface.
USCE				
4F-1	Yes	N5W, 41NE, N15W, 47NE	No	Faulting does not offset bedrock-soil interface.
USCE				
4F-2	No	--	No	--
4F-3	Yes	N15W, 46NE	No	Faulting does not offset bedrock-soil interface.
4F-4	Yes	N2E, 52SE, N22W, 48SW	No	Faulting does not offset bedrock-soil interface.
4F-5	Yes	N32W, 70NE N34W, 70SW	No	Faulting does not offset bedrock-soil interface.

TABLE 1 (Continued)

<u>Lineament, Agency, and Trench Number</u>	<u>Faulting Exposed</u>	<u>Attitude</u>	<u>Cenozoic Movement</u>	<u>Comments</u>
<u>PAYNES PEAK LINEAMENT</u>				
PGandE (WCC) Knapp No. 1	Yes	--	No	--
PGandE (WCC) Burt No. 1 & 2	Yes	--	No	Faulting does not continue into overlying soils.
<u>PRAIRIE CREEK LINEAMENT</u>				
DWR 18	No	--	No	No faults exposed and trench not logged.
PGandE (WCC) O'Brien	No	--	No	--
PGandE (WCC) Wilson No. 1 & 2	Yes	--	No	Faulting does not continue into overlying soils.
<u>SPENCEVILLE LINEAMENT</u> (Southern extension of Prairie Ck. Line.)				
USBR (WCC) Spenceville 1	Yes	N32W, 63SW; N55W, 67SW	Yes	Faulting continues into overlying soils.
(5 trenches) 2	Yes	--	No	Faulting does not continue into overlying soils.
3	Yes	N15-50W, 70-75SW	Yes	Faulting displaces paleo B.
4	No	--	No	--
5	No	--	No	--
<u>DEWITT LINEAMENT</u> (Southern extension of Spenceville and Prairie Ck. Line.)				
USBR (WCC) Henriques & Wilson (10 test pits)	Yes	N20W, 47SW N20W, 55SW	?	No fault assessment made because paleo B too scarce in local area for evaluation
<u>DEWITT LINEAMENT</u>				
USBR (WCC) Hubbard Road (2 trenches)	Yes	N44-50W, 50-60SW	Yes(?)	Faulting in paleo B but gravity also affects rocks making inter- pretations difficult; faulting classified (USBR criteria) "indeterminate" (active).
USBR (WCC) Bean Road (1 trench)	Yes(?)	N60W, 65NE	No	Faulting does not continue upward into paleo B; faults classified (USBR criteria) "indeterminate" (inactive).
USBR (WCC) St. Joseph (3 trenches)	Yes	N38W, 60NE	?	Paleo B locally scarce, therefore, faulting at this locality classi- fied (USBR criteria) "indeterminate".
<u>MAIDU LINEAMENT</u>				
USBR (WCC) Radio Tower (Located on E. splay of Maidu Line.) (6 trenches)	Yes	N55-60E, 30NW-90	?	Paleo B and overlying soils locally scarce, therefore, faulting at this locality classified (USBR criteria) "indeterminate".
USBR (WCC) Maidu (2 trenches) (4 test pits)	Yes	N10E, 45NW	?	Paleo B and overlying soils locally scarce, therefore, no fault assessment made for Late Cenozoic tectonics at this locality.

TABLE 1 (Continued)

<u>Lineament, Agency, and Trench Number</u>	<u>Faulting Exposed</u>	<u>Attitude</u>	<u>Cenozoic Movement</u>	<u>Comments</u>
USBR (WCC) Maidu East (E splay of Maidu Line.) (5 trenches by WCC plus 25 trenches and backhoe pits by USBR)	Yes	N13E, 77SE, N55W, 47SW, N3E, 67SE, N30W, 67SW, N20-25E, 82NW-90, N20-30E, 72-80NW	Yes	Maximum vertical separation of Mehrtens Fm. across fault zone is 5.4 m (18 ft). Slickensides in soil with orientations similar to bedrock faults and steps in colluvial base overlying bedrock fault traces indicate faulting is Cenozoic. To north a buried paleosol at least 100,000 years old is not cut by faulting; therefore, movements are too small to offset soils or fault displace- ments die out to north. Faulting confidence level is 2 on 0-10 scale.
<u>PILOT HILL LINEAMENT</u>				
USBR (WCC) Pilot Hill (3 test pits)	No(?)	--	?	Paleo B and overlying soils scarce, therefore, no fault assessment made for this locality.
USBR (WCC) Salmon Falls (4 test pits)	No(?)	--	?	Thin shears exposed but no faults; lack of local paleo B for offset control. No fault assessment.
<u>SALT CREEK LINEAMENT</u>				
USBR (WCC) Salt Creek (10 test pits)	No(?)	--	?	Paleo B locally lacking, therefore, no fault assessment made for this area.
USBR (WCC) Bayley House (3 trenches) (12 test pits)	No	--	No	Ground water barriers define the lineament but are controlled by clay-rich weathering zones; no evidence of Cenozoic faulting noted.
<u>RESCUE LINEAMENT</u>				
USBR (WCC) Luneman Road (3 trenches)	Yes	N54, 60SW N40W, 40NE	Yes	Faulting trends into overlying colluvium and terminates a paleo B with colluvium on east side of fault thicker than on west side; paleosol indicates 0.55 m (1.8 ft) of down to east displacement. Fault in trench 3 classified as "indeterminate" (active) by USBR criteria; confidence level is 4 on scale 0-10.
USBR (WCC) Knolls (1 trench)	Yes	N20W, 50SW	Yes(?)	Distinct lithologic blocks are bounded in places by clay seams that appear to juxtapose the blocks; basal contact is not obviously offset. Faulting classified by USBR criteria as "indeterminate" (active). Confidence level is 2 on scale of 0-10.

Mesozoic Faults - Northern Foothills

Clark (1960) identified and named the Foothills Fault System (Figure 48). This system, bounded by the Melones Fault zone on the east and the Bear Mountains Fault zone on the west, is formed by numerous north to north-northwest trending preintrusive reverse faults (Clark, 1964, 1976). Major faults within this system can be identified by elongate bodies of serpentine, areas of structural and lithologic discontinuity and zones of intense and well-defined shear cleavage that dip steeply east.

Subsequent to Clark's initial study, Mesozoic faults in the foothills were described and mapped in many geologic investigations. A few of these studies include works by Baird (1962), Burnett and Jennings (1962), Bateman and others (1963), Clark (1964, 1976), Creely (1965), Cebull (1972) and Hietanen (1973a, 1976, 1977).

The Melones Fault zone, named by Clark (1960), strikes northwest along the eastern margin of the Foothills Fault System in its type locality. The fault is defined by strongly sheared zones that, in places, incorporate serpentine and blocks of undeformed or less deformed rock. Shear cleavage within the zone is locally several hundred metres wide and dips vertically or steeply east (Clark, 1960, 1964).

The Melones Fault zone, best exposed south of the Cosumnes River, is the eastern limit of the Foothills Fault System (Jennings, 1975). Clark (1960) noted that north of the American River the Melones Fault splits into several zones. The splay representing the Melones Fault zone in this area is defined as the boundary between Paleozoic rocks to the east and Mesozoic rocks to the west (Clark, 1960, 1964; Duffield and Sharp, 1975).

The Bear Mountains Fault zone of Clark (1960) parallels the trend of the Melones Fault zone to the east and splits into

several faults at its northern end near the Cosumnes River. The regional shear zone mapped by Burnett and Jennings (1962) to the southwest of the area may represent the northern extension of the Bear Mountains Fault zone. This fault zone averages a few hundred metres in width and dips vertically or steeply east (Clark, 1964). Net displacement across the system is unknown but suggested to be large and probably represents several thousand metres of offset (Clark, 1964).

Origin of the Bear Mountains Fault, as with other faults in the Foothills Fault System, is the result of eastward underthrusting during Farallon-American plate interactions in Late Jurassic time. Eastward underthrusting is suggested by some early researchers (Ferguson and Gannett, 1932, p. 90; Knopf, 1929, p. 45-46); however, a strike-slip motion, at least in part, is indicated by Clark (1960) and Cebull (1972).

Mesozoic faults in the study area are considered to be part of the Foothills Fault System. These faults displace the late Oxfordian to early Kimmeridgian (Imlay, 1961, p. D8-D9) Monte de Oro Formation and are truncated by Sierran plutons of the Yosemite intrusive epoch. Radiometric dating of the plutons (Gromme and others, 1967; Evernden and Kistler, 1970) yield a minimum age of about 130 million years. These data suggest that Mesozoic faults developed during the Late Jurassic-Early Cretaceous Nevadan orogeny, about 130 million years ago.

Foothills system faults were driven by a regional east-west compression and are synchronous with late stages of an epidote-albite-amphibole metamorphism. Compressive stresses and subsequent Foothills Fault System displacements were generated during subduction underthrusting and accretion of arc and ophiolitic rocks to Mesozoic California. This deformation generated north-striking, steeply dipping faults, fold axes and slaty cleavage in rocks of the study

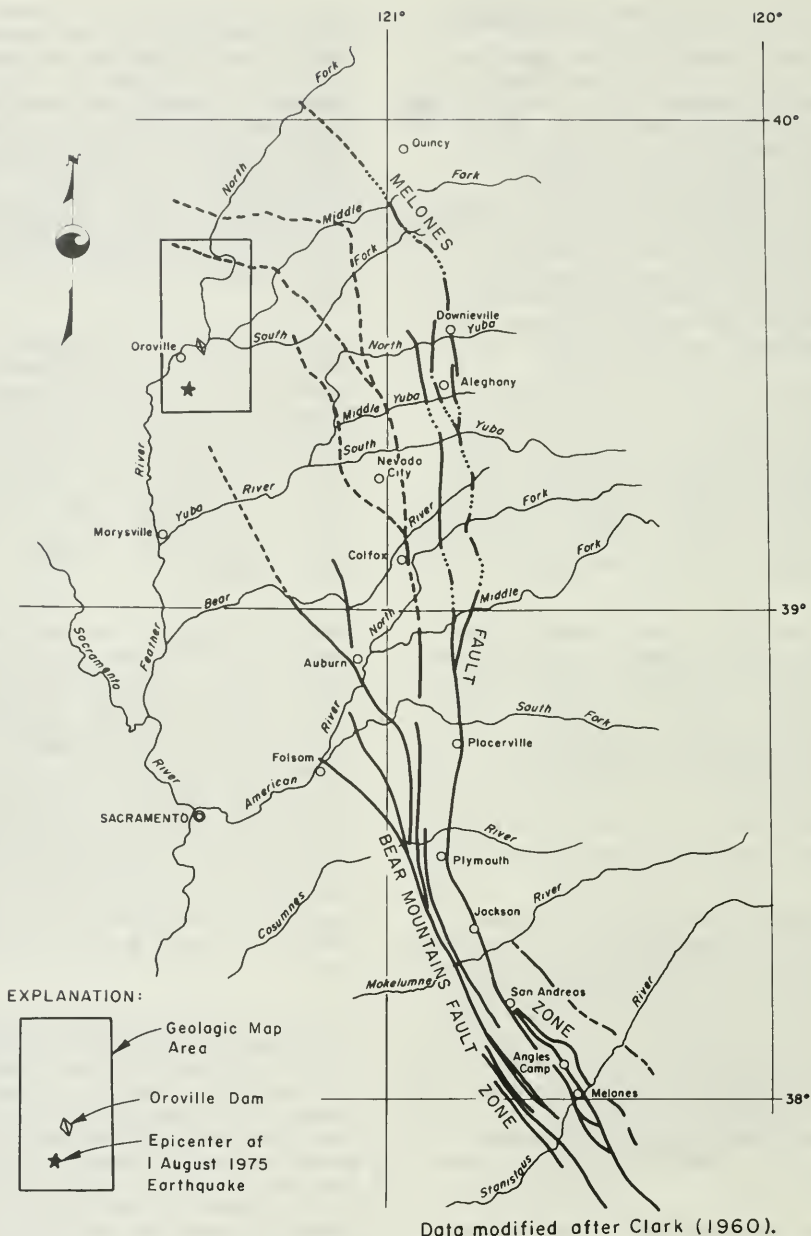


Figure 48. Foothills Fault System of the western Sierra Nevada, California

area. Deformation ceased when these rocks were firmly accreted (obducted) to the continent. Additionally, the westerly migration of subduction was stabilized in areas of the present Coast Ranges terrane at this time.

Mesozoic Faults - Project Area

Mesozoic faults in the study area commonly appear as photo lineaments. These lineaments, sharply defined in high-altitude photography, are commonly aligned with foliation and fold axes in foothill rocks.

Field investigations of major lineaments indicate three are fault zones. Fault features include: (1) pronounced alignment of ridges and valleys along lineament trends, (2) sheared rocks and numerous subordinate faults and shears subparallel with major lineaments, and (3) springs and seeps.

Mesozoic fault movements were probably oblique, however, a large reverse component is indicated by many researchers (Hamilton, 1969; Schweickert and Cowan, 1975; Clark, 1976; Russel, 1978; Standlee, 1978). Reverse, east-dipping Mesozoic faults are predictable in models of eastward subduction which was active at this time; the Glover Ridge thrust fault, an obduction suture, is an exception.

Plate tectonic models for explaining the origin of Mesozoic foothills faults suggest large-scale movements. Displacements on larger foothills system faults such as the Melones Fault zone may exceed several kilometres.

In summary, the Foothills Fault System is a late Paleozoic to Late Jurassic feature. Compression driving these generation faults originated from episodes of plate convergence and consumption along the western edge of Mesozoic North America, and produced major structural elements of the Sierran foothills.

Swain Ravine, Paynes Peak and Prairie Creek Lineament/Fault Zones: The Paynes Peak and Swain Ravine Lineaments are the most striking photo lineaments in the area. Another prominent lineament, the Prairie Creek Lineament, projects into the study area from the south, west of the Swain Ravine Lineament. The trace of the Prairie Creek Lineament within the study area is not well defined.

The Swain Ravine and Paynes Peak Lineaments trend approximately north-northwest and parallel each other in the southern field area. The two lineaments can be traced on the ground by aligned valleys, discontinuous areas of sheared rocks, springs and seeps, and are interpreted to be Mesozoic fault zones.

The Paynes Peak Lineament in the study area has a strong to moderate expression. It lies parallel to, and about 1.6 km (1 mi) east of the Swain Ravine Lineament. Surfically, the only conclusive fault features are exposed in Rocky Honcut Creek (Bangor quadrangle, Section 16, T18N, R5E) where a break in outcrops, a linear drainage and aligned springs define the fault trace.

The northern extension of the Paynes Peak Lineament trends just east of Miners Ranch Reservoir and Bidwell Canyon Saddle Dam. Rock along the lineament is strongly sheared, however, field evidence for faulting north of Rocky Honcut Creek is poor. The Paynes Peak Lineament, as defined in this report, coincides with the eastern margin of the "regional shear zone" as mapped by the U. S. Army Corps of Engineers (1977, Plate V) and terminates about 1 km (0.6 mi) northeast of Bidwell Canyon Saddle Dam.

South of the project area the Paynes Peak Lineament has a strong topographic expression. The lineament terminates north of Paynes Peak in the vicinity of Stone House (U. S. Army Corps of Engineers, 1977, Plate IV).

Surface and subsurface data along the Paynes Peak Lineament were collected and analyzed by Pacific Gas and Electric Company and Woodward-Clyde Consultants. Three trenches, designated Knapp No. 1 and Burt Nos. 1 and 2, were excavated between Bangor and the Yuba River by Pacific Gas and Electric Company. These trenches exposed bedrock faults that do not displace overlying soils.

The Swain Ravine Lineament is the most significant lineament in the area because it coincides with Cleveland Hill Fault cracking that occurred during the 1975 Oroville earthquake. No cracking along the lineament is reported south of Bangor; however, the lineament continues southward as a strong feature. Just south of the Yuba River, the lineament coincides with the eastern margin of a regional shear zone mapped by Burnett and Jennings (1962) and the U. S. Army Corps of Engineers (1977). A more thorough description of the Swain Ravine Lineament is included with the section on Cenozoic faults.

The Prairie Creek Lineament has the least physical expression of the three major lineaments in the study area. The lineament, well-developed south of the Yuba River, is discontinuous to the north. It is prominent in the southeast corner of the Palermo quadrangle, but dies out to the north where the area is overlain by alluvium and late Cenozoic gravels. The length of the Prairie Creek Lineament from the study area to its southern end, where it is truncated by the Rocklin pluton, is approximately 64 km (40 mi).

Investigation of the Prairie Creek Lineament between Bangor and the Yuba River consisted of field mapping and a trench (DWR 18) in the Palermo quadrangle by Department of Water Resources (this study) and three trenches by Pacific Gas and Electric Company. Two of the Pacific Gas and Electric Company trenches (Wilson, 1 and 2), located about 4.8 km (3 mi) northwest of Browns Valley, exposed bedrock faults which did not displace overlying soils. The

third trench (O'Brien) about 3.2 km (2 mi) northwest of Loma Rica exposed no fault structures.

In November 1977, Department of Water Resources personnel trenched the northern end of Prairie Creek Lineament about 855 m (2,800 ft) north of Cox Lane (NE1/4 Section 27, T18N, R4E). Aligned bedrock ridges and a small depression (sag pond-?) define the Prairie Creek Lineament in this area and suggest it is a fault. The trench exposed only strongly weathered, undisturbed bedrock and was backfilled without being logged. That our trench near Cox Lane and the O'Brien trench to the south did not expose faulting may mean that the fault trends east or west of the exploratory trenches, or that it does not continue into this area.

It is assumed the Swain Ravine, Paynes Peak and Prairie Creek Lineaments are complex zones of Mesozoic faulting. These fault zones are probably bands of small, discontinuous faults. Conclusive evidence in the way of trenches or clearly exposed faults is not available to prove that this assumption holds true throughout the extent of the lineaments, however, other field evidence indicates it is a reasonable assumption. The sense of displacement along these lineaments cannot be determined by local field relationships.

Oregon Gulch Fault: The Oregon Gulch Fault juxtaposes arc rocks on the west against ophiolite on the east. The Fault was first mapped by Creely (1965) in his study of the area. Schweickert and Cowan (1975, p. 1,330) show the fault as a continuation of the Bear Mountains Fault zone. Our work indicates this fault is much smaller than the Bear Mountains Fault and that the two are probably not physically continuous. They are, however, interpreted to have formed during the same period of Mesozoic time.

The Oregon Gulch Fault is traceable for approximately 29 km (16 mi) on a north-south trend through the central portion of the area; the fault is obscured lo-

cally along this trend by unconformably-overlying late Cenozoic terrestrial gravel and tuff. The fault zone, moderately defined where exposed, is less than 5 m (16 ft) wide and dips vertically or steeply east. A trench across the fault exposed juxtaposed arc and ophiolitic rocks, but the exact contact was not well-defined (see log, Trench 15 on pages 118-119).

Monte de Oro Fault: The Monte de Oro Fault, first mapped by Creely (1955), is exposed for 6 km (4 mi) in an approximate north-south trend through the central portion of the area. It is overlain in its north and south projections by Tertiary Superjacent Series rocks. The fault dips east and truncates Monte de Oro Formation against arc rocks on the east. Quartz is locally intruded into the fault zone and helps to define its location in poorly exposed areas.

Unnamed Faults: An unnamed fault, subparallel with previously described foothills faults, is exposed 1 km (0.6 mi) north of Oroville Dam. The fault is traceable in a north-south trend for 3 km (2 mi) just west of the North Fork of the Feather River. Gouge, aligned valleys and seeps define the trace.

Small faults and shears are exposed locally through the area. These faults, traceable only for short distances, probably result from sympathetic displacement and fracturing related with Foothills Fault System activity.

Foothills system faults in melange at the north end of the area strike approximately northwest and dip steeply to the northeast. A reason for the change in strike of the Foothills Fault System from north to northwest in this area is uncertain.

Northern area faults can be differentiated into (1) faults that cut melange and (2) faults that are associated with serpentine. Faults associated with serpentine are suggested to represent remnant Benioff zones (Hamilton, 1969;

Bailey and others, 1970; Bateman and Clark, 1974; Coleman, 1977). Occurrences of serpentine were used in this study to identify the location of such faults. Faults that cut melange probably formed at the same time as those associated with serpentine within the subduction complex accretionary prism.

Accretionary prism models (after Karig and Sharman, 1975; Dickinson, 1975) indicate that large numbers of concordant reverse faults are formed in the accumulation and development of these regions. Poor exposure and large areas of similar rock type that are concordant with regional trends preclude identification and mapping of many pre-Cenozoic faults in melange terrane; therefore, the number of these faults shown on the geologic map (Plate 1) is probably fewer than those actually present. Extreme shearing is visible in many melange outcrops suggesting that faults in this terrane are numerous and conform to subduction complex models. Faulting within this complex incorporates and separates individual blocks of rock that contain smaller-scale faults concordant with regional trends.

The amount of offset on faults in melange is not known. Plate tectonic models of continued underthrusting at convergent boundaries suggest cumulative displacements are large and may represent several kilometres.

Glover Ridge Fault: A major Mesozoic thrust fault, informally named the Glover Ridge Fault, is in the southeastern Cherokee quadrangle. Glover Ridge is a klippe (Figure 49) separated from the main thrust sheet of arc rock by incised erosion in Vinton Gulch. The fault was mapped by Creely (1965) as an intrusive contact, however, clay gouge between arc rock and underlying melange indicates a fault, rather than an intrusive contact. Approximately 23 km (14 mi) of fault trace is exposed in the area (Plate 1).

The Glover Ridge Fault trends into the southwestern Berry Creek quadrangle



Figure 49. Aerial southeast view of Glover Ridge (klippe) and the traced location of the Glover Ridge Fault. West Branch Bridge is center-left in photograph.

where its exact location is uncertain. The fault represents a thrust system that overrode melange; its presence should be suspected wherever arc or ophiolitic rocks overlie melange. Several exposures of isolated arc rock in the Big Bend area are in contact with melange metasedimentary rocks and may represent klippen or exotic blocks incorporated in melange from partial subduction of the arc complex.

Topographic configuration indicates the Glover Ridge Fault dips to the southwest. The contact is nearly flat-lying in exposed areas but in the subsurface to the south and west may be more steeply inclined. The Glover Ridge Fault is interpreted to represent a portion of an obduction suture along which arc and ophiolitic rocks were thrust over melange during accretion to continental terrane.

Extent of the obduction suture is uncertain in the Sierran foothills because exposures of the contact are limited. A portion of possibly the same, or a contemporaneous thrust fault is exposed

near the Bear River southeast of Marysville (Xenophontos and Bond, 1978).

Another fault discordant to the Foothill Fault System is exposed near Box Hall Flat, approximately 5 km (3 mi) north of Oroville Dam. The fault, strongly pronounced in aerial photographs and poorly exposed on the ground, can be traced for approximately 3 km (2 mi) in a northeast-southwest direction. Crushed rock and gouge are exposed locally along the fault trace. Sense of slip and total offset on this fault are unknown because faulting is entirely within Smartville ophiolite. Development of this fault is probably synchronous with obduction and therefore represents late-stage development of the Foothills Fault System.

Cenozoic Fault Movement

Cenozoic faulting in the Sierran foothills has been described by several geologists (Lindgren, 1911; Ferguson and Gannett, 1932; Durrell, 1959a; Burnett and Jennings, 1962; Strand and Koenig, 1965; Jennings, 1975, 1977; Alt and others, 1977). Most of the recognized

Cenozoic faults are northwest-striking, east-dipping, high-angle, normal faults (summary in Alt and others, 1977, pp. 33-35).

Cenozoic fault movements commonly occur along older, Mesozoic faults (Alt and others, 1977). Not all Mesozoic faults have experienced reactivation, but they must be considered avenues along which fault movements preferentially occur.

Woodward-Clyde Consultants compiled data on 46 faults in the northern Sierra Nevada having evidence for probable late Cenozoic displacements (Alt and others, 1977). Vertical displacements are undetermined for 11 of these faults. For the remaining faults, vertical displacements are relatively small-scale, ranging from 0.6 m (2 ft) to about 180 m (600 ft). In the Oroville area, displacements range from 4.3 m (14 ft) on the Swain Ravine Lineament fault at the Orange Road trench site, about 17 km (11 mi) south of Oroville, to 46 m (150 ft) on a fault about 27 km (17 mi) north of Oroville.

Surface evidence of Cenozoic faulting is rare. This is attributed to small displacements at sufficiently long recurrence intervals to allow erosion to remove evidence of fault movements. Moreover, much of the study area is not covered by Cenozoic deposits, making determination of younger fault movements difficult.

Within the area of detailed mapping, the Swain Ravine, Prairie Creek and Paynes Peak Lineaments were determined to be Mesozoic fault zones. North of the detail map area several lineaments are apparent on high-altitude infrared and low-altitude black-and-white photographs. For this study the major northern lineaments are informally named the Chico, Soda Springs, Web Hollow and Paradise-Magalia Lineaments. These lineaments were field checked to determine if they are faults. Figure 16 shows these lineaments and associated faults.

Swain Ravine Lineament Fault Zone:

Cenozoic fault movement in Basement Series rocks within the Oroville study area is recognized only in the Swain Ravine Lineament fault zone. This displacement was first noted after the August 1975, movement of the Cleveland Hill Fault. A striking feature of this movement is that it started in a lineament "gap" where there are no lineament features and little topographic evidence of faulting (Figure 50).

The Cleveland Hill Fault can be traced on the ground and in exploration trenches to within 2.3 km (1.4 mi) of the Bidwell Canyon Saddle Dam. The Swain Ravine Lineament fault zone continues to the north and extends into Bidwell Canyon. Hypocenters of aftershocks extend 10 km (6 mi) north of the surface faulting and pass beneath Oroville Dam at a depth of about 5 km (3 mi) (Lahr and others, 1976).

Surface investigations, trenching, and geophysical investigation failed to



Figure 50. Aerial northwest view of the Cleveland Hill Fault along the western side of Cleveland Hill. Note that topographic expression for the fault is lacking.

reveal faulting beyond an olive grove south of Mt. Ida Road, about 2.3 km (1.4 mi) south of Bidwell Canyon Saddle Dam. However, the Swain Ravine Lineament fault zone appears to go northward into Bidwell Canyon. Faulting in the west end of Bidwell Canyon Saddle Dam foundation and a fault exposed in a water tunnel about 1 km (0.6 mi) west of the dam may be parts of a complex system of faults in the Swain Ravine Lineament fault zone. It can be conjectured that the fault system consists of a band of discontinuous, relatively short, small faults along which displacement could jump from fault to fault within the main zone. This kind of fault discontinuity could explain the inability to trace the Cleveland Hill Fault continuously farther north to link up with the faulting at Bidwell Canyon Saddle Dam. The westward tilt indicated by leveling surveys on the saddle dam further suggests that the fault system goes into the Bidwell Canyon arm of the reservoir.

North of Lake Oroville a lineament continues on through Canyon Creek, along the projected northerly trend of the Swain Ravine Lineament fault zone (Figure 16). However, geologic investigation failed to reveal faulting along the lineament. The markedly straight, North Fork of Lake Oroville also is suggestive of faulting, but no faulting could be found along the north side of the lake. Because the Swain Ravine Lineament fault zone is a strong feature of some size, it seems the zone should continue through the reservoir. However, field investigations did not prove this to be true. Therefore it is assumed the fault zone terminates in the reservoir.

The fault movement along the Cleveland Hill Fault in the Swain Ravine Lineament system prompted a number of exploration trenches. These were mostly along the faulted portion, but some were on other parts of the Swain Ravine Lineament and also on the nearby Paynes Peak and Prairie Creek Lineaments. Trenching was done by Department of Water Resources, U. S. Army Corps of Engineers, and by

Woodward-Clyde Consultants for various clients. Purpose of the trenching was to investigate the nature of the faulting in the underlying bedrock and to determine if previous Quaternary fault movement could be detected in soil profile overlying the bedrock. Although exposures of faults in the bedrock were usually obvious and easy to interpret, the exposures of the overlying soil profile were not so clear cut. Interpretation of earlier fault displacements seen in the soil profiles were not necessarily concurred with by all that saw the exposures in the various trenches. For the purposes of this study we have accepted, without necessarily endorsing, the interpretations made in trenches by others.

For displacements of small magnitude, such as along the Cleveland Hill Fault, displacement of the soil profile in trenches is difficult to detect. We are not aware of any trench where such displacement from the August 1, 1975, earthquake could be detected, even though the trenches were excavated across the ground cracking. The cracking could usually be seen at least part way through the soil profile and sometimes, clear through the usually shallow soil profile to bedrock. Although offset of features interpreted to be caused by earlier fault movements could be seen in one trench, other trenches nearby on the same fault might not show offsets, or show displacement of a different magnitude. In short, trenching does not detect all of the previous fault movements with great clarity -- instead very subtle features, subject to varying interpretation, are usually revealed. Earlier small fault movements can easily pass undetected.

Of the 17 Department of Water Resources trenches, 15 were on the Swain Ravine Lineament fault zone. Eight of those trenches (A, B, D, 5, 8, 12, 13 and 16) were excavated across Cleveland Hill Fault ruptures, and each of these exposed a fault in bedrock beneath the ground rupture. Two other trenches (7A and 17) exposed bedrock faults, and the

remaining five trenches on the Swain Ravine Lineament fault zone did not expose any faults.

Only one Department of Water Resources trench exposed convincing evidence of Quaternary movement on the Cleveland Hill Fault prior to the 1975 event. Trench DWR 8, across the Cleveland Hill faulting, exposed a contact between two alluvial units, at a depth of 3.3 m (10.8 ft), with about 30 mm (1.2 in) of apparent down-to-the-west vertical offset on the fault. Soil features near the ground surface were not displaced, indicating movement occurred prior to the 1975 Oroville event. In their Cleveland Hill No. 1 trench, Woodward-Clyde Consultants report 46 cm (18 in) of apparent vertical offset which they interpret as having occurred in at least three, and perhaps more, separate events. This suggests that a 15 cm (6 in) movement would be the maximum displacement expected.

Forty-two exploration trenches were excavated by various investigators on the Swain Ravine Lineament fault zone between Bangor and Lake Oroville (Figure 47 and Table 1). Many of these trenches exposed west-dipping faults showing evidence of multiple, small-scale (less than 1 m), normal Cenozoic movements. An exception to this occurs in the U. S. Bureau of Reclamation Orange Road trenches, where some faults were found to dip east, and one of these showed a 4.3 m (14 ft) normal offset. Five trenches on the lineament just north of the Yuba River, by the Corps of Engineers (1977) exposed Mesozoic faults with no Cenozoic movement.

Ages of movement on the Cleveland Hill Fault and at other places along the Swain Ravine Lineament fault zone are based on displaced soil horizons. The most prominent soil marker is a buried paleosol. Gene Begg (person. commun., 1977) and Roy Shlemon (person. commun., 1977) estimate the paleosol to be at least 100,000 years old, and soils overlying it are 50,000 to 70,000 years

old. Similar paleosols in the Sierran foothills have also been estimated to be at least 100,000 years old by Swan and Hanson (1977, 1978). The U.S. Geological Survey (1978, p. 43) has stated that soils overlying the paleosol may be younger - 10,000 to 25,000 years old - and that a fault which displaces the paleosol and not the overlying soil should be considered to be a minimum of 10,000 years old. In summary, the part of the Cenozoic record available, the soil cover, indicates previous small fault movements within the last 10,000 to 100,000 years.

Where older soil horizons are offset more than successively younger ones, it is interpreted that the fault has moved several times during development of the soil profile. The amount of displacements seen, and the lack of surface fault features along the Cleveland Hill Fault suggest that small movements at relatively long recurrence intervals have occurred over the past 100,000 years.

An east-west channel deposit of late Cenozoic gravel crosses the Paynes Peak and Swain Ravine Lineaments northwest of Bangor (Plate 1), yet shows no field evidence of fault displacement. Moreover, a small diorite plug across the Swain Ravine Lineament in the same area is not displaced, indicating it has not been offset since emplacement, about 130 million years ago.

The fact that fault displacements are seen in soils exposed by trenching, yet no field evidence can be seen for larger displacements of the late Cenozoic gravel channel deposits or pluton, suggests long-term cumulative displacement is too small to detect by normal field techniques. The apparently unbroken pluton in the Swain Ravine Lineament fault zone suggests undetectable displacement for about 130 million years. The same pluton relationship is seen on the Prairie Creek Lineament fault zone which is apparently truncated by the Rocklin pluton.

The evidence indicates a pattern of activity during the last 100,000 years of small, infrequent, vertical fault movements, along the Swain Ravine Lineament fault zone. Presumably, such displacements were produced by earthquakes of about the same magnitude as the 1975 Oroville earthquake. The average slip rate during the last 100,000 years may be faster than during most of the last 130 million years, otherwise the older rocks would be noticeably displaced. For example, cumulative fault displacement of 0.46 m (1.5 ft) in soil was interpreted from relationships in the Cleveland Hill No. 1 trench by Woodward-Clyde Consultants. This gives a maximum slip rate in the Cleveland Hill area of 0.46 m (1.5 ft) per 100,000 years. Assuming the late Cenozoic gravels overlying the Swain Ravine Lineament fault zone are early Quaternary, or about two-million years old, then they should be offset about 9 m (30 ft) if the same slip rate prevailed -- a displacement large enough to be noticed in the field. Applying the same slip rate to the 130 million year-old pluton would produce an offset of about 600 m (1,960 ft).

The Swain Ravine Lineament fault is the only one along which evidence of Quaternary fault displacements was found. However, these kind of fault displacements are subtle and difficult to detect, so it is possible, though not proven, that similar levels of fault activity have taken place along the Prairie Creek and Paynes Peak Lineament faults. South of the study area, the Swain Ravine Lineament fault merges with the Prairie Creek Lineament fault to form one system (Figure 47). Trenches just south of where the two lineaments merge revealed what is interpreted to be Quaternary fault movements (Alt and others, 1977). The persistent evidence of Quaternary movements along the Swain Ravine and the merged Swain Ravine-Prairie Creek Lineament fault zones suggests this may be a preferred avenue along which small Quaternary fault movements occur.

Prairie Creek Lineament Fault Zone:

Several areas of localized ground cracking occurred during the Oroville earthquake and form a crude alignment that extends northwestward from the north end of the Prairie Creek Lineament for 10 km (6 mi) to Oroville. Further to the northwest, Lovejoy basalt on the Campbell and Sorensen Hills is discontinuous with basalt on North and South Table Mountains along a projection of the lineament. This trend, projected still further to the northwest, could coincide with faulting in Tuscan Formation along the Chico monocline. Evidence is lacking, however, these features may result from Cenozoic movement along an underlying Mesozoic bedrock fault.

Even though no evidence of Quaternary fault activity was seen along the Prairie Creek Lineament fault zone, the fact that Quaternary faulting has occurred just south of where it merges with the Swain Ravine Lineament fault zone suggests Quaternary activity has, or could, take place along the Prairie Creek zone. This possibility is reinforced by the occurrence of some small earthquakes along the lineament, and the yet unexplained system of cracks, the "Palermo crack zone", that developed along the northwest projection of the Prairie Creek Lineament fault zone during the Oroville earthquake. For these reasons, the Prairie Creek Lineament fault zone should be regarded as capable of the same kind of activity seen along the Swain Ravine Lineament fault zone. If the Prairie Creek Lineament fault zone does continue northward as an old Mesozoic fault zone more or less concealed by younger rocks of the Super-jacent Series, it would be the longest of the lineament fault zones.

Paynes Peak Lineament Fault Zone: Of the three lineament fault zones in the Oroville area, Paynes Peak is the only one along which no evidence or suggestion of Quaternary activity is seen. Consequently, it is assumed fault activity is

not as likely to occur along the Paynes Peak Lineament as along the other two zones.

Thermalito Powerplant Foundation Faults: During construction, faults were exposed in the foundation excavation for Thermalito Powerplant. The zone consists of several interlaced faults striking from N30-44E, dipping steeply from 70NW to 80SE, and offsetting Miocene age Lovejoy Formation. The fault does not offset overlying gravels of late Cenozoic age. Apparent offsets are both normal and reverse, and apparent cumulative displacement across the zone is as much as 12 m (40 ft), with the southeast side moved downward relative to the northwest side. No evidence for this fault was observed in Lovejoy Forma-

tion exposed on South and North Table Mountains, about 6 km (3.8 mi) to the northeast along projection of strike.

Chico Lineament: The Chico Lineament coincides with the upper hinge of the Chico monocline (Figure 51). A zone of tensional faults, generally small, lies along this hinge line in the area of the lineament. These faults cut Upper Pliocene Tuscan Formation.

A comprehensive study of faulting along the Chico monocline was done by Burnett (1965). Additional studies dealing with faults in Tuscan rocks are by Creely (1965) and Burnett and others (1969); field investigations were also carried out for this report.



Figure 51. Aerial northwest view of the Chico monocline that is locally developed in Tuscan Formation. Note pattern of northwest-trending linear fractures defined by dark vegetation lines. Location is northeast of Chico.



Figure 52. Normal fault (attitude: N3W, 62NE) in Tuscan Formation exhibiting 30 cm (1 ft) of down-to-the-east displacement. Location is a roadcut exposure along Clark Road approximately 6 km (3.7 mi) south of Paradise.

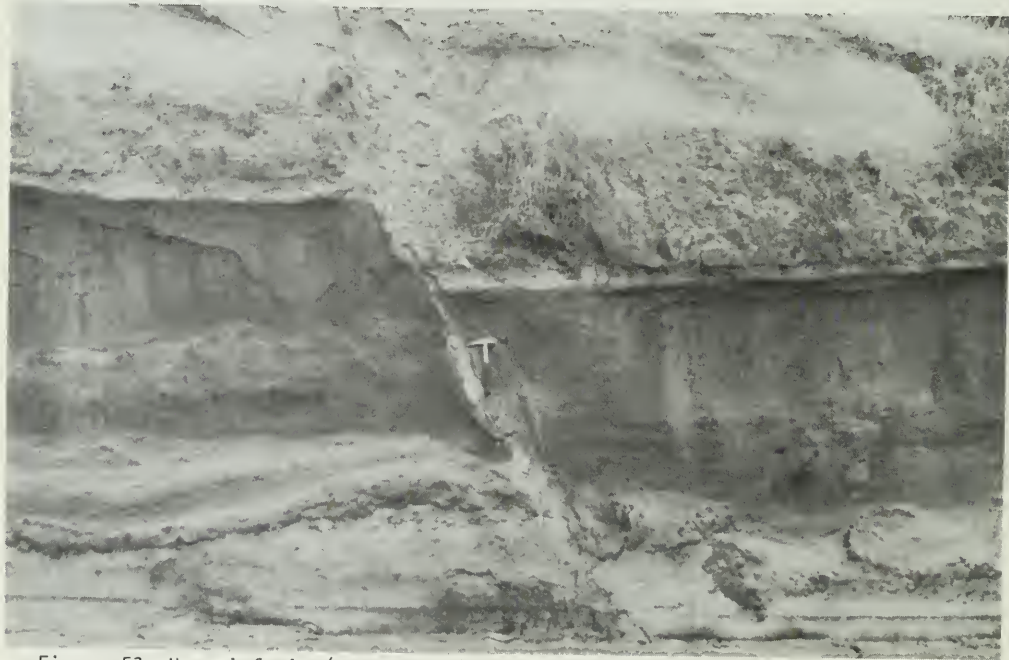


Figure 53. Normal fault (attitude N6W, 65SW) in Tuscan Formation exhibiting 70 cm (2.2 ft) of down-to-the west displacement. Location is a roadcut exposure along Clark Road about 6 km (3.7 mi) south of Paradise.

Faults in Tuscan rocks trend north-northwest and dip either east or west. These are normal faults which usually have little vertical displacement (Figures 52 and 53). Displacements are generally less than 1 m (3 ft); however, displacements of 18 m (60 ft) (Burnett, 1965) and 31 m (100 ft) (Dave Harwood, person. commun., 1978) have been reported.

Soda Springs Lineament: The Soda Springs Lineament is about 16 km (10 mi) long and is composed of linear topographic features and an area of springs. Field investigation along the lineament produced no evidence of faulting. Exposures of Tuscan rock along Ditch Creek (Sect. 9, T26N, R3E) are continuous across the lineament and provide good evidence against faulting. The springs are interpreted to be interflow seeps in the underlying, horizontally-bedded Tuscan Formation.

Web Hollow Lineament: The Web Hollow Lineament is a strong north-south trending feature at least 31 km (19 mi) long and has been suggested to be a fault (Quintin Aune, unpub. data; Alt and others, 1977). A field check of fault features described by Aune was made by Department of Water Resources geologists prior to this study; none of these features could be attributed to faulting (Mark McQuilkin, person. commun., 1977). During this study the entire Web Hollow Lineament was field checked and determined not to be a fault.

A zone of very strong lineaments, parallel to, and just east of the northern end of the Web Hollow Lineament, can be seen in the Tuscan Formation on low-altitude photographs (Figure 54). These cut across the topography in a northwest trend. A check of these lineaments on

the ground failed to substantiate the presence of faulting, however, photographic features so strongly suggest fault control that they are interpreted to be faults. The lack of surficial fault features in the Tuscan Formation suggests these are Upper Pliocene or Pleistocene in age.

Paradise-Magalia Lineament: The Paradise-Magalia Lineament is about 43 km (27 mi) long and trends north from Oroville to Magalia (Figure 16). Linear elements include a section of the Feather River at Oroville, the east edge of South Table Mountain, a drainage on North Table Mountain and a linear ridge on the west side of Magalia Reservoir.



Figure 54. Vertical aerial view of fracture zone developed in Tuscan Formation near Iron Mountain on Deer Creek. Fractures appear as dark vegetation lines which transect topography.

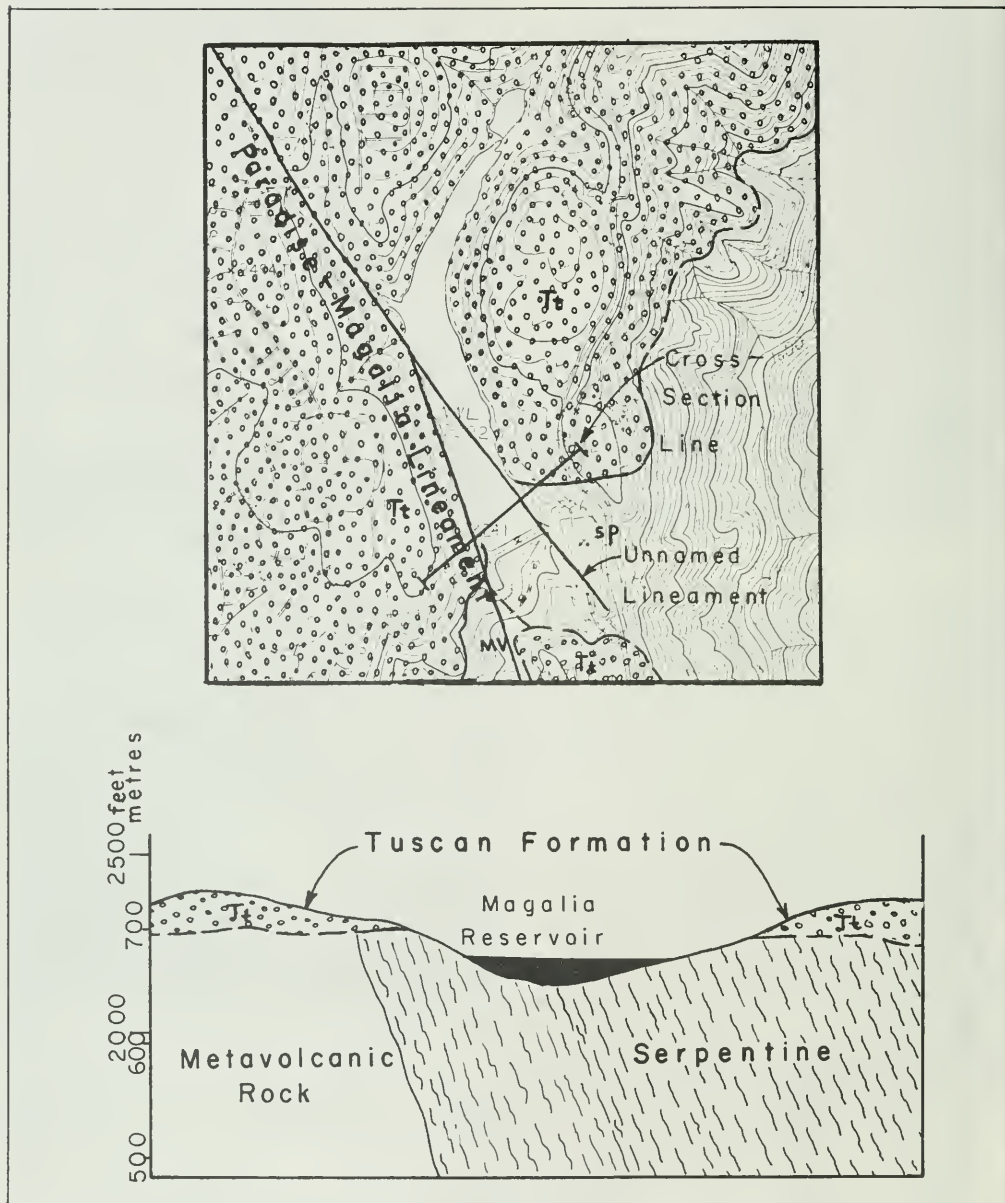


Figure 55. Map with cross section oriented perpendicularly to suspected fault through Maglia Reservoir.

This lineament was investigated throughout most of its length on the ground. Cenozoic fault features could only be found where it contacts Lovejoy Formation on the south side of North Table Mountain. Here a small fault, less than 0.5 km (0.3 mi) long, cuts Lower Pliocene basalt. Another fault of the same size and attitude occurs just to the west -- off the lineament. Poor exposures preclude determining a sense of displacement of either fault, and it is possible that rather than faults they are unusually prominent cooling joints.

Old mining reports indicate faults occur in several mines along the Paradise-Magalia Lineament northwest of Magalia. A report by the California Department of Natural Resources (1930) cites displacements of up to 70 m (225 ft) in Tertiary channel deposits below Tuscan Formation. These faults do not cut overlying Tuscan Formation and must be pre-Pleistocene in age. Faults in the mines as well as a Mesozoic fault at Magalia Reservoir trend more westerly than the Paradise-Magalia Lineament and may not be related to it.

Alt and others (1977, pp. 14-21) state that a prominent Cenozoic fault scarp occurs in Tuscan rocks along the Paradise-Magalia Lineament on the west side of Magalia Reservoir. Detailed mapping of the Tuscan-basement rock contact during this investigation showed no evidence of faulting. A cross-section based on this mapping, drawn perpendicular to this scarp, shows no displacement of the base of the Tuscan Formation (Figure 55).

Summary: Cenozoic fault movements have occurred in the Oroville area on both pre-existing Mesozoic bedrock faults, such as the Cleveland Hill Fault, and on faults in Cenozoic rocks, such as those in the Tuscan and Lovejoy Formations. It is possible that the faults cutting Cenozoic rocks may also be along Mesozoic faults in bedrock concealed by the overlying younger formations.

Potential for future earthquakes and ground rupture in the Oroville area is

considered to be greatest on the Swain Ravine Lineament fault zone, to the north and the south of that portion of fault that ruptured in the 1975 event.

The fault responsible for the magnitude 5.7 earthquake that occurred northeast of Chico, California, in 1940, was not found.

Mesozoic Folds

Smartville ophiolite in the Bangor quadrangle and melange in the Cherokee and Berry Creek quadrangles are isoclinally folded. Exposures of relict pillows provide structural control for tops of section. Near Bangor, pillowed sequences dip east and are inverted; north of this location, pillowed rocks are right-side-up and dip east. Tops of these sections are oriented in opposite directions and suggest that large-scale folding deforms the ophiolite. Large-scale folding is locally confirmed by concordant small-scale folds interpreted to be parasitic deformation.

Mesozoic folds trend north-northwest and plunge south at angles less than 35 degrees. Plunge directions conform with orientations described in several geologic studies of the foothills (Bateman and others, 1963; Clark, 1964, 1976; Creely, 1965; Hietanen, 1973a; Duffield and Sharp, 1975). Axial planes of these folds, oriented subconcordant to metamorphic foliation, dip steeply east or are vertical. Localized folds occur in metamorphosed country rock adjacent to Sierran plutons (Compton, 1955; Clark, 1964; Hietanen, 1973a).

Cenozoic Folding

Cenozoic folding does not affect study area rocks but is described at several locations in the nearby area. At Tuscan Springs, approximately 8 km (5 mi) northeast of Red Bluff, the Tuscan and Chico Formations are gently deformed into open folds (Anderson, 1933). Additionally, Hudson (1951, 1955) has described folded Superjacent Series rocks in the Mount Lincoln-Castle Peak area.

The Chico monocline, as described by Bryan (1923), Anderson (1933), Burnett (1965) and Burnett and others (1969), trends approximately N30W and forms the 24 km (15 mi) straight eastern boundary of the Great Valley between Chico and Red Bluff (Figure 51). The monocline steepens Tuscan Formation dips from 2 degrees east of the fold, to 8 to 10 degrees within the hinge area (Burnett and others, 1969). This is the best developed Cenozoic fold in the immediate area.

Most Cenozoic folding occurred prior to deposition of the Pleistocene (?) Red Bluff Formation as these unconformable gravels are not deformed (Anderson, 1933). The Red Bluff Formation and late

Cenozoic gravels in the study area are incised by actively-downcutting drainages which indicate the foothill region is experiencing uplift; some deformation must be associated with this uplift.

SUMMARY OF GEOLOGIC HISTORY

The geologic history and tectonic movement in the Oroville area is summarized in chronologic order of occurrence. The timing of events is substantiated by field data or referenced from investigators who did particular studies concerning aspects of the geologic history. Absolute dates for events are used if available; relative time, based upon fossils, is used where radiometric dates are lacking.

Table 2

Summary of Geologic Events

<u>Event</u>	<u>Date</u>
<u>Cenozoic Time</u>	
1. Oroville earthquake - small fault movement near Cleveland Hill along Swain Ravine Lineament fault zone	1975
2. Development of "A" and "B" soil profiles. Some small fault movements along Swain Ravine and merged Swain Ravine-Prairie Creek fault zones	10,000-25,000 years before present (USGS, 1978) 50,000-70,000 years before present (Gene Begg and Roy Shlemon, person. commun., 1978)
3. Development of "Paleo B" soil profiles; small fault movements.	100,000 years before present (Gene Begg and Roy Shlemon, person. commun., 1978) 140,000 years old (USGS, 1978)
4. Alluvium deposited	Pleistocene - Recent
5. Development of late Cenozoic faulting in the foothill belt	Post-Pliocene (Alt and others, 1977)
6. Older gravels deposited	Pliocene-Pleistocene(?)

<u>Event</u>	<u>Date</u>
7. Tuscan Formation deposition began	Pliocene, 3.3 million years (Lydon, 1968)
8. Sierran uplift and westerly tilting began	Pliocene, 4-10 million years (Christensen, 1966; Wright, 1976; Hay, 1976)
9. Lovejoy Formation, basalt flows from eastern source	22.2 to 23.8 million years (Dalrymple, 1964)
10. Oroville tuffs (Mehrten Formation-?) deposited	23.8 million years (Dalrymple, 1964)
11. Auriferous gravels deposited	Upper Eocene - Lower Oligocene (Durrel, 1966)
12. Ione Formation deposited	Middle Eocene (Creely, 1965) to early Oligocene
13. Early Sierran uplifts	Cretaceous-early Tertiary

Mesozoic Time

1. Chico Formation deposited	Upper Cretaceous (Taff and others, 1940; Creely, 1965)
2. Plutonism (Yosemite intrusive epoch) - intrusion is responsible for thermally metamorphosing country rocks in the study area	126-138 million years (Gromme and others, 1970; Evernden and Kistler, 1970)
3. Mesozoic faults (Foothills Fault System) - formed by collision of arc and ophiolite with continent	Middle Kimmeridgian to late Tithonian
4. Smartville ophiolite formed	Oxfordian to Kimmeridgian
5. Monte de Oro Formation deposited	Late Oxfordian to early Kimmeridgian (Imlay, 1961)
6. Arc Rocks extruded	Oxfordian (?) to early Kimmeridgian (Creely, 1965)
7. Melange formed	Middle to Upper Jurassic (Kimmeridgian, Bob Treut, person. commun., 1978)

The above tabulation of events indicates tectonic activity is spasmodic. Major activity was in Mesozoic time. The Sierran uplift is a major regional event, but the main influence on rocks of the western foothill belt around Oroville is to tilt Cretaceous and younger rocks gently to the west. Volcanic activity about 22-24 million years ago deposited basalt flows (Lovejoy Formation), lahars and water lain volcanoclastic rocks of the Oroville tuff.

In early Pleistocene time, fault movements began again in response to the most recent Sierran uplift, mostly along the old Mesozoic faults. Some younger rocks, mainly Tuscan Formation, also are faulted. In the Oroville study area, Cenozoic fault displacements are generally small. Elsewhere, Cenozoic displacements up to 197+ m (600 ft) are reported (Alt and others, 1977).

The last 100,000 years has been a period during which small fault displacements on the order of centimetres occurred at infrequent intervals along the older Mesozoic fault zones.

CAUSES OF THE OROVILLE EARTHQUAKE

Geologic investigations reveal that the Oroville earthquake is not unique in the seismic history of the northwestern Sierra Nevada foothill belt. The 1940 magnitude 5.7 earthquake north of what is now Lake Oroville demonstrated that the region is capable of generating moderate-magnitude earthquakes. The trenching and other exploratory work revealed evidence for small displacements in soil during the last 100,000 years or less, depending upon which interpretation is accepted for the age of soils displaced by faulting. Presumably these small fault movements also were accompanied by earthquakes similar to the 1940 and 1975 magnitude 5.7 earthquakes that occurred in the Oroville region.

The geologic investigations of the Oroville area revealed old fault zones

in bedrock. These old fault zones formed during Mesozoic time -- subduction at a plate boundary is postulated as the geologic model for genesis of the faults. Actually, the geologic model assumed for formation of the old fault system is not as critical as the fact that these older fault zones formed in a different tectonic regime than exists today. The imprint of earlier tectonism has left zones of weakness along which fault movements caused by the current Cenozoic tensional regime tend to occur.

The present tectonic pattern clearly seems to be one of general east-west extension. The behavior of the Cleveland Hill Fault, the opening of the fault cracks with time and the geodetic work in the Oroville area, all suggest normal fault movements resulting from east-west tension. A fault plane solution of the August 1975, Oroville earthquake series indicates normal dip-slip movement (Langston and Butler, 1976; Lester and others, 1975), also indicating east-west tension.

Recent leveling work done by Bennett and others (1977) suggests the Sierran block is still undergoing uplift. This uplift is postulated to be the cause of tension in the western foothills. Bennett (1978) continued examination of leveling data and was able to demonstrate noticeable changes in elevation across both the Bear Mountains and Melones Fault zones, again indicating crustal movements prefer to occur along the old fault zones.

In summary, for at least the past 4 million years the foothill region probably has been in east-west tension. It can be speculated that this tension reduced frictional stresses along north-trending older fault systems, allowing small gravitational adjustments and fault movements. These movements probably were accompanied by earthquakes comparable to the 1940 and 1975 magnitude 5.7 earthquakes that occurred in the Oroville area. These fault movements commonly occur along the smaller individual faults within the older fault zone complexes. Possibly not all

movements occur along existing faults, but displacements revealed thus far suggest that most do.

Reservoir-Induced Seismicity

Reservoir-induced seismicity has been greatly studied in the last few decades. Several researchers (for example, Gupta and others, 1973; Rothé, 1973; Božović, 1974) note the following characteristics of reservoir induced seismicity:

1. Earthquake activity begins soon after initial impoundment.
2. Large numbers of foreshocks occur over an extended time period before the main shock.
3. Time versus frequency plots of foreshocks and aftershocks differ from patterns of tectonically induced seismicity.
4. Reservoir-induced earthquakes are shallow focus.
5. Proximity of reservoir-induced seismicity to the triggering dam or reservoir is usual.
6. Relatively high "b" values for foreshocks of reservoir-induced seismic events as established by the equation $\log N = a - bM$ where "b", the slope of the curve, is related to the proportion of large-to-small earthquakes, "N" is the cumulative frequency of magnitude "M" earthquakes, and "a" is a constant determined by area where data were gathered, time duration and areal seismicity.
7. A high ratio of the strongest magnitude aftershock to the magnitude of the main seismic event.

The most consistent characteristic of reservoir-induced seismic activity is the onset of the earthquakes soon after initial impoundment begins (Rothé, 1973). Some examples (after Packer and others, 1977, Appendix A) are listed below.

<u>Reservoir</u>	<u>Elapsed time from beginning impoundment to start of seismicity</u>
Koyna	Immediately
Hsinfengkiang	1 mo.
Hendrik Verwoed	6 mo.
Boulder	9 mo.
Contra	10 mo.
Grandval	15 mo.

In comparison, seismic activity at Oroville occurred more than eight years after water impoundment began.

A second characteristic of reservoir-induced seismicity is that a large number of foreshocks occur over a longer period of time than would be expected for tectonically-induced seismic events (Rothé, 1973; Božović, 1974). For example Kremasta Reservoir had 17 foreshocks in 30 days. Koyna Reservoir had 90 foreshocks in 19 days, and Kariba Reservoir had 20 foreshocks in one day (Gupta and others, 1973). The frequency of foreshocks at Oroville, 21 events in 30 days prior to the main shock, is similar to the Kremasta data.

Mogi (1963) discovered that the plot of time versus frequency for reservoir-induced foreshocks and aftershocks differed from the pattern for tectonically-induced earthquakes. The reservoir-induced seismic pattern (Type II) includes a greater foreshock buildup and a longer period of aftershocks. Figure 56 shows Mogi's "Type II" (reservoir-induced) seismic pattern compared with the pattern of the Oroville earthquake series.

Shallow focal depths for reservoir-induced earthquakes are also a common characteristic (Božović, 1974). Some examples of this characteristic are Monteynard Reservoir, 0.0 km (0.0 mi); Hendrik Verwoed Reservoir, 6 km (3.7 mi); Boulder Reservoir, 1.5 to 9 km (0.9 to 5.6 mi). The main shock of the Oroville series had a depth of 8.8 km (5.5 mi) and aftershock depths from 1.3 to 10.4 km (0.8 to 6.5 mi) (Akers and others, 1977).

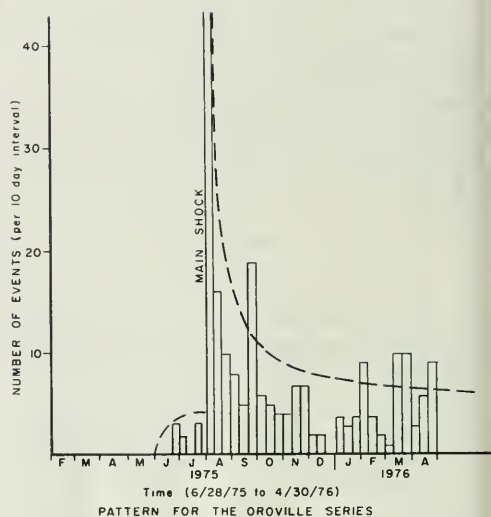
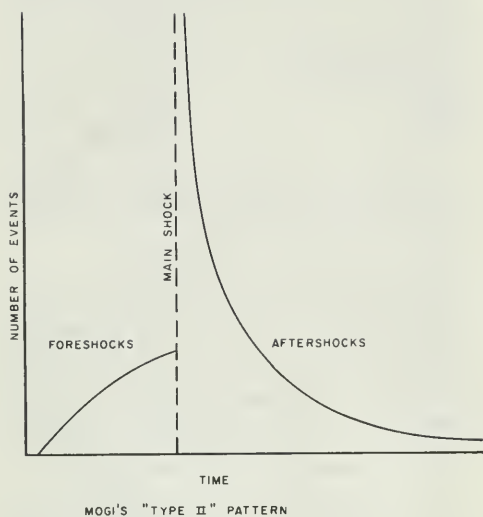


Figure 56. Comparison of foreshock-aftershock patterns for the Oroville earthquake and Mogi's "Type II" (reservoir-induced) earthquakes.

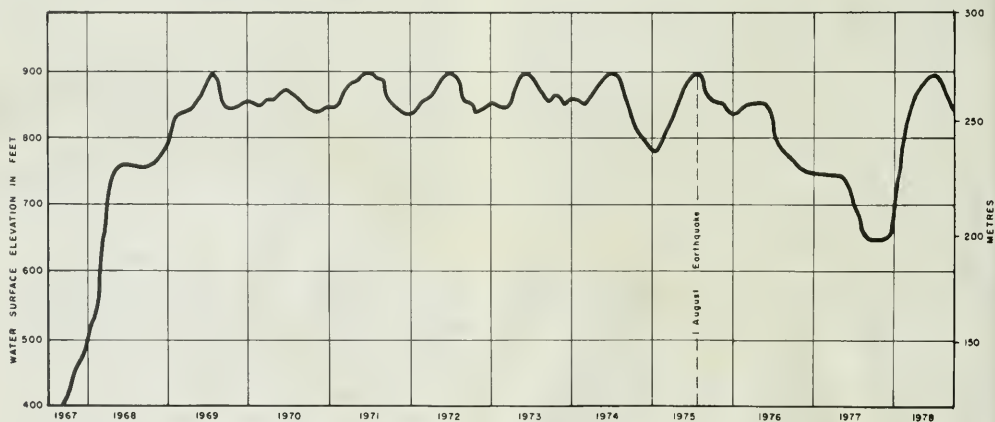


Figure 57. Water level history of Lake Oroville from initial filling to September 1978

In most reservoir-induced seismic events the foci of the earthquakes are very close to, or directly under, the reservoir or dam. This characteristic is noted for earthquakes at Boulder, Monteynard, Grandval, Oued Fodda, Kariba, Kremasta, Marathon and Koyna reservoirs. The most distant earthquake was within 10 km (6.2 mi) of the Koyna Reservoir dam (Gupta and others, 1973). The main shock of the Oroville earthquake series was more distant, approximately 12 km (7.5 mi) from Oroville Dam.

Relatively high "b" values for fore-shocks and aftershocks of reservoir-induced events are common (Gupta and others, 1973). A comparison of "b" values for accepted cases of reservoir-induced seismicity with those of the Oroville earthquake shows a significant difference. Note "b" value comparisons below (after Morison and others, 1976).

"b" Values

<u>Reservoir</u>	<u>Foreshocks</u>	<u>Aftershocks</u>
Kariba	1.1	1.0
Kremasta	1.4	1.1
Koyna	1.9	1.3
Oroville	0.37	0.61

Another feature common to reservoir-induced seismicity is a high ratio, typically 0.8 to 0.9 (Gupta and others, 1973), of the strongest aftershock magnitude to the magnitude of the main shock. The ratio for the Oroville series is 0.91.

A relationship has been postulated between rate of reservoir loading, water depth and induced seismicity (Rothé, 1969). Induced earthquakes seem to be more commonly associated with reservoirs whose water depths are 100 m (328 feet) or greater and during periods of rapid loading (generally the first reservoir filling); large water level fluctuations also induce seismicity (Carder, 1945). Lake Oroville, approximately 200 m (656 ft) deep at maximum pool, reached a depth

of 100 m (328 ft) in February 1968, and has never been lowered beneath that level. A plot of post-construction reservoir elevations with the date of the August 1, 1975, earthquake is shown in Figure 57. The 1975 change from low water in January to high water in late May represents an increase of 29 percent in 5 months; initial reservoir filling during the same time period in 1968 generated an increase in storage of 44 percent with no resulting seismicity.

In comparing data from the Oroville earthquake with reported data from known reservoir-induced earthquakes, the Oroville event has some, but not all, of the characteristics attributed to reservoir-induced earthquakes. The long elapsed time between reservoir filling and the Oroville earthquake is a significant departure from what has occurred in generally accepted cases of reservoir-induced seismicity. The epicentral distance from the reservoir is slightly large and the "b" values are significantly too small. A comparison of accepted characteristics of reservoir-induced earthquakes with those of the Oroville earthquake, does not show whether or not Lake Oroville caused the earthquake series.

The picture is further clouded by the background seismicity which indicates an earthquake comparable to the 1975 Oroville earthquake occurred before the reservoir existed. Small fault displacements in soil profiles exposed by trenching suggest Oroville type events have been occurring for the past 100,000 years. In short, the Oroville earthquake is compatible with the regional pattern of seismicity and, therefore, need not be related to Lake Oroville at all.

The mechanisms customarily used to explain reservoir-induced earthquakes are (1) increase in stress caused by weight of water in the reservoir and (2) increase in pore pressure resulting from the increase in hydrostatic head imposed by the reservoir. The increase

in pore pressure mechanism is more favored. Both theories assume stress conditions in the hypocentral area are in such delicate balance that only small incremental changes in stress will trigger an earthquake.

The epicenter of the August 1, 1975, Oroville earthquake was 12 km (7.5 mi) from Lake Oroville. Although no computations were made by the Department to estimate how much Lake Oroville changes stress in the hypocentral area, at that distance and depth change in stress should be very small.

A reconnaissance survey of springs and wells in the area indicates ground water levels in the foothill area to the east and north of the epicentral area are generally higher than water in Lake Oroville. Assuming hydrostatic pressures in the hypocentral area are controlled by ground water levels, the addition of Lake Oroville in such a hydrostatic regime probably would have no affect on either pore pressure or degree of saturation.

The evidence available does not indicate a causal relationship between Lake Oroville and the earthquake, but the possibility cannot be eliminated conclusively at this time.

POTENTIAL HAZARDS TO STATE WATER FACILITIES

Because the August 1, 1975, Oroville earthquake probably relieved much of the regional strain, it seems unlikely that a similar event will occur in the same place in the near future. Therefore, the next earthquake of comparable magnitude probably would occur north or south of the 1975 earthquake and its zone of aftershocks. Despite the improbability of another local earthquake, estimates of hazards to facilities are based on the assumption that a 1975 type earthquake will happen again in the same area. In other words, the most pessimistic or conservative view was taken.

Hazard posed by regional faults fall into three general categories, (1) hazards created by ground shaking, (2) hazards created by fault displacement, and (3) regional changes in ground elevation.

Ground Shaking

Nothing was seen during the course of geologic investigations that indicates local earthquakes would exceed the magnitude 6.5 Reanalysis Earthquake recommended by the Special Consulting Board for the Oroville earthquake.

The intuitive conclusion to be drawn from the geologic studies would be that the magnitude 5.7 earthquake of August 1, 1975, is close to the strongest to be expected and that the magnitude 6.5 local earthquake assumed for reanalyses of structures is very conservative. Geologic studies suggest the Swain Ravine or Prairie Creek Lineament fault zones are the most likely source of future strong earthquakes.

Fault Displacement

Earthquakes of the size likely to occur in the Oroville area may or may not cause surface rupture. If surface fault displacement does occur it is most likely along the Swain Ravine Lineament fault zone or perhaps the Prairie Creek Lineament fault zone. However, in the east-west tensional environment which apparently prevails in the Oroville area, small displacement could occur along any of the older faults or shear zones. Such an event along the minor faults is considered possible, but improbable.

Maximum displacements in the 1975 earthquake were about 50 mm (2 in) vertical displacement and about 25 mm (1 in) horizontal separation. In a somewhat larger event, displacements might possibly be several times larger than these values along north-south trending faults. Although the displacements along the

Cleveland Hill Fault took considerable time to reach a maximum in 1975, displacements may not always develop so slowly. Therefore, for purposes of analyses, instant displacement should be assumed. It appears that the only important structure which could be subjected to such displacements on north-south trending faults would be the Bidwell Canyon Saddle Dam.

Regional Changes in Ground Elevation

Although regional changes in ground elevation were measurable at Oroville, the maximum change of 60 mm (2.5 in) is not enough to pose a hazard to State water facilities. It is not expected this magnitude of elevation change would be exceeded by any future earthquake. Therefore, elevation changes are not expected to pose a hazard to facilities.

Potential Hazard to Specific Facilities

Oroville Dam and Saddle Dams

The Cleveland Hill Fault could not be traced north of Mt. Ida Road about 2.1 km (1.3 mi) south of Bidwell Canyon Saddle Dam. However, the Swain Ravine Lineament fault zone appears to go into the Bidwell Canyon area of the reservoir. A fault was mapped in the foundation of Bidwell Canyon Saddle Dam near the right abutment. It should be assumed this fault is capable of the maximum displacement cited under "Fault Displacement." Bidwell Canyon Saddle Dam is the only structure at Oroville with this degree of exposure to the probability of future fault displacements.

Numerous faults were mapped in the foundation of Oroville Dam. None of these appear significant and do not appear to be particularly related to the major north-trending Mesozoic fault zones. It is possible that some small displacements could occur along the faults in the dam foundation. It is considered improbable that this would happen. This aspect should be looked at as part of the reanalysis of the main dam.

If the 60-degree westward dip of the Cleveland Hill Fault is assumed to continue at the reservoir, then faulting in the Swain Ravine Lineament fault zone could dip under the dam, passing underneath the dam at a depth of about 5 km (3 mi). It must be assumed that earthquakes can occur right under the dam. However at such shallow depth, the earthquakes would be of small magnitude.

Numerous landslides developed around Lake Oroville since the reservoir has been in operation and there is geologic evidence for a large number of older slides. When the steep slopes bordering the reservoir are heavily saturated by winter rain, the area is landslide-prone and a strong shake during such a period could trigger landslides into the reservoir. While such failure could be dangerous to boaters on the lake, it is not anticipated the dams would be endangered due to the large amount of freeboard which was provided on the Oroville dams. This freeboard of 6.7 m (22 ft) is expected to contain any waves that might be generated by landslides. Large seiches did not develop in the reservoir during the 1975 earthquake, but if they should, the high freeboard is expected to contain seiche waves also.

Thermalito Forebay and Afterbay

Despite the absence of conclusive evidence, it is possible the Prairie Creek Lineament fault zone extends farther northwest on a trend roughly paralleling Highway 70 between Thermalito Power Canal and Wicks Corners. A sequence of three earthquakes (magnitude 2.8-3.0) occurred just east of this stretch of highway on December 12, 1976. Therefore, it should be assumed that an earthquake comparable to the 1975 Oroville earthquake could occur along the northwest projection of the Prairie Creek Lineament fault zone near the east end of Thermalito Forebay. Fault displacements if they were to occur, would probably be in the Power Canal in a section excavated below natural ground and therefore would not pose great hazard.

Thermalito Powerplant

Cenozoic faults underlie Thermalito Powerplant. As much as 12 m (40 ft) of apparent vertical displacement occurs along a system of faults that roughly parallel the longitudinal axis of the powerhouse. The Cenozoic fault activity suggests small displacements could occur again, particularly if a 1975 type earthquake were to occur along the Prairie Creek Lineament fault zone. Such an occurrence is viewed as a possible, though improbable, event.

Other Structures

For the remainder of the Oroville facilities the main hazard would be from ground shaking earthquakes might cause. A number of structures have faults in their foundations and, conceivably, small displacements could occur along these faults. It is considered improbable that displacements would occur, and if they did, it does not seem the damage would be significant. Structures with faults in their foundations are listed below:

Edward Hyatt Powerplant
Oroville Dam Spillway
Thermalito Diversion Dam
Thermalito Power Canal
Parish Camp Saddle Dam

SUMMARY AND CONCLUSIONS

1. The August 1, 1975, Oroville earthquake was accompanied by movement on the previously unrecognized Cleveland Hill Fault. A linear zone of discontinuous ground cracking developed along the fault about 7 km (4.3 mi) east of the main shock epicenter.
2. Initial length of ground rupture on the Cleveland Hill Fault was about 1.6 km (1.0 mi). Over a period of about 12 months the ground cracking extended progressively to the north, reaching a total length of 8.5 km (5.3 mi).
3. Offset along the fault was greatest in the southern segment, where the original cracking occurred. Offset increased with time; movement amounted to about 50 mm (2 in) vertical displacement and 25 mm (1 in) horizontal extension.
4. The Cleveland Hill Fault was not encountered by trenching or geophysical investigation north of Mt. Ida Road. Aftershock hypocenters projected up a calculated fault plane indicate the fault at the ground surface trends into Bidwell Canyon and that it may pass beneath Oroville Dam at depth.
5. Trenching across the Cleveland Hill Fault by Department of Water Resources and others provides evidence for multiple small fault displacements during the past 100,000 years. These displacements would likely have produced earthquakes similar to the 1975 Oroville event.
6. Three major lineament-fault zones, the Paynes Peak, Swain Ravine, and Prairie Creek, have been delineated in the area by geologic studies. These lineament-fault zones are complex bands of discontinuous, intertwined, steeply dipping faults which were formed during Mesozoic or earlier time under the influence of a different tectonic stress regime than exists today. The Cleveland Hill Fault is within the Swain Ravine Lineament fault zone.
7. Most Cenozoic fault movements in the Sierran foothill belt are caused by east-west extensional stresses reactivating pre-existing Paleozoic and Mesozoic faults such as those comprising the lineament-fault zones.
8. Historic (Cenozoic) faulting and historic earthquake records in the foothill region demonstrate that the current and long-range level of seismic activity is one of low- to moderate-magnitude earthquakes at relatively long recurrence intervals,

occasionally resulting in minor ground rupture and offset.

9. Nothing was seen in this geologic study to indicate that earthquakes greater than Richter Magnitude 6.5 should be expected in the Oroville area.
10. Maximum offset that should be anticipated from another Oroville-type earthquake is estimated to be 50 mm

(2 in) of vertical displacement and 25 mm (1 in) horizontal extension. For a somewhat larger event displacement might be several times larger than these values along north-south trending faults.

11. The evidence available does not indicate a causal relationship between Lake Oroville and the earthquake, but the possibility cannot be eliminated conclusively at this time.

REFERENCES CITED

- Akers, R. J., Marlette, J. W., Morrison, P. W., Jr., and Struckmeyer, H. E., 1977, "Performance of the Oroville Dam and Related Facilities During the August 1, 1975 Earthquake." Dept. Water Resources Bull. 203, 102 p.
- Allen, V. T., 1929, "The Ione Formation of California." Univ. Calif. Pub., Bull. Dept. Geol. Sci., v. 18, p. 347-448.
- Allum, J. A. E., 1966, "Photogeology and Regional Mapping." New York, Pergamon Press, 107 p.
- Alt, J. N., Schwartz, D. P., and McCrumb, D. R., 1977, "Regional Geology and Tectonics," in Woodward-Clyde Consultants, Earthquake Evaluation Studies of the Auburn Dam Area, v. 3, 118 p.
- Anderson, C. A., 1933, "The Tuscan Formation of Northern California with a Discussion Concerning the Origin of Volcanic Breccias." Univ. Calif. Pub., Bull. Dept. Geol. Sci., v. 23, p. 215-276.
- Bailey, E. H., Blake, M. C., Jr., and Jones, D. L., 1970, "On-land Mesozoic Oceanic Crust in California Coast Ranges." U. S. Geol. Survey Prof. Paper 700-C, p. 70-81.
- Bailey, E. H., Irwin, W. P., and Jones, D. L., 1964, "Franciscan and Related Rocks, and Their Significance in the Geology of Western California." Calif. Div. Mines and Geol. Bull. 183, 177 p.
- Baird, A. K., 1962, "Superposed Deformations in the Central Sierra Nevada Foothills East of the Mother Lode." Univ. Calif. Pubs. Geol. Sci., v. 42, p. 1-69.
- Bateman, P. C., and Clark, L. D., 1974, "Stratigraphic and Structural Setting of the Sierra Nevada Batholith, California." Pacific Geology, v. 8, p. 79-89.
- Bateman, P. C., Clark, L. D., Huber, N. K., Moore, J. G., and Rinehart, C. D., 1963, "The Sierra Nevada Batholith - a Synthesis of Recent Work Across the Central Part." U. S. Geol. Survey Prof. Paper 414-D, p. 1-46.
- Bateman, P. C., and Wahrhaftig, C., 1966, "Geology of the Sierra Nevada," in Bailey, E. H. (ed.), Geology of Northern California. Calif. Div. Mines and Geol. Bull. 190, p. 107-172.
- Beck, J. L., 1976, "Weight-Induced Stresses and the Recent Seismicity at Lake Oroville, California." Seis. Soc. America Bull., v. 66, n. 4, p. 1121-1131.
- Becker, G. F., Turner, H. W., and Lindgren, W., 1898, "Bidwell Bar, California." U. S. Geol. Survey Folio 43, scale 1:125,000.

- Bennett, J. H., Taylor, G. C., and Topozada, T. R., 1977, "Crustal Movement in the Northern Sierra Nevada." California Geology, Calif. Div. Mines and Geol., p. 51-57.
- Blake, M. C., Jr., and Jones, D. L., 1974, "Origin of Franciscan Melanges in Northern California," in Dott, R. H., Jr., and Shaver, R. H. (eds.), Modern and Ancient Geosynclinal Sedimentation. Soc. Econ. Paleon. Mineral. Spec. Pub. 19, p. 345-357.
- Bond, G. C., Menzies, M., Moores, E. M., D'Allura, J., Buer, K., Day, D., Robinson, L., and Xenophontos, C., 1977, "Paleozoic-Mesozoic Rocks of the Northern Sierra Nevada: Field guide for the Geol. Soc. America Cordilleran Section Meeting," Sacramento, 38 p.
- Bozovic, A., 1974, "Review and Appraisal of Case Histories Related to Seismic Effects of Reservoir Impounding." Engineering Geology, v. 8, p. 9-27.
- Brewer, W., 1930, "Up and Down California in 1860-1864," in Farquhar, F. P. (ed.), Journal, Yale Univ. Press, p. 339.
- Bryan, K., 1923, "Geology and Ground Water Resources of Sacramento Valley California." U. S. Geol. Survey Water Sup. Paper 495, 285 p.
- Buer, K. Y., 1977, "Stratigraphy, Structure and Petrology of a Portion of the Smartsville Complex, Northern Sierra Nevada, California" (abs.): Geol. Soc. America Abstracts with Programs, v. 9, p. 394.
- 1978, "Stratigraphy, Structure and Petrology of a Portion of the Smartsville Ophiolite, Yuba County, California." MS thesis, Univ. California Davis.
- Burchfiel, B. C., and Davis, G. A., 1972, "Structural Framework and Evolution of the Southern Part of the Cordilleran Orogen, Western United States." Am. Jour. Sci., v. 272, p. 97-118.
- 1975, "Nature and controls of Cordilleran Orogenesis, Western United States: Extensions of an Earlier Synthesis." Am. Jour. Sci., v. 275-A, p. 363-396.
- Burk, C. A., 1965, "Geology of the Alaskan Peninsula-Island Arc and Continental Margin." Geol. Soc. America Mem. 99, 250 p.
- Burnett, J. L., 1965, "Fracture Traces in the Tuscan Formation, California." Calif. Div. Mines and Geol. Spec. Rept. 82, p. 33-40.
- Burnett, J. L., Ford, R. S., and Scott, R. G., 1969, "Geology of the Richardson Springs Quadrangle, California." Calif. Div. Mines and Geol., Map Sheet 13, scale 1:62,500.

- Burnett, J. L., and Jennings, C. W., 1962, Geologic Map of California, Chico Sheet: Calif. Div. Mines and Geol., scale 1:250,000.
- Cady, J. W., 1975, "Magnetic and Gravity Anomalies in the Great Valley and Western Sierra Nevada Metamorphic Belt, California." Geol. Soc. America Spec. Paper 168, 56 p.
- California Department of Natural Resources, 1930, "Mining in California." Calif. Div. Mines, v. 26, n. 4, p. 383-412.
- Carder, D. S., 1945, "Seismic Investigations in the Boulder Dam Area, 1940-1944, and the Influence of Reservoir Loading on Local Earthquake Activity." Seis. Soc. America Bull., v. 35, p. 175-192.
- Cebull, S. E., 1972, "Sense of Displacement Along Foothills Fault System: New Evidence from the Melones Fault Zone, Western Sierra Nevada, California." Geol. Soc. America Bull., v. 83, p. 1185-1190.
- Christensen, M. N., 1966, "Late Cenozoic Crustal Movements in the Sierra Nevada of California." Geol. Soc. America Bull., v. 77, n. 2, p. 163-185.
- Churkin, M., Jr., 1974, "Paleozoic Marginal Ocean Basin-Volcanic Arc Systems in the Cordilleran Foldbelt," in Dott, R. H., Jr., and Shaver, R. H. (eds.), Modern and Ancient Geosynclinal Sedimentation. Soc. Econ. Paleon. Mineral., Spec. Pub 19, p. 174-192.
- Clark, L. D., 1960, "Foothills Fault System, Western Sierra Nevada, California." Geol. Soc. America Bull., v. 71, p. 483-496.
- 1964, "Stratigraphy and Structure of Part of the Western Sierra Nevada Metamorphic Belt, California." U. S. Geol. Survey Prof. Paper 410, 70 p.
- 1976, "Stratigraphy of the North Half of the Western Sierra Nevada Metamorphic Belt, California." U. S. Geol. Survey Prof. Paper 923, 26 p.
- Clark, M. M., Sharp, R. V., Castel, R. O., and Harsh, P. W., 1976, "Surface Faulting near Lake Oroville, California in August 1975." Seis. Soc. America Bull., v. 66, n. 4, p. 1101-1110.
- Coleman, R. G., 1971, "Plate Tectonic Emplacement of Upper Mantle Peridotites along Continental Edges." Jour. Geophys. Research, v. 76, n. 5, p. 1212-1222.
- 1977, "Ophiolites." New York, Springer-Verlag, 229 p.
- Coleman, R. G., and Irwin, W. P., 1974, "Ophiolites and Ancient Continental Margins," in Burk, C. A., and Drake, C. L. (eds.), The Geology of Continental Margins. New York, Springer-Verlag, p. 921-931.

- Douglass, R. C., 1967, "Permian Tethyan Fusulinids from California." U. S. Geol. Survey Prof. Paper 593-A, 13 p.
- Duffield, W. A., and Sharp, R. V., 1975, "Geology of the Sierra Foothills Melange and Adjacent Areas, Amador County, California." U. S. Geol. Survey Prof. Paper 827, 30 p.
- Durrell, C., 1959a, "Tertiary Stratigraphy of the Blairsden Quadrangle, Plumas County, California." Univ. Calif. Pub. Geol. Sci., v. 34, p. 161-192.
- 1959b, "The Lovejoy Formation of Northern California." California Univ., Dept. Geol. Sci. Bull., v. 34, n. 4, p. 193-220.
- 1966, "Tertiary and Quaternary Geology of the Northern Sierra Nevada," in Bailey, E. H. (ed.), Geology of Northern California. Calif. Div. Mines and Geol. Bull. 190, p. 185-197.
- Erwin, H. D., 1934, "Geology and Mineral Resources of Northeastern Madera County, California." Calif. Jour. Mines and Geol., v. 30, p. 7-78.
- Evernden, J. F., and Kistler, R. W., 1970, "Chronology of Emplacement of Mesozoic Batholithic Complexes in California and Western Nevada." U. S. Geol. Survey Prof. Paper 623, 42 p.
- Evernden, J. F., Savage, D. E., Curtis, G. H., and James, G. T., 1964, "Potassium-argon Dates and the Cenozoic Mammalian Chronology of North America." Amer. Jour. Sci., v. 262, p. 145-198.
- Ferguson, H. G., and Gannett, R. W., 1932, "Gold Quartz Veins of the Allegheny District, California." U. S. Geol. Survey Prof. Paper 172, 13 p.
- Fontaine, W. M., 1900, "Notes on Mesozoic Plants from Oroville, California," in Ward, L. F. (ed.), Status of the Mesozoic Floras of the United States. U. S. Geol. Survey Ann. Rept., v. 20, p. 342-368.
- Gabb, W. M., 1869, "Cretaceous and Tertiary Fossils." Calif. Geol. Survey, Paleontology of California, v. 2, 299 p.
- Gansser, A., 1974, "The Ophiolite Melange, a World-wide Problem on Tethyan Examples." Eclogae Geol. Helv., v. 67/3, p. 479-507.
- Gass, I. G., and Smewing, J. D., 1973, "Intrusion, Extrusion and Metamorphism at Constructive Margins: Evidence from the Troodos Massif, Cyprus." Nature (London), v. 242, p. 26-29.
- Gilluly, J., 1972, "Tectonics Involved in the Evolution of Mountain Ranges," in Robertson, E. C. (ed.), Nature of the Solid Earth. New York, McGraw-Hill, p. 406-439.

- Compton, R. R., 1955, "Trondhjemite Batholith near Bidwell Bar, California." Geol. Soc. America Bull., v. 66, p. 9-44.
- Creely, R. S., 1955, "Geology of the Oroville Quadrangle." Ph.D. thesis, Univ. of California, Berkeley, 269 p.
- 1965, "Geology of the Oroville Quadrangle, California." Calif. Div. Mines and Geol., Bull. 184, 86 p.
- Dalrymple, G. B., 1964, "Cenozoic Chronology of the Sierra Nevada, California." Univ. Calif. Pubs. Geol. Sci., v. 47, p. 1-41.
- Davis, G. A., 1969, "Tectonic Correlations, Klamath Mountains and Western Sierra Nevada, California." Geol. Soc. America Bull., v. 80, n. 6, p. 1095-1108.
- Day, D., 1977, "Petrology and Intrusive Complexities of Sheeted Dikes in the Smartville Ophiolite, Northwestern Sierra Foothills, California" (abs.): Geol. Soc. America Abstracts With Programs, v. 9, n. 4, p. 410.
- Dewey, J. F., and Bird, J. M., 1970, "Mountain Belts and the New Global Tectonics." Jour. Geophys. Research, v. 75, p. 2625-2647.
- Dickerson, R. E., 1916, "Stratigraphy and Fauna of the Tejon Eocene of California." Univ. Calif. Pub. Bull. Dept. Geol. Sci., v. 9, p. 363-524.
- Dickinson, W. R., 1968, "Circum-Pacific Andesite Types." Jour. Geophys. Research, v. 73, p. 2261-2269.
- 1969, "Evolution of Calc-alkaline Rocks in the Geosynclinal System of California and Oregon." Oregon Dept. Geol. and Min. Industries Bull. 65, p. 151-156.
- 1975, "Time-Transgressive Tectonic Contacts Bordering Subduction Complexes" (abs.): Geol. Soc. America Abstracts with Programs, v. 7, n. 7, p. 1052.
- Dickinson, W. R., and Hatherton, T., 1967, "Andesitic Volcanism and Seismicity around the Pacific." Science, v. 157, p. 801-803.
- Diller, J. S., 1892, "Geology of the Taylorsville Region of California." Geol. Soc. America Bull., v. 3, p. 369-394.
- 1895, "Lassen Peak Folio." U. S. Geol. Survey Atlas, n. 15.
- 1908, "Geology of the Taylorsville Region, California." U. S. Geol. Survey Bull. 353, 128 p.
- Diller, J. S., and Stanton, T. W., 1894, "The Shasta-Chico Series." Geol. Soc. America Bull., v. 5, p. 435-464.

- Gromme, C. S., Merrill, R. T., and Verhoogen, J., 1967, "Paleomagnetism of Jurassic and Cretaceous Plutonic Rocks in the Sierra Nevada, California, and its Significance for Polar Wandering and Continental Drift." Jour. Geophys. Research, v. 72, p. 5661-5684.
- Gupta, H. K., Rastogi, B. K., and Narain, H., 1973, "Earthquakes in the Koyna Region and Common Features of the Reservoir-associated Seismicity," in Ackerman, W. C., White, G. F., and Worthington, E. B. (eds.), Man-made Lakes: Their Problems and Environmental Effects: Amer. Geophys. Union, Geophys. Mono. 17, p. 455-467.
- Hamilton, W., 1969, "Mesozoic California and the Underflow of Pacific Mantle." Geol. Soc. America Bull., v. 80, n. 12, p. 2409-2430.
- Hamilton, W., and Myers, W. B., 1966, "Cenozoic Tectonics of the Western United States." Rev. Geophysics, v. 4, p. 509-549.
- Harland, W. B., Smith, A. C., and Wilcock, B., eds., 1964, "The Phanerozoic Time-scale - A symposium dedicated to Professor Arthur Holmes." Geol. Soc. London Quart. Jour. Supp., v. 1205, 458 p.
- Hay, E. A., 1976, "Cenozoic Uplifting of the Sierra Nevada in Isostatic Response to North American and Pacific Plate Interactions." Geology, v. 4, n. 12, p. 763-766.
- Hess, H. H., 1959, "Nature of the Great Oceanic Ridges." Internat. Ocean. Cong. Preprints, Am. Assoc. Adv. Sci., p. 33-34.
- _____, 1962, "History of Ocean Basins," in Engel, A. E. J., James, H. L., and Leonard, B. F. (eds.), Petrologic studies: a volume to honor A. F. Buddington. Geol. Soc. America, p. 599-620.
- Hietanen, A., 1951, "Metamorphic and Igneous Rocks of the Merrimac Area, Plumas National Forest, California." Geol. Soc. America Bull., v. 62, p. 565-608.
- _____, 1973a, "Geology of the Pulga and Bucks Lake Quadrangles, Butte and Plumas Counties, California." U. S. Geol. Survey Prof. Paper 731, 66 p.
- _____, 1973b, "Origin of Andesitic and Granitic Magmas in the Northern Sierra Nevada, California." Geol. Soc. America Bull., v. 84, p. 2111-2118.
- _____, 1976, "Metamorphism and Plutonism around the Middle and South Forks, Feather River, California." U. S. Geol. Survey Prof. Paper 920, 30 p.
- _____, 1977, "Paleozoic-Mesozoic Boundary in the Berry Creek Quadrangle, Northwestern Sierra Nevada, California." U. S. Geol. Survey Prof. Paper 1027, 22 p.

- Hudson, F. S., 1951, "Mount Lincoln-Castle Peak Area, Sierra Nevada, California." *Geol. Soc. America Bull.*, v. 62, p. 931-952.
- 1955, "Measurement of the Deformation of the Sierra Nevada, California, since Middle Eocene." *Geol. Soc. America Bull.*, v. 66, p. 835-870.
- Hsu, K. J., 1966, "Melange Concept and its Application to an Interpretation of the California Coast Range Geology." (abs.) *Geol. Soc. America Abstracts for 1966*, n. 101, p. 99-100.
- 1968, "Principles of Melanges and Their Bearing on the Franciscan-Knoxville Paradox." *Geol. Soc. America Bull.*, v. 79, p. 1063-1074.
- 1971, "Franciscan Melanges as a Model for Eugeosynclinal Sedimentation and Underthrusting Tectonics." *Jour. Geophys. Research*, v. 76, p. 1162-1170.
- Imlay, R. W., 1961, "Late Jurassic Ammonites from the Western Sierra Nevada, California." *U. S. Geol. Survey Prof. Paper* 374-D, 30 p.
- Irwin, W. P., 1972, "Terranes of the Western Paleozoic and Triassic Belt in the Southern Klamath Mountains, California." *U. S. Geol. Survey Prof. Paper* 800-C, p. C103-C111.
- Irwin, W. P., and Galanis, S. P., 1976, Map showing limestone and selected fossil localities in the Klamath Mountains, California and Oregon. *U. S. Geol. Survey Misc. Field Studies Map* MF-749, scale 1:500,000.
- Irwin, W. P., Jones, D. L., and Pessagno, E. A., Jr., 1977, "Significance of Mesozoic Radiolarians from the Pre-Nevadan Rocks of the Southern Klamath Mountains, California." *Geology*, v. 5, p. 557-562.
- Jackson, E. D., Green, H. W., II, and Moores, E. M., 1975, "The Vourinos Ophiolite, Greece: Cyclic Units of Lineated Cumulates Overlying Harzburgite Tectonite." *Geol. Soc. America Bull.*, v. 86, p. 390-398.
- Jennings, C. W., 1975, Fault map of California: Calif. Div. Mines and Geol., scale 1:750,000.
- 1977, Geologic map of California: Calif. Div. Mines and Geol., scale 1:750,000.
- Karig, D. E., 1970, "Ridges and Basins of the Tonga-Kermadec Island Arc System." *Jour. Geophys. Research*, v. 75, p. 239-255.
- 1971a, "Structural History of the Mariana Island Arc System." *Geol. Soc. America Bull.*, v. 82, p. 323-344.

- 1971b, "Origin and Development of Marginal Basins in the Western Pacific." Jour. Geophys. Research, v. 76, p. 2542-2561.
- 1972, "Remnant Arcs." Geol. Soc. America Bull., v. 83, p. 1057-1068.
- 1974, "Evolution of Arc Systems in the Western Pacific." Ann. Rev. Earth and Planetary Sci., v. 2, p. 51-76.
- Karig, D. E., and Sharman, G. F., III, 1975, "Subduction and Accretion in Trenches." Geol. Soc. America Bull., v. 86, p. 377-389.
- Knopf, A., 1918, "Geology and Ore Deposits of the Yerrington District, Nevada." U. S. Geol. Survey Prof. Paper 114, 68 p.
- 1929, "Mother Lode System of California." U. S. Geol. Survey Prof. Paper 157, 88 p.
- Knowlton, F. H., 1910, "The Jurassic Age of the 'Jurassic Flora of Oregon'." Am. Jour. Sci., v. 30, p. 33-64.
- Lahr, K. M., Lahr, J. C., Lindh, A. G., Bufo, C. G., and Lester, F. W., 1976, "The August 1975 Oroville Earthquakes." Seis. Soc. America Bull., v. 66, n. 4, p. 1085-1099.
- Langstrom, C. A., and Bulter, R., 1976, "Focal Mechanism of the August 1, 1975, Oroville Earthquake." Seis. Soc. America Bull., v. 66, n. 4, p. 1111-1120.
- Lapham, D. M., and McKague, H. W., 1964, "Structural Patterns Associated with the Serpentinities of Southeastern Pennsylvania." Geol. Soc. America Bull., v. 75, p. 639-660.
- Lester, F. W., Bufo, C. G., Lahr, K. M., and Stewart, S. W., 1975, "Aftershocks of the Oroville Earthquake of August 1, 1975," in Sherburne, R. W., and Hauge, C. J. (eds.), Oroville, California Earthquake 1 August 1975. Calif. Div. Mines and Geol. Spec. Rept. 124, p. 131-138.
- Lindgren, W., 1894, "Sacramento, California": U. S. Geol. Survey Geol. Atlas, Folio 5, 3 p., scale 1:125,000.
- 1900, "Description of the Colfax Quadrangle (California)." U. S. Geol. Survey Geol. Atlas, Folio 66, 10 p., scale 1:125,000.
- 1911, "The Tertiary Gravels of the Sierra Nevada of California." U. S. Geol. Survey Prof. Paper 73, 226 p.
- Lindgren, W., and Turner, H. W., 1895 "Smartsville": U. S. Geol. Survey Geol. Atlas, Folio 18, 6 p., scale 1:125,000.

- Lockwood, J. P., 1971, "Sedimentary and Gravity-Slide Emplacement of Serpentinite." *Geol. Soc. America Bull.*, v. 82, p. 919-936.
- 1972, "Possible Mechanisms for the Emplacement of Alpine-type Serpentinite." *Geol. Soc. America Mem.* 132, p. 273-287.
- Lomnitz, C., and Bolt, B. A., 1967, "Evidence on Crustal Structure in California from the Chase V Explosion and the Chico Earthquake of May 24, 1966." *Seis. Soc. America*, v. 57, n. 5, p. 1093-1114.
- Lydon, P. A., 1968, "Geology and Lahars of the Tuscan Formation, Northern California." *Geol. Soc. America Mem.* 116, p. 441-475.
- Lydon, P. A., Gay, T. E., Jr., and Jennings, C. W. (compilers), 1960, *Geologic map of California, Westwood sheet: Calif. Div. Mines and Geol., scale 1:250,000.*
- Mayo, E., 1934, "Geology and Mineral Resources of Laurel and Convict Basins, Southwestern Mono County, California." *Calif. Jour. Mines and Geol.*, v. 30, p. 79-87.
- 1935, "Some Intrusions and Their Wall Rocks in the Sierra Nevada." *Jour. Geol.*, v. 43, p. 673-689.
- Moberly, R., 1972, "Origin of Lithosphere Behind Island Arcs, with References to the Western Pacific." *Geol. Soc. America Mem.* 132, p. 35-55.
- Mogi, K., 1963, "Some Discussions on Aftershocks, Foreshocks and Earthquake Swarms - the Fracture of a Semi-infinite Body caused by an Inner Stress Origin and its Relation to the Earthquake Phenomena." *Earthquake Res. Inst. Bull.*, v. 41, p. 615-658.
- Moore, J. G., 1959, "The Quartz Diorite Boundary Line in the Western United States." *Jour. Geol.*, v. 67, p. 198-210.
- 1973, "Complex Deformation of Cretaceous Trench Deposits, Southwestern Alaska." *Geol. Soc. America Bull.*, v. 84, p. 2005-2020.
- Moore, E. M., 1972, "Model for Jurassic Island Arc-Continental Margin Collision in California" (abs.). *Geol. Soc. America Abstracts with Programs*, v. 4, n. 3, p. 202.
- 1975, "The Smartville Terrane, Northwestern Sierra Nevada, a Major Pre-Late Jurassic Ophiolite Complex" (abs.). *Geol. Soc. America Abstracts with Programs*, v. 7, n. 3, p. 352.
- Moore, E. M., and Jackson, E. D., 1974, "A Comparison of Selected Ophiolites and Oceanic Crust." *Nature*, v. 250, p. 136-139.
- Moore, E. M., and Vine, F., 1971, "The Troodos Massif, Cyprus and Other Ophiolites as Oceanic Crust: Evaluation and Complications." *Royal Soc. London Trans., Se. A.* v. 268, p. 443-466.

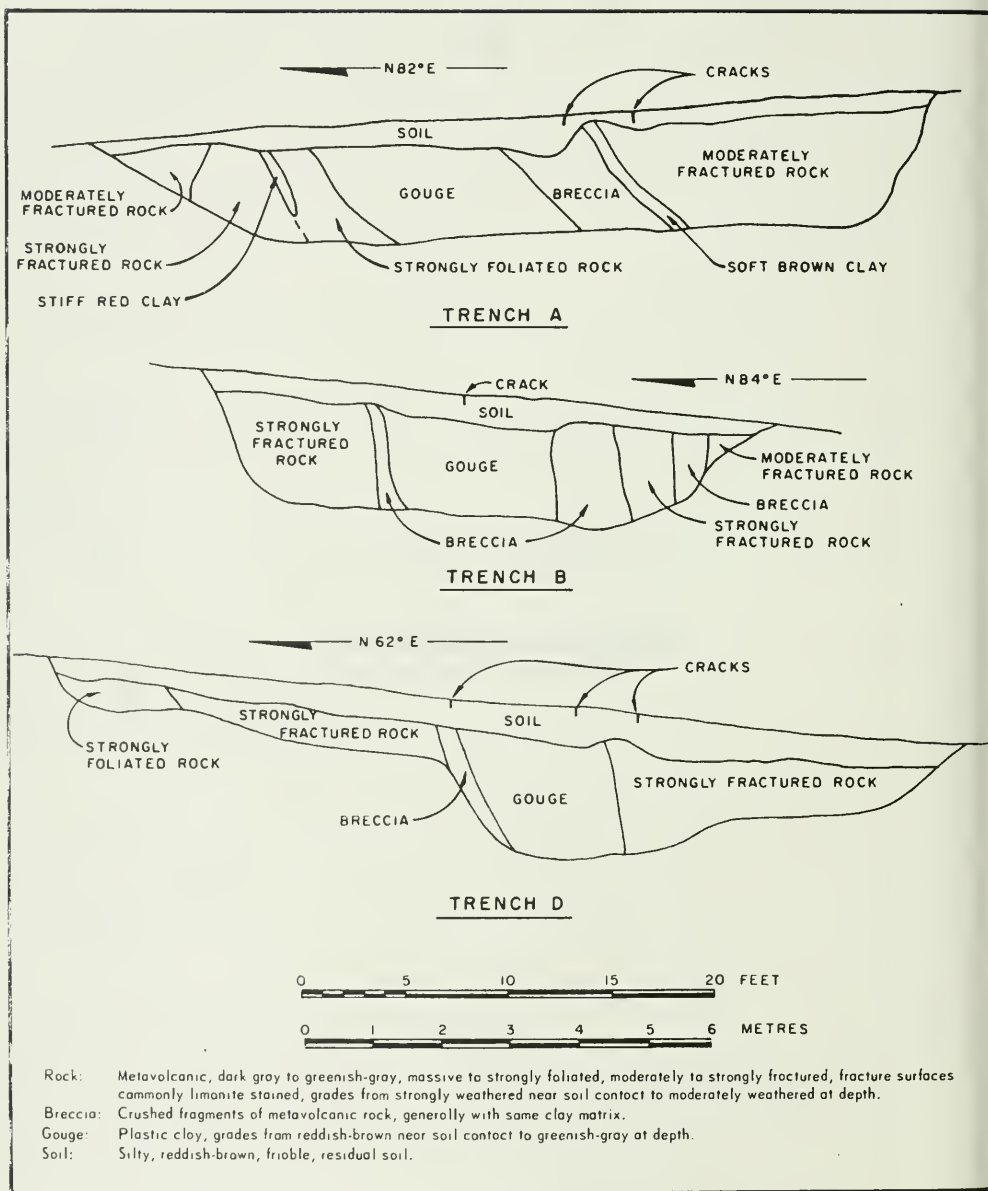
- Morrison, P. W., Jr., 1974, "Report of Seismic Activity Near Lake Oroville January 1969 - December 1972." Calif. Dept. Water Res., Earthquake Engr. Memorandum n. 61, 60 p.
- Morrison, P. W., Jr., Stump, B. W., and Uhrhammer, R., 1976, "The Oroville Earthquake Sequence of August 1975." Seis. Soc. America Bull., v. 66, n. 4, p. 1065-1084.
- Popenoe, W. P., 1943, "Cretaceous, East Side Sacramento Valley, Shasta and Butte Counties, California." Am. Assoc. Pet. Geol. Bull., v. 27, p. 306-312.
- Radbruch-Hall, D. H., Colton, R. B., Davies, W. E., Skipp, B. A., Luchitta, I., and Varnes, D. J., 1976, Preliminary Landslide Overview Map of the Conterminous United States: U. S. Geol. Survey Misc. Field Studies MF-771, scale 1:7,500,000.
- Raymond, L. A., 1977, "Emplacement of Exotic Tectonic Blocks in the Franciscan Complex, Northern Diablo Range, California" (abs.). Geol. Soc. America Abstracts with Programs, v. 9, n. 4, p. 486.
- Rothé, J. P., 1969, "Earthquakes and Reservoir Loading." Proceedings, Fourth World Conference on Earthquake Engineering, Chile, v. 1, p. A28-A38c.
- 1973, "Summary: Geophysics Report," in Ackerman, W. C., White, G. T., and Worthington, E. B. (eds.), Man-Made Lakes: Their Problems and Environmental Effects. Am. Geophys. Union, Geophysical Monograph 17, p. 441-454.
- Russel, L. R., 1978, "The Melones Fault Zone and the Tectonic Framework of the Western Sierra Nevada Between the Middle and South Forks of the American River, California" (abs.). Geol. Soc. America Abstracts with Programs, v. 10, n. 3, p. 145.
- Scholl, D. W., and Marlow, M. S., 1974, "Deposits in Magmatic Arc and Trench Systems: Sedimentary Sequence in Modern Pacific Trenches and the Deformed Circum-Pacific Eugeosyncline," in Dott, R. H., Jr., and Shaver, R. H. (eds.), Modern and Ancient Geosynclinal Sedimentation: Soc. Econ. Paleon. Mineral. Spec. Pub. 19, p. 193-211.
- Schweickert, R. A., 1976, "Early Mesozoic Rifting and Fragmentation of the Cordilleran Orogen in the Western USA." Nature, v. 260, p. 586-591.
- Schweickert, R. A., and Cowan, D. S., 1975, "Early Mesozoic Tectonic Evolution of the Western Sierra Nevada, California." Geol. Soc. America Bull., v. 86, p. 1329-1336.

- Schweickert, R. A., and Wright, W. H., 1975, "Preliminary Evidence of the Tectonic History of the Calaveras Formation of the Western Sierra Nevada, California" (abs.). Geol. Soc. America Abstracts with Programs, v. 7, n. 3, p. 371-372.
- Standlee, L. A., 1978, "Middle Paleozoic Ophiolite in the Melones Fault Zone, Northern Sierra Nevada, California" (abs.). Geol. Soc. America Abstracts with Programs, v. 10, n. 3, p. 148.
- Stanton, T. W., 1896, "The Faunal Relations of the Eocene and Upper Cretaceous on the Pacific Coast." U. S. Geol. Survey Seventeenth Ann. Rept., p. 1005-1060.
- Strand, R. G., and Koenig, J. B., 1965, Geologic Map of California, Olaf P. Jenkins Edition, Sacramento Sheet: Calif. Div. Mines and Geol., scale 1:250,000.
- Swan, F. H., III, and Hanson, K. L., 1977, "Quaternary Geology and Age Dating," in Woodward-Clyde Consultants, Earthquake Evaluation Studies of the Auburn Dam Area: Woodward-Clyde Consultants, unpublished, v. 4, 83 p.
- Swan, F. H., III, and Hanson, K. L., 1978, "Origin and Ages of Late Quaternary Deposits and Buried Paleosols in the Western Sierra Nevada Foothills, California" (abs.). Geol. Soc. America Abstracts with Programs, v. 10, n. 3, p. 149.
- Taff, J. A., Hanna, G. D., and Cross, C. M., 1940, "Type Locality of the Cretaceous Chico Formation." Geol. Soc. America Bull., v. 51, p. 1311-1328.
- Taliaferro, N. L., 1942, "Geologic History and Correlation of the Jurassic of Southwestern Oregon and California." Geol. Soc. America Bull., v. 53, p. 71-112.
- 1943, "Manganese Deposits of the Sierra Nevada, Their Genesis and Metamorphism," in Jenkins, O. P. (ed.), Manganese in California. Dept. Nat. Res., Div. Mines Bull. 125, p. 277-332.
- 1951, "Geology of the San Francisco Bay Counties." Calif. Dept. Nat. Res., Div. Mines Bull. 154, p. 117-150.
- Townley, S. D., and Allen, M. W., 1939, "Descriptive Catalog of Earthquakes of the Pacific Coast of the United States 1769-1928." Seis. Soc. America Bull., v. 29, n. 1, 297 p.
- Turner, H. W., 1893, "Some Recent Contributions to the Geology of California." Am. Geologist, v. 11, p. 307-495.
- 1894, "The Rocks of the Sierra Nevada." U. S. Geol. Survey Fourteenth Ann. Rept., p. 435-495.
- 1896, "Further Contributions to the Geology of the Sierra Nevada." U. S. Geol. Survey Seventeenth Ann. Rept., p. 521-762.

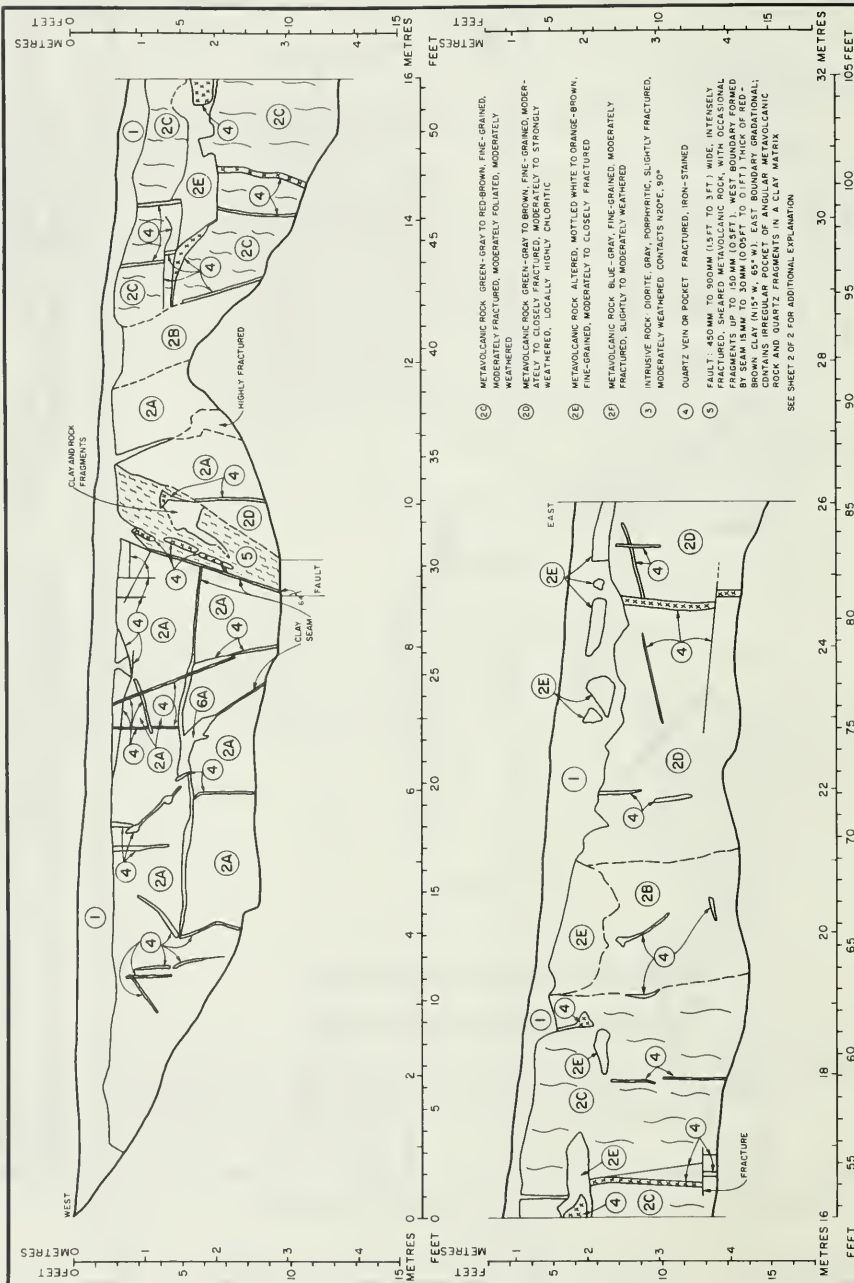
- Tysdal, R. G., Case, J. E., Wrinkler, G. R., and Clark, S. H. B., 1977, "Sheeted Dikes, Gabbro and Pillow Basalt in Flysch of Coastal Southern Alaska." Geology, v. 6, n. 3, p. 377-383.
- U. S. Army Corps of Engineers, 1977, "Fault Evaluation Study, Marysville Lake Project, Parks Bar Alternate, Yuba River, California." U. S. A. C. of Eng., Sacto. Dist., 25 p.
- U. S. Geological Survey Staff, 1978, "Technical Review of Earthquake Evaluation Studies of the Auburn Dam Area (Woodward-Clyde Consultants, 1977)--a report to the U. S. Bureau of Reclamation," U. S. Geol. Survey, 143 p.
- von Huene, R., 1972, "Structure of the Continental Margin and Tectonism at the Eastern Aleutian Trench." Geol. Soc. America Bull., v. 83, p. 3613-3626.
- Whitney, J. D., 1865, "Report of the Progress and Synopsis of the Field Work from 1860-1864." Geol. Survey of Calif., Geology, v. 1, 498 p.
- Williams, H., and Stevens, R. K., 1974, "The Ancient Continental Margin of Eastern North America," in Burk, C. A., and Drake, C. L. (eds.) The Geology of the Continental Margins: New York, Springer-Verlag, p. 781-796.
- Wolfe, J. E., 1967, "Earthquake Hazard Report (n. 28) for the State Water Project - Oroville Dam Site." California Dept. Water Res., 9 p.
- Wood, H. O., and Heck, N. H., 1951, "Earthquake History of the United States, 1769-1950, Part II, Stronger Earthquakes of California and Western Nevada." U. S. Dept. of Commerce, Coast and Geodetic Sur., n. 609.
- Woodward-Clyde Consultants, 1977, "Earthquake Evaluation Studies of the Auburn Dam Area," report prepared for the U. S. Bureau of Reclamation, 8 volumes.
- Wright, L., 1976, "Late Cenozoic Fault Patterns and Stress Fields in the Great Basin and Westward Displacement of the Sierra Nevada Block." Geology, v. 4, n. 8, p. 489-494.
- Xenophontos, C., and Bond, G. C., 1978, "Petrology, Sedimentation and Paleogeography of the Smartville Terrane (Jurassic) - bearing on the Genesis of the Smartville Ophiolite," in Howell, D. G., and McDougall, K. A. (eds.), Mesozoic Paleogeography of the Western United States: Soc. Econ. Paleon. Mineral., Pac. Sect., p. 291-302.

ADDENDA TO CHAPTER II

Department of Water Resources
Exploration Trench Logs



Logs of Exploration Trenches Along Cleveland Hill Crack Zone



EXPLORATION TRENCH LOG

PROJECT: OROVILLE AREA LINEAMENT INVESTIGATION

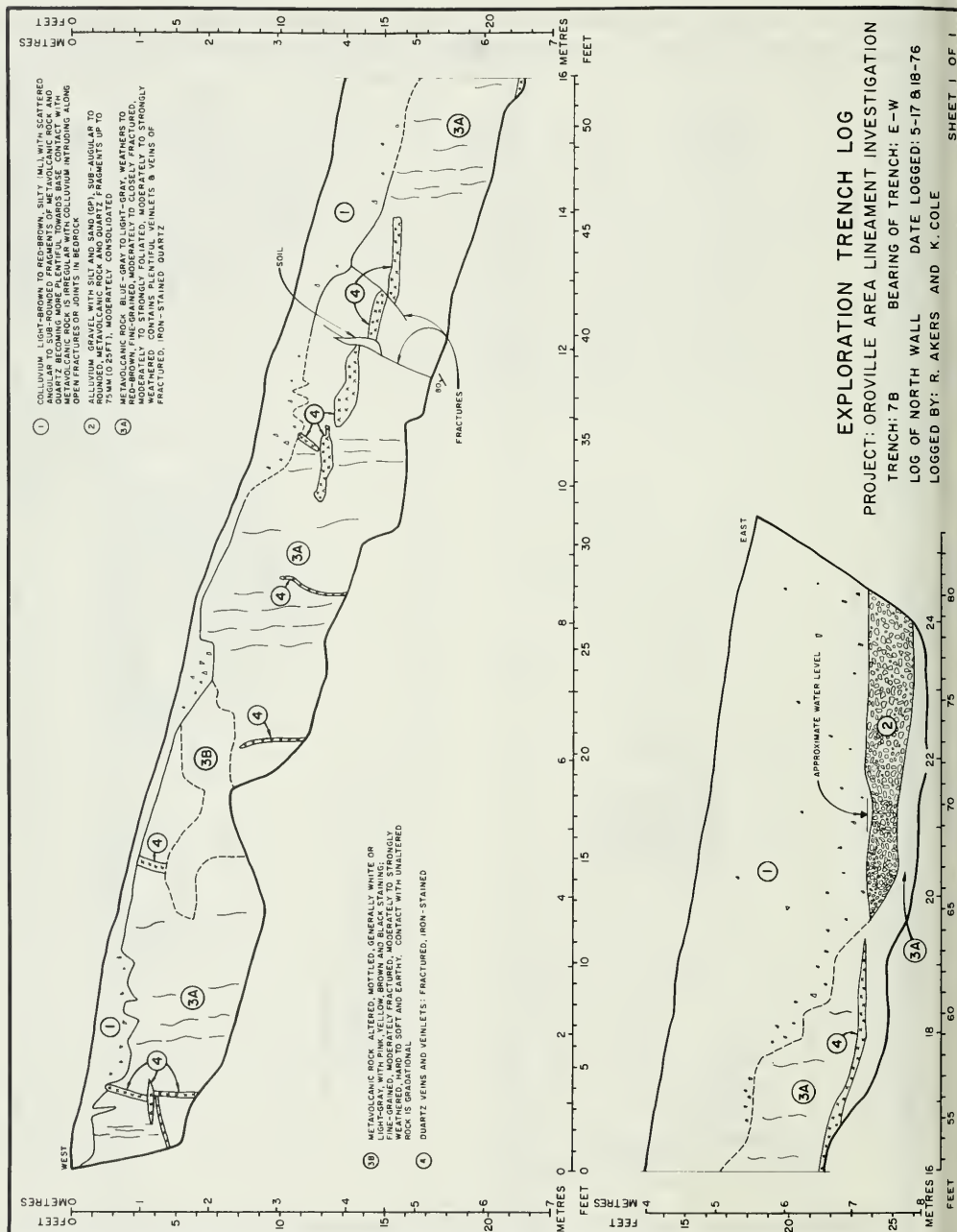
TRENCH: 7-A BEARING OF TRENCH: E-W

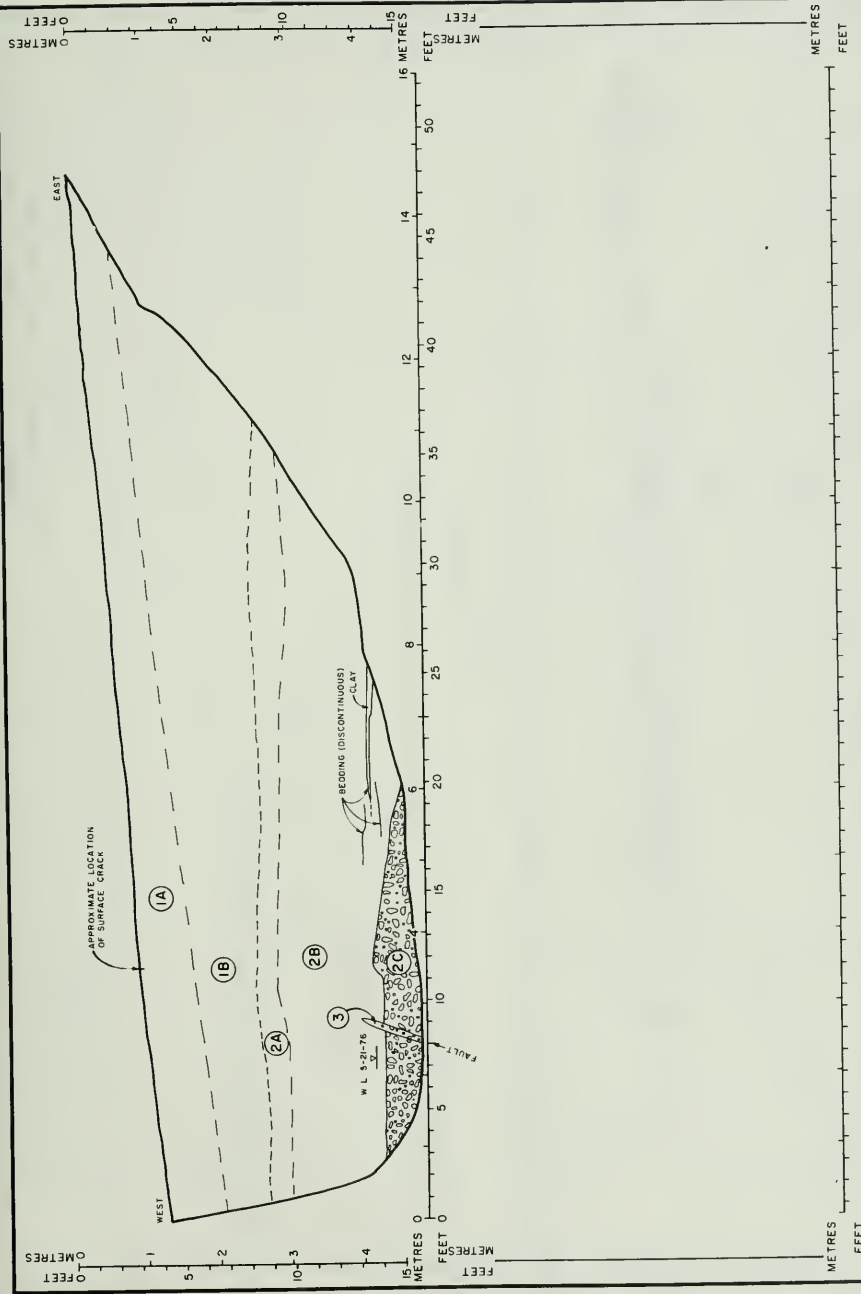
LOG OF NORTH WALL

LOGGED BY: R. AKERS AND K. COLE

- ① COLLUMINARY LIGHT-BROWN TO RED-BROWN, SILTY, MILDLY TO SCATTERED, ANGULAR TO SUB-ANGULAR, GRADES OF METACOLLUMINARY, LIGHT-BROWN TO BROWN, FINE-GRAINED, MODERATELY FOLIATED, SLIGHTLY FOLIATED, GRADES FROM HIGHLY WEATHERED AT UPPER CONTACT TO MODERATELY WEATHERED NEAR BOTTOM OF TRENCH
- ② METACOLLUMINARY ROCK, OLIVE-GRAY TO BROWN, FINE-GRAINED, MODERATELY FOLIATED, SLIGHTLY FOLIATED, GRADES FROM HIGHLY WEATHERED AT UPPER CONTACT TO MODERATELY WEATHERED NEAR BOTTOM OF TRENCH
- ③ METACOLLUMINARY ROCK, SLIGHTLY ALTERED, OLIVE-GRAY TO BROWN, FINE-GRAINED, MODERATELY FOLIATED, MODERATELY TO HIGHLY WEATHERED, WITH NUMEROUS SMALL FRACTURED QUARTZ VEINS AND POCKETS

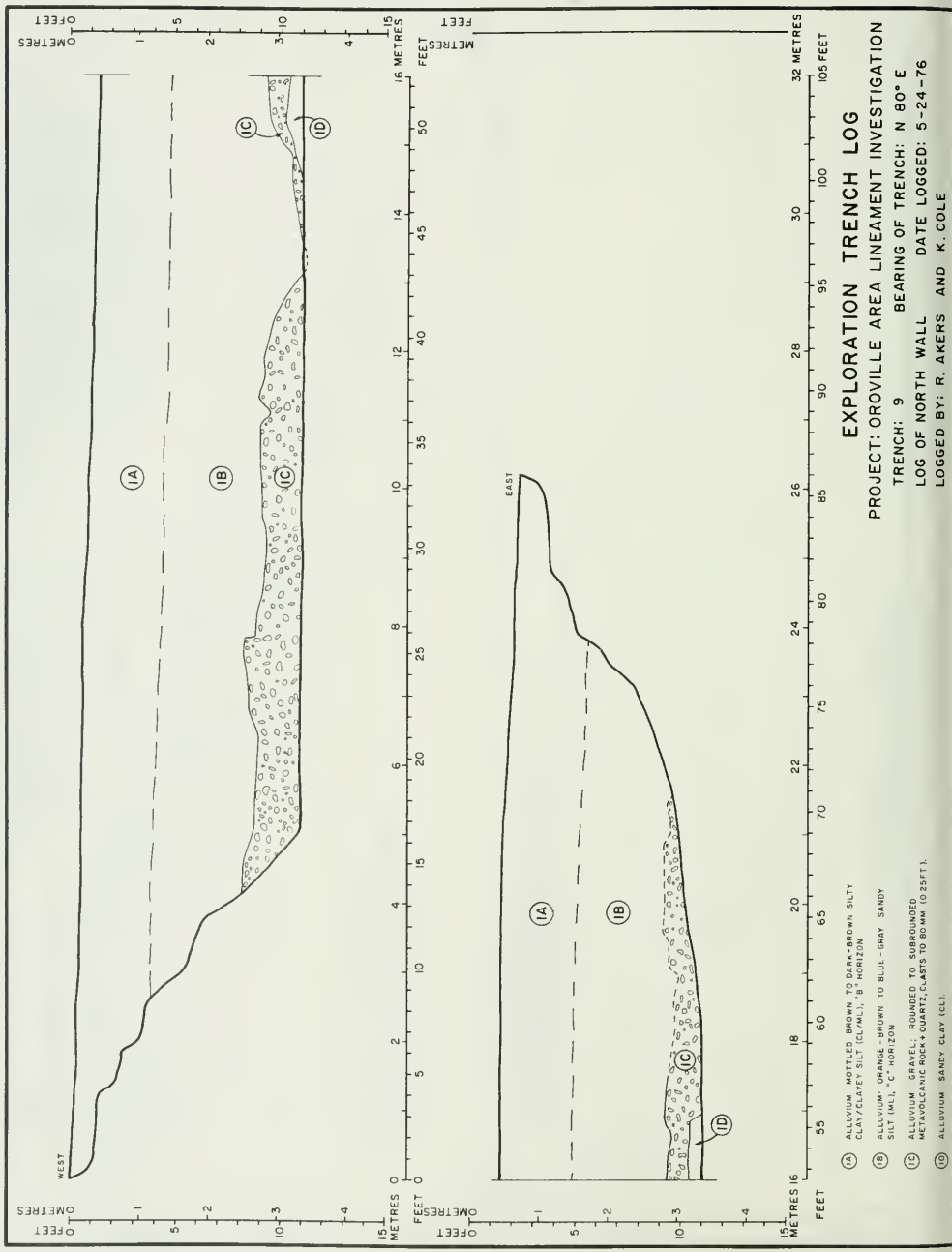
SHEET 2 OF 2 FOR ADDITIONAL EXPLANATION





EXPLOSION TRENCH LOG
 PROJECT: OROVILLE AREA LINEAMENT INVESTIGATION
 TRENCH: 8 BEARING OF TRENCH: N 72° E
 LOG OF NORTH WALL DATE LOGGED: 5-20, 21, 22-76
 LOGGED BY: R. AKERS AND K. COLE
 SHEET 1 OF 1

- 1A COLLUVIUM - RED-BROWN CLAYEY SILT (ML), "B" HORIZON, CONTAINS ANGULAR FRAGMENTS OF METAVOLCANIC ROCK + QUARTZ, AVERAGE SIZE 45 MM TO 15 FT
- 1B COLLUVIUM - MEDIUM-BROWN SILTY CLAY (CL), "C" HORIZON, CONTAINS ANGULAR FRAGMENTS OF METAVOLCANIC ROCK AS 1A
- 2A ALLUVIUM - RED-BROWN SANDY SILT (ML), INCREASING SAND WITH DEPTH, VAGUE LENSES OF SAND AND CLAY NEAR BOTTOM
- 2B ALLUVIUM - GRAVEL (GP), ROUNDED TO SUBROUNDED MEDIUM TO LARGE GRAIN SIZES, SANDY MATRIX, SLIGHTLY CONSOLIDATED, UNSTRATIFIED
- 3 COLLUVIUM - MEDIUM-BROWN SANDY SILT (ML), INCREASING SAND WITH DEPTH, VAGUE LENSES OF SAND AND CLAY NEAR BOTTOM



EXPLORATION TRENCH LOG

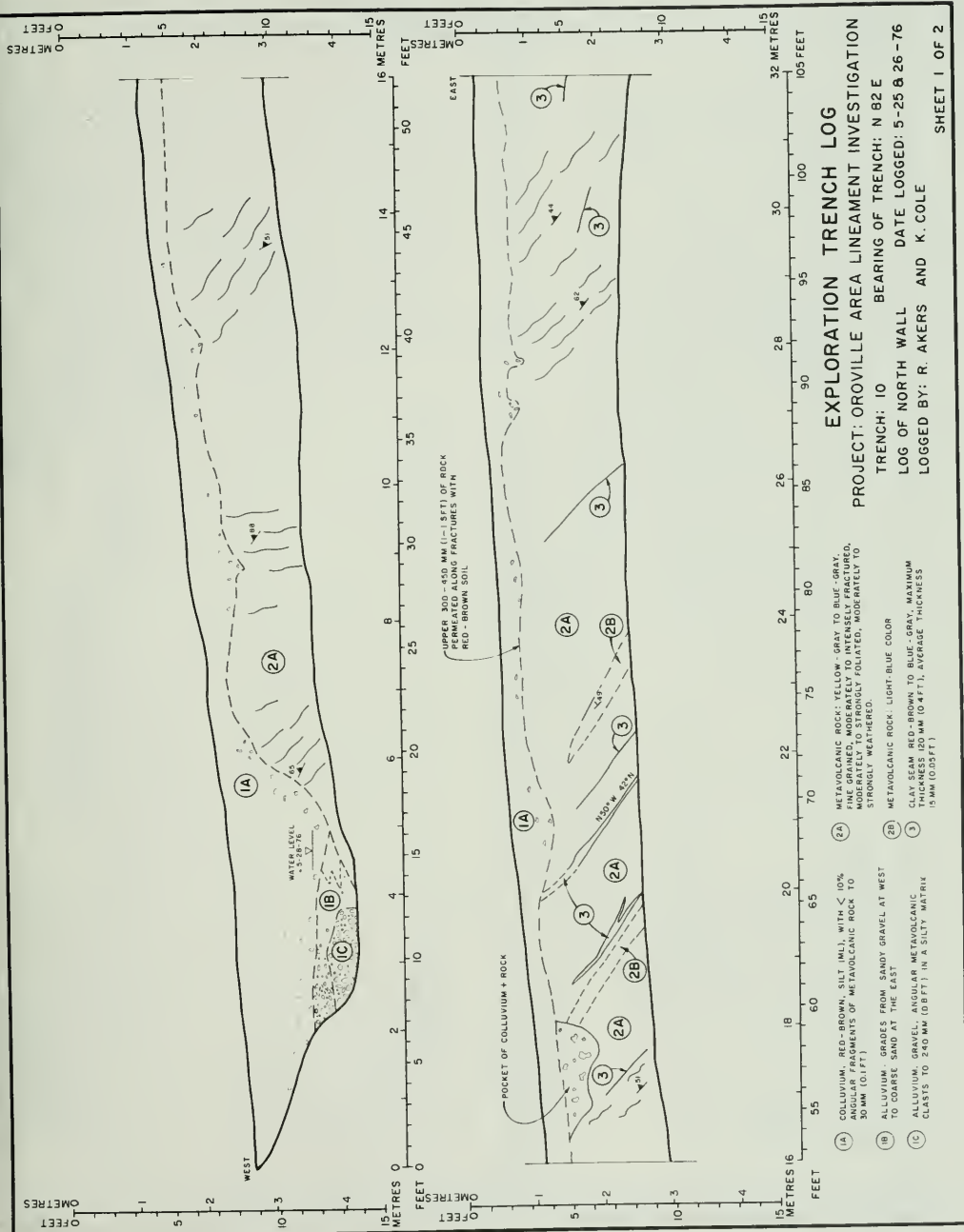
PROJECT: OROVILLE AREA LINEAMENT INVESTIGATION

TRENCH: 9 BEARING OF TRENCH: N 80° E

LOG OF NORTH WALL DATE LOGGED: 5-24-76

LOGGED BY: R. AKERS AND K. COLE

- (A) ALUMINUM MOTTLED BROWN TO DARK-BROWN SILTY CLAY/CLAYEY SILT (CL/ML) "B" HORIZON
- (B) ALUMINUM ORANGE-BROWN TO BLUE-GRAY SANDY SILT (ML), "C" HORIZON
- (C) ALUMINUM GRAY, BOUNDED TO SUBROUNDED METAVOLCANIC ROCK + QUARTZ CLASTS TO 80 MM (3.25 FT.)
- (D) ALUMINUM SANDY CLAY (CL)



EXPLORATION TRENCH LOG

PROJECT: OROVILLE AREA LINEAMENT INVESTIGATION

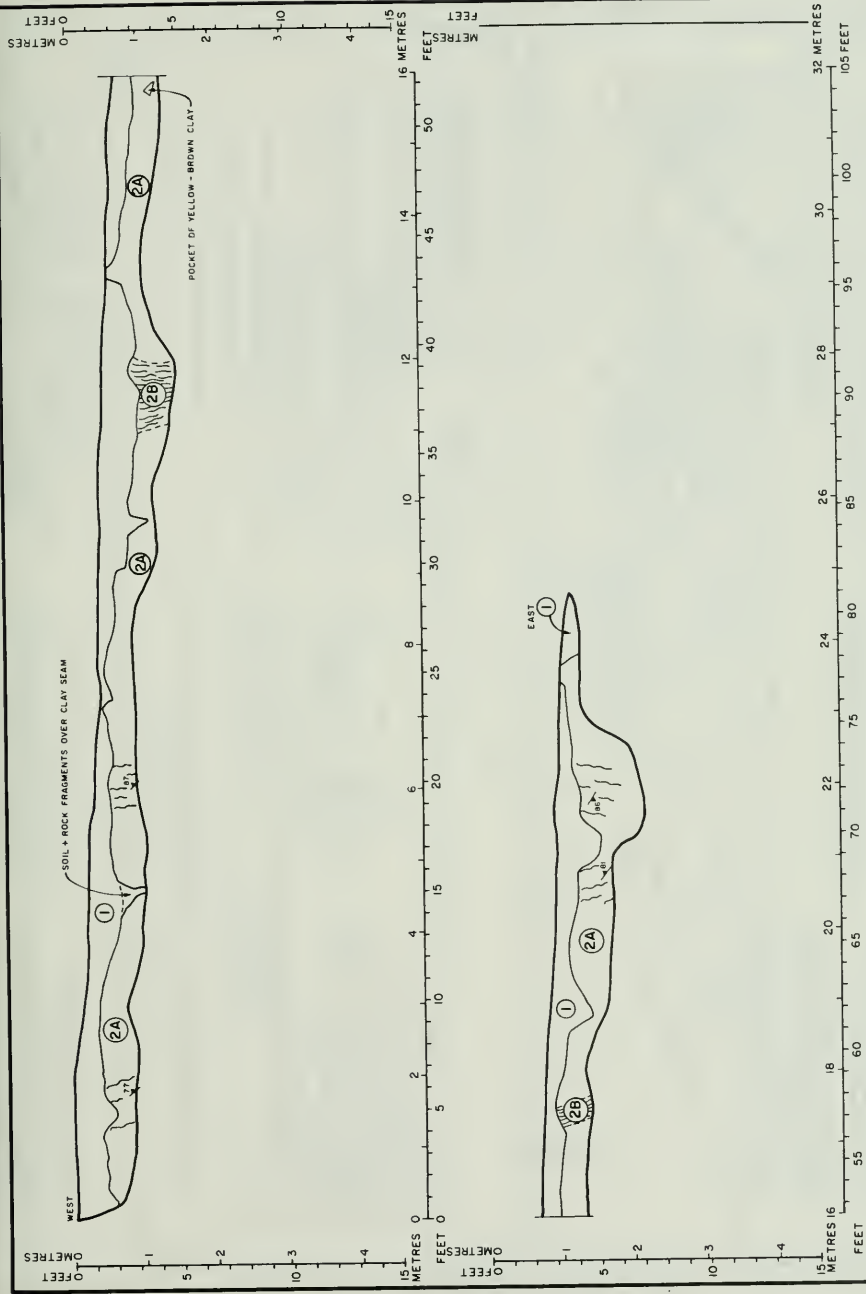
TRENCH: 10 BEARING OF TRENCH: N 82 E

LOG OF NORTH WALL DATE LOGGED: 5-25-82 26-76

LOGGED BY: R. AKERS AND K. COLE

SHEET 1 OF 2

- (1A) COLLUVIUM, RED-BROWN, SILT, ONLY WITH < 10% SAND, 30 MM (0.1 FT)
- (1B) ALLUVIUM, GRAVELS FROM SANDY GRAVEL AT WEST TO COARSE SAND AT THE EAST
- (1C) ALLUVIUM, GRAVEL, ANGULAR METAVOLCANIC CLASTS TO 240 MM (0.8 FT) IN A SILTY MATRIX
- (2A) METAVOLCANIC ROCK: YELLOW-GRAY TO BLUE-GRAY, FINE GRAINED, MODERATELY TO INTENSELY FRACTURED, MODERATELY TO STRONGLY FOLIATED, MODERATELY TO STRONGLY WEATHERED
- (2B) METAVOLCANIC ROCK: LIGHT-BLUE COLOR
- (3) CLAY SEAM, RED-BROWN TO BLUE-GRAY, MAXIMUM THICKNESS 100 MM (0.4 FT), AVERAGE THICKNESS 15 MM (0.05 FT)
- (4A) METAVOLCANIC ROCK: YELLOW-GRAY TO BLUE-GRAY, FINE GRAINED, MODERATELY TO INTENSELY FRACTURED, MODERATELY TO STRONGLY FOLIATED, MODERATELY TO STRONGLY WEATHERED
- (4B) METAVOLCANIC ROCK: LIGHT-BLUE COLOR



EXPLOSION TRENCH LOG

PROJECT: OROVILLE AREA LINEAMENT INVESTIGATION

TRENCH: II BEARING OF TRENCH: N 72° W

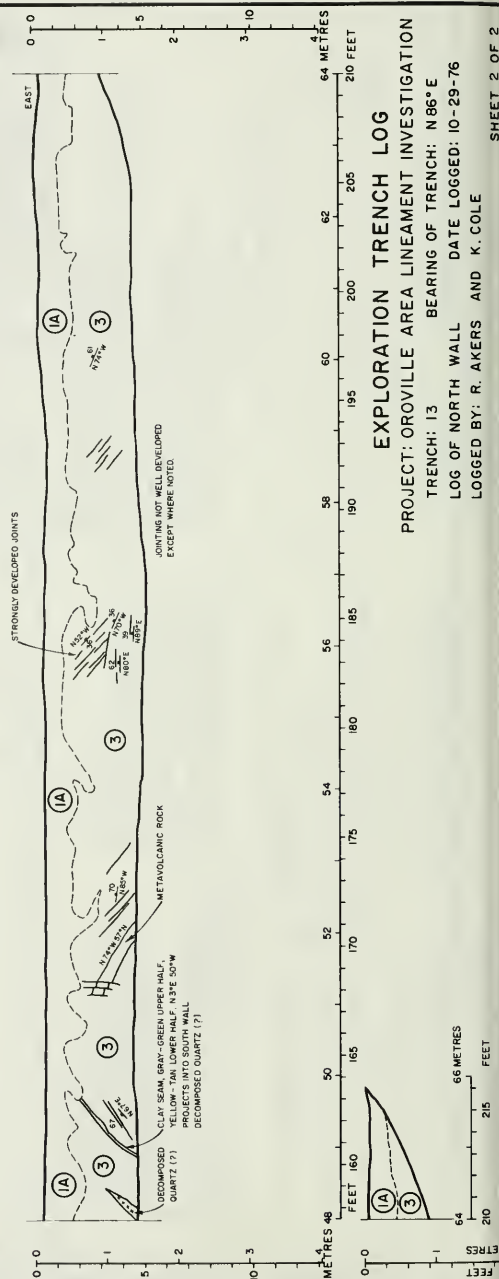
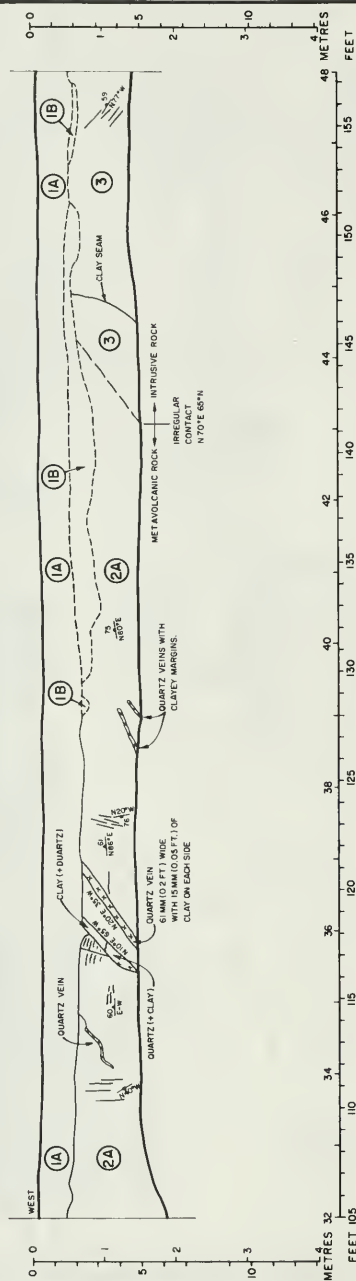
LOG OF NORTH WALL DATE LOGGED: 5-27-76

LOGGED BY: R. AKERS AND K. COLE

SHEET 1 OF 1



- (1) COLLUVIUM RED-BROWN SILT (M.L.), SOIL PROFILE ABSENT
- (2A) METAVOLCANIC ROCK: BLUE-GRAY TO BLUE TO BROWN, MODERATELY FRACTURED, MODERATELY TO STRONGLY WEATHERED.
- (2B) METAVOLCANIC ROCK: ZONE OF INTENSE FOLIATION.



EXPLORATION TRENCH LOG

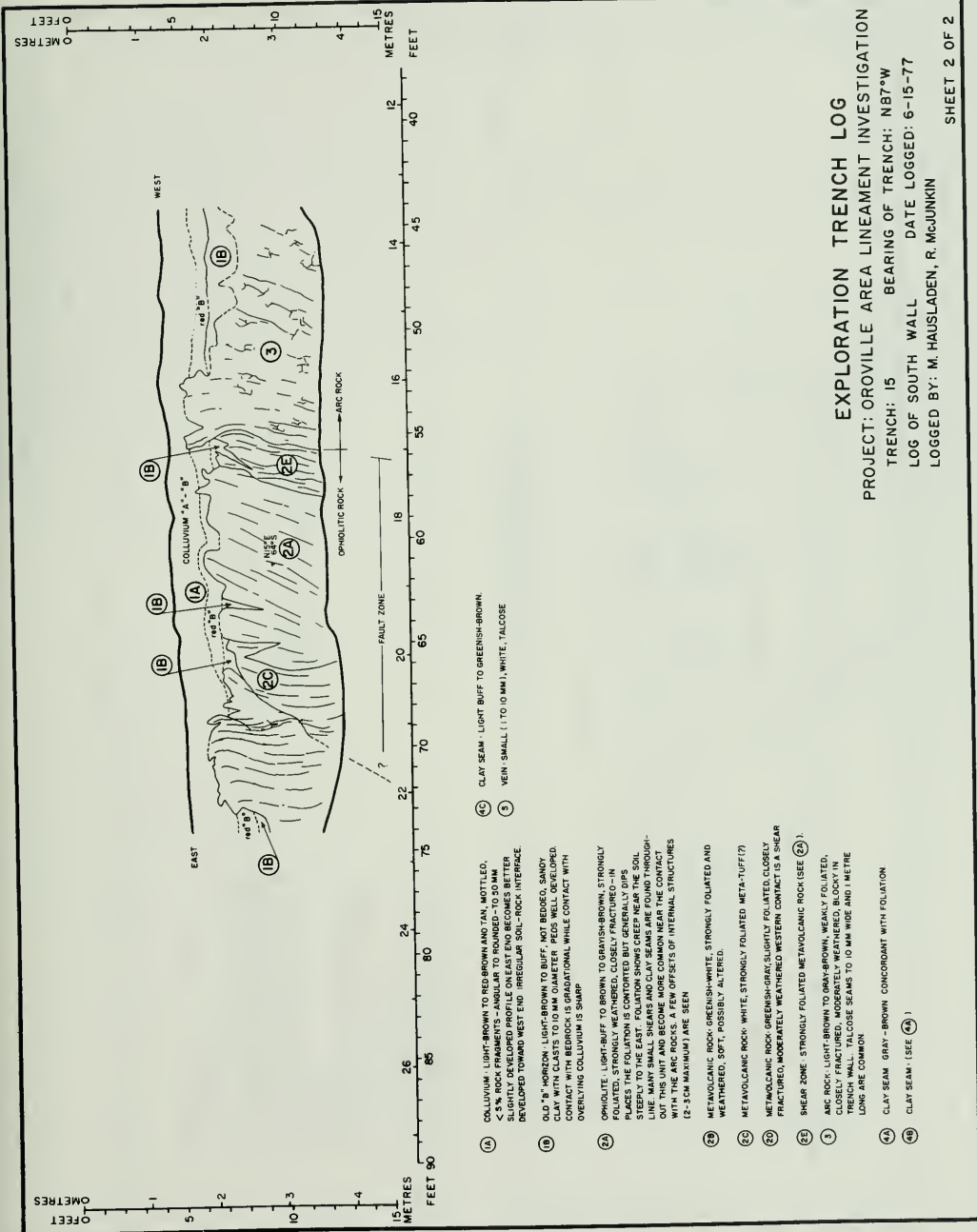
PROJECT: OROVILLE AREA LINEAMENT INVESTIGATION

TRENCH: 13 BEARING OF TRENCH: N 86° E

LOG OF NORTH WALL DATE LOGGED: 10-29-76

LOGGED BY: R. AKERS AND K. COLE

SHEET 2 OF 2



EXPLORATION TRENCH LOG

PROJECT: OROVILLE AREA LINEAMENT INVESTIGATION

TRENCH: 15 BEARING OF TRENCH: N87°W

LOG OF SOUTH WALL DATE LOGGED: 6-15-77

LOGGED BY: M. HAUSLADEN, R. MCJUNKIN

SHEET 2 OF 2

CHAPTER III SEISMOLOGY

Introduction

Bulletin 203, April 1977, reported earthquakes, Richter magnitude 2.5 and greater, of the Oroville sequence through March 1976. This report will present the data recorded from June 1, 1975, through May 31, 1978, Richter magnitude 1.0 and greater.

Figure 58 shows the combined DWR-USGS telemetered seismographic network as it was variously composed throughout the sequence. Since about August 1976, when the USGS network was considerably reduced, the network has remained essentially unchanged. The table in Figure 58 shows the DWR network as it was variously composed from June 1, 1975 to May 31, 1978.

Data

Epicenters of earthquakes of magnitude 1.0 and greater for 1975 and 1976-78 are plotted in Figures 59 and 63, respectively. The hypocenters are listed on Tables 3 and 4. The aftershock zone, as shown in Figures 59 and 63, is partitioned into north, middle, and south sections. The hypocenters from each section are projected onto a vertical east-west striking plane, shown in Figures 60 through 62 and 64 through 66. Figure 67 is a vertical cross-section of the middle section for events recorded between August 2 at 1400 GMT and December 31, 1975.

Surface cracking was observed on Cleveland Hill to the east of the aftershock zone soon after the mainshock. The vertical cross-sections show that the fault plane surfaces near the cracks. The fault was subsequently named the Cleveland Hill Fault. The Department recorded network as recounted in the table on Figure 58, was composed of MGL, ORV, KPK, DOG, BUT and SUT, from July 1975 into

January 1976. Note that OSTI and OHON were added in November 1975. From January 1976 onward, the network included additional stations PAM, and OCAM.

Consequently, to make the Department network of August through December 1975 more nearly equivalent to the network of 1976 onward, the U. S. Geological Survey in Menlo Park supplied the P-times for aftershocks from Woodward-Clyde portable stations WC1, WC2, WC3, and WC4 and USGS Stations OCAM, OHON, OSTI, OWYN and ORAT. Times from Woodward-Clyde stations were available for events recorded on August 2 at 1454 GMT through August 12 at 1945 GMT. Times were available for the event recorded August 5 at 0228 GMT through December 1975.

Installation of the USGS network stations began soon after the August 1 mainshock, and recording was initially accomplished on magnetic tape beginning August 5, 1975. By August 16, 1975, a telemetry link to Menlo Park was established so that their stations were thereafter recorded on 16 mm. film. Woodward-Clyde installed four portable stations in the aftershock area beginning August 2, 1975.

Hypocenters were determined by the USGS Hypo 71 hypocenter program (1) * and the Byerly Crustal model. Station corrections were determined by averaging the hypocenter residuals of a number of well recorded events.

Magnitudes were determined by two methods:

1. The duration method: Magnitude-duration curves were plotted for the Oroville and Jamestown (not shown in Figure 58) short-period vertical seismometers. The elapsed time from the initial seismic P-wave

* (1) Number refers to reference listed at the end of the Chapter.

onset to the time the maximum seismic trace amplitude falls consistently below an arbitrary level is plotted against "known" earthquake magnitudes. This provides a plot whereby the magnitudes of subsequent events are estimated (2).

2. The equivalent Wood-Anderson seismograph magnitude estimate is calculated from the Oroville east-west short-period seismometer response (3).

Figure 68 is a time-plot of the Oroville water surface elevation and the number of aftershocks by month.

Results

Inspection of the epicentral plots Figures 59 and 63 indicates a north-south alignment of aftershocks confined within a rectangle about 15 kilometres north-south and 8 kilometres east-west. Inspection of Table 3 shows that on August 2 the main aftershock activity began to shift to the north and south sections of the apparent fault rupture. After December 31, 1975, about 52 percent of the aftershocks listed in Table 4 occur in the south section (Figure 63) and about 70 percent east of the 121.5 meridian.

A 60° angle to the west has been drawn through the vertical cross sectional plots in Figures 60, 61, 64, and 65 to indicate the approximate dip of the fault break in the north and middle portions of the rupture zone. In Figure 61 at least two alignments seem evident, one near 60° and another about 35°. Most of the hypocenters in Figures 60 through 62 were determined before good depth control was available. Therefore, Figure 67 was plotted beginning with events on August 2 when the first Woodward-Clyde station was available. A near 60° alignment is evident in that figure. In Figure 62 no clear alignment is evident.

Figures 64 and 65 show single alignments near 60° in the north and middle sections.

Figure 66, as in Figure 62, shows no clear alignment of hypocenters and probably indicates more than one rupture plane.

Discussion

As in the seven years before the August 1 1975, Oroville earthquake, subsequent Lake Oroville water surface fluctuations do not appear to affect nearby seismic activity. The rapid filling of the reservoir this past winter and spring (1977-1978) does not, at this time, appear to have influenced the slow decline of the seismicity rate in the aftershock zone.

The near 60° dip of the Cleveland Hill fault plane evident in the north and middle cross-sectional plots is in agreement with that reported by others (Lahr, et al) (4). Savage, et al (5) report that the results of the repeat level survey profiles across the aftershock zone before and after August 1 are consistent with about 0.36 m of normal slip on the fault plane delineated by the aftershock sequence.

Conclusions

Since August 1, 1975, a correlation is not indicated between the Lake Oroville water surface variations and the rate of occurrence of Oroville aftershocks.

Within the boundary of the aftershock zone north of 39°26'N latitude, vertical cross-sectional plots indicate that the Cleveland Hill Fault is a single, well defined break, dipping to the west at about 60° and with a near north-south strike. Vertical cross sectional plots south of 39°26'N indicate that the fault breaks along more than one plane.

STATIONS RECORDED BY DWR
DURING THE OROVILLE SEQUENCE

STATION	DATE ON	DATE OFF
ORV	1963	PRESENT
KPK	1969	PRESENT
MGL	1966	PRESENT
PAM	76/1/20	PRESENT
BUT	75/7/1	PRESENT
SUT	75/7/1	76/12/12
DOG	75/8/2	76/8/6
OCAM	76/1/16	76/9/1
OHON	75/11/5	PRESENT
OSUT	76/9/1	PRESENT
OSTI	75/11/5	PRESENT

□ TELEMETERED STATION

△ PORTABLE STATION

OBL0 "O" PREFIX DESIGNATES USGS STATION
THE USGS STATIONS WERE ESTABLISHED
ON AUG. 6, 1975 OR SHORTLY THEREAFTER.
UNDERLINE DESIGNATES STATIONS CON-
TINUING IN OPERATION AFTER AUG. 1, 1976

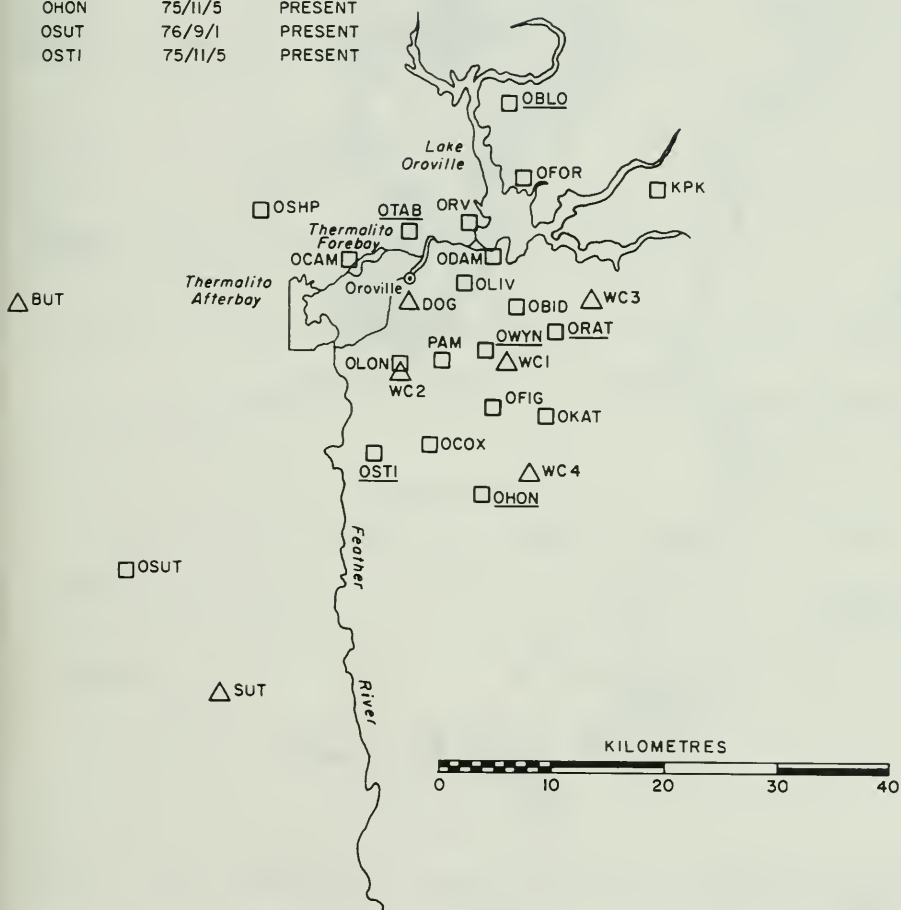


Figure 58. DWR-USGS Oroville Sensitive Seismographic Network

NORTH VERTICAL X-SECTION
EVENTS NORTH OF AND INCLUDING 39° 29.5' N

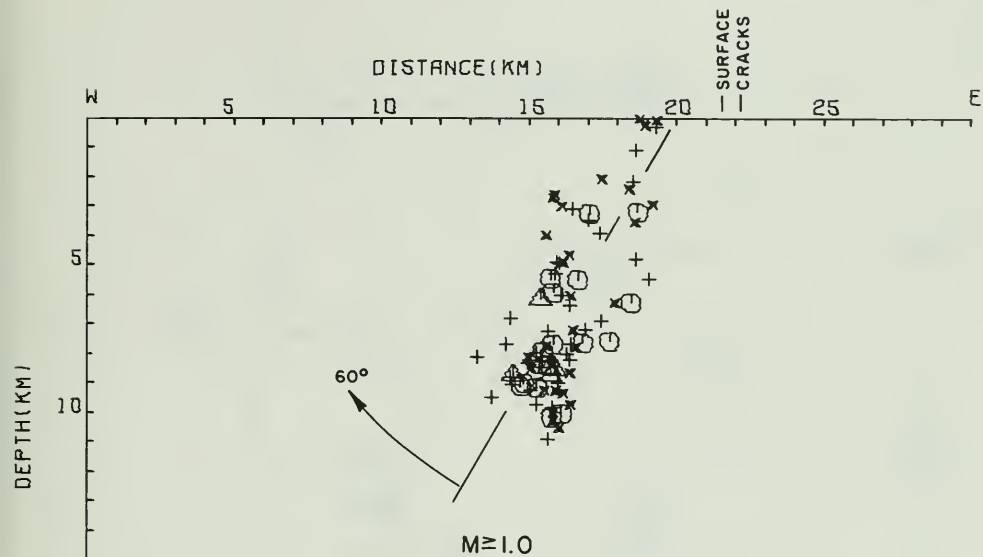


Figure 60. 1975 Oroville Earthquake Hypocenters (North Vertical Cross Section)

MIDDLE VERTICAL X-SECTION
EVENTS BETWEEN 39° 29.5' N AND INCLUDING 39° 26.0' N

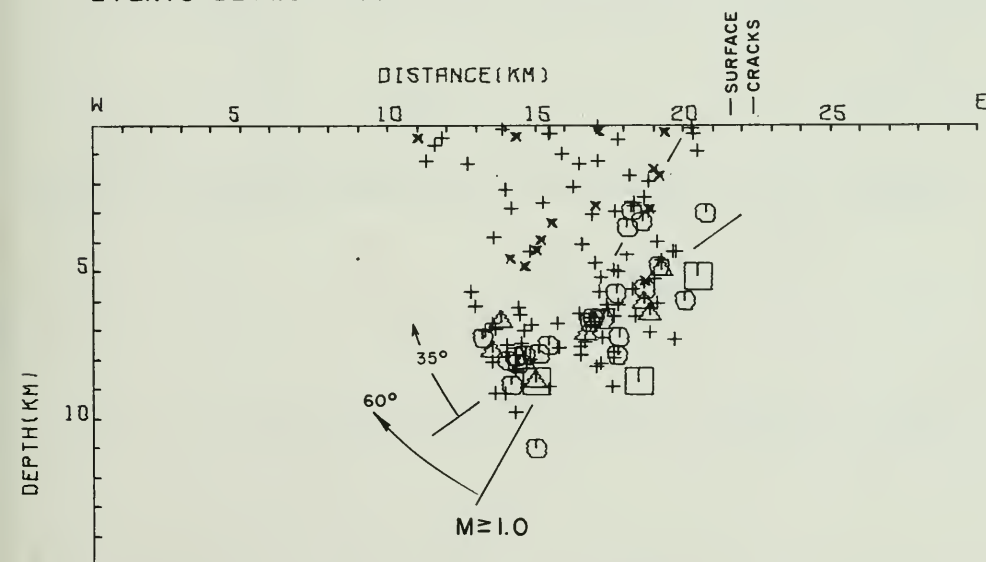


Figure 61. 1975 Oroville Earthquake Hypocenters (Middle Vertical Cross Section)

SOUTH VERTICAL X-SECTION
EVENTS SOUTH OF 39° 26.0' N

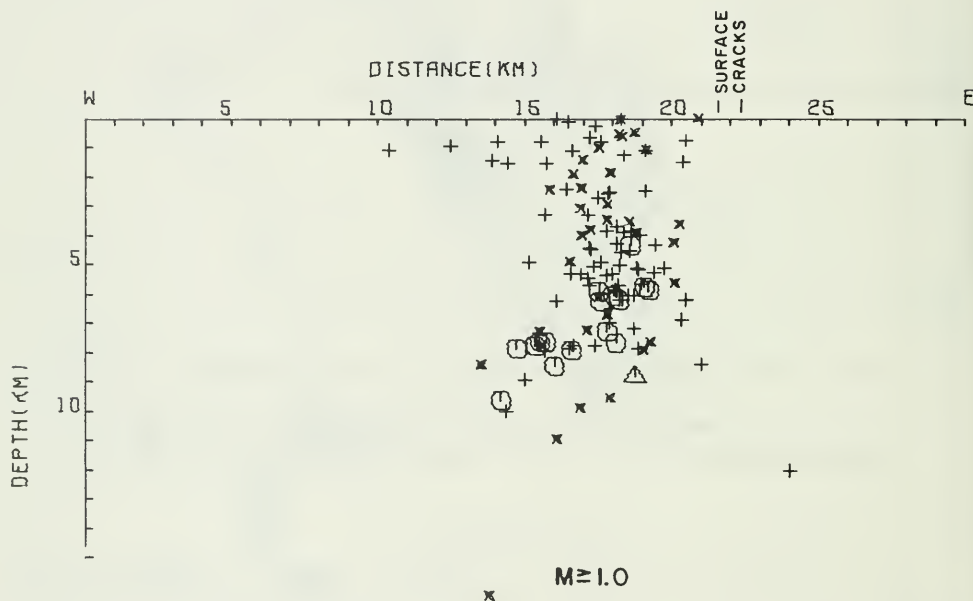


Figure 62. 1975 Oroville Earthquake Hypocenters (South Vertical Cross Section)

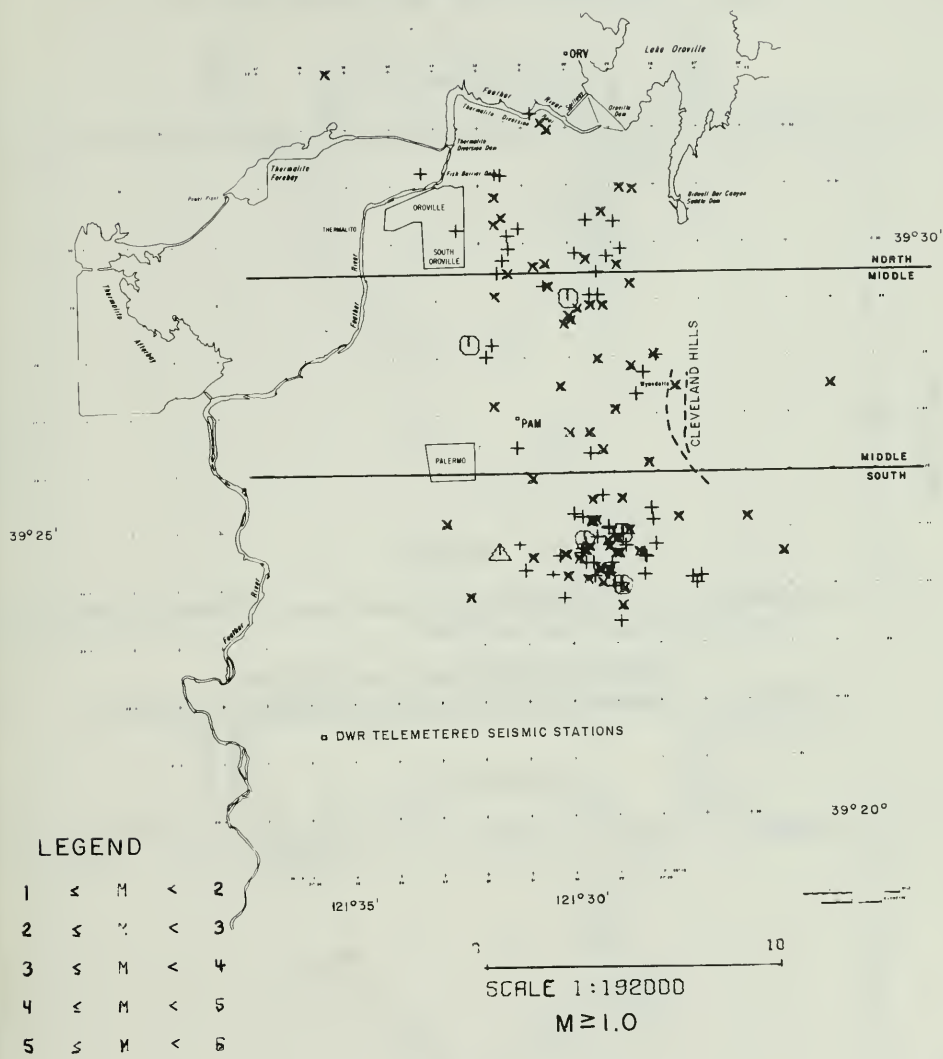


Figure 63. Oroville Earthquake Epicenters (January 1, 1976-May 31, 1978)

NORTH VERTICAL X-SECTION
EVENTS NORTH OF AND INCLUDING 39° 29.5' N

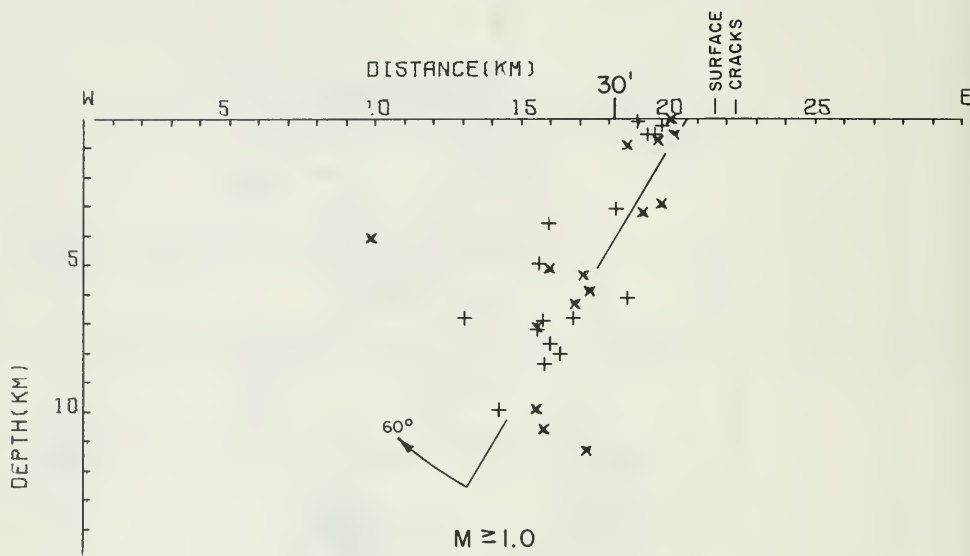


Figure 64. Oroville Earthquake Hypocenters, 1976-May 31, 1978
(North Vertical Cross Section)

MIDDLE VERTICAL X-SECTION
EVENTS BETWEEN 39° 29.5' N AND INCLUDING 39° 26.0' N

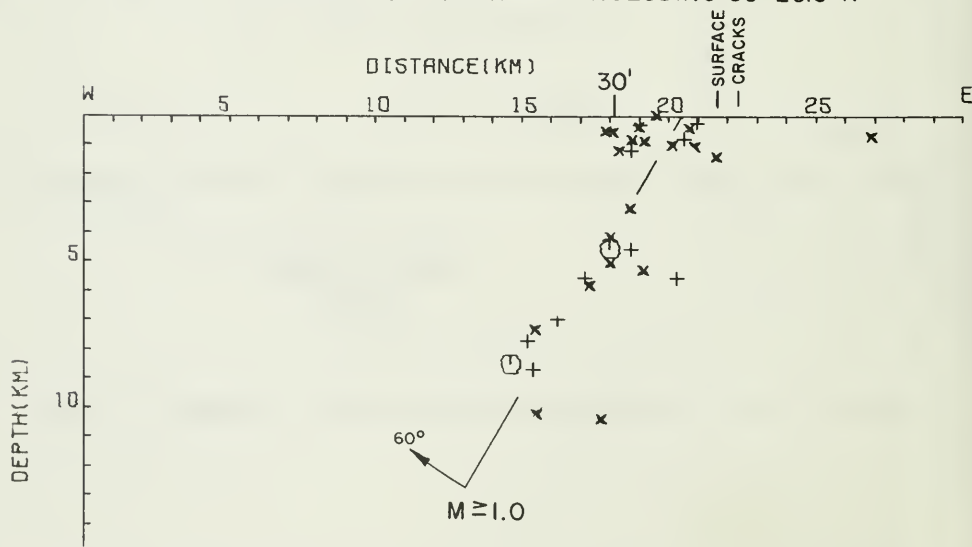


Figure 65. Oroville Earthquake Hypocenters, 1976-May 31, 1978 (Middle Vertical Cross Section)

SOUTH VERTICAL X-SECTION
EVENTS SOUTH OF 39° 26.0' N

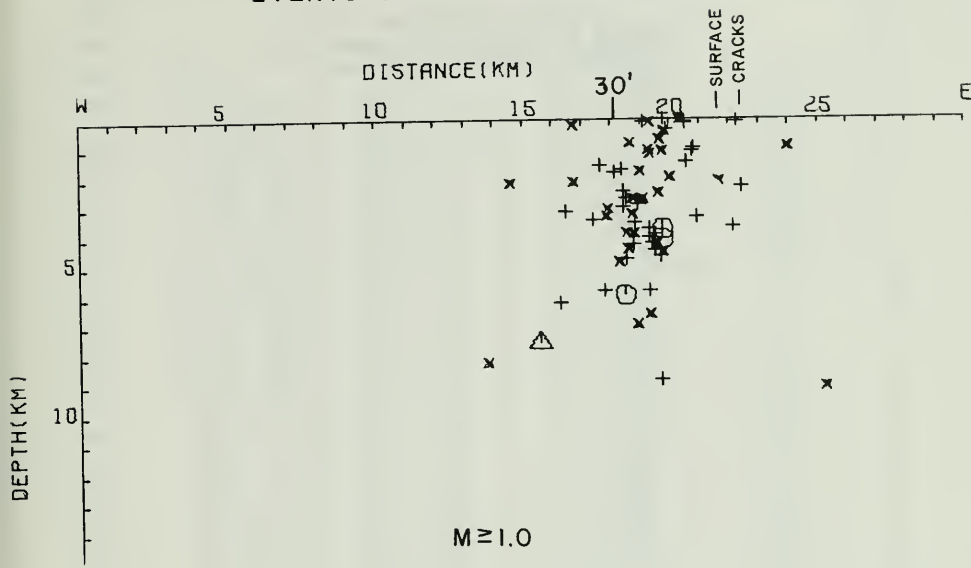


Figure 66. Oroville Earthquake Hypocenters, 1976-May 31, 1978 (South Vertical Cross Section)

MIDDLE VERTICAL X-SECTION
EVENTS BETWEEN 39° 29.5' N AND INCLUDING 39° 26.0' N

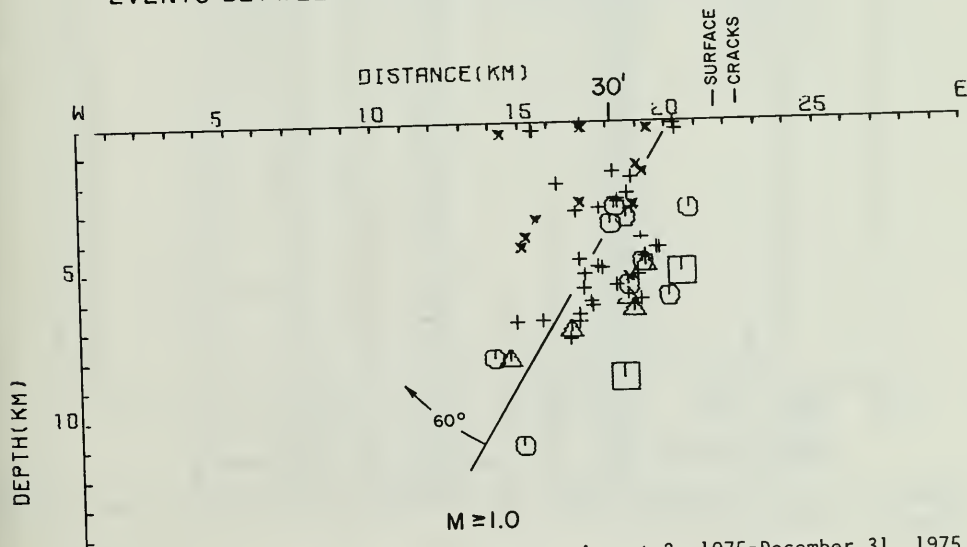


Figure 67. Oroville Earthquake Hypocenters, August 2, 1975-December 31, 1975 (Middle Vertical Cross Section)

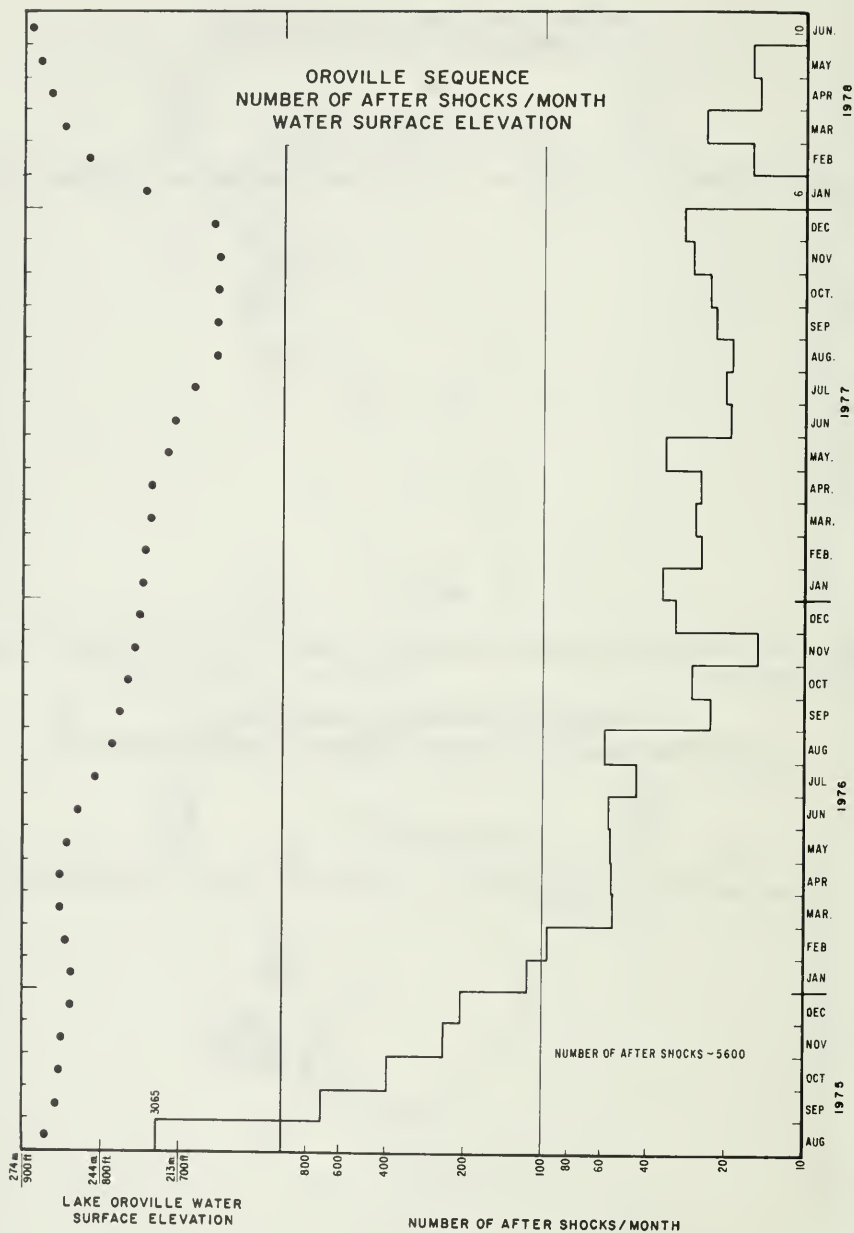


Figure 68. Oroville Sequence, Number of Aftershocks/Month, Water Surface Elevation, (August 1975-June 1978)

TABLE 3. EARTHQUAKE EPICENTERS, JUNE 1975-DECEMBER 1975

EARTHQUAKES WITHIN 15.0 KMS OF OROVILLE MAIN SHOCK 6/1/75-12/31/75									
YR MO DY		(GMT) HR MN SEC	LATITUDE	LONGITUDE	DEPTH	MAG	Q	QUADRANGLE	DIST (KMS)
75/	6/28	1411953.4	39.467	121.538	7.8	3.5	B	PALERMO	2.9
75/	6/28	1413129.9	39.465	121.540	6.5	2.3	C	PALERMO	2.7
75/	6/28	14130140.4	39.466	121.544	7.7	2.1	C	PALERMO	2.9
75/	6/28	14116119.2	39.475	121.540	7.4	2.6	O	PALERMO	3.8
75/	6/29	20120140.0	39.459	121.544	4.6	1.9	C	PALERMO	2.1
75/	7/5	18119116.1	39.460	121.538	4.8	1.0	C	PALERMO	2.1
75/	7/6	111112.4	39.482	121.538	8.3	2.2	B	PALERMO	1.3
75/	7/6	1312158.9	39.456	121.516	4.1	2.8	C	PALERMO	2.3
75/	7/20	01281.9.5	39.461	121.542	6.3	2.5	C	PALERMO	2.3
75/	7/20	101352.4	39.452	121.540	7.1	2.1	C	PALERMO	2.5
75/	7/21	1417137.4	39.470	121.525	7.6	2.5	C	PALERMO	3.3
75/	8/1	15145137.6	39.454	121.542	7.9	3.8	B	PALERMO	1.6
75/	8/1	18127117.6	39.439	121.547	6.7	4.7	B	PALERMO	1.2
75/	8/1	17126149.9	39.463	121.543	8.9	3.0	B	PALERMO	2.5
75/	8/1	18117122.5	39.438	121.577	1.2	2.2	C	PALERMO	3.7
75/	8/1	19135143.0	39.454	121.539	7.0	2.2	C	PALERMO	1.5
75/	8/1	201201.4.5	39.441	121.534	6.7	2.5	B	PALERMO	4.0
75/	8/1	20120112.6	39.441	121.534	8.7	5.7	B	PALERMO	4.0
75/	8/1	20125112.6	39.441	121.534	8.7	4.7	B	PALERMO	4.0
75/	8/1	22120912.6	39.441	121.534	8.7	4.6	B	PALERMO	2.0
75/	8/1	20132139.6	39.443	121.513	4.7	3.0	B	PALERMO	1.8
75/	8/1	20137139.6	39.443	121.513	6.7	3.5	B	PALERMO	1.8
75/	8/1	20140128.2	39.447	121.542	0.8	2.5	B	PALERMO	1.9
75/	8/1	201411.4.4	39.445	121.517	6.4	2.5	C	PALERMO	1.5
75/	8/1	20143123.1	39.434	121.498	4.4	2.5	C	BANGOR	3.2
75/	8/1	20145118.2	39.463	121.501	7.2	3.0	B	PALERMO	3.7
75/	8/1	20148118.2	39.463	121.501	7.2	3.8	B	PALERMO	3.7
75/	8/1	20154154.5	39.424	121.541	1.5	2.5	O	PALERMO	2.0
75/	8/1	2111.31.3.2	39.463	121.551	6.8	2.6	B	PALERMO	2.6
75/	8/1	21113158.6	39.448	121.512	6.6	3.0	B	PALERMO	2.4
75/	8/1	211.91.6.4	39.478	121.542	8.2	2.6	B	PALERMO	4.2
75/	8/1	21110115.6	39.443	121.516	7.8	2.8	B	PALERMO	1.5
75/	8/1	21111132.1	39.410	121.470	7	2.8	D	BANGOR	6.5
75/	8/1	21116123.6	39.440	121.541	8.1	3.2	B	PALERMO	4.2
75/	8/1	21119124.5	39.438	121.546	2.2	2.2	C	PALERMO	1.1
75/	8/1	211201.7.6	39.436	121.508	8.1	2.8	B	PALERMO	2.3
75/	8/1	21121150.5	39.455	121.551	7.7	2.8	C	PALERMO	4.3
75/	8/1	21125158.0	39.479	121.529	7.5	3.3	B	PALERMO	4.3
75/	8/1	21129123.9	39.457	121.555	7.2	3.6	B	PALERMO	2.5
75/	8/1	21130919.4	39.453	121.508	8.6	2.7	B	PALERMO	1.4
75/	8/1	21154135.5	39.416	121.508	6	2.2	D	PALERMO	3.8
75/	8/1	21158114.1	39.435	121.512	6.7	2.0	B	PALERMO	2.0
75/	8/1	221.4155.8	39.433	121.538	7.8	3.4	B	PALERMO	1.9
75/	8/1	221.711.6	39.445	121.571	1.4	2.0	C	PALERMO	3.2
75/	8/1	221.81.4.2	39.490	121.516	7.5	2.5	A	PALERMO	5.7
75/	8/1	221111.4.5	39.447	121.502	7.8	3.1	B	PALERMO	2.8
75/	8/1	221155.6	39.453	121.524	0	2.1	D	PALERMO	1.6
75/	8/1	22115142.5	39.450	121.580	4.5	1.8	D	PALERMO	4.1
75/	8/1	22123143.6	39.455	121.526	7.6	3.2	B	PALERMO	1.9
75/	8/1	221231.4.4	39.436	121.508	7.1	2.5	C	PALERMO	2.3
75/	8/1	22136115.8	39.431	121.486	1.1	2.3	C	BANGOR	4.3
75/	8/1	22150120.3	39.436	121.503	6.5	2.7	C	PALERMO	2.7
75/	8/1	22152156.6	39.435	121.551	8.1	2.6	C	PALERMO	1.6
75/	8/1	231.4112.6	39.482	121.504	8.9	2.5	B	PALERMO	3.5
75/	8/1	23110143.6	39.476	121.550	7.0	2.5	C	PALERMO	4.1
75/	8/1	23114141.4	39.508	121.549	7.5	2.0	C	OROVILLE	7.6
75/	8/1	23131132.6	39.448	121.541	6.2	2.5	B	PALERMO	4.8
75/	8/1	23144140.8	39.491	121.533	7.8	3.4	A	PALERMO	5.6
75/	8/1	23150153.5	39.468	121.545	7.5	2.4	C	PALERMO	3.1
75/	8/1	23151148.6	39.421	121.564	8	2.2	D	PALERMO	3.5
75/	8/2	01.2144.8	39.420	121.479	5.1	2.5	C	BANGOR	5.3
75/	8/2	01.3132.2	39.461	121.558	6.2	2.4	C	PALERMO	3.0
75/	8/2	01.9159.8	39.430	121.584	6.9	2.3	B	PALERMO	2.8
75/	8/2	0113128.1	39.434	121.512	6.6	2.6	C	PALERMO	2.0
75/	8/2	0123152.9	39.464	121.517	1.3	2.0	C	PALERMO	2.9
75/	8/2	01351.4.6	39.433	121.501	6.1	2.6	C	PALERMO	2.9
75/	8/2	01381.11.0	39.461	121.547	1.4	2.2	C	PALERMO	3.2
75/	8/2	0152148.3	39.504	121.528	7.9	3.8	A	OROVILLE	7.0
75/	8/2	0158155.8	39.474	121.550	9.1	2.6	C	PALERMO	3.9
75/	8/2	1131121.6	39.463	121.518	7.0	2.1	D	PALERMO	1.6
75/	8/2	1141137.0	39.447	121.554	7.0	2.3	C	PALERMO	1.8
75/	8/2	1144112.4	39.491	121.529	8.9	2.2	A	PALERMO	5.6
75/	8/2	21271.4.9	39.438	121.563	7.9	2.0	B	PALERMO	2.7
75/	8/2	2131150.7	39.468	121.515	1.1	2.3	C	PALERMO	3.2
75/	8/2	2139149.1	39.473	121.509	1.2	2.3	O	PALERMO	4.2
75/	8/2	3115121.2	39.461	121.479	7.3	2.8	D	BANGOR	5.2
75/	8/2	31471.7.8	39.428	121.517	1.1	2.3	C	PALERMO	2.1
75/	8/2	3151134.7	39.422	121.429	12.0	2.2	D	BANGOR	9.3
75/	8/2	41.9113.4	39.414	121.521	6	2.0	C	PALERMO	3.2
75/	8/2	41161.1.1	39.487	121.561	7.3	2.0	D	PALERMO	5.6
75/	8/2	4123113.7	39.442	121.574	7	2.0	D	PALERMO	3.4
75/	8/2	4143135.6	39.462	121.489	7.0	2.8	B	BANGOR	4.5
75/	8/2	4149122.3	39.435	121.523	7.9	2.9	B	PALERMO	2.7
75/	8/2	51331.5.6	39.483	121.551	3.8	2.2	D	PALERMO	4.9
75/	8/2	5147112.5	39.426	121.588	1.1	2.0	D	PALERMO	4.9
75/	8/2	5148138.4	39.489	121.528	6	2.2	C	PALERMO	3.6
75/	8/2	5152115.4	39.422	121.505	2.2	2.2	C	PALERMO	3.6
75/	8/2	6130113.1	39.432	121.498	5.9	2.0	C	BANGOR	3.3
75/	8/2	613156.9	39.448	121.502	6.7	3.2	B	PALERMO	2.8
75/	8/2	61321.1.1	39.434	121.495	6.5	2.2	C	BANGOR	3.6
75/	8/2	101.7155.6	39.457	121.544	9.1	2.8	B	PALERMO	2.0
75/	8/2	10111153.5	39.495	121.525	7.7	3.1	A	PALERMO	6.1
75/	8/2	10148159.9	39.427	121.485	5.8	3.3	B	BANGOR	4.5
75/	8/2	1115115.5	39.412	121.526	1.5	2.0	D	PALERMO	5.4
75/	8/2	11151150.6	39.485	121.507	6.8	3.4	B	PALERMO	5.4

TABLE 3. EARTHQUAKE EPICENTERS, JUNE 1975-DECEMBER 1975 (Continued)

EARTHQUAKES WITHIN 15.0 KMS OF OROVILLE MAIN SHOCK 6/1/75-12/31/75										
YR	MO	DAY	TIME HR MN SEC	LATITUDE	LONGITUDE	DEPTH	MAG	Q	QUADRANGLE	DIST (KMS)
75	6	2	12129121.8	39.489	121.547	2	2.0	C	PALERMO	3.3
75	6	2	13150142.5	39.485	121.531	2.7	2.2	C	PALERMO	4.7
75	6	2	1412154.4	39.454	121.478	9	2.0	O	BANGOR	5.9
75	6	2	1413110.0	39.483	121.502	5	2.4	C	PALERMO	3.7
75	6	2	14144138.5	39.424	121.504	6.2	3.2	B	PALERMO	3.2
75	6	2	14154135.3	39.435	121.509	5.7	2.2	B	PALERMO	3.0
75	6	2	15128155.1	39.433	121.496	6.2	2.0	B	PALERMO	3.4
75	6	2	15134149.5	39.451	121.502	5.0	2.2	B	PALERMO	3.0
75	6	2	15143140.1	39.433	121.508	4.5	2.0	C	PALERMO	2.4
75	6	2	161111.4	39.455	121.526	6.7	2.1	B	PALERMO	3.2
75	6	2	16151145.0	39.427	121.501	7.3	3.7	A	PALERMO	3.0
75	6	2	17124129.1	39.482	121.489	6.5	4.3	B	BANGOR	6.0
75	6	2	17143124.0	39.485	121.491	6.1	4.0	B	BANGOR	6.1
75	6	2	19121555.2	39.475	121.496	5.6	2.6	A	BANGOR	5.0
75	6	2	191536.7	39.454	121.545	8.0	3.1	A	PALERMO	1.7
75	6	2	20114120.4	39.450	121.535	5.6	2.2	B	PALERMO	1.0
75	6	2	20122116.2	39.450	121.470	4.1	5.1	A	BANGOR	5.6
75	6	2	2013011.4	39.434	121.472	4.3	2.4	C	BANGOR	5.4
75	6	2	20135140.4	39.477	121.491	4.6	3.9	A	BANGOR	3.2
75	6	2	20149144.4	39.459	121.506	4.3	2.1	B	PALERMO	5.1
75	6	2	20150155.5	39.437	121.475	6.0	3.6	B	BANGOR	5.1
75	6	2	20159155.6	39.449	121.493	4.7	5.2	B	BANGOR	4.6
75	6	2	21111144.3	39.458	121.486	4.8	3.4	A	BANGOR	3.3
75	6	2	21131156.3	39.439	121.495	2.8	2.3	B	BANGOR	3.2
75	6	2	221351.8	39.415	121.483	5.3	2.9	B	BANGOR	6.5
75	6	2	23110123.8	39.469	121.489	3.0	2.2	B	BANGOR	3.2
75	6	2	23143121.6	39.444	121.487	1.7	2.2	B	BANGOR	5.7
75	6	3	11131.5	39.492	121.526	4.5	4.5	A	PALERMO	5.2
75	6	3	11191.3	39.486	121.515	7.4	2.4	B	PALERMO	5.5
75	6	3	1240129.4	39.487	121.480	4.3	2.4	B	BANGOR	4.9
75	6	3	21471.8	39.482	121.514	7.1	4.1	A	PALERMO	2.4
75	6	3	5119145.5	39.421	121.489	5.1	2.3	A	BANGOR	5.7
75	6	3	9110122.6	39.465	121.499	4.3	2.1	B	BANGOR	2.7
75	6	3	9144139.7	39.442	121.503	4.9	2.3	B	PALERMO	2.7
75	6	3	1012156.6	39.407	121.502	3.8	2.1	B	PALERMO	2.0
75	6	3	11120122.8	39.438	121.511	4.7	2.5	B	PALERMO	2.0
75	6	3	1513117.8	39.410	121.498	5.6	2.5	A	BANGOR	5.6
75	6	3	1617146.8	39.485	121.485	4.6	2.4	A	BANGOR	5.0
75	6	3	16154156.7	39.431	121.534	8.9	2.6	B	PALERMO	3.1
75	6	3	17140111.8	39.422	121.508	5.7	2.0	C	PALERMO	3.9
75	6	3	17147159.4	39.420	121.497	5.7	2.5	A	BANGOR	4.4
75	6	3	19154112.0	39.412	121.499	5.3	2.0	B	BANGOR	4.6
75	6	3	20136129.2	39.481	121.487	5.2	2.8	B	BANGOR	4.0
75	6	3	20153144.2	39.426	121.492	3.8	2.2	B	BANGOR	6.1
75	6	3	231491.3	39.497	121.517	7.7	2.8	A	PALERMO	4.0
75	6	4	3131.6	39.418	121.470	6.2	2.6	B	BANGOR	2.2
75	6	4	9147144.8	39.421	121.528	7.6	3.5	A	PALERMO	1.7
75	6	4	9154156.4	39.426	121.528	7.3	1.8	B	PALERMO	4.4
75	6	4	1112147.5	39.405	121.512	5.3	2.0	B	PALERMO	5.2
75	6	4	17110120.3	39.486	121.491	7.1	2.7	B	BANGOR	4.7
75	6	5	2128157.1	39.407	121.497	6.2	3.3	A	BANGOR	5.0
75	6	5	511130.6	39.431	121.527	7.7	3.6	A	PALERMO	1.2
75	6	5	9113131.8	39.413	121.508	6.1	1.8	B	PALERMO	3.5
75	6	5	1513155.7	39.422	121.501	6.7	1.8	A	PALERMO	3.5
75	6	5	20144124.4	39.429	121.537	7.9	3.2	B	PALERMO	1.3
75	6	5	23157131.1	39.496	121.534	8.3	2.8	B	PALERMO	6.1
75	6	6	3105129.9	39.495	121.540	8.7	4.7	A	PALERMO	6.1
75	6	6	418140.1	39.499	121.555	8.1	2.6	B	PALERMO	8.6
75	6	6	4129150.8	39.492	121.529	8.2	2.4	A	PALERMO	5.7
75	6	6	415517.5	39.492	121.531	6.2	2.0	A	PALERMO	5.7
75	6	6	814141.9	39.491	121.491	5.3	1.9	B	BANGOR	8.6
75	6	6	9149133.7	39.493	121.541	9.0	2.7	B	PALERMO	5.8
75	6	6	1016143.6	39.504	121.533	8.5	1.9	A	OROVILLE	7.0
75	6	6	10135122.8	39.433	121.505	6.1	1.8	A	PALERMO	2.7
75	6	6	1313126.3	39.502	121.533	9.3	2.9	A	OROVILLE	6.7
75	6	6	1319130.3	39.503	121.523	9.0	2.5	A	OROVILLE	5.9
75	6	6	16125147.2	39.406	121.487	5.7	3.1	A	BANGOR	7.7
75	6	6	18141151.8	39.495	121.537	9.1	3.6	A	PALERMO	3.0
75	6	6	19142148.3	39.504	121.543	7.7	2.8	B	OROVILLE	7.1
75	6	6	2110136.8	39.410	121.522	8.4	3.0	A	PALERMO	6.0
75	6	7	5115148.3	39.400	121.489	7.8	2.3	B	BANGOR	7.8
75	6	7	14120145.1	39.509	121.541	8.6	2.9	A	OROVILLE	7.6
75	6	7	1912155.8	39.504	121.534	8.2	2.4	A	OROVILLE	7.6
75	6	7	2015139.4	39.411	121.482	4.3	2.8	A	BANGOR	5.6
75	6	7	2013120.0	39.503	121.531	9.2	3.1	A	OROVILLE	8.9
75	6	8	0153122.0	39.415	121.526	7.9	2.3	B	PALERMO	6.2
75	6	8	710150.0	39.496	121.524	8.5	4.6	B	PALERMO	5.1
75	6	8	13137153.7	39.500	121.502	7.6	3.2	B	PALERMO	7.1
75	6	8	151501.6	39.488	121.486	6.1	2.4	B	BANGOR	5.1
75	6	8	1913127.3	39.410	121.498	7.6	3.1	A	BANGOR	7.8
75	6	9	7138147.1	39.486	121.499	6.0	3.0	A	BANGOR	5.1
75	6	9	1211138.0	39.510	121.518	6.2	2.4	B	OROVILLE	6.9
75	6	9	20145131.0	39.413	121.489	5.1	2.8	A	BANGOR	2.9
75	6	10	14135125.4	39.406	121.498	4.3	2.2	B	BANGOR	5.0
75	6	10	21125144.8	39.439	121.510	7.1	2.1	C	PALERMO	2.1
75	6	11	2140119.5	39.480	121.467	3.0	3.0	A	BANGOR	6.1
75	6	11	011136.3	39.459	121.484	5.0	4.3	A	BANGOR	5.4
75	6	11	6134150.8	39.423	121.509	5.4	2.8	A	PALERMO	2.9
75	6	11	7141138.8	39.413	121.488	5.6	2.7	A	BANGOR	5.1
75	6	11	151510.5	39.588	121.536	9.0	3.6	A	OROVILLE	5.9
75	6	12	115121.4	39.411	121.492	4.5	2.3	A	BANGOR	4.9
75	6	12	41291.2	39.441	121.486	6.0	2.8	B	BANGOR	4.8
75	6	12	11145121.4	39.408	121.490	3.7	2.1	A	BANGOR	2.6
75	6	12	11150151.9	39.459	121.534	11.0	3.0	B	PALERMO	6.6
75	6	12	181421.8	39.519	121.529	8.4	2.9	B	OROVILLE	2.0
75	6	12	19145112.1	39.439	121.510	6.6	2.7	A	PALERMO	2.1
75	6	16	514111.4	39.415	121.496	4.5	2.2	B	BANGOR	4.4
75	6	16	51481.9	39.471	121.538	8.1	4.0	A	PALERMO	3.3

TABLE 3. EARTHQUAKE EPICENTERS, JUNE 1975-DECEMBER 1975 (Continued)

EARTHQUAKES WITHIN 15.0 KMS OF OROVILLE MAIN SHOCK 6/1/75-12/31/75									
YR MO D	IGMT HR MIN SEC	LATITUDE	LONGITUDE	DEPTH	MAG	Q	DIAGRAM	DIST (KMS)	
75/ 8/16	12123124.3	39.502	121.513	7.6	3.2	A	OROVILLE	7.0	
75/ 8/16	141 01 8.4	39.495	121.506	6.9	2.8	A	PALERMO	6.5	
75/ 8/16	141 9125.8	39.499	121.512	7.2	2.8	B	PALERMO	6.7	
75/ 8/18	3155153.2	39.408	121.506	7.7	2.9	A	PALERMO	4.4	
75/ 8/20	2110133.3	39.413	121.500	7.0	2.9	B	PALERMO	4.3	
75/ 8/21	191 0138.0	39.424	121.472	4.9	2.6	B	BANGOR	5.7	
75/ 8/23	18131153.0	39.436	121.494	6.3	3.1	A	BANGOR	7.0	
75/ 8/24	9110117.2	39.485	121.498	3.5	3.3	A	BANGOR	5.8	
75/ 8/24	9155157.2	39.503	121.492	4.8	2.1	B	OROVILLE OAM	7.8	
75/ 8/25	13135111.0	39.484	121.496	2.9	3.2	B	BANGOR	5.8	
75/ 8/25	19139143.9	39.472	121.519	2.1	2.0	B	PALERMO	3.6	
75/ 8/26	18127143.3	39.411	121.545	.8	2.7	C	PALERMO	3.4	
75/ 8/29	9145131.8	39.476	121.511	6.8	2.9	A	PALERMO	4.4	
75/ 8/29	9148126.5	39.484	121.529	3.3	2.9	B	PALERMO	2.6	
75/ 8/29	1411252.5	39.462	121.528	7.9	2.9	B	PALERMO	2.3	
75/ 8/31	0132114.4	39.408	121.500	6.5	2.6	B	BANGOR	4.7	
75/ 9/ 3	21120153.9	39.498	121.487	5.5	2.2	B	BANGOR	7.5	
75/ 9/ 4	11171 1.9	39.412	121.543	9.6	3.0	B	PALERMO	3.3	
75/ 9/ 4	15139125.6	39.506	121.518	6.4	2.1	A	OROVILLE	7.3	
75/ 9/ 4	161 3143.8	39.411	121.497	5.0	2.0	A	BANGOR	4.6	
75/ 9/ 5	211 1138.9	39.406	121.515	7.9	3.2	A	PALERMO	4.2	
75/ 9/ 6	11391 5.0	39.406	121.516	7.8	2.9	A	PALERMO	4.2	
75/ 9/ 6	9142138.0	39.414	121.493	6.0	2.5	A	BANGOR	4.6	
75/ 9/ 8	21110157.3	39.405	121.514	7.7	2.5	B	PALERMO	4.3	
75/ 9/ 7	0131130.1	39.559	121.531	9.7	2.3	C	OROVILLE	13.1	
75/ 9/ 7	0136111.9	39.427	121.563	.9	2.0	C	PALERMO	3.0	
75/ 9/ 7	121 7110.2	39.412	121.489	4.0	2.0	A	BANGOR	5.0	
75/ 9/10	12138130.9	39.518	121.526	5.5	3.2	B	OROVILLE	8.6	
75/ 9/10	1711013.5	39.517	121.524	6.4	2.5	A	OROVILLE	8.0	
75/ 9/10	171391 4.9	39.521	121.526	2.4	3.5	B	OROVILLE	8.9	
75/ 9/10	18150139.7	39.516	121.522	4.0	2.3	B	OROVILLE	8.4	
75/ 9/12	21 0148.0	39.511	121.491	3.2	3.5	B	OROVILLE OAM	4.3	
75/ 9/13	18127150.3	39.395	121.516	4.9	1.9	C	PALERMO	5.4	
75/ 9/15	14147111.4	39.409	121.521	6.2	2.7	B	PALERMO	3.7	
75/ 9/20	81531 9.9	39.503	121.506	3.9	2.0	B	OROVILLE	7.3	
75/ 9/20	12122135.2	39.411	121.500	1.8	1.6	A	BANGOR	4.5	
75/ 9/21	17149158.5	39.402	121.516	5.3	2.4	C	PALERMO	4.7	
75/ 9/22	121251 9.0	39.434	121.508	5.2	2.4	B	PALERMO	5.4	
75/ 9/25	13148123.1	39.425	121.495	1.9	2.0	A	BANGOR	4.9	
75/ 9/26	21311 7.0	39.494	121.526	4.8	4.0	B	PALERMO	2.9	
75/ 9/26	31 8132.7	39.488	121.527	3.3	1.7	B	PALERMO	5.2	
75/ 9/26	41152152.7	39.402	121.509	4.4	1.9	B	PALERMO	3.9	
75/ 9/26	8151 8.5	39.410	121.515	1.9	1.9	B	PALERMO	3.9	
75/ 9/26	9157115.9	39.424	121.505	5.9	3.2	B	PALERMO	3.2	
75/ 9/26	12149131.8	39.418	121.501	3.5	1.9	A	PALERMO	3.8	
75/ 9/27	2147110.3	39.392	121.495	6.2	2.8	B	BANGOR	7.9	
75/ 9/27	131 5151.1	39.504	121.492	1.1	2.5	B	OROVILLE OAM	8.0	
75/ 9/27	22134136.2	39.513	121.529	6.2	4.6	B	OROVILLE	8.4	
75/ 9/27	2214114.6	39.525	121.529	4.4	2.9	A	OROVILLE	9.0	
75/ 9/27	221481 6.7	39.524	121.525	10.3	1.3	A	OROVILLE	9.3	
75/ 9/27	22153144.9	39.516	121.524	9.3	1.5	A	OROVILLE	8.3	
75/ 9/27	22154126.3	39.527	121.522	10.5	1.6	A	OROVILLE	9.6	
75/ 9/27	231 4130.6	39.519	121.521	10.0	3.0	B	OROVILLE	8.6	
75/ 9/27	231281 4.7	39.515	121.525	10.2	3.0	A	OROVILLE	9.3	
75/ 9/27	231381 8.4	39.509	121.526	7.2	2.6	B	OROVILLE	7.6	
75/ 9/28	01 3149.5	39.520	121.525	9.8	1.8	B	OROVILLE	8.0	
75/ 9/28	0134123.4	39.515	121.525	10.0	1.5	A	OROVILLE	8.3	
75/ 9/28	1146157.3	39.508	121.519	4.7	1.8	B	OROVILLE	7.5	
75/ 9/28	4122115.7	39.523	121.527	13.9	2.0	A	OROVILLE	9.2	
75/ 9/28	91 51 2.0	39.502	121.520	9.3	1.7	A	OROVILLE	6.8	
75/ 9/28	9125137.4	39.415	121.506	4.2	2.2	B	PALERMO	3.8	
75/ 9/28	19159150.6	39.529	121.520	9.3	1.6	A	OROVILLE	9.8	
75/ 9/28	211 7114.7	39.529	121.524	5.9	3.4	B	OROVILLE	9.8	
75/ 9/29	21 3136.3	39.441	121.512	3.1	2.4	B	PALERMO	1.9	
75/ 9/29	101 9137.0	39.504	121.518	4.7	1.3	A	OROVILLE	7.1	
75/ 9/29	11151111.8	39.514	121.505	2.1	1.3	B	OROVILLE	8.4	
75/ 9/30	171 8133.9	39.408	121.524	2.4	1.9	C	PALERMO	3.7	
75/10/ 2	21142125.6	39.464	121.490	1.9	2.8	B	BANGOR	4.6	
75/10/ 2	221511 3.3	39.466	121.496	2.6	2.8	B	BANGOR	4.3	
75/10/ 2	22138128.5	39.458	121.491	2.5	2.0	B	BANGOR	4.4	
75/10/ 3	1137120.4	39.416	121.551	8.4	1.8	B	PALERMO	3.1	
75/10/ 3	211 11 1.2	39.411	121.541	10.0	2.2	B	PALERMO	4.9	
75/10/ 3	21281 8.4	39.511	121.490	.0	1.5	B	OROVILLE OAM	8.6	
75/10/ 3	6145118.6	39.498	121.500	6.3	1.7	A	PALERMO	6.9	
75/10/ 4	0119118.8	39.410	121.532	4.9	2.6	B	PALERMO	3.5	
75/10/ 4	12128139.9	39.513	121.519	4.0	2.0	A	OROVILLE	8.1	
75/10/ 8	9156142.5	39.411	121.548	16.2	1.9	B	PALERMO	3.5	
75/10/10	7144147.4	39.462	121.492	3.7	3.5	A	BANGOR	4.3	
75/10/11	2154158.8	39.522	121.518	9.9	1.3	B	OROVILLE	8.1	
75/10/12	4140153.6	39.467	121.485	1.7	1.4	A	BANGOR	5.1	
75/10/12	151 5135.2	39.507	121.527	7.8	1.3	A	OROVILLE	7.4	
75/10/12	21341117.4	39.400	121.511	4.0	1.4	B	PALERMO	4.9	
75/10/13	14156137.0	39.492	121.511	3.5	2.8	B	PALERMO	6.0	
75/10/13	161 8151.2	39.492	121.515	5.5	3.0	B	PALERMO	5.9	
75/10/13	211201 1.1	39.428	121.486	4.4	2.8	A	BANGOR	4.0	
75/10/14	2144158.5	39.506	121.527	4.0	1.2	B	OROVILLE	7.3	
75/10/14	91 11 5.7	39.406	121.512	2.4	1.3	B	PALERMO	4.3	
75/10/14	211321 6.4	39.471	121.509	.3	1.4	B	PALERMO	4.0	
75/10/16	3120148.9	39.400	121.488	1.1	1.9	A	BANGOR	6.2	
75/10/18	13159142.2	39.408	121.509	7.2	1.3	B	PALERMO	4.2	
75/10/20	141411 5.7	39.512	121.522	5.0	2.5	B	OROVILLE	8.8	
75/10/20	151221 5.7	39.506	121.520	7.7	1.3	B	OROVILLE	7.2	
75/10/21	13126125.0	39.414	121.512	3.1	1.5	A	PALERMO	3.5	
75/10/23	201 7144.5	39.475	121.534	6.3	1.6	B	PALERMO	5.9	
75/10/26	8121139.3	39.414	121.498	4.7	1.4	A	BANGOR	4.0	
75/10/27	211 2144.4	39.505	121.517	3.1	2.7	C	OROVILLE	7.3	
75/10/28	3141118.0	39.498	121.510	3.3	3.3	B	PALERMO	6.6	
75/10/28	5113148.0	39.525	121.534	4.1	1.8	B	OROVILLE	9.3	

TABLE 3. EARTHQUAKE EPICENTERS, JUNE 1975-DECEMBER 1975 (Continued)

EARTHQUAKES WITHIN 15.0 KMS OF OROVILLE MAIN SHOCK 6/1/75-12/31/75									
(G M T)			LATITUDE	LONGITUDE	DEPTH	MAG	O	QUADRANGLE	DIST (KMS)
YR	MO	DAY							
			HR	MIN	SEC				
75/10/30	141	9118.7	39.410	121.495	.6	1.8	A	BANGOR	4.8
75/10/30	15124138.7	39.485	121.542	.4	1.3	C	PALERMO	4.9	
75/10/31	1110122.7	39.416	121.493	3.5	1.9	B	BANGOR	4.6	
75/11/1	21461.3.6	39.428	121.495	1.2	2.2	A	BANGOR	3.7	
75/11/3	161.3137.3	39.398	121.509	3.3	2.8	B	PALERMO	5.3	
75/11/3	23117138.7	39.400	121.507	5.0	2.6	B	PALERMO	5.2	
75/11/4	211.4147.7	39.497	121.517	6.1	1.8	A	PALERMO	6.7	
75/11/5	5137147.0	39.408	121.492	4.3	3.4	B	BANGOR	5.2	
75/11/5	19130138.8	39.503	121.521	7.0	1.8	B	OROVILLE	7.0	
75/11/5	231161.6.4	39.440	121.489	2.9	1.4	B	BANGOR	3.9	
75/11/7	23158142.5	39.409	121.517	2.4	2.3	B	PALERMO	3.9	
75/11/8	41441.8.1	39.492	121.484	.3	2.0	A	BANGOR	7.2	
75/11/9	6115146.4	39.405	121.491	.5	1.3	B	BANGOR	5.5	
75/11/10	4136154.7	39.403	121.585	1.0	1.8	B	PALERMO	4.9	
75/11/13	111461.3.2	39.456	121.487	1.5	1.6	B	BANGOR	4.3	
75/11/15	31351.1.6	39.419	121.490	4.8	4.0	B	BANGOR	4.5	
75/11/15	31451.8.4	39.428	121.501	5.3	2.1	A	PALERMO	3.2	
75/11/15	4122134.3	39.420	121.484	6.4	2.1	C	BANGOR	6.5	
75/11/15	13141116.9	39.409	121.508	3.8	1.8	B	PALERMO	4.2	
75/11/16	51.0135.1	39.492	121.492	3.6	1.0	A	BANGOR	6.7	
75/11/16	10111714.6	39.414	121.526	3.3	2.2	B	PALERMO	3.1	
75/11/18	81471.6.5	39.415	121.487	7.9	1.0	B	BANGOR	5.0	
75/11/18	13110143.1	39.408	121.472	.1	2.4	A	BANGOR	6.1	
75/11/20	12136118.8	39.421	121.484	7.8	1.7	B	BANGOR	4.8	
75/11/23	7132153.5	39.410	121.500	2.5	2.1	A	PALERMO	4.5	
75/11/23	211421.7.1	39.406	121.490	3.9	1.8	C	BANGOR	5.4	
75/11/24	9141139.8	39.420	121.521	10.9	1.7	B	PALERMO	2.6	
75/11/25	1113128.5	39.406	121.500	9.5	1.0	C	PALERMO	4.9	
75/11/26	121.8124.2	39.505	121.521	4.9	1.2	B	OROVILLE	7.2	
75/11/26	12151153.3	39.408	121.496	.0	2.4	B	BANGOR	4.9	
75/11/26	13153153.7	39.498	121.488	.3	1.7	B	BANGOR	7.4	
75/11/26	15159123.7	39.502	121.485	3.0	1.2	B	OROVILLE DAM	8.0	
75/11/27	23159120.6	39.427	121.512	9.8	1.3	B	PALERMO	2.4	
75/11/30	10123120.9	39.511	121.493	2.2	2.1	A	OROVILLE DAM	8.6	
75/12/1	7150129.5	39.472	121.483	.3	1.1	B	BANGOR	5.5	
75/12/1	23126127.3	39.404	121.496	.6	1.3	C	BANGOR	5.2	
75/12/3	11331124.0	39.403	121.500	1.0	1.7	B	PALERMO	5.1	
75/12/3	7112113.1	39.424	121.491	6.0	2.5	A	BANGOR	4.2	
75/12/3	101131.9.5	39.398	121.465	.0	1.2	B	BANGOR	7.6	
75/12/4	171591.9.6	39.396	121.475	4.2	1.5	C	BANGOR	7.1	
75/12/5	12125142.5	39.411	121.471	1.5	2.0	A	BANGOR	6.3	
75/12/5	21151141.9	39.408	121.501	2.9	1.7	B	PALERMO	4.6	
75/12/6	141.4153.8	39.507	121.484	.1	1.7	B	OROVILLE DAM	8.5	
75/12/7	7131421.7.9	39.513	121.517	7.2	1.1	B	OROVILLE	8.2	
75/12/9	211201.4.9	39.497	121.524	2.8	1.4	B	PALERMO	6.3	
75/12/10	31.8148.3	39.507	121.541	4.8	2.8	B	OROVILLE	7.4	
75/12/12	8152132.4	39.457	121.510	2.8	1.9	A	PALERMO	2.7	
75/12/12	13133115.1	39.536	121.494	2.4	1.0	C	OROVILLE DAM	11.1	
75/12/13	2154143.4	39.447	121.503	2.9	2.1	A	PALERMO	2.8	
75/12/19	6144150.0	39.454	121.532	3.9	1.9	B	PALERMO	1.5	
75/12/20	7138119.0	39.507	121.523	4.9	2.0	B	OROVILLE	7.3	
75/12/21	41.81.4.4	39.406	121.475	5.6	1.0	B	BANGOR	6.4	
75/12/23	2155119.6	39.523	121.516	7.8	1.0	A	OROVILLE	9.3	
75/12/23	71.4120.1	39.431	121.473	3.6	1.0	B	BANGOR	5.4	
75/12/26	1114124.8	39.414	121.511	1.4	1.9	B	PALERMO	3.6	
75/12/27	5144150.3	39.410	121.501	2.6	2.0	A	PALERMO	4.4	

TABLE 4. EARTHQUAKE EPICENTERS, JANUARY 1976-MAY 1978

EARTHQUAKES WITHIN 15.0 KMS OF OROVILLE MAIN SHOCK 1/1/76-5/31/78

YR MO DY	(GMT)	HR MN SEC	LATITUDE	LONGITUDE	DEPTH	MAG	Q	QUADRANGLE	OIST (KMS)
76/1/1	18:58:39.3		39.421	121.494	2.4	2.1	B	RANGOH	4.1
76/1/2	10:22:9.7		39.454	121.481	.0	1.2	C	BANGOR	4.8
76/1/4	14:12:9.7		39.432	121.514	2.2	1.9	B	PALERMO	2.0
76/1/4	10:48:32.6		39.410	121.472	.0	1.1	B	BANGOR	6.3
76/1/4	15:11:13.7		39.510	121.528	.9	1.7	B	OROVILLE	7.7
76/1/4	15:50:1.4		39.498	121.508	11.3	1.2	C	PALERMO	6.7
76/1/9	17:54:28.6		39.488	121.487	.3	2.1	B	BANGOR	6.6
76/1/10	21:52:1.7		39.394	121.472	1.1	1.2	C	BANGOR	7.1
76/1/16	23:31:45.3		39.521	121.473	.6	1.9	B	OROVILLE DAM	10.3
76/1/17	7:15:20.0		39.424	121.467	1.1	2.0	B	BANGOR	6.1
76/1/18	0:37:22.9		39.417	121.484	5.8	2.9	B	BANGOR	5.1
76/1/23	13:31:18.8		39.413	121.484	1.1	1.6	B	BANGOR	5.3
76/1/26	2:11:42.6		39.420	121.466	1.0	2.5	B	BANGOR	6.3
76/1/26	19:40:1		39.416	121.474	3.8	3.2	B	BANGOR	5.5
76/1/26	21:01:14.6		39.437	121.468	.5	1.4	B	BANGOR	5.7
76/1/28	13:52:19.5		39.405	121.517	3.1	2.3	B	PALERMO	4.3
76/1/28	23:41:34.9		39.396	121.502	5.8	2.3	B	PALERMO	5.7
76/2/1	18:17:56.7		39.526	121.557	6.8	2.2	C	OROVILLE	9.6
76/2/2	19:11:58.4		39.441	121.486	.3	1.7	C	BANGOR	4.9
76/2/2	21:43:59.7		39.460	121.503	10.4	1.3	D	PALERMO	3.5
76/2/9	9:16:47.4		39.495	121.490	.8	1.5	C	BANGOR	6.2
76/2/9	10:19:33.5		39.485	121.485	.9	1.0	C	BANGOR	6.5
76/2/9	11:16:44.6		39.464	121.495	1.2	1.8	B	BANGOR	5.8
76/2/9	13:33:1		39.503	121.523	7.7	2.5	B	OROVILLE	6.9
76/2/9	13:47:39.3		39.492	121.475	.1	1.0	B	BANGOR	7.6
76/2/9	13:57:14.2		39.495	121.523	.1	1.9	C	PALERMO	6.0
76/2/19	11:31:30.6		39.497	121.513	6.3	1.0	C	PALERMO	5.8
76/2/23	9:59:13.3		39.481	121.498	.6	1.0	C	BANGOR	5.4
76/3/6	12:16:30.4		39.446	121.499	4.2	1.1	B	BANGOR	3.1
76/3/12	5:38:28.8		39.480	121.501	.5	1.0	C	PALERMO	5.7
76/3/15	15:52:31.7		39.470	121.466	1.1	1.0	B	BANGOR	6.1
76/3/15	17:14:15.5		39.469	121.503	1.6	1.6	B	PALERMO	4.5
76/3/19	2:14:56.3		39.541	121.509	5.4	1.7	B	OROVILLE	11.3
76/3/20	12:19:42.1		39.409	121.470	.1	2.0	B	BANGOR	6.6
76/3/21	14:31:58.1		39.397	121.539	7.2	2.1	B	PALERMO	4.9
76/3/27	15:41:14.2		39.500	121.484	.6	2.5	B	OROVILLE DAM	7.9
76/3/28	8:42:1		39.499	121.525	4.3	2.2	A	PALERMO	6.5
76/4/3	22:49:32.2		39.414	121.480	2.5	1.2	B	BANGOR	5.5
76/4/4	18:41:31.6		39.415	121.489	2.2	2.2	B	BANGOR	5.9
76/4/4	9:41:22.4		39.491	121.507	6.8	1.2	B	PALERMO	6.0
76/4/12	7:43:4.5		39.410	121.415	.1	1.2	C	BANGOR	10.8
76/4/16	17:11:15.7		39.501	121.497	3.1	2.9	B	OROVILLE DAM	7.4
76/4/16	17:41:30.4		39.498	121.480	.8	1.2	B	BANGOR	6.8
76/4/30	20:51:39.2		39.428	121.466	.1	2.1	A	BANGOR	4.4
76/5/7	7:14:43.4		39.405	121.469	.8	2.4	C	BANGOR	6.1
76/5/7	13:48:1		39.419	121.491	3.3	1.7	B	BANGOR	6.4
76/5/12	11:47:41.1		39.420	121.490	2.7	1.6	B	BANGOR	5.8
76/5/15	13:16:1		39.418	121.484	4.0	2.2	B	BANGOR	5.0
76/5/17	17:13:0.1		39.447	121.491	3.2	1.1	B	BANGOR	3.7
76/5/18	9:46:16.8		39.470	121.465	.2	2.5	B	BANGOR	6.8
76/5/19	11:01:3.1		39.514	121.486	3.2	1.8	B	OROVILLE DAM	9.1
76/5/20	17:27:34.5		39.489	121.491	1.2	2.3	C	BANGOR	6.5
76/5/21	18:14:40.7		39.409	121.514	.7	1.3	C	PALERMO	4.0
76/5/26	3:55:25.3		39.495	121.527	.0	2.4	B	PALERMO	6.0
76/5/31	21:36:1.1		39.507	121.523	3.6	2.6	B	OROVILLE	7.3
76/6/31	5:30:1		39.412	121.477	.3	2.5	B	BANGOR	5.9
76/6/1	8:31:14.0		39.509	121.518	4.0	2.4	B	OROVILLE	7.6
76/6/6	12:14:10.7		39.420	121.489	7.0	1.2	B	BANGOR	4.6
76/6/14	6:17:28.2		39.473	121.529	.7	2.5	B	PALERMO	3.6
76/6/14	18:36:1		39.525	121.525	.9	2.1	B	OROVILLE	4.3
76/6/14	23:30:26.2		39.473	121.536	.5	3.4	B	PALERMO	3.6
76/6/14	23:51:54.6		39.470	121.532	7.7	2.1	B	PALERMO	3.2
76/6/25	19:12:27.2		39.413	121.465	3.4	2.6	B	BANGOR	6.7
76/6/26	6:13:31.5		39.407	121.490	4.3	2.4	B	BANGOR	5.3
76/6/29	7:31:56.4		39.425	121.528	7.2	2.0	A	OROVILLE	9.4
76/7/1	01:59:15.4		39.511	121.492	6.1	2.6	A	OROVILLE DAM	8.6
76/7/6	6:35:17.5		39.409	121.527	7.6	4.1	A	PALERMO	3.6
76/7/6	7:59:33.2		39.413	121.519	4.2	3.4	A	PALERMO	3.4
76/7/7	11:43:40.1		39.584	121.513	4.8	2.6	B	OROVILLE	11.6
76/7/11	23:19:20.3		39.403	121.489	3.5	2.6	B	BANGOR	5.7
76/7/20	5:33:1		39.404	121.484	3.7	2.3	C	BANGOR	6.0
76/7/23	16:57:15.7		39.512	121.525	1.6	1.2	C	OROVILLE	7.9
76/7/24	12:57:1		39.462	121.499	6.1	1.8	B	BANGOR	5.5
76/7/30	17:27:14.5		39.488	121.528	13.2	1.0	B	PALERMO	5.2
76/8/10	15:11:57.9		39.411	121.494	3.0	2.5	B	BANGOR	4.8
76/8/16	18:53:33.7		39.409	121.501	3.3	1.0	B	PALERMO	4.5
76/8/16	23:13:14.9		39.403	121.506	3.5	1.4	C	PALERMO	4.8
76/8/15	5:43:14.5		39.539	121.507	5.9	1.4	B	OROVILLE	11.1
76/8/19	8:15:1		39.456	121.473	5.5	2.9	A	BANGOR	5.6
76/8/24	7:15:14.5		39.422	121.497	.1	2.6	B	BANGOR	7.9
76/8/31	19:29:35.2		39.508	121.543	.9	2.7	B	OROVILLE	7.5
76/9/16	22:12:14.9		39.499	121.492	.9	1.1	O	BANGOR	7.4
76/10/21	0:38:11.5		39.489	121.480	.4	2.3	B	BANGOR	7.4
76/10/22	13:16:12.5		39.497	121.483	4.2	2.9	B	BANGOR	5.8
76/11/10	8:14:57.2		39.412	121.491	.8	1.0	C	BANGOR	4.9
76/11/23	12:58:1		39.464	121.488	.4	1.9	C	BANGOR	5.0
76/12/15	11:32:32.2		39.408	121.496	6.9	1.5	B	BANGOR	4.9
76/12/25	15:59:15.5		39.425	121.488	.1	2.0	B	BANGOR	7.2
76/12/29	3:31:55.7		39.416	121.478	.0	2.9	B	BANGOR	5.5
77/1/9	23:24:40.3		39.487	121.499	4.5	3.4	B	BANGOR	6.0
77/1/9	23:27:14.1		39.491	121.509	5.5	2.3	B	PALERMO	6.0
77/1/12	3:30:47.7		39.413	121.493	2.7	2.5	A	BANGOR	7.4
77/1/23	11:21:50.0		39.401	121.486	2.7	1.0	B	BANGOR	6.1
77/1/30	6:35:24.9		39.440	121.491	.6	2.8	A	BANGOR	3.7
77/3/5	17:55:32.8		39.487	121.493	.8	2.9	B	BANGOR	5.2
77/3/7	0:46:15.5		39.466	121.490	1.9	2.2	B	BANGOR	4.1

TABLE 4. EARTHQUAKE EPICENTERS, JANUARY 1976-MAY 1978 (Continued)

EARTHQUAKES WITHIN 15.0 KMS OF OROVILLE MAIN SHOCK 1/1/76-5/31/78

YR MO (Y		(G M T)	LATITUDE	LONGITUDE	DEPTH	MAG	Q	QUADRANGLE	DIST (KM)
		HQ MN SEC							
77/ 3/14	22:37:21.7		39.401	121.447	.1	2.5	B	BANGOR	8.6
77/ 4/15	11:10:40.2		39.410	121.493	3.9	1.0	B	BANGOR	4.9
77/ 4/27	4:26:29.2		39.404	121.487	2.8	1.9	B	BANGOR	5.7
77/ 4/28	16:23:13.0		39.416	121.482	3.9	2.0	B	BANGOR	5.3
77/ 4/28	17:45:52.1		39.410	121.481	4.2	1.2	B	BANGOR	5.7
77/ 5/ 4	6:11:11.4		39.400	121.482	4.5	2.9	B	BANGOR	6.4
77/ 5/ 4	6:15:36.3		39.401	121.479	4.6	2.7	B	BANGOR	6.5
77/ 5/ 4	6:59:10.2		39.400	121.479	4.1	3.4	B	BANGOR	6.6
77/ 5/ 6	7: 1:53.2		39.399	121.478	.4	1.5	C	BANGOR	6.7
77/ 5/11	16:44: 7.3		39.502	121.479	.2	2.4	C	OROVILLE DAM	8.3
77/ 5/17	17:18:28.0		39.405	121.484	6.6	1.0	C	BANGOR	5.9
77/ 5/18	17:20:22.4		39.461	121.457	1.4	1.7	D	BANGOR	7.0
77/ 5/25	1:11:01:58.4		39.417	121.476	2.0	1.6	B	BANGOR	5.7
77/ 7/14	0:39:58.1		39.518	121.526	7.1	1.8	B	OROVILLE	8.6
77/ 7/19	9:43:20.7		39.405	121.488	1.8	1.3	C	BANGOR	5.6
77/ 7/19	0:57:23.6		39.421	121.456	2.1	1.4	C	BANGOR	7.1
77/ 7/20	8:48:16.4		39.427	121.478	4.5	1.6	C	BANGOR	5.0
77/ 8/ 8	10:35:40.7		39.414	121.494	6.0	3.0	A	BANGOR	4.6
77/ 8/30	22:07:44.3		39.419	121.546	8.3	1.1	D	PALEOMO	2.7
77/ 9/13	4:28:26.5		39.403	121.447	3.3	2.5	B	BANGOR	8.6
77/ 9/13	6:39:49.8		39.403	121.451	3.7	2.3	B	BANGOR	8.3
77/10/ 3	18:22:38.2		39.442	121.520	7.0	2.5	B	PALEOMO	1.2
77/10/16	10:36:10.2		39.556	121.594	4.1	1.0	B	OROVILLE	13.8
77/11/10	20:24:42.2		39.410	121.495	1.7	2.9	B	BANGOR	4.8
77/11/23	8:28: 2.7		39.402	121.492	4.4	1.2	B	BANGOR	5.6
77/12/ 6	14:14:57.5		39.403	121.470	.2	2.0	B	BANGOR	6.9
77/12/ 9	4:1 3:11.5		39.403	121.500	3.1	1.9	B	PALEOMO	5.1
77/12/ 9	9:39: 7.8		39.404	121.483	1.2	1.9	B	BANGOR	6.0
77/12/11	8:42:41.9		39.412	121.484	.1	1.0	B	BANGOR	5.4
77/12/27	12:33: 8.9		39.451	121.396	.7	1.1	C	BANGOR	12.1
78/ 1/ 4	20:56:22.8		39.410	121.490	.7	1.0	B	BANGOR	5.8
78/ 1/31	22: 9:57.9		39.521	121.478	2.9	1.0	C	OROVILLE DAM	10.1
78/ 3/ 1	13:55:14.7		39.454	121.529	7.3	1.0	C	PALEOMO	1.6
78/ 3/28	16:20:30.6		39.407	121.474	1.0	1.0	C	BANGOR	5.9
78/ 4/ 2	14:40:53.9		39.421	121.429	1.0	1.0	D	BANGOR	9.3
78/ 5/ 8	16:48:34.8		39.511	121.481	.6	2.2	B	BIDWELL BAR	9.0
78/ 5/29	20:27:31.0		39.469	121.469	1.5	2.0	B	BANGOR	6.6

References

1. Lee, W. H. K., J. C. Lahr, Hypo 71 (revised). "A Computer Program for Determining Hypocenter, Magnitude, and First Motion Pattern of Local Earthquakes." USGS Open File Report 75-311.
2. Lee, W. H. K., R. E. Bennett and K. L. Meagher (1972). "A Method of Estimating Magnitude of Local Earthquakes from Signal Duration." U. S. Geological Survey Open File Report.
3. Hofmann, R. B., and R. W. Wylie (1964), "Proceedings of the VESIAC Conference on Seismic Event Magnitude Determination." Institute of Science and Technology, University of Michigan.
4. Lahr, K. M., J. C. Lahr, A. G. Sindh, C. G. Bufe and F. W. Winter (1976), "The August 1975 Oroville Earthquakes." BSSA, 66, 4, p. 1085-1099.
5. Savage, J. C., M. Lisowski, W. H. Prescott, and J. P. Church (1977) "Geodetic Measurements of Deformation Associated with the Oroville, California Earthquake." JGR, 82,11, p. 1667-1671.

CHAPTER IV

VERTICAL AND HORIZONTAL GEODESY

Vertical Crustal Movements

Introduction

Due to the August 1, 1975, Oroville earthquake (magnitude 5.7, main shock located about 12 kilometres southwest of Oroville Dam), the Department began an intensive surveying program to reobserve previously established vertical and horizontal control networks to determine locations, magnitude of movement, and trends of the major faulting.

A monitoring network to measure horizontal and vertical movement at Lake Oroville was established in 1967. In April 1968, the horizontal network was remeasured, and in late 1968 releveled of most of the network was completed. In 1969, about half of the level network was releveled.

1975 August - September:	Leveling and Horizontal Control.
1976 January - April:	About half releveled.
1976 September - November:	All level lines rerun.
1977 September - November:	All level lines rerun.
1978 August - September:	About 90 percent of total length to be rerun.

Precise Survey Programs

September 1967. The Lake Oroville Monitoring Network was the original program to monitor the area around Oroville Dam and Lake Oroville for movement caused by the filling of the lake. Figure 71 shows the level net for study of Lake Oroville - 1967.

The program consisted of establishing 106 new bench marks as well as leveling an additional 139 bench marks for a total network of 94.15 kilometres (58.5 miles). The leveling accuracy was Class 1 first-order^{1/}, which means the closure error

Figure 69 shows a plot of the filling of Lake Oroville to Elevation 274.3 metres (900 feet) starting in 1967 and the normal cycling of the lake. Also shown is the effect of the California Drought; beginning in 1976, Lake Oroville receded to its lowest water elevation since filling (198.1 metres (650 feet) in December 1977). Between December 1977 and June 1978, the lake refilled to within a few metres of full.

The location of the Oroville area level lines (1977) are shown on Figure 70. The end points of the lines are not connected on this figure for purposes of identification.

The following precise surveys were made in response to the August 1, 1975, Oroville earthquake:

for each line may not exceed 3.0 millimetres (0.010 foot) times the square root of the distance in kilometres.

The leveling was run from an established U. S. Coast and Geodetic Survey (USC&GS) network in and near the City of Oroville. The leveling was extended easterly and northerly to diorite rock masses. The USC&GS established the elevations along the lines and terminal bench marks and the Department completed first-order leveling over the net interior. These elevations are used as the base reference elevations.

^{1/} Classification, Standards of Accuracy, and General Specifications of Geodetic Control Surveys, U. S. Department of Commerce (February 1974).

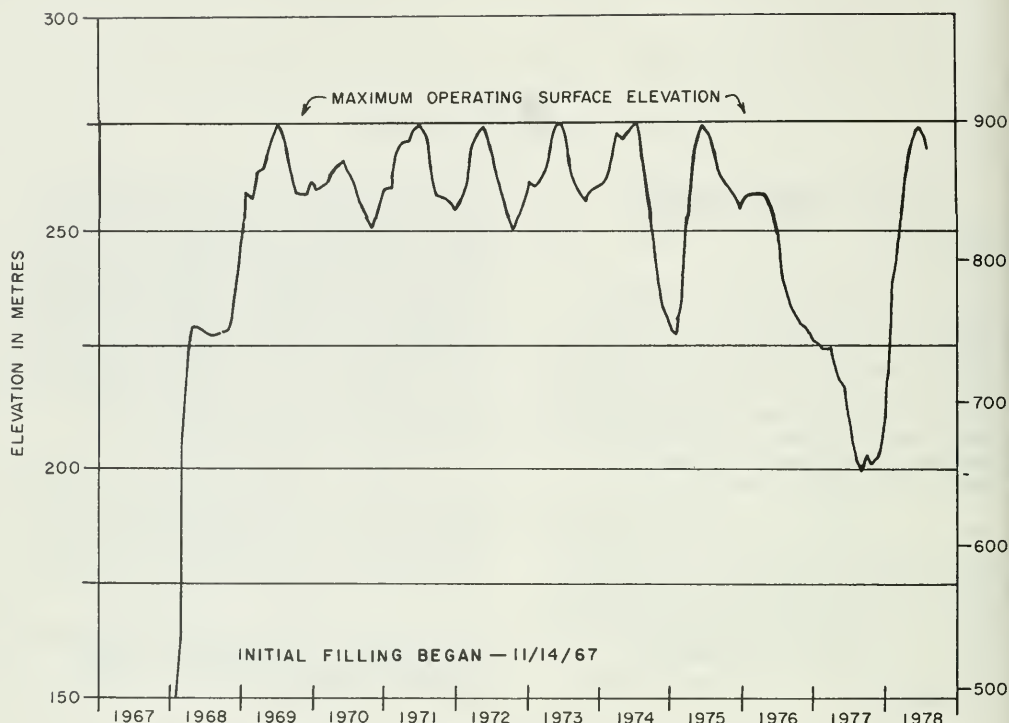


Figure 69. Lake Oroville Water Surface Elevation

July - September 1968. Because the funds allotted to survey the entire 1967 network were inadequate, Line Olive leveling was omitted (12.1 kilometres, 7.5 miles), and the Line Bald Rock leveling was shortened by 9.7 kilometres (6.0 miles). This leveling was performed using second-order methods, single run, except where differences in elevations between bench marks previously established were in excess of first-order tolerances, then reruns were made for confirmation. A total of 57.6 kilometres (35.8 miles) were run in one direction between July 1 and September 27.

October - November 1969. Twenty-six kilometres (16 miles) of Class 1 first-order leveling was conducted during October and November.

August - September 1975. Because of the

earthquake, 117 kilometres (73 miles) of Class 1 first-order levels were made between August 13 and September 12.

January - April 1976. Seventy-five kilometres (47 miles) of Class 1 first-order levels were made between January 19 and April 8.

September - November 1976. One hundred sixty-two kilometres (101 miles) of Class 1 first-order leveling was accomplished between September 15 and November 11.

September - November 1977. This Class 1 first-order survey releveled the September - November 1976 network of 162 kilometres (101 miles), between September 13 and November 3. The level net, for study of Lake Oroville - 1977, is shown on Figure 72.

Precise Survey Adjustment

Free Adjustment. Independent free adjustments for each epoch of leveling were made using the variation-of-parameters method of least squares. In free adjustments, the net is not constrained to fit previously established elevations. Only Bench Mark OM-27, Elevation 540.468 metres

(1773.19 feet), (1967 USC&GS adjustment), is assumed to be stable at the fixed elevation, and all other elevations are adjusted in relation to it. Therefore, any comparison of the free adjusted elevation of a bench mark in one epoch to that of another epoch indicates apparent movement between two levelings.

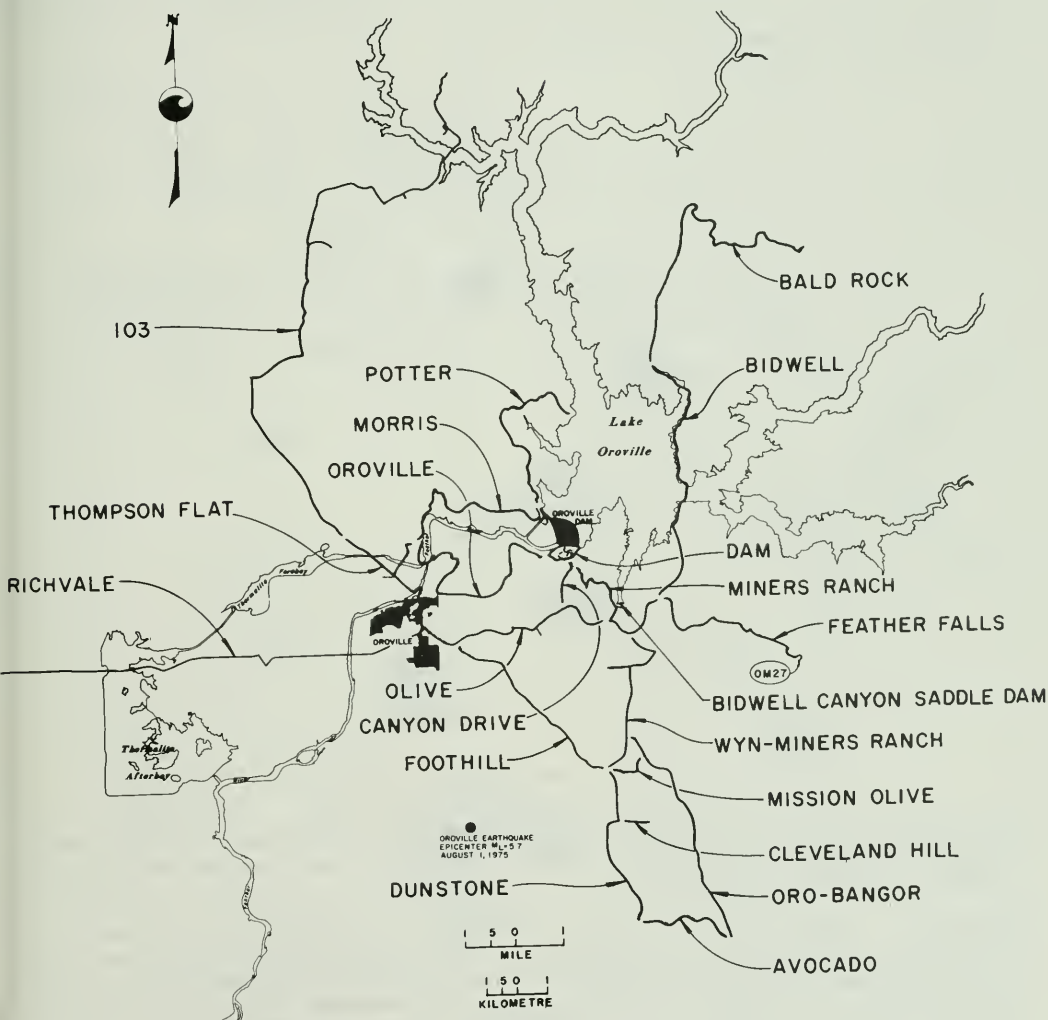


Figure 70. Oroville Area Level Lines (1977)

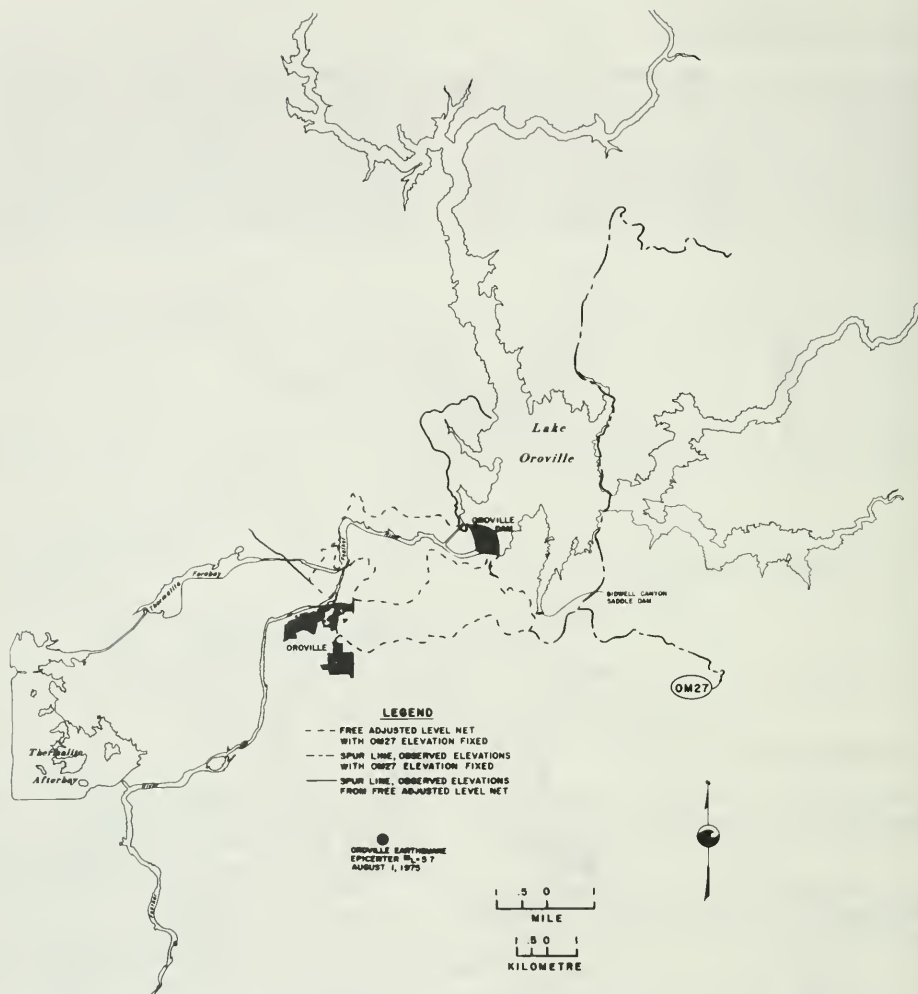


Figure 71. Precise Level Net for Study of Lake Oroville - 1967

The level net used for the October 1977 adjustment typifies the basic network as refined to that date (Figure 72).

Spur Lines. Six main spur lines are connected to the main net without benefit of closure back to the net; therefore, these lines are not adjusted and reflect only observed elevations. The lines are Feather Falls, Bidwell, Bald Rock, Rich-

vale, Potter and Line 103. Also, several short spur lines are connected to the net.

Line Feather Falls is the connecting link between the fixed Bench Mark OM-27 and OM-20 (main connector to the level net); therefore, Feather Falls line is the actual observed elevations with no adjustments.

Lines Bidwell and Bald Rock are connected to the net at OM-20 and are observed elevations without any adjustments. The 1977 elevation on the Bald Rock Terminal Bench Mark (L1092) is 22 millimetres (0.072 foot) lower than the established 1967 elevation. This elevation difference is within Class 2 first-order leveling limits and, therefore, may not be indicative of a 22-millimetre (0.072-foot) subsidence.

Line Richvale is also a spur line connected to the level net at the west side with excellent agreement between October 1977 and October 1976. The extreme west bench mark indicates 16 millimetres (0.052 foot) of subsidence and the entire line varies between (1976-77) 10 and 20 millimetres (0.033 and 0.066 foot).

After Line 103 leaves the level net, this spur line indicates the same type

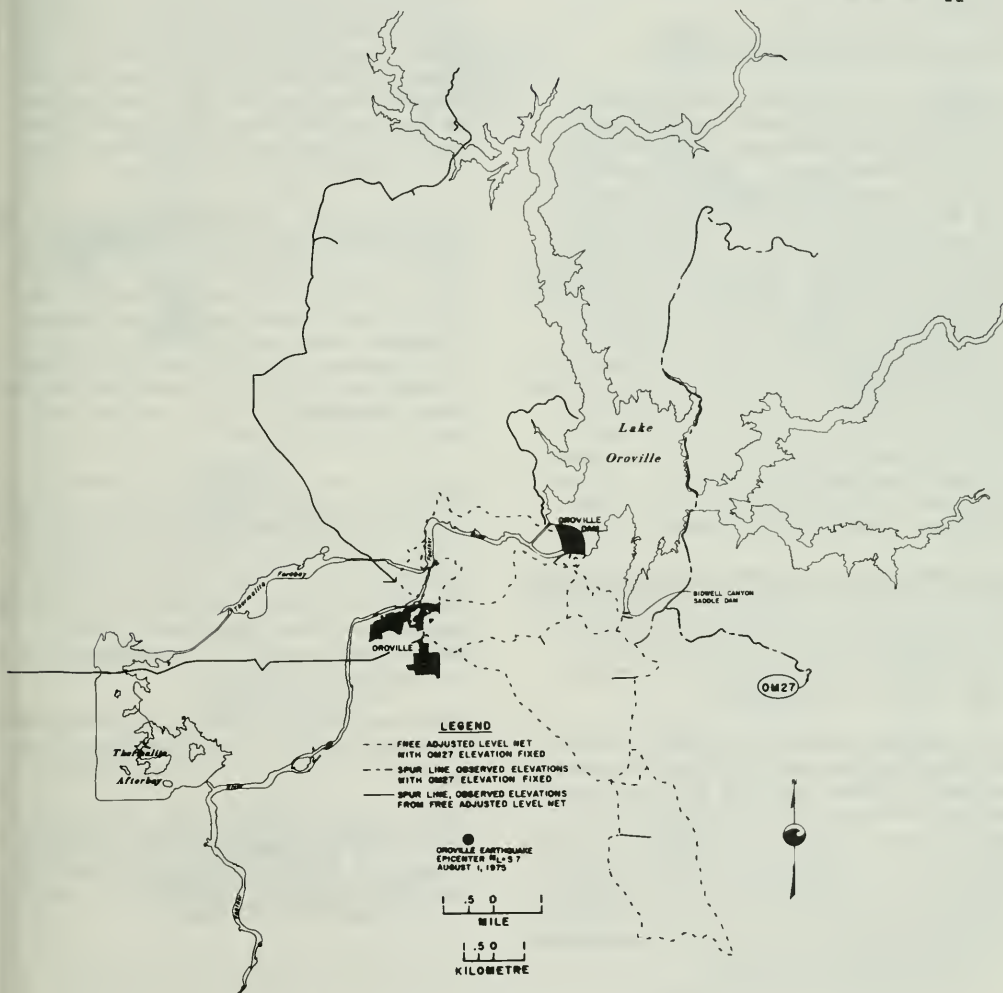


Figure 72. Precise Level Net for Study of the Oroville Earthquake - 1977

divergence between 1976 and 1977; that is about 20 millimetres (0.066 foot) lower than 1976, using observed elevations. The 1976 data show uplift, and the 1977 data indicate subsidence.

Potter shows approximately 10 millimetres (0.033 foot) of uplift in 1977 compared to October 1976. The 1977 subsidence is more than 20 millimetres (0.066 foot) compared to the reference date of September 1967.

Elevation Differential Isograms

General. The elevation differential isograms are hand-drawn representation lines of equal vertical elevation differences for each epoch. By necessity, a certain amount of judgement is used in the determination of the contour lines. Generally, the contours developed from the spur lines are less credible because they are observed elevations. Therefore, these elevation-differential isograms (Figures 73 through 78) are limited in the area of the spur line, and care must be used in interpretation of the contours in these areas. The interpretation of these spur line contours was intentionally limited by not developing contours to their extremities; however, all data for these spur lines are shown on the vertical elevation differential plots.

September 1967 - October 1969 (Figure 73). This epoch shows elevation differentials during initial filling of Lake Oroville starting in October 1967 and reaching maximum lake elevation of 274.3 metres (900 feet) in July 1969.

This isogram shows no subsidence south of Lake Oroville and only minor subsidence on the southeast side of the lake up to a maximum of only 20 millimetres (0.066 foot), based on spur line observed elevations. This isogram is limited in extent because only 26 kilometres (16.2 miles) of the original 1967 net were releveled. It shows that only very minor subsidence occurred during this period.

October 1969 - August 1975 (Figure 74). This epoch is the result of (a) the normal lake cycling from 1969 to 1974, (b) the lower-than-normal cycle in winter of 1974 to elevation 228.6 metres (750 feet), (c) refilling to maximum lake elevation in June 1975, and (d) the effects of the August 1, 1975, Oroville earthquake.

This isogram is also limited in extent because of the short survey in 1969; however, it does show that only minor subsidence was measured during August 1975 after the main shock, with most of the subsidence occurring after this survey. The maximum 1975 subsidence contour is only 15 millimetres (0.049 foot) along the southeast side of the lake.

September 1967 - October 1977 (Figure 75). The 1967-1977, ten-year epoch, encompasses all measurable elevation differentials from all causes. They include the previous items plus the earthquake aftershock sequence, and the effect of the California drought, which resulted in Lake Oroville being drawn down to its lowest elevation of 198.1 metres (650 feet) in October 1977.

Generally, the subsidence adjacent to Lake Oroville and Dam is fairly uniform, ranging between 20-25 millimetres (0.066-0.082 foot). A significant subsidence area to the south and west of the dam indicates increased subsidence away from the lake and dam, especially in the southern direction, to a maximum of 60 millimetres (0.20 foot).

Throughout the area south of Lake Oroville the subsidence is quite predominant and may be attributed to the fault zone.

August 1975 - October 1976 (Figure 76). This epoch includes only the immediate aftershock sequence and decreasing lake elevation from 274.3 metres (900 feet) to 233.2 metres (765 feet).

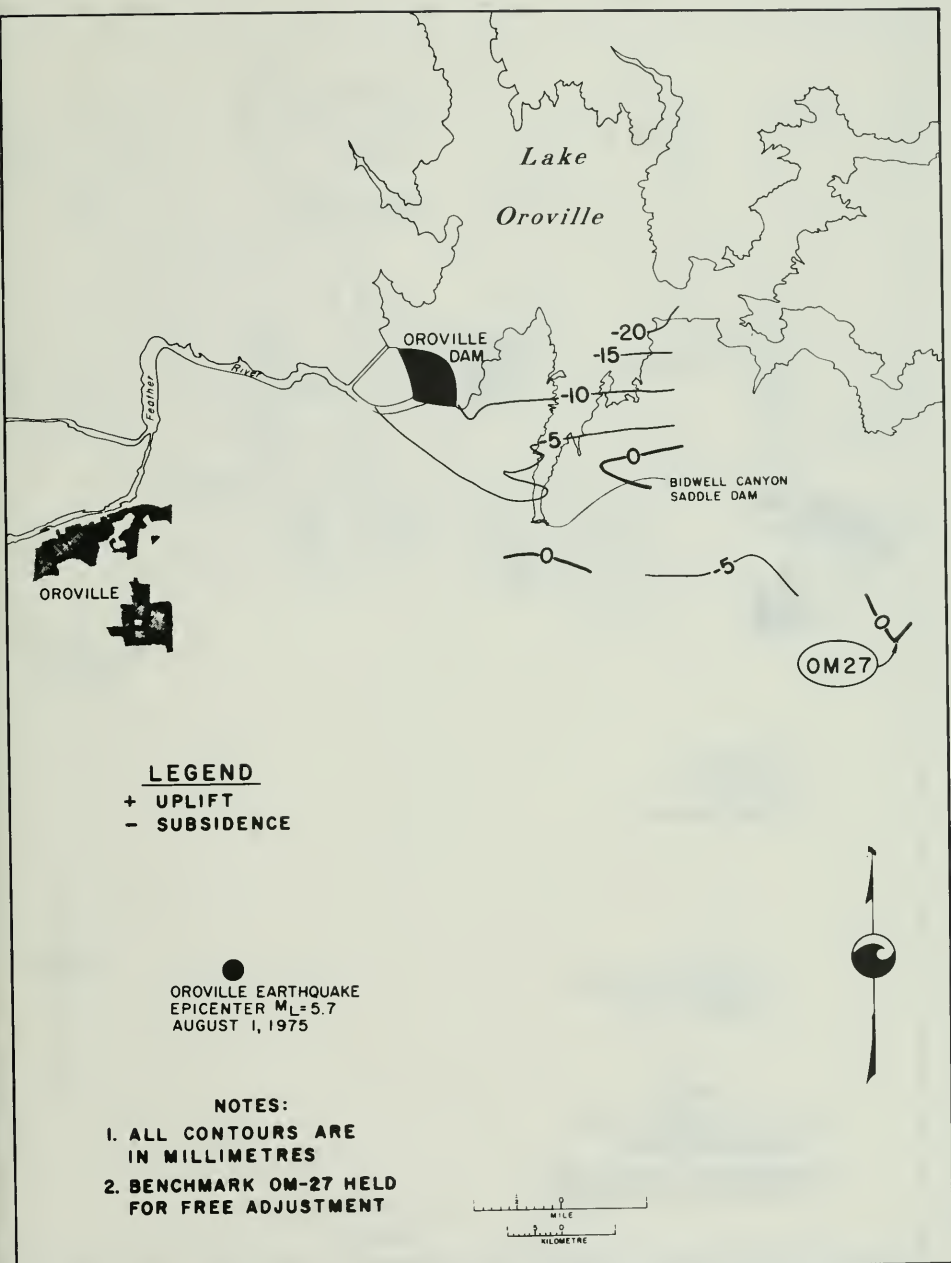


Figure 73. Elevation Differential Isogram--September 1967-October 1969

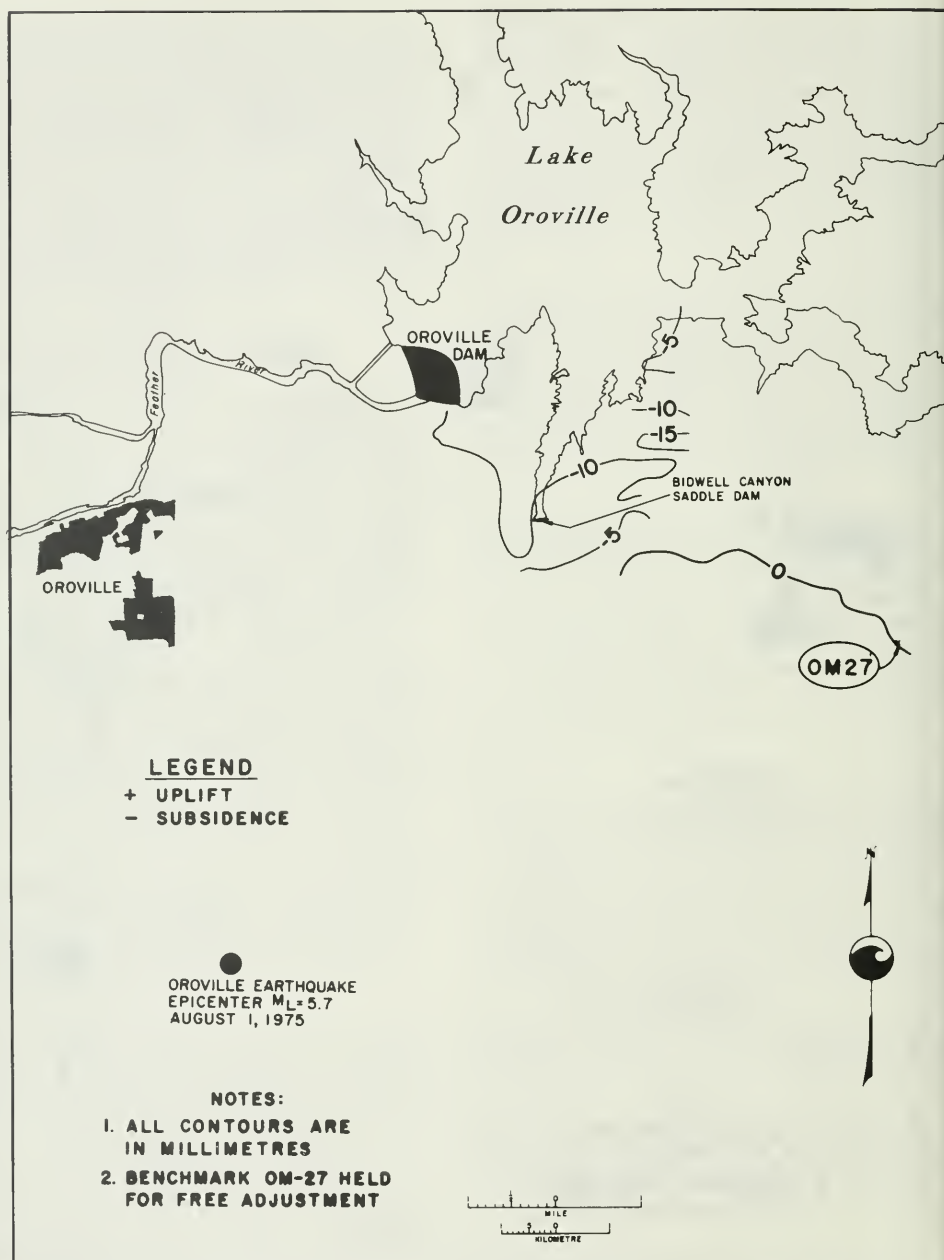


Figure 74. Elevation Differential Isogram--October 1969-August 1975

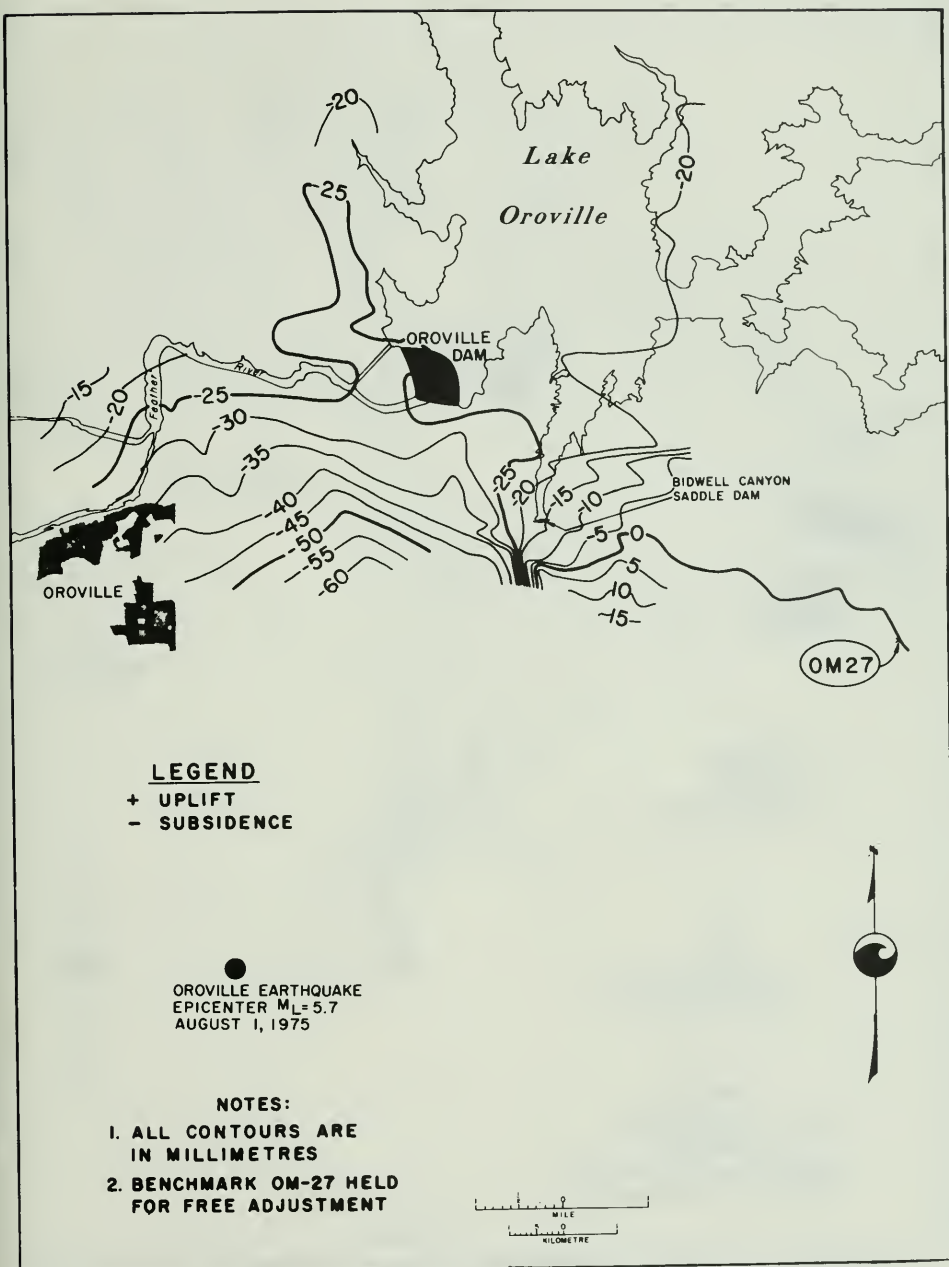


Figure 75. Elevation Differential Isogram--September 1967-October 1977

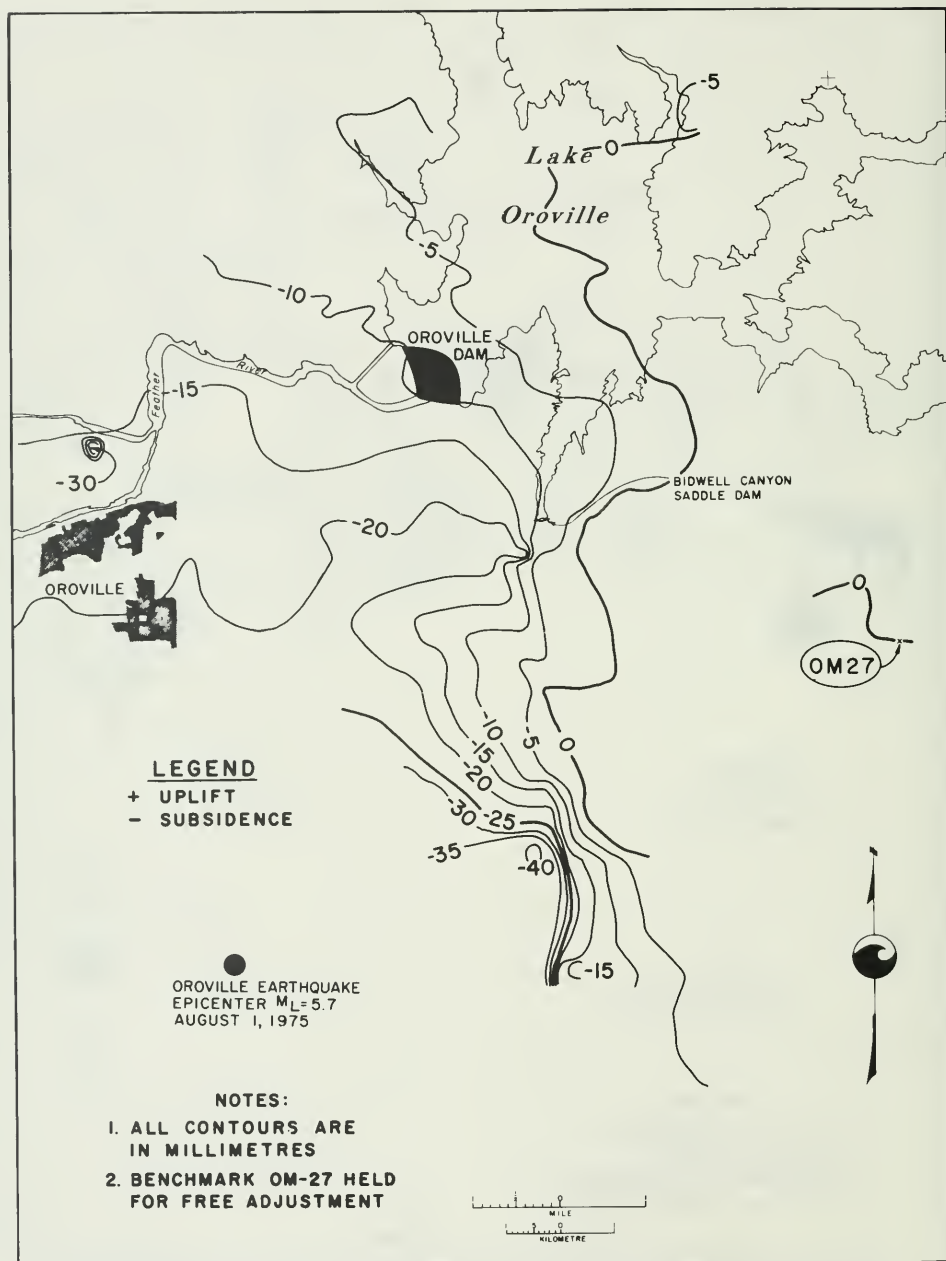


Figure 76. Elevation Differential Isogram--August 1975-October 1976

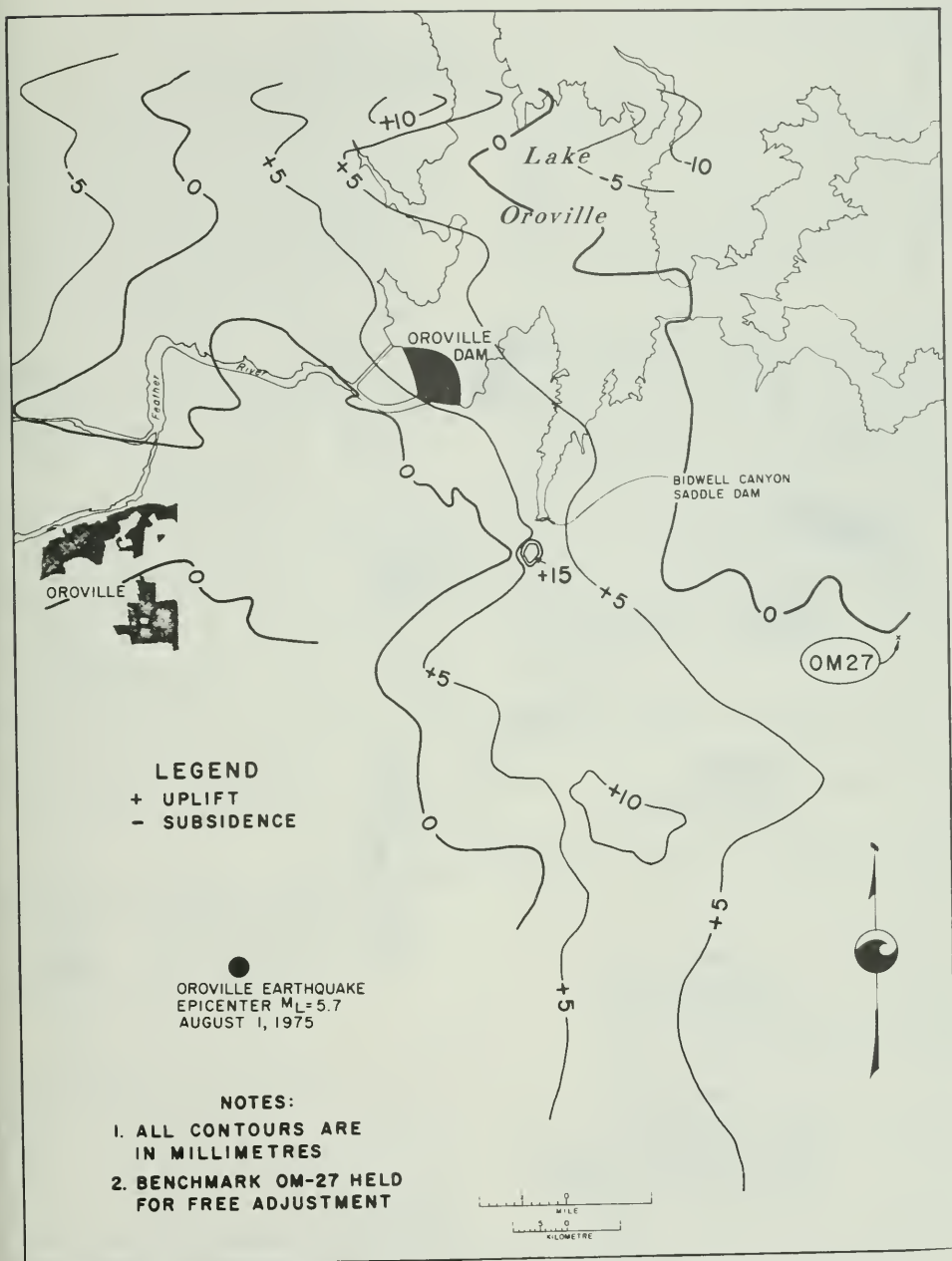


Figure 77. Elevation Differential Isogram--October 1976--October 1977

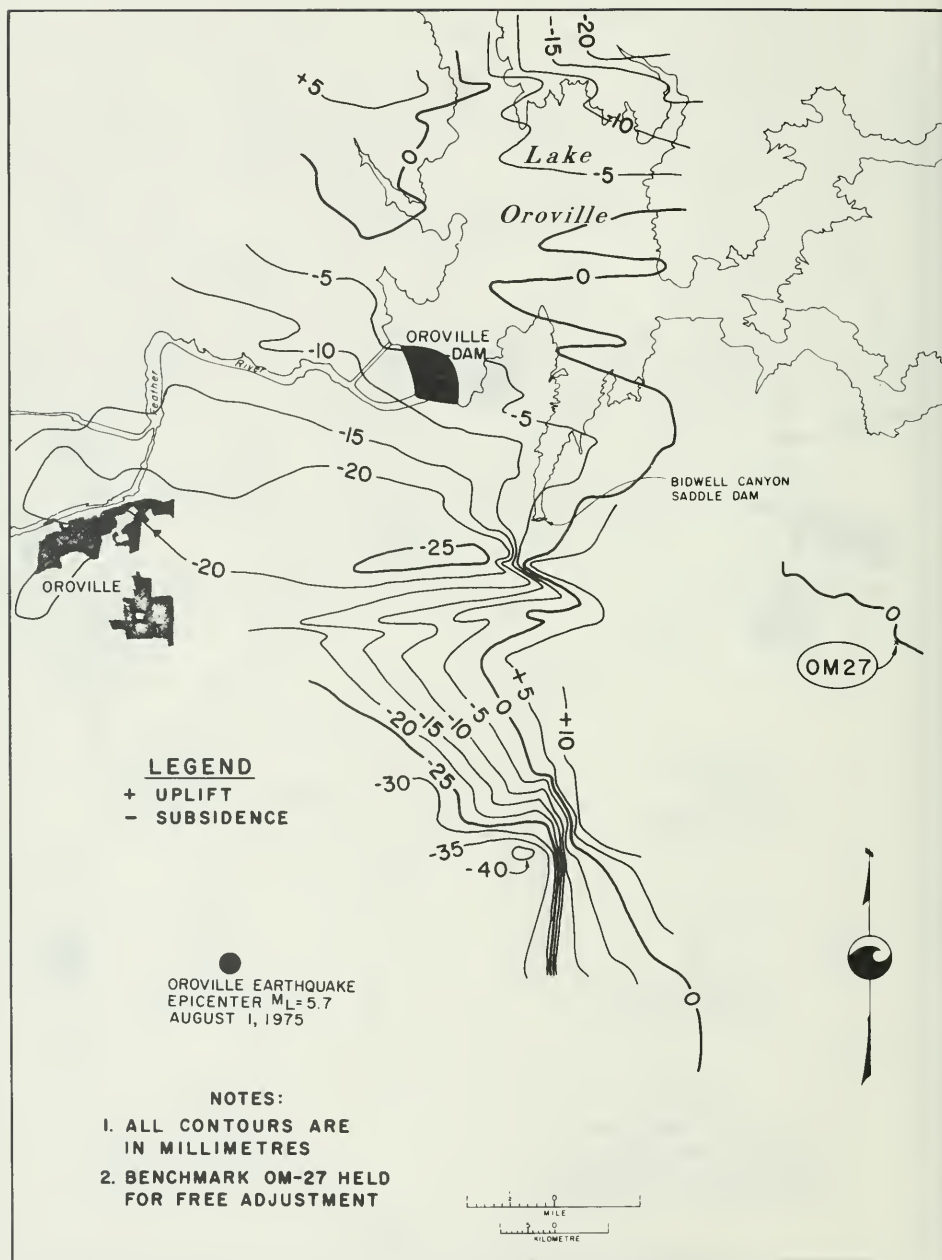


Figure 78. Elevation Differential Isogram--August 1975-October 1977

This epoch clearly shows subsidence to the west of the nearly north-south zero line. The magnitudes are small near the dam and lake; however, significant trends developed south of the lake. The contours south of the Lake show a north-south trending fault zone through lines Mission Olive and Cleveland Hill. The ground surface to the west shows a net subsidence of 40 millimetres (0.131 foot) across this zone, with ground rupture present in this fault zone.

October 1976 - October 1977 (Figure 77). This epoch includes continued lowering of Lake Oroville -- due to the drought -- of approximately 35.1 metres (115 feet) and the declining aftershock sequence.

North-south uplift between the two north-south zero lines is predominant for this epoch. Significant uplift between the two north-south 5-millimetre (0.016-foot) contours is well defined with two areas of 10-millimetre (0.033-foot) uplift.

The fault zone through lines Cleveland Hill and Mission Olive is not clearly defined during this time period. However, the area south of the dam defines that previous area, although it shows uplift of plus 5 millimetres (0.016 foot) compared to the previous subsidence in this area.

August 1975 - October 1977 (Figure 78). This epoch includes the reduced lake elevation of approximately 76.2 metres (250 feet) and the entire aftershock sequence shortly after the August 1, 1975, main shock.

This time period clearly shows the fault zone through lines Cleveland Hill, Mission Olive, and just south of the lake. The north-south zero line separates the subsidence to the west and the uplift to the east with the dam and lake in the subsidence area. The magnitude of movement adjacent to the dam and lake is very small and insignificant. The net subsidence across the fault zone is approximately 50 millimetres (0.164 foot)

with lowering of ground surface to the west.

Elevation Differential Along Lines

General. The plots of the elevation differential for each of the lines are based on a free adjustment holding OM-27 fixed. Spur lines are observed elevations based on the adjusted junction bench mark elevation.

The Oroville area level lines are shown on Figure 70 and the locations of the bench marks are shown on Plate 2 (inside rear cover). The reference dates for the individual lines vary according to when the line was first established for monitoring of the Oroville area. Also shown on each figure is a plot of the approximate ground profile along the line for topographical referencing.

The lines listed below are presented in alphabetical order along with comments concerning significant movements and anomalies.

Avocado (Figure 79) (Reference Date February 1976)

1. Possible southern extension of fault zone.

Bald Rock (Figure 80) (Reference Date September 1967)

1. Spur line, observed elevations only.
2. The October 1977 plot is approximately 20 millimetres (0.066 foot) below the August 1975 plot although within first-order survey error limits.

Bidwell (Figure 81) (Reference Date September 1967)

1. Spur line observed elevations only.

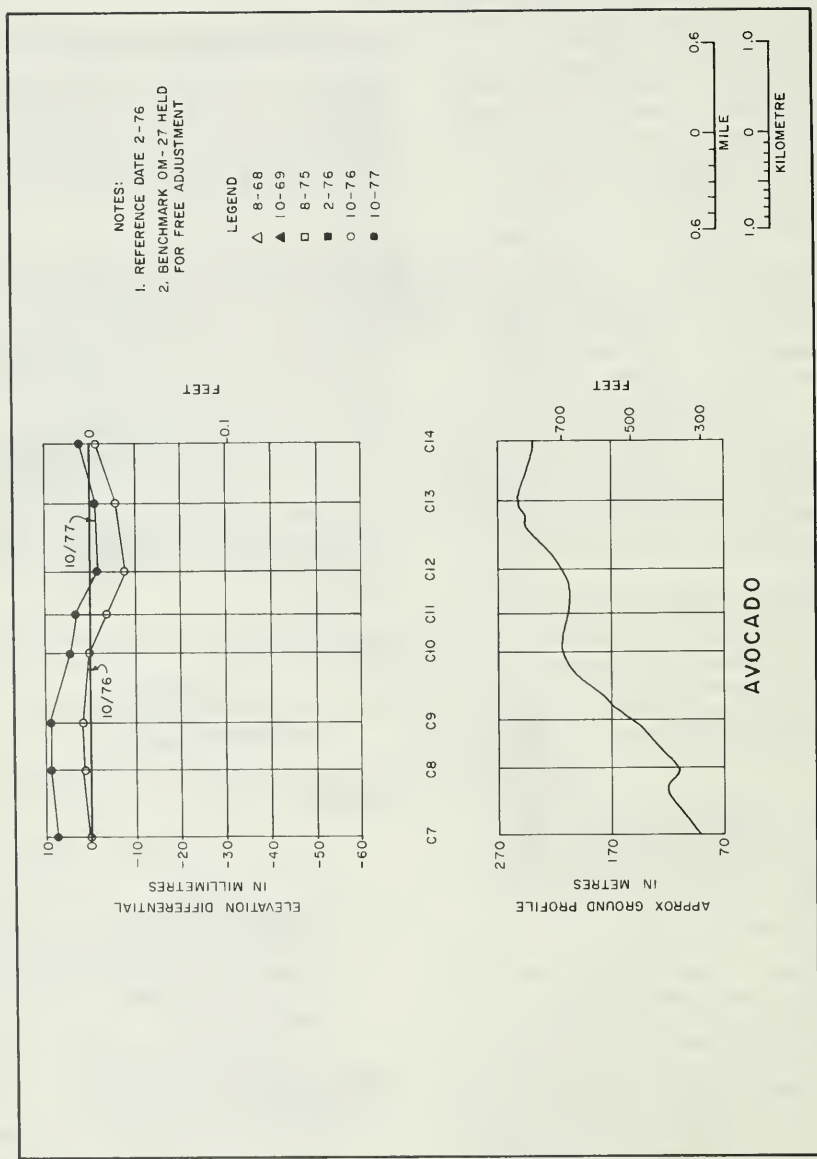


Figure 79. Avocado Elevation Differentials

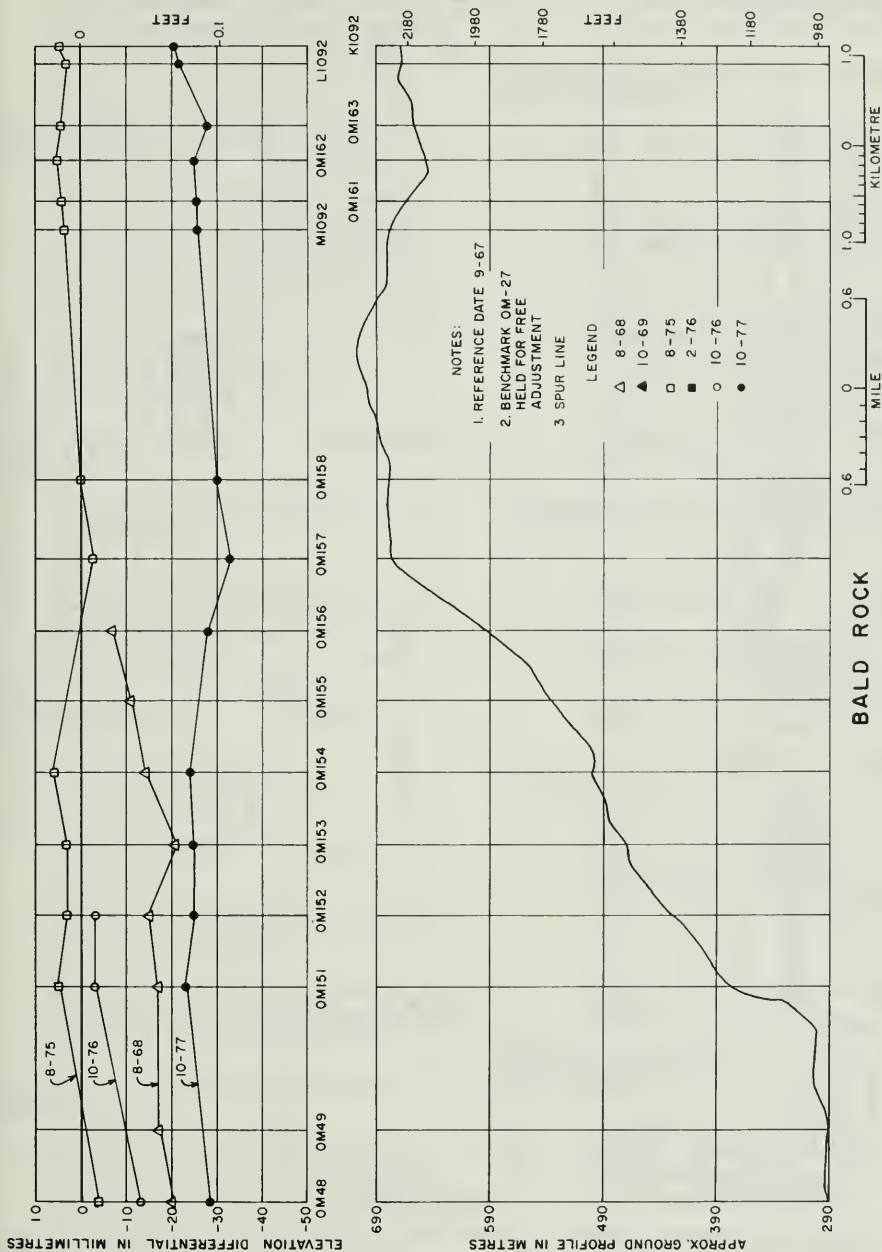


Figure 80. Bald Rock Elevation Differentials

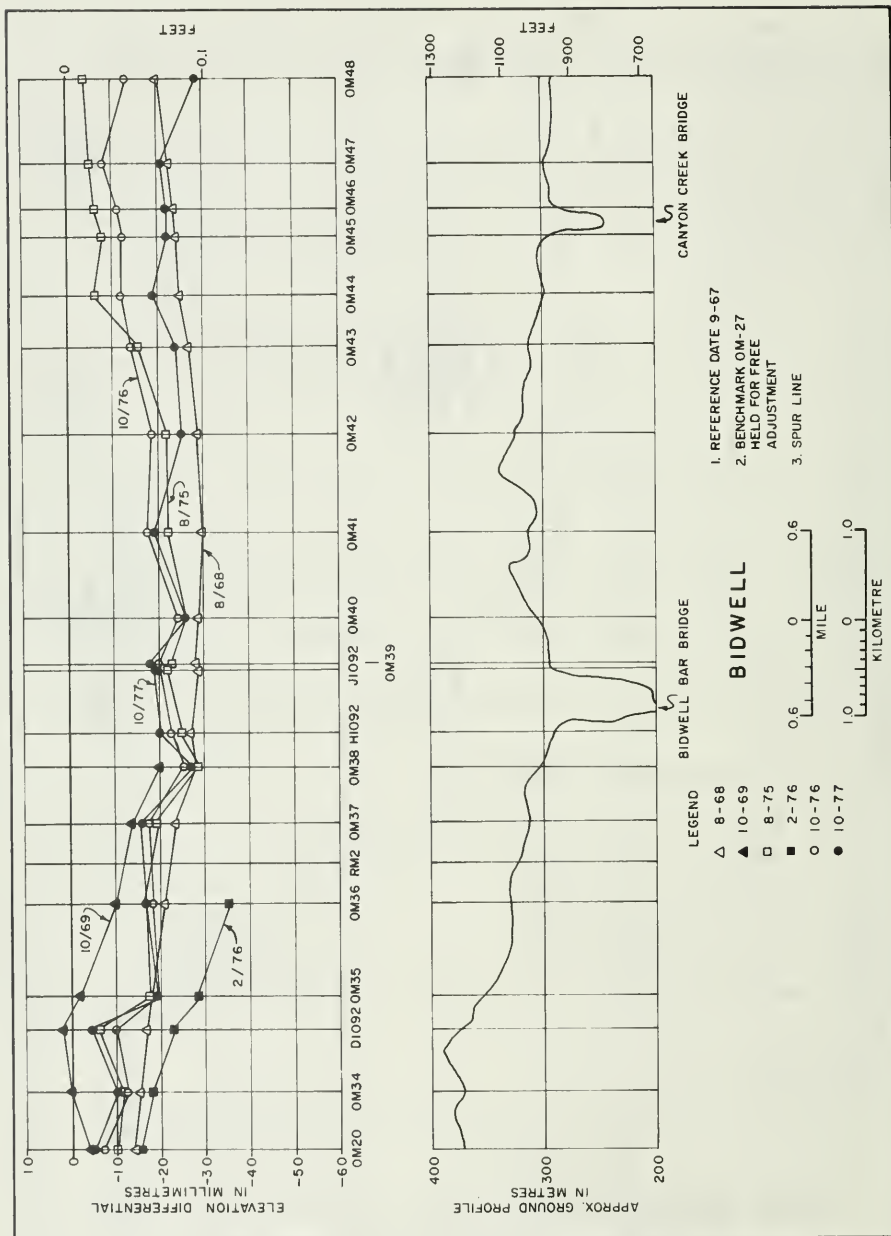


Figure 81. Bidwell Elevation Differentials

2. Close agreement of plots, except that divergence starts at about OM-42 to OM-48 where this line connects to Bald Rock.

Bidwell Canyon Saddle Dam (Figure 82)
(Reference Date September 1967)

1. Spur line from OM-33.
2. Only minor subsidence is evident up to about 20 millimetres (0.066 foot).
3. Normal embankment consolidation is shown at Monuments 2, 3 and 6 through 10.

Canyon Drive (Figure 83) (Reference Date August 1975)

1. No significant subsidence after the February 1976 survey.
2. Fifteen to 20 millimetres (0.049 to 0.066 foot) subsidence measured between August 1975 and February 1976.

Cleveland Hill (Figure 84) (Reference Date October 1975)

1. Spur line, observed elevations only.
2. Ground cracking occurred between N and M.
3. Definite subsidence to the west of the ground cracking.
4. Significant subsidence occurred at the ground rupture between November 1975 and February 1976.

Dam (Figure 85) (Reference Date September 1967)

1. Subsidence fairly consistent at 25 to 35 millimetres (0.082 - 0.115 foot).

Dunstone (Figure 86) (Reference Date February 1976)

1. Only minor variations of less than 10 millimetres (0.033 foot).

Feather Falls (Figure 87) (Reference Date September 1967)

1. Spur line fixed from Bench Mark OM-27.
2. OM-27 is the fixed elevation bench mark for the entire level net and spur lines.
3. Consistency of the adjacent bench marks (OM-26, H-925, H-80, and OM-25) shows a stable area for the fixed reference Bench Mark OM-27.
4. Localized discontinuity between G1092 and OM25.

Foothill (Figure 88) (Reference Date August 1975)

1. Consistent elevation after February 1976.
2. Fifteen to 40 millimetres (0.049 - 0.131 foot) of subsidence shown between August 1975 and February 1976.

Miners Ranch (Figure 89) (Reference Date September 1967)

1. Anomaly occurs at OM-17 (17 millimetres (0.056 foot) uplift October 1976 to October 1977), possibly disturbed by power pole installation.
2. Significant subsidence west of Q-925.

Mission Olive (Figure 90) (Reference Date October 1975)

1. Significant fault zone movement between 4RBR and 5RBR. Ground cracking observed between MO-4 and MO-5, MO-7 and MO-8.
2. Movement occurred between November 1975 and February 1976.

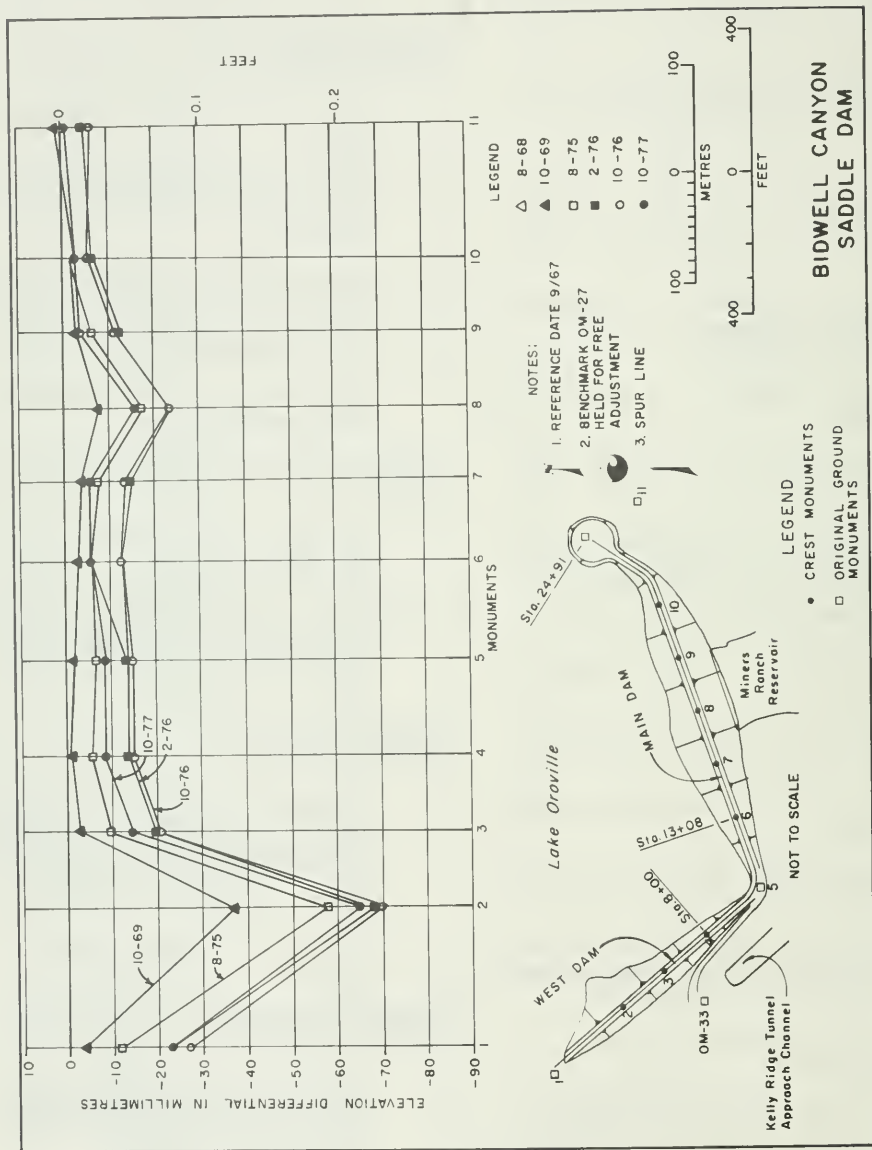


Figure 82. Bidwell Canyon Saddle Dam Elevation Differentials

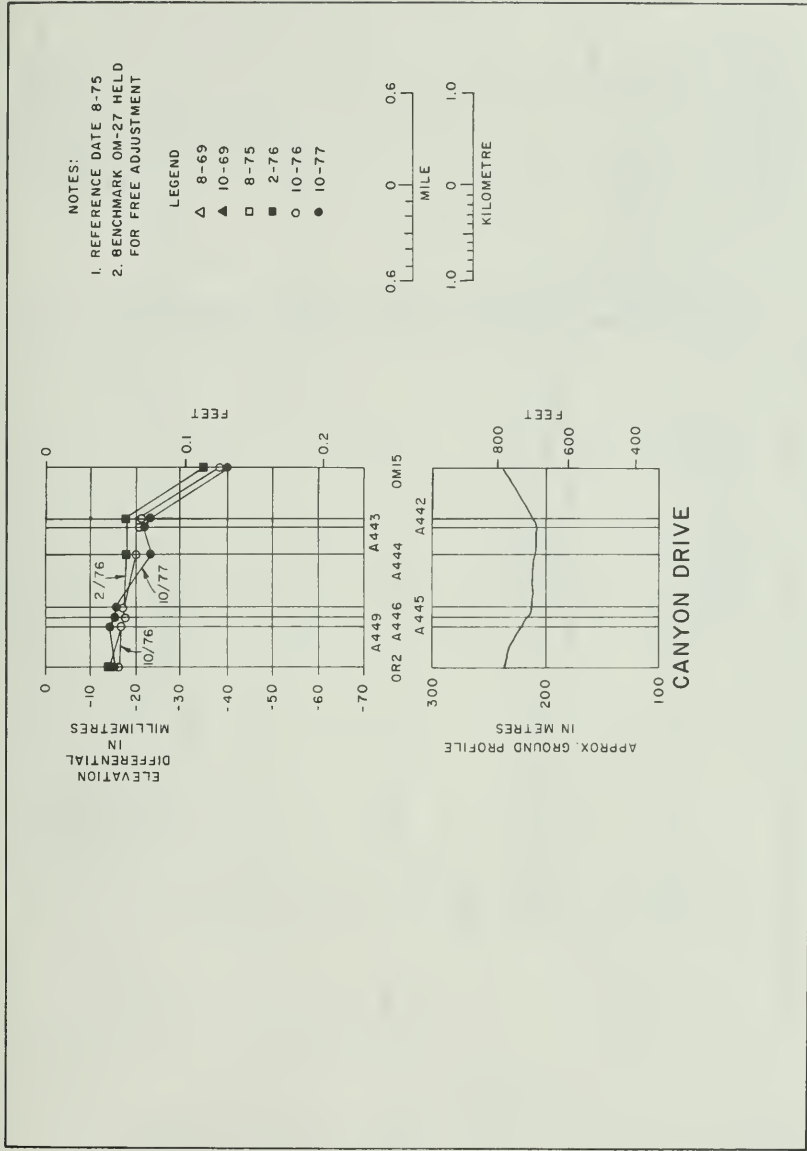


Figure 83. Canyon Drive Elevation Differentials

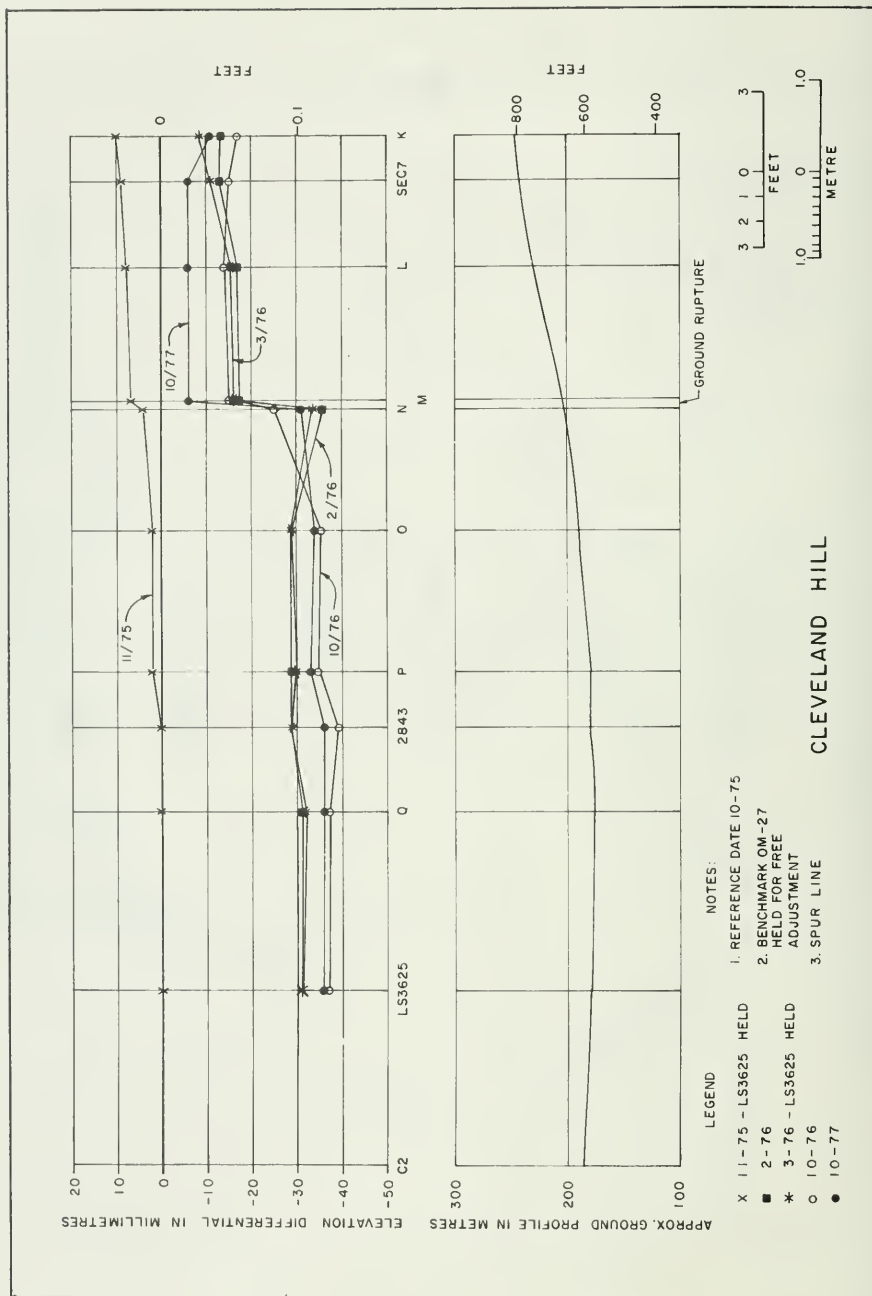


Figure 84. Cleveland Hill Elevation Differentials

- NOTES:
1. REFERENCE DATE 9-67
 2. BENCHMARK OM-27 HELD FOR FREE ADJUSTMENT
- LEGEND
- △ 8-68
 - ▲ 10-69
 - 8-75
 - 2-76
 - 10-76
 - 10-77

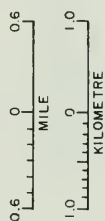
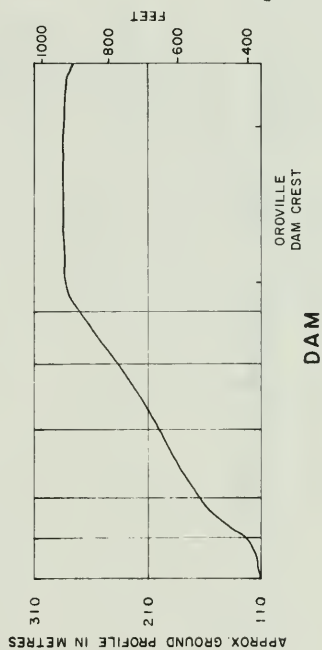
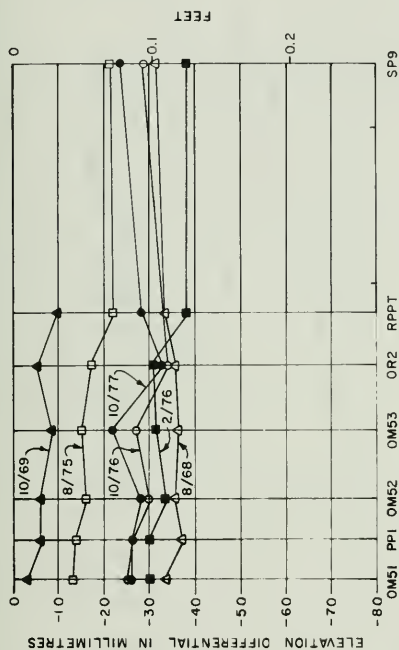


Figure 85. Dam Elevation Differentials

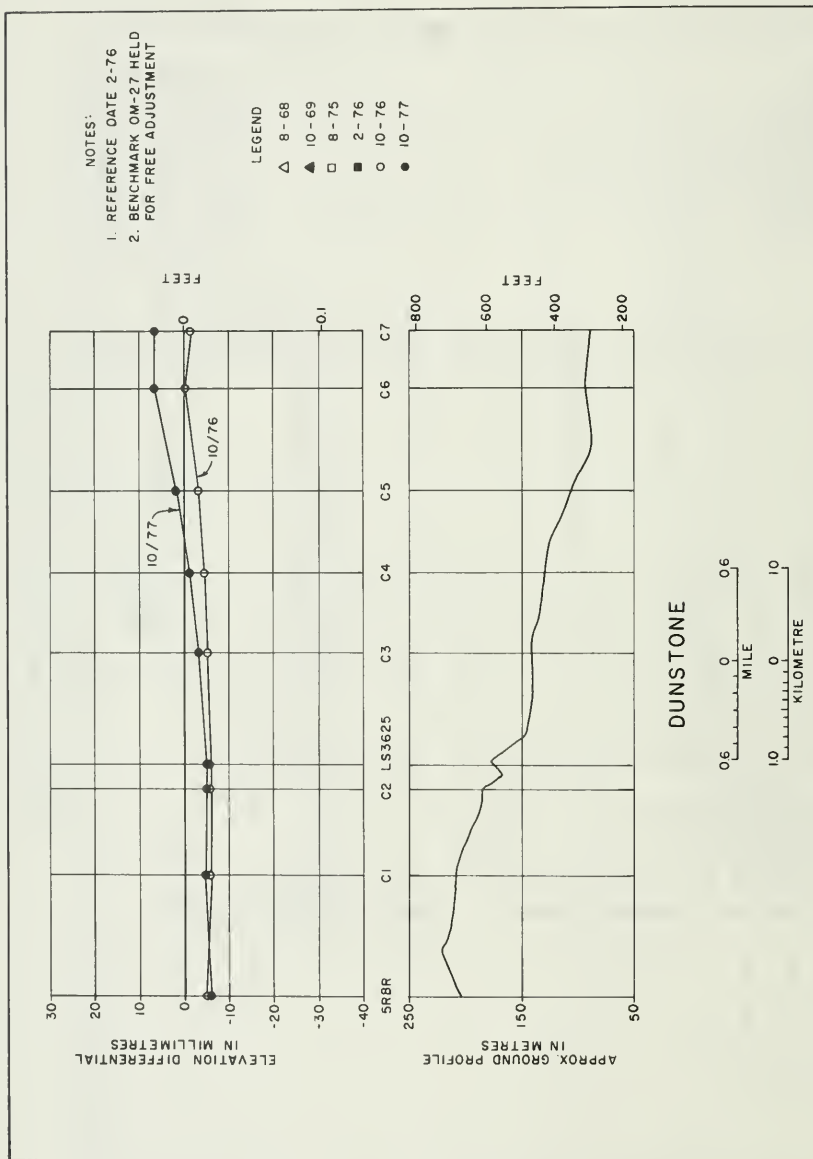


Figure 86. Dunstone Elevation Differentials

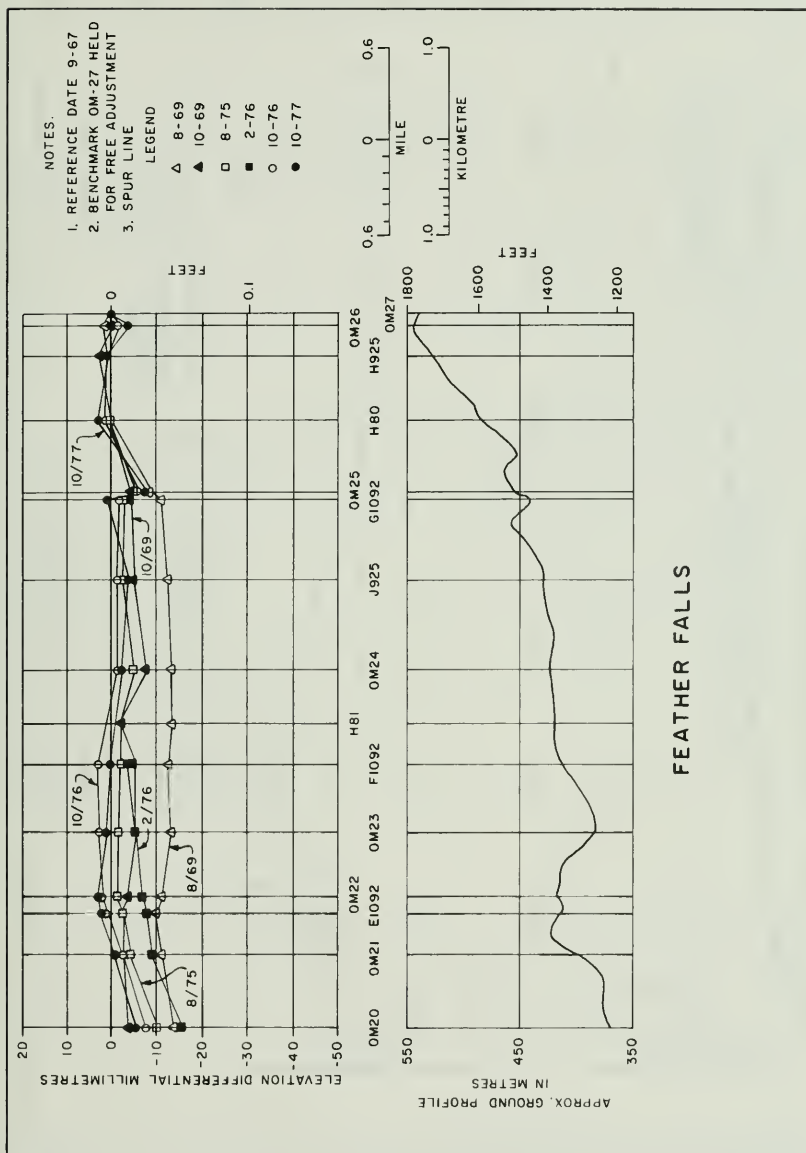


Figure 87. Feather Falls Elevation Differentials

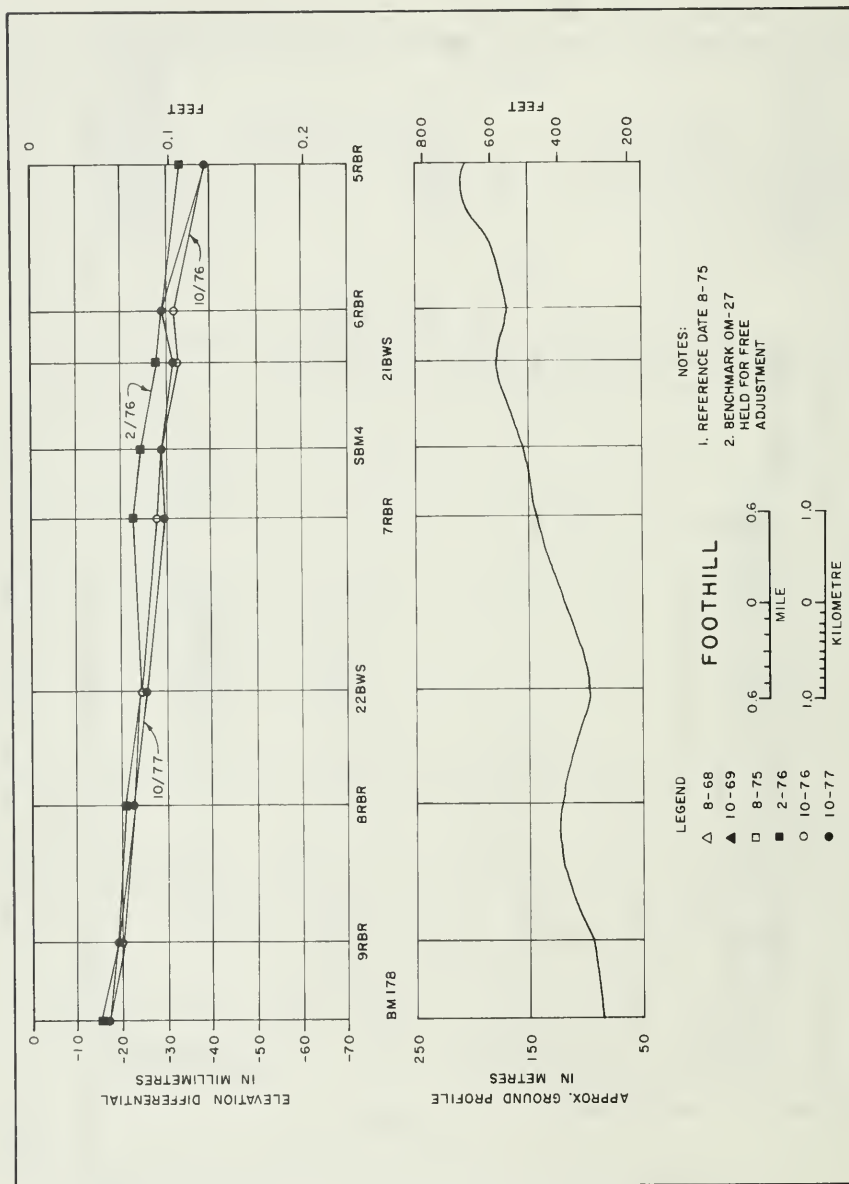
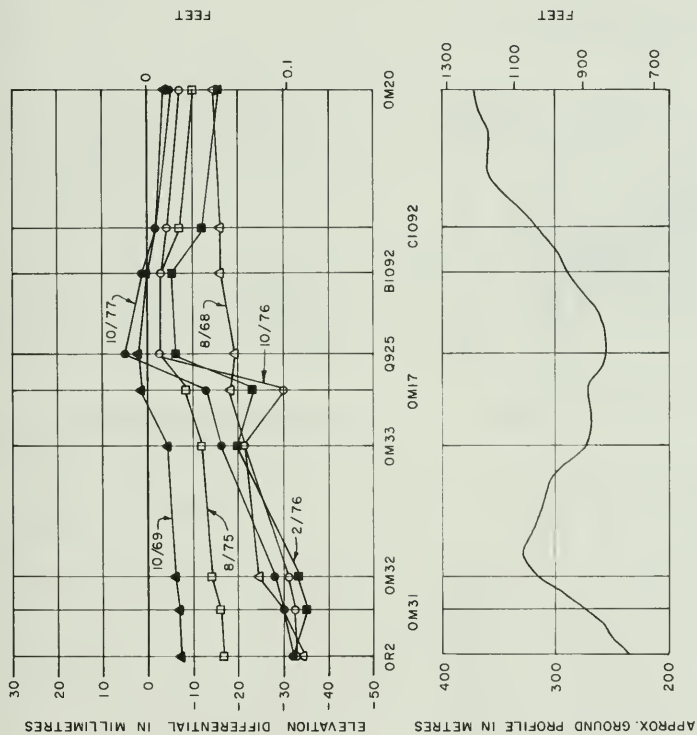


Figure 88. Foothill Elevation Differentials



- NOTES:
1. REFERENCE DATE 9/67
 2. BENCHMARK OM-27 HELD CONSTANT FREE ADJUSTMENT
 3. NEW POWER POLE WAS PLACED CLOSE TO OM17 IN APRIL 1977

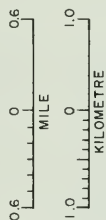


Figure 89. Miners Ranch Elevation Differentials

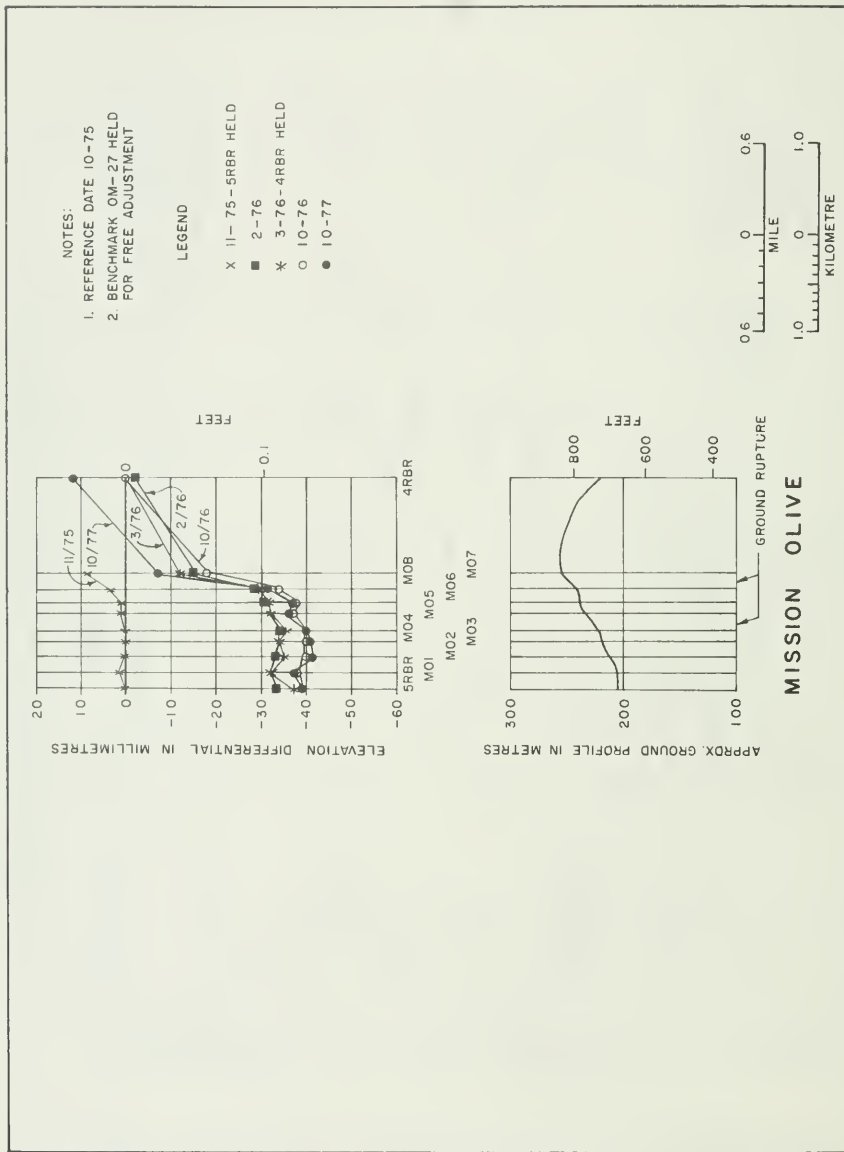


Figure 90. Mission Olive Elevation Differentials

3. Magnitude of fault zone is approximately 40 millimetres (0.131 foot).

Morris (Figure 91) (Reference Date August 1968)

1. Shows only minor uplift.

Olive (Figure 92) (Reference Date September 1967)

1. Significant subsidence trend at OM-13 to a maximum of 63 millimetres (0.207 foot).

Oro-Bangor (Figure 93) (Reference Date August 1975)

1. Almost stable line with the exception of minor uplift between October 1976 and October 1977 between 20 BWSRM and SBM-2 up to about 10 millimetres (0.033 foot).

Oroville (Figure 94) (Reference Date September 1967)

1. Anomalies at OM-6, W-145 and OM-50 indicate uplift from previous trends, probably localized conditions.
2. A major portion of the line has subsided up to 40 millimetres (0.131 foot) since September 1967.

Potter (Figure 95) (Reference Date September 1967)

1. Spur line, observed elevations only.
2. Consistent pattern with some variation.
3. The 1977 range of settlement is approximately 20 millimetres (0.066 foot).

Richvale (Figures 96 and 97) (Reference Date August 1975)

1. Spur line, observed elevations only.
2. Almost perfect agreement between October 1976 and October 1977.
3. Line subsidence of approximately 10 to 20 millimetres (0.033 to 0.066 foot).

Thompson Flat (Figure 98) (Reference Date September 1967)

1. Spur line, observed elevations only.
2. Subsidence trend range from 10 to 20 millimetres (0.033 to 0.066 foot).

Wyn-Miners Ranch (Figure 99) (Reference Date August 1975)

1. Significant subsidence at the southern end of this line between A-234 and 5RBR ranging to 40 millimetres (0.131 foot) entering into the fault zone.

103 (Figures 100, 101, 102) (Reference Date 1957)

1. Spur line, observed elevations only.
2. Minor variation of the October 1976 and 1977 surveys referenced to the 1957 datum but all are within the error limits.

Oroville Dam Crest Differential Settlement (Figure 103) (Reference Date April 1969) (Referenced to Abutments)

General. Figure 103 is included only to show the relationship of the earthquake to the consolidation rate of the Oroville Dam embankment. The graph shows that the consolidation rate increased after the July 1975 survey due to the August 1 earthquake; however, the same settlement pattern continues. The lake elevations

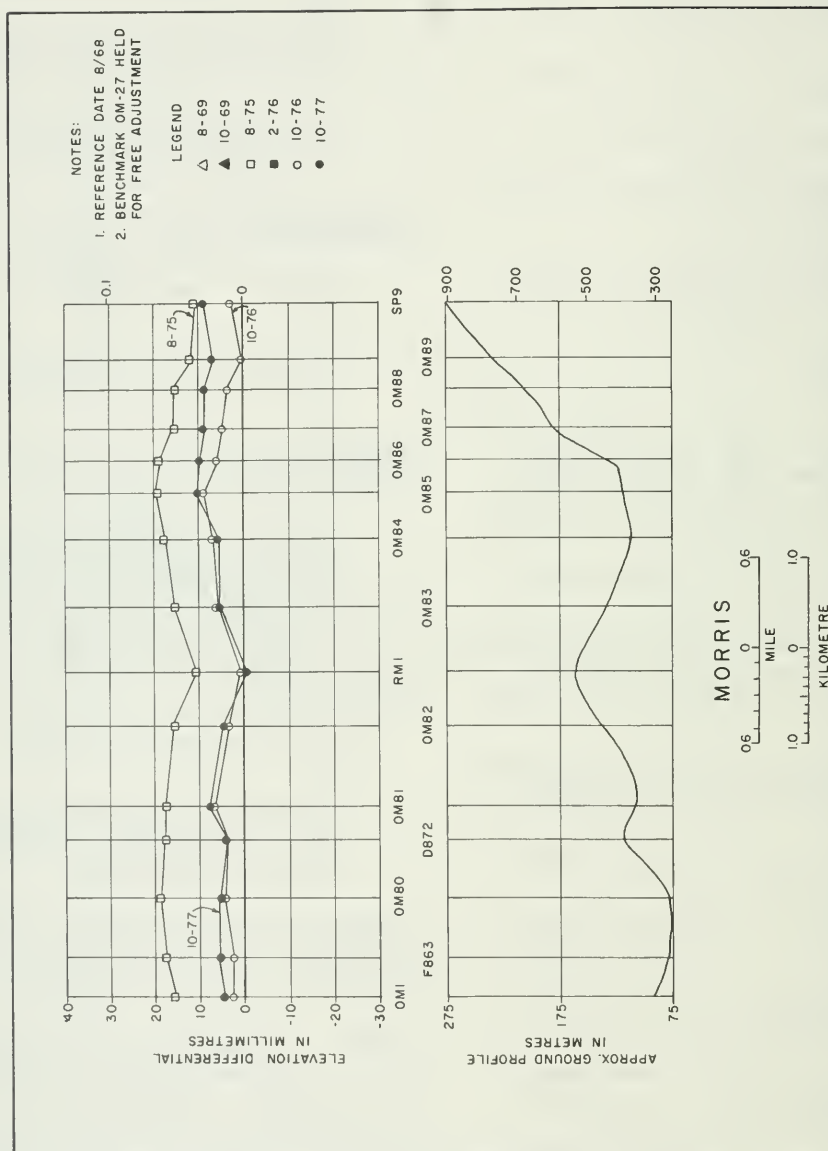


Figure 91. Morris Elevation Differentials

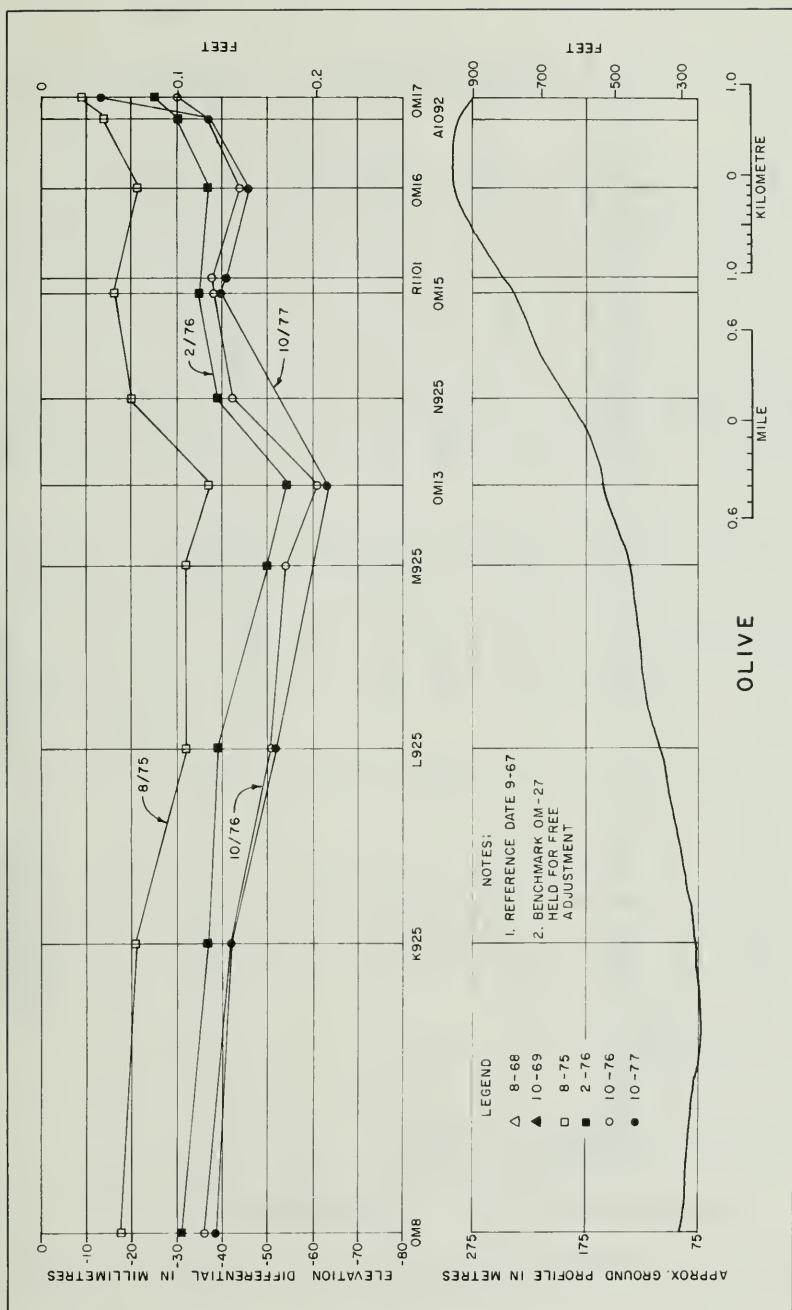


Figure 92. Olive Elevation Differentials

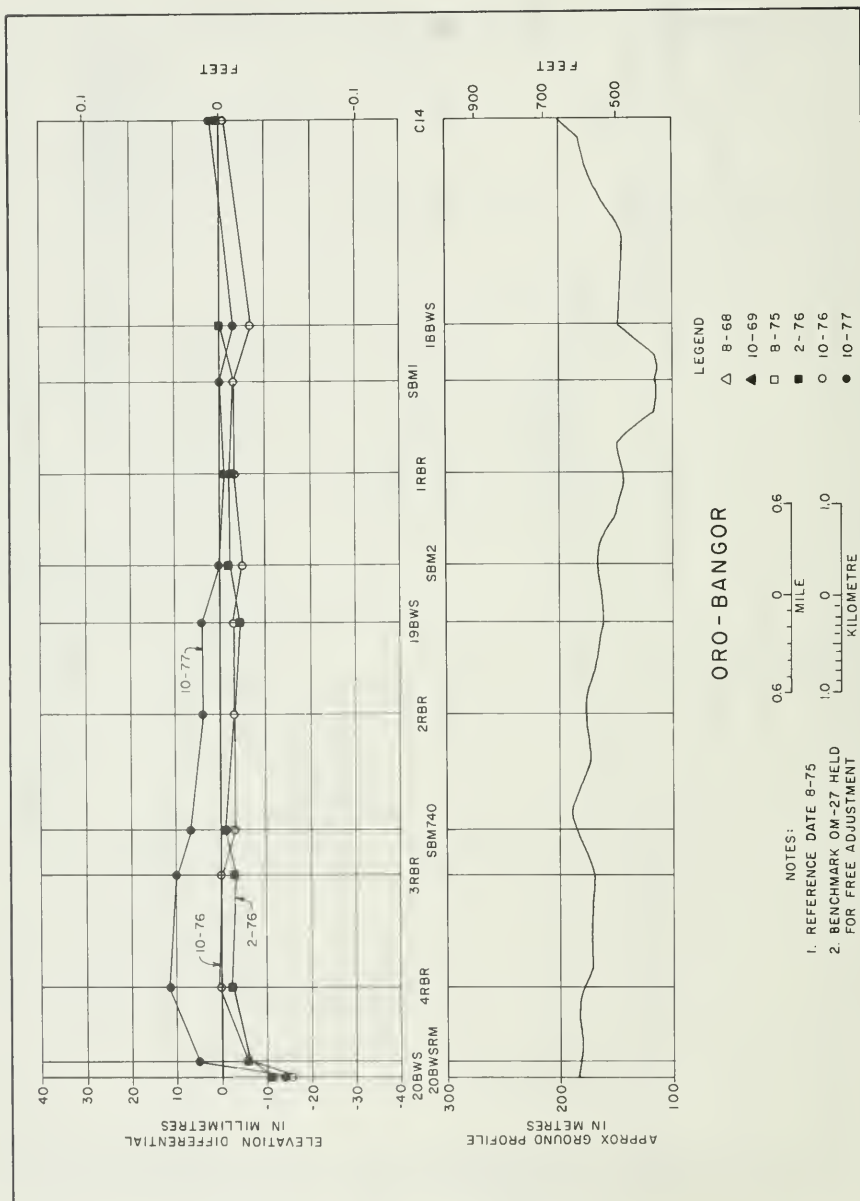


Figure 93. Oro-Bangor Elevation Differentials

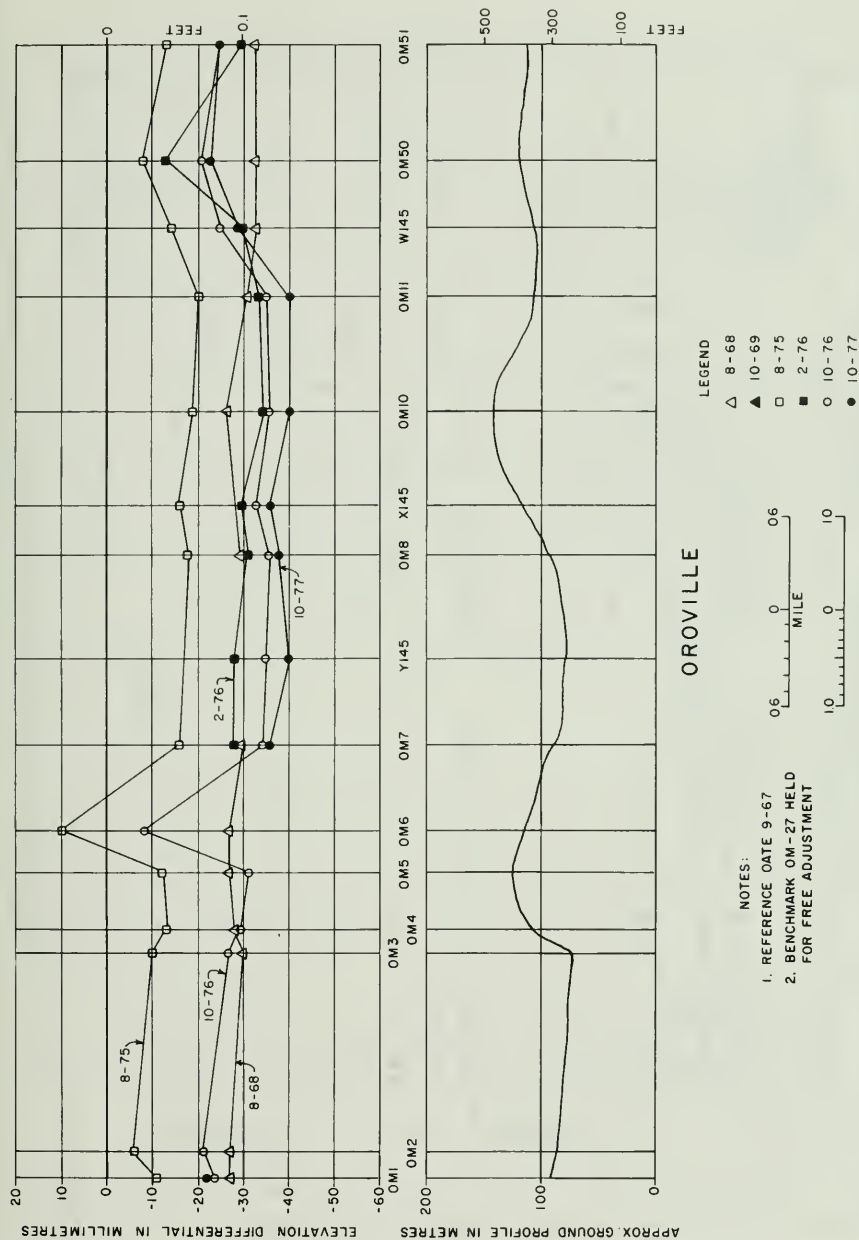


Figure 94. Oroville Elevation Differentials

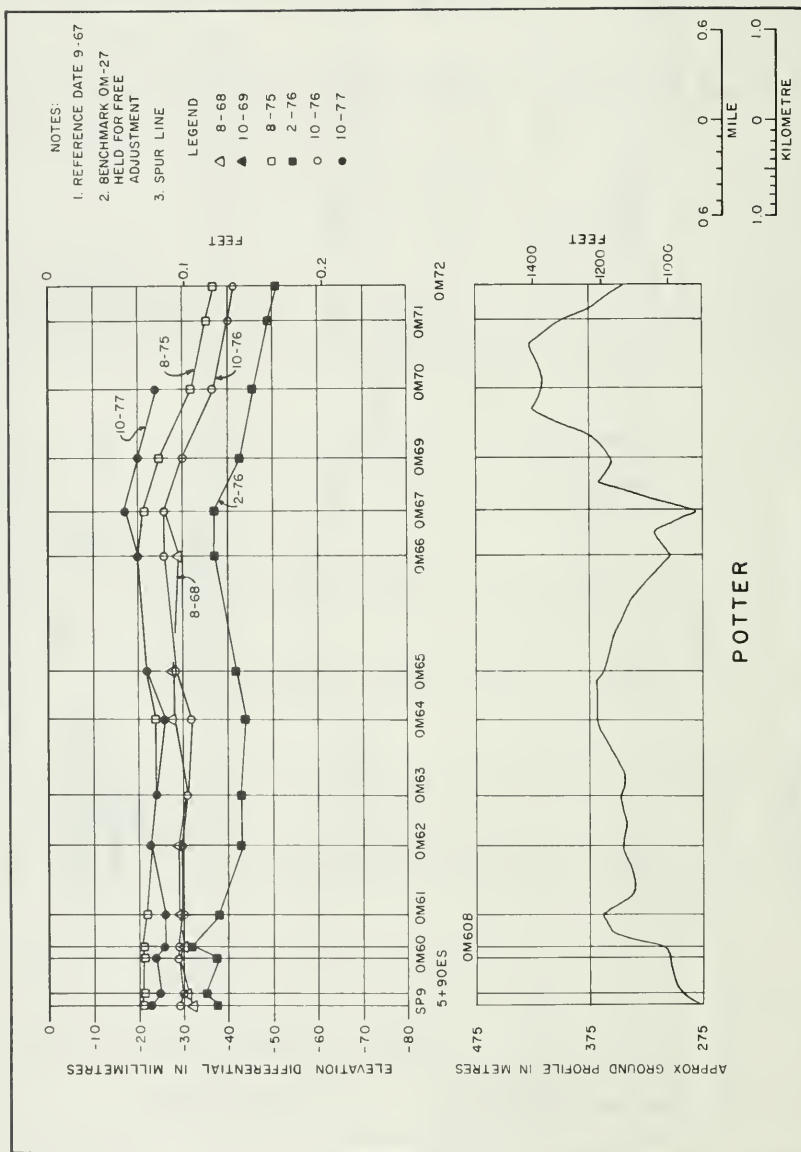


Figure 95. Potter Elevation Differentials

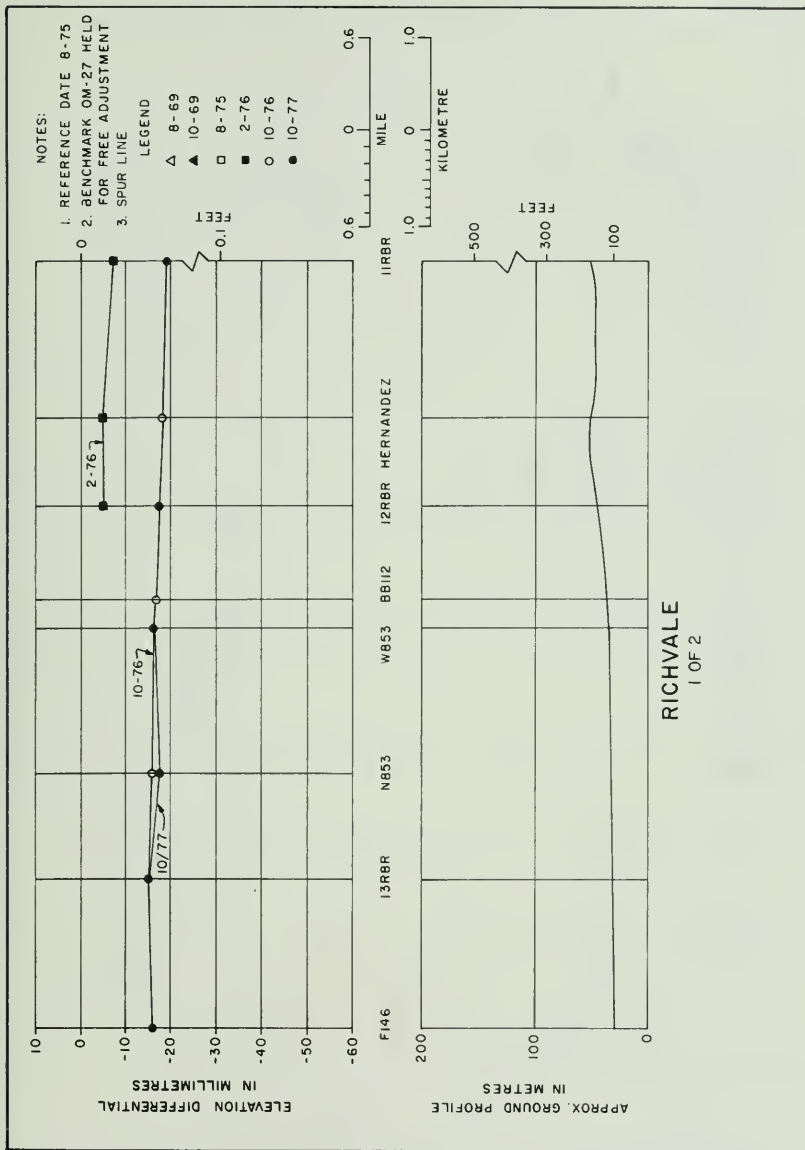


Figure 96. Richvale Elevation Differentials (1 of 2)

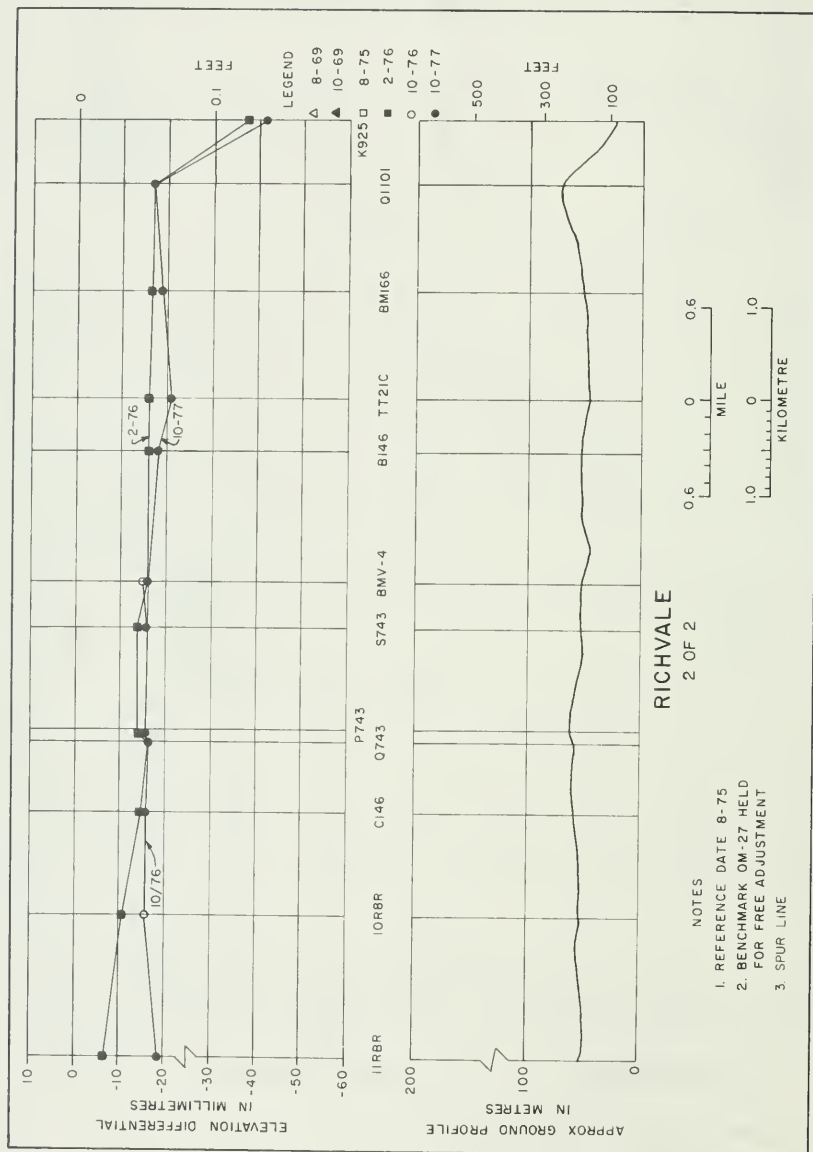


Figure 97. Richvale Elevation Differentials (2 of 2)

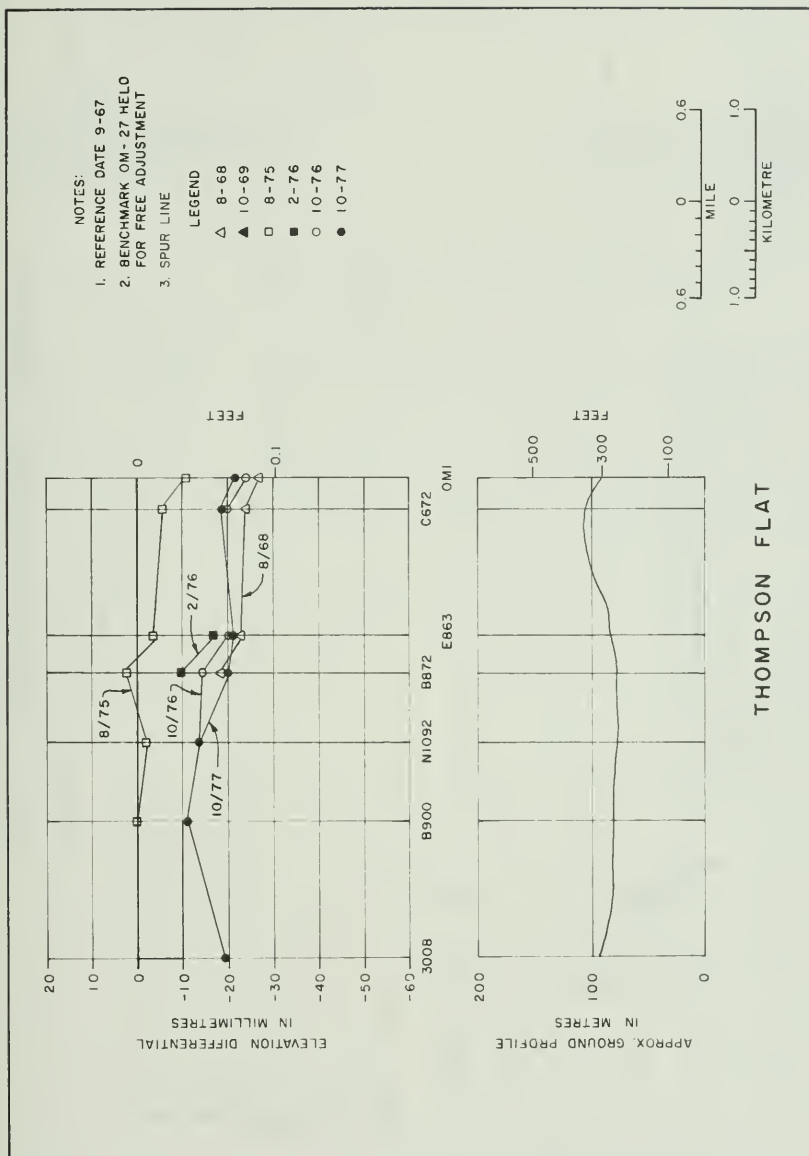


Figure 98. Thompson Flat Elevation Differentials

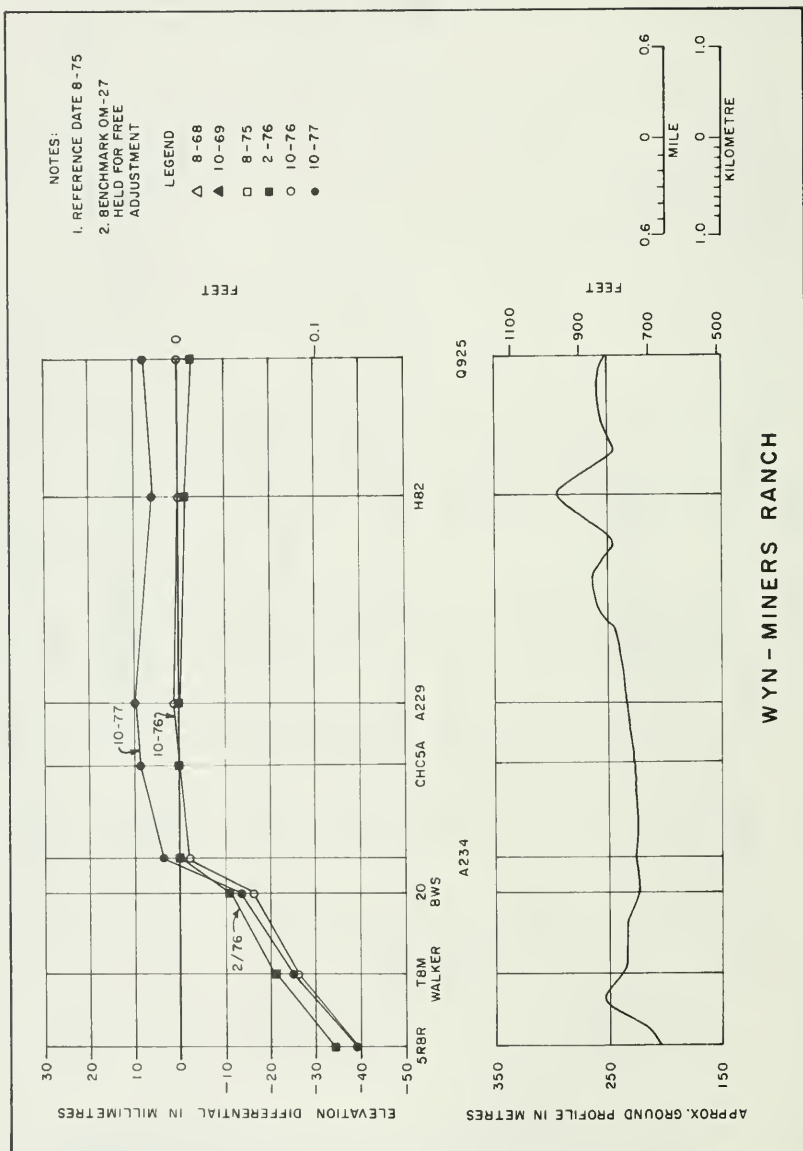


Figure 99. Wyn-Miners Ranch Elevation Differentials

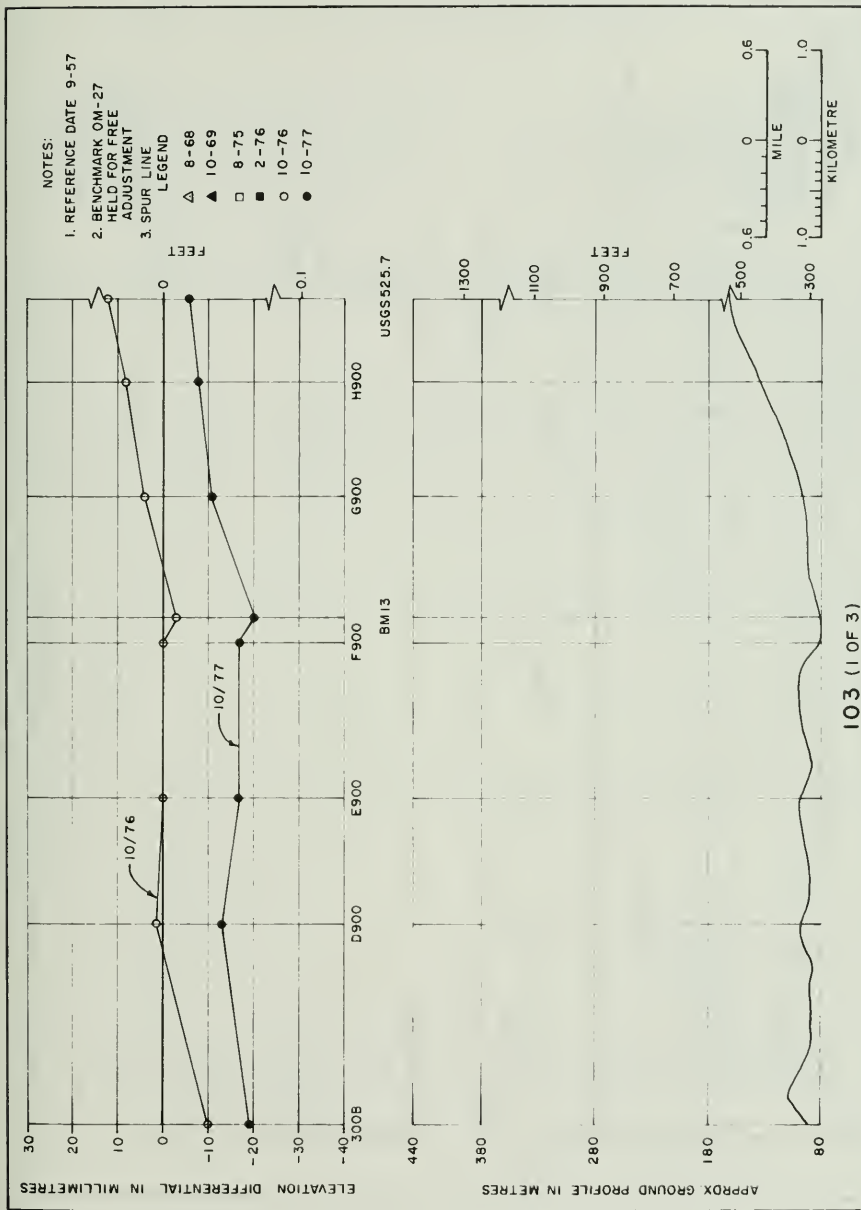
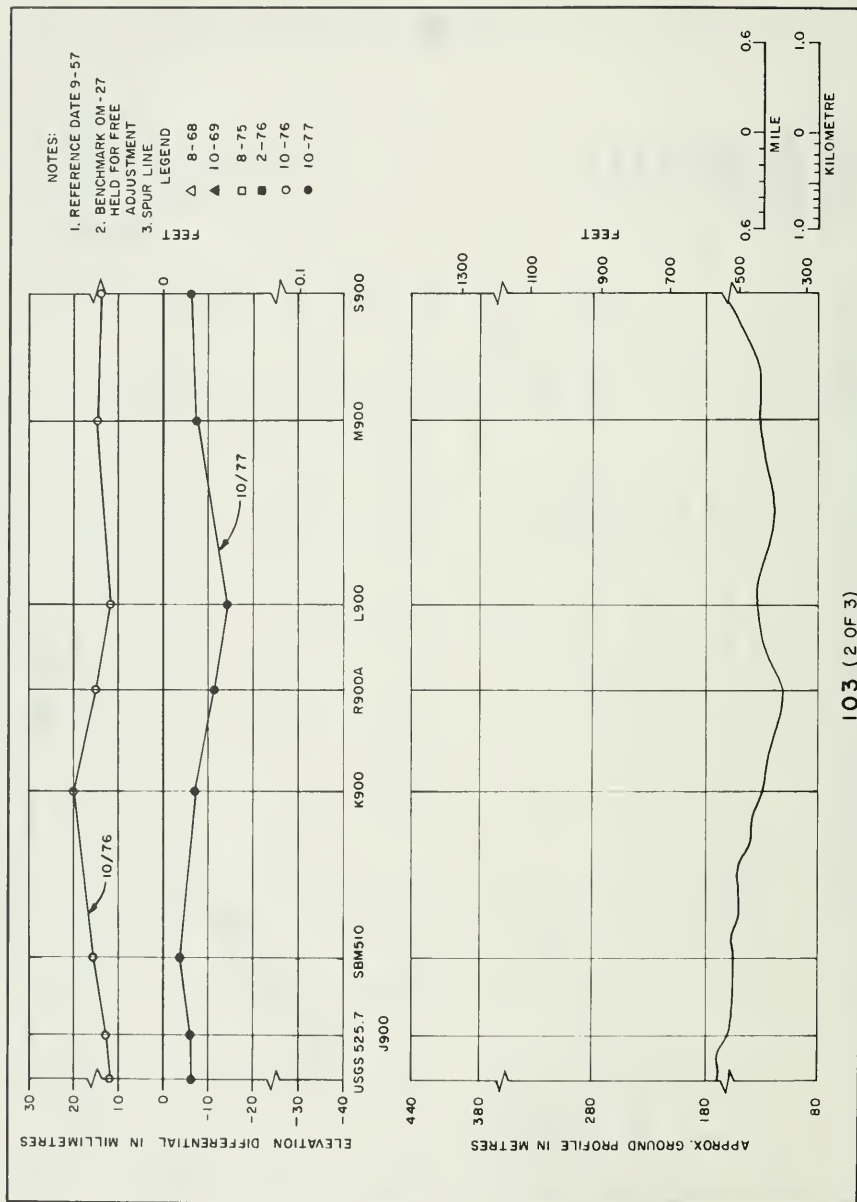


Figure 100. 103 Elevation Differentials (1 of 3)



103 (2 OF 3)

Figure 101. 103 Elevation Differentials (2 of 3)

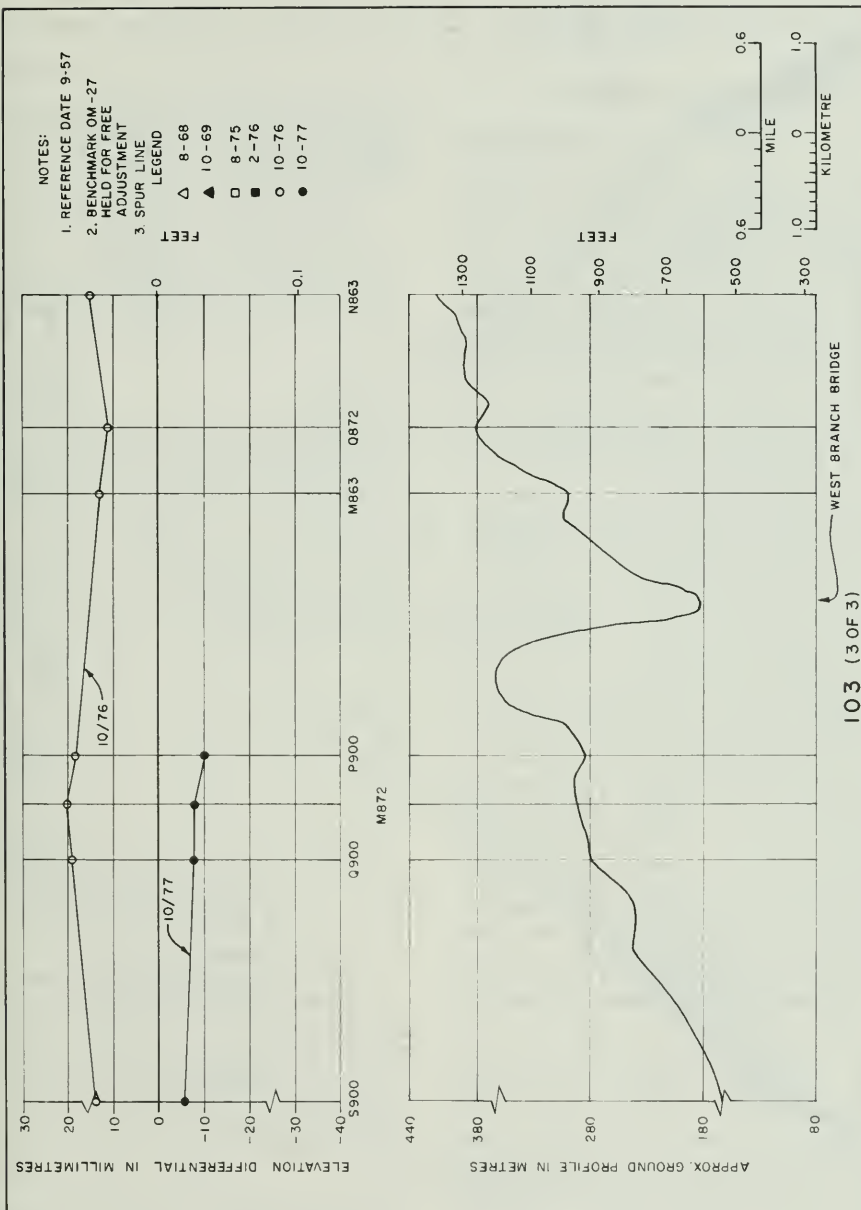
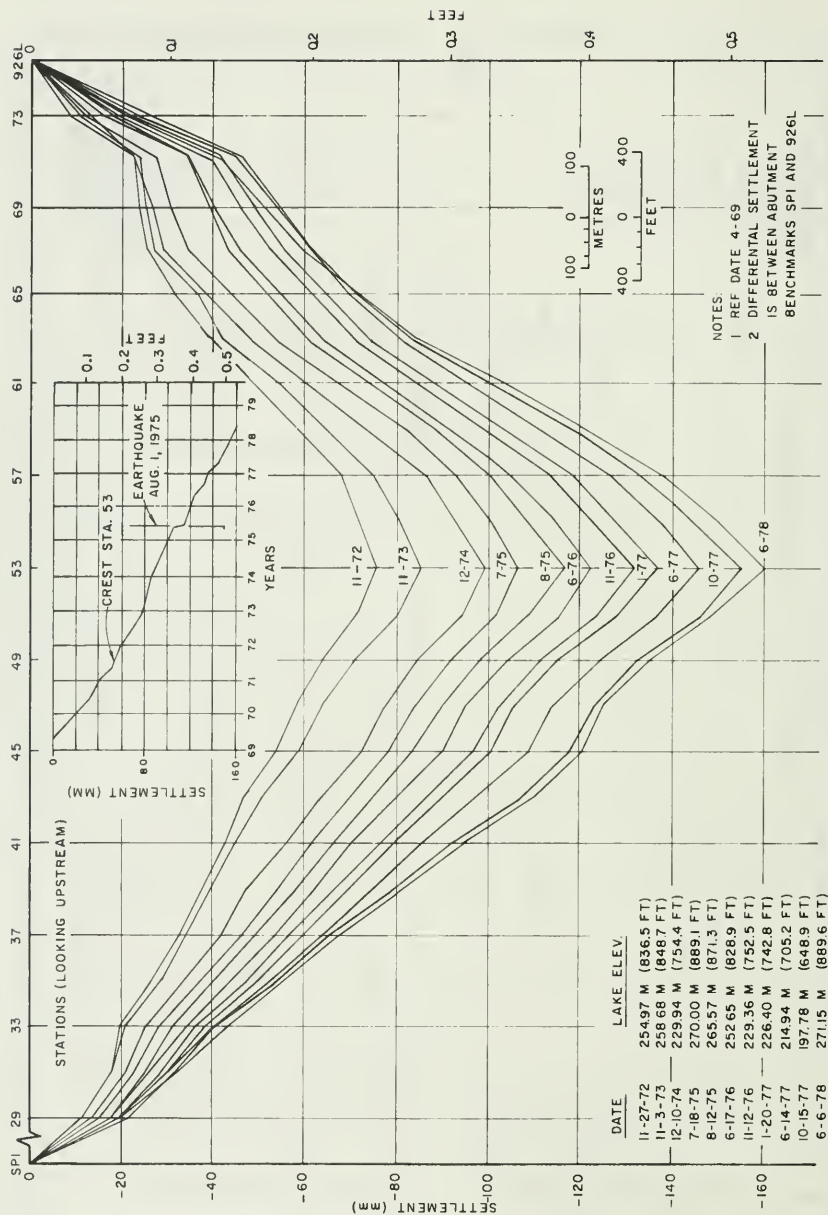


Figure 102. 103 Elevation Differentials (3 of 3)



OROVILLE DAM CREST DIFFERENTIAL SETTLEMENT

Figure 103. Oroville Dam Crest Differential Settlement
(Referenced to the Abutments)

at the time of the surveys are tabulated on the plot.

Commentary

The Department is requesting the National Oceanic and Atmospheric Administration (NOAA) to releve key bench marks, especially OM27, when they rerun their first order network in the Oroville area.

The annual releve frequency of the Oroville area network will be decreased to a longer interval not to exceed five years.

Conclusions

The following conclusions are based on free adjustment holding the elevation of OM-27 fixed (1967 USC&GS adjustment) and therefore, all elevation differentials are relative to OM-27.

1. Based on the preearthquake datum of 1967, the greatest elevation differential was only 63 millimetres (0.207 foot) on line Olive during the ten-year epoch (1967-1977).
2. The August 1, 1975, Oroville earthquake is associated with minor subsidence in the Oroville area, mainly south and southwest of Lake Oroville.
3. Most of the subsidence associated with the August 1, 1975, Oroville earthquake was measured between late August 1975 to October 1976.
4. The elevation differentials show movement of the fault zone that passes through the level lines Cleveland Hill and Mission Olive (ground cracking was evident before the lines were established). A fault zone may pass through the level lines Miners Ranch south of Lake Oroville; however, no ground cracking was found there.
5. Minor subsidence of less than 25 millimetres (0.082 foot) has been

measured adjacent to Oroville Dam and Lake between 1967 to 1977 due to all causes.

Horizontal Earth Movements

Introduction

During 1967, the Lake Oroville horizontal monitor network was established to identify movement that might be associated with filling of Lake Oroville and changes that could occur in the event of major tectonic activity. Figure 104 shows the Horizontal Geodetic Control and Triangulation Net, 1967-1975, as refined to this latter date.

Horizontal Geodetic Control and Triangulation Programs

September 1967. The 1967 original horizontal monitoring, Class 1 first-order triangulation, included four base lines measured by a geodimeter. A total of 14 stations were established. Ten concrete piers, with stainless-steel instrument adapters cast into them, were constructed. A permanent tower 6.1 meter (20 feet) high, constructed with 103-millimetre (4-inch) galvanized pipe with a stainless-steel instrument adapter, was built on Kelly Ridge because of restrictions regarding the cutting of trees and brush set forth by the Division of Beaches and Parks. The remaining stations were those of the U. S. Coast and Geodetic Survey. Metal instrument stands were erected over them and bolted to rocks to avoid disturbing the station marks. Triangulation station Bald Rock is located in the same diorite rock mass as the northernmost bench mark.

Observations were made at night and consisted of 16 sets of directions taken with a first-order theodolite.

The observation at Gaub did not have pointings to Oroville that would have established an azimuth at the westerly extreme of the net and did not have any observations to or from Bald Rock to fix

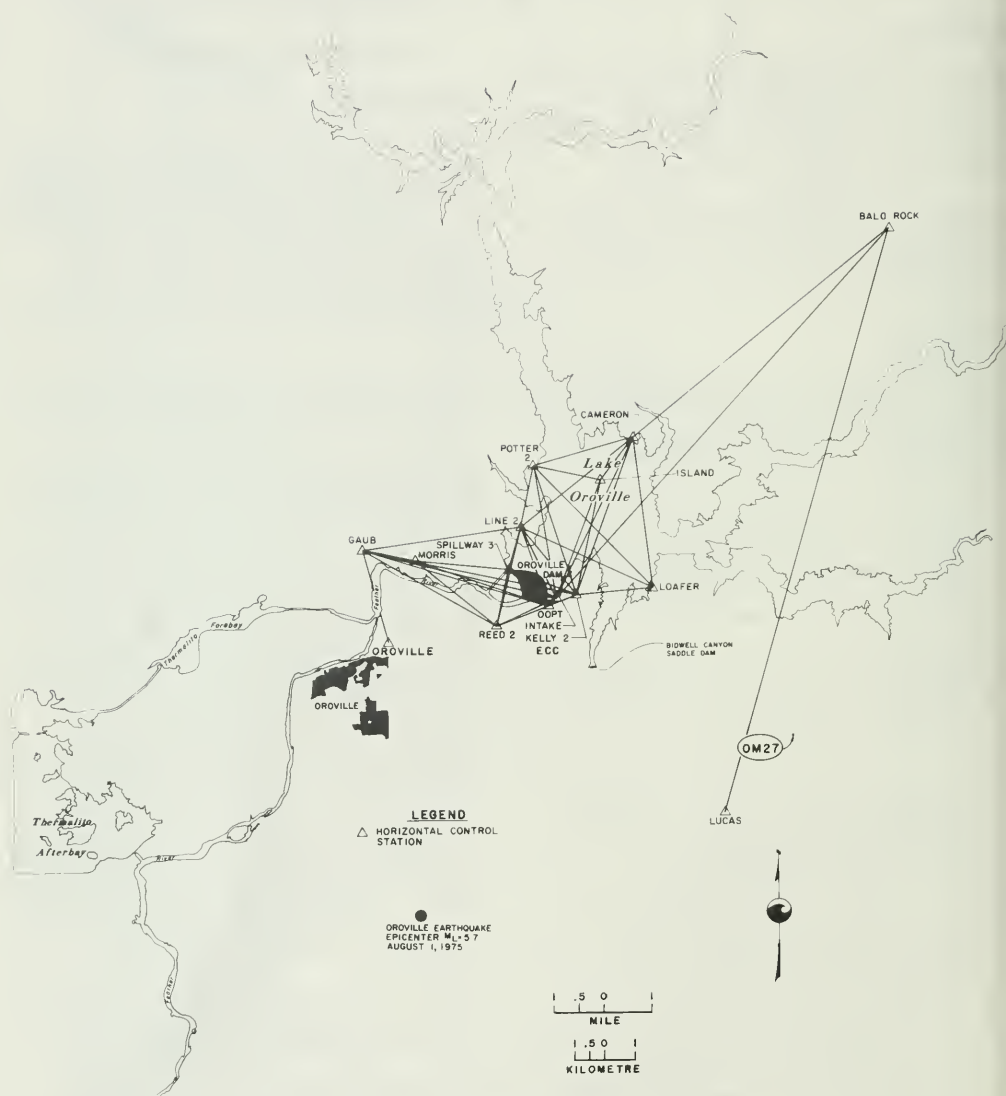


Figure 104. Horizontal Geodetic Control and Triangulation Net (1967-1975)

any orientation at the northeasterly extreme, nor was an astronomical azimuth observed from any station.

Seven lines were measured with a Model 2A Geodimeter providing the scale for the net. Three lines were measured on two successive nights; the remaining four were single observations. The 2A Geodimeter was considered a first-order base-line instrument.

April 1968. The second observation program of the horizontal net at Lake Oroville was conducted during the period from April 1 through April 12, 1968. A small change was made in the original triangulation net. Observations from the original station Spillway became blocked by a fence; therefore, it was reestablished in the other spillway abutment. A property owner requested the removal of station Potter. Hence, Potter 2 was established on State property. Observations were made to and from the original station Potter before it was removed.

Observations were made at night and consisted of 16 sets of directions (32 pointings) with a first-order theodolite. Three of the lines measured in 1976 were remeasured.

Comparison at that time between the initial observation in 1967 and that in April 1968 resulted in no detectable horizontal movement.

August - September 1975. During August and September 1975, after the August 1, 1975, Oroville earthquake, the Lake Oroville horizontal monitor net was reobserved. Night-time observations from the 16 existing stations were made with a Wild T-3 Theodolite, using the 16-set criteria at each station.

Several stations have been replaced since the original 1967 work:

Potter 1 replaced by Potter 2 in 1968
Spillway replaced by Spillway 3 in 1968

Kelly 2 replaced by Kelly 2 Eccentric in 1972

Computations and Analyses

In general, the comparison of observed angles for 1967, 1968, and 1975 shows little change. The observations at Spillway 3 (1968 vs. 1975) indicate a five-second difference; however, an examination of the triangle closures revealed that the 1968 index pointing from Spillway 3 to ODPT was in error, and this line was deleted from the recomputation of the 1968 work.

The lack of any direct azimuth orientation for the 1967 observation was corrected in 1968. The original computations show the Department's 1968 position for Bald Rock instead of the U. S. Coast and Geodetic Survey (USC&GS) published value. This 1968 value determination had been used in both the original 1967 and 1968 computations. Difficulties were encountered when the 1968 repositioning of USC&GS second-order station Bald Rock was checked. Apparently, computations had progressed from Bald Rock through a fully-observed traverse to USC&GS first-order station Gaub. This closure error was somehow transferred back to Bald Rock and a new position established.

Using the original 1967/68 field data, this traverse was recomputed with a closure error on the Bald Rock USC&GS published position of 24 millimetres (-0.08 foot) north, and 9 millimetres (-0.03) foot) east. The standard deviation of the direction work was 0.44 second and the length error ratio was one part in 377,640. This closure error was much less than the 88 millimetres (-0.29 foot) north and 49 millimetres (+0.16 foot) east, indicated in the original 1968 computations. Since it appeared that the USC&GS published position of Bald Rock was actually compatible with the other first- and second-order stations in the area, all work was recomputed on this basis.

Length measurements were used in the computations to check the position of

Bald Rock, but only one length (Line 2 to Bald Rock) has been used for the 1967/1968 and 1975 complete net computations. All computation and recomputation was by the Department of Transportation "Cosmos" Computer Program, which is a least squares adjustment by variation of geographic coordinates. Probabilities as computed in the program were:

1967 Monitor Net - 0.45 seconds standard deviation for directions - lengths 1 part in 467,049.

1968 "Bald Rock" Traverse - 0.53 seconds standard deviation for directions - lengths 1 part in 391,512

1968 Monitor Net - 0.74 seconds standard deviation for directions - lengths 1 part in 282,029

1975 Monitor Net - 0.78 seconds standard deviation for directions - lengths 1 part in 267,022

Although the errors and adjustments appear quite small, the computed distances have not matched measured lengths

as well as could be expected. The computed lengths are plus or minus 50 millimetres (0.164 foot) long, as compared to measured lengths. During the 1975 observations, the U. S. Geological Survey measured two lines in the Oroville Monitor Net, incidental to other work they were involved with. The measured length, Kelly 2 Eccentric to Cameron, is 103 millimetres (0.338 foot) shorter than the computed length. The measured length, Kelly 2 Eccentric to Line 2, is 46 millimetres (0.151 foot) shorter than the computed length. Five short lines were measured with the MA/100 tellurometer by the Department during February 1976; the Line Kelly 2 Eccentric to Line 2 was within 5 millimetres (0.016 foot) of the USGS measured distance. The other four lines were about 50 millimetres (0.164 foot) shorter than the computed distances. The Line Kelly 2 Eccentric to Cameron is beyond the MA/100 range.

Comparative coordinate position changes, in millimetres, from the 1967 observation are:

		<u>1968</u>		<u>1975</u>	
		<u>mm</u>	<u>feet</u>	<u>mm</u>	<u>feet</u>
<u>Loafer</u>	North	-37	-0.12	-37	-0.12
	East	-12	-0.04	+85	+0.28
<u>Island</u>	North	-37	-0.12	+18	+0.06
	East	+21	+0.07	+85	+0.28
<u>Reed 2</u>	North	- 9	-0.03	-43	-0.14
	East	+15	+0.05	+ 9	+0.03
<u>Spill 3</u>	North	-	-	- 6	-0.02
	East	-	-	- 3	-0.01
<u>OPDT</u>	North	-12	-0.04	-49	-0.16
	East	- 9	+0.03	+ 9	+0.03
<u>Morris</u>	North	- 6	-0.18	-15	-0.05
	East	+3	+0.01	+ 3	+0.01
<u>Cameron</u>	North	-55	-0.18	+30	+0.10
	East	+ 9	+0.03	+94	+0.31

		<u>1968</u>		<u>1975</u>	
		<u>mm</u>	<u>feet</u>	<u>mm</u>	<u>feet</u>
<u>Intake</u>	North	-27	-0.09	-34	-0.11
	East	- 3	-0.01	+27	+0.09
<u>Line 2</u>	North	-21	-0.07	-12	-0.04
	East	+18	+0.06	+ 9	+0.03
<u>Potter 2</u>	North	-	-	+ 6	+0.02
	East	-	-	0	0

The computed movements of the stations of this net are insignificant; and, in many cases, within the accuracy of the surveys. It appears that there is a scale problem in the network, but the effect on comparative position differences would be slight. Results of the 1975 survey indicate a north and east expansion of the easterly portion of the net. However, the measured lengths from Kelly 2 Eccentric to Loafer and Cameron as compared to computed lengths, do not support this indicated change.

Commentary

The 1975 observations and calculations were to be a duplicate of the 1967 and 1968 work. However, all stations visible from each occupied station were observed, and all directions used in the computations. Therefore, some of these observed lines form extremely poor figures and adversely affect the final station positions.

Based on the comparison of preearthquake (1967) and postearthquake (1975) values, using all observations, the greatest computed movement occurred at station Cameron, with a movement of +98 millimetres (+0.32 foot) northeasterly.

The Oroville Horizontal Geodetic Control and Triangulation Net is being refined to include only strong figures. All the previous surveys will be recalculated on this basis for comparison to future surveys.

Conclusions

1. All computed horizontal movements are minor and in many cases within the accuracy of the existing surveys and computations.
2. The August 1, 1975, Oroville earthquake did not cause sufficiently large horizontal movements that could be reliably measured and calculated within the Lake Oroville Monitoring Network.

CHAPTER V
OROVILLE DAM:
EVALUATION OF SEISMIC STABILITY

Acknowledgements for Chapter V

For some time before the earthquakes of 1975, the Division of Safety of Dams had been working on static and dynamic analyses of Oroville Dam as part of their program for developing dynamic analysis capability. After the earthquakes, the Divisions of Operations and Maintenance and Design and Construction undertook the analysis of seismic preparedness and safety of the Oroville Complex, including an evaluation of seismic stability of Oroville Dam. Much of the work already completed by Division of Safety of Dams was used in this evaluation, and they were requested to participate in the additional studies following the earthquake.

John Vrymoed performed the static and most of the dynamic finite element analyses, and interpreted the acceleration records of the 1975 earthquakes. He also provided advice on additional dynamic analyses. His office report, "Dynamic Analysis of Oroville Dam," provided most of the material for several chapters and much of the additional information for this report.

Bill Bennett planned the cyclic test program for Oroville gravel and carried out the first 20 tests. His report, "Evaluation of Sample Density for Triaxial Testing of Oroville Gravel," is the basis of the discussion of sample density in Section 8.

Emil Calzascia made the modifications to the Pacoima and Taft acceleration records to develop the acceleration time history for the reanalysis earthquake; and did the filtering and corrections to acceleration records of the 1975 earthquakes to produce acceleration time histories and response spectra.

Through many discussions, Rashid Ahmad, Emil Calzascia, Bill Bennett, and John Vrymoed of the Division of Safety of Dams contributed immeasurably to the understanding of complex aspects of the analysis, and suggested methods for solving problems associated with three-dimensional effects.

Harry Kashiwada of the Soils Laboratory made many trips to Richmond to assist in conducting the cyclic triaxial tests, first with Bill Bennett and later with N. Banerjee.

N. Banerjee took over the cyclic testing and completed the program, under the direction of Professor H. B. Seed.

The guidance and advice provided by Professor Seed during the studies is especially appreciated.

1. INTRODUCTION

Background

Oroville Dam is situated on the Feather River in the foothills of the Sierra Nevada above the Sacramento Valley. The

dam is 8 kilometres (5 miles) east of the City of Oroville and about 113 kilometres (70 miles) north of Sacramento (see Figure 105).

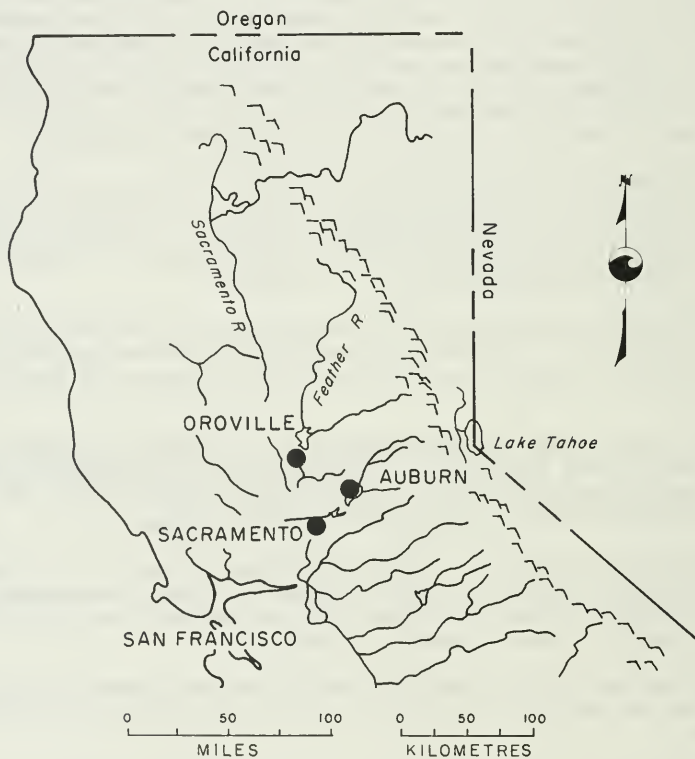


Figure 105. Location Map

It has a maximum embankment height of 235 metres (770 feet) and crest length of 1 707 metres (5,600 feet) from the gated spillway to the left abutment. The 61 000 000 cubic metre (80,000,000 cubic yards) embankment is made up of an inclined impervious gravel-clay core founded on a concrete core block, with sand-gravel-cobble transitions and shells upstream and downstream.

Historically, there have been some moderately strong earthquakes in the Oroville region. However, when the dam was built in the early 1960's, there were no known active faults within 32 kilometres (20 miles) of the dam. Design to resist earthquakes was a major consideration, and the best methods available at the time were used. Embankment slopes were analyzed by modified Swedish slip-circle,

sliding-wedge, and infinite-slope methods, with a 0.1g horizontal acceleration force included to represent earthquake loading. The upstream slope of the embankment was investigated to find the critical conditions for stability with several reservoir levels. The minimum safety factor found was 1.2 for the upstream slope, with the reservoir lowered 90 metres (300 feet).

In addition, a series of shake table tests, using a 1:400 scale embankment model, were conducted by Professor Seed at the University of California at Berkeley; he also performed analytical studies to calculate seismic coefficients for the dam for the El Centro earthquake (maximum acceleration = 0.25g), to estimate soil strengths that would exist in the gravel shell during an earthquake, and to determine safety factors for upstream sliding wedges. Seismic coefficients varied from 0.1g to 0.25g, strengths (friction angle of gravel shell) varied from 42° to 38°, the inclination of contact force between wedges varied from 0 to 20°, and resulting safety factors varied from 1.75 to 1.

On August 1, 1975, an earthquake of Richter Magnitude 5.7 occurred about 12 kilometres (7.5 miles) from the dam. The Oroville earthquake series began with a number of foreshocks on June 28, 1975. Then on August 1, twenty-nine foreshocks occurred within 5 hours of the main shock. The largest of these foreshocks had a magnitude of 4.7. Many aftershocks, with magnitudes up to 5.1, occurred throughout August, and scattered shocks continued for many months.

The embankment performed well in all the shocks of the Oroville earthquake sequence, which produced accelerations at the base of the dam of about 0.1g on three different occasions. Instrumentation results indicated maximum permanent displacements of about 25 millimetres (1 inch), pore-pressure rise in the core of 15 metres (50 feet), and maximum transitory pore-pressure response in the upstream transition of 83 kilopascals (0.8

TSF). Performance of all Oroville area water-project structures is detailed in DWR Bulletin No. 203, "Performance of the Oroville Dam and Related Facilities During the August 1, 1975 Earthquake".

Even though the embankment performed well in the 1975 Oroville earthquake, it became apparent that active faults were quite close to the dam. The question became: What earthquake is now appropriate for analysis of Oroville Dam, and how will the dam perform in that earthquake? To answer this question, the Department of Water Resources began the comprehensive investigation described in this report.

The dam performance was to be evaluated by the latest state-of-the-art procedures, which included cyclic-strength testing of gravels, studies of the observed embankment response to ascertain the in-place shear modulus of the gravel shells, and static and dynamic finite-element-method analyses to determine stresses in the embankment. To assist in the evaluations, the Department convened a special consulting board of foremost specialists in geology, seismology, dynamic analysis, and practical dam design. This board has provided guidance in completing the studies discussed in this report and has reviewed the findings.

Commentary

1. It is generally accepted that very dense cohesionless soils will not develop liquefaction flow slides. The cyclic triaxial tests on Zone 3 gravels provide additional support for this concept. Pore water pressures might rise momentarily to the value of the confining pressure on any loading cycle, but would then drop quickly as the sample strained. In order for a flow slide to be possible, pore pressure would have to remain high as strain progressed.

In evaluating embankment performance, liquefaction flow slides were not considered possible. The objective was

to make the best estimate possible of the extent of deformations that would be caused by earthquake shaking.

2. An apparent discrepancy has been noted by the profession between strains in laboratory test samples and strains calculated by dynamic analyses. For dynamic stresses developed in an embankment during strong earthquake shaking, calculated linear elastic shear strains may approach 1 percent. At the same stresses, laboratory samples could reach 5- to 10-percent shear strain. Developers of dynamic analysis procedures generally contend that calculated stresses are correct even though the strains may be incorrect.

In situations where initial static shear stresses are high, the strain in any one cycle may be about the same in a test sample as that calculated for a field element. Sample strain accumulates incrementally in one direction until the accumulated strain is 5 to 10 percent. On any one cycle, shear strain may not be much greater than 1 percent.

However in other situations, where initial static shear stress is smaller, the strain on any one cycle generally reaches several percent.

3. There has not been any method developed and verified for calculating embankment deformations caused by earthquake shaking, other than the rough estimate of average shear strain potential times height, made for Upper San Fernando Dam. This dam developed very high strain potentials, and probably a liquefied interior zone. It is not at all clear that the same method would apply to a case with much smaller strain potentials and no liquefied zone. For example, it is commonly accepted that a dam which develops compressive strain potentials of less than 5 percent will not suffer significant deformations. But, if the described method is used, displacements

of many feet would be calculated for a high dam with average compressive strain potential of only 2 or 3 percent.

4. The investigation was limited to the upstream shell whose strength might be reduced during earthquake shaking because of saturation and possible lack of drainage. The downstream shell is essentially dry and would presumably retain full drained strength and therefore would develop smaller strains. The core is a compacted clay-gravel, a type of material found to perform well in strong earthquake shaking. On the basis of these considerations, the maximum deformations would be expected in the upstream shell.

Summary of Findings

1. Oroville Dam is in a narrow canyon relative to the height of the dam, which complicates the problem of analyzing earthquake response. Abutment restraint has a significant effect on natural period, accelerations, displacements, and stresses. Two-dimensional methods of dynamic analysis will not give correct values for these response factors. However, a two-dimensional analysis can be forced to give the correct period and crest accelerations (when they are known from crest acceleration records) by deliberately using an incorrect (pseudo) modulus for the embankment soil. An extension of this approach was used to take into account the abutment restraint effects on shear stresses generated by the Reanalysis Earthquake. A basic assumption was that the same pseudo shear modulus which gave the correct response in the recorded earthquake will also give the correct response in a stronger earthquake. The effect of abutment restraint is to reduce shear stresses significantly in the upper part of the embankment.

2. The cyclic strength of dense cohesionless soil is difficult to assess, particularly at consolidation stresses lower than the critical confining pressure. Cyclic triaxial tests were carried out on dense samples of Monterey "O" sand and Oroville sand at low isotropic consolidation stresses, with special attention given to observing sample behavior. The results indicate that dense samples strain as uniformly as do loose samples, and that higher strains are produced when higher cyclic stresses are applied. These observations hold true even for cyclic stresses higher than the consolidation stress. However, it was found that strain occurs only in the extension direction for dense sands.

Studies by others on dense Monterey "O" sand also showed that triaxial sample strain is all in the extension direction, but that triaxial stress-strain behavior still correlates with shaking-table stress-strain behavior. These tests all used cyclic triaxial stresses less than the consolidation stress.

On the basis of all these studies, the cyclic triaxial test is considered to be as applicable for evaluating cyclic strain behavior at consolidation stresses lower than critical confining pressure as at consolidation stresses above critical confining pressure. However, further studies are needed at higher cyclic stresses to extend the correlation between cyclic triaxial and shaking-table tests.

The cyclic triaxial tests on Oroville gravel were used to determine cyclic shear strength envelopes. For some tests, curves of strain vs. number of cycles were conservatively extrapolated, because cyclic load dropped or apparent sample necking occurred early in the test.

3. Many of the analysis conditions and soil properties could not be determined precisely. Ranges of supportable choices and values were defined

by testing, analysis of observed performance, and comparison with other published data. Embankment displacements were estimated for two cases defined as follows:

- a) Best Judgment Case -- For each analysis condition and soil property, use the value within the defined range that is best supported by available evidence and judgment.
- b) Conservative Case -- For each analysis condition and soil property, use the end of the defined range that produces the higher estimated displacement.

Predicted behavior of the dam, based on the "best judgment case," is that no slides or large movements will develop; but permanent displacements on the order of a metre could develop at the surface of the upstream slope. This predicted behavior is considered conservative in many respects, and the possibility of greater displacements is considered remote.

Displacements were also estimated for the "conservative case," which is considered the extreme behavior that could be postulated from the defined ranges of soil properties and conditions. The surface of the upstream slope might undergo displacements of 10 metres (33 feet) between the two berms, slumping near the upper berm, and bulging near the lower berm. Although uncomfortably large, these movements would not threaten the safety of the dam. Remember, this is not the predicted behavior, but the extreme limit that could be postulated if all soil properties and conditions were more adverse than the best judgment choices.

Conclusions

- 1. The seismic stability of Oroville Dam was investigated for the Reanalysis Earthquake of Richter Magnitude 6.5, at a hypocentral distance of 5 kilometres (3 miles) from the dam, and producing the following ground motion

characteristics at the base of the dam:

maximum acceleration	0.6 g
predominant period	0.4 seconds
duration	20 seconds
acceleration time history	modified Pacoima plus modified Taft

It was concluded that this ground shaking was more severe than any future shaking likely to affect the dam.

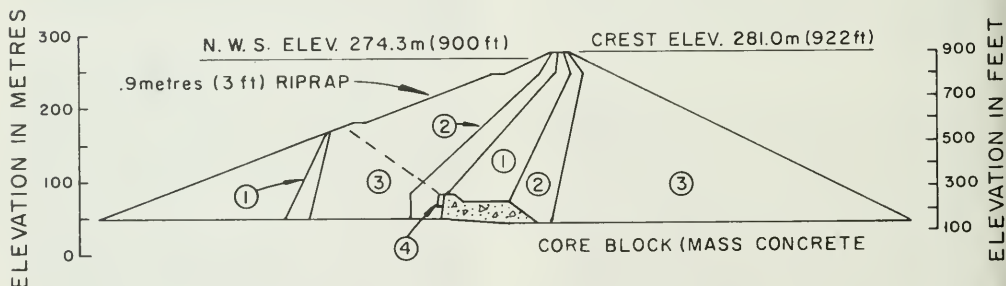
2. Using "best judgment" choices for input soil properties and conditions, relatively small embankment deformations were estimated by the seismic evaluation procedures. It is concluded that Oroville Dam would perform satisfactorily if subjected to the Reanalysis Earthquake.

2. DESCRIPTION OF EMBANKMENT MATERIALS AND DYNAMIC INSTRUMENTATION

Embankment Materials

Materials comprising the various zones of the dam considered in the analyses are shown on Figure 106. Gradation

curves for these materials are shown on Figure 107.



ZONE 1 & 4 -	6 900 000 CUBIC METRES (9,000,000 CUBIC YARDS)
	IMPERVIOUS
ZONE 2 -	7 260 000 CUBIC METRES (9,500,000 CUBIC YARDS)
	TRANSITION
ZONE 3 -	46 710 000 CUBIC METRES (61,100,000 CUBIC YARDS)
	PERVIOUS
RIPRAP -	315 700 CUBIC METRES (413,000 CUBIC YARDS)
CONCRETE -	222 500 CUBIC METRES (291,000 CUBIC YARDS)

Figure 106. Oroville Dam Maximum Section

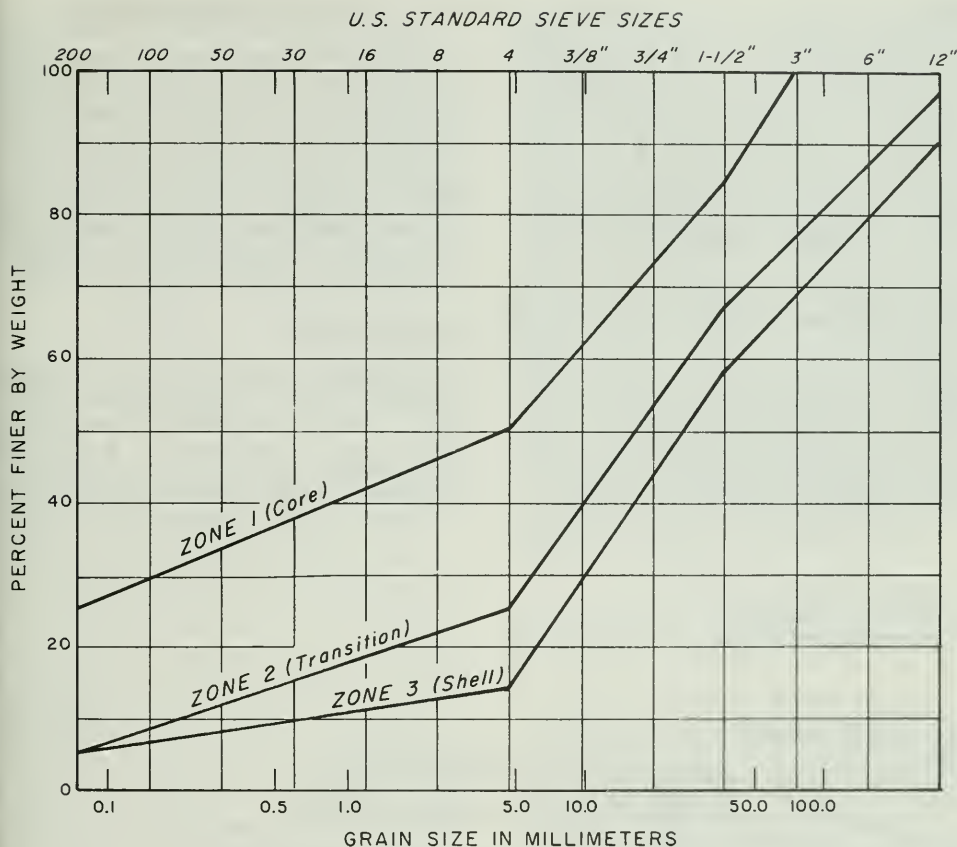


Figure 107. Average Gradation Curves of Oroville Dam Materials

The materials used in each zone and the compaction methods were:

Zone 1--Impervious core consisting of a well-graded mixture of clays, silts, sands, gravels, and cobbles to 8 centimetre (3-inch) maximum size. Compaction was in 25-centimetre (10-inch) lifts by 90.7-tonne (100-ton) pneumatic rollers. Average in-place dry density achieved was 2 243 kilograms per cubic metre (140 pounds per cubic foot) at 8.0 percent moisture (average 100 percent compaction, DWR standard 20,000 ft-lbs per cubic foot).

Zone 2--Transition consisting of a well-graded mixture of silts, sands, gravels, cobbles, and boulders to 38-centimetre (15-inch) maximum size (6-percent limit on minus No. 200 U. S. Standard sieve). Compaction was in 38-centimetre (15-inch) lifts by smooth-drum vibratory rollers. Average in-place dry density achieved was 2 419 kilograms per cubic metre (151 pounds per cubic foot) at 3.9 percent moisture (average 99 percent compaction, DWR standard vibratory maximum density test).

Zone 3--Shell of predominantly sands,

gravels, cobbles, and boulders to 61-centimetre (24-inch) maximum size (up to 25 percent minus No. 4 U. S. standard sieve sizes permitted). Compaction was in 61-centimetre (24-inch) lifts by smooth-drum vibratory rollers. Average in-place dry density achieved was 2 355 kilograms per cubic metre (147 pounds per cubic foot) at 3.1-percent moisture (average 99 percent compaction, DWR standard vibratory maximum density test).

Zone 4--Buffer zone designed to compress, contains between 15 and 45 percent passing No. 200 U. S. standard sieve with 20-centimetre (8-inch) maximum size. Compaction was in 38-centimetre (15-inch) lifts by a smooth-drum vibratory roller. Average density was 1 666 kilograms per cubic metre (104 pounds per cubic foot). (Average 82-percent compaction, DWR standard 20,000 ft-lb per cubic foot.)

- PORE PRESSURE CELLS
- ACCELEROMETERS
- ▽ SOIL STRESS CELLS

Dynamic Instrumentation

The embedded dynamic instrumentation system at Oroville Dam has been operating on a limited basis since the August 1975 earthquake. Since then the system has deteriorated to a point requiring a completely new present "state-of-the-art system" in order to obtain reliable, consistent dynamic records. Following is a description of the original system and the upgraded system.

Original System

The originally installed dynamic instrumentation system at Oroville is inoperable. This system included four force-balance type accelerometers, 6 pore pressure sensors, and 15 soil-stress cells, installed at the maximum section (Station 53 + 05) as shown on Figure 108.

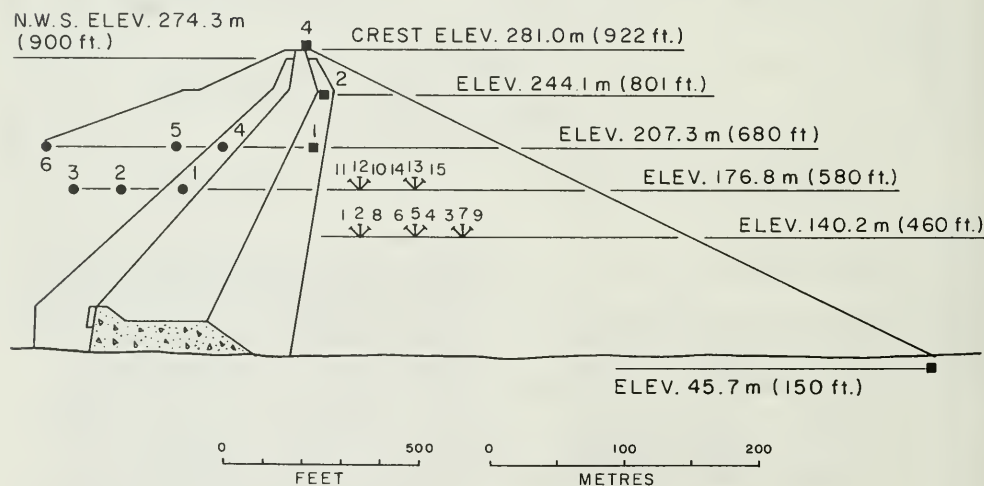


Figure 108. Oroville Dam Embankment, Original Dynamic Instrumentation

Two accelerometers were located in the embankment, one at the crest, and one in an abutment near the toe of the dam. The exact locations are as follows:

- No. A-1 Beneath the crest at Elevation 207.3 metres (680 feet).
- No. A-2 Beneath the crest at Elevation 244.1 metres (801 feet).
- No. A-3 Downstream toe, on rock at Elevation 45.7 metres (150 feet).
- No. A-4 On the crest at downstream edge Elevation 281.0 metres (922 feet).

These instruments measured accelerations along three orthogonal axes: Vertical, upstream-downstream (N46°E) and cross canyon. In cooperation with the U. S. Geologic Survey, (USGS), three strong-motion accelerographs were placed at the site. One was located at the crest in the same vault with A-4, one in the core block gallery, and one on rock at Elevation 341.4 metres (1,120 feet) about 1.6 kilometres (1 mile) northwest of the dam (Seismograph Station ORV). The core-block and crest instruments were oriented as described above. The seismograph station instrument was oriented with one of the horizontal axes at N37°E. With the exception of the core-block unit, all strong-motion instruments were operable during the 1975 earthquake activity.

All six dynamic pore-pressure cells installed in the upstream shell and transition zones showed a response during one event or another of the August earthquake series. The five groups of stress cells were located in the downstream shell. Each cell group measures stresses vertically and at 45 degrees to vertical in the upstream and downstream direction. Each cell has two transducers; one measures both static and dynamic stresses (CEC), and the other measures static stress only (MAIHAK). Cell Numbers 1, 2, 5, 6, 7, 10, 11, 12, and 14 were operable during the 1975 earthquake activity.

Upgraded System

Following the August 1, 1975 Oroville earthquake, the special consulting board recommended improvements to the seismic-data-acquisition system at Oroville. In March, 1977, the system was upgraded by adding new strong-motion accelerographs at two stations on the dam crest, in the grout-gallery adits on each abutment, and in the core block. These five instruments were all connected to a trigger at the toe of the dam and to a time-signal receiver (WWVB). In December 1978, the system was further upgraded by replacing failed accelerometers and pore-pressure signal-conditioning equipment, and by connecting all but two sensors to a digital recorder located in the Area Control Center. However, the dynamic soil-stress cells, which were rendered inoperable by a lightning strike at the dam in September 1976, were not replaced.

The following is a detailed description of the upgraded system as of December 1978 (Figure 109):

1. Installed four new SMA-1A strong-motion accelerographs in the two instrument vaults on the crest, in the left grout gallery portal, and in the toe seepage vault. These replaced existing SMA-1 units. These units will provide film record of acceleration at the unit and digital record in the Area Control Center. (The two existing SMA-1 units in the right grout-gallery portal and core block will provide film record at the unit only).
2. Installed three new FBA-3 force-balance accelerometers. Two of these, at the toe seepage vault and at crest Station 53 instrument vault, replaced failed units and provide redundancy with the SMA-1A records, which are on separate power supply. The third FBA-3 was installed in instrument house T on the downstream slope of the dam at midheight. This unit is a replacement for two existing FBA units buried in the embankment. The

buried units were at the limit of their life expectancy and were giving questionable readings. All the FBA-3 units will provide digital record of accelerations in the Area Control Center.

3. Installed two EFM-1 earthquake force monitors in the Area Control Center. They are connected to the SMA-1A units in the toe seepage vault and at crest Station 53. They will display the maximum acceleration experienced

since the last reset.

4. Installed new power-supply and calibration - signal conditioning equipment for the six pore-pressure cells.
5. Installed new DDS-1105 digital recorder in the Area Control Center, and connected it to four new SMA-1A, three new FBA-3, and six pore-pressure cells. All units are connected to a common trigger. A common time base (WWVB) will be recorded on all records.

- 6 - ● PORE PRESSURE CELLS
- 3 - ■ ACCELEROMETERS
- 6 - ▲ STRONG MOTION ACCELEROGRAPH (SMA-1 OR SMA-1A)

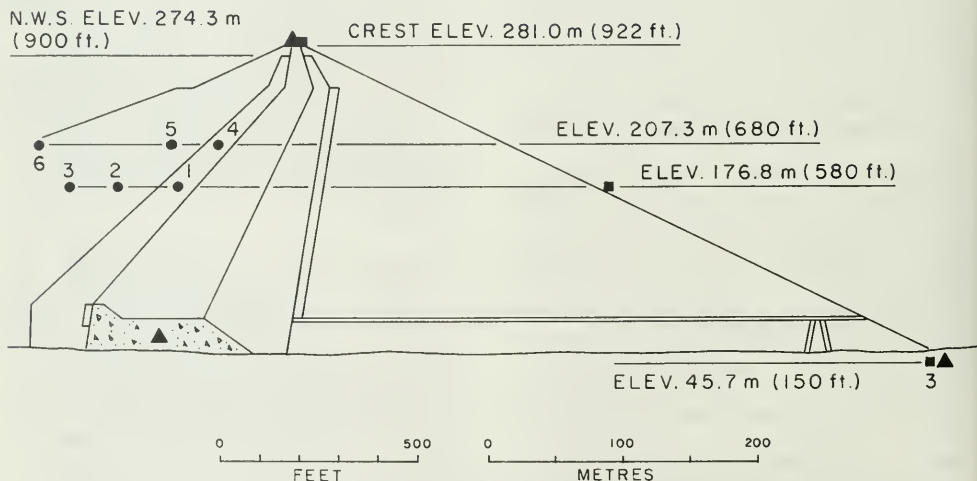
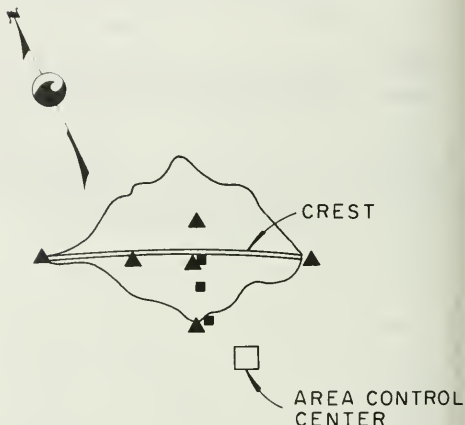


Figure 109. Oroville Dam Embankment, Present Dynamic Instrumentation (December, 1978)

3. RECORDED EMBANKMENT RESPONSE TO THE 1975 EARTHQUAKE

General

If complete and clear records had been obtained for the three or four larger shocks of 1975, a rare chance would have been available to test the mathematical models used for dynamic analysis by comparing the computed response with the observed response of the embankment. Unfortunately, the recording system was beset with problems and failures, and only partial records were obtained for the strongest shocks. One complete, clear set of records was obtained - for the September 27 aftershock.

The main use made of the records was to estimate the natural period of the dam. Secondly, computed and recorded crest motions were compared for the August 1 and September 27 events (Section 5). These comparisons were complicated by the three-dimensional effect of the canyon. Recorded dynamic pore pressures in the upstream shell and transition zones were not significantly large. All dynamic normal stresses were small.

Embankment response was evaluated for the following events:

<u>Seismic Event</u>	<u>Epicenter Lat. Long.</u>	<u>Richter Magnitude</u>	<u>Distance from dam (Km/mi)</u>	<u>Depth (Km/mi)</u>
Aug. 1 (main shock)	39° 26-33' 121° 31-71'	5.7	11/7	9/5.5
Aug. 5	39° 28-73' 121° 31-46'	4.7	7/4	9/5.5
Sept. 27	39° 30-65' 121° 32-69'	4.6	3.5/2	5.5/3.5

Many other foreshocks and aftershocks were recorded but were not used in these analyses.

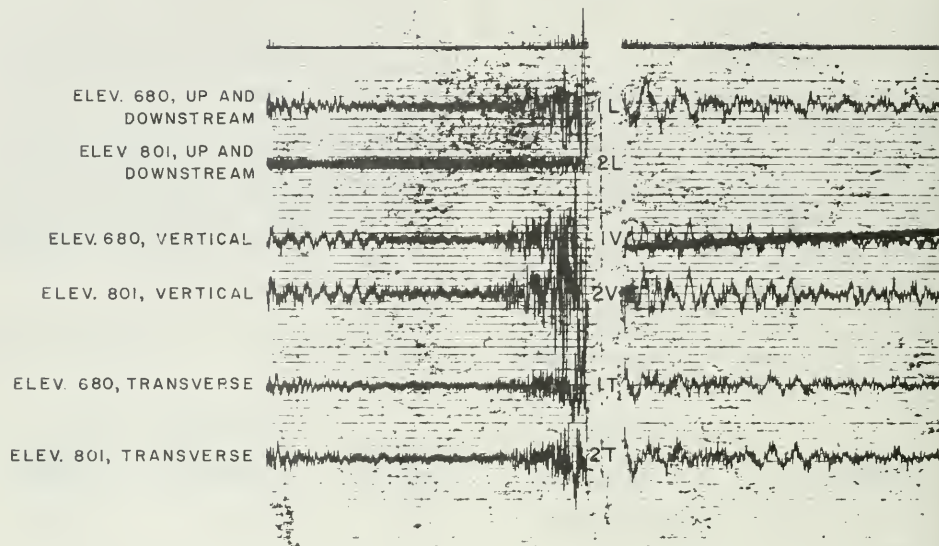
Recorded Events

August 1, 1975

For the August 1 and August 5 events, there were gaps in the records during the strongest shaking. However even if records had been obtained during this interval, they could not have been deciphered because of the overlap of adjacent records (Figures F110 and F112). The aftershock of September 27, produced the only complete, clear records; however, the acceleration was of lower amplitude and higher frequency than the first two.

The DWR accelerometers were triggered by a minor foreshock and were still recording when the main shock occurred. With the arrival of the large accelerations of the main shock, other instruments (pore pressure and stress cells) were triggered, resulting in an overload and a temporary loss of power. This loss of power caused all of the instruments to stop recording for most of the duration of the strong motion. After several seconds, the back-up power source was activated and all of the instruments started to record again. The record is shown in Figure 110.

RECORDER NO. 1



RECORDER NO. 2

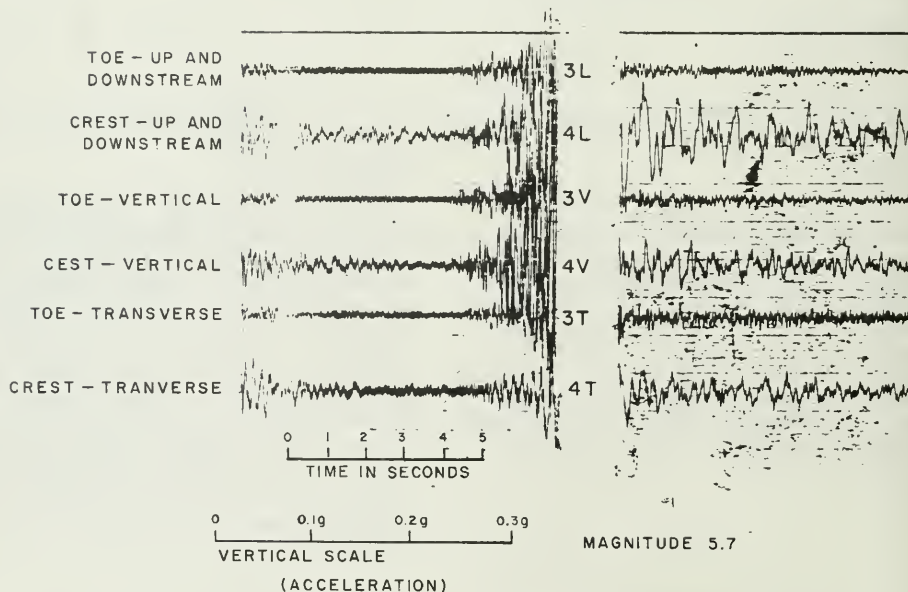


Figure 110. Acceleration Records, Main Event of August 1, 1975

Examination of aftershock records on recorder No. 2 showed the space between two events to be about 1.5 centimetres (0.6 inch), the same length as the gap in the August 1 record. After August 8, the speed of the recorders was increased 2-1/2 times. From then on, the space between events was about 2.5 centimetres (1 inch). Therefore, it was presumed that the gap in the August 1 records represented the distance the accelerometer drum rolled after power had been cut off, and the time gap could not be indicated correctly by the time scale on the chart.

The power failure was reenacted to find out how much time elapsed between main power cutoff and activation of the back-up power source. It was determined that the generator, which is the source for the back-up power supply, needed a minimum of 5 to 6 seconds to start and supply power to the recorders once the main power supply was cut off. Therefore, the time gap in the main event record was set at 6 seconds.

Recordings of stress for the August 1 event were also marred by a gap due to the power loss. Before the gap, a maximum vertical normal stress of 159 kilopascals (23 psi) was recorded by cell No. 5. Pore pressure cell No. 1 registered a maximum pressure increase of 90 kilopascals (13 psi), which was dissipated during the 6-second gap. Pore-pressure cells 4, 5, and 6 also showed minor fluctuations, on the order of 14 to 34 kilopascals (2 to 5 psi).

To gain an insight into what occurred during the time represented by missing portions of the DWR acceleration records, USGS recordings of accelerations at the seismic station and at the crest of Oroville Dam were obtained and compared with the corresponding DWR records. Unfortunately, the first few seconds of the USGS crest record were lost, as noted in California Division of Mines and Geology Special Report 124, "Oroville, California Earthquake, 1 August, 1975". However, the last portions of the DWR

and USGS crest records are nearly identical. Any differences are due to baseline and instrument corrections performed on the USGS record. The DWR record was not corrected. The last portion of the two crest records (following the gap) can be lined up as shown in Figure 111. This leaves 2-1/2 seconds where the record is missing from both the USGS and DWR instruments.

The record at the USGS seismograph station, 1.6 kilometres (1 mile) NW of Oroville Dam, was positioned so that its two highest peaks line up with the two high peaks recorded on the DWR base accelerometer. This positioning of the USGS base record shows that the strong base motion had essentially ceased by the start of the USGS recorded crest motion. The USGS seismograph station and dam crest records were digitized for use in making analyses by computers.

August 5, 1975

As can be seen on Figure 112, the DWR record again has a vital part of the event missing and hence could not be used in any subsequent analysis. It can be seen, however, that like the August 1 recorded motions, the dam is freely oscillating while the amplitudes of the accelerations of the crest are decreasing in a typical decay curve pattern. This again occurs with the amplitudes of the recorded base motion being negligible.

The USGS does not have records of the August 5 event.

September 27, 1975

The seismic event of September 27, 1975, (Magnitude 4.6) was recorded in its entirety on the DWR accelerometers, Figure 113. These records were digitized for use in subsequent analyses. The digitized records were processed using the routine computer processing methods for strong-motion accelerograms developed at Cal Tech. Some changes, however, were made in this standard processing technique. The instrument correction was not

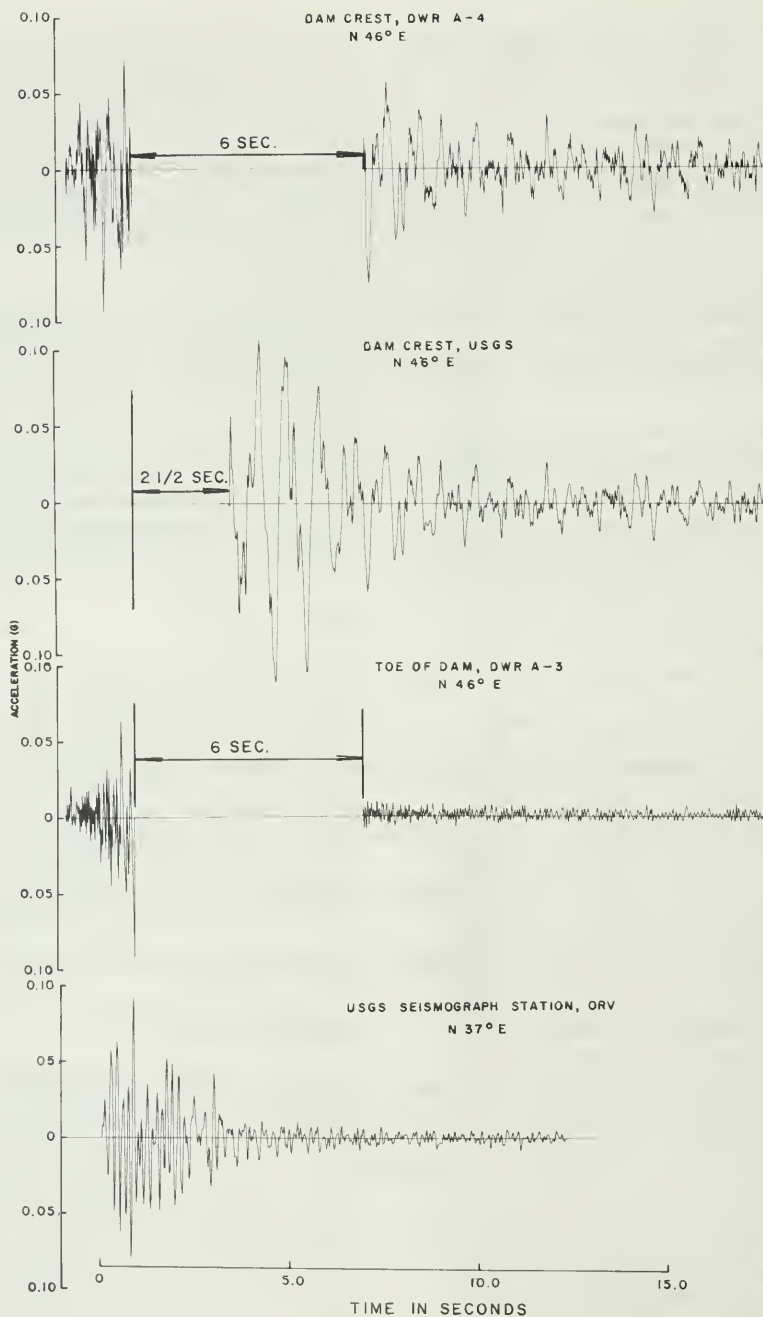


Figure 111. Acceleration Records with Corrected Time Scales, August 1, 1975

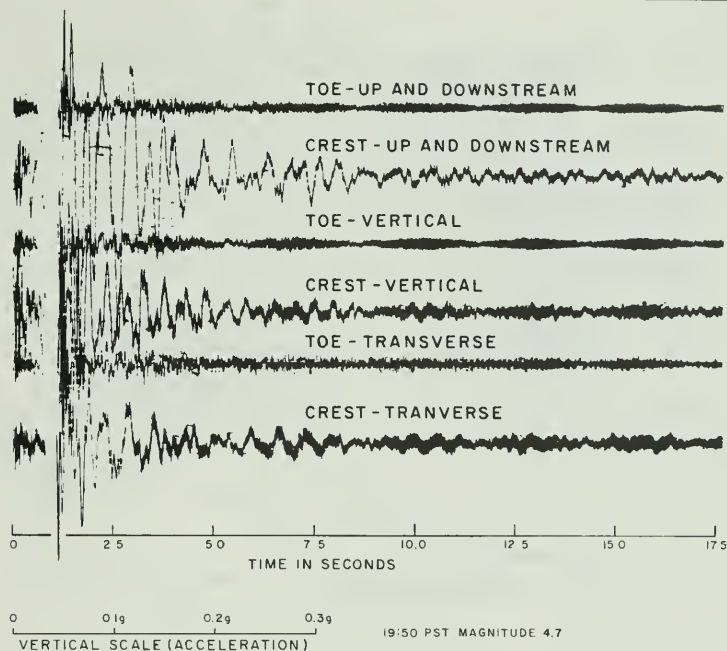


Figure 112. Acceleration Records, Event of August 5, 1975

performed because the accelerometers are of a force-balance type. It was assumed that the instrument response was unaffected throughout the frequency range of interest.

The records of the base and crest motions (horizontal and vertical) were baseline corrected and put through an Ormsby filter to obtain equally spaced acceleration points between 1.4 and 48 hertz. This filter bandwidth deviates from the standard filter used at Cal Tech, because of the high frequency content, low amplitude, and short duration of the records. Acceleration-time histories plotted from the digitized records, along with corresponding response spectra, are in Appendix B.

The USGS has no records of any seismic events for September 27, 1975.

A maximum vertical normal stress of 62 kilopascals (9 psi) was recorded by cell No. 5. Using methods which will be described later, the vertical normal stress computed for cell No. 5 location was 41 to 62 kilopascals (6 to 9 psi).

Observed Natural Period

For both the August 1 and August 5 events, the dam continued to vibrate after the earthquake had stopped. As shown in Figures 111 and 112, after the base accelerations had dropped to less than 0.01g, long period crest accelerations continued for several seconds, starting at an amplitude of about 0.1g and decreasing in a typical decay curve pattern for free vibration.

For the August 1 record, 5 or 6 success-

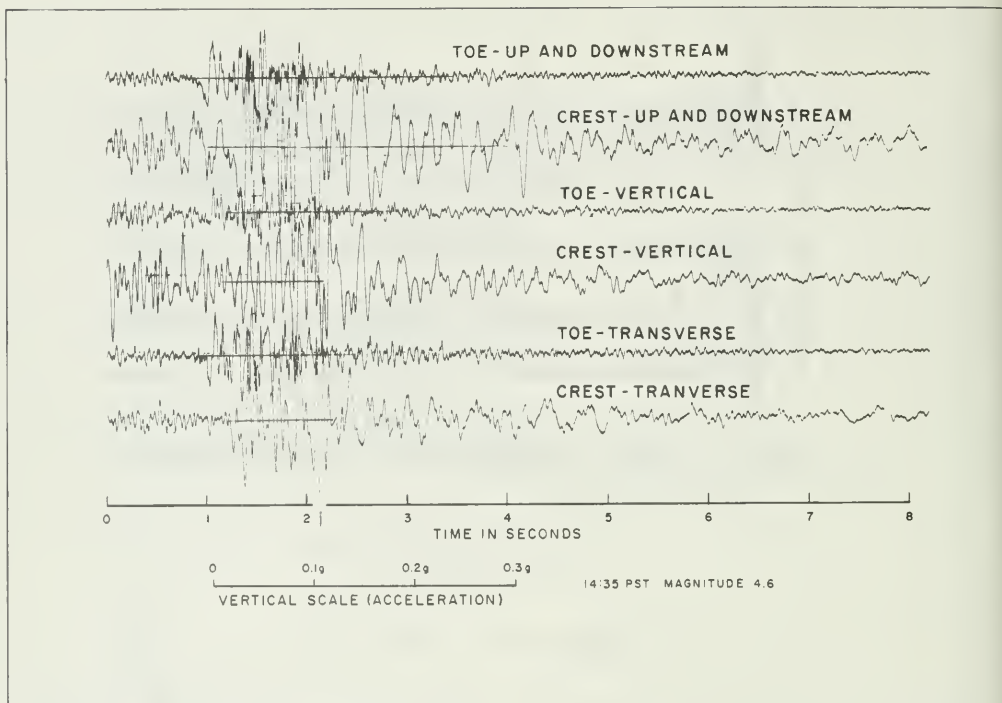


Figure 113. Acceleration Records, Event of September 27, 1975

ive cycles have periods close to 0.8 seconds. For the August 5 record, there are 3 or 4 cycles in the decay curve with a period of about 0.7 seconds. Acceleration response spectra for the August 1 USGS crest record show a predominant period of 0.8 seconds (Figure 114). Response spectra were not calculated for the August 5 event, because the extreme overlap of adjacent records made accelerations indistinguishable for the strong motion portions. The September 27 event was not used for estimating period be-

cause it did not develop a clear decay curve pattern for free vibration.

Since these observed periods are for free vibration conditions, they are the natural periods of the dam; and since the fundamental period is known to be dominant in an earth dam, the observed periods are presumed to be the fundamental periods. Thus the fundamental natural period is determined to be 0.8 seconds for the intensity of shaking produced by the August 1 main shock.

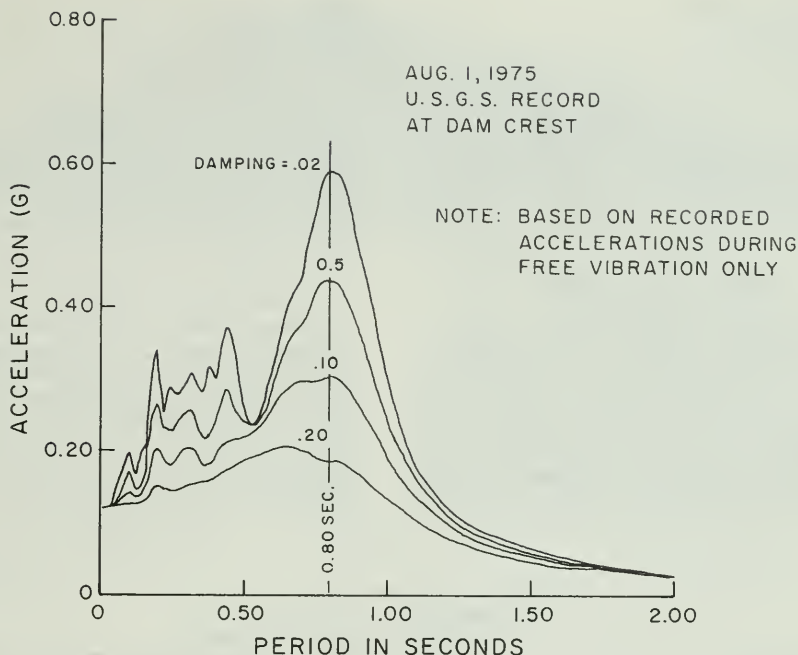


Figure 114. Acceleration Response Spectra for Crest Motions, Event of August 1, 1975

4. ANALYSIS OF STATIC STRESSES BY FINITE ELEMENT METHOD

General

The behavior of an embankment dam subjected to dynamic loading by an earthquake is significantly influenced by the stress condition existing in the embankment prior to the earthquake. Current methods of analysis for evaluating the seismic stability and permanent deformations require knowledge of the static stress distribution for the maximum section of Oroville Dam. These static stresses can best be calculated by the finite element method, which permits the evaluation of stresses and deformations in an embankment through a series of steps or increments to simulate construction and reservoir filling. The following sequence was used in this analysis:

1. Construction of the core block in four layers.
2. Construction of the cofferdam, upstream of the core block, in 14 layers.
3. Construction of the remaining embankment in 27 layers.
4. Application of water load in four stages, simulating filling of the reservoir.

The finite-element representation of Oroville Dam is shown on Figure 115. This mesh, used in the static and dynamic analyses, contains 564 elements and 585 nodes.

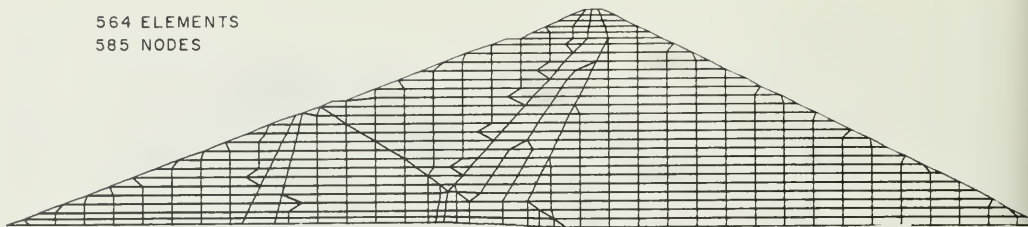


Figure 115. Finite Element Mesh, Maximum Section Oroville Dam

Material Properties

The success of finite-element analyses to model the behavior of an earth dam depends in a large part on how well the nonlinear response of soil and rock materials under load can be described analytically. Because of the good comparison between observed and computed settlements in a previous analysis by Kulhawy

and Duncan (1970), the same stress-strain parameters were used in this analysis. The difference between the parameters for the transition (Zone 2) and shell (Zone 3) materials, shown in Table 5 is negligible. Therefore, Zone 3 parameters were used for both Zones 2 and 3 in all the finite-element-method analyses.

Table 5

Values of Stress-Strain Parameters
for Analysis of Oroville Dam
(From Kulhawy and Duncan)

Parameter	Values Used in Analyses					
	Symbol	Shell	Transition	Core	Soft Clay ^{a/}	Concret
Unit weight (lb/ft ³)	Y	150	150	150	125	162
Cohesion (tons/ft ²)	c	0	0	1.32 ^{b/}	0.3	216 ^{c/}
Friction angle (degrees)	φ	43.5	43.5	25.1 ^{b/}	13.0	0
Modulus number	K	3780	3350	345	150	137,500
Modulus exponent	n	0.19	0.19	0.76	1.0	0
Failure ratio	R _f	0.76	0.76	0.88	0.9	1.0
Poisson's)	G	0.43	0.43	0.30	0.49	0.15
ratio)	F	0.19	0.19	-0.05	0	0
parameters)	d	14.8	14.8	3.83	0	0

^{a/} Zone of soft clay at upstream end of core block.

^{b/} c and φ for $(\sigma_1 + \sigma_3) \leq 50$ tsf; $(c = 10.2 \text{ tons/ft}^2, \phi = 4^\circ; \text{ for } (\sigma_1 + \sigma_3) > 50 \text{ tsf})$

^{c/} Tensile strength of concrete = 14 tons/ft² (200 psi).

Static Stress Analysis

Computer program ISBILD was used to carry out the static-stress analysis. This program is similar to the one used in the earlier analysis of Oroville Dam by Kulhawy and Duncan. The major difference is the type of element used. Kulhawy and Duncan used a quadrilateral element divided into two triangles. Within each triangle the strains vary linearly; then, for compatibility reasons, the strain along the sides of the quadrilateral element is kept constant.

Program ISBILD uses a quadrilateral incompatible isoparametric element. This means that in addition to 8 regular degrees of freedom at 4 nodes, the element has 4 internal degrees of freedom to improve its bending behavior. These additional nodes of displacement, in general, make the elements incompatible at the interelement boundaries.

Seepage Forces

Reservoir effects are simulated by consi-

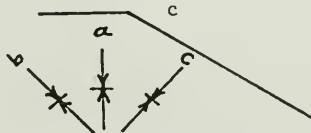
dering the water load in two parts: total stress forces and water pressure forces. To account for the effects of the seepage forces in the core, piezometer readings were used as input to the computer program NODALFOR (developed by Division of Safety of Dams). This program uses the water pressures at nodes and computes the forces at the sides of elements due to these pressures. The sum of these side forces is the resultant water force on the element. Resultant water forces are then distributed to element nodes in proportion to the contributing area of each node. The values distributed to a node from adjacent elements are added to yield the net water force at the node. This net water force is added to the total soil force (based on saturated unit weight) at the node to get the effective soil force.

Table 6 shows the comparison between the measured and calculated static stress values.

Table 6

Static Stress Comparison

Cell No.*	Direction of Stress	Compressive Stress (tsf)	
		Maihak Cell	FEM Analysis
1	b	13.8	16.6
2	a	29.5	28.2
3	b	14.4	11.1
4	c	-	23.0
5	a	30.9	25.6
6	b	15.1	14.2
7	a	22.3	21.0
8	c	11.0	24.5
9	c	-	20.8
10	c	7.9	18.9
11	b	11.5	12.1
12	a	25.4	20.2
13	a	18.0	17.0
14	b	10.0	9.1
15	c	-	17.1



*Note: All but three of the static stress cells were functioning during the 1975 earthquakes.

There is good agreement between measured and calculated vertical stresses. Inclined stresses, compression toward the downstream toe, also show good agreement. However, the two operable cells measuring compression toward the upstream toe measure only about half the calculated stresses.

The computed static stresses in the

shells are compared with results by Nobari and Duncan (1972) in Figures 116 through 119.

Stress comparisons are not valid in the core because Nobari and Duncan present total stresses, where the stresses computed in this study are effective stresses. Plots of stresses in all elements are included in Appendix C.

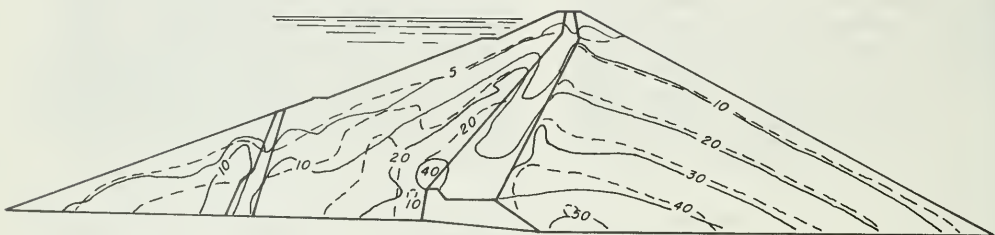


Figure 116. Contours of Effective Maximum Principal Stress in Oroville Dam, Full Reservoir

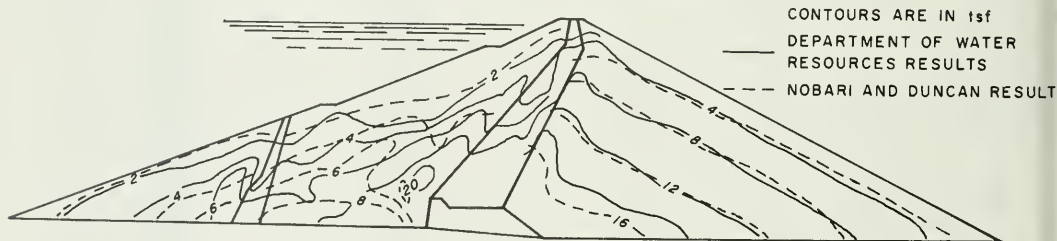


Figure 117. Contours of Effective Minimum Principal Stress in Oroville Dam, Full Reservoir

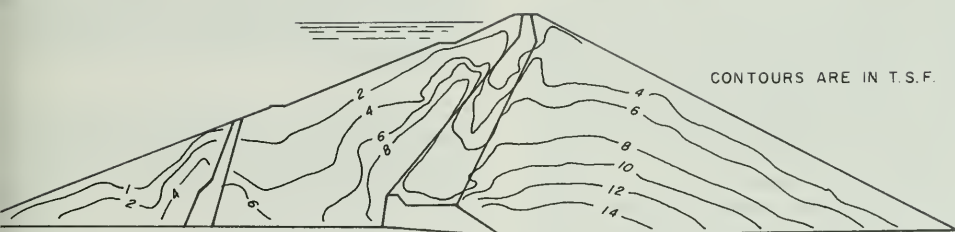


Figure 118. Contours of Maximum Shear Stress in Oroville Dam, Full Reservoir

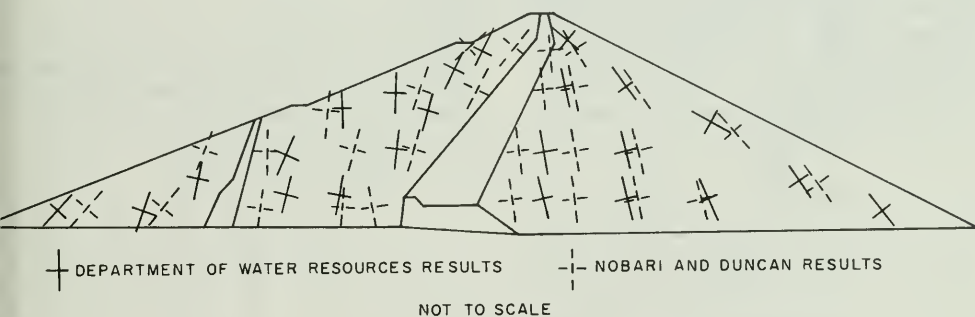


Figure 119. Orientation of Principal Stresses

5. DETERMINATION OF DYNAMIC SHEAR MODULUS AND DAMPING VALUES FOR EMBANKMENT SHELL MATERIAL

General

Dynamic shear modulus values at low strains can be measured in the field using geophysical methods or in the laboratory using vibration tests. Values at higher strains can be measured in the laboratory using cyclic shear tests. If recorded motions during an earthquake are available, calculations can be made to determine the modulus corresponding to those recorded motions. Damping is usually measured in the laboratory during the same test used to measure the modulus.

Measurement of dynamic shear modulus and damping for the Oroville Dam shell material is a difficult task: Field measurements of shear wave velocity would require deep borings in the gravel and cobbles; undisturbed samples for laboratory tests would be next to impossible; remolded samples for laboratory tests cannot reproduce field conditions of particle size, stress, time of loading, or variability of grading and compaction

in the shell. In spite of the difficulties, a considerable effort was made to determine the modulus and damping because they are the most important parameters controlling the response of the dam to an earthquake.

Studies by Seed and Idriss (1970) have shown that the dynamic shear modulus of granular soils can be related to the effective mean normal stress as follows:

$$G = 1000 K_2 (\sigma'_m)^{1/2}$$

G = dynamic shear modulus in psf
 K_2 = a parameter relating G and σ'_m
 σ'_m = effective mean normal stress in psf

K_2 is a function of strain level and void ratio. $K_{2\max}$, the maximum value of K_2 , is obtained at low shear strain ($10^{-4}\%$).

For clays, Seed and Idriss found that shear modulus could be related to static undrained shear strength and dynamic shear strain as shown in Figure 120.

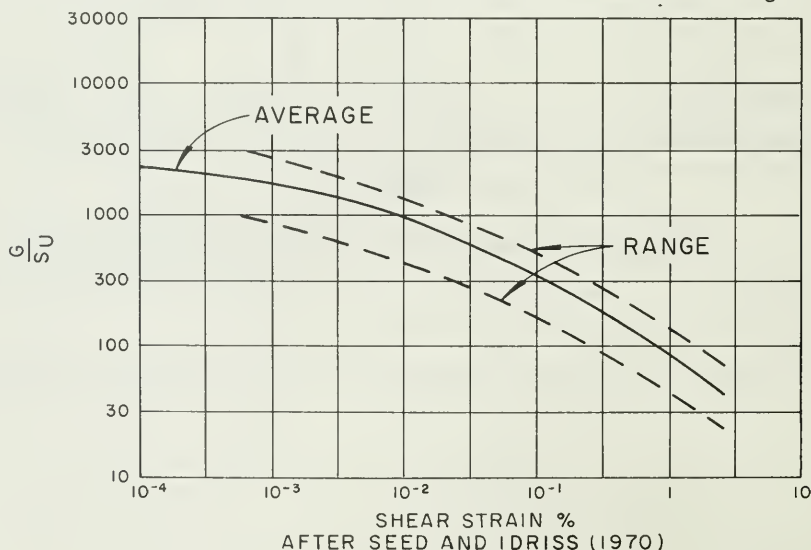


Figure 120. In-Situ Shear Moduli for Saturated Clays

It was presumed that the gravel shells would dominate the response behavior during earthquake shaking because they occupy about 90 percent of the embankment. Therefore, the testing and analysis for shear modulus were done only for the gravel shell material. The core modulus and damping were assumed equal to published values for clays.

Two methods were used to determine the modulus of the gravel shell material: cyclic triaxial tests on remolded samples, and analysis of recorded embankment response during the Oroville earthquakes of 1975. Damping values for the gravel material were estimated from the cyclic triaxial tests.

Cyclic Triaxial Tests

Laboratory test data to define the dynamic properties of gravel material are very limited. Presently available cyclic test equipment can test specimens up to 30 centimetres (12 inches) diameter. The average gradation of the Oroville shell material has a maximum particle size of 15 centimetres (6 inches) and would require a specimen diameter of 90 centimetres (36 inches).

Comparison studies by Becker, (1972) have shown the same static strength for samples with modeled gradation of 5 centimetre (2-inch) and samples with field gradation of 15 centimetre (6-inch)

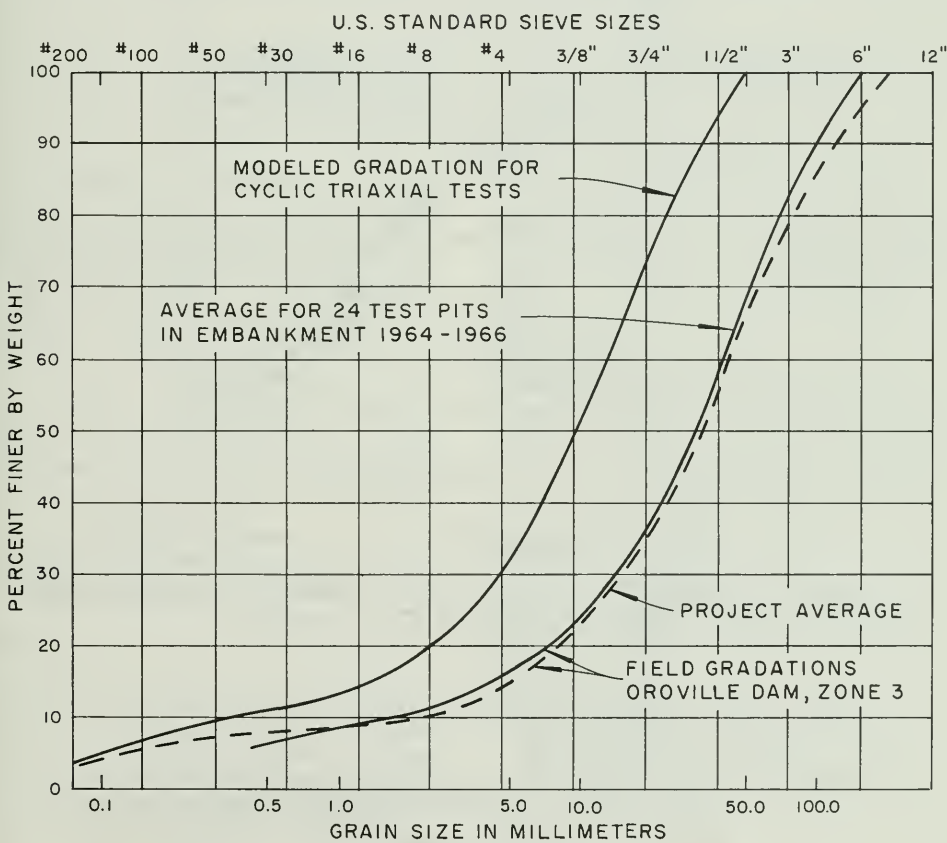


Figure 121. Sample Gradation for Cyclic Triaxial Tests

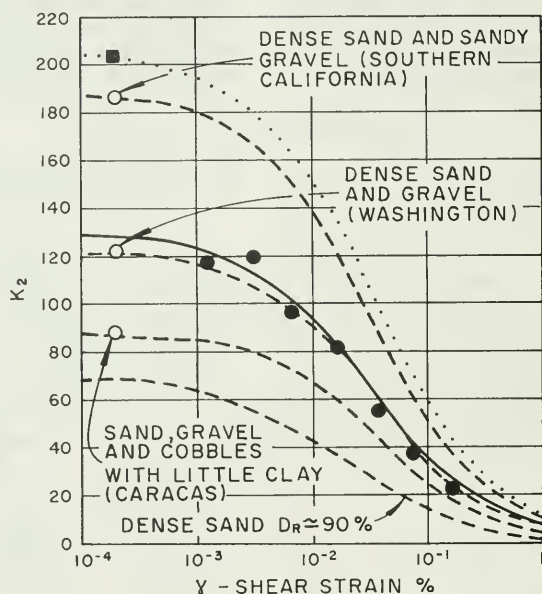
maximum particle size. It seems reasonable to extend this kind of modeling to cyclic testing.

A general study was undertaken by Wong (1973) to determine the cyclic strength, dynamic shear modulus, and damping of gravels. Strain controlled cyclic triaxial tests of 30 centimetre (12-inch) diameter samples of modeled Oroville gravel gradation were part of that study. Samples tested were composed of Oroville gravel with 5 centimetre (2-inch) maximum particle size and a grad-

ation curve parallel to the average shell grading (Figure 121).

The sample density used was about 2 430 kilograms per cubic metre (152 pounds per cubic foot). Average density of Zone 3 is 2 360 kilograms per cubic metre (148 pcf). All samples were isotropically consolidated with a pressure of 196 kilopascals (4,096 pounds per square foot).

Figure 122 shows the results of these cyclic tests compared with the results



--○--

FROM FIELD SHEAR WAVE VELOCITY MEASUREMENTS, SEED AND IDRISS 1970.

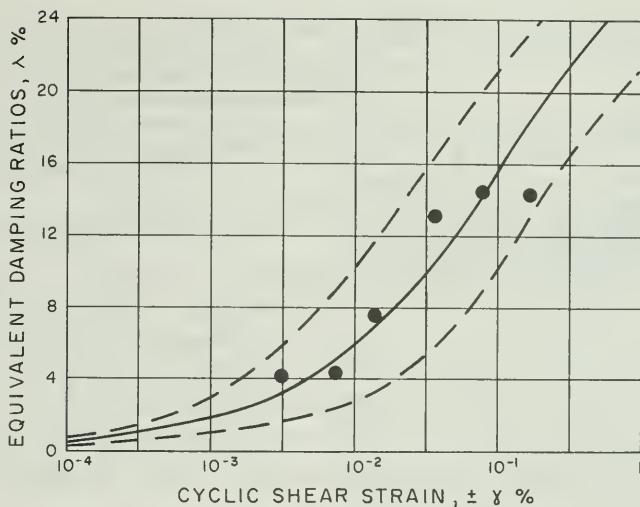
●

TRIAXIAL TESTS ON MODELED OROVILLE GRAVEL BY WONG
 MAXIMUM PARTICLE SIZE = 2 INCHES
 SAMPLE DIAMETER = 12 INCHES
 $\sigma_{3c} = 4100$ psf
 RELATIVE DENSITY = 100 %
 SET UP DENSITY = 152 pcf
 N = 5 CYCLES

■

FROM DYNAMIC ANALYSIS OF EMBANKMENT FOR 1975
 RECORDED EARTHQUAKES (PERIOD = ONE SECOND)

Figure 122. Modulus Determinations for Gravelly Soils



- DATA FOR OROVILLE MODEL GRADATION, THIS INVESTIGATION
- AVERAGE VALUE FOR SANDS, FROM SEED AND IDRIS, 1970
- - UPPER AND LOWER BOUNDS FOR SANDS

Figure 123. Comparison of Damping Ratios for Gravelly Soils and Sands

reported by Seed and Idriss. The Seed-Idriss curves are based on field shear wave velocity measurements for K_{2max} , and the average K_2/K_{2max} reduction curve for sands. Using the same reduction curve to fit the triaxial test data gives a K_{2max} value of 130.

Figure 123 shows the damping results compared with the range of values for sands reported by Seed and Idriss. The test data points are very close to the average curve for sands.

Analysis of Recorded Embankment Response During the 1975 Earthquakes

General

Even though there were gaps in the records of the stronger shocks, the 1975 Oroville earthquakes afforded an opportunity for analyzing embankment response to determine the dynamic shear modulus of the embankment materials. Acceleration time histories were recorded at

both the base and the crest of the dam for several events. The August 1 main shock provided the best definition of the natural period of the embankment - the key to the analysis.

The natural period is dependent upon stiffness (shear modulus) and mass distribution. Knowing the mass distribution and the period allows calculation of the shear modulus. Knowing the shear modulus and embankment strain allows calculation of shear modulus parameter K_{2max} .

Computer program QUAD4 was used in the analyses. It determines the natural period by solution of the eigenvalue problem:

$$\begin{aligned}
 [K] &= w^2 [M] & (5-2) \\
 [K] &= \text{system stiffness matrix} \\
 [M] &= \text{system mass matrix} \\
 w &= \text{natural circular frequency}
 \end{aligned}$$

The stiffness matrix is developed from

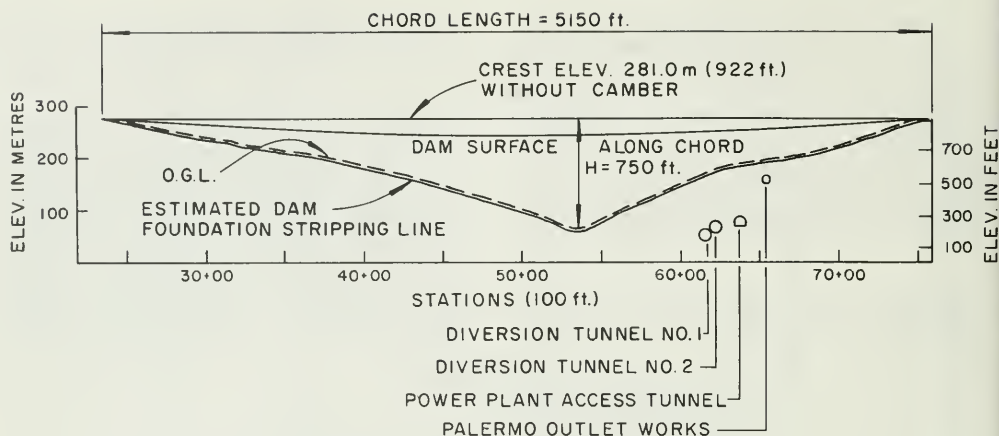


Figure 124. Section on Long Chord of Dam Axis

the shear modulus values for all the elements in the maximum section FEM mesh -- and is therefore a function of shear modulus parameter K_2 .

The Oroville embankment is located in a triangular canyon and has a crest length to maximum height ratio of approximately 7. A longitudinal profile is shown in Figure 124.

A three-dimensional (3D) analysis of the dam to determine K_{2max} of the gravel shell material is not possible, because present computer capabilities are inadequate for dams as large as Oroville. The solution to this problem is to find the appropriate values of natural period and shear strain to use in a two-dimensional (2D) analysis.

Makdisi (1976) has derived a relationship between the natural periods computed by 3D and 2D analyses for a 30-metre (100-foot) high dam with slopes of 2:1 and a constant shear modulus throughout. Assuming this relationship is valid for the much higher Oroville Dam with variable shear modulus as defined by equation 5-1, the 2D period can be computed corresponding to the observed period in the August 1, 1975 earthquake.

The same value of shear modulus, G , was

used in the 2D and 3D analyses in deriving the natural period relationship. Since the parameter to be calculated, G_{max} , would have to be the same for 2D and 3D, then G/G_{max} and consequently the shear strain are also the same for the 2D and 3D cases. Thus the same strain and modulus reduction factor must be used for the 2D and 3D analyses when applying the natural period relationship

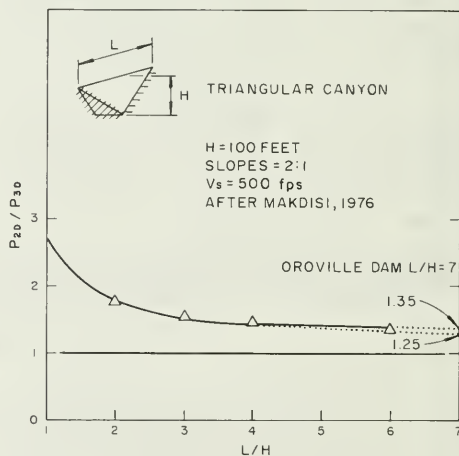


Figure 125. Comparison of Natural Periods for Two-Dimensional and Three-Dimensional Embankment in Triangular Canyon

It is important to note that this relationship would not give the correct period for a very long (2D) dam subjected to the August 1, 1975 earthquake shaking. But it does give a correct relationship among period, strain, and K_{2max} , allowing the calculation of K_{2max} .

Natural Period for Two-Dimensional Analysis

Makdisi's correlation of 2D and 3D periods only goes to an L/H of 6. Extrapolating to an L/H of 7 gives a period ratio of 1.25 to 1.35 (Figure 125). The natural period of Oroville Dam Embankment in the August 1, 1975 earthquake was estimated to be 0.8 seconds (see page). The natural period range to be used in the 2D analysis is 1.0 to 1.1 seconds.

Shear Strain for Two-Dimensional Analysis

The maximum displacement computed from the August 1 recorded (USGS) crest motion is 1.5 centimetres (0.6 inch). The assumption is made that the peak shear

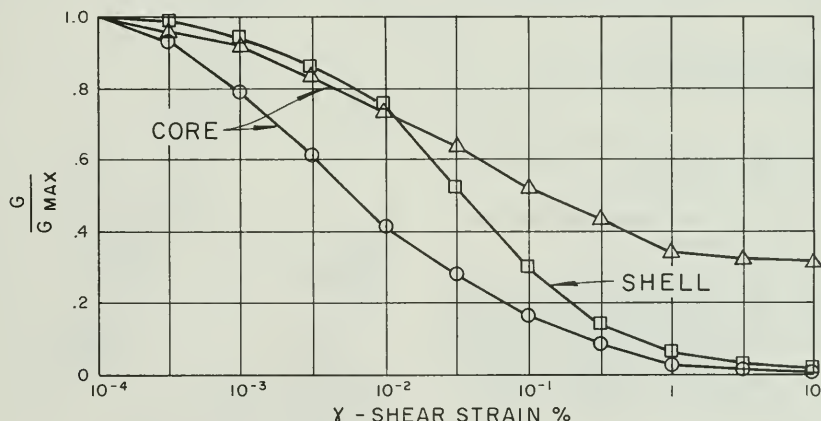
strain (γ_{max}) is constant throughout the dam and is equal to maximum crest displacement (D) divided by embankment height (H).

$$\gamma_{max} = \frac{D}{H} \times 100\% = 0.007\%$$

A ratio of average strain to peak strain of 0.6 has been used in this study. Thus the average shear strain is about 0.004 percent for the actual (3D) dam, which is also the value to use in the Two Dimensional Analysis.

Shear Modulus Reduction Factor

The average shear modulus reduction curve for sands shown in Figure 126 was used for the gravel shells. At a shear strain level of 0.004 percent, the modulus reduction factor is 0.86. This value agrees well with the results of a dynamic response analysis for the August 1, 1975 earthquake, which will be discussed later in this chapter. The range of reduction factors in that analysis was generally only 0.78 to 0.88. An average value of 0.85 was used in the calculation of K_{2max} .



- AVERAGE REDUCTION CURVE SANDS, FROM SEED AND IDRIS
- AVERAGE REDUCTION CURVE CLAYS, FROM SEED AND IDRIS
- △ REDUCTION CURVE CLAYS, $S_u = 8000$ psf FROM SEED (PRIVATE COMMUNICATION)

Figure 126. Shear Modulus Reduction Curve for Embankment Soils

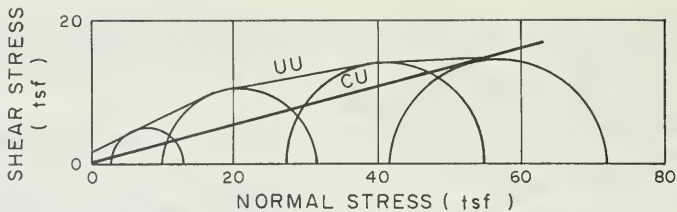


Figure 127. Static Shear Strength Envelopes for Core Material

$K_{2\max}$ vs. Natural Period

Computer program QUAD4 was used to calculate natural periods for the following input properties and conditions:

- A. Finite element mesh of Maximum Section (Figure 115)
- B. Static stresses determined from static FEM analysis
- C. Shell and Core Material Densities used in static FEM analysis
- D. Core shear modulus - three trial values of G_{\max}/S_u - 1100, 2200, 4400
 - CU shear strength envelope (Figure 127)
- E. Shell $K_{2\max}$ - four trial values - 100, 200, 300, 400
- F. Shear Modulus Reduction Factor for both shell and core - 0.85

The results are plotted in Figure 128 as a family of curves of $K_{2\max}$ vs. natural period. Each curve is for a different value of core modulus. Varying the core modulus by a factor of four changes the shell $K_{2\max}$ by 20 percent to 25 percent.

Range of $K_{2\max}$ - The range of $K_{2\max}$ is 135 to 210 for a natural period from 1.0 second to 1.1 second and core G_{\max}/S_u of 1100 to 4400.

Comparison of Observed and Computed Crest Motions

Ideally, the value found for shell $K_{2\max}$ would be used in a three-dimensional dynamic analysis using the recorded base motion. A comparison of the computed crest motion with recorded crest motion would then be a direct check on the mathematical model and material properties used. However, a three-dimensional analysis is not presently possible for Oroville Dam, and a

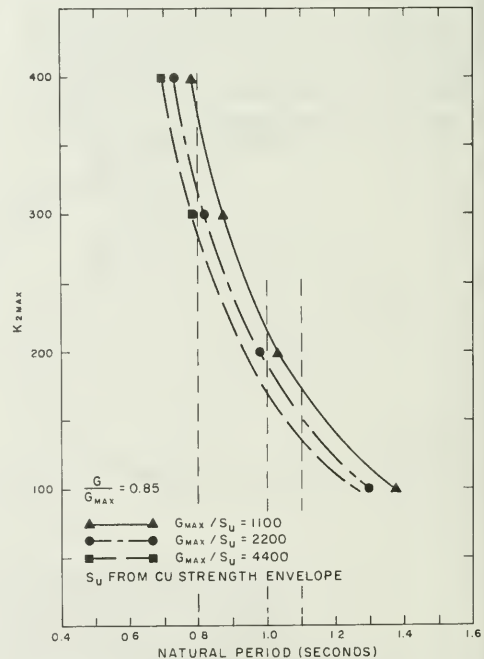
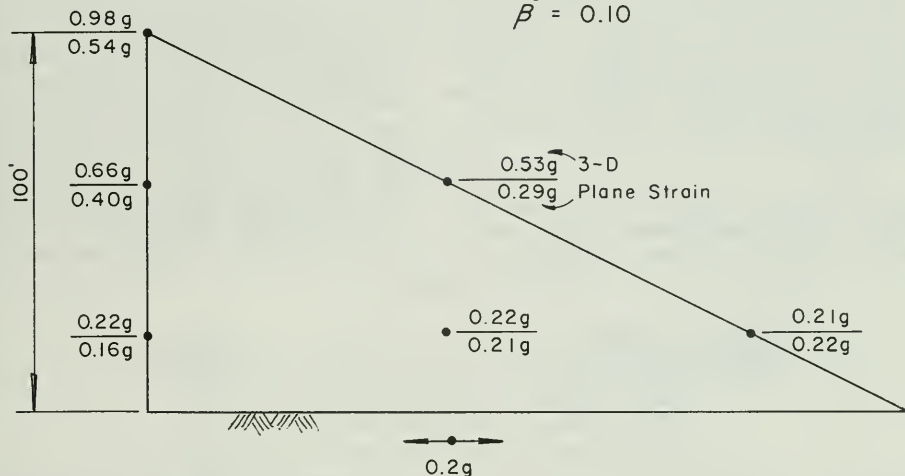


Figure 128. $K_{2\max}$ vs. Natural Period

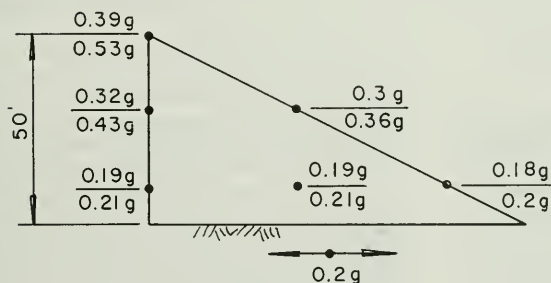
two-dimensional analysis would give a different response acceleration as shown by Makdisi (Figure 129). His study was done for a 30 metre (100 feet) high dam, Taft earthquake, and $L/H = 3$. In some locations particularly at the crest, the difference is large -- up to 100 percent.

This is because the restraint or stiffening effect of the abutments is ignored in a plane strain analysis. Therefore, the two-dimensional analysis needs to be modified to account for the abutment restraint.

$$\begin{aligned} L/H &= 3 \\ V_s &= 500 \text{ fps} \\ \beta &= 0.10 \end{aligned}$$



MID-SECTION



QUARTER SECTION

Figure 129. Maximum Accelerations Computed from 3D and Plane Strain Analyses Using Base Motions from Taft Record (After Makdisi)

Embankment Response Model

The Embankment Response Model is a two-dimensional analysis with a modified K_{2max} (pseudo K_{2max}) value that gives a computed natural period equal to the observed period (3D) for the actual embankment during the August 1, 1975 earthquake. It is an implied assumption that the same adjustment which accounts for the three-dimensional effects on natural period will also account for the three-dimensional effects on acceleration and strain. The pseudo K_{2max} value is higher than the K_{2max} representing shear modulus because the stiffening or restraint effects of the abutments are included.

By definition, the model applies to the August 1, 1975 earthquake. This same model may apply to other, stronger,

earthquakes, but the 1975 earthquake series did not provide enough information to test this question.

The value of pseudo K_{2max} corresponding to the observed natural period of 0.8 sec. is 285 to 370 (Figure 128).

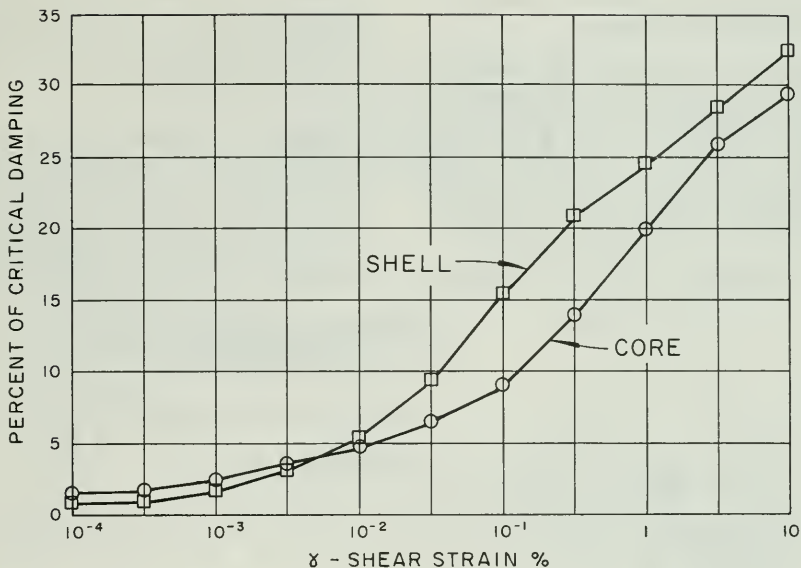
August 1 Event

The acceleration record at the toe of the dam was not usable because of the six-second gap. The bedrock record from seismograph station ORV was used, even though it is a mile from the dam, 275 metres (900 feet) higher in elevation, and oriented 9 degrees different than the dam instruments. Where both records are present, accelerations are similar for seismograph station ORV and the toe of the dam. Other input was as follows:

Computer Program	LUSH
Highest Frequency Used	8 Hertz
Shell - Pseudo K_{2max}	350
- Average Modulus Reduction Curve for Sands (Figure 126)	
- Average Damping Curve for Sands (Figure 130)	
Core - G_{max}/S_u	1750
- Shear Strength Envelope	UU
- Higher Modulus Reduction Curve for Clays (Figure 126)	
- Average Damping Curve for Clays (Figure 130)	
Poisson's Ratio	0.3

The comparison between the computed and observed crest accelerations is shown in Figure 131 along with the input bedrock motion. Comparisons of displacement time history and acceleration response spectra are shown in Figure 132. The shapes and magnitudes of the computed patterns are generally similar to those observed. The response spectra of the computed crest motion show the dam to oscillate with two distinct periods. The first period of 0.15 seconds is not

evident in the response spectrum of the observed crest motion, probably because the period of 0.15 second corresponds to the forced vibrations during base shaking, which is the missing portion of the crest record. The second period shown in the response spectrum of the computed crest motion occurs at 0.75 seconds, slightly different from the period of 0.8 seconds for the recorded motion. This may mean that 350 is too high a choice for pseudo K_{2max} , or that



- AVERAGE DAMPING CURVE SANDS, FROM SEED AND IDRIS
 —○— AVERAGE DAMPING CURVE CLAYS, FROM SEED AND IDRIS

Figure 130. Damping Ratios for Embankment Soils

the frequency content was different for the bedrock motions at the base of the dam and at seismograph station ORV.

September 27 Event

The bedrock motion of the September 27 event recorded at the dam toe was used as input to the dynamic finite element model. Other input was the same as for analysis of the August 1 event, except the highest frequency used for LUSH was 16 Hertz instead of 8 Hertz.

Response was computed at the crest and at 74 metre (240 foot) depth. Comparisons of computed and observed acceleration time histories and response spectra are shown in Figure 133.

Accelerations at the crest are much smaller than in the August 1 main shock, and the duration of shaking is much shorter. The response is all at high

frequency -- 2 to 10 hertz. Either the shaking is not strong enough to excite the dam into definitive free vibration motion, or the fundamental period is much smaller for the September 27 event.

Dynamic Properties Adopted for the Gravel Shell

The shear modulus parameter, K_{2max} , was determined for the gravel shell by cyclic triaxial tests and analysis of embankment response to the August 1, 1975 earthquake. Both methods have serious limitations including:

1. Remolded samples cannot faithfully model variations in gradation and compaction in the embankment.
2. The triaxial test does not correctly model the stresses in the embankment.
3. Shear strain is assumed constant

throughout the dam in the analysis of observed response.

4. Makdisi's correlation for natural periods was developed for a 30 metre (100 foot) high dam with constant shear modulus and damping throughout. This correlation was assumed applicable to Oroville Dam with a height of 230 metres (750 feet) and a shear modulus that varies throughout.

The two different methods gave different

answers. However, these results bracket published values for dense gravels (Figure 122). Therefore, it was decided to use two values, 130 and 205, to represent the range.

Because the damping results determined in the cyclic triaxial tests agreed so well with the published average values for sands, it was also decided to use an approximation of the average damping curve in computing dynamic stresses generated by the Reanalysis Earthquake.

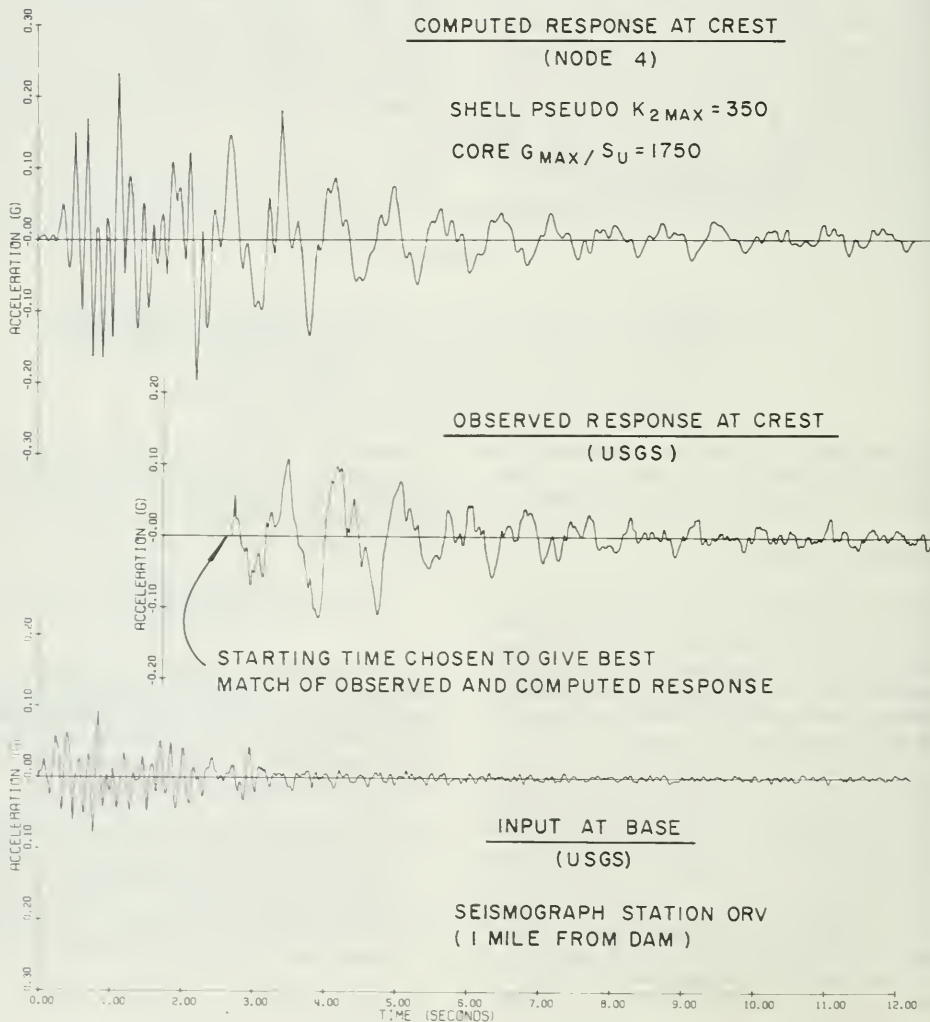
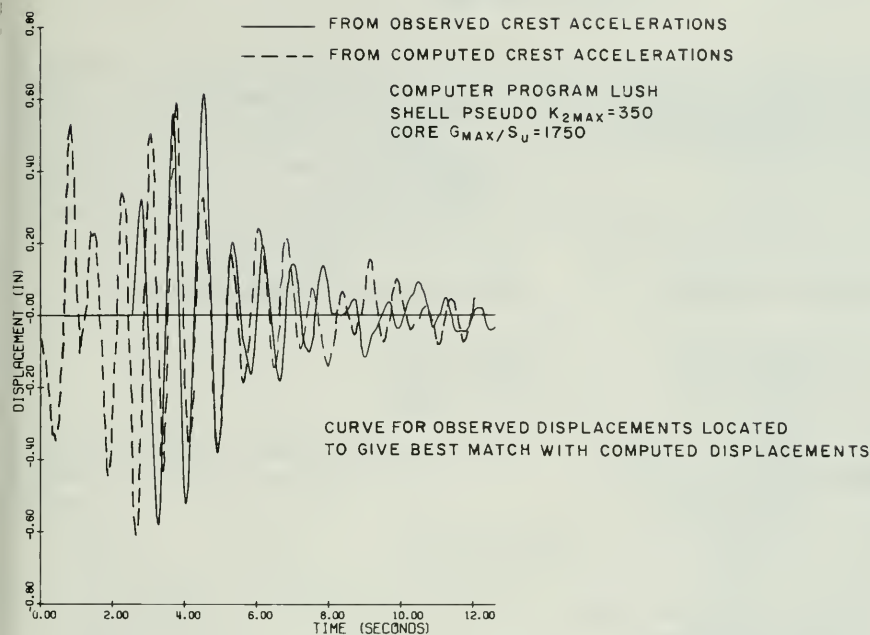
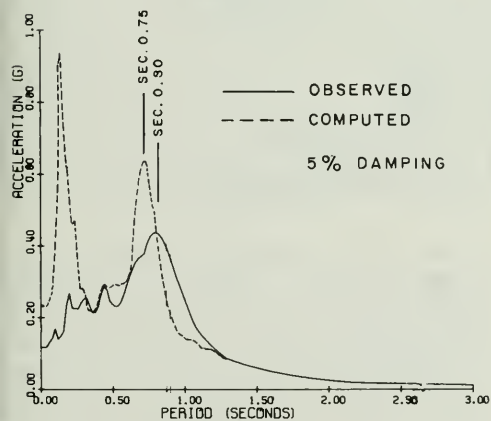


Figure 131. Comparison of Acceleration Time Histories, August 1 Main Shock



ACCELERATION RESPONSE SPECTRA FOR CREST MOTIONS



ACCELERATION RESPONSE SPECTRA FOR BASE MOTION USED IN LUSH ANALYSIS

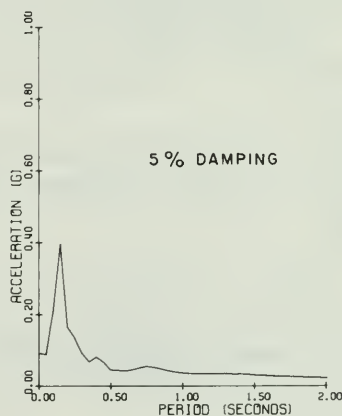
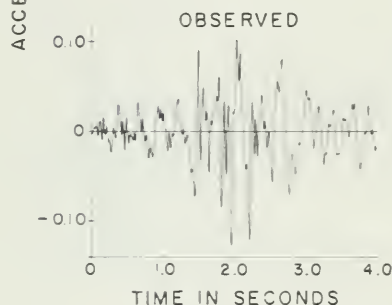
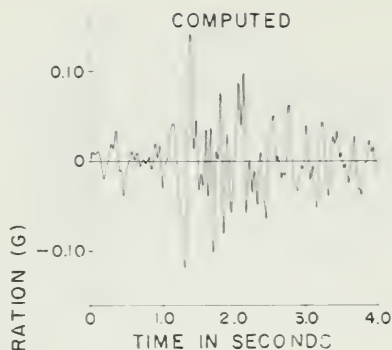
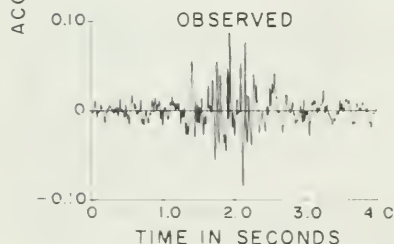
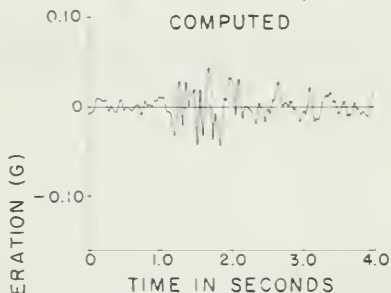


Figure 132. Comparison of Displacement Time Histories and Acceleration Response Spectra for Crest Motions, August 1 Main Shock

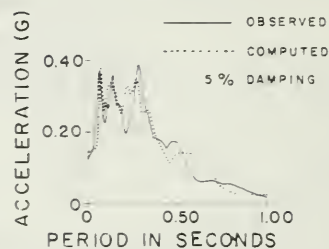


NODE 4 (CREST) ELEVATION 922 FEET



NODE 88 ELEVATION 680 FEET

ACCELERATION RESPONSE SPECTRA



ACCELERATION RESPONSE SPECTRA

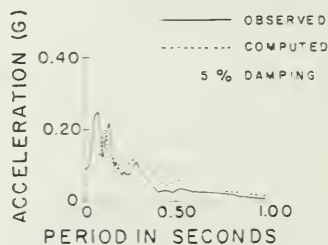


Figure 133. Comparison of Acceleration Time Histories and Response Spectra, September 27 Aftershocks

6. REANALYSIS EARTHQUAKE

On August 1, 1975, a Magnitude 5.7 earthquake occurred approximately 12 kilometres (7.5 miles) southwest of Oroville Dam. The associated surface cracking, traced to within 5 kilometres (3.1 miles) of the dam, revealed a previously unidentified "active" fault (see Figure 134). For a more detailed discussion, refer to

Chapters II, III, AND IV of this bulletin, which describe geological and seismological studies as well as vertical and horizontal geodesy.

Historically, other local events include the following earthquakes:

<u>Richter Magnitude</u>	<u>Date</u>	<u>Location from Dam</u>
5.7	February 8, 1940	50 km (31 miles) north
4.7	May 24, 1966	37 km (23 miles) northwest
4.7	April 29, 1968	48 km (30 miles) west
4.7	August 1, 1975	14 km (9 miles) southwest

In addition, other known faults and maximum credible earthquakes are as follows:

<u>Fault</u>	<u>Richter Mag.</u>	<u>Distance from Dam</u>
San Andreas	8.5	195 km (122 miles)
Honey Lake	7.5	117 km (73 miles)
Mohawk Valley		72 km (45 miles)
Bear Mountains - Melones		58 km (36 miles)

See Figure 135 for fault locations.

Based on the hypocenter locations of the August 1 main shock and the subsequent aftershocks, the causative fault was defined as dipping to the west from the ground surface cracking. This fault system is presumed to extend northward beyond the limit of identified surface cracking. Thus, as illustrated in Figure 136, at depth it would pass directly under Oroville Dam.

The main shock hypocenter was about 9 kilometres (5.5 miles) deep; the after-shock hypocenters were 3 to 8 kilometres (2 to 5 miles) deep. It is assumed for purposes of developing Reanalysis Earthquake motions, that for an earthquake larger than magnitude 5.7, the hypocenter would be 5 kilometres (3 miles) from the base of the dam.

In view of the 1975 earthquake activity, the Consulting Board for Earthquake Analysis and the Special Consulting Board for the Oroville Earthquake recommended the following:

- A. "In view of the developments, it is appropriate to consider that earthquakes ranging up to magnitude 6.5 may occur within a few miles of the dam site."
- B. "The Board considers that an appropriate earthquake motion for reevaluation of structures critical to public safety in the Oroville-Thermalito complex would be one producing a peak acceleration of 0.6g and having characteristics similar to those developed near Pacoima dam during the San

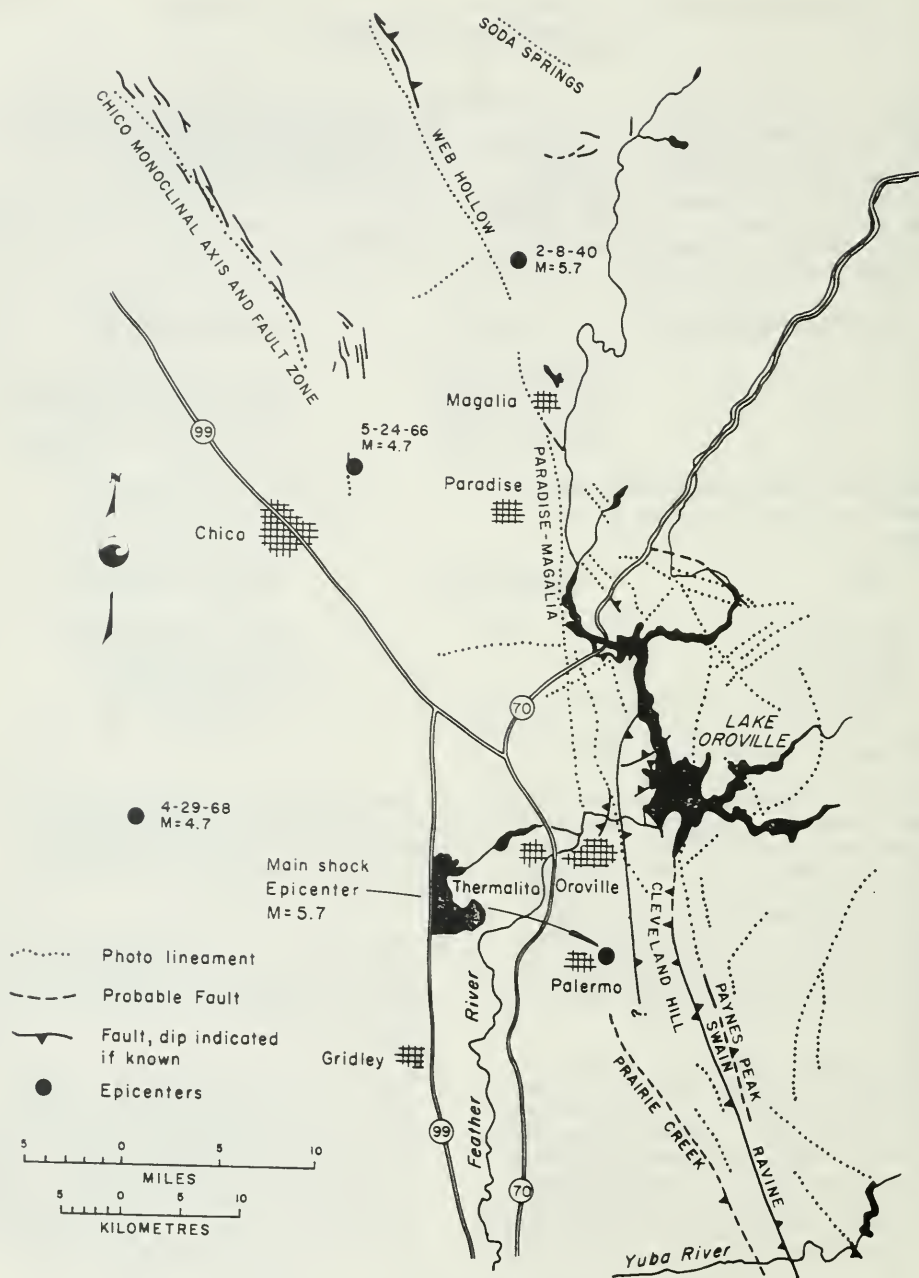


Figure 134. Lineaments, Faults and Recorded Epicenters Around Oroville

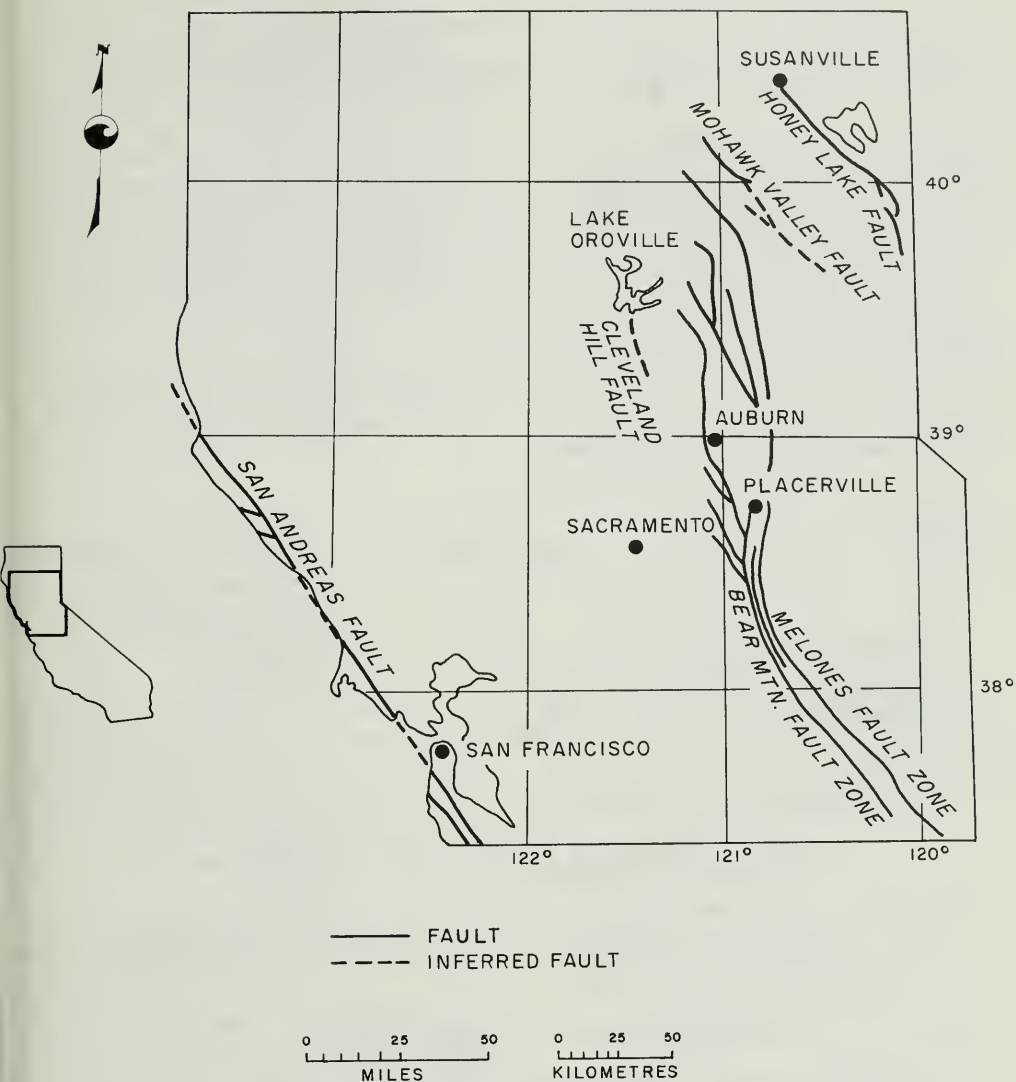
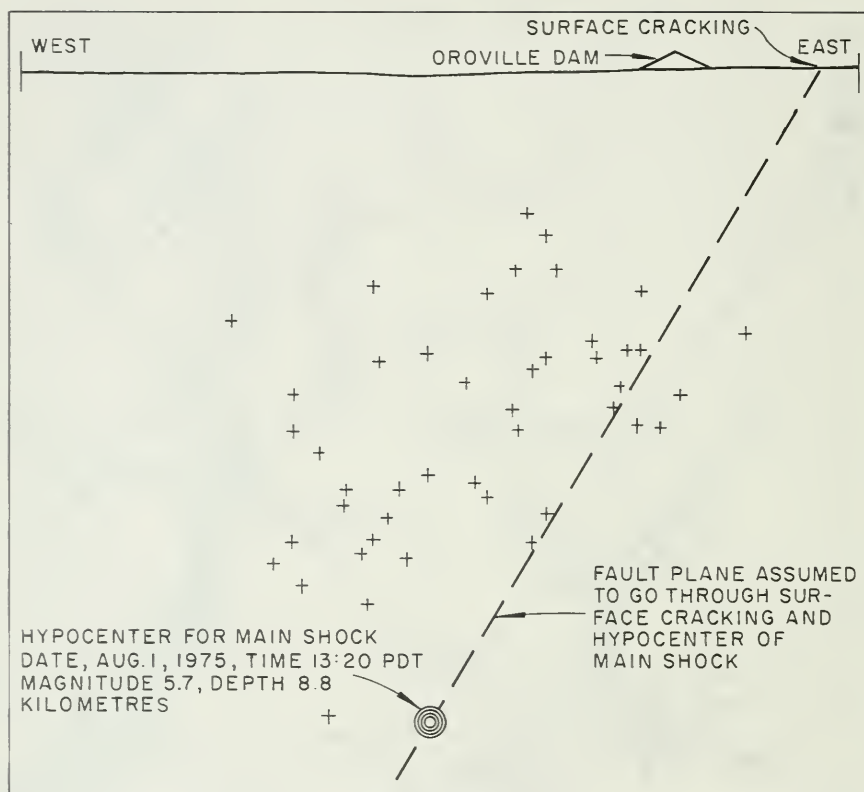
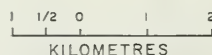
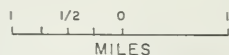


Figure 135. Location of Faults in Relation to Oroville Dam



CROSS SECTION AT MAIN SHOCK HYPOCENTER
PROJECTED NORTHWARD 10 KILOMETRES

+ DENOTES ESTIMATED HYPOCENTER FOR EARLY AFTERSHOCKS,
AUGUST 1 THRU 7, 1975.



SECTION BEARING EAST-WEST

Figure 136. Relationship of Oroville Dam to Assumed Northward Extension of Fault

Fernando earthquake of February 9, 1971. The time-history of such a motion should be obtained from a modified form of the Pacoima dam record, as discussed in the "Report of the Consulting Board for Earthquake Analysis" dated May 22, 1973. The actual time-history could be the same as that forwarded to Mr. Jansen by Clarence R. Allen with his letter of January 16, 1974, except that the duration of shaking should be limited to the first 20 seconds of the record provided, and all ordinates of the record should be multiplied by a suitable scaling factor to give a peak acceleration of 0.6g.

"In addition the structures should be checked for the motions produced by the following earthquakes:

- (a) a magnitude 8.5 earthquake occurring at a distance of 161 kilometres (100 miles)
- (b) a magnitude 7.25 earthquake occurring at a distance of 56 kilometres (35 miles)

It is unlikely that these latter two earthquakes will produce conditions more critical than the motion discussed in detail above, but the check should be made to verify that this is so. Design earthquakes for noncritical structures can be less severe in intensity than those discussed above, and the Board will defer this recommendation until the evaluation of critical structures is completed."

Ground motion characteristics are estimated for the recommended earthquakes as follows (Figure 137):

<u>Magnitude</u>	<u>Distance Km/Mi</u>	<u>Peak Acceleration</u>	<u>Predominant Period Sec.</u>	<u>Duration (a > .05g) Sec.</u>
6.5	5/3	0.6g	0.29	20
7.25	56/35	0.15g	0.4	23
8.5	161/100	0.05g	0.8	3

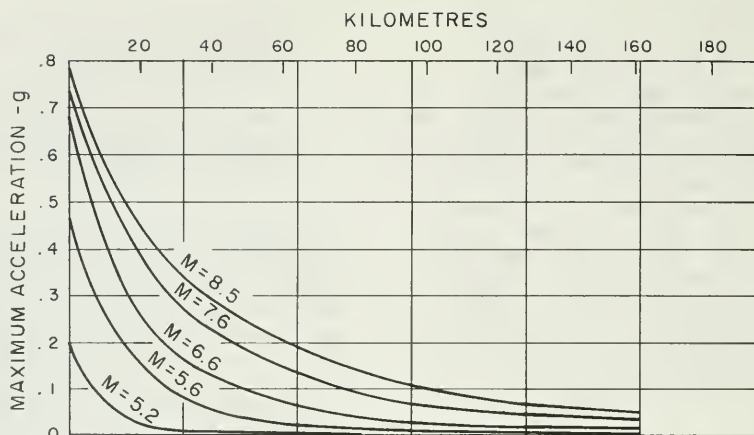
Based on these characteristics, the ground acceleration for the nearby event of magnitude 6.5 exceeds that from the others; and the duration is generally as great or greater; therefore, the 7.25 and 8.5 magnitudes will not be considered further in the analysis.

The acceleration time history shown in Figure 138 is essentially the one recommended by the consulting board. The accelerogram was derived by scaling the Pacoima S16E record down by 0.6/1.17 and adding the Taft record scaled up by 0.3/1.15. The first 2.6 seconds of the Taft record were dropped and the joining made at time 11.2 seconds of the Pacoima. Accelerations in the Taft portion are about 30 percent higher by this procedure than by scaling all ordinates of the time history provided by Clarence R. Allen, to give a peak acceleration of

0.6g. However, the Taft portion peaks are still small in comparison to the Pacoima peaks, and do not produce significant stresses in the embankment. The resulting Reanalysis Earthquake has the following characteristics:

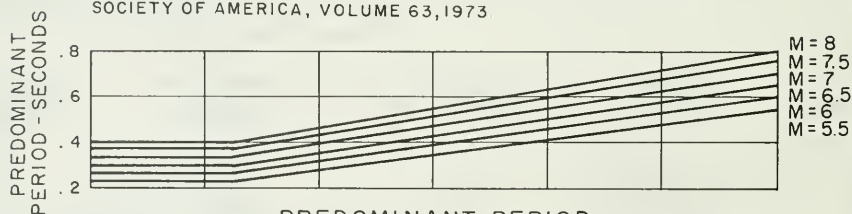
Richter Magnitude	6.5
distance from energy source to dam	5 kilometres (3 miles)
maximum acceleration	0.6g
predominant period	0.4 seconds
duration	20 seconds
acceleration time history	modified Pacoima plus modified Taft

Figures 138 and 139 show the acceleration time history and response spectra.



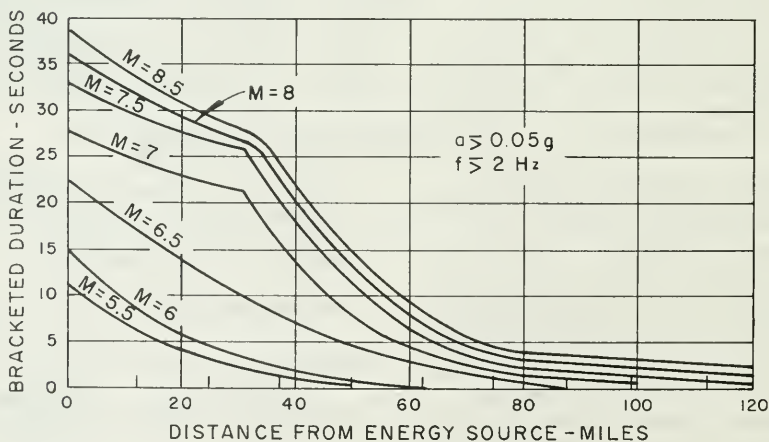
MAXIMUM ACCELERATION

AFTER SCHNABEL AND SEED "ACCELERATIONS IN ROCK FOR EARTHQUAKES IN THE WESTERN UNITED STATES" BULLETIN SEISMOLOGICAL SOCIETY OF AMERICA, VOLUME 63, 1973



PREDOMINANT PERIOD

AFTER SEED, IDRIS AND KIEFER, "CHARACTERISTICS OF ROCK MOTIONS DURING EARTHQUAKES" JOURNAL, SMFE, SEPT, 1969.



BRACKETED DURATION

AFTER BOLT "DURATION OF STRONG GROUND MOTION" PROCEEDINGS FIFTH WORLD CONFERENCE ON EARTHQUAKE ENGINEERING, ROME, 1974.

Figure 137. Earthquake Ground Motion Characteristics

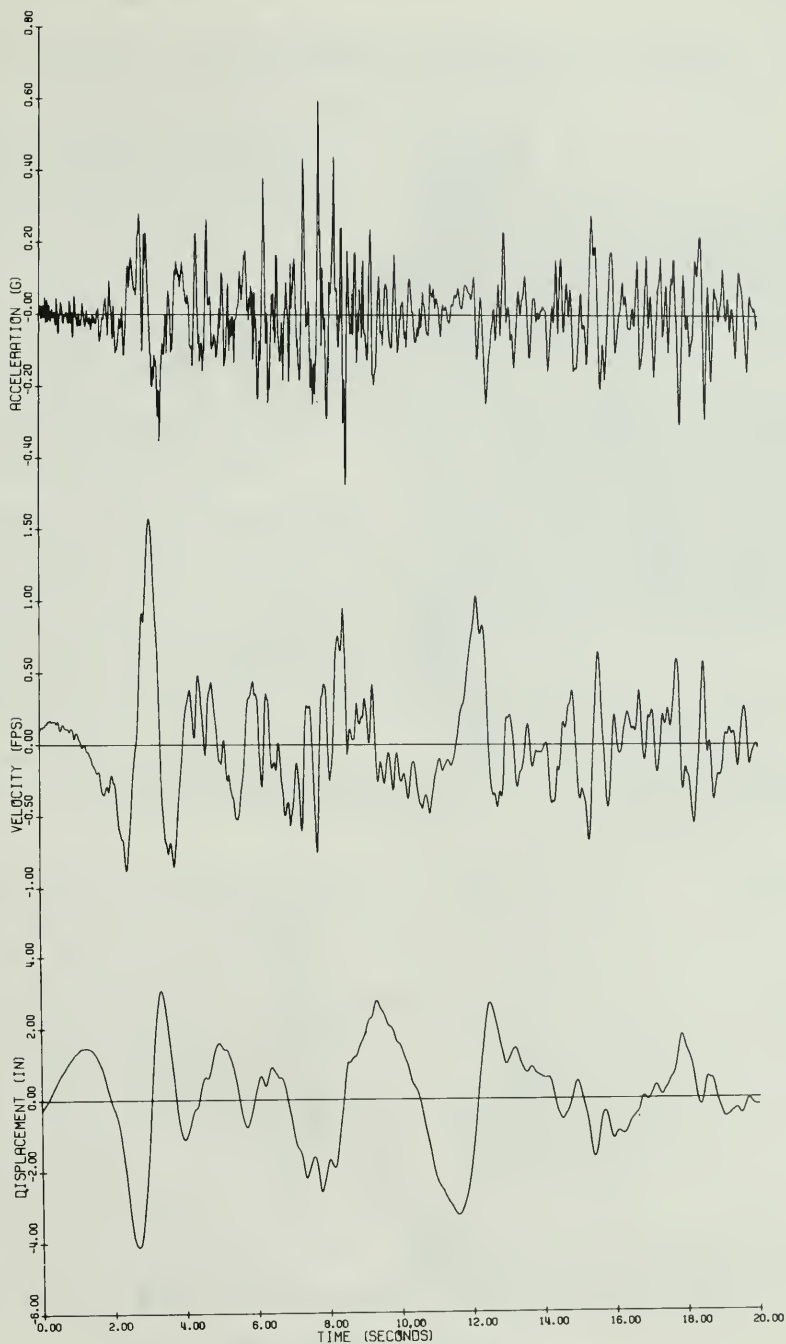


Figure 138. Reanalysis Earthquake

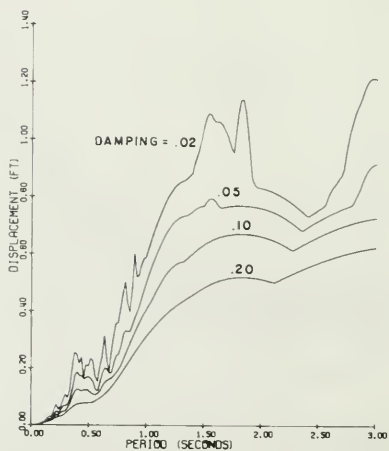
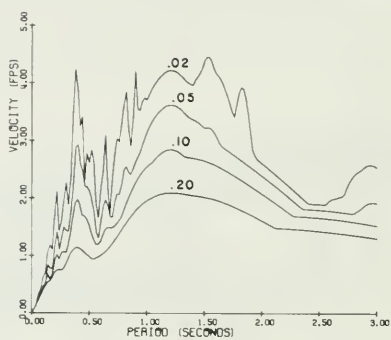
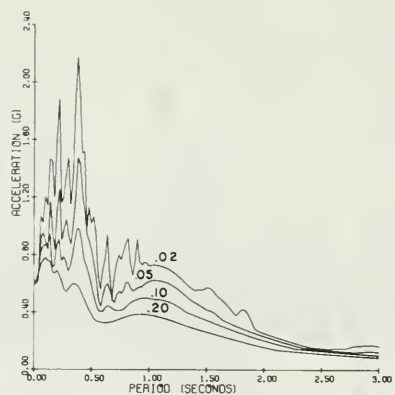


Figure 139. Response Spectra for the Reanalysis Earthquake

7. ANALYSIS OF DYNAMIC STRESSES FOR THE REANALYSIS EARTHQUAKE

Methods of Response Computation

The response of a multiple-degree-of-freedom structure may be determined by solution of the following set of equations:

$$[M] \{\ddot{u}\} + [C] \{\dot{u}\} + [K] \{u\} = F(t)$$

[M] = mass matrix for the structure
[C] = damping matrix for the structure
[K] = stiffness matrix for the structure

\ddot{u} , \dot{u} , u = nodal accelerations, velocities, and displacements

$F(t)$ = earthquake load vector.

Two of the most commonly used programs in the United States for solving these equations are QUAD4 (Idriss, et al, 1973) and LUSH (Lysmer, et al, 1974). Both of these programs are currently in use in the Department of Water Resources for computing the seismic response of finite-element models of embankment dams. Some modifications have been made to them so the LUSH will generate stress time histories, as well as acceleration and displacement time histories, and QUAD4 will take input in the same format as LUSH.

Both programs use the equivalent linear method to account for the nonlinearity in the soil shear modulus and damping ratio. Every element in the structure is assigned an independent value of damping ratio and shear modulus, depending upon the average shear strain anticipated during the earthquake. These properties remain constant during the shaking. After the response has been computed, the average shear strain and corresponding soil properties for every element are evaluated. If the difference between the assumed and computed soil properties is less than a given tolerance, the solution is assumed converged. The average shear strain is computed as a fixed fraction of the maximum shear strain experienced during

the shaking.

QUAD4 solves the equations of motion by a direct integration method. Integration may be carried out by either the linear acceleration technique or Wilson's Theta Method. Rayleigh damping is used which filters out the structure's response in the higher frequency range.

LUSH uses a complex number formulation of the elastic moduli and a method of complex response which assumes that the input motion is harmonic. This formulation allows viscous damping to be introduced in the construction of the stiffness matrix. The program was developed to analyze the response of high-frequency structures, such as nuclear power plants, and has the advantage of providing a more accurate response and a faster solution time.

Acceleration Response of Dam to Reanalysis Earthquake

Acceleration time histories were computed at four elevations in the embankment for the following conditions:

Computer Program	QUAD4
Shell K_{2max}	130
Core Shear Modulus	
G_{max}/S_u	2200
Undrained Strength Envelope	CU
Average Shear Modulus Reduction Curves and Damping Curves	
Poisson's Ratio	0.3

Figure 140 illustrates how the motions are modified in progressing upward through the dam.

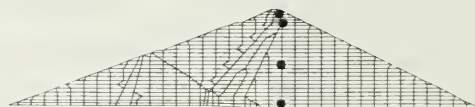
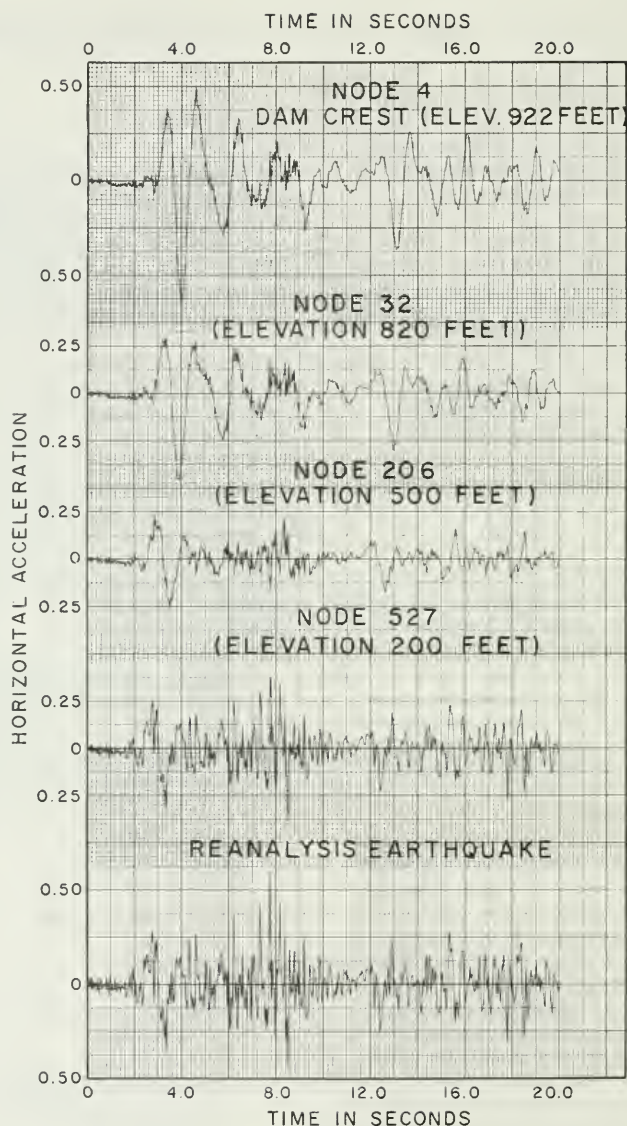


Figure 140. Acceleration Response to Reanalysis Earthquake

Input Variables and Computed Shear Stresses

Comparative studies were made to evaluate the influence of several variables on computed shear stresses. Two computer programs, LUSH and QUAD4, were used for the dynamic stress analyses. Both programs are in general use for computing dynamic shear stresses of embankments.

Shear stresses were calculated for two values of K_{2max} for the shell -- 130 and 205. These values were considered to represent a reasonable range for the highly compacted gravels. The 130 value was determined by cyclic triaxial tests on 30 centimetre (12-inch) diameter samples of gravelly sand with 5 centimetre (2-inch) maximum particle size. The 205 value was chosen to represent the upper

limit of the range estimated by a two-dimensional analysis for observed crest motions in the August 1, 1975 earthquake.

Two of the soil properties used in the analysis, namely shear modulus of the core and Poisson's ratio, were assumed based on published information for other soils. Therefore, stresses were calculated for a range of values of these properties to determine their influence on shear stresses.

Although most of the study was concentrated on the maximum section of the dam, shorter abutment sections could be more critical. Consequently, dynamic shear stresses were also calculated for dam sections 100 metres (330 feet) high and 64 metres (210 feet) high.

The following table summarizes the different values used in the comparison studies:

<u>Variable</u>	<u>Values Used in Comparison Studies</u>		
Shell Shear Modulus			
Parameter K_{2max}	130	205	
Core Shear Modulus	Low	High	
Parameter G_{max}/S_u	2200	1120	
Shear Strength Envelope	CU	UU	
Modulus Reduction Curves	Low*	High*	
Computer Program	QUAD4	LUSH	
	(Wilson's Theta Method)	(Highest frequency =	
	(.02 second time step)	8 Hertz)	
Poisson's Ratio	0.3	0.45	.3/.49**
Embankment Section	750 ft.	330 ft.	210 ft.

*The modulus reduction curves and damping curves used are shown in Figures 20 and 24. The low-modulus reduction curve for clays is the average curve by Seed and Idriss. It is generally for low values of S_u . The high-modulus reduction curve for clays was provided by Professor Seed to John Vrymoed. It is for an S_u of 8000 psf. It was used for core elements with S_u greater than 6000 psf.

**0.3 in unsaturated downstream zone
0.49 in submerged upstream zone

Appendix E includes plots of maximum dynamic horizontal shear stress and shear strain for the several conditions studied, shear stress time histories for $K_{2\max}$ of 205 and 130, and acceleration time histories for $K_{2\max}$ of 205 and 130.

The following embankment properties and conditions were held constant for all analyses:

Acceleration time history for Reanalysis Earthquake

Shell

- moist density 150 pcf
- saturated density 153 pcf
- average modulus reduction curve for sands
- average damping curve for sands

Core

- saturated density 153 pcf
- average damping curve for clays

Core Block

- density 150 pcf
- constant shear modulus 187,200,000 psf
- constant damping

Static stresses from static finite element method analyses.

Average shear strain = $0.6 \times$ maximum shear strain.

Iterations continued until computed G was within 10 percent of trial G in nearly all elements.

OROVILLE DAM — MAXIMUM SECTION
REANALYSIS EARTHQUAKE — MAXIMUM ACCELERATION = 0.6g
LUSH DYNAMIC RESPONSE ANALYSIS

CORE $\frac{G_{\max}}{S_u} = 1120$ (HIGHER CORE MODULUS)

Influence of Shear Modulus of Shell Material

Response analyses were conducted for two values of $K_{2\max}$, 130 and 205, as discussed previously (page 214). The following embankment properties and conditions were used for both analyses:

Computer Program LUSH

Maximum Section

Poisson's Ratio 0.3

Core - $G_{\max}/S_u = 1120$

- UU static shear strength envelope
- Higher shear modulus reduction curve for clays

Table III shows the average maximum shear strains throughout the embankment.

Table III

Shell $K_{2\max}$	Average Maximum Shear Strain (%)
130	0.18
205	0.09

Increasing the modulus from 130 to 205 increases the shear stresses by 20-70 percent in the lower portion of the upstream shell as shown in Figure 141. Unfortunately, comparisons were not possible in the upper portion of the dam because LUSH stresses for $K_{2\max}$ of 130 were incorrect in this area (see section on computer programs).

$$\frac{\text{MAXIMUM } \Delta T_{xy} (K_{2\max}=205)}{\text{MAXIMUM } \Delta T_{xy} (K_{2\max}=130)}$$

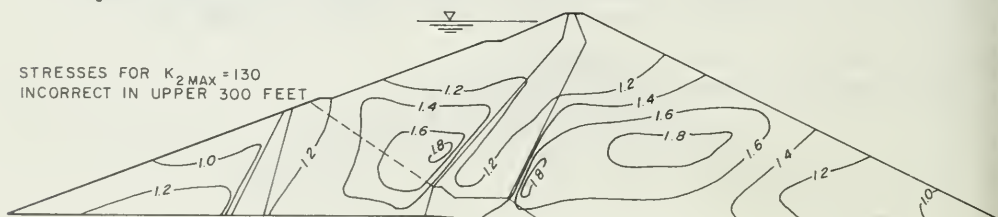


Figure 141. Influence of Shear Modulus of Shell Material on Computed Maximum Horizontal Dynamic Shear Stresses

Influence of Shear Modulus of Core Material

A comparison of maximum dynamic shear stresses was made for two sets of core modulus input data. Both analyses were made using the following embankment properties and conditions:

Computer Program LUSH
Maximum Section
Shell $K_{2max} = 130$
Poisson's Ratio = 0.3

The two sets of core modulus parameters were as follows:

Core Material Parameter	Figure	High Core Modulus	Low Core Modulus
G_{max}/S_u	120	1120 (Lower bound value reported by Seed & Idriss, 1977)	2200 (Average value reported by Seed & Idriss, 1977)
Undrained Strength Envelope	127	Unsaturated UU (End of construction condition)	Saturated CU (End of embankment consolidation condition)
Normal Stress	116	$1/2(\sigma'_{1c} + \sigma'_{3c})$ (From static FEM analysis this study)	$1/2(\sigma'_{1c} + \sigma'_{3c})$ (From static FEM analysis by Nobari and Duncan, 1972)*
Modulus Reduction Curve	126	Higher curve for most elements because $S_u = 6000$ psf or more	Lower curve for all elements because S_u generally less than 6000 psf

*Normal stresses by Nobari and Duncan were used because their finite element mesh was finer in the core and transition zones than the mesh used in the present study, and the stresses were therefore better defined. However, after the analysis was completed it was discovered that these were total stresses, not effective stresses. Their figures 67 and 68 incorrectly defined the plotted contours as effective stresses. The net result is that the low core modulus is somewhat higher than intended, but still four times less than the high core modulus.

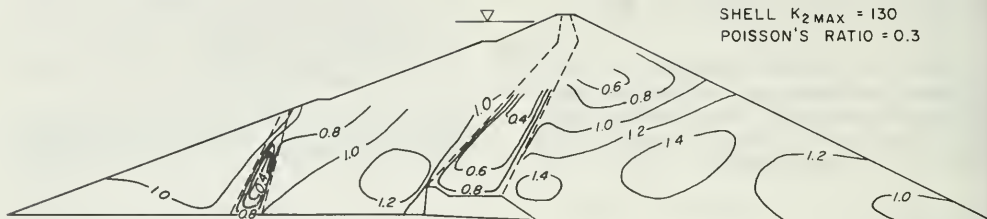
Of the listed parameters, the undrained strength envelope and modulus reduction curve were most significant. The CU strength envelope gave S_u values about half as great as the UU envelope, generally less than 8000 psf. This, in turn caused the lower reduction curve to be used which has about four times as much reduction in modulus as the higher curve at the strain levels in question. The net effect of all four parameters was that the low core modulus values were

about one fourth the high core modulus values.

A comparison of maximum dynamic horizontal shear stresses for the two core modulus conditions is shown in Figure 142 for the bottom 135 metres (450 feet) of embankment. A comparison for the top 90 metres (300 feet) is not shown because the LUSH stresses are incorrect for these upper elements (see next section).

STRESSES BY LUSH FOR $K_{2\text{MAX}}$ OF
130 INCORRECT IN UPPER 300 FEET

REANALYSIS EARTHQUAKE
COMPUTER PROGRAM LUSH
SHELL $K_{2\text{MAX}} = 130$
POISSON'S RATIO = 0.3



NOTE: HIGHER CORE MODULUS ABOUT
4 X LOWER CORE MODULUS

ΔT_{xy} WITH LOWER CORE MODULUS
ΔT_{xy} WITH HIGHER CORE MODULUS

Figure 142. Influence of Shear Modulus of Core on Computed Maximum Horizontal Dynamic Shear Stresses

Reducing the core modulus lowers the core stresses, and raises the stresses somewhat in the shells. The downstream shell has the greatest increase -- up to 40 percent. Most of the upstream shell has very little stress increase. A small zone adjacent to the base and the core has a 20-percent increase. And a narrow zone adjacent to the surface of the upstream slope actually has a 20-percent decrease.

Computer Programs LUSH and QUAD4

In order to resolve a question of unusual shear stress time histories by LUSH, and for general comparison, computed stresses by LUSH and QUAD4 were compared.

Questionable shear stress time history patterns were found mainly in the upper 90 metres (300 ft) of the maximum section for the LUSH analysis with $K_{2\text{MAX}}$ of 130, for both the high and low core shear modulus values. There were significant shear stresses at time zero and large-amplitude, long-period stress fluctuations thereafter. A typical pattern is shown in Figure 143. (These unusual patterns were not found in any elements for the LUSH analysis using $K_{2\text{MAX}}$ of 205).

The induced stresses should be zero at time zero, and should be insignificant for the first two seconds because the input accelerations are insignificant for the first two seconds. Furthermore,

these questionable patterns bear no resemblance to other stress time histories throughout the embankment, which start at zero and have patterns consistent with the input acceleration time history

Dynamic stresses were computed by QUAD4 for the same input used for LUSH:

Maximum section
Shell $K_{2\text{MAX}} = 130$
Core, low shear modulus
Poisson's ratio = 0.3

All time histories produced by QUAD4 had patterns consistent with that of the input earthquake motion. Shear stress patterns by LUSH and QUAD4 are the same in the lower part of the embankment, and are distinctly different in the upper 90 metres, as illustrated by Figures 143 and 144. It is concluded that the LUSH stresses in the upper 90 metres are incorrect for the analyses using a $K_{2\text{MAX}}$ of 130.

The LUSH program was checked by analyzing a sample problem. It gave the prescribed results. Cause of the abnormal behavior is still undetermined.

Figure 145 compares the maximum dynamic horizontal shear stresses for LUSH and QUAD4. In the lower part of the dam, where the LUSH stresses are valid, the two programs give about the same stresses except in a zone adjacent to the upstream slope, where LUSH stresses are

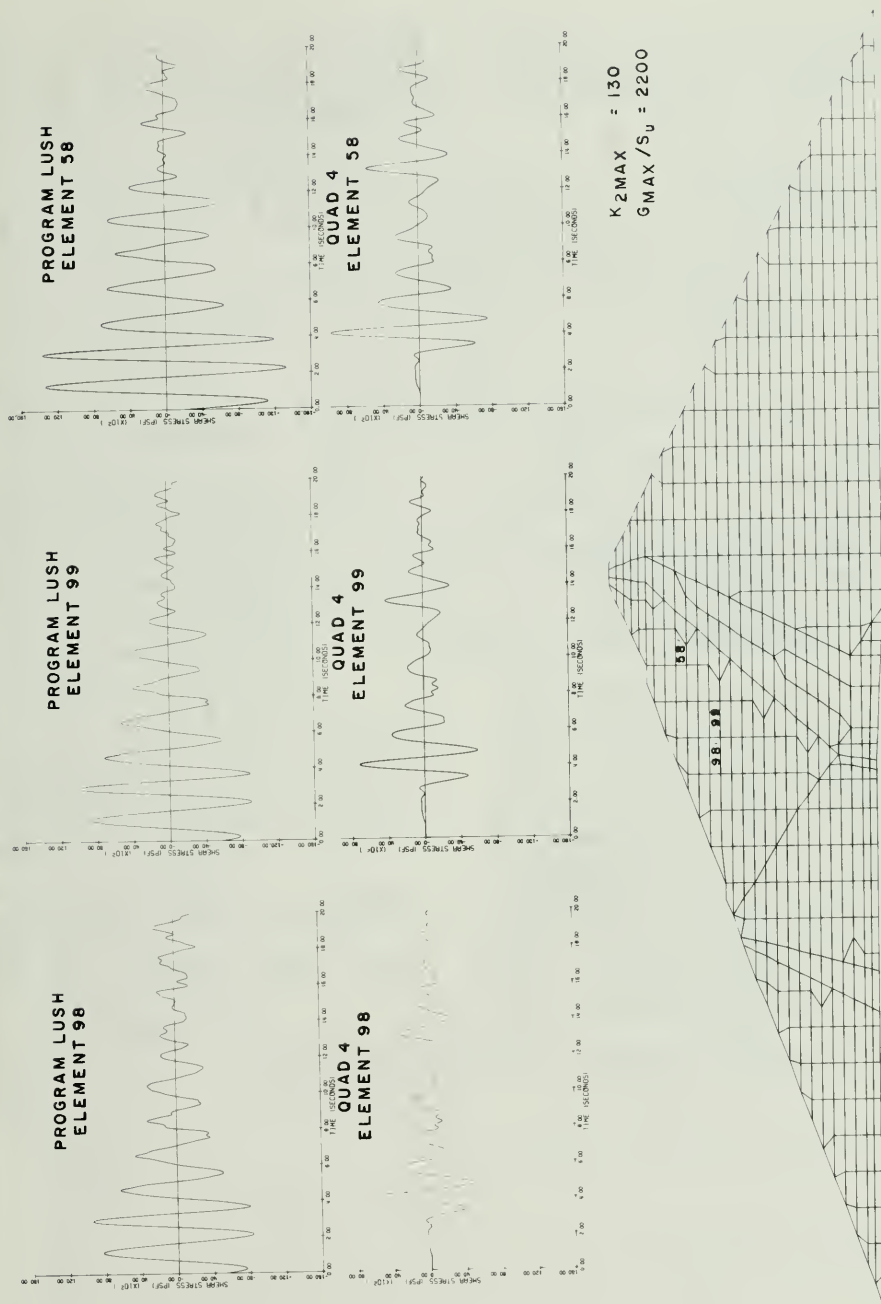
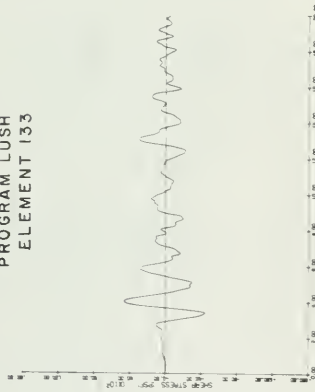


Figure 143. Comparison of Horizontal Dynamic Shear Stress Time Histories from LUSH and QUAD4

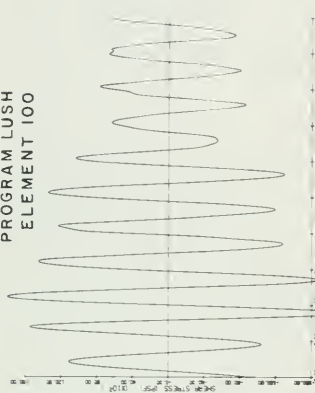
PROGRAM LUSH
ELEMENT 133



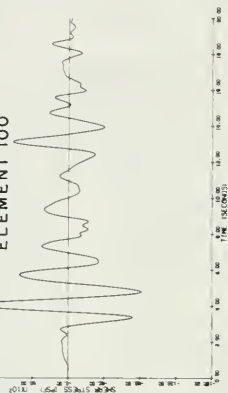
QUAD 4
ELEMENT 133



PROGRAM LUSH
ELEMENT 100



QUAD 4
ELEMENT 100



K2MAX = 130
GMAX / S₀ = 2200

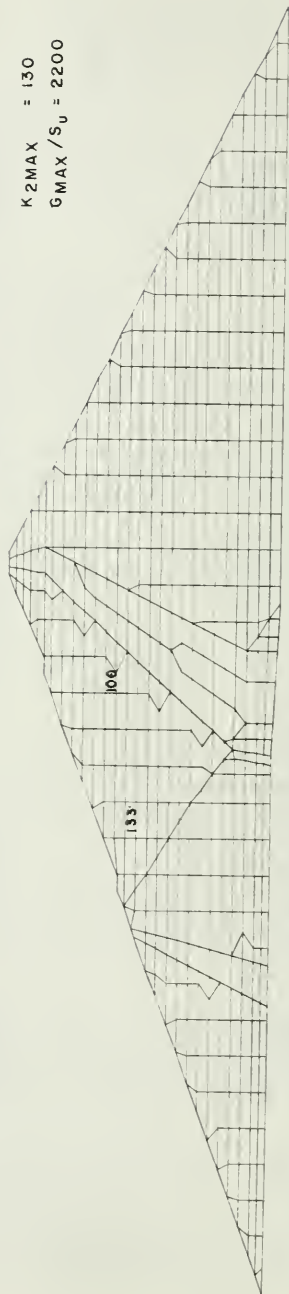


Figure 144. Comparison of Horizontal Dynamic Shear Stress Time Histories from LUSH and QUAD4

about 20 percent higher. In the upper 90 metres, particularly on the upstream side, the LUSH stresses are as much as 60 percent greater than the QUAD4

stresses. No conclusions may be drawn in the upper elements other than that the LUSH stresses are in error.

STRESSES BY LUSH FOR $K_{2\text{MAX}}$ OF
130 INCORRECT IN UPPER 300 FEET

REANALYSIS EARTHQUAKE
SHELL $K_{2\text{MAX}} = 130$
LOWER CORE MODULUS
POISSON'S RATIO = 0.3

ΔT_{xy} BY LUSH

ΔT_{xy} BY QUAD 4

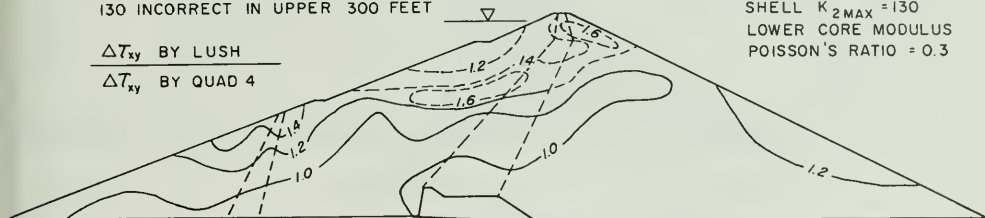


Figure 145. Comparison of Computed Maximum Horizontal Dynamic Shear Stresses by Computer Programs LUSH and QUAD4

It is recommended that in general use of program LUSH, if stresses appear to be out of line for any reason, the time histories should be checked to see if high stresses are occurring at time zero and for the period of time before input accelerations are significant.

Influence of Poisson's Ratio

A Poisson's ratio value of 0.3 was used for all the dynamic analyses of the Oroville embankment. On later reflection it was realized that a value of 0.5 is more appropriate for saturated soils during undrained loading.

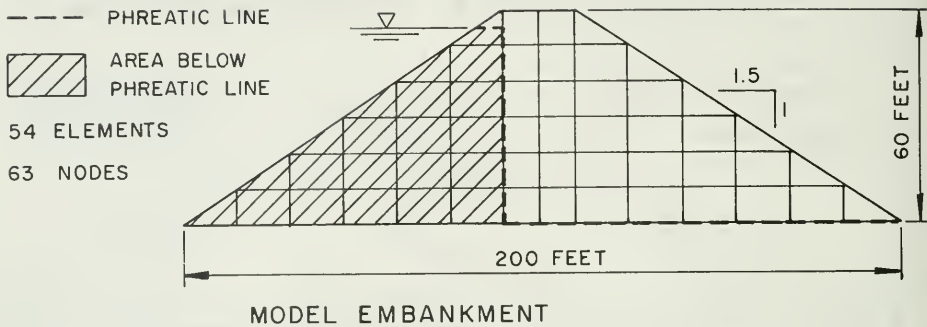
The influence of Poisson's ratio was examined using the following input:

Model embankment (Figure 146)
Computer program LUSH
Shell $K_{2\text{MAX}} = 130$
Static stresses = γH (soil
density x depth
of overburden)

Three Poisson's ratio conditions were analyzed:

1. 0.3 for entire embankment
2. 0.45 for the entire embankment
3. 0.49 for saturated zone (upstream half) and 0.3 for unsaturated zone (downstream half)

Figure 147 shows the influence of Poisson's ratio on dynamic shear stresses. The higher Poisson's ratios generally cause about 10 percent higher dynamic horizontal shear stresses in the central portion of the embankment, but hardly any difference at the base or crest. Comparisons of horizontal and vertical dynamic normal stresses are included in Appendix E. Although the comparisons were not made on the Oroville maximum section directly, it is considered reasonable to generalize them for application to the Oroville section.



STUDIES PERFORMED :

3 ANALYSES CONDUCTED WITH IDENTICAL INPUT VARIABLES EXCEPT POISSON'S RATIO (ν)
 POISSON'S RATIO CONDITIONS ANALYZED

- 1). POISSON'S RATIO = 0.30 FOR ENTIRE EMBANKMENT SECTION
- 2). POISSON'S RATIO = 0.45 FOR ENTIRE EMBANKMENT SECTION
- 3). POISSON'S RATIO = 0.49 FOR ELEMENTS BELOW PHREATIC LINE
 POISSON'S RATIO = 0.30 FOR ELEMENTS ABOVE PHREATIC LINE

METHOD OF ANALYSIS = LUSH PROGRAM

HIGHEST FREQUENCY USED IN ANALYSIS = 8.0 HERTZ

EFFECTIVE STRAIN RATIO = 0.60

INPUT MOTION = REANALYSIS EARTHQUAKE

MAXIMUM ACCELERATION = 0.6g

AVERAGE MODULUS REDUCTION CURVE FOR SANDS

AVERAGE DAMPING CURVE FOR SANDS

STRESS CONDITIONS ASSUMED FOR STUDY

H = HEIGHT OF SOIL ABOVE ELEMENT CENTROID

γ = DENSITY, 153 pcf FOR ELEMENTS ABOVE PHREATIC LINE
 91 pcf FOR ELEMENTS BELOW PHREATIC LINE

$\sigma_{y'}'$ = EFFECTIVE VERTICAL NORMAL STRESS (psf) = $\gamma * H$

$\sigma_{h'}$ = EFFECTIVE HORIZONTAL NORMAL STRESS (psf) = $K_0 * \sigma_{y'}'$

K_0 = COEFFICIENT OF EARTH PRESSURE AT REST = 0.60

σ_m' = EFFECTIVE MEAN NORMAL STRESS (psf) = $\frac{\sigma_{y'}' + 2\sigma_{h'}}{3}$

K_{2MAX} = SHEAR MODULUS PARAMETER = 130

G_{MAX} = MAXIMUM SHEAR MODULUS AT LOW STRAINS (psf) = $1000 * K_{2MAX} * (\sigma_m')^{\frac{1}{2}}$

Figure 146. Model Embankment for Determining Influence of Poisson's Ratio on Dynamic Shear Stresses

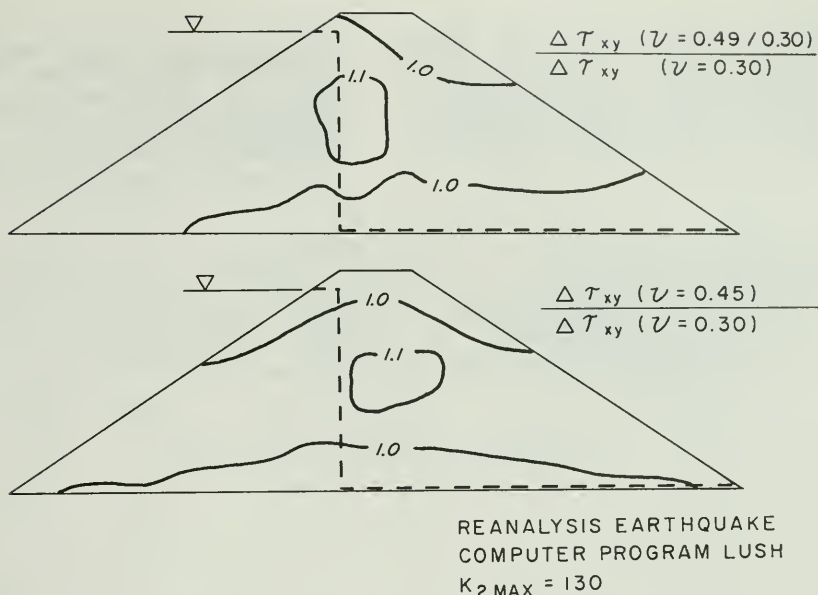


Figure 147. Influence of Poisson's Ratio on Computed Dynamic Shear Stresses

Influence of Embankment Section

Most dynamic analyses of dams are done for the maximum section. However, other sections could be more critical. To cover the range of possibilities, two other sections were analyzed using the same input properties and conditions as used for the maximum section:

Computer program QUAD4
 Poisson's ratio = 0.3

Shell $K_2 \text{ max} = 130$
 Core $G_{\text{max}}/S_u = 2200$
 CU shear strength envelope
 Average modulus reduction curve
 for clays

Finite-element meshes for the two sections were the upper rows of elements of the maximum section mesh. Natural periods and maximum crest accelerations for the three sections are:

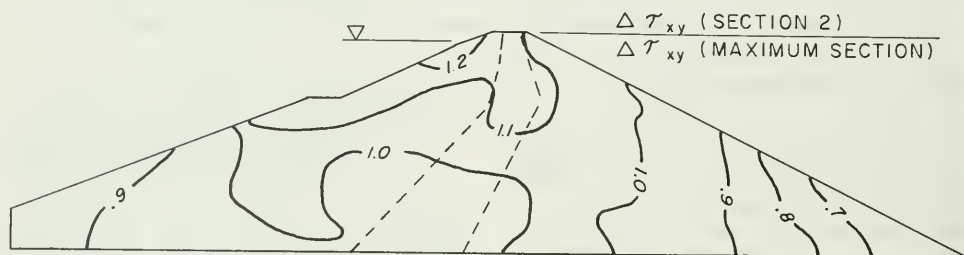
	<u>Maximum Section</u>	<u>Section 2</u>	<u>Section 3</u>
Elements	564	128	66
Height, metres/feet	225/750	100/330	64/210
First mode natural period, sec.	1.98	1.22	.83
Maximum horizontal crest acceleration, g	0.64	0.75	0.79
Maximum vertical crest acceleration, g	0.38	0.51	0.66

Figure 148 shows comparisons of the two shorter sections to the maximum section for maximum dynamic horizontal shear stresses. With respect to the maximum section, both short sections develop

less stress in the outer parts of the shells, and about the same stress in the center; on the average, most of the upstream shell develops about the same stresses.



SECTION 3 (64 METRES HIGH)



SECTION 2 (100 METRES HIGH)

REANALYSIS EARTHQUAKE
COMPUTER PROGRAM QUAD 4
SHELL $K_{2\text{MAX}} = 130$

Figure 148. Comparison of Computed Maximum Horizontal Dynamic Shear Stresses for Different Embankment Sections

Combined Influence of Variables

The submerged upstream gravel shell is the area of concern for seismic stability. The following table summarizes the influence on stresses in that area by the variables studied:

<u>Variable (Figure)</u>		<u>Range</u>	<u>Influence on Dynamic Horizontal Shear Stresses in Upstream Shell (Percent Difference)</u>
Shell K_{2max}	(35)	205 vs. 130	+20 to +70*
Core Shear Modulus	(36)	Lower vs Higher	0 to $\pm 20^*$
Computer Program	(39)	LUSH vs. QUAD4	0 to +20*
Poisson's Ratio	(41)	0.45 vs. 0.3	0 to +5
Embankment Height	(42)	100 metre vs. 230 metre	0 to ± 10

*Not defined in upper 90 metres because LUSH stresses with $K_{2max} = 130$ are incorrect in this area.

For the dynamic shear stresses in the upstream shell, the influence of Core Shear Modulus, Computer Program, Poisson's ratio, and Embankment Height are relatively minor over the range of values studied. However, for the combination of Program LUSH and higher shear modulus in the core, the 20 percent differences are cumulative in a shallow zone along the upstream slope. This is the combination used to calculate stresses for evaluation of embankment performance and will give the highest stresses in this zone.

The major influence is shear modulus of the shell. Increasing shell K_{2max} by a factor of 1.6 causes shear stresses to increase by 1.2 to 1.7. The choice of K_{2max} within the range 130-205 will be a major determinant of computed embankment performance. The conservative approach would be to use a value around 200 - near the upper end of the range.

Three-Dimensional Effect

Comparisons of stresses by two-dimensional (plane strain) and three-dimensional analyses are shown in Figure 149 (after Makdisi, 1976) for a dam with:

H = 30 metres (100 ft)
L/H = 3
Slopes = 2:1
 V_s = 150 metres per second (500 feet per second)
Damping = 10%
Earthquake = Taft (first 15 seconds)
 $a_{max} = 0.2g$

For the maximum section, the three-dimensional analysis gives stresses at the crest, base, and slope areas that are 50 percent to 100 percent lower than those for the plane strain analysis. In the central portion, stresses are the same for 2D and 3D analyses.

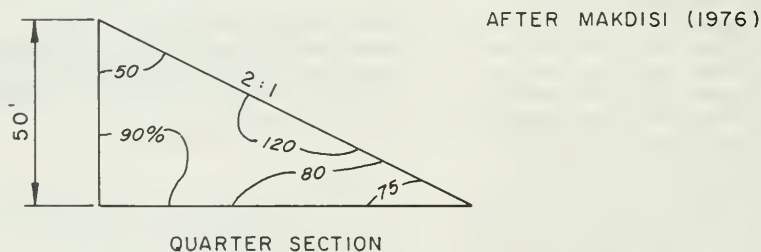
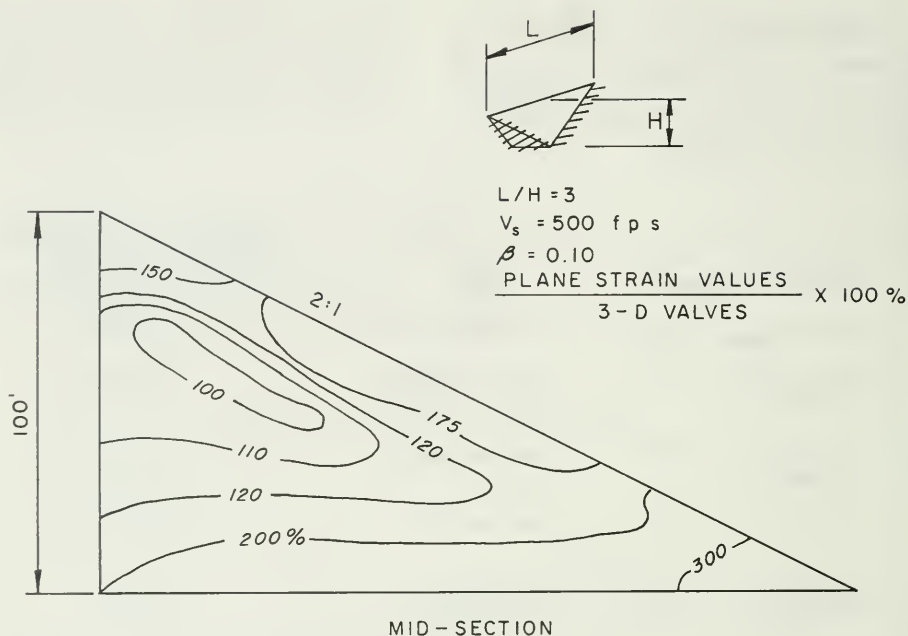


Figure 149. Comparison of Maximum Horizontal Shear Stresses Determined from 3D and Plane Strain Analyses Using Base Motions from Taft Record

For the quarter section, stresses by 2D and 3D analyses differ by less than 20 percent for most locations, but near the

crest the 3D stresses are twice as high as 2D stresses.

For Oroville Dam with $L/H = 7$, smaller differences would be expected between 2D stresses and 3D stresses.

One way to estimate the 3D stresses for the Oroville maximum section is to use the embankment response model defined in Section 5. The implied assumption here is that the same pseudo $K_{2\max}$ value (350) which accounted for abutment restraint effects in the August 1, 1975 earthquake will also correctly account for abutment restraint effects in the Reanalysis Earthquake. Then the model will give the correct period and acceleration response, and the correct computed linear elastic shear strains in the maximum section of the actual (3D) embankment.

The effect of abutment restraint is to reduce the strains of the maximum section by developing shear stresses on its sides. Thus all the inertia forces do not have to be borne by shear stresses on the tops and bottoms of elements. It is these top and bottom stresses that are usually of concern in relation to embankment behavior. These element top and bottom shear stresses can be calculated by multiplying the shear modulus of the material by the 3D shear strains

obtained from the embankment response model.

The embankment response (3D) was calculated for the following conditions:

Computer Program LUSH

Maximum Frequency Used 10 Hertz

Maximum Section

Shell - Pseudo $K_{2\max} = 350$

- Average Modulus Reduction Curve for Sands

- Average Damping Curve for Sands

Core - $G_{\max}/S_u = 1750$

- Shear Strength Envelope UU

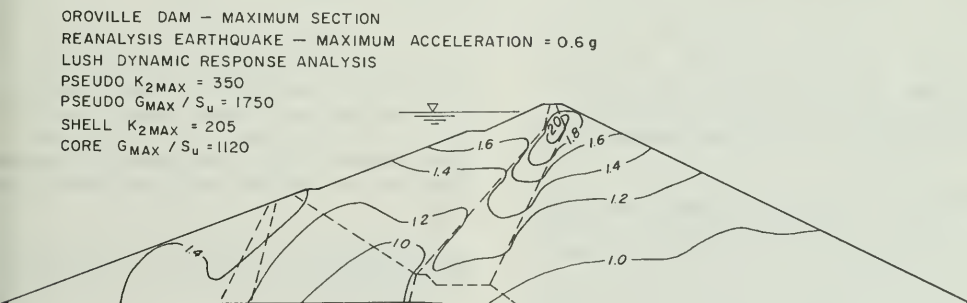
- Higher Modulus Reduction Curve

- Average Damping Curve for Clays

Poisson's Ratio 0.3

Appendix E includes 2D shear stresses for pseudo $K_{2\max} = 350$; Appendix F explains the method used to calculate 3D stresses.

Figure 150 shows the ratio of 2D to 3D stresses in the upstream shell computed for shell $K_{2\max}$ of 205. In the lower interior part of the upstream shell, 2D and 3D stresses are the same; in the central part and upstream of the cofferdam core, 2D stresses are 25 percent higher; in the upper part, 2D stresses are over 50 percent higher. These results are similar to Makdisi's in the upper part of the dam, but the differences between 2D and 3D stresses is much less than those (Makdisi's) along the slope and base.



$$\frac{\text{MAXIMUM } \Delta T_{xy} \text{ FOR PLANE STRAIN CONDITIONS}}{\text{MAXIMUM } \Delta T_{xy} \text{ FOR PSEUDO - 3D CONDITIONS}} = \frac{\text{MAXIMUM } \Delta T_{xy} (K_{2\max} = 205)}{\text{MAXIMUM } \Delta T_{xy} (K_{2\max} = 350)} \times \frac{350}{205}$$

Figure 150. Estimated Three-Dimensional Effect on Computed Maximum Horizontal Dynamic Shear Stresses

8. CYCLIC SHEAR STRENGTH

Cyclic Strength Test Program

Cyclic strength testing was carried out only for the saturated upstream gravel shell and transition. The downstream shell is not saturated and would be much stronger -- with cyclic strength essentially equal to the static effective strength. The two clayey gravel cores occupy a relatively small proportion of the embankment. Also, studies have shown that compacted clayey embankments perform well during earthquakes (Seed, Makdisi, & DeAlba, 1978).

Minor Principal Consolidation Stress

196 kilopascals (4100 psf)
784 kilopascals (16,400 psf)
1370 kilopascals (28,700 psf)
2550 kilopascals (53,300 psf)

Consolidation Stress Ratio $K_c = \sigma'_{1c} / \sigma'_{3c}$

1, 1.5 & 2
1
1, 1.5 & 2
1, 1.5 & 2

Sample Gradations and Density

Modeling Embankment Shell Gradation

Zone 3 materials are sands, gravels, and cobbles up to 15 cm (6 in.) size. Figure 151 shows the average gradation. Even for gradations coarser than the average, maximum particle size rarely exceeds 22.5 cm (9 in.) with only a small percent of material larger than 15 cm (6 in.).

Testing of smaller size particles to represent full-scale material has been done for many years. Lowe (1964) was the first to use a model gradation parallel to the field gradation. This modeling method has since been used by others, notably Marachi *et al* (1969), Becker *et al* (1972), and Wong (1973). Marachi and Becker did static shear tests on full-size field gradations of Oroville Zone 3 material as well as on

The cyclic triaxial testing was carried out under the direction of Professor H. B. Seed at the University of California, Richmond Field Station. The program consisted of about 90 cyclic triaxial tests on 30-cm (12-inch) diameter samples to measure the cyclic strength of the gravel; and about 12 cyclic triaxial tests on 7.1-cm (2.8-inch) diameter samples to determine the effects of aging. Tests of the larger samples included the following consolidation conditions to represent a wide range of locations within the upstream shell:

the modeled gradation. When compared at equal relative densities, the friction angle for the two parallel gradations was the same (maximum difference was one degree).

The same modeled gradation has been used in this study for the cyclic triaxial tests on gravels. Additionally, a second modeled gradation was used for cyclic triaxial tests of smaller samples (Figure 151). The ratio of sample diameter to maximum particle size is six.

Relationship of Test Sample Density to Field Density

The objective was to prepare test samples at the same percent compaction as achieved for the Zone 3 shell material compacted into the embankment. Figure 152 shows the statistical distribution of percent compaction in the shell.

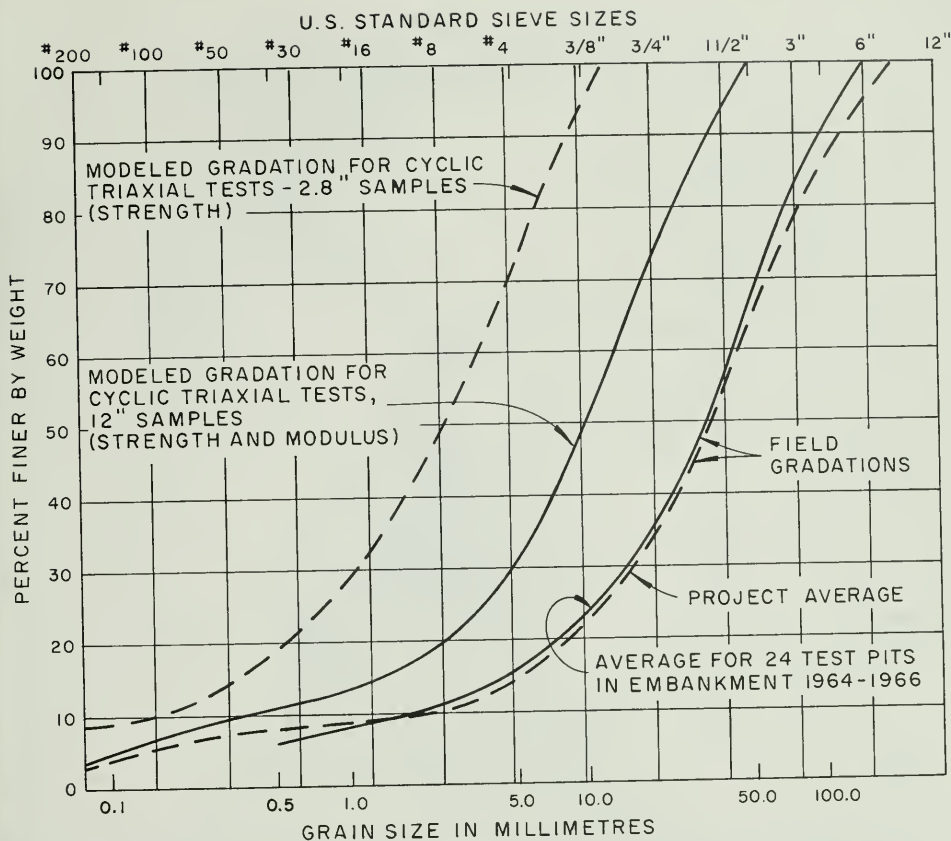


Figure 151. Field and Modeled Oroville Gravel Gradations

Average = 99%
 Standard Deviation = 4%
 Significant Range = 90% - 110%

Figure 153 shows that most of the gravel shell contained between 5 percent and 20 percent minus No. 4, with an average of 14 percent; and that for this average gradation, the average compaction achieved was 100 percent at a dry density of 2 387 kilograms per cubic metre (149 pcf).

Maximum density tests were carried out on samples of minus 5-cm (2-in.) material (modeled gradation) to be used for

the cyclic triaxial tests. The same equipment and procedures were used for these tests as for the control tests run during construction. Test procedures are described in the Oroville Dam Embankment Materials Report. In summary, the test consists of vibrating a 500 kilogram (110-lb.) saturated sample in a 67.5-cm (27-in.) diameter mold for five minutes with a 13.8-kilopascal (2-psi) surcharge. Vibration is with a foundry type air-driven vibrator at a frequency not less than 7,000 VPM. During vibration the mold is lifted off the floor.

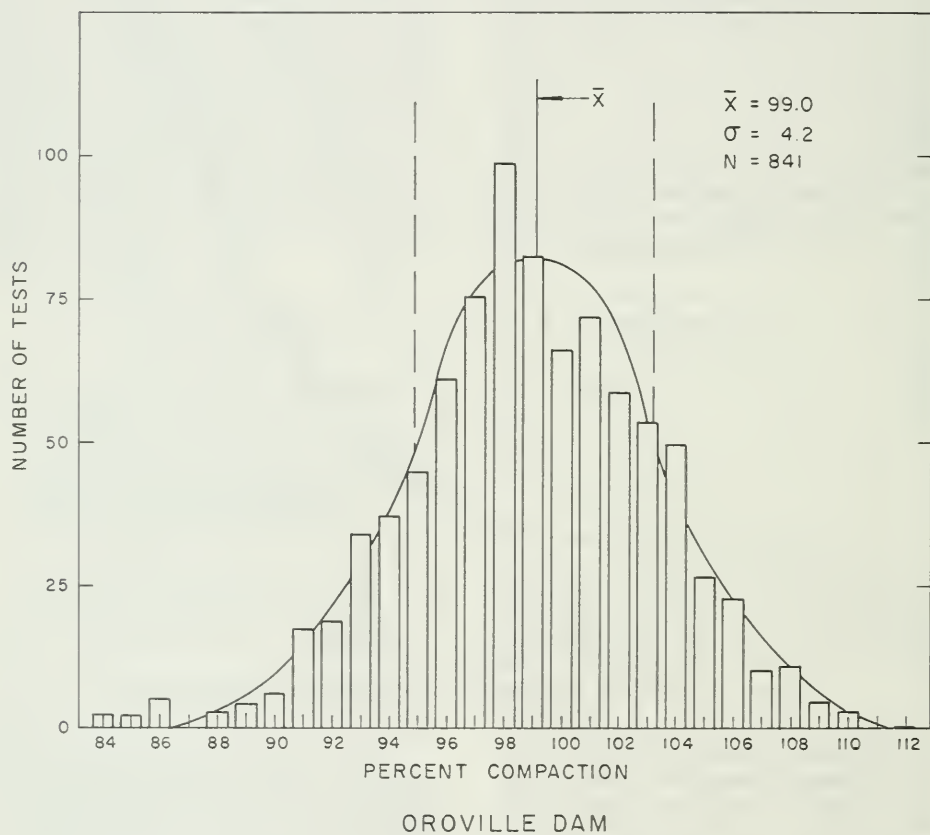


Figure 152. Final Statistical Analysis - Zone 3, Percent Compaction

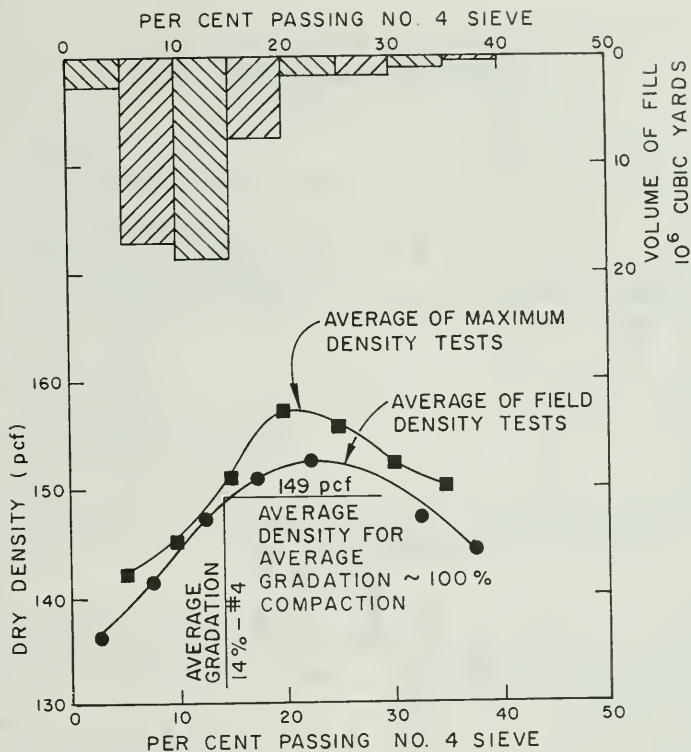


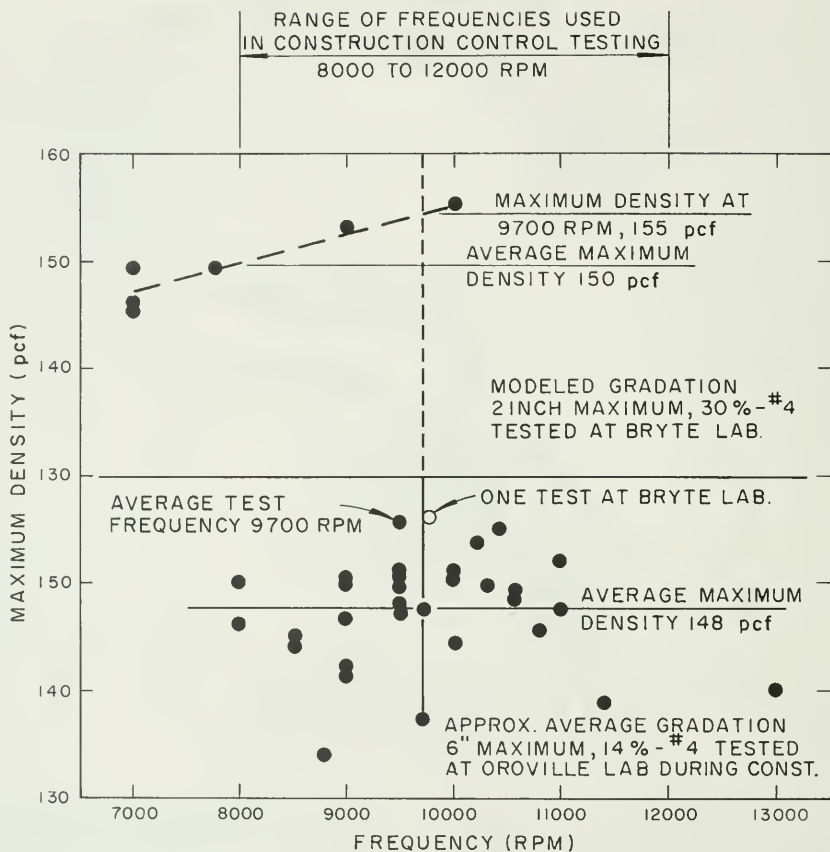
Figure 153. Field Control Tests - Zone 3

Figure 154 shows the results of these tests, along with construction control test results of samples with 14 percent minus No. 4. For the six tests on modeled gradation samples, maximum density appears to be a function of vibration frequency. However, the construction control tests show a general scatter with no apparent correlation.

This difference is understandable. For the tests on modeled gradation material, the gradation and specific gravity were exactly the same for all tests; and the tests extended over a period of two weeks during which vibrator characteristics would not be expected to change drastically. By contrast, the construction control tests were run over a

period of several years on materials with varying gradations and specific gravity.

The frequency of vibration generally varied from 8,000 to 12,000 VPM, averaging 10,000 VPM during construction control testing. Therefore, it seems appropriate to use a frequency of 10,000 VPM for maximum density testing of the modeled gradation material. An average density of 2 390 kilograms per cubic metre (149 pcf) was used for setting up cyclic triaxial test samples. The range was 2 360 to 2 410 kilograms per cubic metre (147 to 151 pcf) and the standard deviation was 18 kilograms per cubic metre (1.1 pcf). Both maximum density at about 10,000 VPM and



27 INCH MOLD
AIR VIBRATOR
1100 POUND SAMPLE
2 psi SURCHARGE
5 MINUTE VIBRATION

Figure 154. Maximum Density Tests - Zone 3

average maximum density for 7,000 to
10,000 VPM are considered in comparing

sample compaction with field compaction
in the following table:

<u>Compaction Conditions</u>	<u>All Zone 3 Material</u>	<u>Material With Average Gradation in Zone 3 Embankment</u>	<u>Cyclic Triaxial Samples</u>
<u>Average Maximum Density for All Frequencies</u>		148 pcf	150 pcf
Average Placed Density		149 pcf	149 pcf
Average Percent Compaction	99%	101%	99%
<hr/>			
<u>Average Maximum Density for Frequencies From 9,500 to 10,000 VPM</u>		150 pcf	155 pcf
Average Placed Density		149 pcf	149 pcf
Average Percent Compaction		99%	96%
<hr/>			
Range of Percent Compaction	91% - 107% (+2 standard deviations)		95% - 100%

The average percent compaction of the cyclic triaxial test samples is slightly (2 percent to 3 percent) less than the average percent compaction of Zone 3 material with average gradation; and also slightly less (0 to 3 percent) than the average percent compaction of all Zone 3 material.

Summary of Test Procedures

30 cm Diameter Samples

The sample was manufactured in 10 layers in a membrane-lined mold on the triaxial test base. Material for each layer was weighed, mixed, placed in the mold, and vibrated for four minutes by a vibrating weight placed on top of the layer. The top cap was placed on the sample, a vacuum applied, the mold removed, and a second membrane installed. The chamber was assembled on the base, filled with water, and pressurized. The sample was soaked by flowing water upward through it, and then backpressured until pore pressure parameter B was 0.9 or higher. Back pressure for

most tests was 392 kilopascals (8,200 psf). After consolidation was complete, cyclic loading was applied at a frequency of one cycle per minute, beginning with the compression half. Loads were set to be sinusoidal and symmetrical about the static axial deviator stress. The slow frequency was necessary for the hydraulic loading system to maintain scheduled loads as the sample underwent large displacements. Continuous records were made of load, displacement and pore pressure.

7.1 cm Samples

Procedures were basically the same as for the larger samples. Exceptions were:

1. Material was not mixed individually for each layer.
2. Sample was made in five layers rather than ten.
3. Half of the samples were allowed to consolidate for two months before testing.

4. Loading frequency was one cycle per second.

Results of Cyclic Triaxial Tests

The testing report (Appendix L), which is now being prepared, will be provided on request when it becomes available.

Copies of the test records and associated data, plots of cyclic stress vs. number of cycles for specified strains, and cyclic strength envelopes, all for tests of 30-cm (12-in.) samples, have been provided to DWR. Summaries of the test records are included in Appendix G. The cyclic strength envelopes are discussed in the next section.

Detailed results of the aging tests on 7.1-cm (2.8-in.) samples have not been provided yet. A verbal report was made that aging did not produce any strength gain.

Most of the tests were successful, but some records show deficiencies. Typical test records for successful tests are shown in Figures 155 and 156. The deficiencies were mainly found on tests with isotropic consolidation ($K_c = 1$) and include the following:

1. Loading was more than 10 percent asymmetric and drifted or jumped during the test. In addition, the loading amplitudes often attenuated quite severely with succeeding cycles. About half of the samples consolidated isotropically at 785 kilopascals (16,400 pounds per square foot) suffered from severe attenuation. An example of such load attenuation is shown in Figure 157.
2. Load jumps and unusual pore pressure jumps rendered about the first 20 cyclic tests questionable. It was unfortunate that most of the isotropically-consolidated tests at an initial confining pressure of 196 kilopascals (4,100 psf) were in this group. Examples of such tests are shown in Appendix G.

3. Many samples which developed significant strain produced symptoms of necking.
4. Many samples which developed only a small amount of strain were tested for only a relatively few number of cycles. For example, except for two tests which experienced severe load attenuation, all of the samples consolidated isotropically to 784 kilopascals (16,400 psf) were stressed only to 12 cycles or less.
5. After the testing program was completed, the load calibration was found to be different from the designated value. The actual applied loads were approximately 15 percent higher than those recorded. The correction not only changes the values of the cyclic stresses but also alters the values of the anisotropic consolidation stress ratios, because the hydraulic actuator was used to increase the major principal consolidation stress to a higher value than the minor principal consolidation stress. There were some check tests performed in an attempt to ascertain when the calibration actually deviated from its designated value. On the basis of these tests, this point was found to be about halfway through the testing program. However, the 15 percent difference would be virtually impossible to find by check tests, because the variations of cyclic test results are at least that large. It is also quite reasonable to assume that the calibration error was present throughout the testing program.

Several corrections must be made to the cyclic triaxial stresses on the rest records:

1. The C_c correction is made because the triaxial test does not duplicate the stresses present in an actual soil element. A C_c value of 1.0 is usually used for anisotropically-consolidated samples; a value of

about 0.6 is used for isotropically-consolidated samples.

2. Axial stresses should be multiplied by 1.15 to correct for the load calibration error. For the anisotropically consolidated samples this will also give slightly higher consolidation stress ratios. K_c values of 1.5 and 2 should be changed to 1.57 and 2.15 respectively.

3. Membrane Strength Correction: This correction is used to account for the fact that the membranes surrounding the sample carry some of the applied axial load. The correction is a function of the induced strain and is shown in Appendix L (available later in 1979). This correction becomes significant only at the lowest effective consolidation stress used in this study.

4. Membrane Compliance Correction - During consolidation, the membrane penetrates into spaces between particles around the surface of the sample. During cyclic loading, pore pressure increases are a controlling factor in sample behavior. The system is intended to be undrained, keeping the pore volume constant. However, if the membrane penetration decreases slightly, the pore volume expands slightly and the pore pressure increase is less than if the volume was kept constant. Verbal reports are that cyclic stresses should be multiplied by 0.9 to account for membrane compliance.

Investigation of Sample Behavior of Dense Sands in Static and Cyclic Triaxial Tests

Objective

Many limitations of the cyclic triaxial test have been pointed out by Seed and Peacock (1970) and by Seed (1976) and include:

1. The cyclic triaxial test does not reproduce the correct initial stress conditions within the ground.
2. There is a 90° rotation of the direction of the major principal stress during the extension and compression halves of the loading cycle.
3. The intermediate principal stress does not have the same relative value during the two halves of the loading cycle.
4. Unless special precautions are taken, friction may develop between the sample and the end caps, which will cause stress concentrations.
5. During the extension half of the stress cycle, necking may develop and invalidate the test data beyond this point in the test.

These limitations are legitimate, but the test is used despite them, because triaxial test results have been successfully related to other cyclic shear tests such as the cyclic simple shear by an appropriate correction factor.

However, consideration of these limitations played an important role in the interpretation of the cyclic triaxial tests carried out for the modeled Oroville gravel samples. The cyclic test results for the isotropically consolidated samples produced many questions concerning the development of sample strain. These samples produced strain almost totally in the extension direction. There was debate over whether some samples developed only a limited amount of strain during testing. It seemed that many samples required cyclic "tension" stresses ($\sigma_{dp}/2\sigma'_{3c} > 0.5$) to produce significant strain levels. Other samples exhibited so much extension strain that necking was suspected. A single cause for this behavior was difficult to isolate due in part to the severe load attenuation during many of these tests.

It was not clear whether the previously mentioned test limitations were the cause of the described behavior, or whether the test results were valid (as valid as triaxial tests that don't produce this observed strain behavior). Of particular concern was resolving whether these test results could be used to evaluate the performance of the embankment during earthquake shaking.

Since available information on the behavior of very dense samples is limited, it was decided to conduct a laboratory investigation to examine more closely the behavior of dense samples and to document the results photographically. The specific objective was to answer these three questions:

1. Is the development of primarily extension strain a valid result for isotropically consolidated dense samples, or is it a product of an erroneous test condition such as sample necking?
2. Did the isotropically consolidated cyclic tests on the modeled Oroville gravel develop necking problems?
3. What happens to an isotropically consolidated sample when the cyclic stress ratio ($\sigma_{dp}/2\sigma'_3$) exceeds 0.5 (tension) and does this constitute a valid test condition?

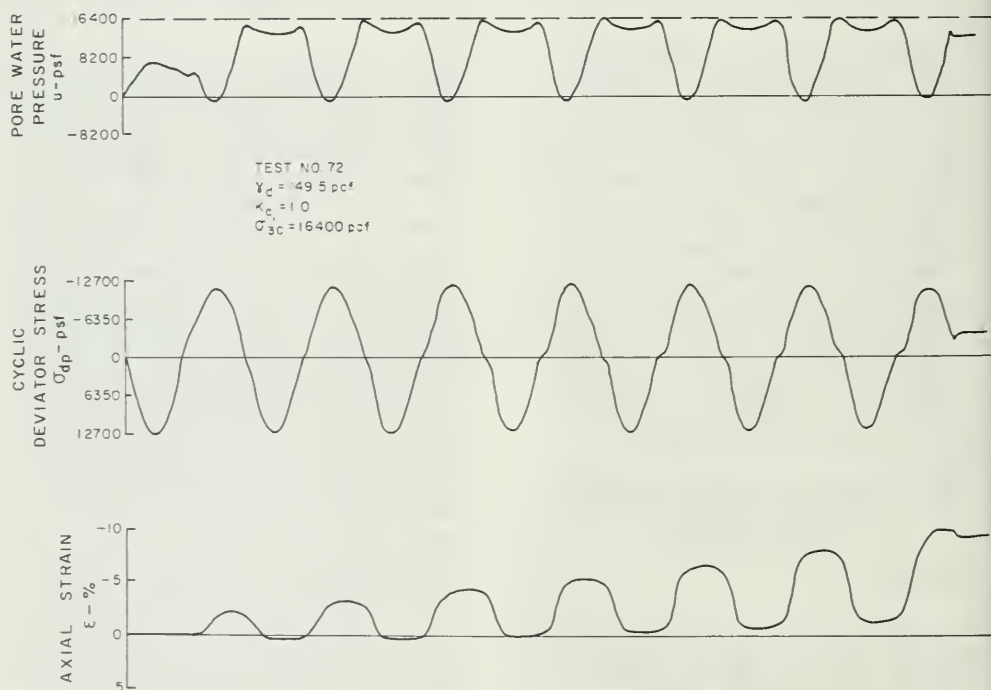


Figure 155. Cyclic Triaxial Test Records for Modeled Oroville Gravel

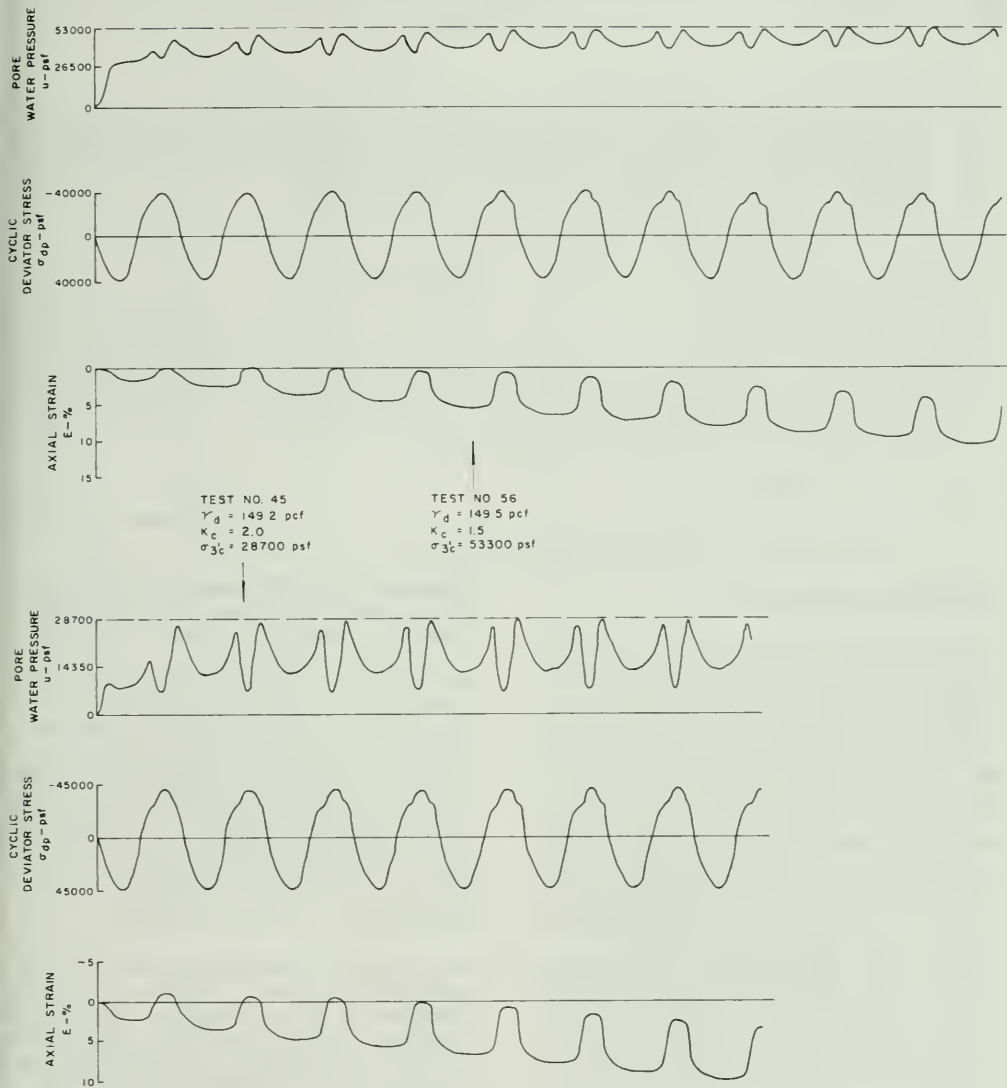


Figure 156. Cyclic Triaxial Test Records for Modeled Oroville Gravel

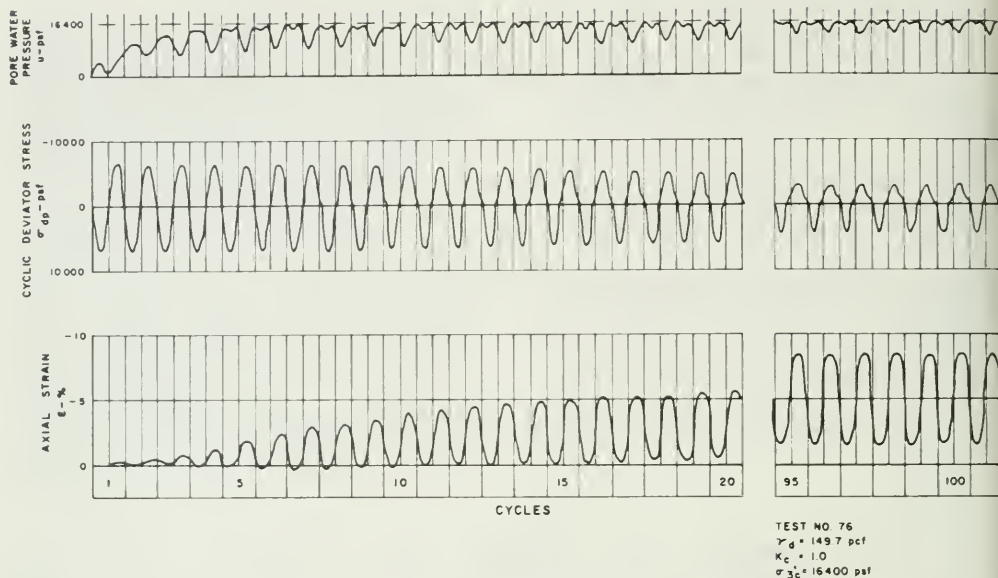


Figure 157. Cyclic Triaxial Test Records for Modeled Oroville Gravel

Program and Procedures

Approximately 60 static and cyclic triaxial tests were carried out on dense samples with particular attention to observing sample behavior and relating it to strain and pore pressure characteristics. The tests were conducted at the Department of Water Resources' Laboratory at Bryte and at the Department of Transportation Laboratory in Sacramento. The two materials tested were Monterey "O" sand and the minus 1.27-cm (1/2-inch) portion of the modeled Oroville gravel, designated Oroville sand. The gradations of these two test materials are shown in Figure 158. Films, slides, and photographs were taken during the tests to document sample behavior and aid in the interpretation of the test measurements.

Monterey "O" sand was used to investigate the behavior of dense, cohesionless samples that were constructed as uniformly as possible and tested under ideal conditions. The behavior of these uniform samples could then be

compared to the behavior of samples that simulated the sample characteristics of the modeled Oroville gravel.

The Monterey "O" sand was chosen because it has a uniform gradation and has been used extensively in previous investigations. These samples were prepared by pluvial compaction through air in an attempt at producing the most uniform sample possible. In addition, the samples were capped with "frictionless" lucite platens lubricated with silicon grease and covered with a circular piece of rubber membrane.

The Oroville sand material was used to represent the sample characteristics of the modeled gravel samples. Both types of samples had gradation curves parallel to the average field gradation and had the same ratio of sample diameter to maximum grain size. Both types of samples would also be constructed using the same preparation technique (high-frequency vibration in layers). No special precautions were taken to minimize the friction at the end platens.

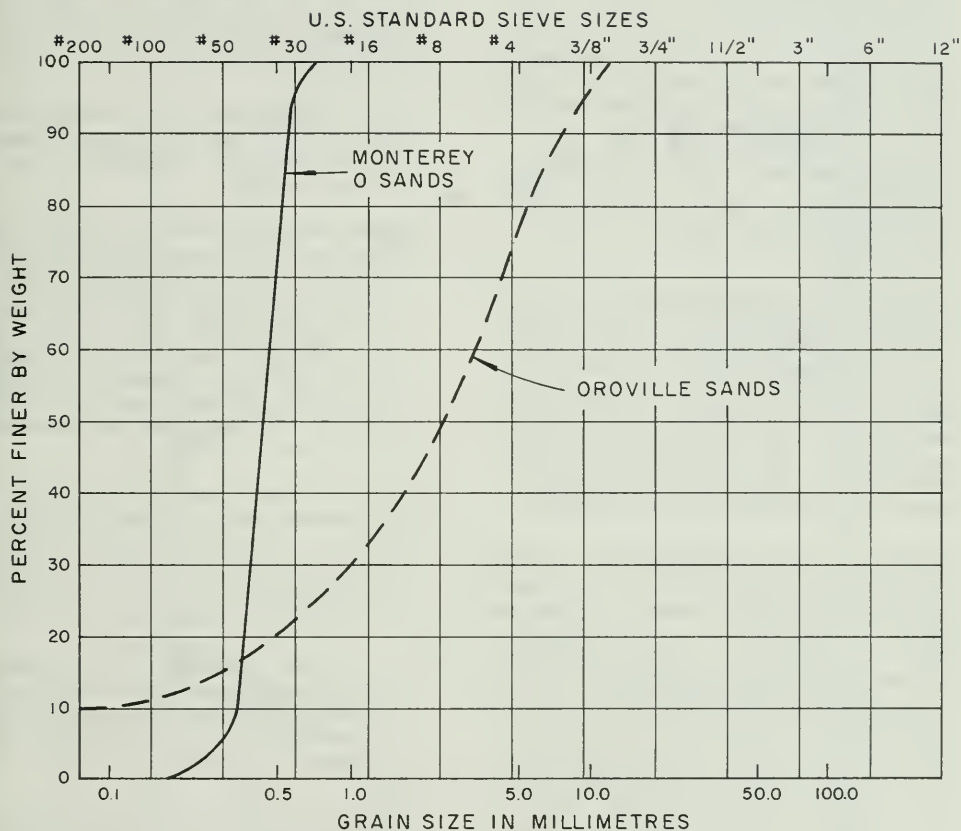


Figure 158. Monterey #0 Sand and Oroville Sand Gradations

All of the samples constructed were 12.7 centimetres (5 inches) high and 6.4 centimetres (2.5 inches) in diameter. Monterey "0" sand samples were confined by a 0.3-millimetre (0.012-inch) rubber membrane and the Oroville sand samples by either a 0.3- or 0.6-millimetre (0.012- or 0.025-inch) rubber membrane. Most of the Monterey "0" sand samples had dry densities ranging from 1 698 to 1 714 kilograms per cubic metre (106 to 107 pounds per cubic foot). A few additional static test samples, however, were constructed with dry densities of about 1 569 to 1 586 kilograms per cubic metre (98 to 99 pounds per cubic foot).

The Oroville sand samples were prepared in five 2.5-centimetre (1-inch) layers and had dry densities of approximately 2 275 kilograms per cubic metre (142 pounds per cubic foot). The relative density of the very dense Monterey "0" sand samples was estimated to be 95 to 100 percent. The relative density of the Oroville gravel samples was estimated to be about 85 to 90 percent.

Saturation details are similar to those used by Mulilis *et al* (1975). Carbon dioxide gas is first passed through the sample to replace the air within the voids and cell lines. Carbon dioxide is used because its solubility in water is much greater than that of air. After the carbon dioxide stage, de-aired water is slowly introduced into the sample from the bottom. The water moves into the sample at a very slow rate, filling most of the voids in the sample. After passing water through the sample, back pressure is applied to dissolve any remaining gas bubbles. The degree of saturation is checked by measuring the pore pressure parameter B. Almost all samples tested had B values of 0.90 or greater and back-pressure values equal to 393 kilopascals (8,200 pounds per square foot). All samples tested were consolidated isotropically to an effective consolidation pressure of 196 kilopascals (4,100 psf).

Static Tests on Monterey "0" Sand

Static tests were conducted only for the Monterey "0" sand samples. Consolidated undrained tests were carried out for medium and very dense samples in both the compression and extension directions, with a strain rate of 0.03 percent per minute.

Typical stress and pore pressure development with strain are shown on Figures 159 and 160. The following observations may be made:

1. For all of the tests conducted, the pore water pressure increases at low strains. After a certain strain value is reached, the pore pressure begins to decrease. This drop in pore pressure continues until the sample fails. The pore pressure development with strain is nearly identical in both the extension and compression directions.
2. The maximum stress and the slope of the stress-strain curves are much greater for the compression tests than for the extension tests, thus indicating the relative weakness of the extension direction.
3. At a given axial stress, the lower density samples strain farther than do the higher density samples. This is true for both the extension and compression directions.
4. The difference in the slopes of the stress-strain curves in the extension and compression directions is more pronounced in the samples of higher density.

Figure 161 summarizes eight stress-strain curves for the static tests conducted on the very dense samples of the Monterey "0" sand. The compression modulus is about five times the extension modulus.

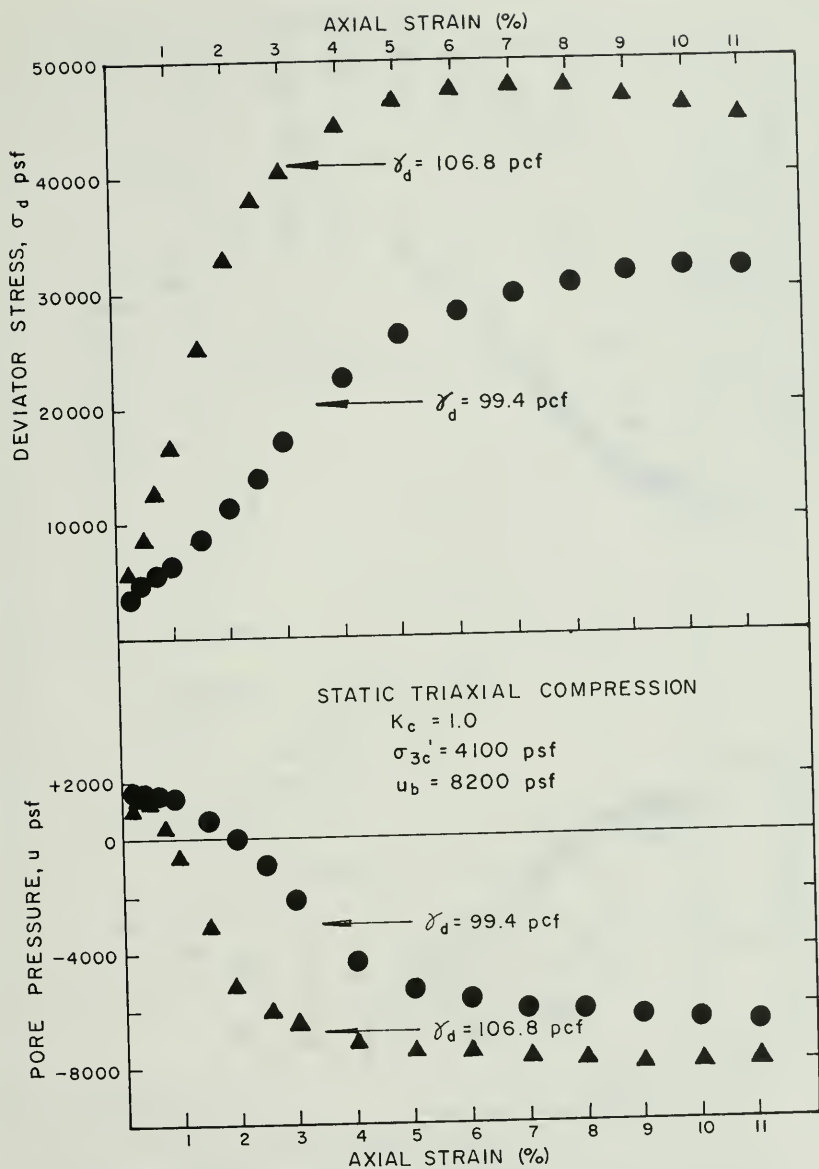


Figure 159. Typical Static Triaxial Compression Test Results for Monterey #0 Sand

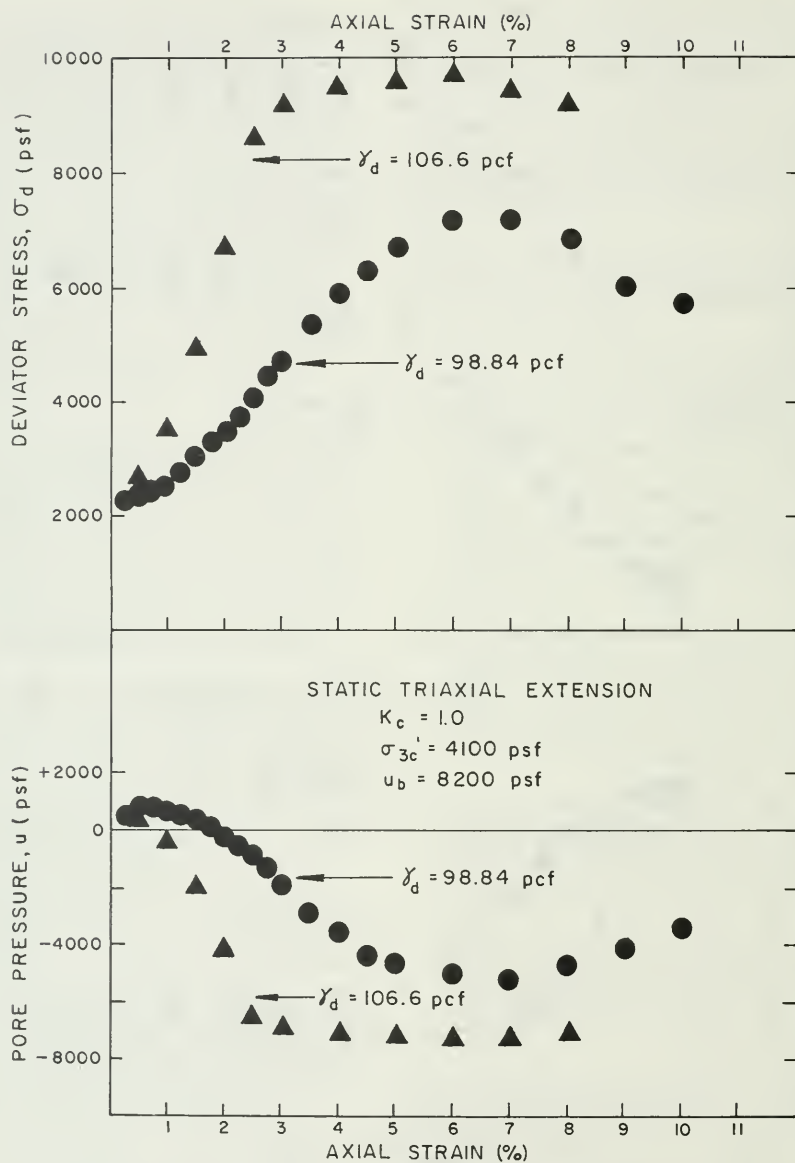
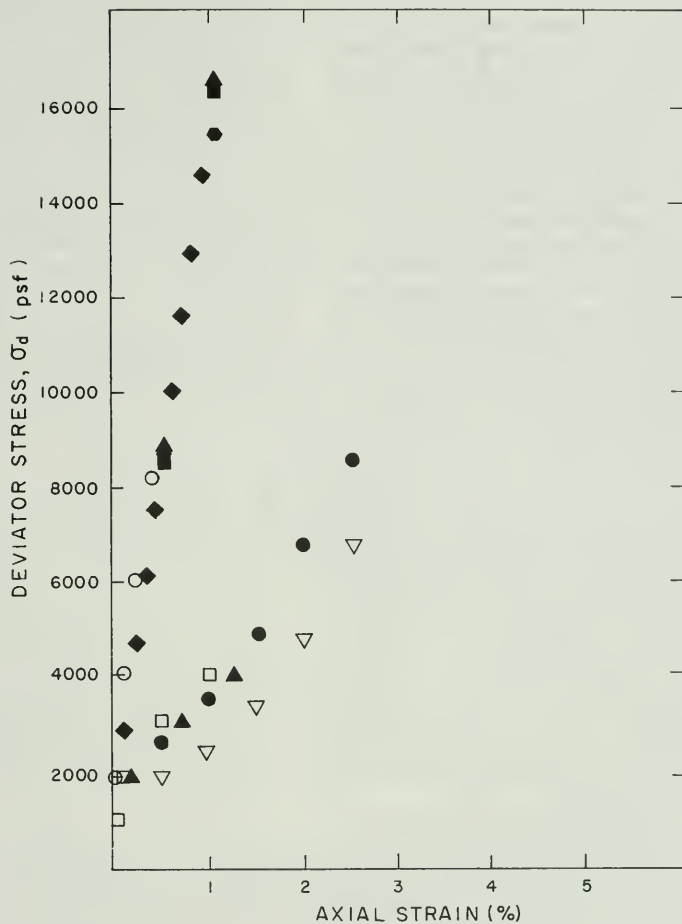


Figure 160. Typical Static Triaxial Extension Test Results for Monterey #0 Sand



$$K_c = 1.0, \sigma'_{3c} = 4,100 \text{ psf}$$

STATIC COMPRESSION TESTS

- TEST NO. A, $\sigma'_d = 106.5 \text{ pcf}$
- TEST NO. F, $\sigma'_d = 106.8 \text{ pcf}$
- ◆ TEST NO. N, $\sigma'_d = 106.6 \text{ pcf}$
- TEST NO. CB, $\sigma'_d = 106.4 \text{ pcf}$

STATIC EXTENSION TESTS

- ▽ TEST NO. B, $\sigma'_d = 106.9 \text{ pcf}$
- TEST NO. E, $\sigma'_d = 106.6 \text{ pcf}$
- TEST NO. CD, $\sigma'_d = 107.1 \text{ pcf}$
- ▲ TEST NO. CE, $\sigma'_d = 107.1 \text{ pcf}$

Figure 161. Summary of Static Triaxial Test Results for Dense Monterey 10" Sand.

Cyclic Tests on Monterey "0" Sand

Cyclic stress ratios ($\sigma_{dp}/2\sigma'_{3c}$) varying from 0.3 to 2.2 were used in the testing of very dense Monterey "0" sand samples. Results of these tests showed that the axial strain developed almost totally in the extension direction. This was true despite the fact that the samples were carefully prepared and composed of uniformly graded sand. This behavior is illustrated in Figure 162, which presents the cyclic strain envelopes for several tests. Observations, photographs and movies made during testing show that the asymmetric strain is not caused by sample necking. Most samples retained a uniform cylindrical shape until the final two or three cycles, when distinct failure occurred.

The strain levels (1/2 peak-to-peak) developed in ten cycles for the tests shown in Figure 162 plotted against cyclic deviator stress (σ_{dp}) in Figure 163. Also shown are the average static stress-strain curves for both the compression and extension directions. The cyclic test results plot along the static extension stress-strain curve.

After the first few cycles, the rate of strain increase is quite gradual for all of the cyclic triaxial tests depicted in Figure 162. This was true despite the fact that the peak pore water pressure values are at, or close to, the initial confining pressure and that the cyclic stress ratios were extremely high. The highest strain level reached was only ± 5 percent. For each test, despite the

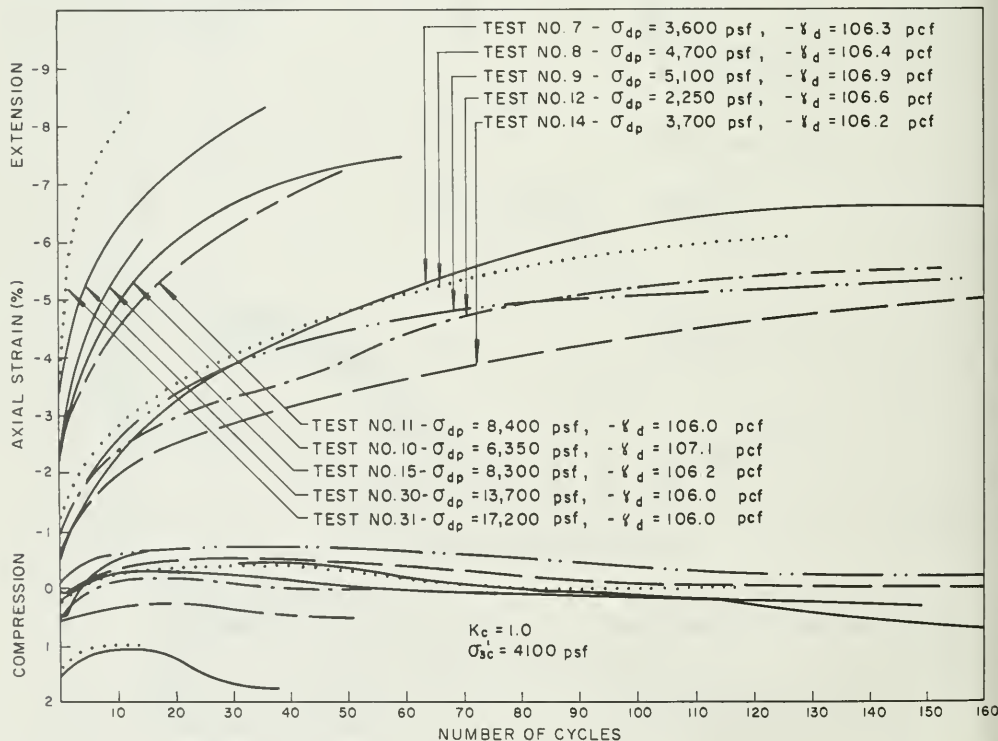


Figure 162. Cyclic Triaxial Strain Envelopes for Monterey "0" Sand

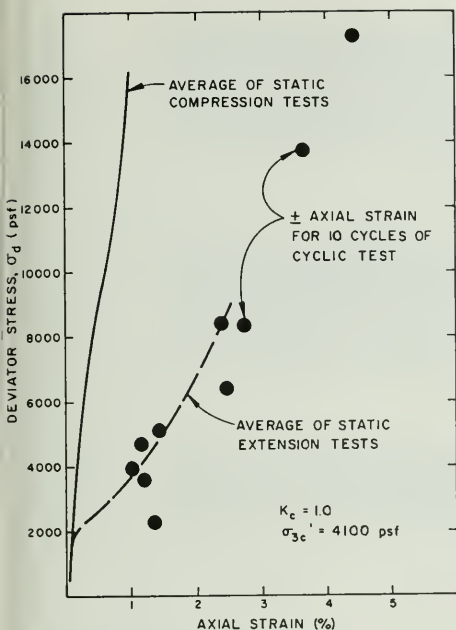


Figure 163. Static and Cyclic Triaxial Test Results for Dense Monterey "0" Sand

value of the stress level, the sample reached a point where the rate of strain increase was so low that it would have required tens or hundreds more cycles to develop an additional one percent of axial strain. This behavior has been described as limiting strain by Mulilis *et al* (1975) and DeAlba *et al* (1975), who also tested samples of Monterey "0" sand. Mulilis performed his tests using cyclic triaxial equipment, whereas DeAlba used large-scale simple shear (shaking table) apparatus. Both studies found a general increase in the limiting strain as the relative density decreased.

In Figure 164, the cyclic test results are presented as the number of stress cycles required to produce a specified amount of strain for different stress levels. Extremely high cyclic stress ratios ($\sigma_{dp}/2\sigma'_{3c}$) were required to cause significant strains in relatively

low numbers of cycles. These cyclic stress ratios ranged as high as 2.2 for these tests. However, tests having cyclic stress ratios greater than 0.5 have often been classified as having erroneous tensile stresses. Many references, including the U. S. Bureau of Reclamation (1976) and Seed *et al* (1975), state that exceeding the 0.5 cyclic stress ratio boundary can cause the sample cap to lift off, which may result in the sample failing prematurely by necking near the top.

The tests carried out for the dense samples of Monterey "0" sand showed that large cyclic stress ratios (greater than 0.5) do not necessarily produce cap lift off and necking at the top of the sample. The large stress ratios produced uniform strains throughout the length of the sample, the same as for samples tested at much lower stresses. Figure 165 shows portions of the cyclic test records for samples tested with cyclic stress ratios of 0.27 and 1.0. The only difference that may be observed in the strain development in the two tests is that the larger stress ratio produces a higher level of strain in the first few cycles. This characteristic was generally true for all the cyclic tests conducted on the Monterey "0" sand. The larger the applied stress, the higher the strain level became in the first few cycles.

It should be noted that all of the cyclic tests were continued until the samples eventually necked. The necking developed despite the fact that these samples were carefully prepared and tested. However, this was not caused by the cap lifting off and causing a neck at the top of the sample. Necking developed at different locations for different samples anywhere from the bottom of the sample to the top. In addition, most Monterey "0" sand samples only indented slightly before the development of a shear plane. A typical shear plane is shown in Figure 166. After the development of a shear plane, the samples quickly necked completely.

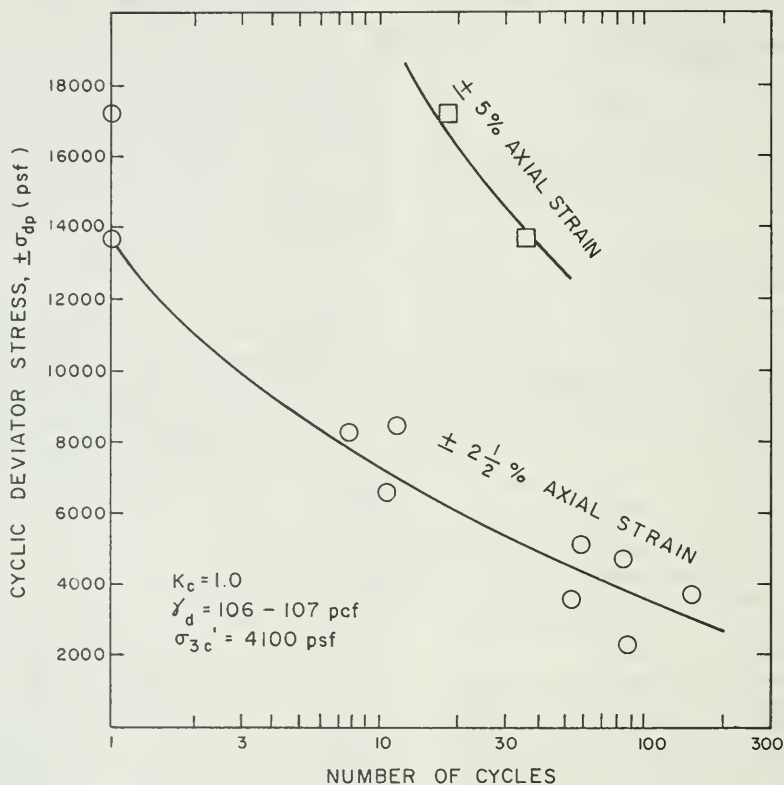


Figure 164. Cyclic Triaxial Test Results for Monterey "0" Sand

The development of this necking behavior is illustrated in Figure 167.

Cyclic Tests on Oroville Sand. Ten cyclic triaxial tests were carried out for the Oroville sand samples. The cyclic stress ratios ranged from 0.3 to 1.0 and the samples were cycled until they necked.

These samples also developed predominant extension strain although the magnitudes were slightly higher than for the Monterey "0" sand samples. In addition, observations and photographs reveal that

the necking was different for these samples than for the Monterey "0" sand samples. Instead of developing a shear plane in the final stage of necking, the Oroville sand samples developed strain concentrations and indentation in the middle portions of the samples. These necks seemed to always be concentrated in one of the middle layers. In general, these samples did not remain as uniform as the Monterey "0" sand samples prior to the final stages of necking. Figures 168 and 169 illustrate this behavior.

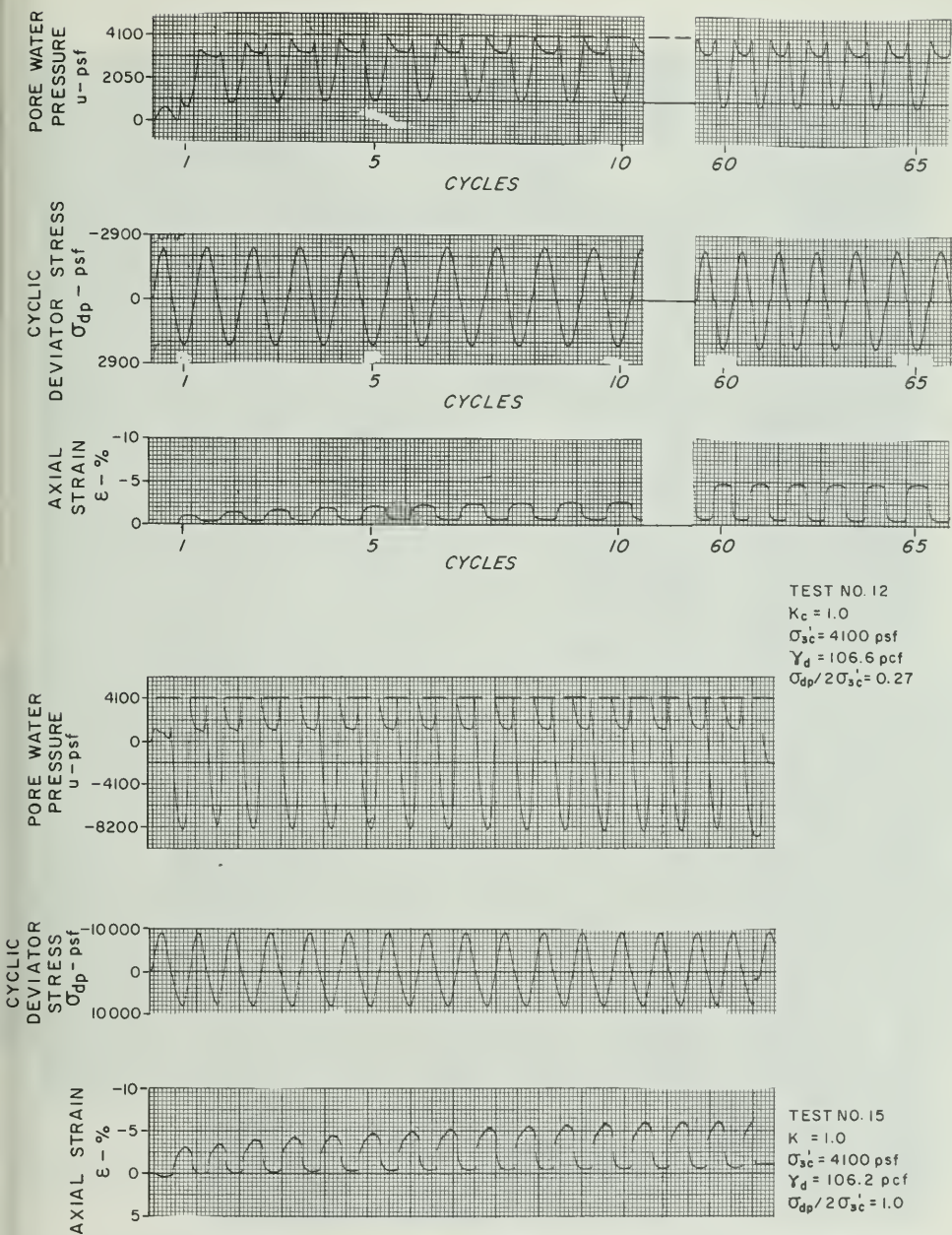
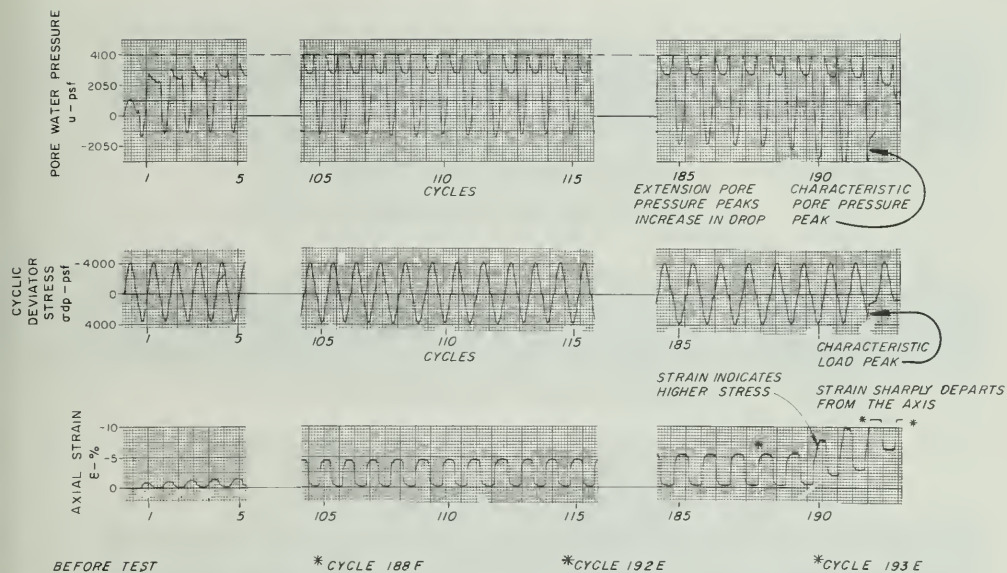


Figure 165. Cyclic Triaxial Test Records for Monterey #10 Sand

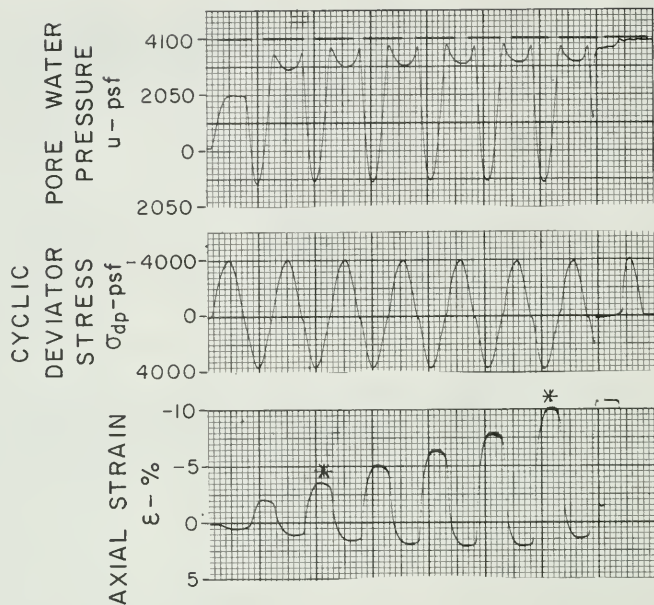


Figure 166. Shear Plane Development during Final Stage of Necking for Monterey "0" Sand



TEST NO. 14 ($\gamma_D = 106.9 \text{ pcf}$, $K_c = 1.0$, $\sigma_{3c}' = 4100 \text{ psf}$)

Figure 167. Cyclic Triaxial Test Records for Monterey "0" Sand



TEST NO. 16
 $\gamma_d = 138.2$ pcf
 $K_c = 1.0$
 $\sigma'_{3c} = 4100$ psf

BEFORE TEST

* CYCLE 2E

* CYCLE 5E

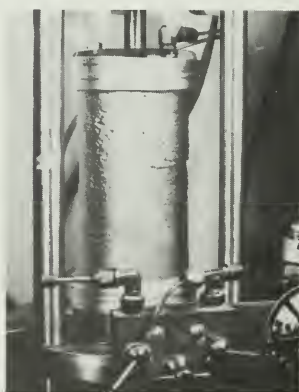
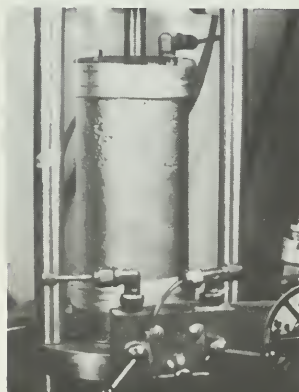
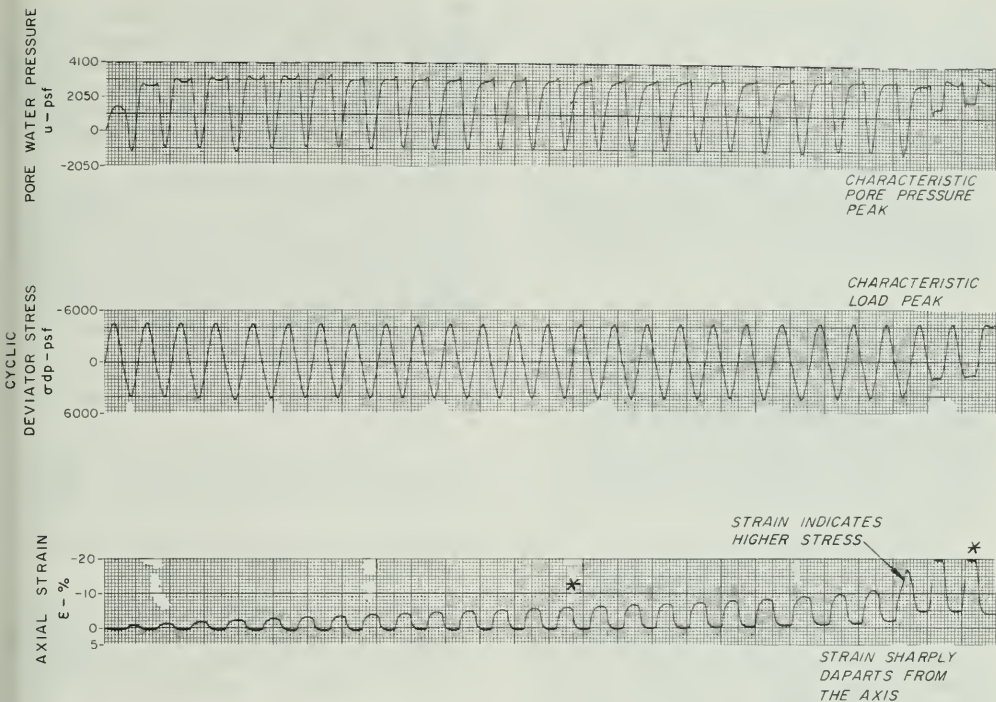


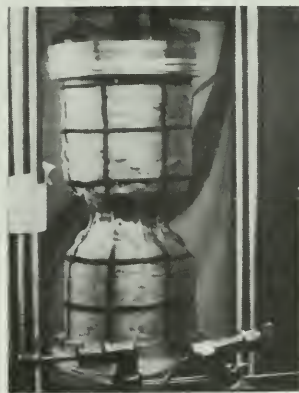
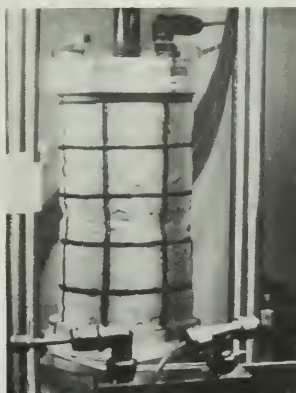
Figure 168. Cyclic Triaxial Test Records for Oroville Sand



BEFORE TEST

* CYCLE 14E

* CYCLE 26E



TEST NO. 25 ($\gamma_D = 142.9 \text{ pcf}$, $K_c = 1.0$, $\sigma_{3c} = 4100 \text{ psf}$)

Figure 169. Cyclic Triaxial Test Records for Oroville Sand

Analysis of Test Results

Extension Strain

The results of the cyclic tests show that predominant extension strain is not unusual for isotropically-consolidated samples of dense, cohesionless material. Visual observations show that this behavior is not a result of necking.

Analysis of cyclic triaxial test records produced by Mulilis et al (1975) and other testing programs reveals that the extension strain is consistently greater than the compression strain. This effect increases with increasing density so that very dense samples strain almost totally in the extension direction.

The asymmetry could possibly be explained by the inherent limitations of the test. The stress conditions do not have the same relative values during the extension and compression halves of the stress cycle. Samples of higher densities require higher cyclic stress ratios to cause significant strain levels. With higher cyclic stress ratios, the stress conditions in the two halves of the stress cycle become more asymmetric. This would explain why the extension strain becomes more pronounced than the compression strain for higher densities. Although the extension direction is weaker than the compression direction, an average of the two strains produced seems to be appropriate because it has been successfully related to cyclic simple shear conditions (see Figures 175 and 176).

Necking Behavior

The cause of necking is theorized to be non-uniformities and stress concentrations with the sample. As cycling continues, the sample strains and will eventually develop a stress concentration until all the axial strain occurs primarily in one location and the sam-

ple necks. As the uniformity of the sample increases, a higher number of cycles is required to cause necking. This would explain why the more uniform Monterey "O" sand samples held together better than the Oroville sand samples.

Necking can sometimes be detected in the test records alone. This is because drastic necking leaves characteristic readings in the pore pressure, strain, and loading measurements. These characteristic readings are illustrated for both materials in Figures 167 through 169 and include:

1. A sharp increase in the extension strain.
2. The strain goes significantly into extension during compression loading.
3. The pore water pressure drop during extension loading increases.
4. Pore water pressure and axial load records develop characteristic shapes during the final stage of necking, when the sample separates.

These necking symptoms develop only during drastic necking. The samples may develop necks of smaller magnitudes without producing these symptoms. Without producing detectable symptoms in the test records, severe necking has been observed in the samples as far back as 12 cycles before complete separation. Symptoms of drastic necking have also been found in some of the test records for the modeled Oroville gravel samples. This leads to the conclusion that some of the modeled Oroville gravel samples developed drastic necking. Examples of the test records where drastic necking has been found are shown in Figures 170 through 172.

Sample "Tension"

Many sand samples were tested well beyond the "tension" boundary of 0.5 cyclic stress ratio, but still behaved like samples tested at lower stress ratios.

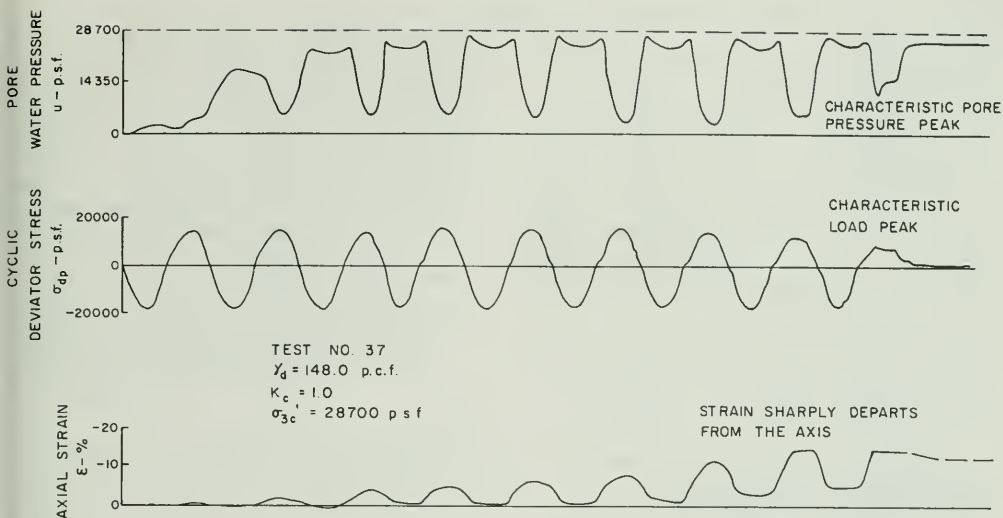


Figure 170. Cyclic Triaxial Test Records for Modeled Oroville Gravel

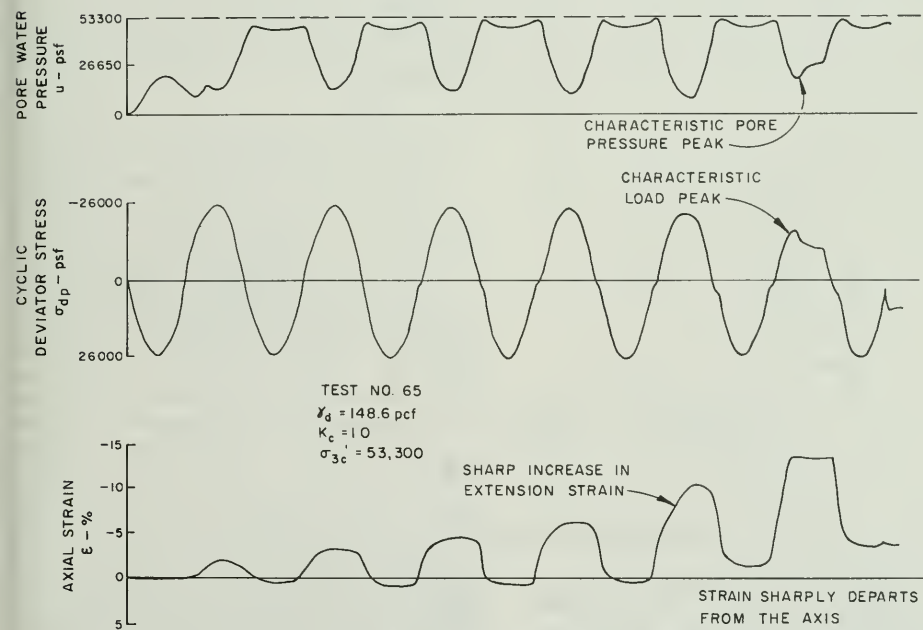


Figure 171. Cyclic Triaxial Test Records for Modeled Oroville Gravel

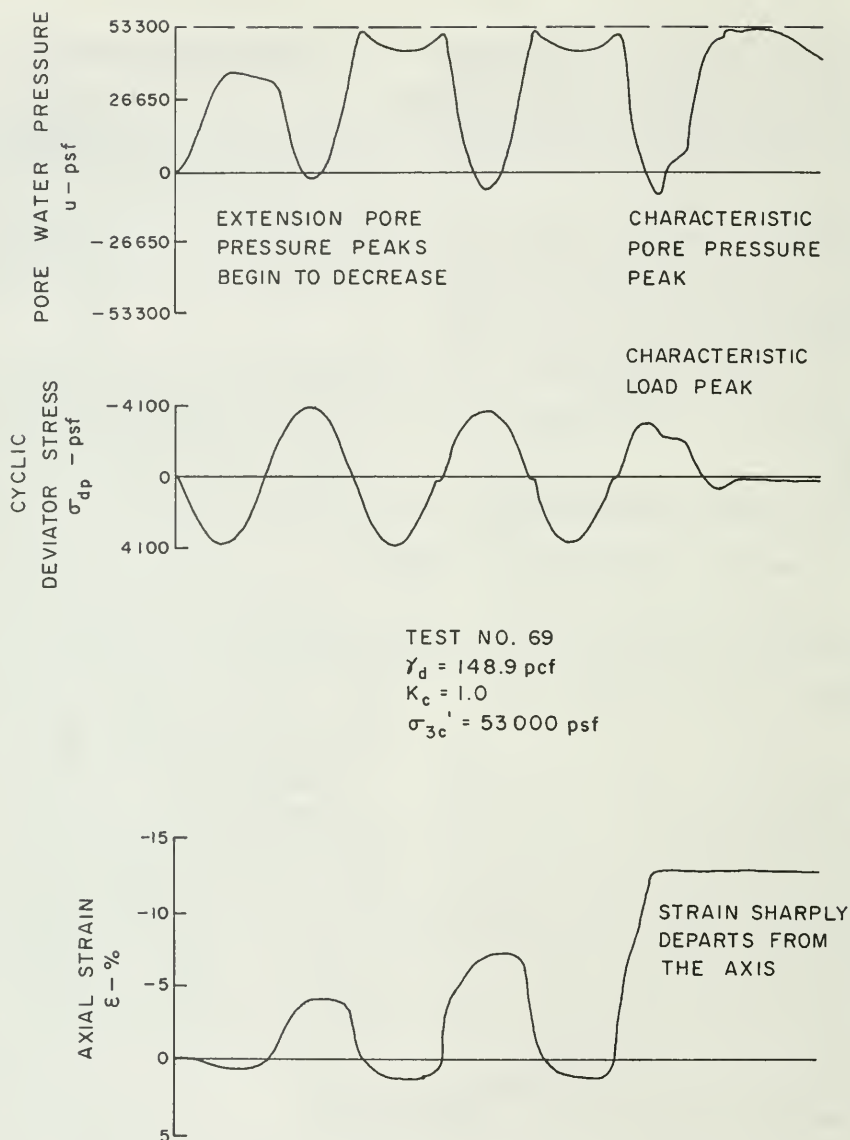


Figure 172. Cyclic Triaxial Test Records for Modeled Oroville Gravel

This is because the designation of a cyclic stress ratio of 0.5 as the boundary for sample "tension" and cap lift-off has little meaning. This definition was probably developed assuming that when the cyclic stress ratio was greater

than 0.5, the extension stress would be greater than the effective confining pressure and the sample cap would have to lift off. This would be a total stress definition. Soil behavior, however, is controlled by effective stresses

The idea of a constant "tension" boundary throughout a cyclic triaxial test is incorrect. During a cyclic triaxial test, the residual pore water pressure at the end of each complete stress cycle tends to increase with each applied cycle. As the residual pore pressure approaches the chamber pressure, the effective confining pressure is reduced. The cyclic load, however, remains constant. Thus, if an isotropically consolidated sample is cycled long enough to approach initial liquefaction, it experiences a "tension" condition regardless of the cyclic stress ratio being applied.

The question that must be addressed is why the sample hold together during "tension" and how does this relate to actual soil behavior during earthquake loading.

First it should be noted that the static extension test produced normal uniform sample behavior up to a stress ratio ($\sigma_{dp}/2\sigma'_{3c}$) of 1.0; and could have gone higher if a higher back-pressure had been used.

In Figures 167 through 172, which show cyclic test results, the pore water pressure develops into a repetitive steady-state pattern after the first few cycles. Examination of the steady-state pore pressure patterns presented reveals that, as the cyclic stress curve crosses the zero axis, the pore pressure approaches the chamber pressure, and the effective confining pressure drops to virtually zero. At this time, the sample begins to strain quite rapidly. As the sample strains, the pore pressure begins to drop and the sample strain begins to level off. Most of the strain develops at relatively low percentages of the applied stress. This behavior is the same for both extension and compression halves of the stress cycle. The main differences between the two halves of the stress cycle during this steady-state pore pressure pattern are in the magnitudes of the pore pressure drop and the amounts of axial

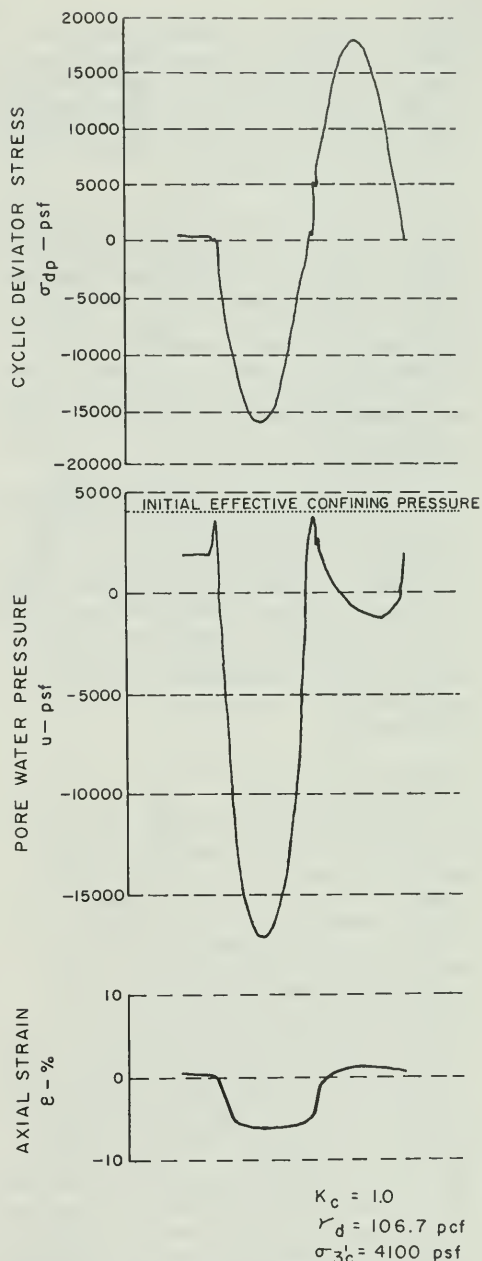


Figure 173. Extension/Compression Cycle for Monterey "0" Sand Cyclic Triaxial Test

strain. For cyclic triaxial tests on dense isotropically consolidated samples, the axial strain is concentrated in the extension direction, and the pore pressure drop in the extension direction is approximately four times the drop in the compression direction.

The pore pressure drop is what holds the sample together. Without the drop in pore pressure, the sample would experience unlimited strain in either direction of loading. The drop in pore pressure has often been explained by the tendency of the sample to dilate. However, the drop in pore pressure during the extension half of the stress cycle could possibly be caused by an erroneous feature of the cyclic triaxial test. If the cap lifted off, the resistance to extension loading would be a result of suction on the water alone and not represent actual sample behavior. Necking might not result; but the test would no longer represent a shearing test. It is very important to note that, if this behavior exists, it exists for every isotropically consolidated cyclic triaxial test that approaches initial liquefaction.

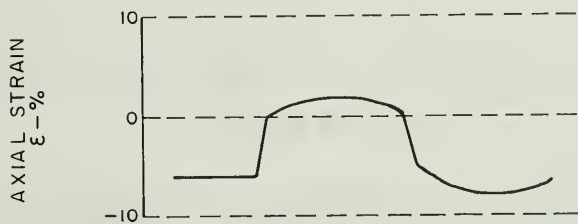
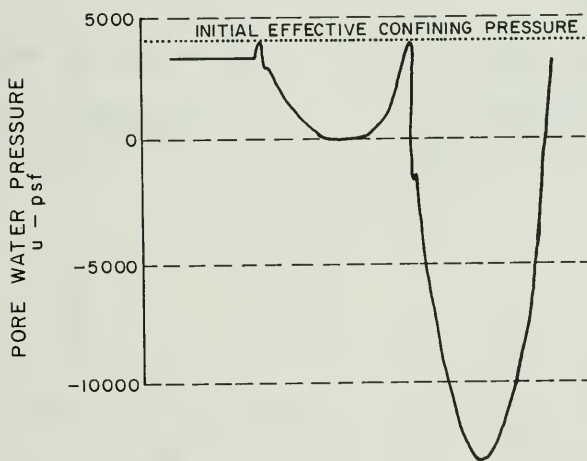
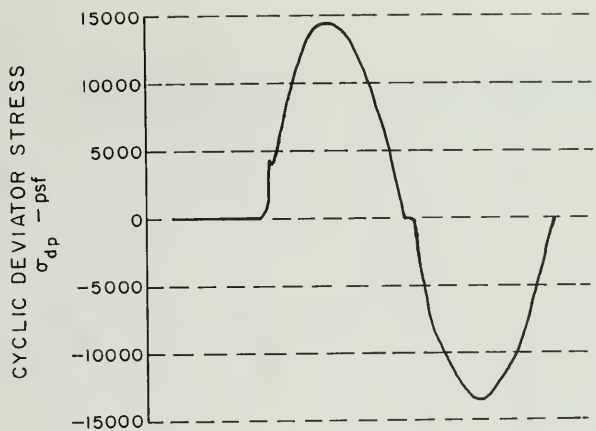
Although the possibility of this erroneous "suction" behavior exists, it is not believed responsible for the behavior of the sample. Instead, it is presumed that the extension half of the stress cycle is actually analogous to lateral compression. This idea is supported by the fact that the extension and compression halves of the stress cycle yield similar patterns of pore pressure change. In Figures 173 and 174 are detailed plots of single stress cycles for two cyclic triaxial tests on isotropically-consolidated samples of dense Monterey "0" sand. One cycle begins with compression and the other begins with extension. It may be seen that a pore pressure rise occurs during the initial loading in either direction. Then, after the sample has experienced axial strain, the pore pressure drops. Although the magnitude of the drops are

different for the extension and compression directions, the general behavior is the same. This same behavior is shown in Figures 159 and 160, which depict static extension and compression test results. Every time axial stress is applied in either direction, in static or cyclic loading, the pore water pressure rises first and then drops with increasing strain.

The cyclic triaxial test behavior can also be related to static test behavior by the development of strain. Results of studies by Mulilis, et al (1975), DeAlba, et al (1975), Seed and Lee (1966), and many others show that cyclic triaxial tests develop higher strains for samples composed of lower densities. Examination of the static test results presented in Figures 159 and 160 reveals that, to produce the same amount of pore pressure drop, samples of lower densities require much more strain.

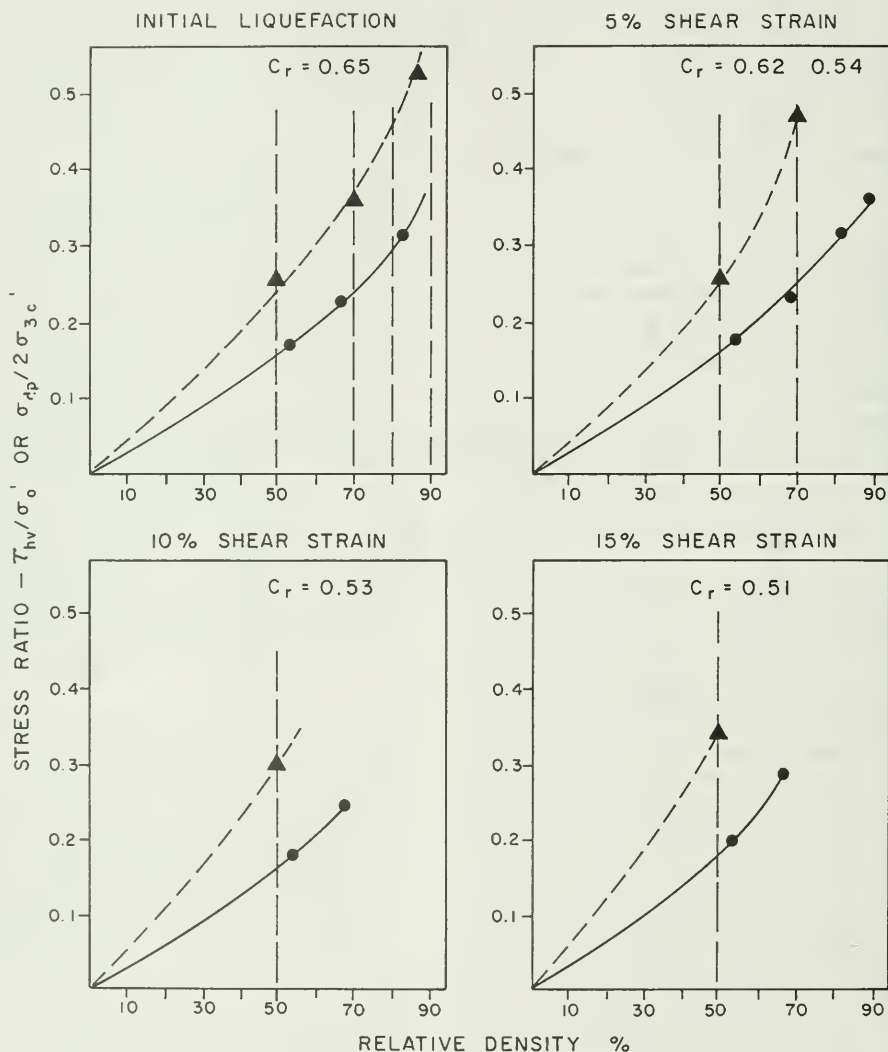
The testing system that has been considered the best measure of the deformation potential of isotropically consolidated samples is the large-scale simple shear (shaking table) device. Comparisons between shaking-table and cyclic triaxial test results carried out for isotropically consolidated samples of Monterey "0" sand are depicted in Figures 175 and 176. The shaking-table results are consistently weaker than the results of the cyclic triaxial test. The ratio of the two strengths ranges between 0.5 and 0.6 for the conditions depicted. This range of cyclic strength ratios is consistent with the theoretical range of 0.55 to 0.70 developed by Seed and Peacock (1970) for the C_r correction needed to account for the difference in stress conditions.

The similar pore pressure tendencies exhibited in both the static and cyclic triaxial tests, the observed effects of sample density on both static and cyclic triaxial sample strains, similarity of sample behavior at cyclic stress ratios ($\sigma_{dp}/2\sigma'_{3c}$) above and below 0.5,



$K_c = 1.0$
 $\gamma_d = 106.2$ pcf
 $\sigma_{3c}' = 4100$ psf

Figure 174. Compression/Extension Cycle for Monterey "0" Sand Cyclic Triaxial Test



NOTES :

▲ = TRIAXIAL TEST ($\sigma_{dp}/2\sigma'_{3c}$) - MULILIS ET AL (1975)

● = SHAKING TABLE TEST (τ_{hv}/σ'_o) - DE ALBA ET AL (1975)

$C_r = (\tau_{hv}/\sigma'_o) / (\sigma_{dp}/2\sigma'_{3c})$

Figure 175. Comparison for Shaking Table and Cyclic Triaxial Test Results for 5 Cycles

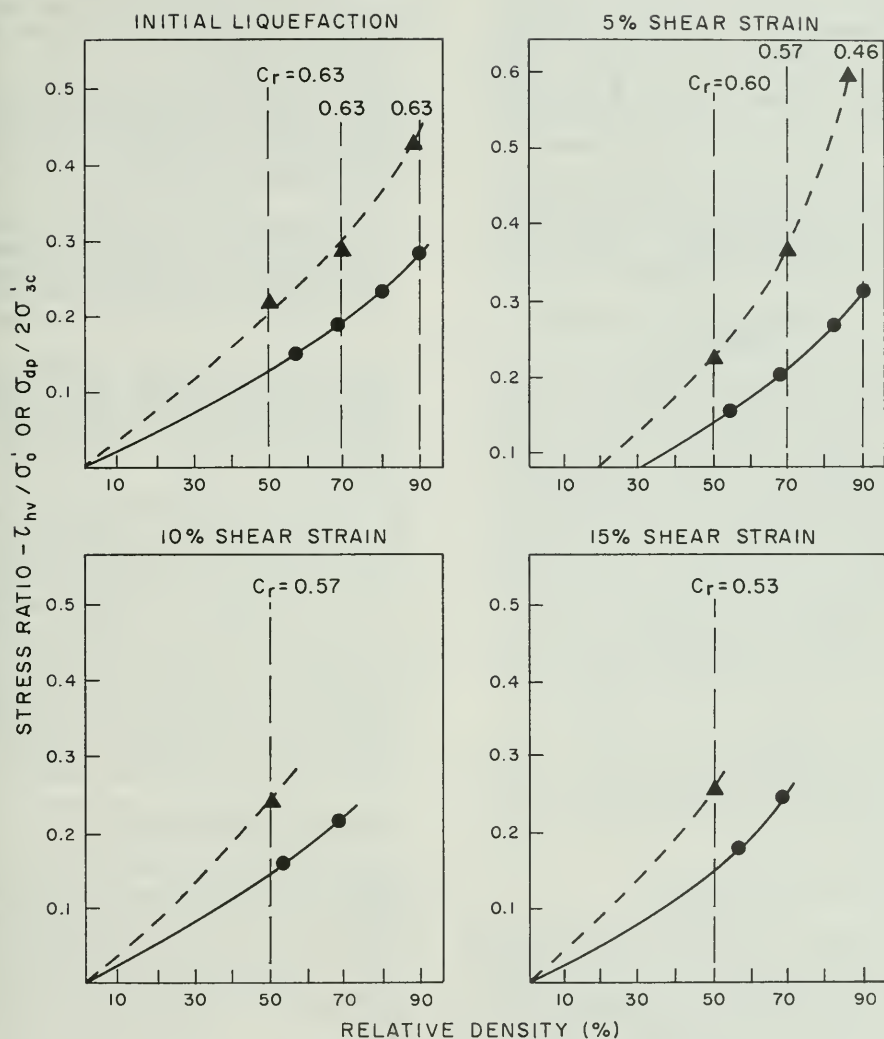


Figure 176. Comparison of Shaking Table and Cycle Triaxial Test Results for 10 Cycles

and the comparisons between the cyclic triaxial test and shaking-table results all indicate that the cyclic triaxial test can be used to estimate the deformation potential of a soil during cyclic loading. In addition, the development of a shear plane during cyclic loading indicates that a shearing behavior is indeed taking place. Since the question of sample "tension" eventually occurs in every sample, it would seem that cyclic stress ratios greater than 0.5 are just as valid as lower stress ratios.

Cyclic Strength Interpretations Considered

Because of the uncertainties generated by the cyclic triaxial tests performed for the modeled Oroville gravel samples, two different strength interpretations were considered. The two interpretations are contrasted by different judgments concerning strain development. Strength interpretation I was based upon the observation that the isotropically consolidated gravel samples did not seem to develop significant strain levels at low confining pressures and that the static strength might be appropriate to use at these consolidation stresses. Strength interpretation II was developed using the results of the laboratory investigation of dense sands to interpret and extrapolate the test results of the modeled Oroville gravel samples.

Strength Interpretation I

The results of the cyclic triaxial tests for the modeled Oroville gravel are summarized in Appendix K. The assumptions used in defining the strain levels, load levels, corrections, and other parameters will be included in the final report on testing (Appendix L), which will be available on request when completed.

The results of these tests were converted into the cyclic strength envelopes shown in Figure 177. The strengths are designated as the shear stress required

to cause a specified strain in six cycles. A C_c correction of 0.6 for tests with $K = 1$, and a ϕ' of 41.5° were used in the C_c conversion.

Static undrained strength results were used to define the cyclic strengths for alpha values of 0 and 0.1 at low consolidation pressures because:

1. The samples that were isotropically consolidated at 196 and 784 kilopascals (41,000 and 16,400 psf) developed only a limited amount of strain -- generally less than ± 5 percent.
2. The critical confining pressure is about 800 kilopascals (about 17,000 psf) based on static triaxial tests done by the U. S. Army Corps of Engineers in 1964.

At consolidation pressures lower than the critical confining pressure, static test samples have very high strength because negative pore pressure develops. The basic assumption of interpretation I is that negative pore pressure will also develop in cyclic tests, and therefore the cyclic strength has to be as high as static strength. This assumption seems to be verified by the limited strains that developed in cyclic tests at low consolidation pressures.

Strength Interpretation II

The assumption for interpretation I is probably valid for liquefaction considerations, i.e., at confining pressures less than critical, a cohesionless material probably will not liquefy if subjected to cyclic stresses lower than the static shear strength. However, liquefaction is not a concern for the Oroville gravels. The cyclic triaxial samples never showed any tendencies to develop sudden unlimited strains. The objective of the cyclic testing was to define strain behavior as related to consolidation stress conditions and cyclic stress levels.

As shown in Figures 159 and 160, positive pore pressure develops at low strain levels in static tests, even for very dense samples and low consolidation pressure. Furthermore, in the shaking table tests reported by DeAlba, positive pore pressures developed and eventually reached the value of the overburden pressure. In both cases, the pore pressure then decreased during further increase in strain. The pore pressure drop is the mechanism which prevents liquefaction. However, the sample can strain to an extent consistent with the effective stresses that develop.

Cyclic triaxial test behavior was complicated by the severe load attenuation and necking problems encountered in the testing program. For example, many of the samples that did not develop large amounts of strain had either significant load attenuation or were not tested to large numbers of cycles. Tests at the higher consolidation pressures that did develop large strains also exhibited symptoms of necking behavior.

If the samples consolidated at the lower consolidation pressures were tested at higher stresses and numbers of cycles, higher cyclic strain levels would have been produced. Based on the tests of dense Monterey "O" sand, cyclic strain would be expected to increase proportionately with an increase in cyclic stress. This would not lead to a sudden jump in shear strength envelope as is the case for interpretation I. Thus, it is probable that the actual cyclic strength values at alphas of 0.0 and 0.1 at the lower confining pressures are not as high as the static strength values presented in Figure 177.

The second strength interpretation was developed from the cyclic triaxial test

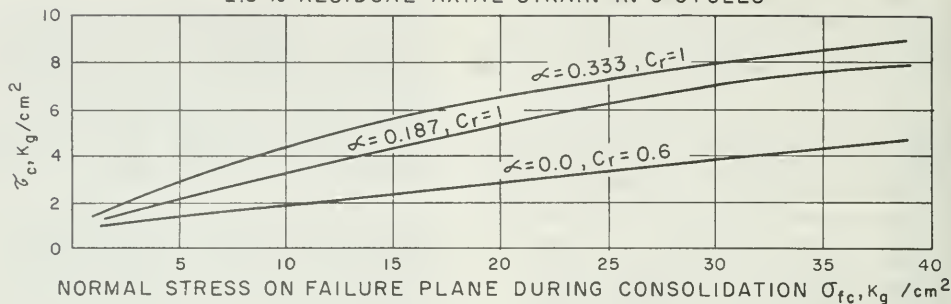
records. It was assumed that the increase in strength due to the calibration error canceled out the reduction in strength due to the membrane corrections. However, the consolidation stress ratios (K_c) were corrected for the calibration change. This assumption was judged to be conservative.

Axial strain was defined as follows: cumulative peak compressive strain for anisotropically consolidated samples; one-half peak to peak strain for isotropically consolidated samples. For tests with load attenuation or necking, strain curves were extrapolated to higher cycles based on the early portions of the tests (prenecking or preattenuation). Typical extrapolations of strain are shown in Figure 178.

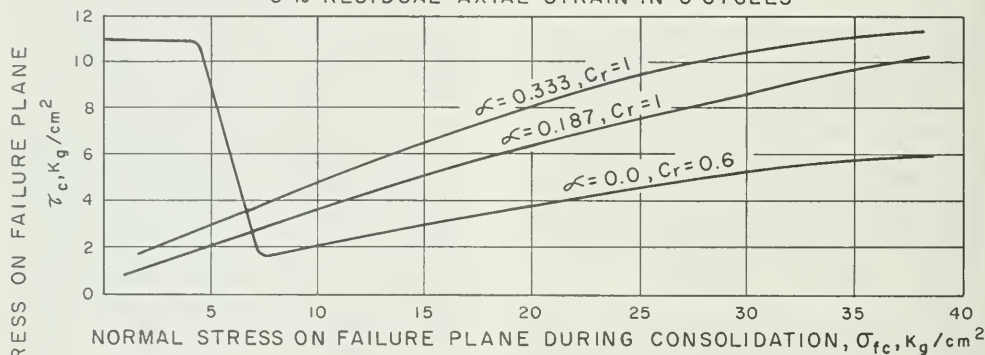
The conservatism shown in the figure was used to account for the severe load attenuation and necking behavior experienced in the isotropically consolidated cyclic tests. The strain extrapolations for the remaining tests are shown in Appendix H. Presented in Appendix I are the cyclic-stress vs. number-of-cycles curves developed for this second strength interpretation.

The resulting cyclic strength envelopes for 5- and 10-percent strain in 10 cycles are shown in Figure 179. The procedures used in developing these cyclic strength envelopes are illustrated in Appendix J. A C_c correction of 0.63 (for $K_c = 1.0$ tests), and a ϕ' of 44° were used in the conversion. It should be noted that this second strength interpretation is judged to be conservative, because cyclic strain envelopes have a tendency to level off as cycling continues. A straight line extrapolation, therefore, can be considered relatively conservative.

2.5 % RESIDUAL AXIAL STRAIN IN 6 CYCLES



5 % RESIDUAL AXIAL STRAIN IN 6 CYCLES



10 % RESIDUAL AXIAL STRAIN IN 6 CYCLES

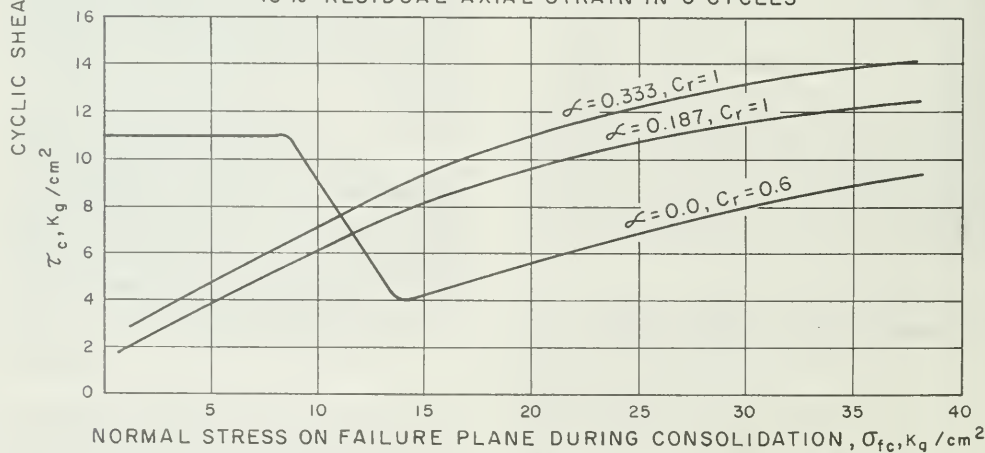


Figure 177. Cyclic Strength Envelopes for Strength Interpretation I - Static and Cyclic Test Results

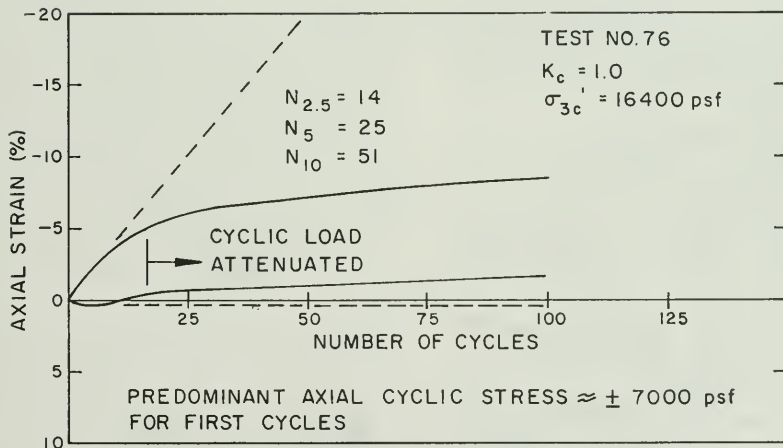
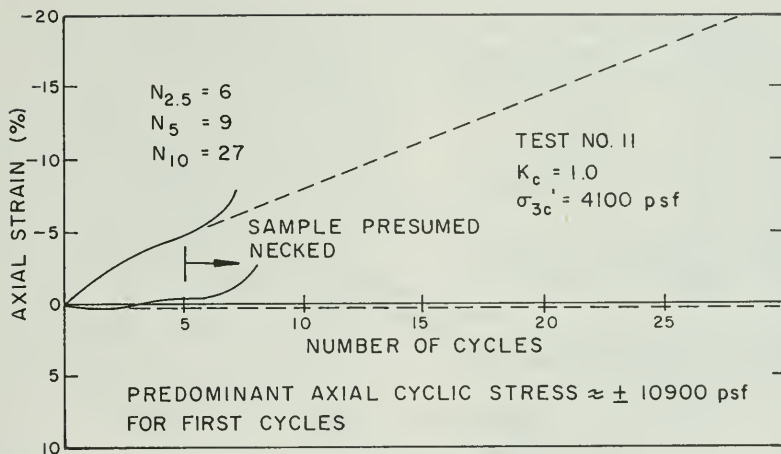


Figure 178. Typical Extrapolations of Isotropically-Consolidated Cyclic Triaxial Tests on Modeled Oroville Gravel

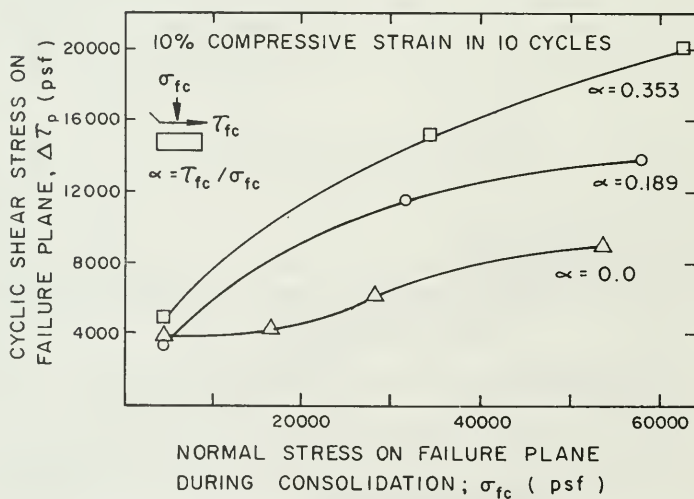
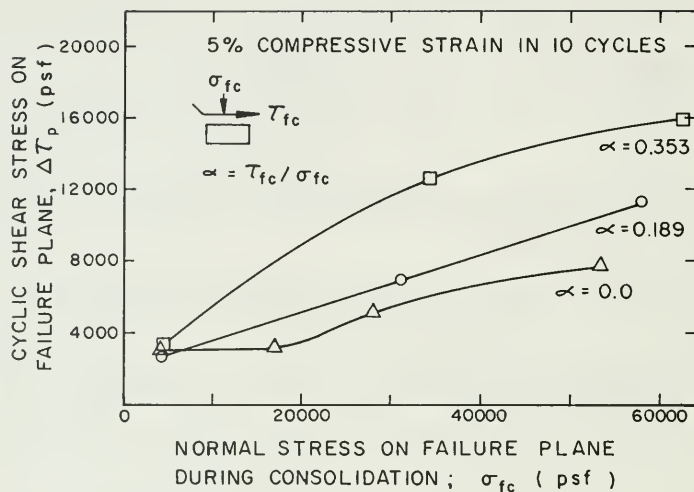


Figure 179. Cyclic Strength Envelopes for Strength Interpretation II - Extrapolated Cyclic Test Results

9. EVALUATION OF PERFORMANCE

General Considerations

So far, this chapter has dealt mostly with the concerted efforts to determine the input properties and conditions for a complete dynamic evaluation of embankment performance during the Reanalysis Earthquake. A fairly wide range of interpretations was possible for dynamic shear modulus and cyclic shear strength. Other properties were found to have only a minor effect on computed stresses. Thus, even though the procedures used are sophisticated -- the current state-of-the-art -- the inability to define all input properties closely limits the confidence level of the results.

This is not meant to imply that the dynamic analysis procedures are inferior to other methods of evaluating seismic performance of dams. It is only meant to emphasize that a fairly wide range of answers will often be found, even with the most diligent efforts to measure or otherwise determine dynamic material properties and other conditions affecting embankment behavior. Generally, other methods of analysis suffer the same limitations as dynamic analysis procedures, plus additional shortcomings of their own. Carefully documented observations of dam performance during strong earthquakes are needed.

Meanwhile, each engineer tries to apply the lessons learned from the few dams shaken by moderately strong earthquakes. Unfortunately, there is not always agreement among dam design engineers on just what the lessons are from a given set of observations. One area of general agreement is that evaluation of seismic stability of dams requires the exercise of sound judgment by engineers experienced in dam design.

Method of Evaluation

The seismic stability analysis of an earth dam involves four major steps:

1. Determine the stresses induced into the soil in the field -- both static and dynamic.
2. Simulate as closely as possible these stresses on samples of similar soil in the laboratory and observe the behavior.
3. Extrapolate back from the laboratory to the field to estimate probable behavior of the actual earth dam.
4. Compare the predicted performance of the dam with established criteria for acceptability.

The static and dynamic stress analyses and the laboratory testing have already been discussed in Sections 4, 7 and 8. The remainder of this section deals with steps 3 and 4.

Two assumptions are needed to relate test sample stresses to field stresses -- that the failure planes are known in both cases, and that the irregular field stress time history can be represented by an equivalent uniform stress time history.

Failure Planes

It is assumed that horizontal planes in field elements should be related to failure planes in test samples. For consolidation conditions, normal and shear stresses must be the same on field horizontal planes and sample failure planes. For cyclic loading conditions, cyclic shear stresses on these planes are compared in order to relate field

behavior to test sample behavior. This comparison is usually in the form of a safety factor or strain potential for each field element. Either form is a measure of the amount of strain that a test sample would develop if subjected to the same stress history as the field element.

For triaxial test samples consolidated anisotropically, the failure plane is assumed to be inclined at an angle of $\phi = 45 + \phi/2$ degrees from the major principal plane. For samples consolidated isotropically, ϕ is assumed to be 45 degrees, and the correction factor C_r is used to account for the inability of the triaxial test to duplicate all the field stresses correctly.

Equivalent Regular Stress Time History

Two procedures have been developed for converting an irregular shear-stress time history to an equivalent regular shear-stress time history (Lee and Chan, 1972, and Seed et al, 1975). Both procedures were derived from essentially the same basic assumption -- that the irregular, and equivalent regular, stress patterns would produce the same accumulated strain. The amount of strain produced by each cycle is related to the stress level of the cycle and assumed to be independent of its location

within the time history. However, studies by Harder (1977) show that computed equivalent regular stresses may vary by as much as 30 percent, depending on the location of the higher peaks within the irregular pattern.

Weighting curves are used to determine the relative contribution of each cycle. The cyclic stress (τ) vs. number of cycles (N) curves from the cyclic tests are used as weighting curves. Each location (element) within the embankment requires a different τ vs. N curve specifically for the consolidation stress conditions of that location, thus requiring many interpolations from the test curves. Also, triaxial test curves have different shapes than do simple shear test curves.

Variations in choice of procedures, weighting curve interpolations, and test method can lead to different results. To remedy this situation, Seed et al (1975), have presented a universal weighting curve based on large-scale shaking-table tests on sand.

This curve, shown in Figure 180, was used in the calculations of equivalent uniform shear-stress time histories. Two different combinations of regular stress level and number of cycles at this level were computed:

	Combination No.	
	1	2
Ratio of regular stress to peak irregular stress	0.65	0.5
Number of regular stress cycles	6	10

Combination No. 2 was used in the performance evaluations.

No attempt was made in this study to account for the location of the larger stress peaks within the time history.

Cases Analyzed and Assumptions

One assumption made at the beginning of this study was that only the submerged upstream shell would be of concern.

The downstream shell is unsaturated and is assumed to have essentially full static drained strength, which is much greater than the cyclic undrained strength of the upstream shell. Equally pertinent, observations of embankment performance in earthquakes, theory, and judgment all lead to the conclusion that a well-compacted, dry rockfill or gravel

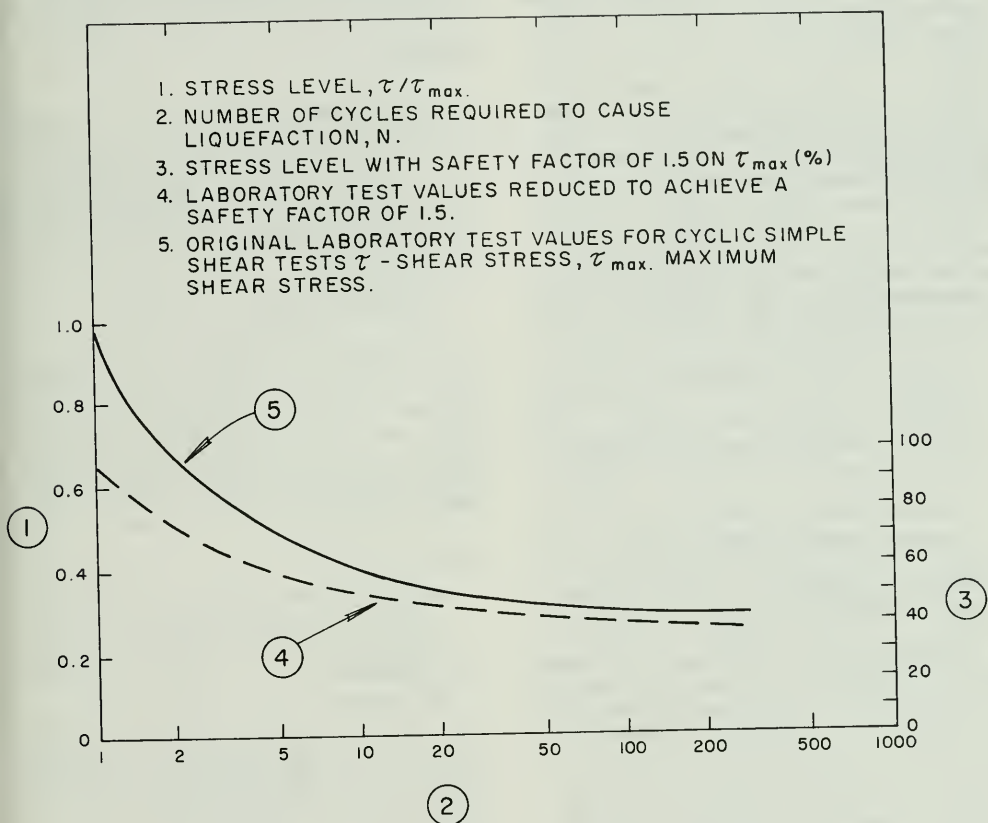


Figure 180. Representative Relationship Between τ/τ_{max} and Number of Cycles Required to Cause Liquefaction (Seed et al, 1975)

embankment will perform well in a strong earthquake.

The core is a well-compacted, clay-gravel material. It should perform as well as compacted clay embankments that have withstood strong earthquake shaking without any detrimental effects (Seed et al, 1978).

Many of the input properties and analysis conditions could vary over a wide range without significantly affecting the predicted behavior. Some, such as material density, are well defined. However, there are four items which can vary over a wide range, which have a major effect on the predicted behavior, and on which there are differences in opinion as to the best defined or most reasonable value:

1. Dynamic shear modulus of shell material.
2. Cyclic shear strength of upstream shell material.
3. Abutment restraint (3D) effects on dynamic shear stresses.
4. Degree of drainage in the upstream shell during earthquake shaking.

The influence of items 1 and 3 on stresses has already been examined in Section 7. On item 2, two different strength interpretations have been discussed in Section 8. Item 4, drainage, has not been discussed previously, but it was observed in Section 3 that in the August 1 earthquake, pore pressure in the upstream transition rose 90 kilopascals (13 psi) and then dissipated during the six second gap in the record.

Strain potentials in the upstream shell were computed for four cases involving different assumptions for these properties and conditions. Other properties and conditions were either well defined or were chosen from the conservative end of the defined range. (Conservative means that the value chosen produces the

highest strain potential of any value in the range.) The rationale for each case is supportable, and to a large degree is a matter of judgment, or of philosophy in dealing with level of risk. Strain potential contours for all four cases are shown in Appendix M.

Case a

Shell $K_{2max} = 165$

Strength Interpretation II (lower), but with consideration of effect of conservatism in data extrapolations and of possible strengthening effect of seismic history.

Abutment restraint (3D) effects included.

Drainage effects considered qualitatively.

In the authors' judgment, these values and conditions are the most supportable choices based on considerations of the data and evidence developed in this study, and many other studies over the last few years. Case a is called the "best judgment case."

Case b

Shell $K_{2max} = 205$

Strength Interpretation II (lower)
Abutment restraint (3D) effects NOT included
NO drainage

Each of these choices is at the end of the defined range which produces the higher estimated displacement. Case b is called the "conservative case."

Case c

Shell $K_{2max} = 205$

Strength Interpretation I (higher)
Abutment restraint (3D) effects NOT included
NO drainage

The choices for the first two items represent the viewpoint of some of the many engineers who contributed to this study. For the last two items, the

usual conservative assumptions were used.

Case d

Shell $K_{2max} = 130$
Strength Interpretation II (lower)
Abutment restraint (3D) effects NOT
included
NO drainage

For the last two items the usual conservative assumptions were used. The first two items are from cyclic triaxial tests of 30-centimetre (12-inch) remolded samples. Several studies have shown that dynamic strength and shear modulus are higher in situ than in remolded samples. The assumption is that the strength and modulus from the tests, although both too low, give about the same strain potentials as the correct in situ strength and modulus would give.

Comparison of Cases

Cases c and d result in slightly higher strain potentials than case a; case b strain potentials are substantially higher than any of the other three. Therefore only cases a and b will be considered further in assessing behavior of the dam.

Predicted Behavior - Best Judgment Case

The best judgment choices of input values and conditions have already been described. The reasoning for these choices is presented here.

The predicted behavior is the assessment of permanent displacements that the re-analysis earthquake would cause in the upstream shell.

Shell K_{2max}

Two extrapolations were made to extend the natural period ratio curve to L/H of 7. The more consistent one gives a period ratio of 1.35 (Figure 125). The corresponding 2D period is 1.1 seconds, and range of K_{2max} is 135 to 165 (Figure 128).

Cyclic Shear Strength

There is probably some conservatism in the use of remolded samples to represent the behavior of in-place materials -- even though the two-month aging tests did not indicate a gain in strength. For example, the recent past seismic history probably strengthened the gravel shell material against possible future earthquakes.

Also, there is some conservatism in the extrapolation of the cyclic strain envelopes for Strength Interpretation II.

Three-Dimensional Effect

Both Makdisi's work and analyses of this study indicate that lower shear stresses will develop for three-dimensional conditions than for two-dimensional conditions -- particularly in the area of higher strain potentials in the upper part of the shell. Makdisi's results for a narrower canyon (L/H = 3) than Oroville give 0 to 75 percent lower stresses. Estimates by this study for the actual Oroville Canyon (L/H = 7) give about 20 percent lower stresses. The San Fernando Dams should have had a much smaller or negligible 3D effect because the L/H were 12 and 13. Therefore, it is assumed that the 3D effect is not "built in" to the procedure which was developed and tested against the observed earthquake performance of the San Fernando Dams.

Drainage

All the strength evaluations are based on the assumption of completely undrained conditions in the upstream shell. However, drainage does take place as indicated by the rapid dissipation of the pore pressure developed in the August 1, 1975 earthquake. At cell No. 1, a cyclic pore pressure of 90 kilopascals (13 psi) developed early and dissipated during the six-second gap in the records. This cell is located in the upstream transition zone near the core, and indicates that the gravel shell

and transition do experience some degree of drainage during earthquake shaking, even in interior locations. Drainage relief of pore pressures presumably would be greater at locations closer to the surface of the slope, where the strain potentials tend to be higher.

Predicted Behavior

Stresses were calculated for a shell $K_{2\text{max}}$ of 165 corresponding to the 1.1

PSEUDO THREE DIMENSIONAL ANALYSIS

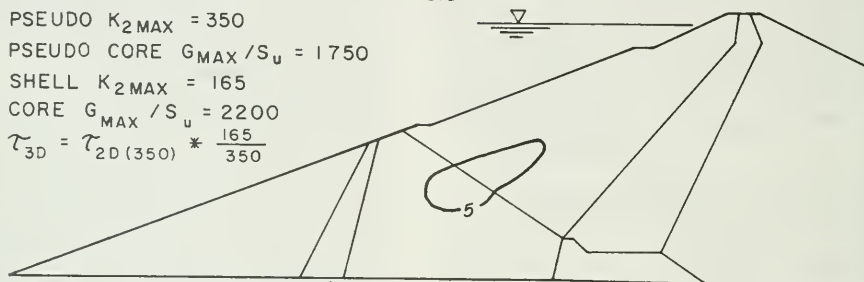
PSEUDO $K_{2\text{MAX}} = 350$

PSEUDO CORE $G_{\text{MAX}} / S_u = 1750$

SHELL $K_{2\text{MAX}} = 165$

CORE $G_{\text{MAX}} / S_u = 2200$

$$\tau_{3D} = \tau_{2D(350)} * \frac{165}{350}$$



PREDICTED FOR BEST JUDGMENT CASE

NOTES :

REANALYSIS EARTHQUAKE

COMPUTER PROGRAM LUSH

CYCLIC STRENGTH INTERPRETATION II - EXTRAPOLATED CYCLIC TRIAXIAL TEST RESULTS

UNDRAINED CONDITIONS

Figure 181. Computed Compressive Strain Potentials in Upstream Shell - Percent

Calculations were not made for the effect of higher strength or drainage because information is not complete enough to quantify these factors. However, the strain potentials would be even lower, and could be described as less than 5 percent everywhere in the upstream shell.

An interesting question here is what displacements would result from the method of calculation used at Upper San Fernando Dam. If average compressive strain is assumed to be 2 percent, then average shear strain is only 3 percent, and a 91-metre (300-feet) high section would produce a surface displacement

second natural period, and for the three dimensional effect (abutment restraint). As shown in Figure 181, the resulting compressive strain potentials are less than 5 percent except for a small zone in the middle of the upstream shell. This would generally be regarded by dam design engineers as indicating acceptable behavior involving only minor displacements.

of 2.7 metres (9 feet), which is not what most engineers would think of as minor displacement.

It may well be that the method of calculating displacement applies to cases with high strain potentials and liquefaction, as at Upper San Fernando Dam, but does not apply to cases with low strain potentials and no liquefaction. It may also be that dams of great height would experience substantial displacements corresponding to low strain levels, and that not enough experience is available with earthquake performance to realize it. It is likely a little of both.

From all the considerations discussed, it is concluded that compressive strain potentials will be small -- less than 5 percent -- and that no slides or "large" movements will develop. It is not so clear just how "large" might be the displacements associated with the predicted strain potentials. Because of the great height of the dam, it is considered conceivable that permanent displacements on the order of a metre could develop at the surface of the upstream slope as a result of the small shear strains within the upstream shell.

Estimated Displacements for Conservative Assumptions

The predicted behavior for the best judgment case is considered conservative in many respects, and the possibility of greater displacements is considered remote. Nevertheless, it is worthwhile to check this remote possibility to see how bad the situation would be if soil properties and conditions proved to be more adverse than the best judgment choices. The four pertinent input values and conditions for the conservative case were:

Shell $K_{2max} = 205$
 Strength Interpretation II (lower)
 Abutment restraint (3D) effects
 NOT included
 No drainage

The strain potential pattern and the method of estimating displacements are included in Appendix M. The extreme of deformations of the upstream slope might be as follows:

- horizontal displacement of the surface by a few tens of feet in the interval between the two berms.
- slumping of the shell material near the upper berm.
- bulging of the shell material near the lower berm.

The displacement and slumping would be limited to the upstream shell material. Slumping would not be expected to extend upslope to the crest (judgment based on extent of slumping at Lower San Fernando Dam). The compacted gravel in the upstream shell would be as strong and perform as well after deformation as before.

Based on the behavior of triaxial test samples, there is no concern over sudden massive shear slides or liquefaction flow slides. Movement would occur only in short-duration increments and only during the highest peaks of earthquake acceleration, the several increments accumulating to a total of perhaps 10 metres.

Remember that this is the most extreme case that could be supported by the results of the analysis -- by adopting simultaneously the most conservative values for material properties and other input conditions. Although these postulated movements are uncomfortably large, they would not threaten the safety of the dam.

REFERENCES

- Becker, E., Chan, C. K. and Seed, H. B. "Strength and Deformation Characteristics of Rockfill Materials in Plane Strain and Triaxial Compression Tests". Report No. TE 72-3 to State of California, Department of Water Resources. 1972
- Bolt, Bruce A. "Duration of Strong Ground Motion". Proceedings - Fifth World Conference on Earthquake Engineering. Rome, 1974.
- DeAlba, P., Chan, C. K. and Seed, H. B. "Determination of Soil Liquefaction Characteristics by Large-Scale Laboratory Tests". Report No. EERC 75-14. University of California, Berkeley. 1975
- Harder, Leslie F., Jr. "Liquefaction of Sand Under Irregular Loading Conditions". Thesis, submitted in partial satisfaction of requirements for the Degree of Master of Science in Engineering, Graduate Division, University of California, Davis. 1977.
- Idriss, I. M., Lysmer, J., Hwang, R. and Seed, H. B. "A Computer Program for Evaluating the Seismic Response of Soil Structures by Variable Damping Finite Element Procedures". Report No. EERC 73-16. University of California, Berkeley. 1973.
- Kulhawy, F. H. and Duncan, J. M. "Nonlinear Finite Element Analysis of Stresses and Movements in Oroville Dam". Report No. TE 70-2 to State of California, Department of Water Resources. 1970.
- Lee, Kenneth L. and Kwok Chan. "Number of Equivalent Significant Cycles in Strong Motion Earthquakes". Proceedings, Conference on Microzonation for Safer Construction, Seattle. November 1970.
- Lowe, J. "Shear Strength of Coarse Embankment Dam Materials". Proceedings, 8th Congress on Large Dams, pp. 745-761. 1964.
- Lysmer, J., Udaka, T., Seed, H. B. and Hwang, R. "LUSH - A Computer Program for Complex Response Analysis of Soil-Structure Systems". Report No. EERC 74-4. University of California, Berkeley. 1974.
- Makdisi, F. I. "Performance and Analysis of Earth Dams During Strong Earthquakes". Dissertation, submitted in partial satisfaction of the requirements for the Degree of Doctor of Philosophy in Engineering, Graduate Division, University of California, Berkeley. 1976.
- Marachi, N. D., Chan, C. K., Seed, H. B. and Duncan, J. M., "Strength and Deformation Characteristics of Rockfill Materials". Report No. TE 69-5 to State of California Department of Water Resources. 1969.
- Mulilis, J. D., Chan, C. K. and Seed, H. B. "The Effects of Method of Sample Preparation on the Cyclic Stress-Strain Behavior of Sands". Report No. EERC 75-18. University of California, Berkeley, 1975.

REFERENCES (Continued)

- Nobari, E. S. and Duncan, J. M. "Effect of Reservoir Filling on Stresses and Movements in Earth and Rockfill Dams". Report No. TE-72-1. University of California, Berkeley. 1972.
- Schnabel, Per B. and Seed, H. Bolton. "Accelerations in Rock for Earthquakes in the Western United States". Bulletin, Seismological Society of America. Volume 63. 1973.
- Seed, H. Bolton. "Evaluation of Soil Liquefaction Effects on Level Ground During Earthquakes". State-of-the-art paper presented at Symposium on Soil Liquefaction, ASCE National Convention, Philadelphia. October 2, 1976.
- Seed, H. Bolton and Idriss, I. M. "Soil Moduli and Damping Factors for Dynamic Response Analysis". Report No. EERC 70-10. University of California, Berkeley. 1970.
- Seed, H. Bolton, Idriss, I. M. and Kiefer, Fred W. "Characteristics of Rock Motions During Earthquakes". Journal, SMFE. September 1969.
- Seed, H. B., Idriss, I. M., Makdisi, F. and Banerjee, H. "Representation of Irregular Stress Time Histories by Equivalent Uniform Stress Series in Liquefaction Analyses". Report No. EERC 75-29. University of California, Berkeley. 1975.
- Seed, H. Bolton and Lee, Kenneth L. "Liquefaction of Saturated Sands During Cyclic Loading". Journal of the Soil Mechanics and Foundations Division, ASCE. Vol. 92, No. SM6, Proc. Paper 4972, pp. 105-134. November 1966.
- Seed, H. B., Lee, K. L., Idriss, I. M. and Makdisi, F. "Analysis of the Slides in the San Fernando Dams During the Earthquake of February 9, 1971". Report No. EERC 73-2. University of California, Berkeley. 1973.
- Seed, H. Bolton, Makdisi, Faiz, I., and DeAlba, Pedro "Performance of Earth Dams During Earthquakes". Journal of the Geotechnical Engineering Division, ASCE. Volume 104, No. GT7, Proc. Paper 13870, pp. 967-994. July 1978.
- Seed, H. Bolton and Peacock, W. H. "Applicability of Laboratory Test Procedures for Measuring Soil Liquefaction Characteristics Under Cyclic Loading". Report No. EERC 70-8. University of California, Berkeley. 1970.
- U. S. Bureau of Reclamation. "Dynamic Analysis of Embankment Dams". For Submission to the International Commission on Large Dams for Publications as a State-of-the Art Paper. 1976.
- Vrymoed, John, et al. "Dynamic Analysis of Oroville Dam". Final Draft of Office Report, Department of Water Resources, Division of Safety of Dams. June 1978.
- Wong, R. T. "Deformation Characteristics of Gravels and Gravelly Soils Under Cyclic Loading Conditions". Dissertation, submitted in partial satisfaction of the requirements for the Degree of Doctor of Philosophy in Engineering, Graduate Division, University of California, Berkeley. 1973.

CHAPTER VI
SEISMIC ANALYSIS OF THE OROVILLE
DAM FLOOD CONTROL OUTLET STRUCTURE

Commentary

As a result of the August 1, 1975 Oroville earthquake, of magnitude 5.7, the Department found it appropriate to reanalyze the Oroville Dam Flood Control Outlet structure (Figures 182 and 183) using a stronger earthquake (magnitude 6.5) and the latest techniques in seismic investigation.

A seismic study, monitored by the Department, was conducted under a consulting agreement between Dr. Edward L. Wilson and the Department of Water Resources. The results were presented in the report, "Earthquake Analysis of the Oroville Dam Flood Control Outlet Structure", by Edward L. Wilson, Frederick E. Peterson, and Ashraf Habibullah. Their report is included as the final part of this chapter.

The finite-element method and dynamic techniques were utilized in this study to perform a linearly elastic three-dimensional analysis of the reinforced-concrete structure. The three-dimensional analysis was chosen because of the complexity of the structure. In this analysis, dead and hydrostatic loads were applied to the same finite-element model; the interaction of the reservoir was not included due to limitations of the present state of the art. However, to include the full participation of the reservoir, a finite-element two-dimensional analysis with hydrodynamic interaction was also performed. This resulted in stresses approximately 20 percent higher.

The modified Pacoima and Taft, 6.5 magnitude earthquake accelerogram (see

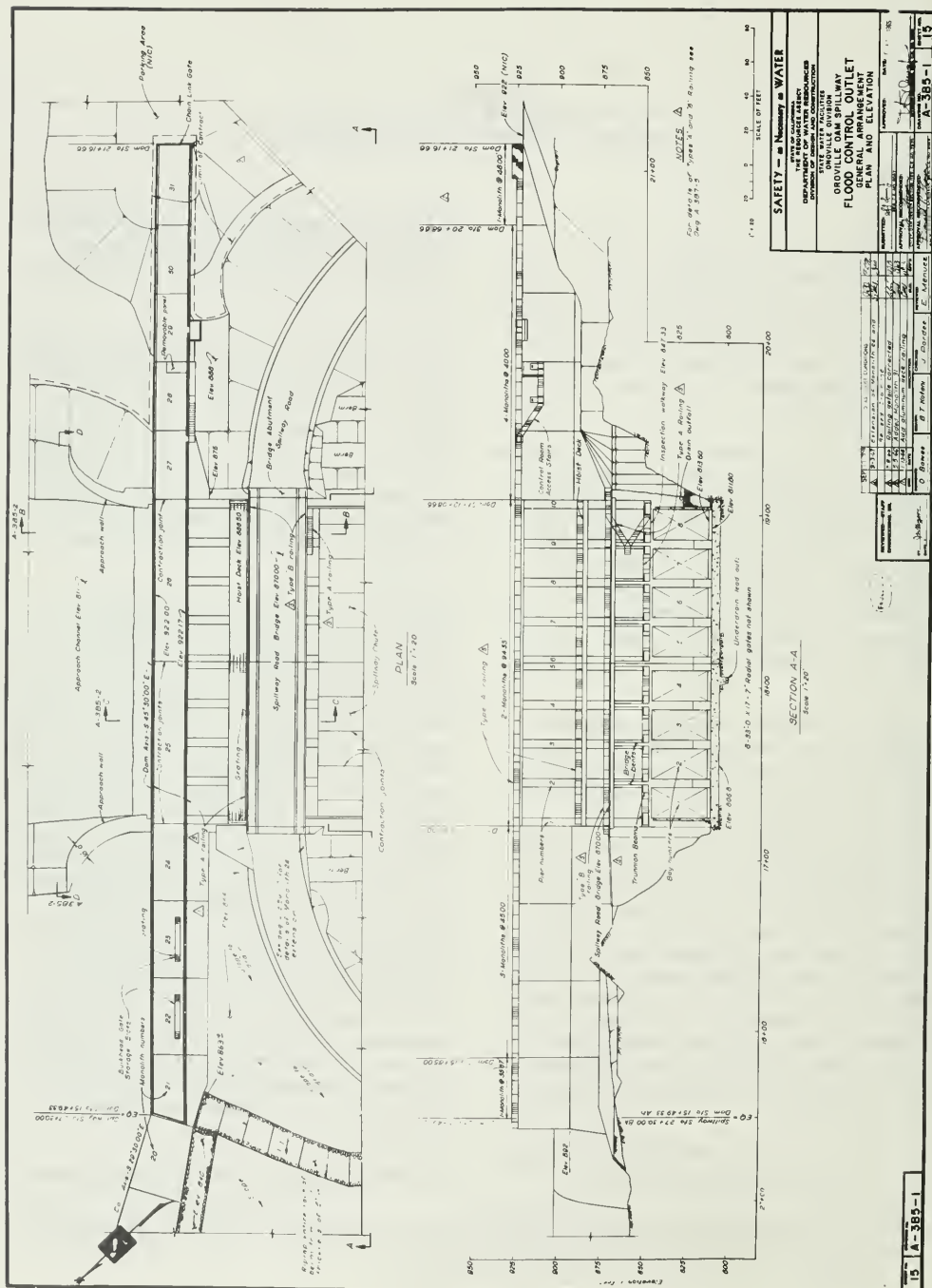
Chapter V), was used in these analyses. Horizontal acceleration of the ground was applied parallel to the outlet centerline. This produced the largest stresses in the piers.

The effects of a horizontal acceleration in the transverse direction were examined by the Department. For this case the piers were assumed fixed at the breast wall and bottom slab. Displacement of the supports equal to the width of two contraction joints was assumed. Stresses produced were below allowable working stresses and therefore no further investigation for this case was necessary.

Maximum stresses from Dr. Edward L. Wilson's report were utilized by the Department to perform a reinforced-concrete-theory analysis of the structure, which resulted in the tensile stresses shown in Figures 184 through 186. These are peak instantaneous stresses with the occurrence time shown at the bottom of each figure. The largest concrete tensile stress of any concern is 2172 kPa (315 psi). It was obtained in an area of the piers where the reinforcing steel available is almost negligible (Figure 185, Elevation 850, Station 12+68). However, experimental research and prototype observation have shown^{1/} that the dynamic tensile strength of mass concrete is at least 10 percent of its static compressive strength or, in this instance, 3792 kPa (550 psi); therefore, the peak stress of 2172 kPa (315 psi) at the downstream end of the piers is well within the tensile strength of the concrete.

Maximum concrete tensile-stress values

^{1/} Refer to text and references of Chapter VII ("Earthquake Response Analysis of Thermalito Diversion Dam" by Anil K. Chopra).



values shown in Figure 184 are not considered critical, because the reinforcing steel available in that area is capable of resisting the total earthquake tensile force without any contribution from the surrounding concrete (see Figure 186).

Although piers 1 and 10 were not investigated numerically by the Department, they are not expected to develop critical stresses because they carry half as much load as do the adjacent piers, and a significant portion of their height is in direct contact with the rock abutment.

The Department also investigated the structure for stability against sliding through the shear-friction equation

$$Q = \frac{CA + N \tan \phi}{H} \quad \text{The use of a}$$

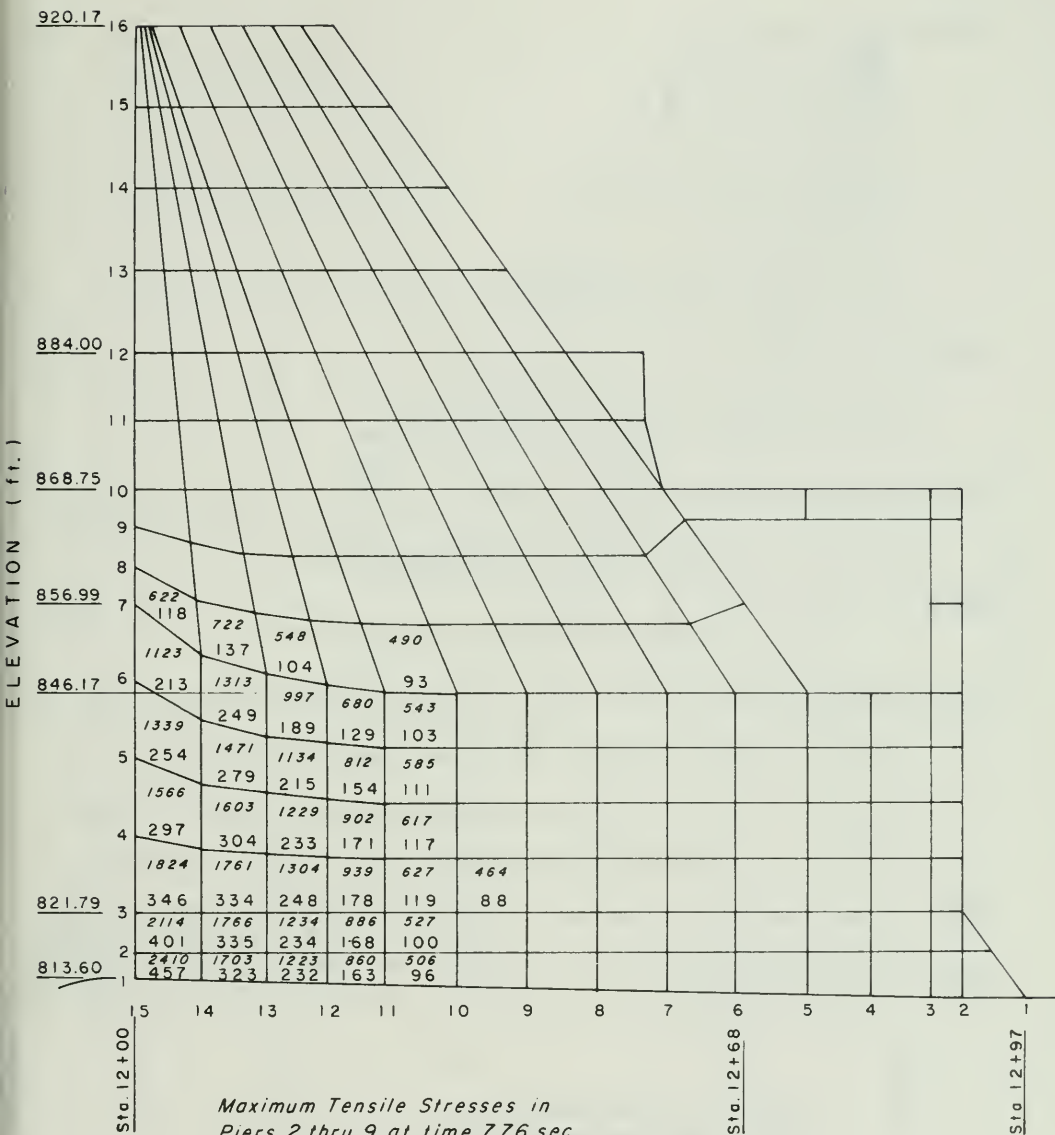
cohesion value of 3447 kPa (500 psi) produced a shear-friction factor of 11.6, which is ample against sliding.

Conclusion

The investigations performed indicate that when the Oroville Flood Control Outlet Structure is subjected to the Reanalysis Earthquake ground motion, it is stable, and that expected compressive and tensile stresses are within the allowable limits established for the structure.

Introduction to Figures 184 through 186

1. Smaller tensile stresses and compressive stresses were intentionally left out due to their uncritical magnitudes.
2. Although stresses in piers 5 and 6 are somewhat different from those in piers 2, 3, 4, 7, 8 and 9, the small variation did not justify showing them independently.
3. Figures 184 through 186 show the elevation of a pier with an element mesh layout. Actual stresses are tabulated inside the elements.



Maximum Tensile Stresses in
Piers 2 thru 9 at time 7.76 sec.
Top: Reinforcing Steel Stress (psi)
Bot: Concrete Stress (psi)

Figure 184. Maximum Tensile Stresses at Time 7.76 Seconds

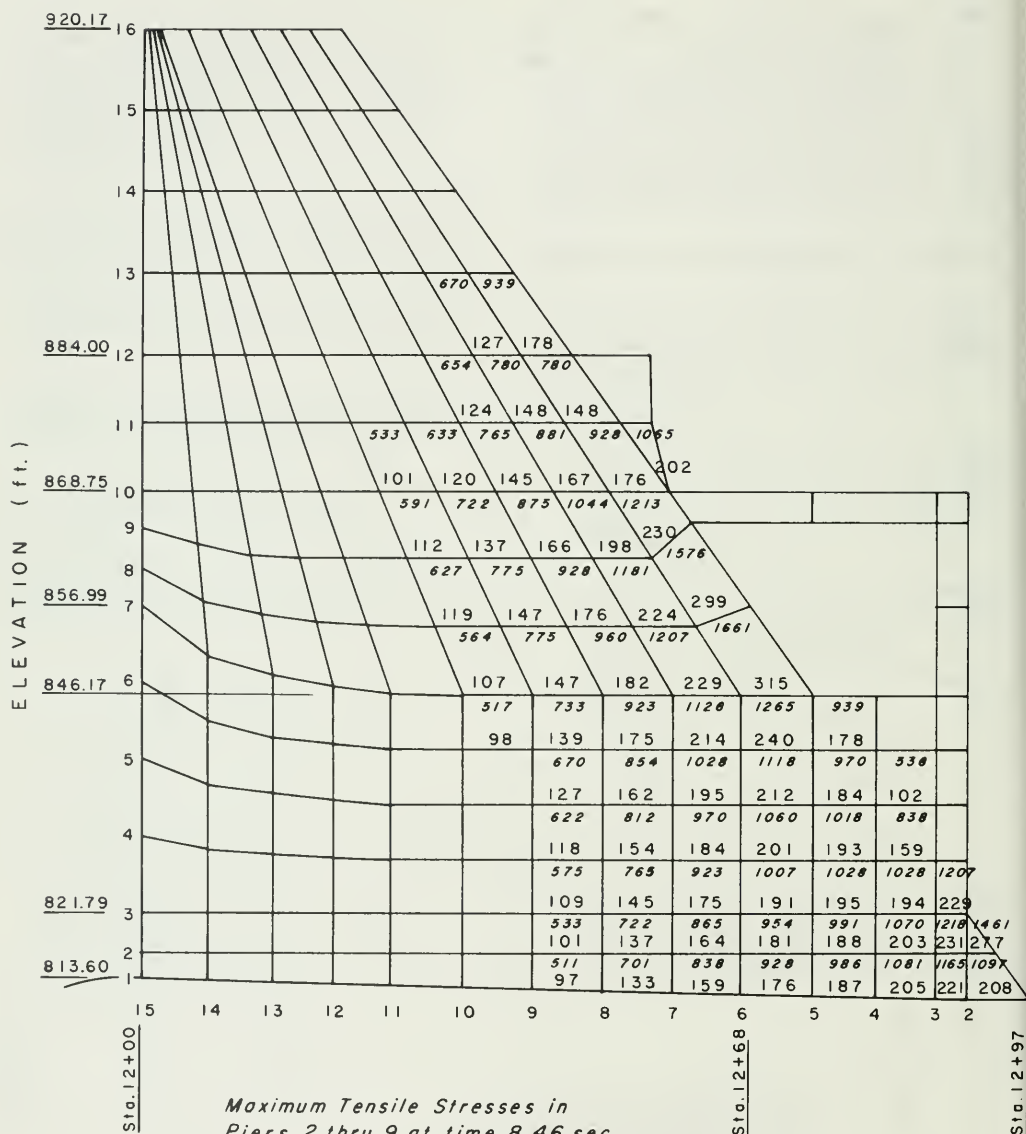
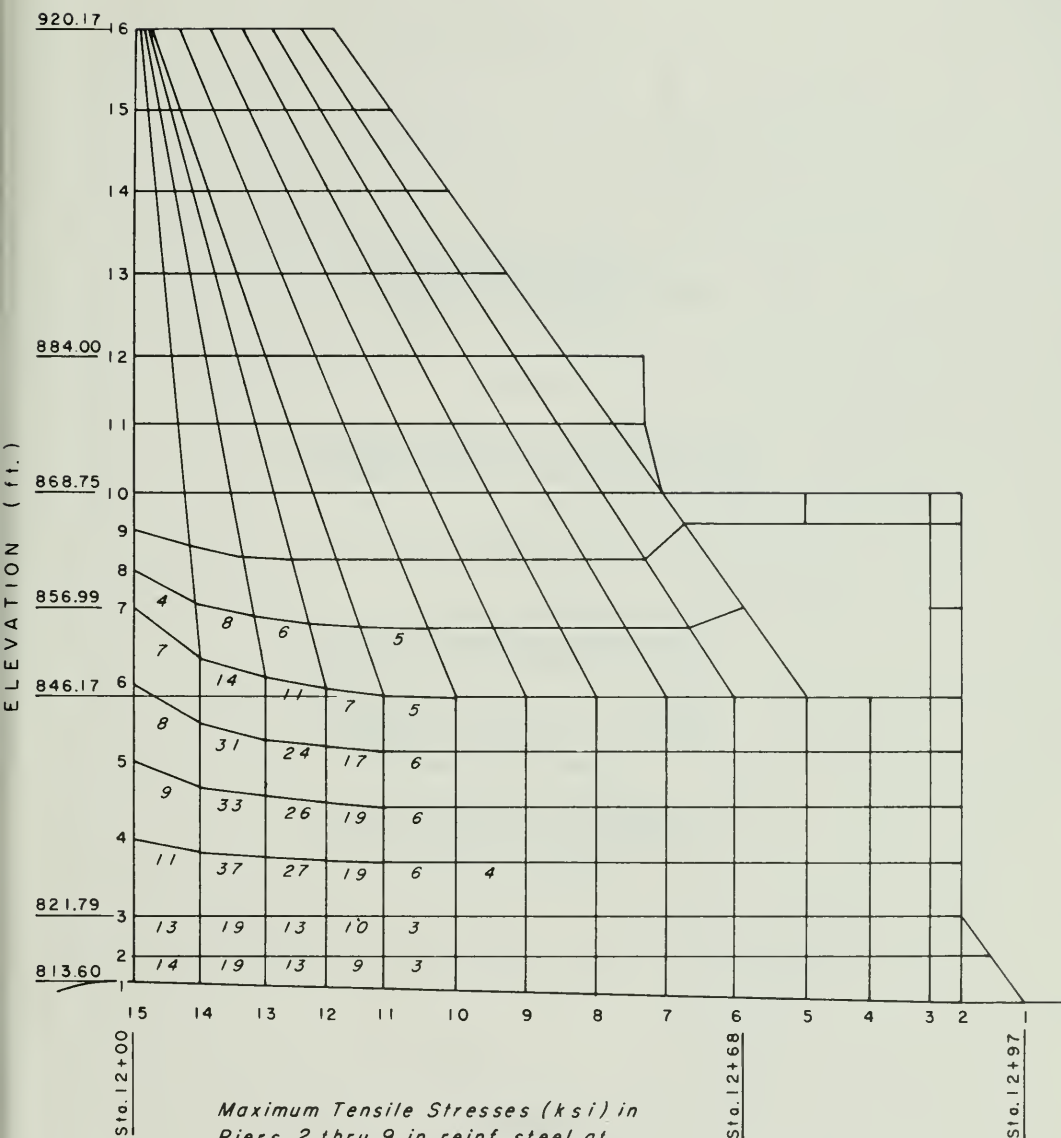


Figure 185. Maximum Tensile Stresses at Time 8.46 Seconds



Maximum Tensile Stresses (ksi) in
Piers 2 thru 9 in reinf. steel at
time 7.76 secs. disregarding
contribution from concrete

Figure 186. Maximum Tensile Stresses at Time 7.76 Seconds in Steel

A REPORT TO THE
DEPARTMENT OF WATER RESOURCES
STATE OF CALIFORNIA

on the

Earthquake Analysis of the Oroville Dam
Flood Control Outlet Structure

by

Edward L. Wilson
Professor of Civil Engineering
University of California, Berkeley

Frederick E. Peterson, President
Engineering/Analysis Corporation
Berkeley, California

Ashraf Habibullah, President
Computers/Structures International
Oakland, California

June 1977

TABLE OF CONTENTS

	PAGE
I. Introduction	1
A. Background.	1
B. Basic Assumptions	1
II. Three-Dimensional Analysis Without Hydrodynamic Interaction .	3
A. Objective and Scope	3
B. Analysis Procedure.	6
1. Idealization.	6
2. Analysis process.	6
3. Output of results	8
C. Structural Model.	8
1. Finite element mesh	8
2. Material properties	9
3. Displacement boundary conditions.	9
4. Mass distribution	9
D. Analysis Cases and Results.	9
1. Static Analysis	9
a. applied loads	13
b. results	15
2. Analysis for mode shapes and frequencies.	22
3. Response spectrum analysis.	22
4. Time history response analysis.	29
a. solution parameters	29
b. results	31
III. Two-Dimensional Analysis With Hydrodynamic Interaction . . .	44
A. Analysis Without Interaction.	44
B. Analysis With Interaction	44
C. Extension to Three Dimensional Analysis	46
IV. Transverse Earthquake Analysis.	47
V. Vertical Earthquake Analysis.	48
VI. Final Remarks	49

I. INTRODUCTION

A. Background

The analysis presented in this report was conducted under a consulting agreement between the Department of Water Resources of the State of California and E. L. Wilson. The analysis was monitored by personnel of the Division of Design and Construction.

The purpose of the report is to present an Earthquake Analysis of the Oroville Dam Flood Control Outlet Structure utilizing the finite element method and dynamic techniques suitable for this particular structure. It is not the objective of this report to assess the structural safety of the structure but to present the results (stresses and displacements) of a specific analyses based on the given loadings and stated assumptions.

B. Basic Assumptions

The structure to be analyzed is a complex three dimensional structure given in detail in drawings A-3B5-1 to A-3B5-7 which were supplied by Department of Water Resources. Since the three dimensional dynamic analysis of the complete series of monoliths is beyond the present state-of-the-art with respect to computer capabilities it was necessary to study the three dimensional dynamic behavior of a typical monolith only. For elastic behavior this idealization should introduce only minor errors--less than 10 percent.

The specified earthquake loading produces stresses and displacements which must be combined with the results of other load conditions if the total state of stress is to be evaluated. In order for the results of the various load conditions to be combined in a rational manner dead loads and static hydrostatic loads were applied to the same three dimensional finite element model and are presented in this report as separate results.

Also, the upstream-downstream direction was assumed to be the critical direction with respect to the dynamic earthquake loading. A separate simplified analysis is presented to evaluate the significance of the earthquake loading in the transverse direction. In addition, potential vertical earthquake stresses must be considered separately.

At the present time an exact three dimensional analysis of a dam-reservoir system is not possible. Therefore, it was necessary to estimate this effect by examining this effect on a two-dimensional structure with similar dynamic properties.

Only linearly elastic behavior was considered. After the results from the various analysis are combined it will be necessary to apply experience and engineering judgment in order to estimate the significance of nonlinear behavior and to estimate the realistic behavior of the structure under the specified earthquake.

II. THREE DIMENSIONAL ANALYSIS WITHOUT HYDRODYNAMIC INTERACTION

A. Objective and Scope

This section describes the three dimensional static and dynamic analysis of a typical section of the mass concrete spillway structure. The objective of the analysis is to compute stresses in the concrete due to seismic excitation.

A critical exposure condition for the spillway structure occurs when seismic input acts parallel to the direction of flow. For this case, horizontal motion is induced in the breast wall which must be resisted by overturning (i.e., vertical stresses) in the piers. From the proportions of the structure, it is reasonable to approximate the horizontal translation of the foundation as a rigid body; i.e., at any instant, the acceleration at the base of all piers is identical. The ends of the spillway structure terminate in substantial embankments; thus, it is reasonable to neglect horizontal motion transverse to the direction of flow for an earthquake acting in the direction of flow.

A typical section of the spillway structure is bounded between two vertical planes as shown schematically in Figure II.1. One plane bisects the pier and the other coincides with a mid-plane of the breast wall. The X, Y, Z reference system shown in the figure is chosen as follows. X is horizontal and transverse to the direction of flow. Y is vertical and directed up. Z is horizontal, parallel to flow and directed upstream. A plan view of this same section is shown in Figure II.2. Assuming that the X-translation is zero on both vertical planes and that the same Z-direction ground input acts at the base of all piers, an analysis of the section shown in Figure II.1 will predict a response typical of that for the entire structure.

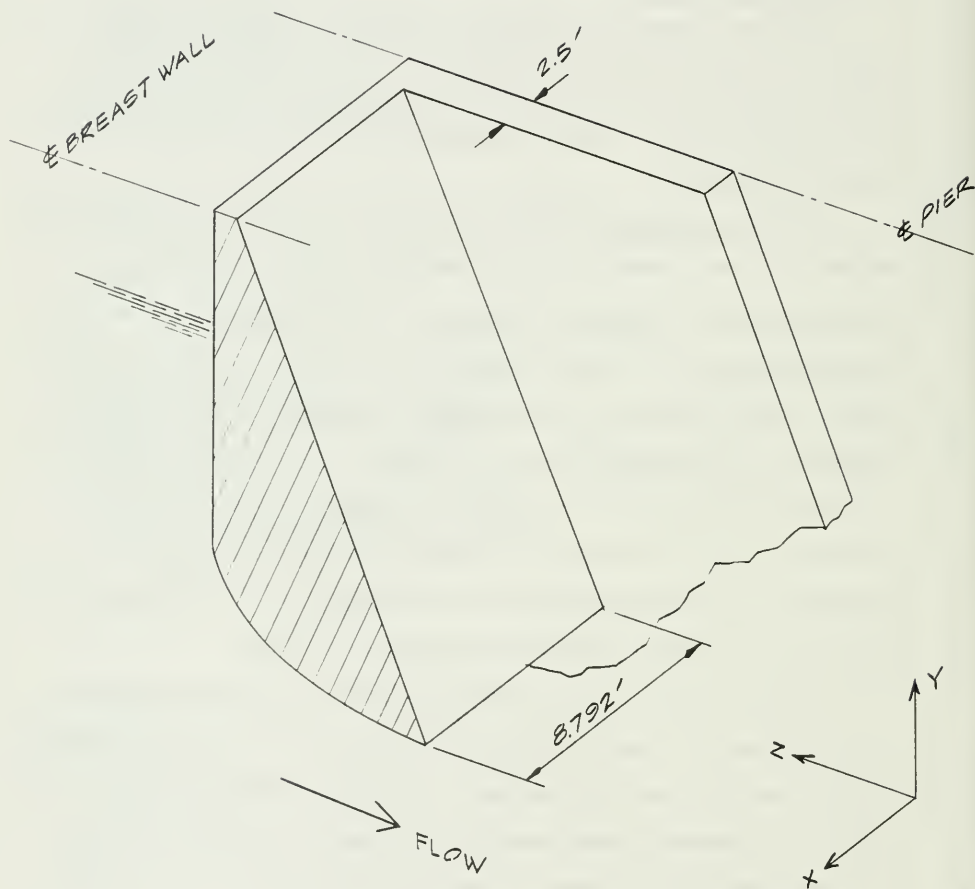


FIGURE II.1 OROVILLE SPILLWAY STRUCTURE
SCHEMATIC OF TYPICAL SECTION

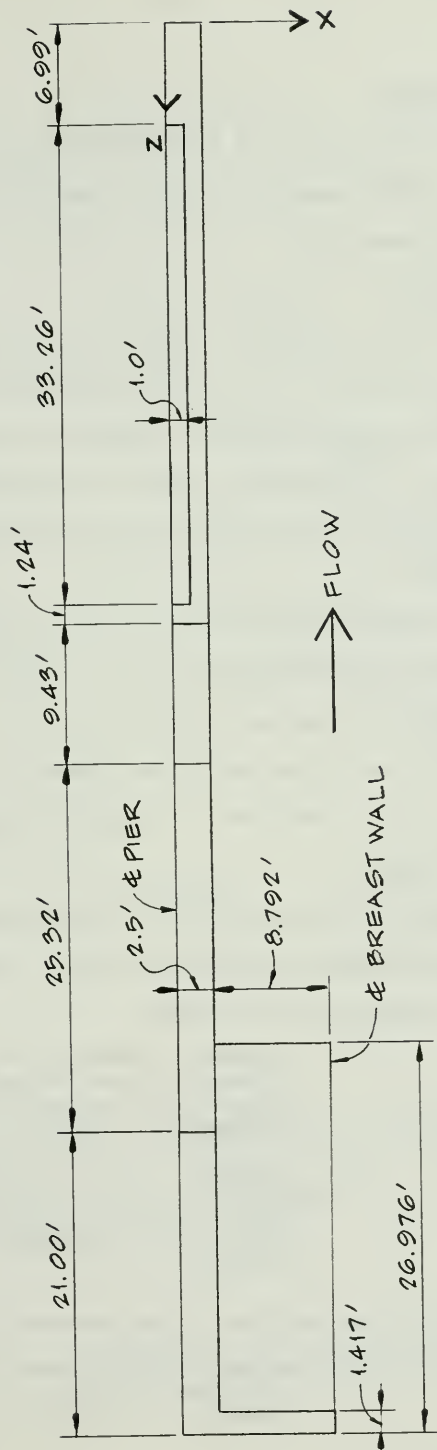


FIGURE II.2 OROVILLE SPILLWAY STRUCTURE
PLAN VIEW OF TYPICAL SECTION

B. Analysis Procedure

The purpose of the analysis is to predict seismic stresses in the concrete structure. For comparison, static stresses under operating conditions are also calculated.

1. Idealization

The typical section isolated in Figure II.1 is idealized as a three dimensional elastic continuum. The structure considered is the mass concrete only. Non-structural masses are lumped at various locations in the structure; e.g., the gate mass is lumped at the trunnion. Added mass due to structure/reservoir interaction is not considered in the three dimensional analysis.

An elevation view of a typical section is shown in Figure II.3. Ground acceleration is applied through the base of the pier and is directed in the global Z-direction. The structure is free to deform in the Y,Z plane, but is restrained against displacement normal to the vertical planes: $X = 0$ (pier) and $X = 11.292'$ (breast wall).

2. Analysis Process

The three dimensional stress analysis was performed using the linear elastic finite element computer code known as EASE2. Usage and theoretical basis for EASE2 are described in the reports:

- (1) "EAC/EASE2 - Elastic Analysis for Structural Engineering", User Information Manual, Control Data Corporation, Cybernet Services, Publication No. 84002700, Revision B (6-15-76).
- (2) "EAC/EASE2 - Dynamic Analysis for Structural Engineering", User Information Manual, Control Data Corporation, Cybernet Services, Publication No. 84000040, Revision A (6-15-76).

The EASE2 analysis was performed in the sequence outlined below:

- (1) prepare a finite element mesh consisting of the three dimensional, eight-node solid elements;

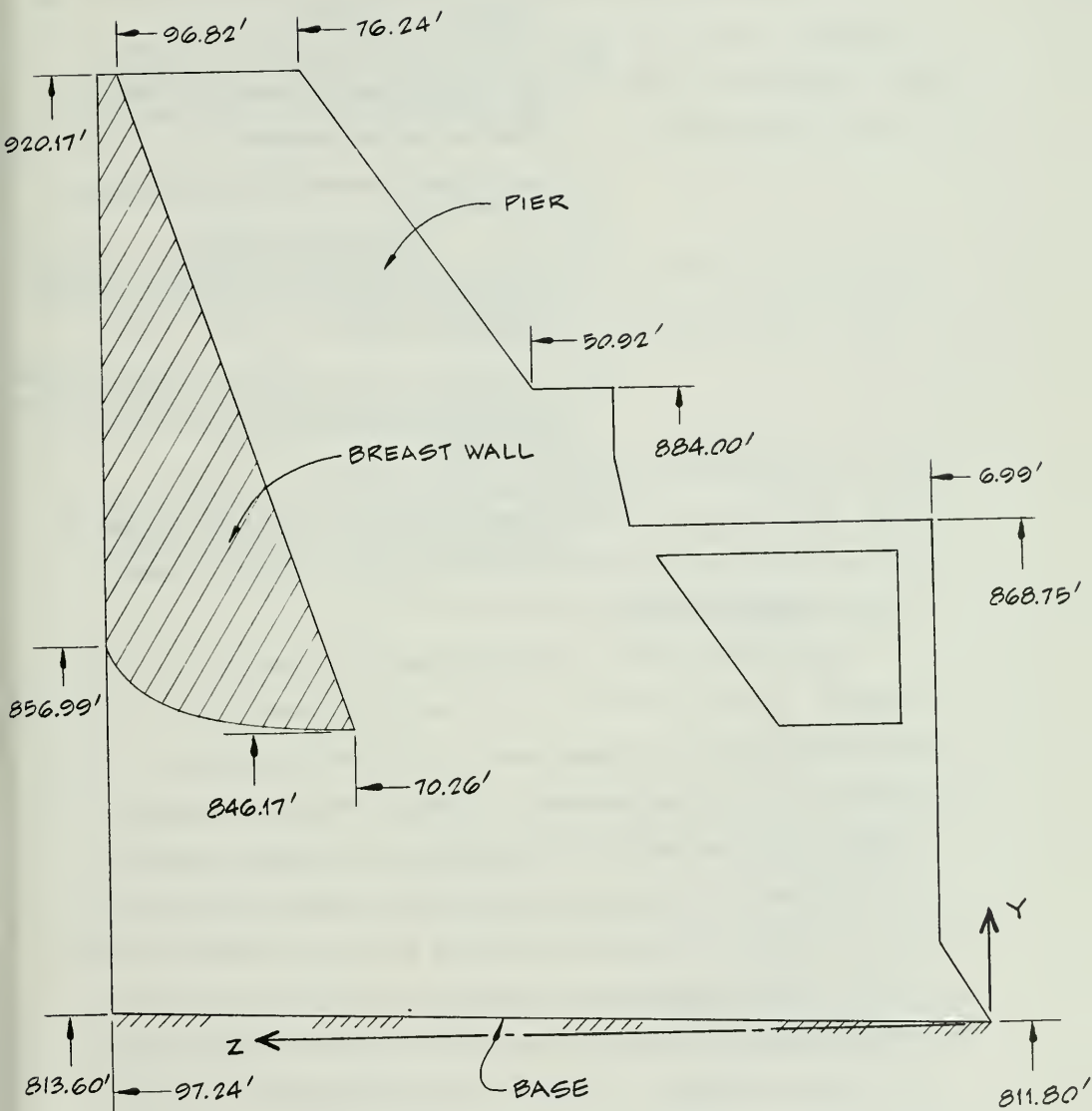


FIGURE II.3

OROVILLE SPILLWAY STRUCTURE
ELEVATION OF TYPICAL SECTION

- (2) lump non-structural masses at corresponding locations in the model;
- (3) calculate static loads due to gravity, hydrostatic pressure and trunion prestress and analyze the structure for operating condition static stresses;
- (4) analyze the structure for mode shapes and frequencies;
- (5) knowing the structure frequencies, calculate the spectral response due to the earthquake time history (modified Pacoima and Taft, 20 seconds duration);
- (6) to locate regions of critical stress, perform a response spectrum analysis of the structure assuming Z-direction input at the base of the pier;
- (7) requesting output at locations of high stress, calculate the dynamic response of the structure due to Z-direction ground input acting at the base of the pier.

3. Output of Results

Complete output from a three dimensional time history analysis is enormous. To reduce print-out to manageable proportion, it is necessary to limit output to those quantities of primary concern. For the spillway structure, this primary quantity is principal tension in the concrete. The static and response spectrum analyses produce complete spatial distributions of stress and thus can be used to locate regions of high stress. Output from the seismic response analysis is limited to principal tension plotted versus time, one plot for each location of potentially critical stress. From the plots, the times at which maximum stresses occur can be determined. Finally, complete distributions of principal tension are displayed at those times at which maxima were found to occur.

C. Structural Model

1. Finite Element Mesh

The section of Figure II.1 is modeled with 285 eight-node solid elements. The mesh is built up of four vertical layers of elements as shown in Figure II.4. Figure II.5 plots the +X face of elements 1-to-177 which represent the pier, and Figure II.6 is an enlargement of one of the three breast wall element layers.

2. Material Properties

The modulus of elasticity and Poisson's ratio of the concrete are taken as 5000 ksi and 0.2, respectively. The weight density of the concrete is 160 pcf.

3. Displacement Boundary Conditions

The base of the pier is fixed. Transverse X-displacement is zero for all nodes in the pier mid-plane and breast wall mid-plane. These boundary conditons allow free Y,Z translation of the structure at all nodes above the base, and X- translation is free at all nodes except those on the vertical boundary planes.

4. Mass Distribution

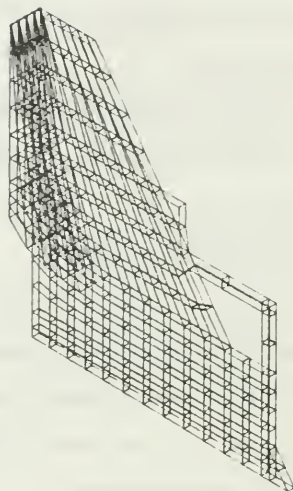
The total mass of the structure model is the sum of the mass due to element volume (i.e., structural mass) plus non-structural added mass. The total mass due to element volume was computed by EASE2 as 3906^k. This is 6% lower than the working drawing estimate of 4153^k (corrected to 160 pcf concrete). The total non-structural mass is 337^k. Each non-structural mass item (e.g., inspection walkway, maintenance deck, etc.) has its mass distributed to the node or line of nodes nearest its actual location in the structure.

D. Analysis Cases and Results

1. Static Analysis

Three static loading conditions:

UNDEFORMED GEOMETRY



/STATE OF CALIFORNIA/DEPARTMENT OF WATER RESOURCES/OROVILLE DAM SPILLWAY/
 /STATIC AND DYNAMIC THREE DIMENSIONAL FINITE ELEMENT ANALYSIS/
 ISOMETRIC VIEW OF TOTAL MODEL -- NODE AND ELEMENT NUMBERS SUPPRESSED



ERC/CSI/ERSE2/E2PLOT

VIEW NUMBER 1

FRAME NUMBER 1

PUN DATE 10/14/76

FIGURE II.4 OROVILLE SPILLWAY STRUCTURE
 3/D FINITE ELEMENT MODEL

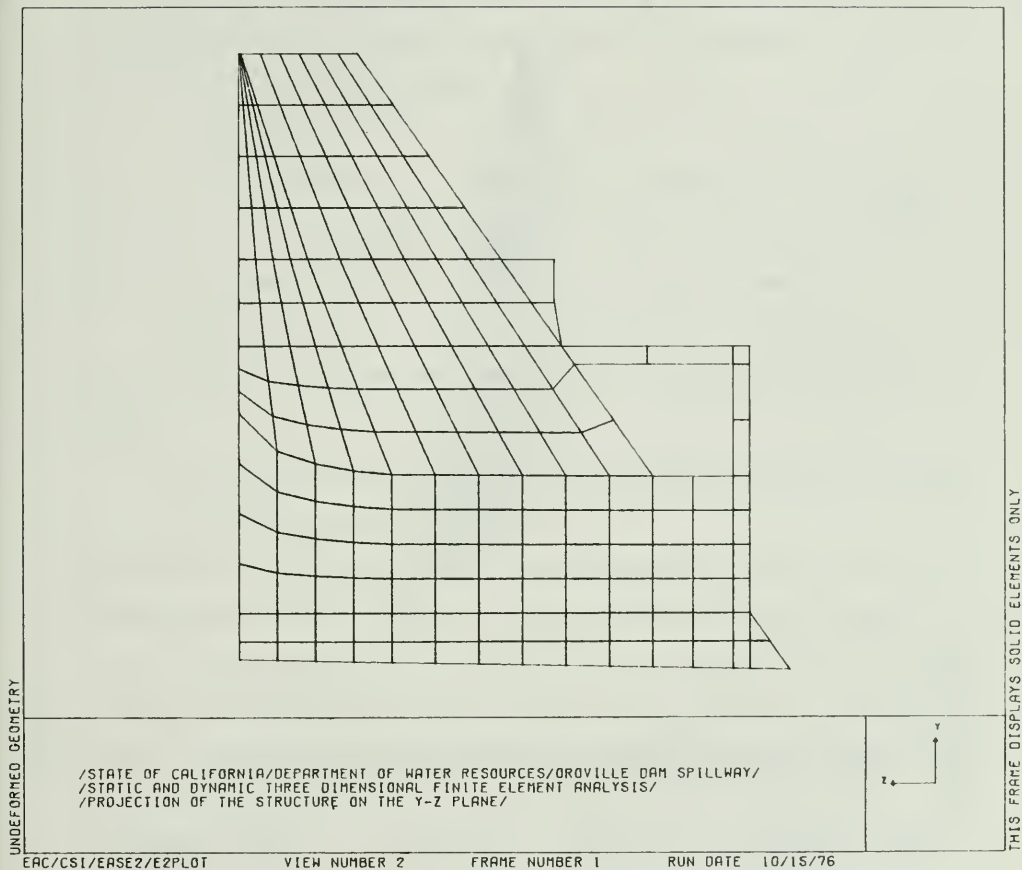


FIGURE II.5 OROVILLE SPILLWAY STRUCTURE
 PIER ELEMENT LAYER

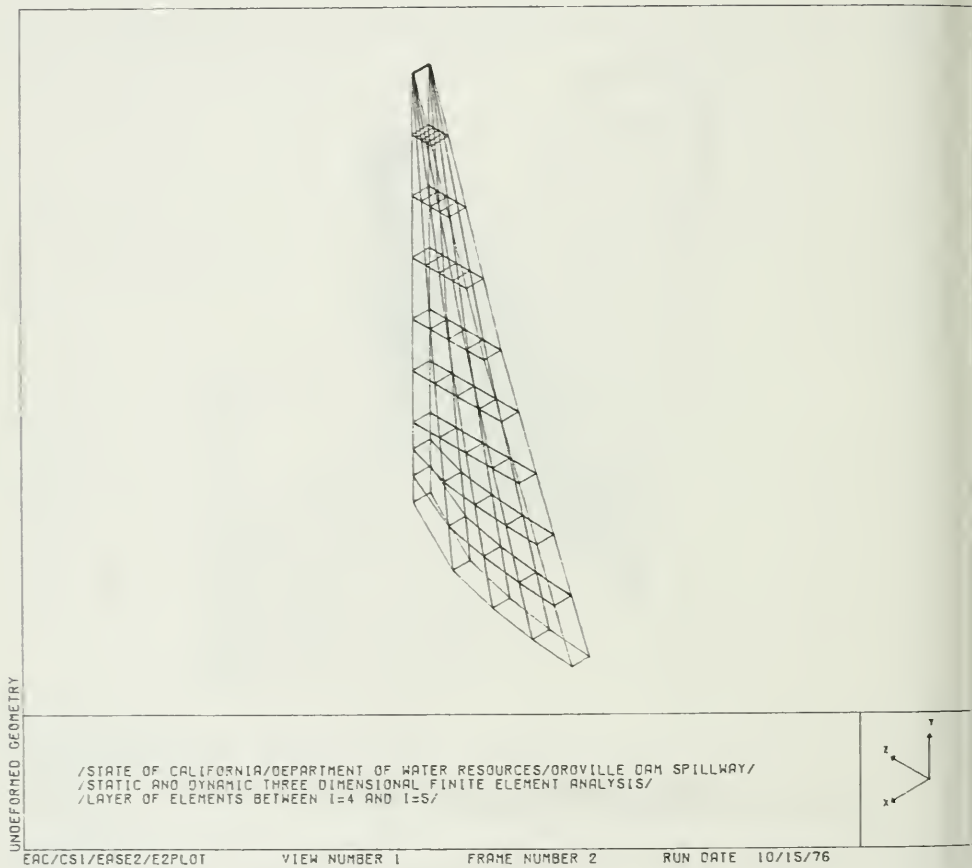


FIGURE II.6 OROVILLE SPILLWAY STRUCTURE
 BREAST WALL ELEMENT LAYER

- (1) gravity;
- (2) hydrostatic pressure (closed gate, water surface elevation of 900 feet);
- (3) trunnion anchorage prestress

are analyzed individually and in combination. The combined loading case is called the "operating condition".

a. Applied Loads

Gravity loading is a 1-g static acceleration applied in the minus Y-direction. The total gravity loading is 4243^k ; this includes 3906^k due to structure plus 337^k due to non-structural mass items.

Hydrostatic loads are computed assuming that the water surface is at an elevation of 900.00 feet. The loading is separated into two major parts:

- (1) pressure on the exposed surface of the mass concrete structure; and,
- (2) pressure on the radial gate.

The structure is loaded by applying pressure normal to the face of all exposed solid elements. Integrating the pressure distribution applied on the finite element model, we obtain a total horizontal force of 1377^k (-Z) and a total vertical force of 752^k (+Y); see Figure II.7. Actual uplift acting on the elliptical underside of the breast wall was calculated as 757^k . The horizontal and vertical resultants due to hydrostatic pressure on the gate are 1296^k (-Z) and 880^k (+Y), respectively. These forces act on the pier at the trunnion.

A self-equilibrating load set simulating trunnion anchorage prestress was applied to the pier to offset the hydrostatic gate load. Twenty four (24) tendons (in 1/2 of the pier) at 142.6^k per tendon results in a total prestress force of 3422^k . The line of action of the opposing prestress forces was aligned through the average trajectory of the tendon array.

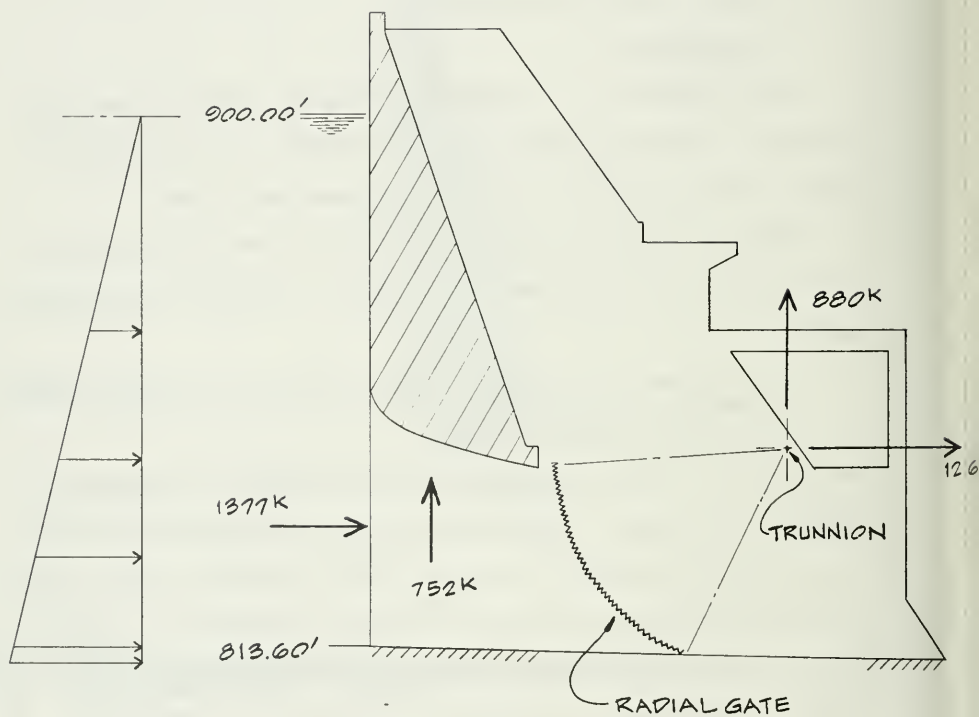


FIGURE II.7 HYDROSTATIC LOAD RESULTANTS

b. Results

Static analysis results are described in this section. Stresses due to gravity alone and stresses for the operating condition (i.e., gravity + hydrostatic + prestress) are presented.

The spatial distribution of stress in the concrete is displayed as follows. A Y,Z projection of the 177 solid elements used to model the pier is shown in Figure II.8(A). Figure II.8(B) is an elevation view of the same 177 elements transformed to an integer coordinate system in which all element faces have the same area. If element centroidal stresses were printed at their respective physical (Y,Z) locations, the result would be unreadable. Values printed in the integer system (Figure II.8(B)) form a regular array as maybe seen in Table II.1. This table lists the vertical (Y) stress in psi calculated in each pier element for the gravity loading condition; negative values indicate compression. Maximum vertical compression is 300 psi in element 14 which is located in the heel of the pier. Tables II.2 and II.3 are distributions of minimum and maximum principal stress, respectively, due to gravity only. Note that the vertical and minimum principal stresses in the vicinity of the heel are nearly the same; this indicates that the minimum stress is approximately vertical in the heel region. Stresses in the breast wall due to gravity are low; the min/max principal stresses fall in the range -100 psi/10 psi.

The principal stresses for the operating condition (sum of all static loads) are shown in Tables II.4 and II.5. One notes that principal stresses are not an exact sum at the principal stresses due to the individual load conditions; since their directions are not the same. However; near the heel where all load conditions tend to produce vertical stresses

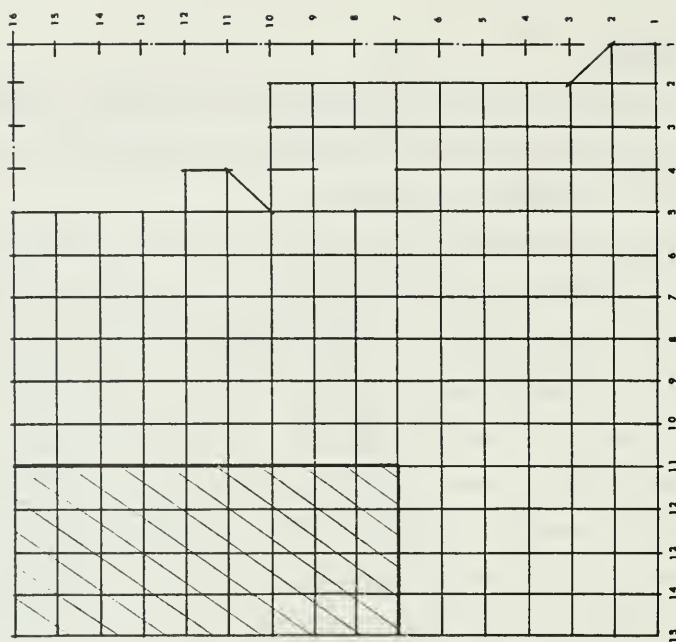


FIGURE II.8.B ELEVATION VIEW OF PIER ELEMENTS
MAPPED INTO THE PRINTER DISPLAY
COORDINATE SYSTEM

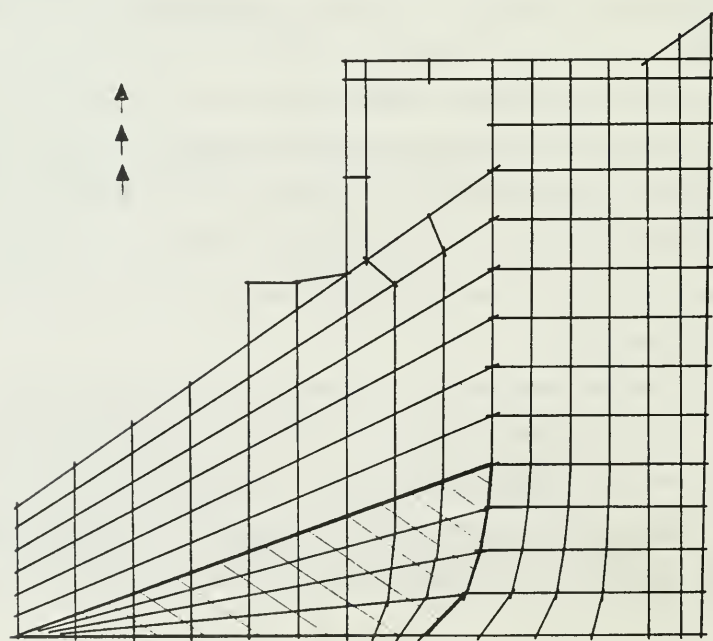


FIGURE II.8.A ELEVATION VIEW OF PIER ELEMENTS
PHYSICAL COORDINATE SYSTEM

```

HEADING LINE THREE          = ( GRAVITY LOADS / VERTICAL STRESS / PSI UNITS
STATIC LOAD CASE NUMBER    = (      1)
ELEMENT DISPLAY SET NUMBER = (      1)
SCALE FACTOR               = (      .1000E+04)
OUTPUT STRESS COMPONENT    = (      2)

```

```

OROVILLE DAM SPILLWAY/ HALF OF TYPICAL BAY/ STATIC ANALYSIS RESULTS/
PIER ELEVATION VIEW/ ELEMENTS 001-TO-177/
GRAVITY LOADS / VERTICAL STRESS / PSI UNITS

```

SOLID ELEMENT CENTROIDAL STRESSES

-13	-13	-12	-12	-12	-11	-11	-10	-9	-8										
-16	-16	-16	-18	-20	-18	-17	-14	-12	-9										
-21	-22	-22	-23	-26	-24	-21	-17	-13	-9										
-27	-27	-28	-30	-32	-29	-26	-21	-15	-5										
-32	-32	-33	-36	-42	-40	-36	-30	-21	-7	-25									
-39	-38	-38	-40	-47	-46	-43	-36	-23	-19	-3									
-49	-47	-44	-45	-54	-56	-52	-40	-27	16	-53	2	-8							
-69	-67	-58	-55	-67	-71	-59	-43	-20	-14				-41						
-126	-134	-117	-100	-90	-81	-62	-41	-23	22				-46						
-226	-239	-217	-174	-122	-88	-66	-45	-18	2	-1	-13	-48							
-244	-236	-215	-180	-138	-101	-74	-50	-27	-9	-6	-20	-36							
-254	-240	-216	-184	-147	-112	-83	-58	-36	-21	-16	-22	-26							
-265	-247	-219	-188	-154	-120	-91	-66	-45	-32	-26	-23	-23							
-281	-252	-219	-190	-159	-127	-98	-74	-54	-41	-33	-27	-18	-13						
-300	-246	-219	-191	-162	-131	-104	-80	-61	-48	-39	-30	-22	-10						

TABLE II.1 STATIC GRAVITY STRESSES
VERTICAL (Y) COMPONENT

HEADING LINE THREE = (GRAVITY LOADS / MINIMUM PRINCIPAL STRESS / PSI UNITS
 STATIC LOAD CASE NUMBER = (1)
 ELEMENT DISPLAY SET NUMBER = (1)
 SCALE FACTOR = (.1000E+04)
 OUTPUT STRESS COMPONENT = (7)

OROVILLE DAM SPILLWAY/ HALF OF TYPICAL BAY/ STATIC ANALYSIS RESULTS/
 PIER ELEVATION VIEW/ ELEMENTS 001-TO-177/
 GRAVITY LOADS / MINIMUM PRINCIPAL STRESS / PSI UNITS

SOLID ELEMENT CENTROIDAL STRESSES

-14	-13	-13	-13	-13	-12	-11	-10	-10	-10				
-16	-16	-17	-19	-21	-19	-17	-14	-12	-11				
-21	-22	-22	-24	-27	-24	-21	-18	-13	-10				
-27	-27	-28	-30	-33	-30	-26	-22	-15	-5				
-32	-32	-33	-36	-43	-40	-37	-31	-22	-12	-32			
-39	-38	-38	-40	-48	-47	-44	-37	-28	-26	-9			
-49	-47	-44	-45	-54	-57	-53	-43	-31	7	-59	-12	-10	
-70	-68	-59	-56	-67	-71	-61	-47	-29	-28			-42	
-129	-137	-121	-102	-91	-81	-63	-44	-27	-2			-46	
-227	-240	-219	-178	-124	-88	-66	-46	-18	-4	-4	-13	-50	
-244	-236	-215	-181	-139	-101	-74	-51	-27	-13	-15	-27	-36	
-254	-240	-216	-184	-148	-112	-83	-58	-36	-23	-24	-27	-27	
-265	-247	-219	-188	-154	-121	-91	-66	-45	-32	-29	-26	-23	
-281	-253	-219	-190	-159	-127	-99	-74	-54	-41	-34	-27	-18	-13
-304	-247	-220	-192	-163	-133	-105	-81	-62	-48	-39	-30	-22	-10

TABLE II.2 STATIC GRAVITY STRESSES
 MINIMUM PRINCIPAL COMPONENT

HEADING LINE THREE = (GRAVITY LOADS / MAXIMUM PRINCIPAL STRESS / PSI UNITS
 STATIC LOAD CASE NUMBER = (1)
 ELEMENT DISPLAY SET NUMBER = (1)
 SCALE FACTOR = (.1000E+04)
 OUTPUT STRESS COMPONENT = (-9)

OROVILLE DAM SPILLWAY/ HALF OF TYPICAL BAY/ STATIC ANALYSIS RESULTS/
 PIER ELEVATION VIEW/ ELEMENTS 001-10-177/
 GRAVITY LOADS / MAXIMUM PRINCIPAL STRESS / PSI UNITS

SOLID ELEMENT CENTROIDAL STRESSES

0	0	0	1	2	0	0	0	0	0				
0	0	1	3	5	4	2	1	0	0				
0	1	2	4	9	7	6	4	2	0				
0	1	2	5	11	11	10	9	7	5				
0	1	2	5	13	12	12	11	9	8	1			
0	0	1	4	13	14	15	14	16	20	12			
0	0	0	3	11	14	15	16	15	23	1	9	7	
3	5	5	7	6	9	11	15	23	23				-2
-6	-8	-10	-4	0	0	5	12	21	50				1
6	-4	-10	-14	-4	1	0	4	13	27	30	14	5	
3	5	5	3	1	0	0	0	0	4	10	6	0	
2	0	0	0	0	0	0	0	0	0	0	2	1	
0	-1	-1	-1	-1	0	0	0	0	0	0	0	0	
5	3	4	3	3	2	2	2	1	1	1	1	1	0
-33	-27	-24	-20	-17	-14	-11	-8	-7	-5	-4	-3	-2	-1

TABLE II.3 STATIC GRAVITY STRESSES
 MAXIMUM PRINCIPAL COMPONENT

```

HEADING LINE THREE          = (GRAVITY+HYDROSTATIC+PRESTRESS/ MINIMUM PRINCIPAL STRESS/ PSI UNITS
STATIC LOAD CASE NUMBER    = (      4)
ELEMENT DISPLAY SET NUMBER = (      1)
SCALE FACTOR               = (      .1'00E+04)
OUTPUT STRESS COMPONENT    = (      7)

```

OPPOVILLE DAM SPILLWAY/ HALF OF TYPICAL BAY/ STATIC ANALYSIS RESULTS/
 PIER ELEVATION VIEW/ ELEMENTS 001-TO-177/
 GRAVITY+HYDROSTATIC+PRESTRESS/ MINIMUM PRINCIPAL STRESS/ PSI UNITS

SOLID ELEMENT CENTROIDAL STRESSES

-12	-12	-12	-12	-13	-12	-12	-11	-10	-8								
-14	-15	-17	-19	-21	-20	-18	-15	-12	-10								
-22	-22	-22	-24	-27	-24	-21	-18	-15	-11								
-30	-28	-27	-28	-30	-27	-25	-23	-19	-13								
-36	-33	-31	-32	-36	-37	-38	-35	-30	-15	-33							
-41	-37	-36	-37	-42	-47	-48	-46	-36	-34	-23							
-46	-42	-41	-44	-57	-62	-64	-61	-53	-21	-43	-18	-11					
-56	-51	-47	-56	-80	-83	-84	-82	-72	-67							-45	
-83	-80	-72	-86	-110	-103	-99	-112	-142	-100								-49
-129	-124	-120	-123	-130	-115	-107	-135	-265	-169	-131	-27	-55					
-127	-114	-112	-115	-107	-135	-147	-210	-202	-280	-150	-57	-24					
-115	-113	-116	-113	-95	-161	-259	-217	-207	-165	-177	-75	-31					
-97	-116	-127	-126	-122	-128	-297	-249	-120	-148	-137	-99	-74					
-80	-122	-130	-141	-144	-139	-196	-198	-153	-153	-139	-112	-34	-96				
-73	-127	-142	-157	-156	-146	-103	-151	-180	-165	-146	-120	-103	-84				

TABLE II.4

STATIC OPERATING CONDITION STRESSES
 MINIMUM PRINCIPAL COMPONENT

HEADING LINE THREE = (GRAVITY+HYDROSTATIC+PRESTRESS/ MAXIMUM PRINCIPAL STRESS/ PSI UNITS
 STATIC LOAD CASE NUMBER = (4)
 ELEMENT DISPLAY SET NUMBER = (1)
 SCALE FACTOR = (.1000E+04)
 OUTPUT STRESS COMPONENT = (9)

020VILLE DAM SPILLWAY/ HALF OF TYPICAL BAY/ STATIC ANALYSIS RESULTS/
 2100 ELEVATION VIEW/ ELEMENTS 001-10-177/
 GRAVITY+HYDROSTATIC+PRESTRESS/ MAXIMUM PRINCIPAL STRESS/ PSI UNITS

SOLID ELEMENT CENTROIDAL STRESSES

0	0	1	1	7	1	0	0	0	0				
0	0	0	1	7	1	0	0	0	0				
-2	-2	-2	-2	-1	0	0	0	0	0				
-5	-5	-5	-5	-3	1	0	0	0	0				
-7	-7	-6	-6	-4	1	0	0	0	1	-1			
-9	-8	-6	-6	-4	1	0	0	0	-2	1			
-9	-8	-6	-7	-5	1	0	0	0	21	1	7	19	
-7	-5	-7	-6	-6	2	0	0	0	-4			-3	
-9	-9	-4	-11	-10	3	0	2	-7	49			4	
-7	-9	-5	-7	-6	2	0	4	-9	-6	52	17	12	
1	2	1	2	1	0	4	-6	6	-12	24	-5	2	
-1	0	7	12	18	19	-7	7	-5	5	0	1	2	
-1	4	22	40	75	214	-27	-3	3	-1	0	-1	-1	
0	10	30	55	121	361	206	3	5	4	3	2	3	1
27	14	23	46	155	221	140	18	-16	-15	-13	-9	-6	-3

TABLE II.5

STATIC OPERATING CONDITION STRESSES
 MAXIMUM PRINCIPAL COMPONENT

a direct summation is a good approximation. Also, the stresses in the breast wall for this combined load case are in the range -100 psi to 10 psi.

2. Analysis for Mode Shapes and Frequencies

The ten (10) lowest natural frequencies and mode shapes were determined using EASE2. Table II.6 lists the first five (5) frequencies and their associated global (X,Y,Z) mass modal participation factors. By definition, the X-direction mass modal participation factor for the i-th mode is:

$$\psi_x^i = \phi_i^T \underline{M} \underline{I}_x$$

where ϕ_i is the i-th mode eigenvector, \underline{M} is the system mass matrix and \underline{I}_x is a vector containing ones at X translational degrees of freedom and zeroes elsewhere. If ψ_x^i is small (in comparison to ψ_y^i and ψ_z^i), it means that the i-th mode has practically no X component. From Table II.6 it is seen that the ψ_x^i are negligible from which we conclude that the mode shapes are essentially two-dimensional in the vertical Y,Z plane.

Figures II.9, II.10 and II.11 plot eigenvectors for modes 1, 2 and 3 respectively. The undeformed structure is shown dashed in these plots. The second mode represents localized vibrations in the bent which supports the road bridge. Generally, however, the modes are combinations of shear and flexure involving the entire pier. The breast wall responds essentially as a rigid mass atop the pier cantilever.

3. Response Spectrum Analysis

The "modified Pacoima and Taft" acceleration time history (shown for 20 seconds in Figure II.12) is assumed to act at the base of the pier in the global Z-direction. The response spectrum for 5% damping for the modified Pacoima and Taft is plotted in Figure II.13. Note that the spectral acceleration approaches the peak acceleration (0.6g) at the high frequency end.

MODE NUMBER, i	NATURAL FREQUENCY, f_i	MASS MODAL PARTICIPATION FACTORS		
		ψ_x^i	ψ_y^i	ψ_z^i
1	10.07 hz	.0005	0.7057	2.4645
2	22.60 hz	-.0028	0.8632	0.1599
3	24.84 hz	-.0058	2.0934	1.5704
4	28.14 hz	-.0073	1.6520	-0.7618
5	36.39 hz	-.0067	-0.0664	0.2202

TABLE II.6 OROVILLE SPILLWAY STRUCTURE
 NATURAL FREQUENCIES AND ASSOCIATED
 MASS MODAL PARTICIPATION FACTORS
 FOR THE LOWEST FIVE MODES

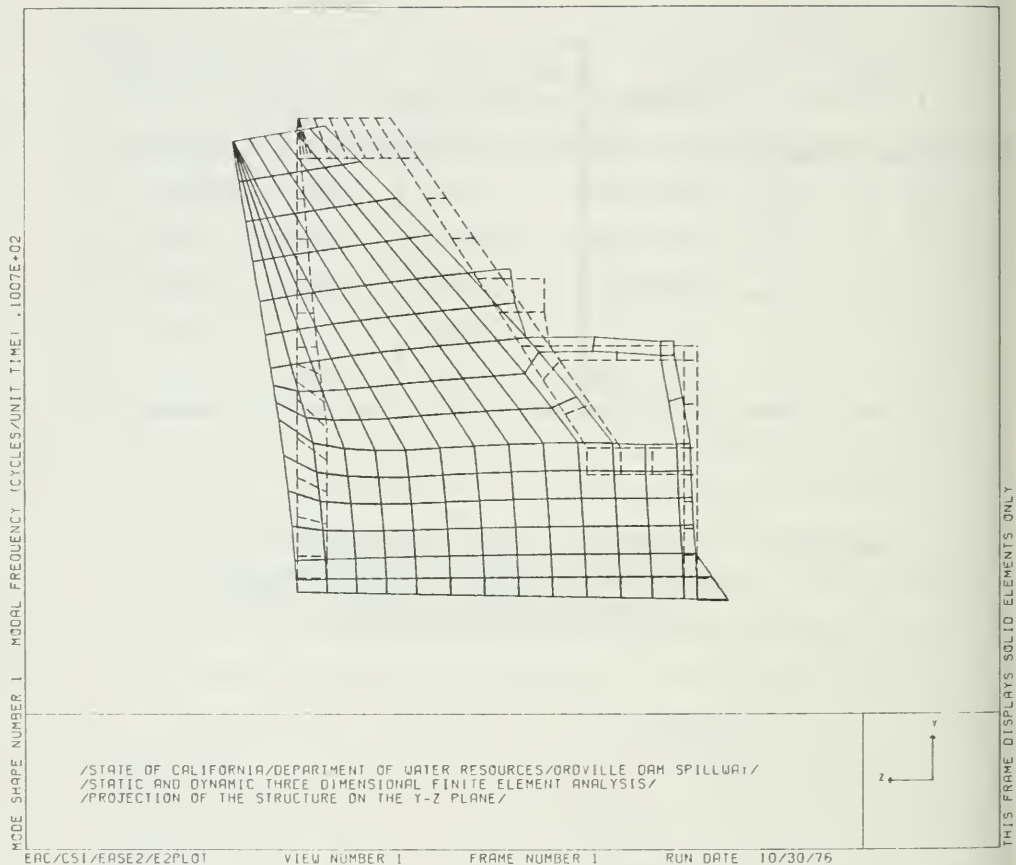
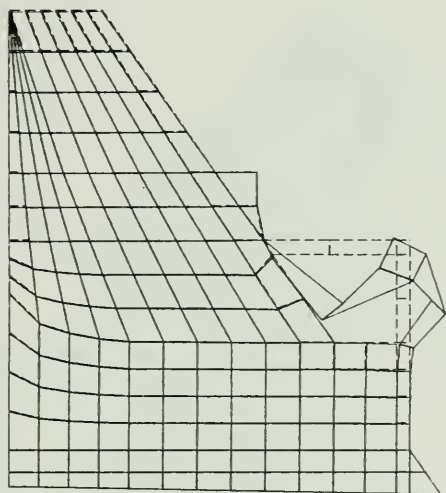


FIGURE II.9 OROVILLE SPILLWAY STRUCTURE
 PLOT OF MODE SHAPE NUMBER ONE

MODE SHAPE NUMBER 2 MODAL FREQUENCY (CYCLES/UNIT TIME) .2260E+02



/STATE OF CALIFORNIA/DEPARTMENT OF WATER RESOURCES/OROVILLE DAM SPILLWAY/
 /STATIC AND DYNAMIC THREE DIMENSIONAL FINITE ELEMENT ANALYSIS/
 /PROJECTION OF THE STRUCTURE ON THE Y-Z PLANE/



THIS FRAME DISPLAYS SOLID ELEMENTS ONLY

EAC/CSI/ERSE2/E2PLOT

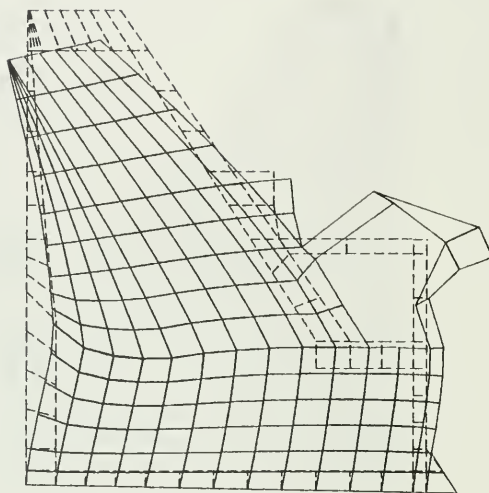
VIEW NUMBER 1

FRAME NUMBER 2

RUN DATE 10/30/76

FIGURE II.10 OROVILLE SPILLWAY STRUCTURE
 PLOT OF MODE SHAPE NUMBER TWO

MODE SHAPE NUMBER 3 MODAL FREQUENCY (CYCLES/UNIT TIME) .2484E-02



/STATE OF CALIFORNIA/DEPARTMENT OF WATER RESOURCES/ROVILLE DAM SPILLWAY/
 /STATIC AND DYNAMIC THREE DIMENSIONAL FINITE ELEMENT ANALYSIS/
 /PROJECTION OF THE STRUCTURE ON THE Y-Z PLANE/



EAC/CSI/ERSE2/E2PLOT

VIEW NUMBER 1

FRAME NUMBER 3

RUN DATE 10/30/76

FIGURE II.11 OROVILLE SPILLWAY STRUCTURE
 PLOT OF MODE SHAPE NUMBER THREE

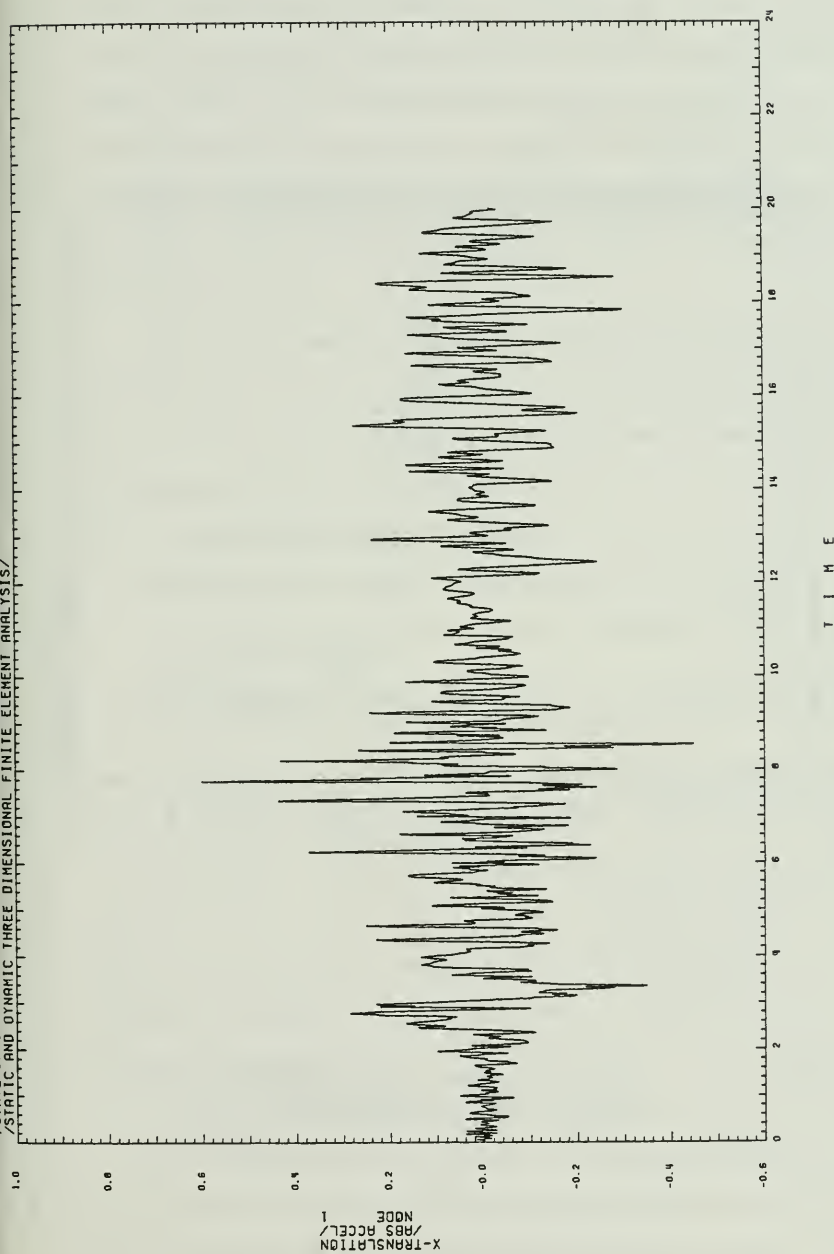


FIGURE II.12 ACCELERATION TIME HISTORY FOR
 MODIFIED PACOIMA AND TAIT

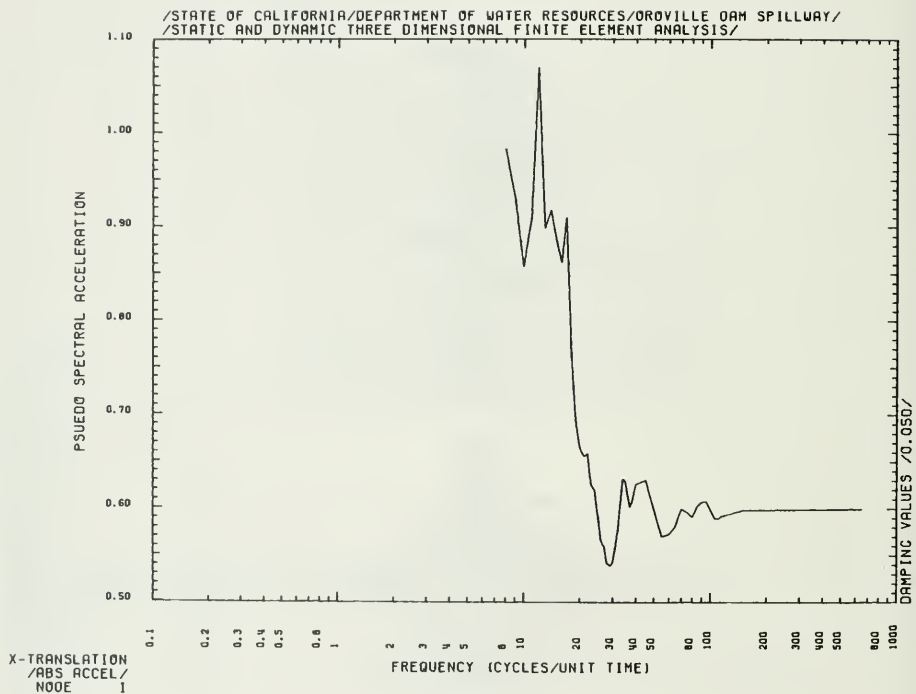


FIGURE II.13 RESPONSE SPECTRUM (5% DAMPING) FOR
MODIFIED PACOIMA AND TAIT

A response spectrum analysis using a square root of the sum of the squares combination of the lowest ten modes was performed with EASE2. Vertical (Y) stresses in the pier due to Z-direction base input are listed in Table II.7. Note that the critically stressed region is the pier heel; 457 psi is predicted in element 14 at the base. Stresses in the breast wall are considerably lower than those predicted in the pier. The maximum X-direction stress in the wall occurs at the crest and is estimated to be 32 psi.

The maximum component of deflection calculated by EASE2 is 0.136 inch (Z) at the crest. A hand estimate of the crest displacement shows that the first mode contributes over 95%; this means that the structure is responding primarily in its first mode.

4. Time History Response Analysis

From the response spectrum analysis we note the following:

- (1) the first mode is the principal contributor to the response of the structure;
- (2) stresses are largest in the pier heel region but are also significant in the vicinity of the pier toe;
- (3) the pier provides horizontal support to an essentially rigid, massive breast wall; stresses in the breast wall are low because it responds nearly rigidly.

The essential characteristics of the time history analysis can be inferred from the results of the response spectrum solution. The results of both analyses should be practically identical because the principal contribution to overall response is contained in the lowest modes, particularly the first mode.

a. solution parameters

The forcing function is applied as Z-direction ground input acting at the base of the pier. The same "modified Pacoima and Taft" acceleration history used for the response spectrum analysis (Figure II.12) is

HEADING LINE THREE = (VERTICAL (Y-DIRECTION) STRESS/ PSI UNITS/

RESPONSE CASE NUMBER = (1)
 ELEMENT DISPLAY SET NUMBER = (1)
 SCALE FACTOR = (.1000E+04)
 OUTPUT STRESS COMPONENT = (2)

OROVILLE DAM SPILLWAY/ HALF OF TYPICAL BAY/ RESPONSE SPECTRUM ANALYSIS/
 PIER ELEVATION VIEW/ ELEMENTS 001-TO-177/
 VERTICAL (Y-DIRECTION) STRESS/ PSI UNITS/

SOLID ELEMENT CENTROIDAL STRESSES

29	24	21	18	14	10	6	4	7	17										
27	25	23	25	26	17	8	10	25	47										
36	32	30	29	32	18	7	22	47	76										
46	39	33	32	34	17	12	35	62	108										
54	44	35	32	36	16	19	47	84	84	50									
62	48	37	32	37	14	26	61	85	111	188									
72	57	42	33	38	15	33	65	107	179	25	6	14							
96	80	56	38	40	16	41	82	141	210										
164	155	107	59	38	21	58	108	155	205										
293	277	199	108	42	26	69	115	156	161	82	6	29							
327	278	206	125	55	27	68	112	147	153	113	63	30							
354	289	212	134	63	27	66	108	137	143	128	114	84							
385	303	216	138	68	27	63	102	128	137	135	143	200							
421	310	215	139	71	28	59	96	121	133	138	161	192	211						
457	299	214	139	73	28	55	91	116	130	143	166	183	162						

TABLE II.7 RESPONSE SPECTRUM ANALYSIS STRESSES
 VERTICAL (Y) COMPONENT

also used in the time history response analysis. The structure is subjected to ground motion for the full 20 second duration.

Even though the response is principally represented by the first mode, contributions for all ten (10) of the structure's lowest modes are included in the transient response analysis. Five (5) percent damping is assumed uniformly for all modes. The time interval at which output is displayed is limited to 1/5 of the period of the first mode or 0.02 second (i.e., 20% of 1/10.07 hertz). Since the excitation is applied for 20 seconds, output is produced at 1000 time points. Using the predictions from the response spectrum analysis, the amount of time history output can be narrowed considerably; i.e., principal stresses in the pier are of major concern, and output is limited to these stress versus time histories. Complete spatial distributions of principal stresses in the pier are recovered only at those times at which maxima occur.

b. results

The histories of absolute Z-direction acceleration for four nodes along the crest of the pier were averaged and plotted versus time; the resulting acceleration time history is shown in Figure II.14. Although the earthquake acts on the structure for 20 seconds, peak values were found to occur in the 7-to-9 second interval; consequently, only the first 10 seconds of response are shown. From Figure II.14 it is seen that the peak crest acceleration is about 1.2 g's.

Figures II.15, II.16, II.17 and II.18 are principal stress time histories covering the first 10 seconds of response. Figures II.15 and II.16 show minimum and maximum principal stress, respectively, developed at the centroid of element 14; element 14 is located at the pier base, upstream face (i.e., at the pier "heel"). Figures II.17 and II.18 are

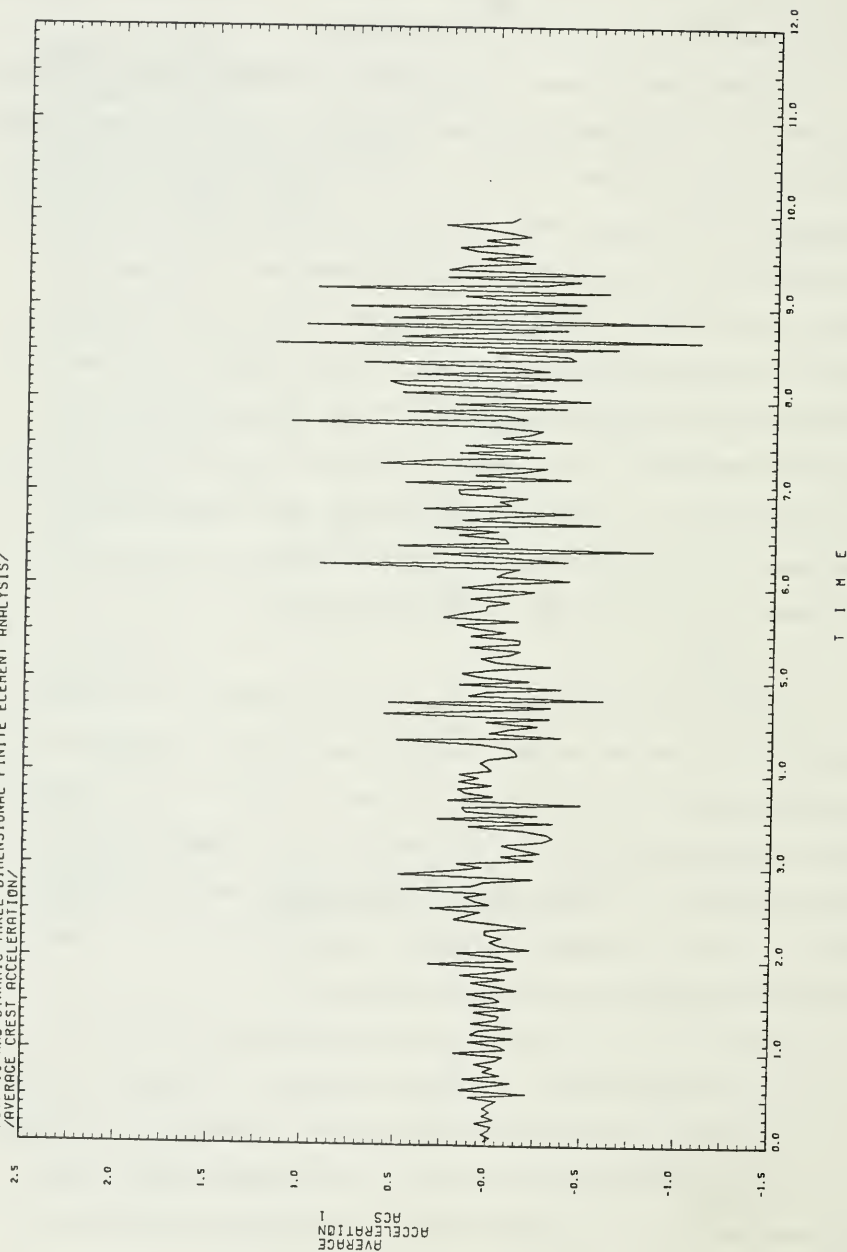


FIGURE II.14 AVERAGE CREST ACCELERATION DUE TO
 MODIFIED PACOIMA AND TAFT
 SEISMIC EXCITATION

/STATE OF CALIFORNIA/DEPARTMENT OF WATER RESOURCES/OROVILLE DAM SPILLWAY/
 /STATIC AND DYNAMIC THREE DIMENSIONAL FINITE ELEMENT ANALYSIS/
 /MINIMUM PRINCIPAL STRESS/HEEL OF PIER/

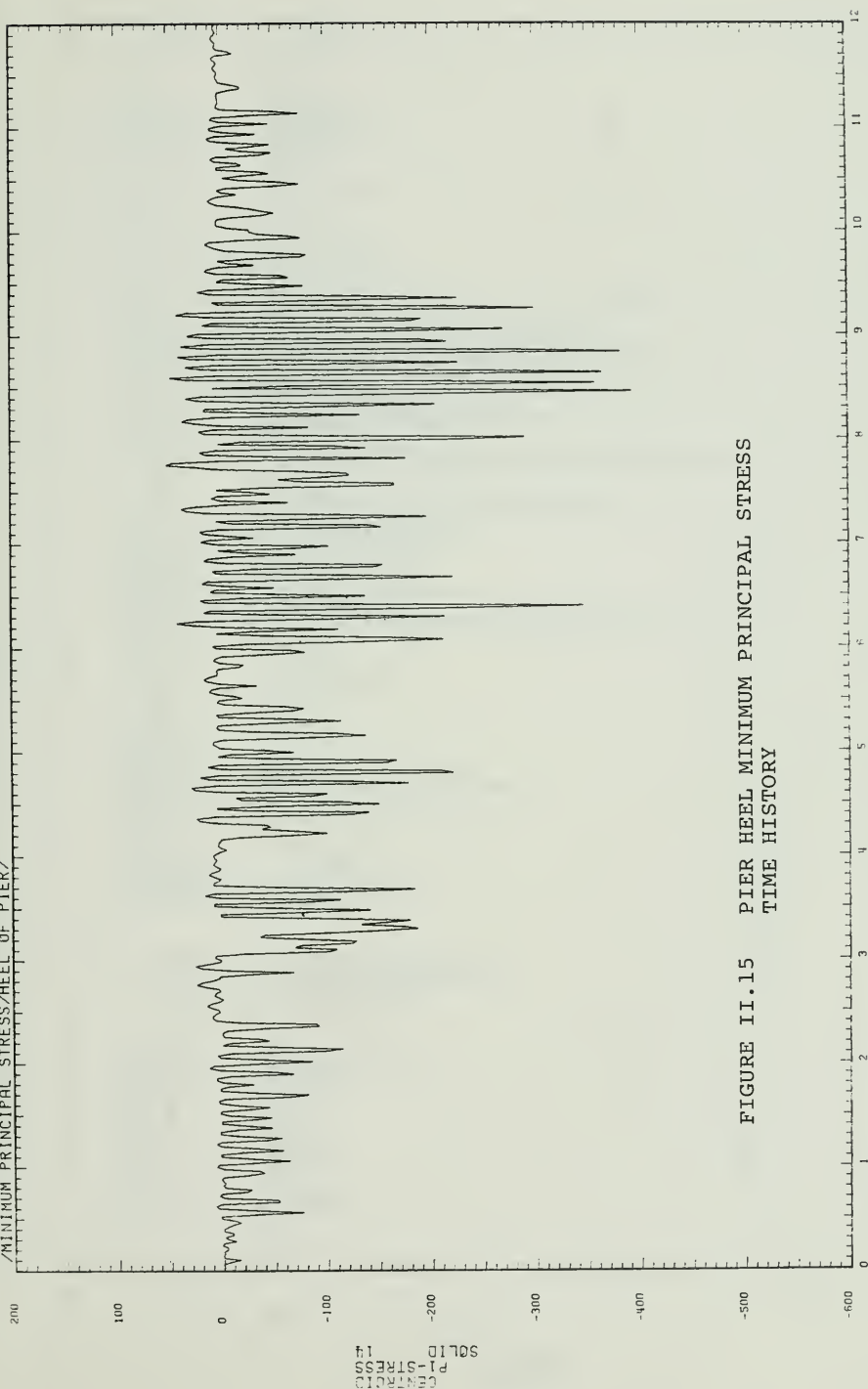


FIGURE II.15 PIER HEEL MINIMUM PRINCIPAL STRESS
 TIME HISTORY

T I M E

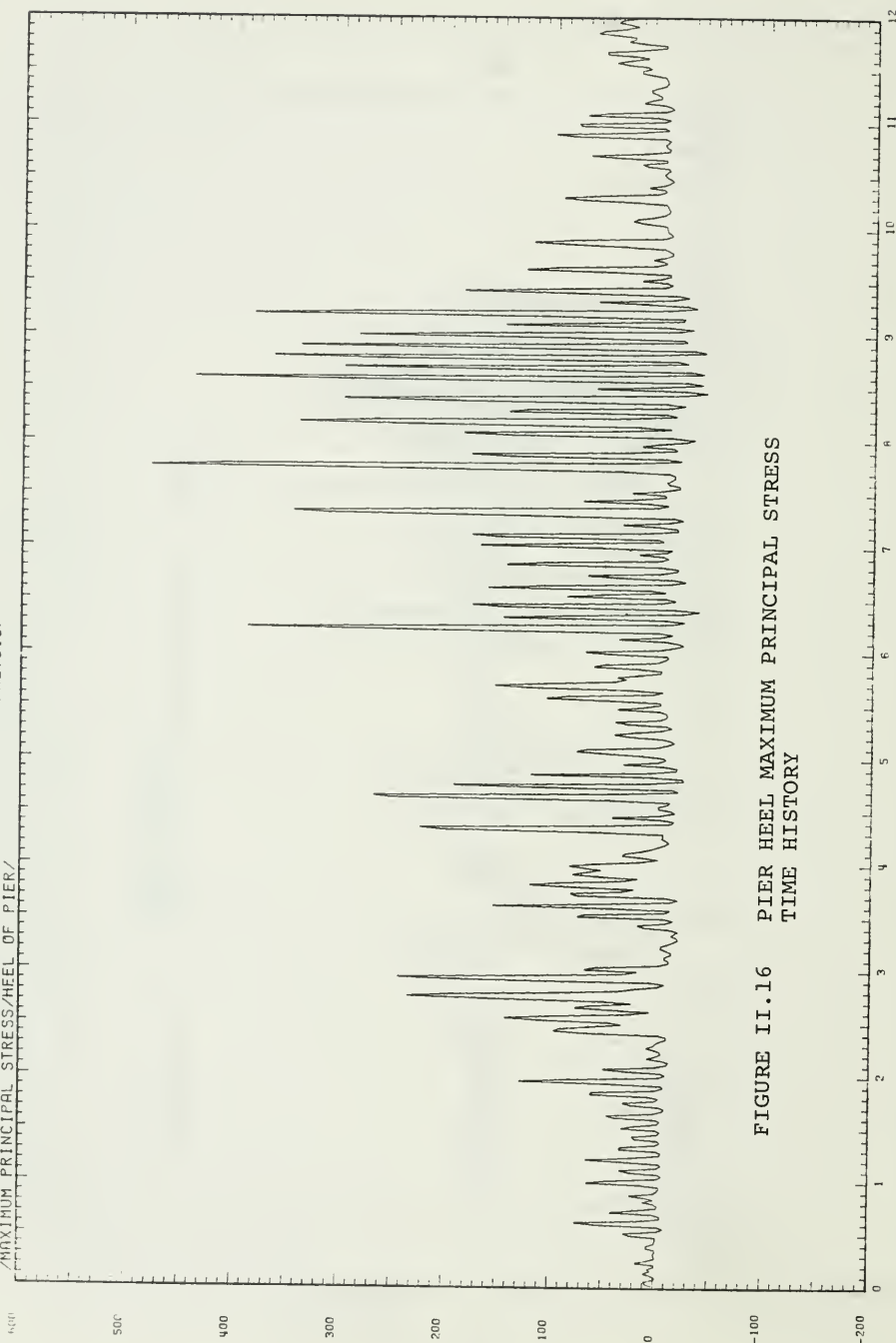


FIGURE II.16 PIER HEEL MAXIMUM PRINCIPAL STRESS
 TIME HISTORY

/STATE OF CALIFORNIA/DEPARTMENT OF WATER RESOURCES/OROVILLE DAM SPILLWAY/
 /STATIC AND DYNAMIC THREE DIMENSIONAL FINITE ELEMENT ANALYSIS/
 /MINIMUM PRINCIPAL STRESS/TOE OF PIER/

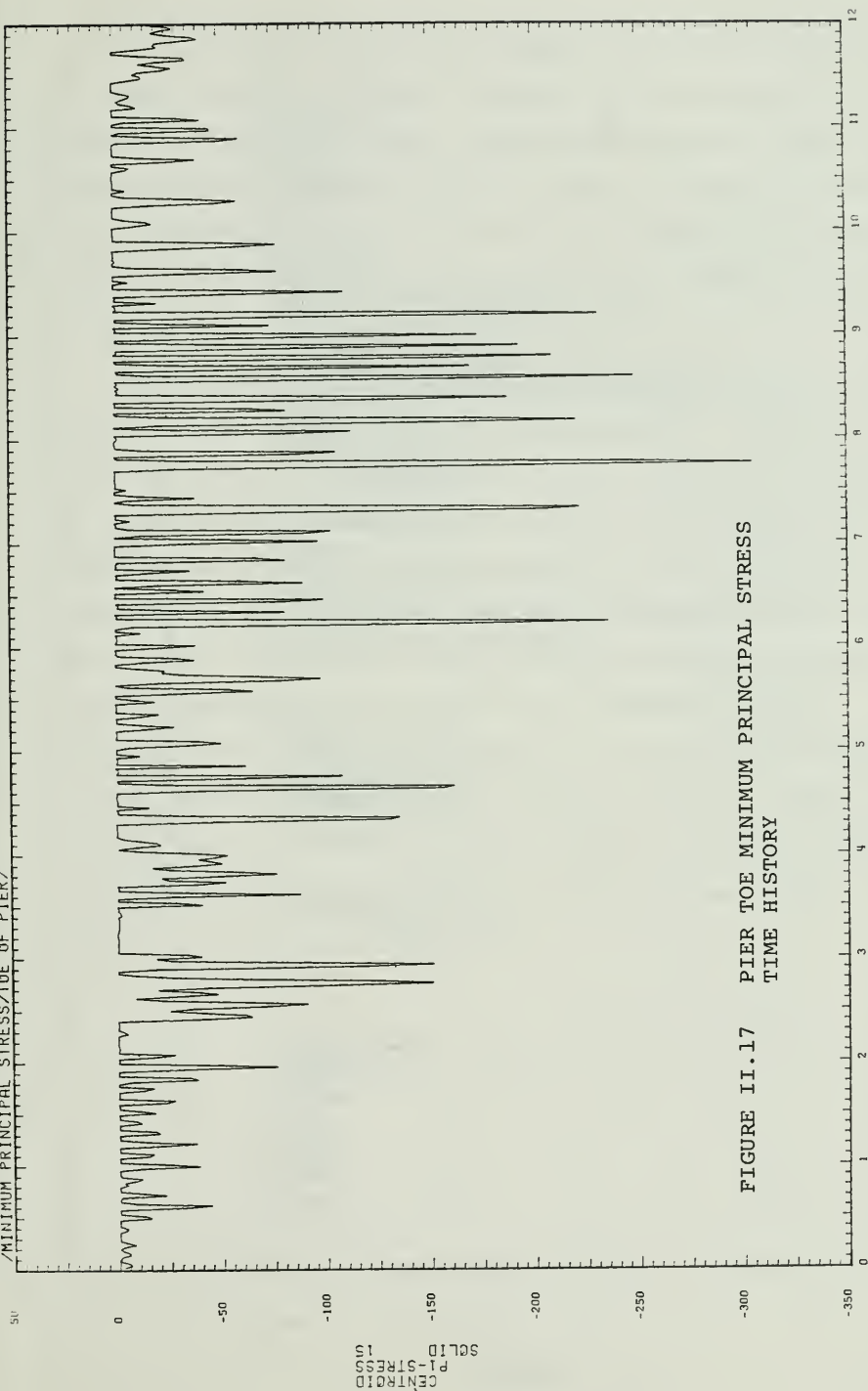


FIGURE II.17 PIER TOE MINIMUM PRINCIPAL STRESS
 TIME HISTORY

T I M E

/STATE OF CALIFORNIA, DEPARTMENT OF WATER RESOURCES, GROSVILLE DAM SPILLWAY/
 /STATIC AND DYNAMIC THREE-DIMENSIONAL FINITE ELEMENT ANALYSIS/
 /MAXIMUM PRINCIPAL STRESS/TOE OF PIER/

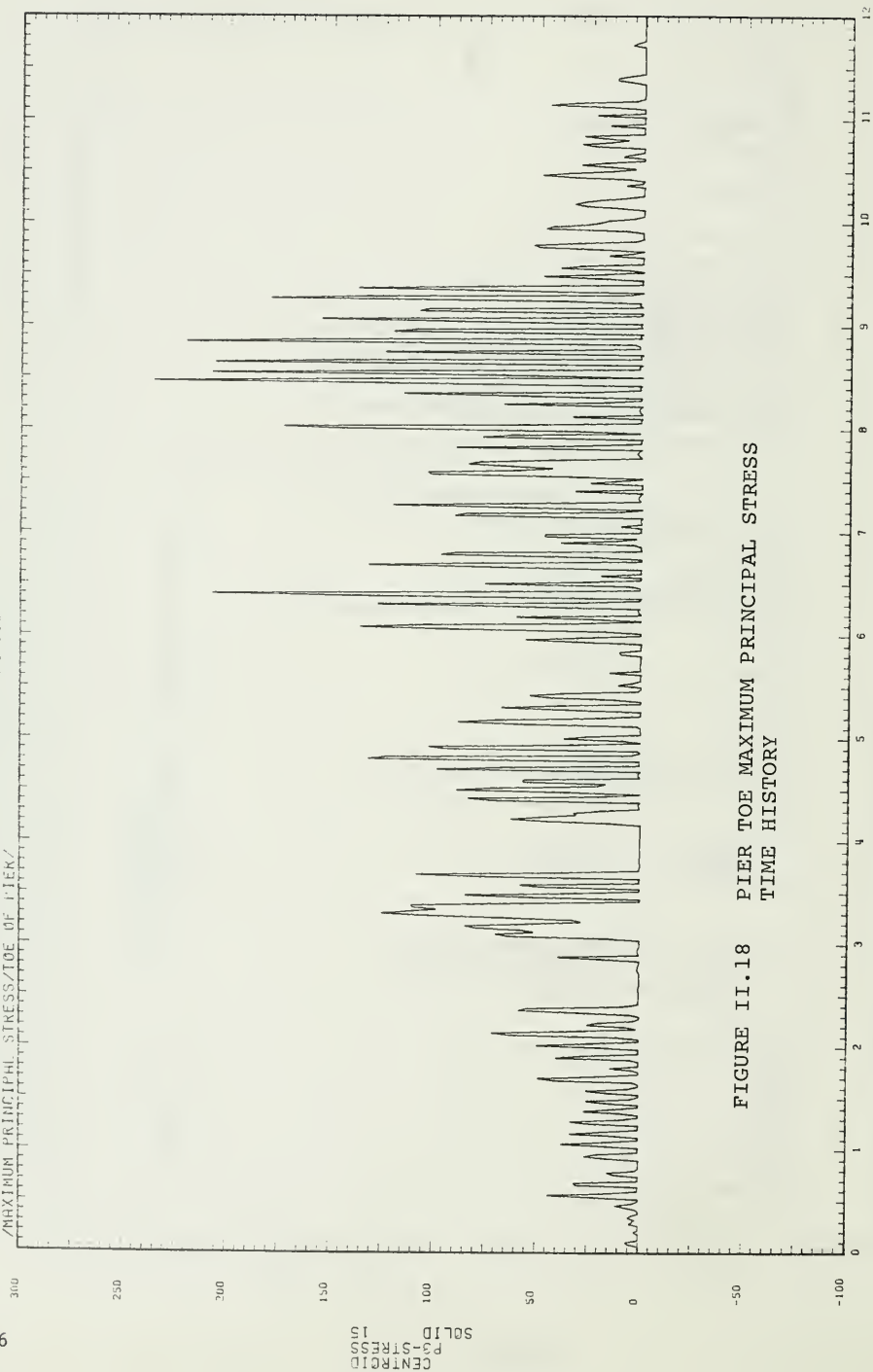


FIGURE II.18 PIER TOE MAXIMUM PRINCIPAL STRESS
 TIME HISTORY

T I M E

plots of minimum and maximum stress, respectively, predicted at the c.g. of element 15 (at the pier "toe"). The peak values of principal stress predicted in the pier heel and toe regions are summarized in Table II.8. Note that the critical values occur at two times: 7.76 and 8.46 seconds. Since the earthquake can act in either the +Z or -Z direction the maximum seismic stresses (irrespective of sign) are 480 psi in the heel and 305 psi in the toe.

Tables II.9 and II.10 list the minimum and maximum principal stresses, respectively, in all pier elements at time 7.76 seconds. Similarly, Tables II.11 and II.12 show the min/max stresses, respectively, developed in the pier at 8.46 seconds. Note that the peak stresses always occur either in the heel or toe. Table II.13 shows the vertical (Y) stress distribution in the pier at time 7.76 seconds. By comparing Tables II.10 and II.13 it is seen that the critical stresses in the pier are nearly vertical in the heel at 7.76 seconds (e.g., in element 14, 480 psi maximum principal versus 464 psi vertical). Also, from the time history analysis the maximum vertical stress in the pier heel (i.e., element 14) was calculated to be 464 psi (see Table II.13); this prediction agrees very well with the 457 psi value predicted by the response spectrum analysis (see Table II.7).

PIER LOCATION	MINIMUM PRINCIPAL STRESS	TIME OF OCCURRENCE	REFERENCE FIGURE NUMBER	MAXIMUM PRINCIPAL STRESS	TIME OF OCCURRENCE	REFERENCE FIGURE NUMBER
HEEL	-394 psi	8.46 sec.	II.15	480 psi	7.76 sec.	II.16
TOE	-305 psi	7.76 sec.	II.17	236 psi	8.46 sec.	II.18

TABLE II.8 PEAK (PRINCIPAL) STRESSES IN THE PIER HEEL AND TOE REGIONS
CAUSED BY MODIFIED PACOIMA AND TAFT SEISMIC INPUT


```

HEADING LINE THREE          = (/MINIMUM PRINCIPAL STRESS/PSI UNITS/TIMESTEP NUMBER 388/
TIME STEP NUMBER           = ( 388)
ELEMENT DISPLAY SET NUMBER = ( 1)
SCALE FACTOR               = ( .1000E+04)
OUTPUT STRESS COMPONENT    = ( 1)
TIME OF OUTPUT             = ( .7760E+01)

```

```

OROVILLE DAM SPILLWAY/ HALF OF TYPICAL RAY/ TIME HISTORY ANALYSIS/
PIER ELEVATION VIEW/ ELEMENTS 001-10-117/
/MINIMUM PRINCIPAL STRESS/PSI UNITS/TIMESTEP NUMBER 388/

```

SOLID ELEMENT CENTROIDAL STRESSES

0	-1	-2	-12	-26	-25	-27	-28	-27	-27			
-1	-5	-11	-20	-35	-42	-45	-50	-54	-62			
-2	-7	-15	-28	-51	-58	-66	-75	-88	-101			
-2	-7	-16	-31	-63	-72	-84	-98	-116	-159			
-2	-7	-16	-35	-75	-87	-101	-117	-137	-136	-81		
-2	-8	-17	-39	-86	-100	-117	-139	-157	-164	-186		
-2	-8	-18	-42	-96	-113	-136	-161	-190	-217	10	-7	-1
-3	-8	-19	-45	-105	-124	-148	-176	-218	-287			-7
5	1	-11	-49	-111	-128	-152	-184	-225	-309			-8
-6	-1	-8	-46	-103	-122	-148	-178	-216	-262	-180	-24	-27
-5	-15	-20	-35	-73	-110	-138	-164	-200	-217	-190	-107	-38
-4	-7	-13	-28	-54	-96	-130	-162	-191	-208	-201	-167	-102
1	1	-3	-20	-49	-86	-123	-156	-183	-200	-205	-206	-247
-8	-3	-4	-12	-42	-74	-117	-150	-175	-193	-203	-219	-254 -305
51	30	19	-4	-36	-75	-113	-146	-172	-198	-201	-222	-243 -228

TABLE II.9 MINIMUM PRINCIPAL STRESSES IN THE PIER
AT TIME 7.76 SECONDS

HEADING LINE THREE = (/MAXIMUM PRINCIPAL STRESS/PSI UNITS/TIMESTEP NUMBER 388/

TIME STEP NUMBER = (388)
 ELEMENT DISPLAY SET NUMBER = (1)
 SCALE FACTOR = (.1000E+04)
 OUTPUT STRESS COMPONENT = (2)
 TIME OF OUTPUT = (.7760E+01)

OROVILLE DAM SPILLWAY/ HALF OF TYPICAL BAY/ TIME HISTORY ANALYSIS/
 PIER ELEVATION VIEW/ ELEMENTS 001-TO-177/
 /MAXIMUM PRINCIPAL STRESS/PSI UNITS/TIMESTEP NUMBER 388/

SOLID ELEMENT CENTROIDAL STRESSES

10	20	14	12	11	11	11	10	7	2				
21	15	15	19	24	22	19	14	7	2				
20	19	20	24	34	29	22	15	8	1				
26	23	23	28	41	32	23	14	5	-1				
32	28	25	31	48	39	29	19	9	12	10			
39	32	27	33	56	46	37	30	34	27	8			
44	40	33	37	66	56	46	41	27	3	47	17	20	
68	60	47	46	78	64	50	30	8	11				0
124	127	96	70	98	68	46	19	2	2				8
224	222	174	119	97	72	44	24	7	6	11	17	5	
267	243	188	135	104	78	54	36	29	38	48	12	2	
312	265	204	149	110	82	61	48	45	50	45	26	6	
364	291	216	155	112	83	64	53	49	45	36	12	-6	
421	309	216	155	110	80	62	52	46	39	24	3	7	3
480	298	214	151	105	74	55	44	38	31	15	-3	-9	-8

TABLE II.10 MAXIMUM PRINCIPAL STRESSES IN THE PIER
 AT TIME 7.76 SECONDS

```

HEADING LINE THREE          = (/MINIMUM PRINCIPAL STRESS/PSI UNITS/TIMESTEP NUMBER 423/
TIME STEP NUMBER            = ( 423)
ELEMENT DISPLAY SET NUMBER  = ( 1)
SCALE FACTOR                = ( .1000E+04)
OUTPUT STRESS COMPONENT    = ( 1)
TIME OF OUTPUT              = ( .8460E+01)

```

```

ODONVILLE DAM SPILLWAY/ HALF OF TYPICAL BAY/ TIME HISTORY ANALYSIS/
PIER ELEVATION VIEW/ ELEMENTS 001-10-177/
/MINIMUM PRINCIPAL STRESS/PSI UNITS/TIMESTEP NUMBER 423/

```

SOLID ELEMENT CENTROIDAL STRESSES

-31	-20	-15	-13	-12	-12	-12	-10	-7	-2				
-20	-16	-16	-20	-25	-23	-19	-14	-7	-2				
-22	-21	-21	-25	-34	-28	-21	-14	-7	-1				
-29	-26	-24	-28	-34	-30	-21	-12	-4	1				
-35	-30	-26	-29	-44	-35	-25	-15	-7	-9	-8			
-42	-33	-27	-30	-49	-39	-30	-24	-28	-23	-7			
-50	-40	-31	-33	-55	-46	-37	-33	-20	3	-32	-13	-18	
-68	-59	-43	-39	-64	-51	-39	-22	-2	-8			0	
-121	-119	-96	-89	-70	-52	-32	-11	0	1			-6	
-215	-210	-153	-96	-74	-53	-30	-14	-1	-1	-4	-11	-4	
-247	-217	-163	-110	-79	-57	-37	-23	-18	-26	-35	-8	-2	
-278	-231	-174	-121	-83	-59	-42	-33	-32	-36	-33	-20	-5	
-312	-248	-182	-126	-85	-59	-44	-37	-34	-33	-26	-9	5	
-351	-261	-181	-126	-83	-56	-42	-35	-31	-27	-17	-3	-5	-2
-394	-251	-174	-123	-79	-51	-35	-28	-24	-20	-9	3	7	6

TABLE II.11 MINIMUM PRINCIPAL STRESSES IN THE PIER
AT TIME 8.46 SECONDS

HEADING LINE THREE = (/MAXIMUM PRINCIPAL STRESS/PSI UNITS/TIMESTEP NUMBER 423/
 TIME STEP NUMBER = (423)
 ELEMENT DISPLAY SET NUMBER = (1)
 SCALE FACTOR = (.1000E+04)
 OUTPUT STRESS COMPONENT = (2)
 TIME OF OUTPUT = (.2460E+01)

OROVILLE DAM SPILLWAY/ HALF OF TYPICAL DAY/ TIME HISTORY ANALYSIS/
 PIER ELEVATION VIEW/ ELEMENTS 001-TO-177/
 /MAXIMUM PRINCIPAL STRESS/PSI UNITS/TIMESTEP NUMBER 423/

SOLID ELEMENT CENTROIDAL STRESSES

0	1	3	9	20	24	26	27	28	26				
1	4	10	19	33	37	42	47	51	60				
2	6	13	25	47	53	61	69	82	95				
1	6	14	28	56	65	75	89	106	148				
1	6	13	30	65	76	89	104	124	124	75			
2	6	14	32	73	85	101	122	140	148	170			
1	6	13	33	79	94	115	139	166	193	-5	6	2	
2	6	13	34	82	100	123	148	188	251			9	
-5	-4	3	31	87	100	123	153	192	265			9	
5	-2	-1	23	70	92	117	147	180	202	150	18	24	
4	0	0	16	46	80	107	136	164	178	155	86	28	
3	2	3	11	34	67	99	129	155	169	162	133	79	
0	-1	-1	4	26	59	92	122	147	161	164	163	192	
7	3	3	2	21	53	86	117	140	154	161	173	197	236
-43	-26	-18	-8	16	49	83	113	136	150	160	175	189	177

TABLE II.12 MAXIMUM PRINCIPAL STRESSES IN THE PIER AT TIME 8.46 SECONDS

```

HEADING LINE THREE          = (/VERTICAL STRESS IN PIER/Y-DIRECTION/PSI UNITS/TIME STEP NUMBER 388/
TIME STEP NUMBER            = ( 388)
ELEMENT DISPLAY SET NUMBER  = ( 1)
SCALE FACTOR                = ( .1000E+04)
OUTPUT STRESS COMPONENT     = ( 2)
TIME OF OUTPUT              = ( .7760E+01)

```

```

DROVILLE DAM SPILLWAY/ HALF OF TYPICAL BAY/ TIME HISTORY ANALYSIS/
PIER ELEVATION VIEW/ ELEMENTS 001-10-177/
/VERTICAL STRESS IN PIER/Y-DIRECTION/PSI UNITS/TIME STEP NUMBER 388/

```

SOLID ELEMENT CENTROIDAL STRESSES

17	14	12	10	7	5	2	-1	-5	-13										
15	14	13	15	16	10	2	-8	-20	-36										
20	18	18	19	21	11	-2	-18	-38	-61										
26	23	21	22	25	11	-7	-28	-52	-91										
32	27	23	23	28	9	-14	-39	-71	-71	-42									
39	31	25	24	31	7	-20	-52	-74	-96	-163									
48	39	30	26	33	5	-27	-57	-95	-159	14	-6	9							
67	58	42	30	35	0	-34	-73	-127	-191									-3	
120	120	84	42	28	-10	-51	-99	-144	-197									-4	
221	223	159	77	20	-17	-64	-107	-150	-154	-80	-4	-24							
266	235	171	97	32	-19	-63	-106	-141	-148	-113	-68	-36							
311	255	181	108	41	-16	-63	-103	-132	-140	-131	-125	-98							
362	277	189	113	46	-13	-61	-98	-124	-136	-140	-158	-230							
416	290	190	115	49	-10	-57	-94	-119	-133	-145	-179	-221	-244						
464	280	191	117	51	-7	-54	-90	-115	-133	-152	-185	-209	-188						

TABLE II.13 VERTICAL (Y) STRESSES IN THE PIER
AT TIME 7.76 SECONDS

III. TWO DIMENSIONAL ANALYSIS WITH HYDRODYNAMIC INTERACTION

A. three dimensional dynamic analysis which includes hydrodynamic interaction is beyond present research development for a structure of this type. It is possible to estimate the magnitude of this effect from the analysis of a two dimensional model with similar dynamic properties.

A. Analysis Without Interaction

A two dimensional finite element model was selected with the same mesh idealization as used in three dimensional model of the pier (Figure II.5). Normal concrete properties were used except the weight density was scaled so that the fundamental period of the two dimensional model was the same as the fundamental period of the three dimensional model without hydrodynamic interaction. From Table III.1 one notes that the maximum stresses obtained from this two dimensional model are in excellent agreement with the three dimensional analysis. This confirms the results from the three dimensional analysis which indicated very low stresses in the breast wall.

B. Analysis With Interaction

The analysis of the two dimensional model with hydrodynamic interactions was accomplished using the following program:

*EADHI - "A Computer Program for Earthquake Analysis of Gravity Dams Including Hydrodynamic Interaction," by P. Chakradarti and A. K. Chopra, May 1968, College of Engineering, U.C. Berkeley, California.

From Table III.1 the results indicate an increase in critical stresses at the toe and heel of approximately 20 percent due to hydrodynamic interaction.

LOCATION	3/D ANALYSIS W/O HYDRODYNAMIC INTERACTION		2/D ANALYSIS W/O HYDRODYNAMIC INTERACTION		2/D ANALYSIS W/ HYDRODYNAMIC INTERACTION	
	$\sigma_{\max}/\text{time}$	$\sigma_{\min}/\text{time}$	$\sigma_{\max}/\text{time}$	$\sigma_{\min}/\text{time}$	$\sigma_{\max}/\text{time}$	$\sigma_{\min}/\text{time}$
HEEL ELEMENT 14	480 / 7.76	394 / 8.46	496 / 7.76	419 / 8.46	596 / 7.76	570 / 8.46
TOE ELEMENT 15	236 / 8.46	305 / 7.76	269 / 8.46	330 / 7.76	366 / 8.46	398 / 7.76

TABLE III.1 SUMMARY OF ANALYSIS

C. Extension to Three Dimensional Analysis

A reasonable engineering approximate solution to the three dimensional hydrodynamic interaction is to apply the ± 20 percent correction to the results obtained from the three-dimensional analysis without interaction. This is a suggested approach for a horizontal earthquake. The effects of hydrodynamic interaction due to a vertical earthquake have not been considered.

IV. TRANSVERSE EARTHQUAKE ANALYSIS

The monoliths of the flood control outlet structure are separated by contraction joints. The actual size of these joints must be measured in the field. The monoliths which do not contain gates are solid and are short relation to the two monoliths with gates. Therefore, it is reasonable to evaluate the stresses in the gate monoliths only due to a transverse earthquake. Because of the special geometry of these structures the maximum possible transverse displacement would be equal to the size of two contraction joints regardless of the magnitude of the earthquake.

Furthermore, transverse displacement of the gate monoliths will cause bending in the piers between the foundation and the roof of the intake which is a distance of approximately 34 ft. A good estimate of bending developed in the pier can be calculated by assuming the pier to act as a fixed end beam subjected to a support displacement equal to the size of two construction joints. For a 5 ft. pier, the extreme fiber strain will be 0.0012Δ where Δ is the contraction joint displacement. Since these piers are reinforced a damage evaluation can be made from normal reinforced concrete theory.

V. VERTICAL EARTHQUAKE

For a structure of this type the modes of vibration which have significant vertical components have a very high frequency--greater than 50 cycles per second. For this high frequency the structure moves as a rigid body at the earthquake acceleration. Therefore, a very good approximation of the maximum stresses due to vertical earthquakes can be calculated by multiplying the gravity stresses by the maximum acceleration (given as a fraction of gravity).

The vertical stresses due to gravity are given in Table II.1. If the maximum acceleration due to a vertical earthquake was 30% of gravity the vertical stress at the heel will vary ± 90 psi or from -210 psi to -390 psi.

VI. FINAL REMARKS

This report summarizes the results of a three dimensional finite element analysis of the Oroville Dam Flood Control Outlet Structure. Hydrostatic, prestress, gravity and horizontal earthquake results are presented separately. In addition, approximate methods of analysis are given for hydrodynamic interaction and for transverse and vertical earthquake behavior.

CHAPTER VII
SEISMIC ANALYSIS OF THE
THERMALITO DIVERSION DAM

Commentary

As a result of the August 1, 1975 Oroville earthquake, of magnitude 5.7, the Department found it appropriate to reanalyze the Thermalito Diversion Dam (Figures 187 and 188) using a stronger earthquake (see Chapter V), and the latest techniques in seismic investigation.

An earthquake study, monitored by the Department, was conducted under a consulting agreement with Dr. Anil K. Chopra. Dr. Chopra's results and conclusions were presented in his report, "Earthquake Response Analysis of Thermalito Diversion Dam". That report is presented in this chapter (beginning on page 355).

Dr. Chopra performed a dynamic two-dimensional response analysis of the dam using the finite-element method. The Department agrees with the methods used and conclusions presented in his report.

The Department investigated the Dam for sliding, utilizing the shear-friction equation

$$Q = \frac{CA + N \tan \phi}{H}. \quad \text{A cohesion value, } C = 3447$$

kPa (500 psi), produced a shear-friction factor of approximately 5. This is considered a safe value against sliding.

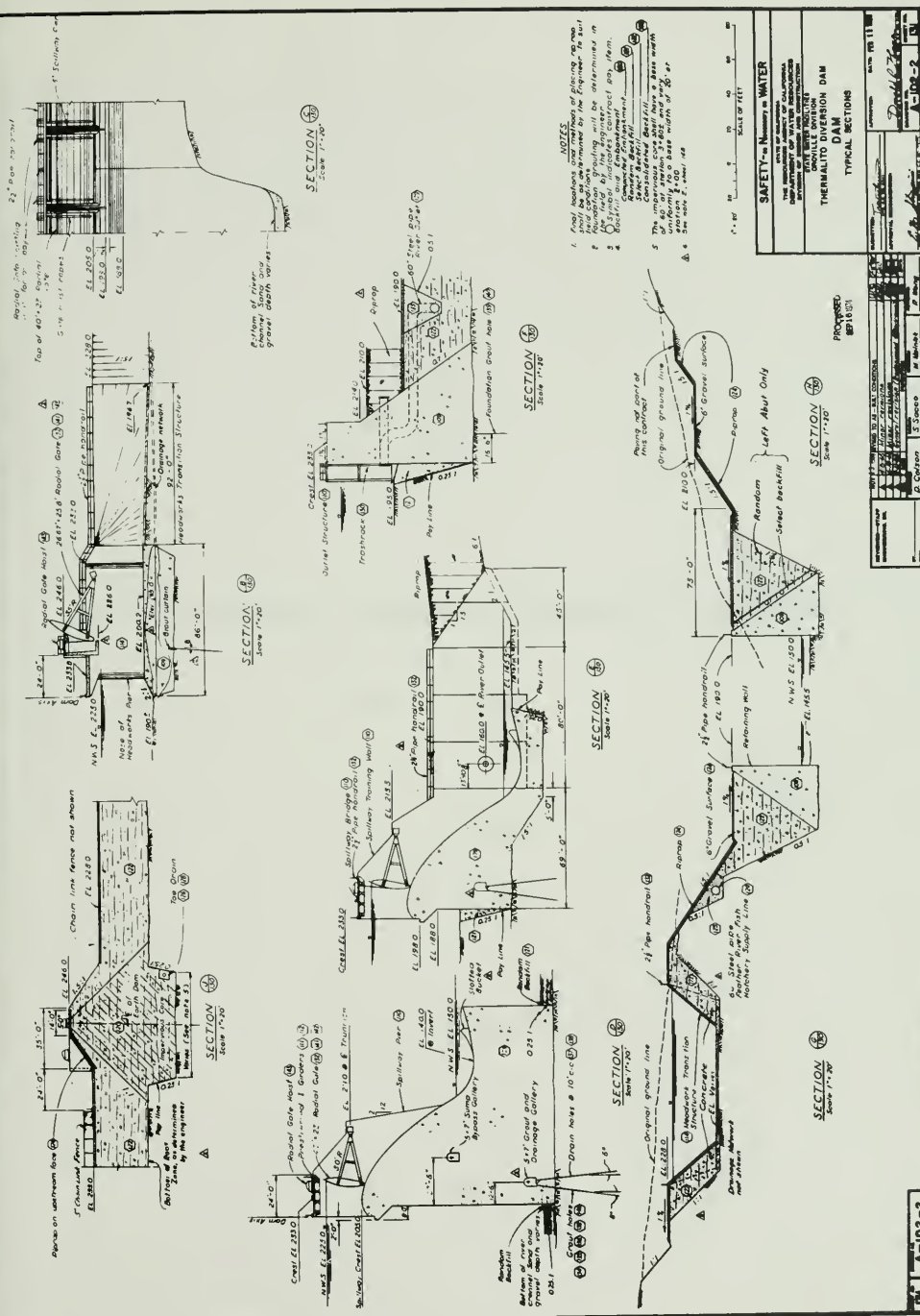


Figure 188. Typical Sections

EARTHQUAKE RESPONSE ANALYSIS OF THERMALITO DIVERSION DAM

by

Anil K. Chopra

EARTHQUAKE RESPONSE ANALYSIS OF THERMALITO DIVERSION DAM

by

Anil K. Chopra

Introduction

The Department of Water Resources, State of California, entered into an agreement with Dr. A. K. Chopra to "perform structural analysis using finite element techniques of Thermalito Diversion Dam". The agreement stipulated that "the analysis will employ the most suitable dynamic methods applicable to the specific structures".

Results of this analysis for the ground motion specified by the Department of Water Resources, State of California, are presented in this report.

The scope of the work necessary for structural analysis of Thermalito Diversion Dam was first discussed and outlined in a preliminary meeting between Dr. Chopra and Denzil Carr of the State Department of Water Resources. Subsequently, results from preliminary analyses were discussed at a meeting on September 7, 1976 between Dr. Chopra and Messrs. Sam Linn, Edgar Najera, and Vernon Persson of the State Department of Water Resources. The series of analyses and results required by the State Department of Water Resources were defined. In accordance with these requirements, a draft report was submitted on November 4, 1976.

Messrs. Linn, Najera and Don Steinwert, State Department of Water

Resources, commented on the draft report at a meeting on February 25, 1977 with Dr. Chopra.

The draft report has been revised and expanded to account for these comments, resulting in this final report.

The draft report of November 4, 1976 was based on analyses of the dam for the ground motion originally recommended by the Special Consulting Board for the August 1, 1975 Oroville Earthquake (Fig. 1). The Board made supplementary recommendations regarding ground motions to be considered in their report of November 23, 1976. After a study of this supplementary recommendation, it was concluded in a report of March 4, 1977 (see Appendix) that, for analysis of Thermalito Diversion Dam and Oroville Dam Flood Control Outlet Structure, there is no need to supplement the ground motion originally recommended by the Board, for which the structures had already been analyzed. All results presented in the main body of this report are therefore based on analyses for the original ground motion.

Finite Element Models

The dynamic response analysis of gravity dams is done by the finite element method, assuming that monoliths act independently of each other and in a condition of plane stress; in practice a one-foot thick slice of the dam is analyzed. If the foundation material is significantly softer than the dam concrete, then it may have a significant effect on the dynamic behavior of the dam and must be included in the finite element idealization. In the case of Thermalito Diversion Dam, however, the properties of the foundation rock are such that it should have only insignificant influence on the dynamic response of the dam. Furthermore the degree to which the response is affected depends strongly on the depth of rock included in the finite element model, and where rock essentially similar to the rock under the dam and near the ground surface may be asumed to extend to great depths -- as in the present case -- there is no rational basis for defining the limits of the finite element model. Consequently, in this investigation the

concrete monoliths were assumed to be supported on a rigid base, and the specified earthquake ground motion was applied at the base. It was concluded that no greater reliability in the dynamic response results could have been achieved by including an arbitrary layer of rock under the monoliths in the finite element model, even though it is common practice to include such a layer in performing purely static analysis.

The finite element models defined for the analysis of monoliths 10, 12 and 18 are shown in Figs. 2-5. They all employ the isoparametric quadrilateral element used in the SAP program developed by Professor E. L. Wilson at the University of California, Berkeley. They have graded meshes, with slender elements near the monolith faces to better define the stresses in those regions. In each case, the number of elements through the upstream-downstream direction and the number of rows of elements through the height, are considered to be sufficient to provide good definition of the stress, especially in the critical zones.

Two different finite element models were used to represent monolith 12: The one shown in Fig. 2 which includes only the monolith itself was defined for purposes of preliminary analysis. The other shown in Fig. 3 includes an approximate two-dimensional model of the appurtenances: pier, bridge and radial gate. This model, although not appropriate for determining the details of dynamic response of the appurtenances themselves, is believed to be adequate to represent effects of the appurtenances on the dynamic response of the monolith, which is the main concern of this investigation.

The modulus of elasticity of the finite elements included in the model of Fig. 3 to represent the piers was set at $5/45$ (=width of pier/width of monolith) of the value for concrete. The density of these elements was set in a slightly different ratio to include the weight of the radial gate and other equipment. For the top-most row of elements, the density was increased to include the weight of the bridge, but the modulus of elasticity was taken as that of the concrete

The static and dynamic analysis of all finite element models were performed by the computer program EADHI¹ developed at the University of California, Berkeley. This program includes the effects of interaction between the dam and water, and of water compressibility.

The properties of concrete were taken as those provided by the Department of Water Resources, State of California, for the 2-1/2 sack mix, which is used throughout the monoliths except for a small thickness near the exposed surfaces and galleries:

- Modulus of Elasticity = 5.1×10^6 psi
- Poisson's Ratio = 0.17
- Unit Weight = 155 pcf

Earthquake Response Analysis

Before proceeding with analysis of the dam, the computer program EADHI was extended to handle water level above the crest of a monolith. This capability is necessary to analyze overflow monoliths 10 and 12.

Several preliminary results were generated to obtain an overall impression of the dynamic response of the dam. For this purpose the finite element model of Fig. 2 for monolith 12, excluding the appurtenances, was analyzed.

The frequencies of the first three natural modes of vibration are shown in Table 1. It is apparent that the dam has rather high vibration frequencies.

Stress analyses were performed considering the static loads assumed to be acting prior to occurrence of an earthquake. These include the dead weight of the monolith, and the hydrostatic pressure of the water when the reservoir is at the normal level (El. 225).

The dynamic response of the finite element model of Fig. 2 to the specified ground motion (Fig. 1) assumed to act in the upstream-downstream direction was determined. Only those modes with frequencies less than 30 Hz were considered

Table 1: Natural Frequencies of Vibration of
Monolith 12 without Appurtenances

Mode No.	Natural Frequencies, cps	
	Dam Only	Dam with Water at EL. 225.0
1	14.5	8.5
2	30.4	29.1*
3	34.8	28.9*

* The natural vibration modes of the dam without water are numbered according to standard convention: The natural mode having the lowest vibration frequency is called the first mode, that having the next higher frequency is the second mode, etc. Because hydrodynamic interaction effects depend on the frequency and shape of the vibration mode², the vibration frequencies of the three modes of the dam are not in increasing order when effects of water are considered. However, this is of no consequence in the analysis, because all the modes which have significant contributions to the total response are included.

in the dynamic response analysis, because the earthquake motions are not defined accurately for higher frequencies. Analysis by the computer program EADHI leads to the time history of horizontal and vertical displacements at all nodal points of the finite element system and the time history of the three components of total stress -- static plus dynamic -- in all finite elements. Only a small portion of these results which is most pertinent to evaluating safety of the dam is included here.

Fig. 6 shows the contours of "envelope" values of the maximum principal stress. These are peak values of maximum principal stress -- the most tensile stress -- developed in each element at any time during the earthquake; they are not all concurrent values. The static stresses have been combined with the dynamic stresses (taking proper account of the tensorial nature of the stress components) so that these contours indicate the absolute magnitude of the tensile stresses that must be resisted by the monolith during the earthquake. Of major significance are the zones of tensile stress at the downstream face just above the bucket and at the upstream edge of the base. The latter zone is in part a consequence of the discontinuity between the concrete and the assumed rigid base. It is in part the result of a singularity in the mathematical model under study and that part could be removed by changing the mathematical model. However, this singularity is of little concern in this case because the maximum tensile stress is about 310 psi, which, as will be discussed later, is considerably below the tensile strength of concrete.

The final results of critical stresses in Monoliths 10, 12 and 18 which are obtained from dynamic analysis of the response of finite element models of Figures 3-5 produced by the specified ground motion (Fig. 1) are presented next.

Fig. 7 shows the contours of "envelope" values of the maximum principal stresses in Monolith 12. These are total stresses including those due to static loads. As mentioned earlier, the two-dimensional finite element model for the

appurtenances above the monolith is suitable for including their effects on stresses in the monolith, but is too crude for determining the response of the appurtenances themselves. Consequently stresses in the appurtenances are not presented. Of major significance in Fig. 7 are the zones of tensile stress on the downstream face just above the bucket and the upstream edge of the base. It is of interest to note that these envelope values of stresses do not differ significantly from those computed without including the effects of appurtenances (Fig. 6).

In order to further examine the response, contours of the instantaneous maximum tensile stresses are presented in Figs. 8 and 9 at two instants of time: when the tensile stresses on the downstream face attain their peak value (7.35 secs after beginning of the earthquake motion) and when the tensile stresses at the upstream edge of the base reach their peak value ($t = 8.47$ secs). It is apparent that at each of these time instants, stresses in a significant portion of the dam are compressive.

Fig. 10 shows the contours of "envelope" values of the minimum principal stresses -- the most compressive stresses -- developed in each element at any time during the earthquake, including both static and earthquake effects.

The corresponding contours of "envelope" values of the maximum and minimum principal stresses for Monolith 10 are shown in Figs. 11 and 12 and those for Monolith 18 in Figs. 13 and 14. These are similar in general form to the results obtained for Monolith 12 but are significantly smaller in magnitude. These shorter monoliths, which have very high natural vibration frequencies, do not respond dynamically to any great extent.

Summary of Results

The principal features of these dynamic analysis results may be summarized as follows:

1. The maximum compressive stresses (Figs. 10, 12 and 14) due to both static and dynamic effects were about 200, 425 and 350 psi respectively in Monoliths 10, 12 and 18. These are well within the capacity of this concrete and constitute no cause for further consideration.
2. The maximum tensile stresses due to both static and dynamic effects were about 200, 310 and 225 psi respectively in Monoliths 10, 12 and 18. Later, these will be compared with the tensile strength of concrete.

Tensile Strength of Concrete

Although standard criteria for design of concrete dams do not allow tensile stresses of these magnitudes, evidence is available to support the conclusion that significant dynamic stresses in tension can be supported by sound concrete. Experiments conducted in Japan^{3,4} showed that static tensile strength of concrete is about 8 to 9 percent of the static compressive strength, which is similar to the usual assumption of a 10 percent ratio. Moreover, under dynamic conditions, at loading rates to be expected in concrete gravity dams subjected to intense earthquake motions, these experiments showed that the concrete strengths are significantly -- up to 50 percent -- higher (both in tension and compression) than under static loading. Similarly, recent tests in the United States on mass concrete cores from three dams showed, on the average, a corresponding increase in tensile strength of 67 percent⁵.

Further evidence of the dynamic tensile strength of concrete was provided by the performance of Pacoima Dam during the San Fernando Earthquake of 1971. The ground motion experienced by this structure must have been very intense; accelerations exceeding 1g were recorded near the dam. Analyses carried out at University of California, Berkeley, of dynamic response to that motion indicated that the dam must have developed maximum tensile stresses in the order of 750 psi. Yet no evidence of cracking could be found on either face of the dam.

On the basis of both the laboratory test data and the experience at Pacoima Dam, it is reasonable to assume that the concrete in Thermalito Diversion Dam can resist tensile stresses of at least 10 percent of the static compressive strength, increased by 50 percent to account for the faster loading rates during vibration of the dam.

Comparison of Analytical Results and Tensile Strength

As mentioned earlier, the maximum compressive stresses predicted by analyses are well within the capacity of concrete and are therefore of no concern.

The corresponding maximum tensile stresses in various parts of Monoliths 10, 12 and 18 are summarized in Table 2. Also included are the static compressive strength values, provided by the State Department of Water Resources, and estimates for dynamic tensile strength, based on the preceeding section of this report, for the four concrete mixes employed in the dam (Fig. 15).

It is apparent that the tensile stresses predicted by analyses are less than one-half of the tensile strength of the concrete. The concrete is therefore capable of safely resisting these tensile stresses.

The earthquake ground motion specified by the State Department of Water Resources, for which only a single horizontal component of motion was provided, is the excitation for which all the analyses presented above were carried out. However, research studies² have shown that the contributions of the vertical component of ground motion to the response of concrete gravity dams are significant. Even for vertical ground motion, hydrodynamic pressures act in nearly the horizontal direction on a nearly vertical upstream face, thus causing lateral response. Although this additional lateral response can be quite significant for short dams, the available margin in tensile strength (see Table 2) should be sufficiently large to keep the total (due to horizontal

Table 2: Comparison of Analytical Results and Tensile Strength

Part of the Dam	Concrete Mix	Static Compressive Strength, psi	Dynamic Tensile Strength, psi	Maximum Tensile Stress		
				Monolith 10	Monolith 12	Monolith 18
Interior	2 $\frac{1}{2}$ sack	3500	525	150	250	150
Upstream Face	3 sack	4500	675	200	310	225
Downstream Face	3 $\frac{1}{2}$ sack	5000	750	75	200	170
Ogee & Bucket	4 sack	5800	870	[†] NA	240	[†] NA

[†] Not applicable

and vertical ground motion) tensile stresses within the available tensile strength.

Conclusion

Based on results of dynamic analyses and available data for concrete strength it is concluded that Thermalito Diversion Dam should be able to resist the stresses expected during the earthquake ground motion specified by the State Department of Water Resources.

References

1. Chakrabarti, P., and Chopra, A.K., "A Computer Program for Earthquake Analysis of Gravity Dams Including Hydrodynamic Interaction," Report No. EERC 73-7, Earthquake Engineering Research Center, University of California, Berkeley, May 1973.
2. Chakrabarti, P., and Chopra, A.K., "Earthquake Response of Gravity Dams Including Reservoir Interaction Effects," Report No. EERC 72-6, Earthquake Engineering Research Center, University of California, Berkeley, December 1972.
3. Hatano, T., and Tsutsumi, H., "Dynamical Compressive Deformation and Failure of Concrete Under Earthquake Load," Report No. C-5904, Central Research Institute of Electric Power Industry, Tokyo, September 30, 1959.
4. Hatano, T., "Dynamical Behavior of Concrete Under Impulsive Tensile Load," Report No. C-6002, Central Research Institute of Electric Power Industry, Tokyo, November 5, 1960.
5. Raphael, J.M., "The Nature of Mass Concrete in Dams," Douglas McHenry Symposium Volume, American Concrete Institute, Detroit, Michigan, 1977.

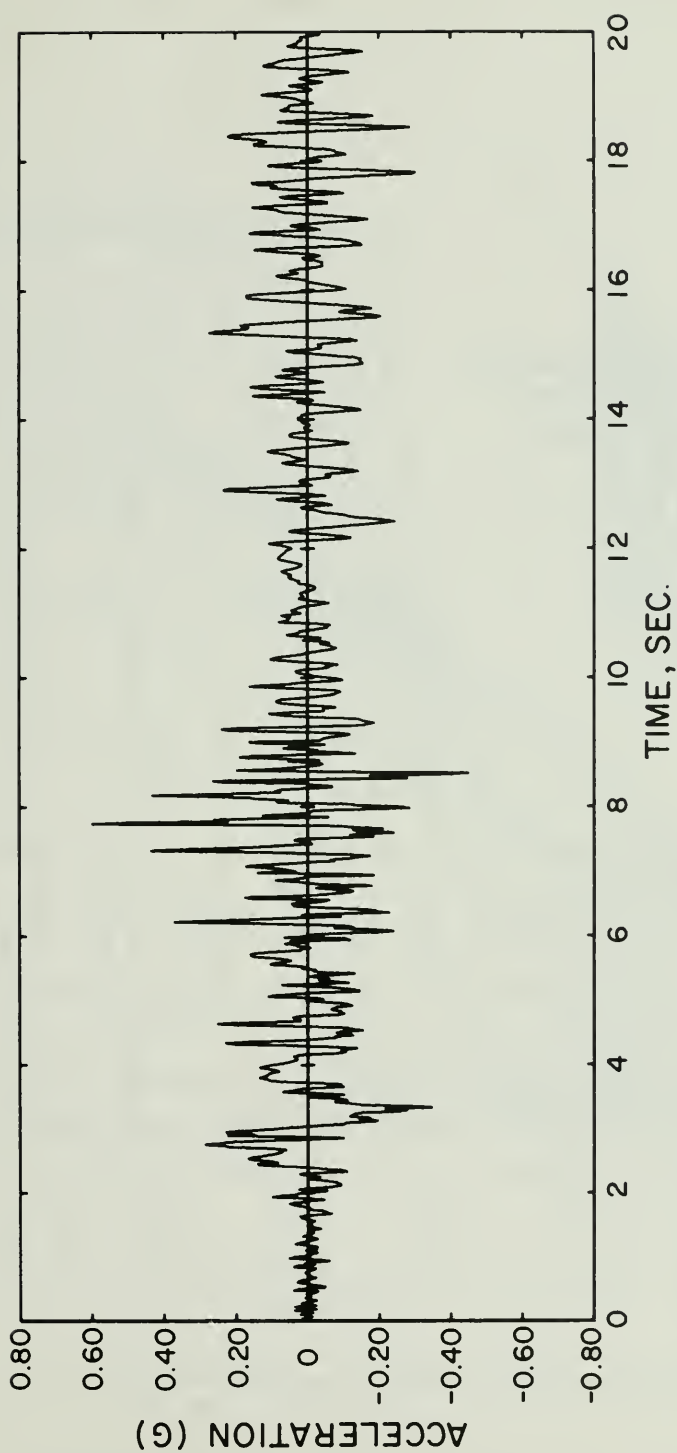


Fig. 1 Horizontal Ground Acceleration Specified by the Department of Water Resources, State of California

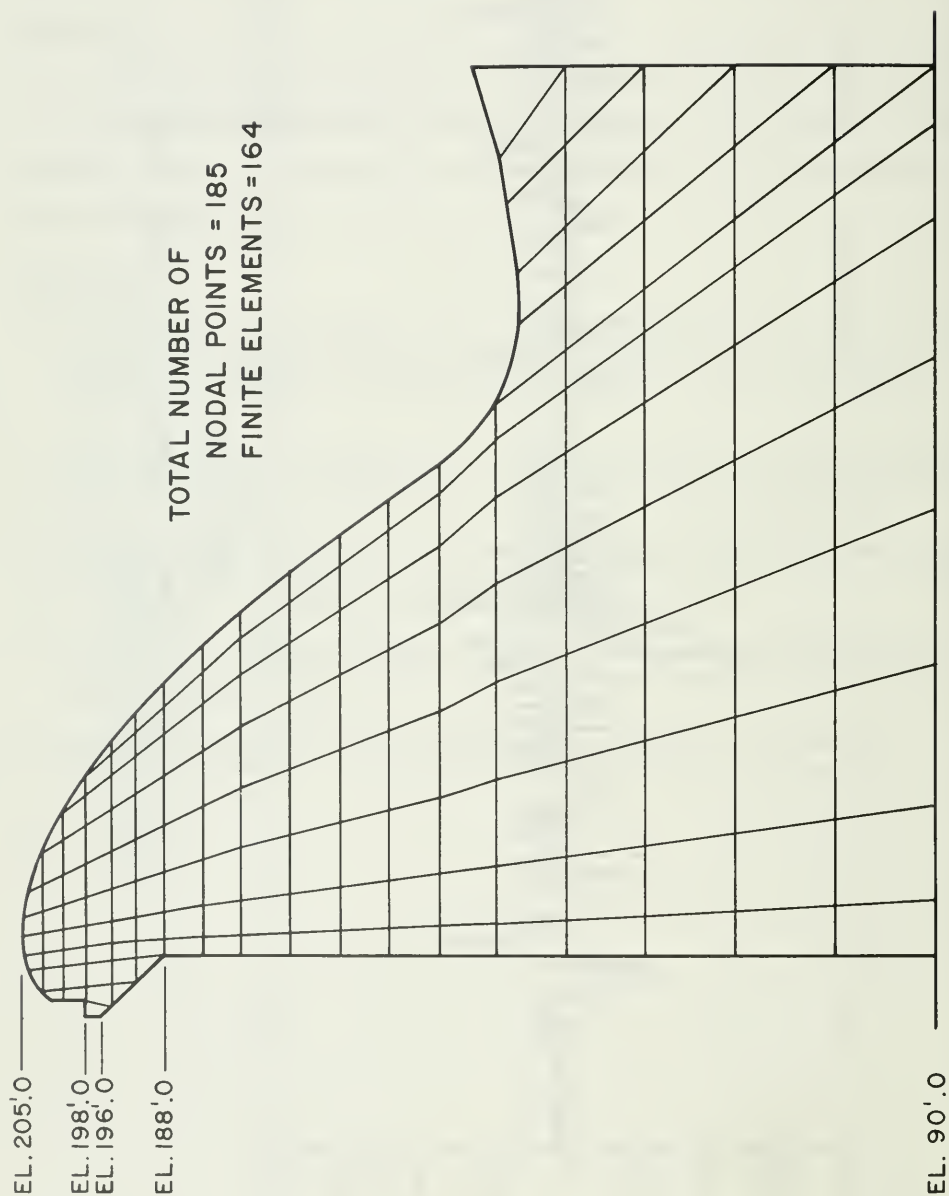


Fig. 2 Finite Element Mesh: Monolith 12 without Appurtenances

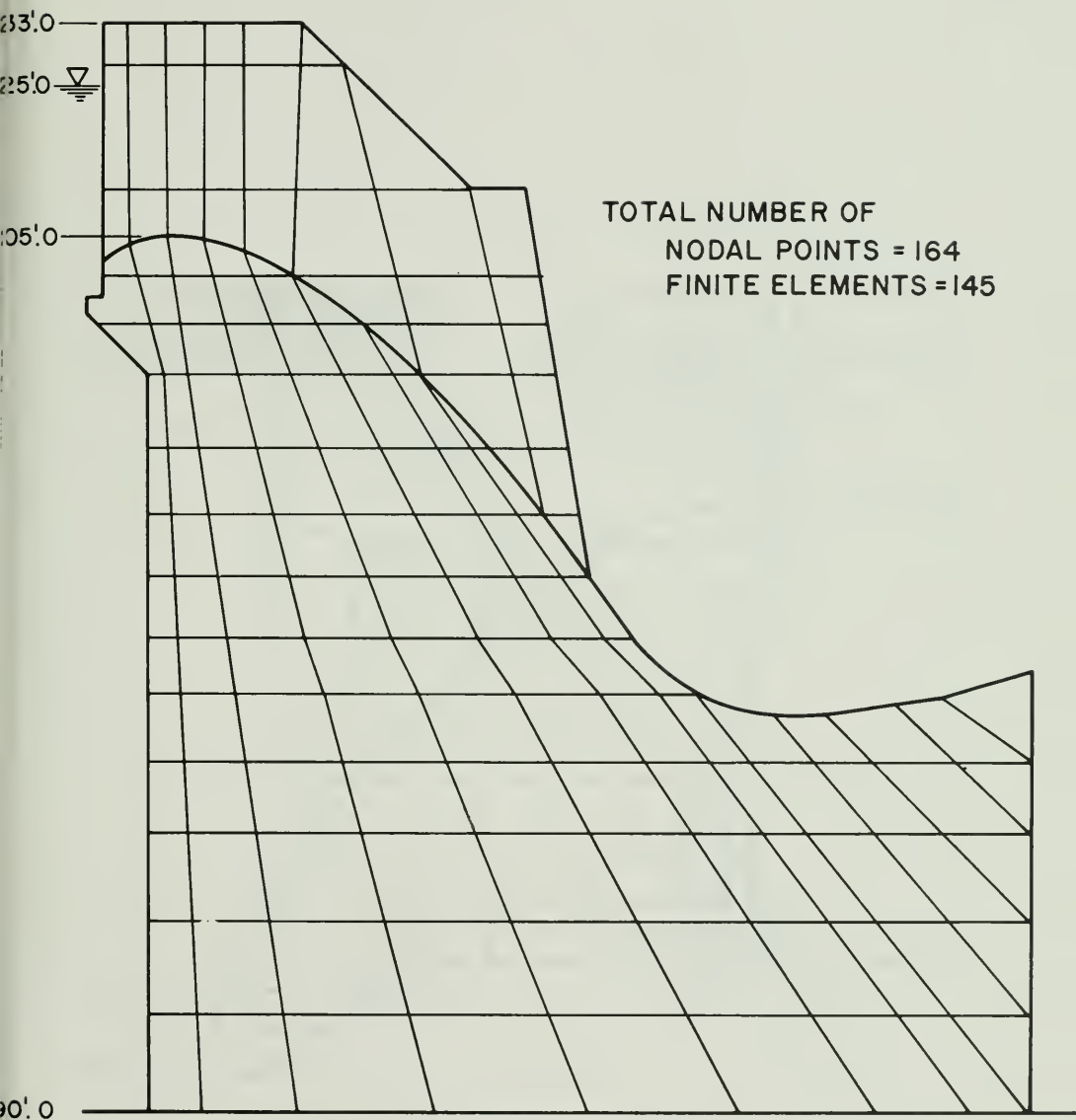


Fig. 3 Finite Element Mesh: Monolith 12 with Appurtenances

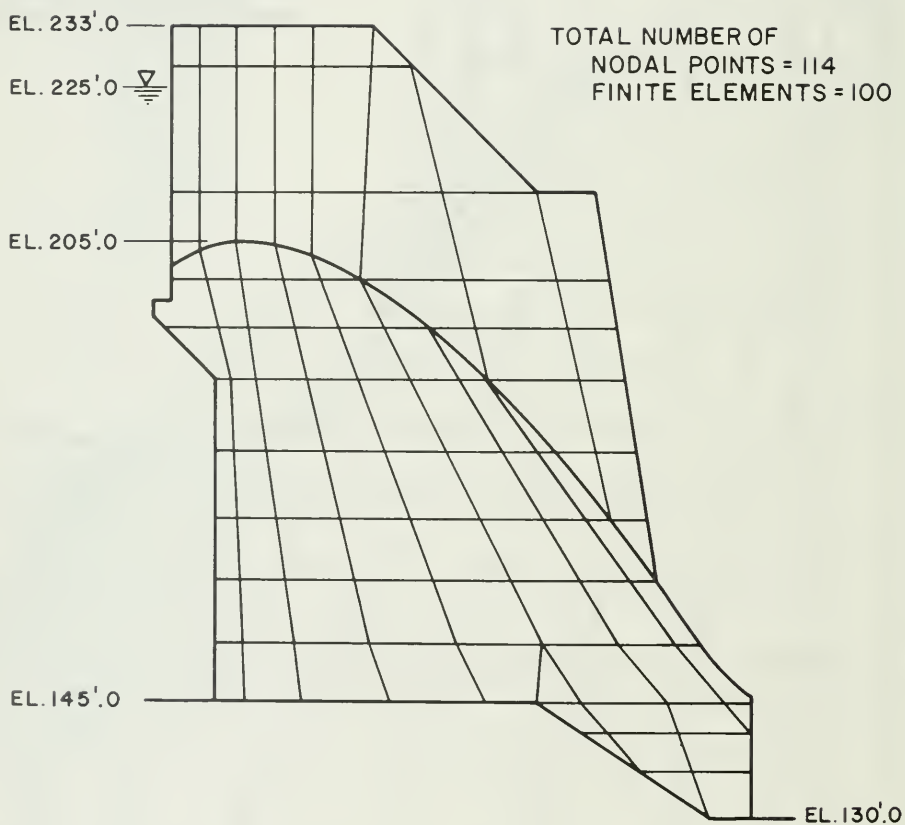


Fig. 4 Finite Element Mesh: Monolith 10

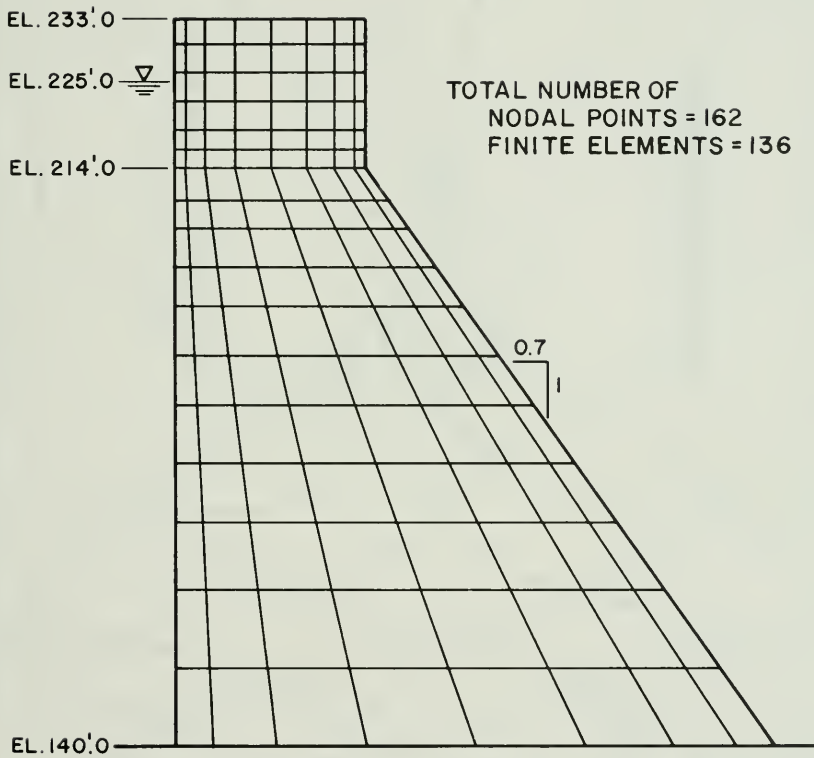


Fig. 5 Finite Element Mesh: Monolith 18

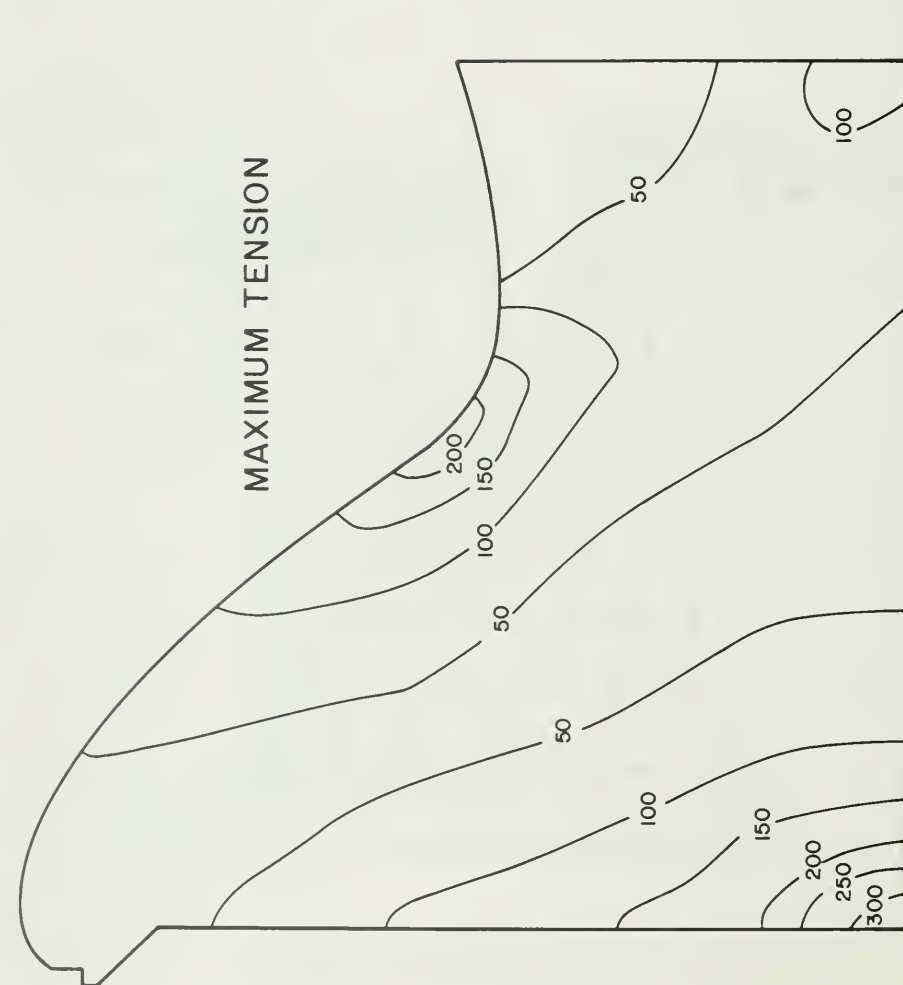


Fig. 6 Envelope Values of Maximum Principal Stress (Static + Dynamic);
Monolith 12 without Appurtenances

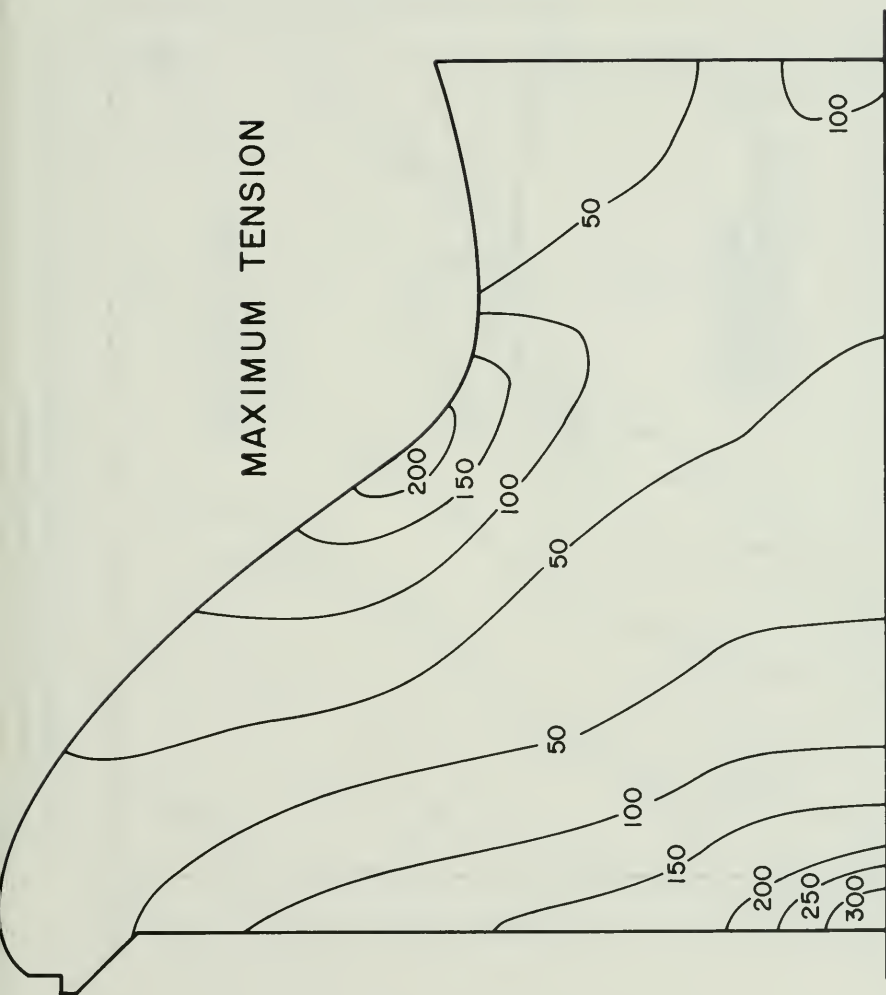


Fig. 7 Envelope Values of Maximum Principal Stress (Static + Dynamic);
Monolith 12 with Appurtenances

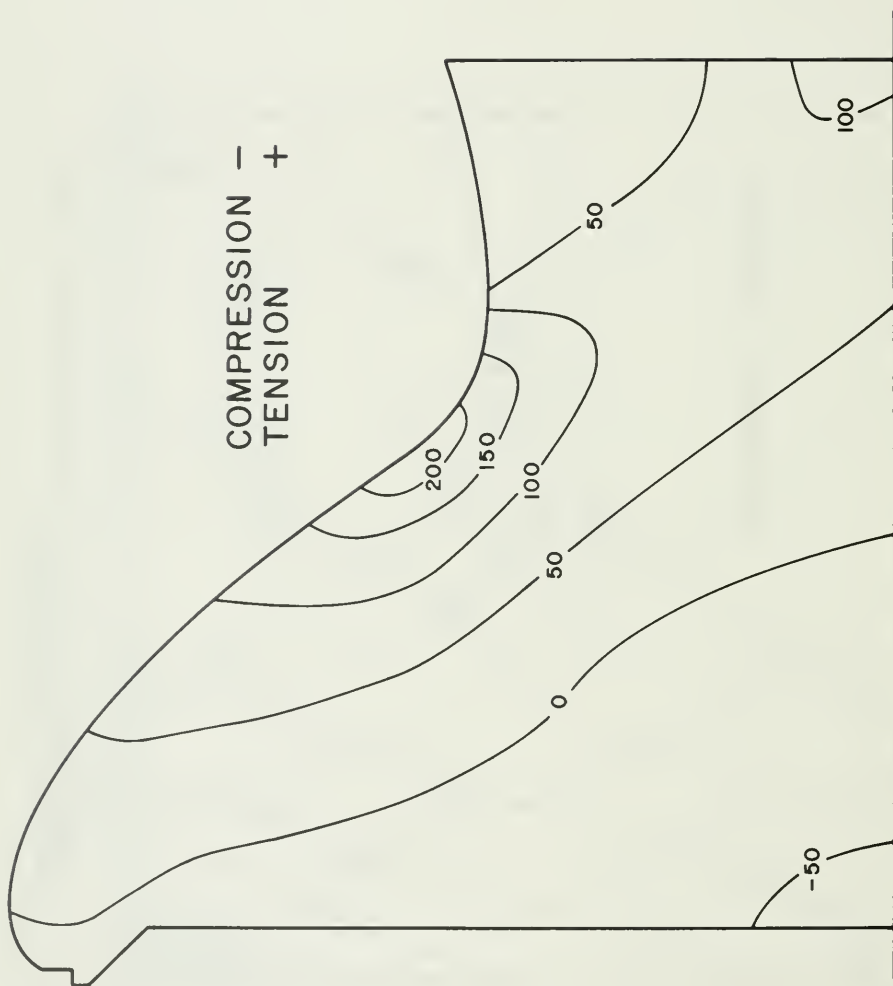


Fig. 8 Maximum Principal Stress (Static + Dynamic) at $t = 7.35$ secs;
Monolith 12 with Appurtenances

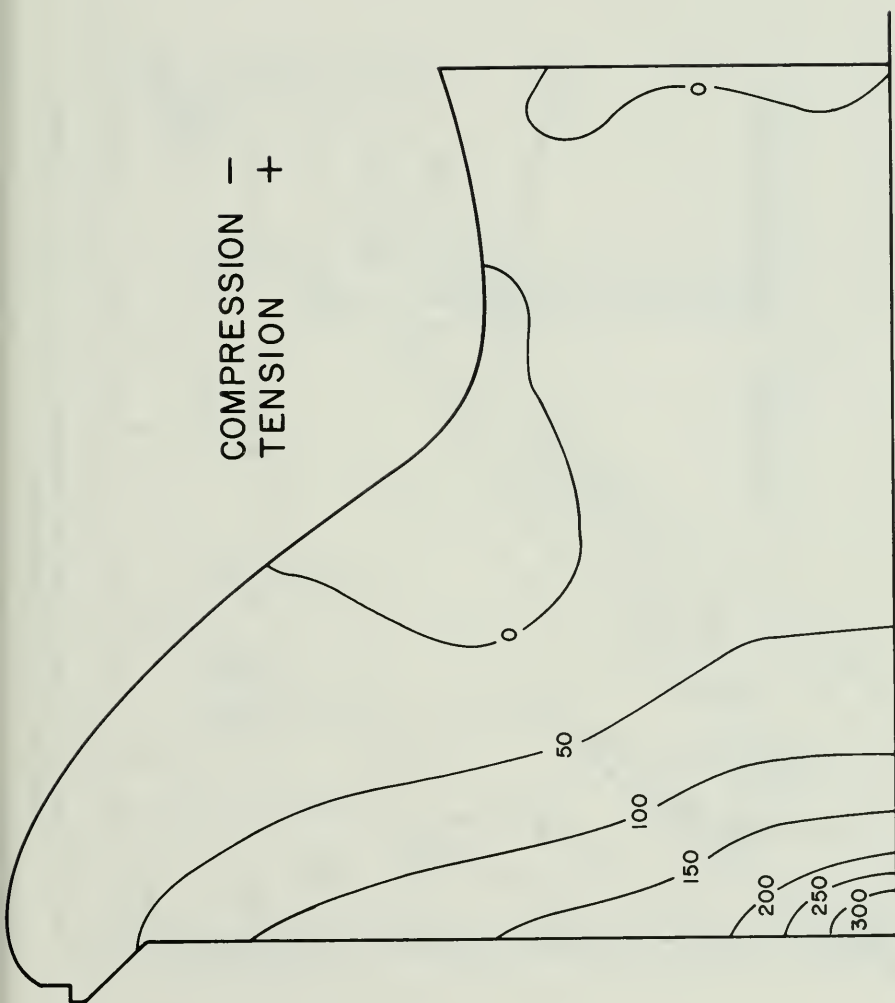


Fig. 9 Maximum Principal Stress (Static + Dynamic) at $t = 8.47$ secs;
Monolith 12 with Appurtenances

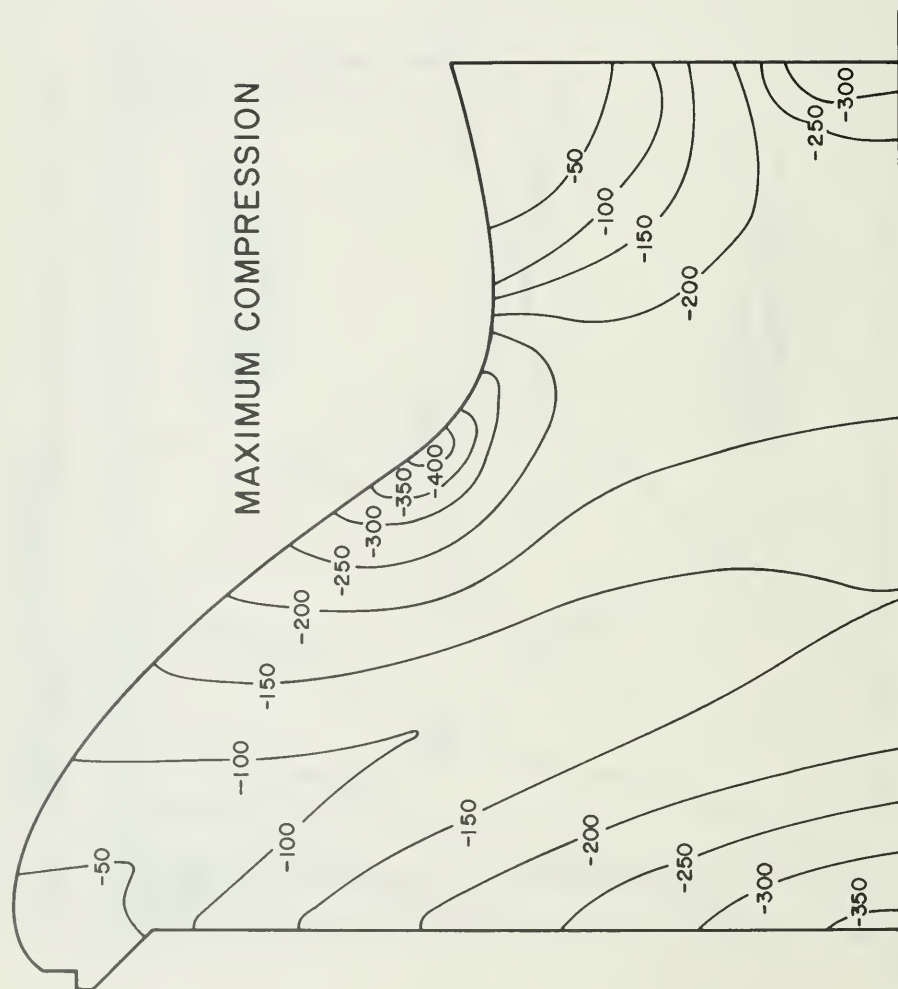


Fig. 10 Envelope Values of Minimum Principal Stress (Static + Dynamic);
Monolith 12 with Appurtenances

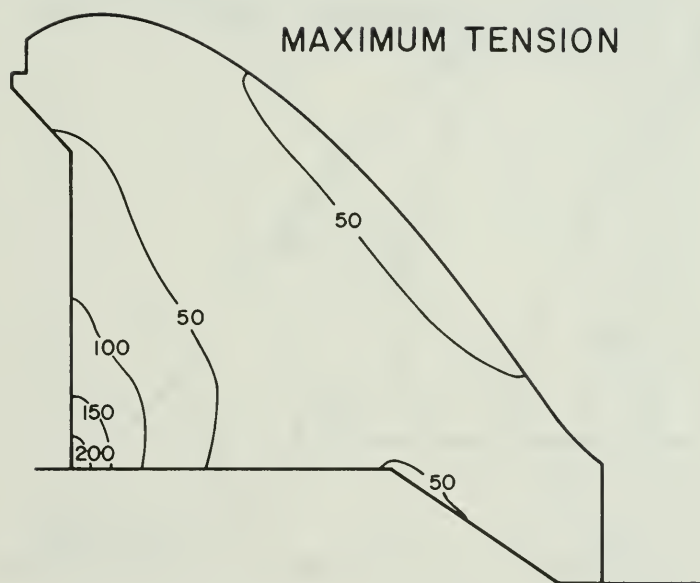


Fig. 11 Envelope Values of Maximum Principal Stress (Static + Dynamic);
Monolith 10

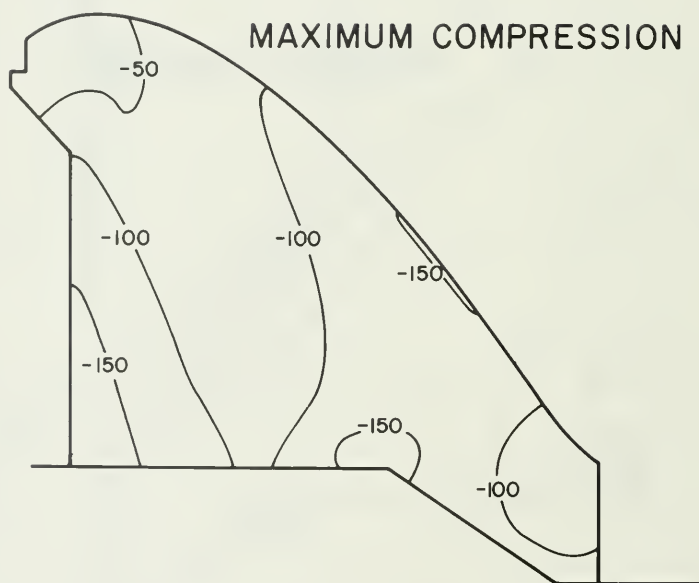


Fig. 12 Envelope Values of Minimum Principal Stress (Static + Dynamic);
Monolith 10

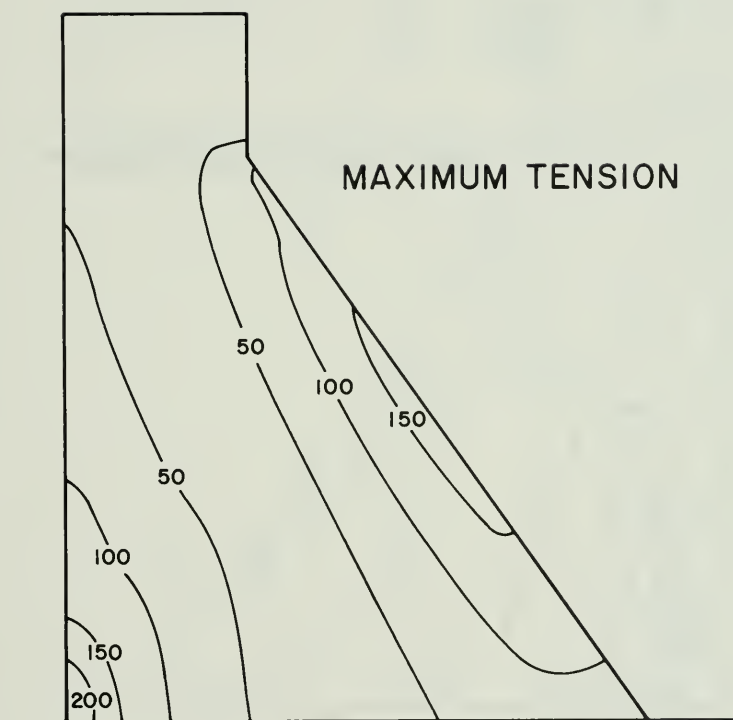


Fig. 13 Envelope Values of Maximum Principal Stress (Static + Dynamic),
Monolith 18

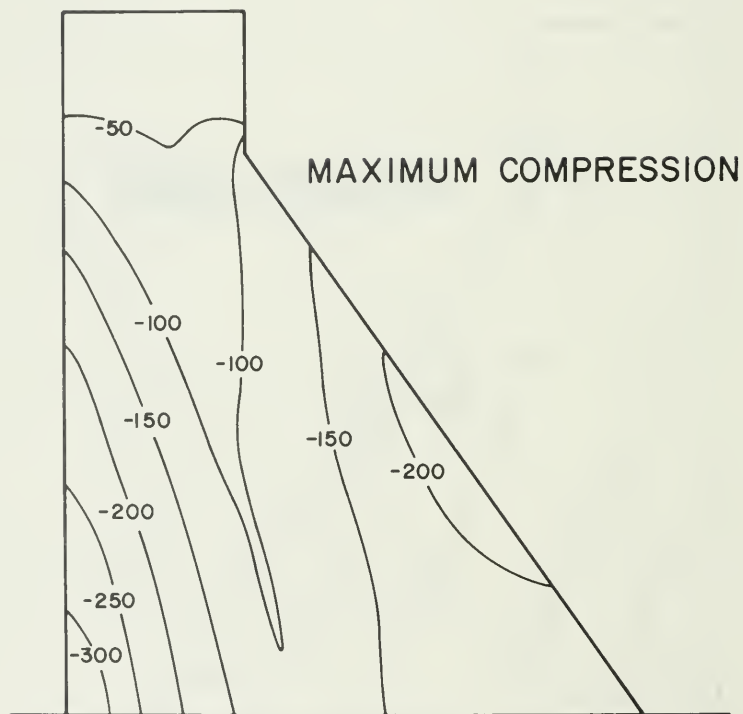


Fig. 14 Envelope Values of Minimum Principal Stress (Static + Dynamic);
Monolith 18

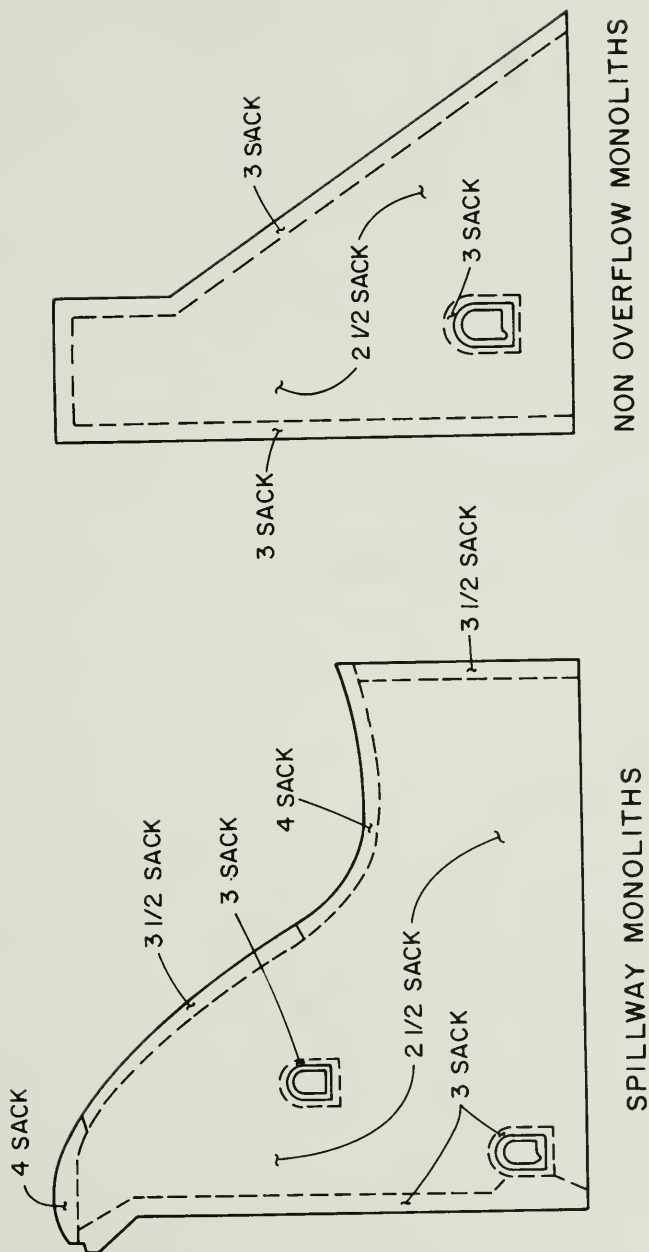


Fig. 15 Concrete Mixes in Thermalito Diversion Dam

APPENDIX

RE: Report (dated November 23, 1976) of the Special Consulting Board for the August 1, 1975 Oroville Earthquake to Mr. R. B. Robie, Director, Department of Water Resources, State of California.

Board Recommendation:

"The Board recommends that for critical structures with high fundamental frequencies, the previously recommended time-history of earthquake be supplemented by a time history meeting the high frequency (10 Hz or greater) requirements specified by the Nuclear Regulatory Commission in its Regulatory Guide No. 1.60, with the spectrum scaled to 0.4g at zero period."

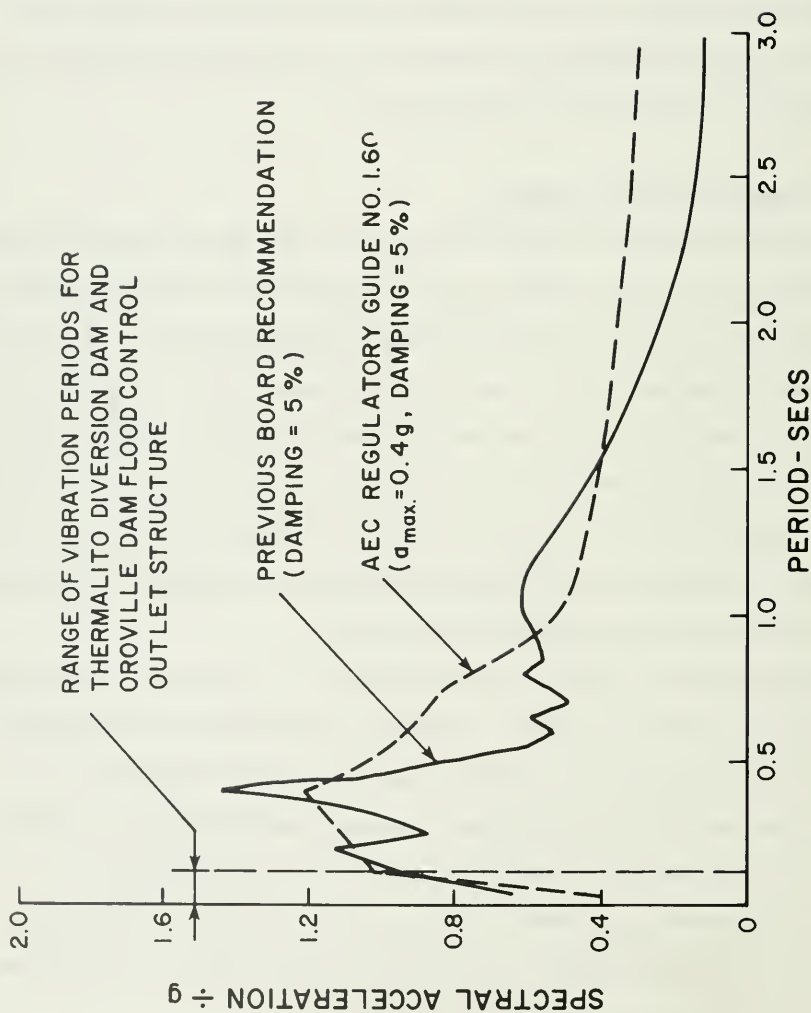
Response (Prepared by Anil K. Chopra)

Two pseudo-acceleration response spectra, both for damping ratio of 5 percent, are presented in the attached figure: one for the earthquake motion previously recommended by the Board; and the other is the spectrum specified in the AEC (now NRC) Regulatory Guide No. 1.60, scaled to 0.4g at zero period. The natural periods of vibration of Thermalito Diversion Dam and Oroville Dam Flood Control Outlet Structure lie within the period range 0 to 0.15 sec shown in the attached figure.

It is apparent that in the range of vibration periods of interest there is little need to supplement the ground motion previously recommended by the Board, for which the structures have already been analyzed.

If each spectrum was normalized with respect to its ordinate at zero period, in the range of periods of interest, ordinates of the normalized AEC Regulatory Guide No. 1.60 spectrum would be significantly larger than ordinates of the normalized spectrum for the ground motion previously recommended by the Board. However, the actual (without normalizing) spectra do not have the same relationship because the ordinates at zero period are different by a factor of 50 percent: 0.6g for the ground motion previously recommended by the Board, and 0.4g for the AEC Regulatory Guide No. 1.60 spectrum.

March 4, 1977



Comparison of Response Spectrum for Ground Motion Recommended by the Consulting Board and AEC Reg. Guide No. 1.60 Response Spectrum.

April 13, 1977

Professor George W. Housner
Division of Civil Engineering
and Applied Mathematics
California Institute of Technology
1201 East California Boulevard
Pasadena, CA 91109

Dear Professor Housner:

In the November 23, 1976 report of the Special Consulting Board for the August 1, 1975 Oroville Earthquake, the Board recommended that the adopted time history of earthquake motion be supplemented by a time history of higher frequencies. Dr. Anil Chopra of UCB investigated the effect of this recommendation. His findings are enclosed.

Please give us your comments at your earliest convenience.

Sincerely,

Donald C. Steinwert, Chief
Structural Unit
Design Branch
Division of Design and
Construction

Enc.

ENajera:mrs

bcc: H. H. Eastin w/attach
R. B. Jansen w/attach
K. G. Barrett w/attach
E. C. James w/attach

GEORGE W. HOUSNER
1201 EAST CALIFORNIA BLVD.
PASADENA, CALIFORNIA 91125

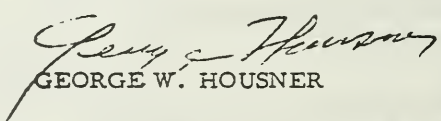
April 26, 1977

Mr. Donald C. Steinwert
Division of Design and Construction
Department of Water Resources
P. O. Box 388
Sacramento, California 95802

Dear Mr. Steinwert:

This is in reply to your letter of April 13th, concerning Dr. Chopra's investigation on the Oroville facilities. I am satisfied from Dr. Chopra's statement and the spectrum curves that he shows that further analysis need not be made with the ground motion specified by the Nuclear Regulatory Commission in its Regulatory Guide No. 1.60, with a spectrum scaled to 0.4 g at 0. The ground motion originally recommended by the consulting board is adequate.

Yours truly,



GEORGE W. HOUSNER

GWH:bb

CHAPTER VIII

REAPPRAISAL OF SECONDARY STRUCTURES

Introduction

As a result of the August 1, 1975 Oroville earthquake, the Department of Water Resources found it appropriate to reanalyze the major structures of the Oroville complex using both the "latest state-of-the-art" dynamic analysis and the Reanalysis Earthquake described in Chapter V. It was determined that non-critical structures could be reassessed using a lesser seismic force if a reanalysis was necessary. The Board would defer its recommendation as to the need for reappraisal of these secondary structures until the evaluation of the critical structures is complete.

After evaluating how a structural failure would affect project operation, possible loss of life and property, and the possibility of failure, the Department recommended what further seismic analysis is needed for the facilities in this report. The locations of these facilities are shown in Figures 189 and 193.

Fish Barrier Dam

Description

The Fish Barrier Dam is a concrete gravity structure (Figures 190 through 192) founded on generally fresh and hard rock consisting of meta-andesite and meta-conglomerate rocks. The dam consists of a central low-overpour section 250 feet long, a high-overpour section on either side of the lower section with a total length of 54 metres (176 feet), and a non-overpour section on the right abutment 53 metres (174 feet) long. The low-overpour section consists of a gravity section with a cantilevered reinforced-concrete crest apron extending 2.7 metres (9 feet) downstream of the dam face, and two aeration piers. The other two sections are gravity concrete sections. The maximum structural height

of the dam is 28 metres (91 feet). A thorough inspection of the dam after the August 1, 1975 earthquake revealed no damage to this facility.

Original Seismic Analysis

The original seismic analysis consisted of a pseudostatic analysis; an acceleration coefficient of 0.1g acting either downstream or upstream was used. The hydrodynamic force was determined using the Westergaard formula and an assumed natural period of 1 second for the structure. In addition to the earthquake force, the pseudostatic analysis included all normal forces including river flows up to 50,000 cfs. Utilizing these loading conditions, the structure was analyzed at several levels for maximum and minimum principal stresses, safety against sliding (f), and the shear friction factor of safety

$$(s_{sf} = \frac{f V + r A}{H}). \text{ In addition,}$$

the overturning safety factor was checked for the Federal Power Commission review in 1972.

On the basis of the preceding analysis, the maximum principal compressive stress was approximately 120 psi, and maximum tensile stress was about 10 psi. Both are considerably lower than the allowable stress established for this structure.

The analysis for sliding on the foundation indicated that the allowable sliding factor (ratio of total horizontal forces to total vertical forces) of 0.7 is exceeded by as much as 57 percent. This is offset by the high values of the shear friction factor of safety for this structure, in excess of 17 compared to minimum allowable for seismic loading of 3.25.

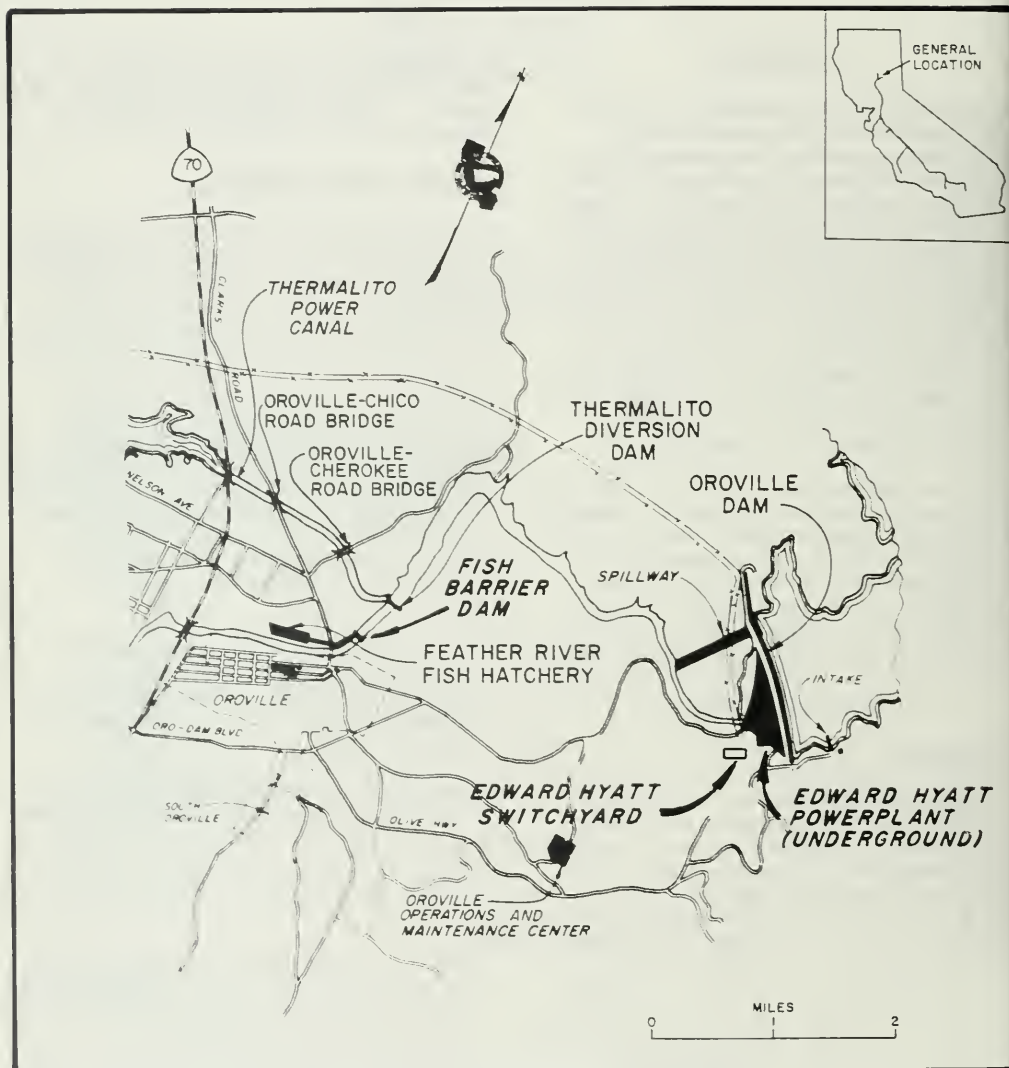


Figure 189. Location Map, Edward Hyatt Powerplant Facilities

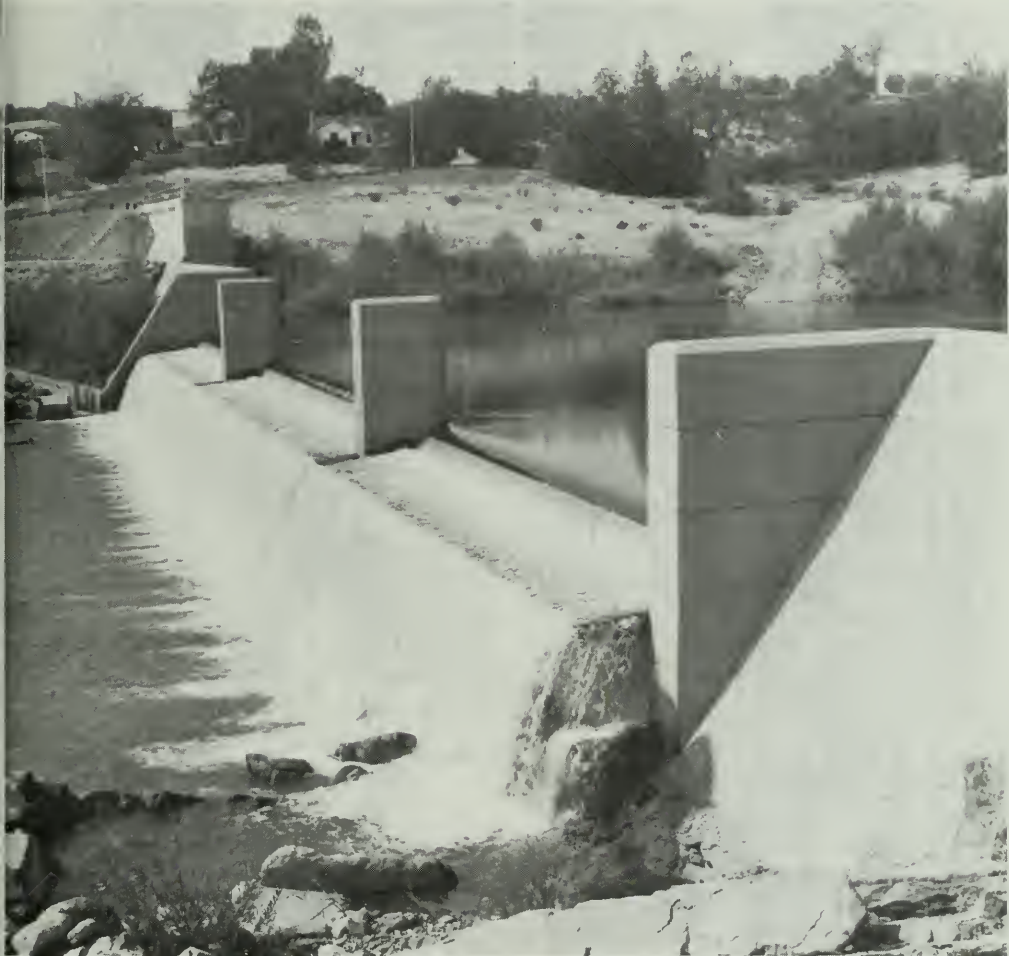


Figure 190. Fish Barrier Dam

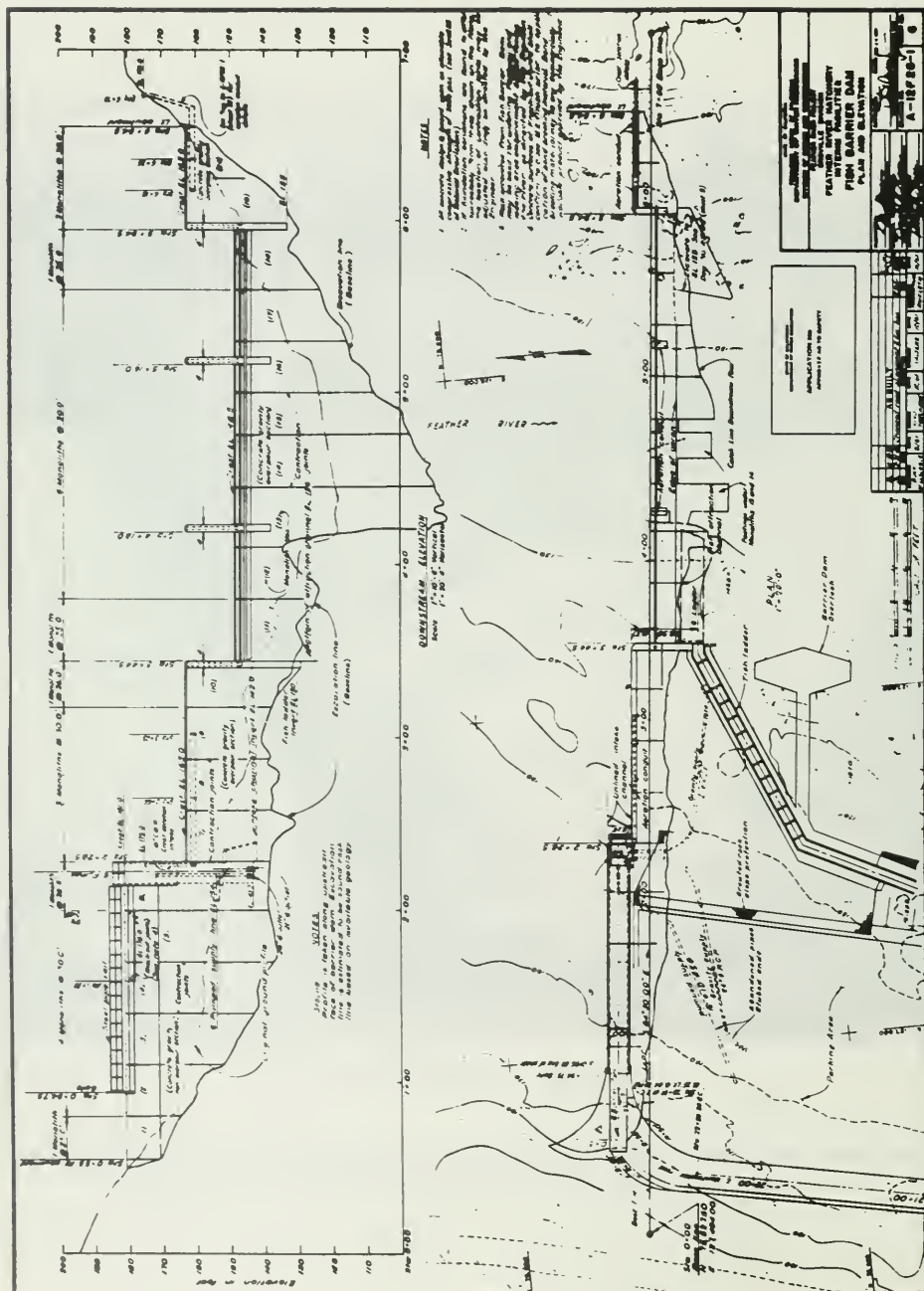


Figure 191. Fish Barrier Dam, Plan and Elevation

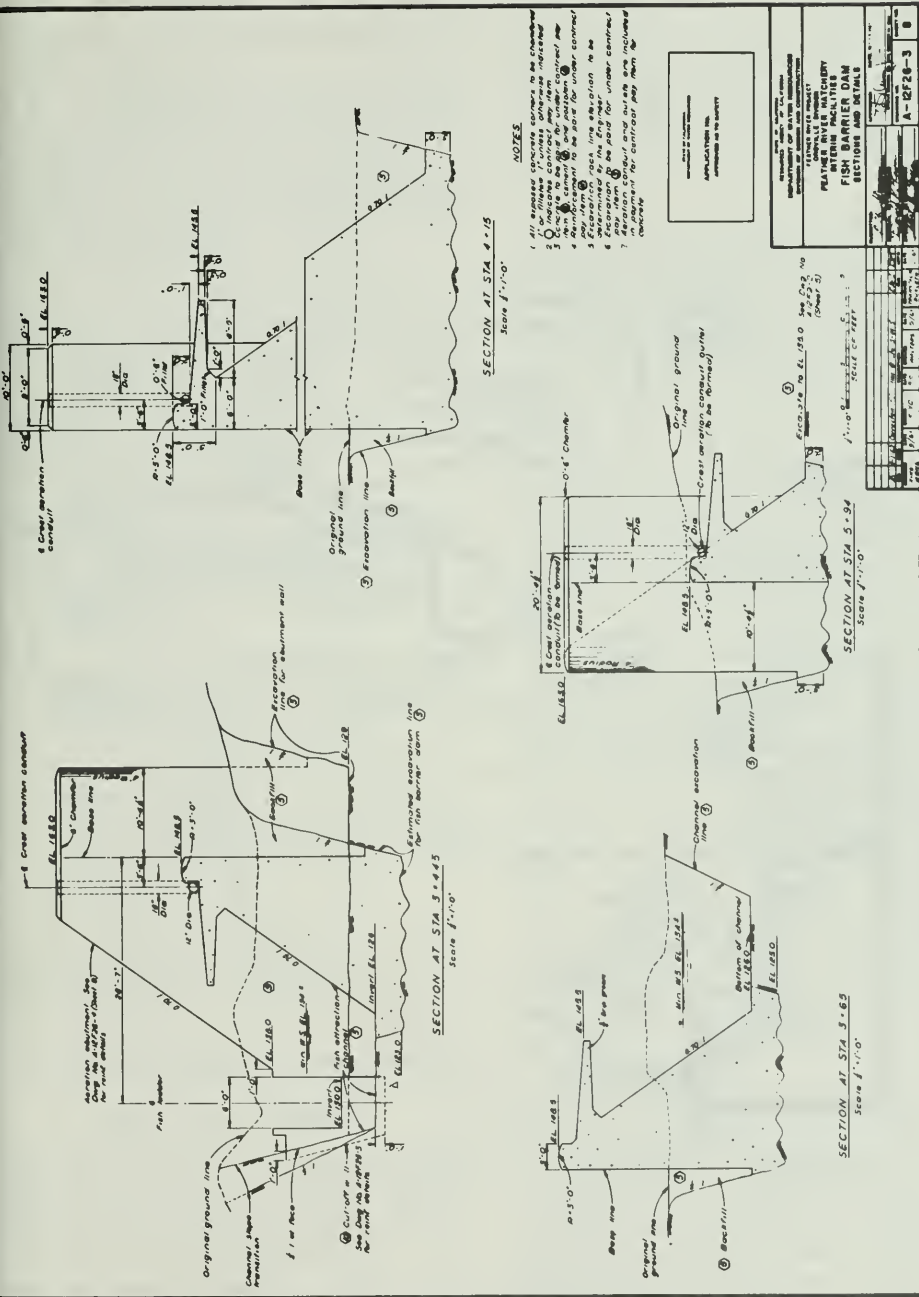


Figure 192. Fish Barrier Dam, Section and Details

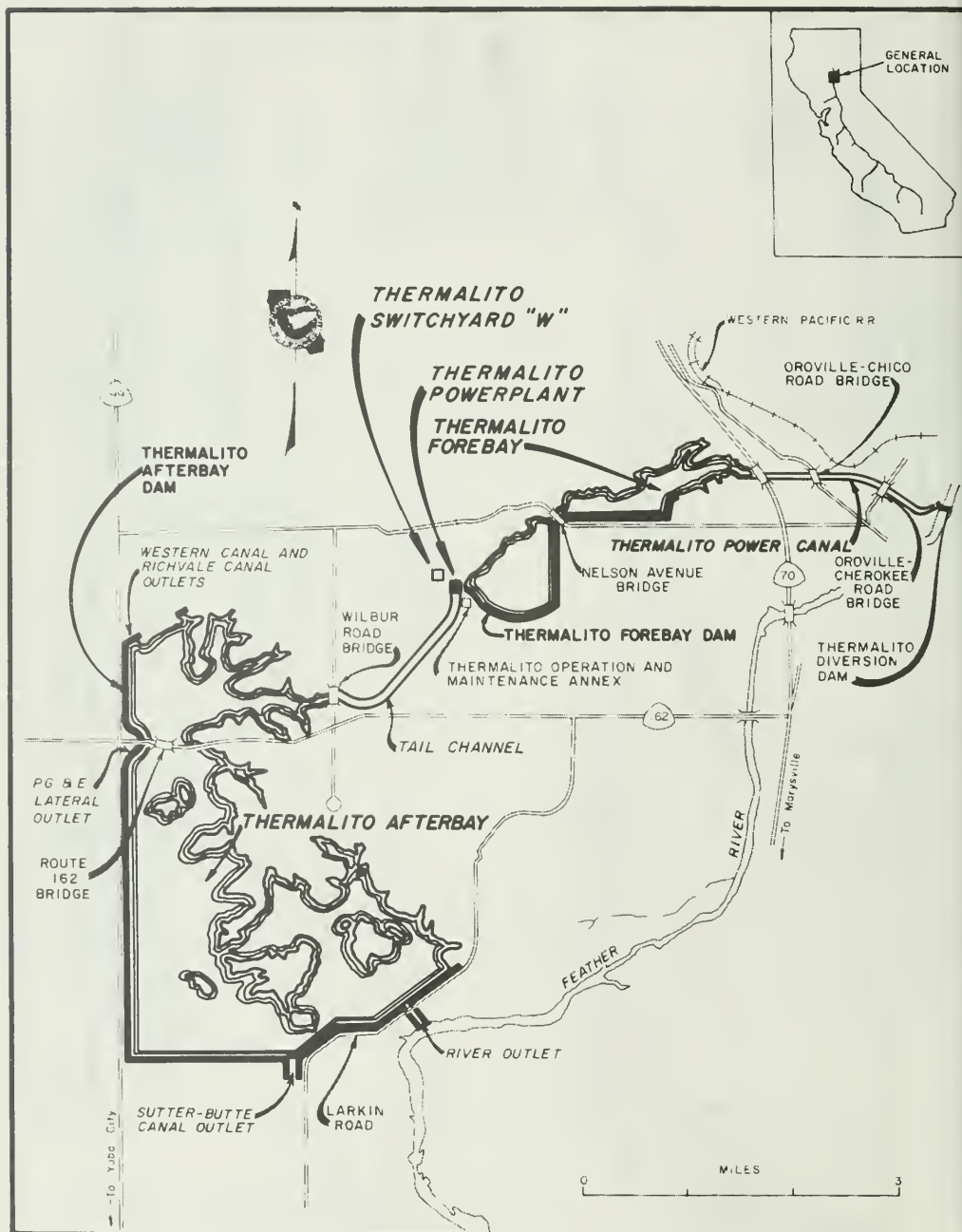


Figure 193. Location Map, Thermalito Powerplant, Forebay, and Afterbay

Recommendation for Seismic Reanalysis

The Department recommended using a pseudostatic analysis and a seismic coefficient of 0.25 to reanalyze the secondary structures, in lieu of the rigorous dynamic analysis used for the critical structures. The chairman of the Earthquake Consulting Board concurred with this recommendation.

A quick check using the pseudostatic analysis and a seismic coefficient of 0.25 and 0.6 indicated a minimum shear friction factor of safety in excess of 9.

A brief study of the consequences of failure of this structure indicates the following:

1. Possible loss of life would be limited to fishermen along the river at the time of the event. This would be further limited to those fishermen to close to the dam to be warned.
2. Property damage would be minor and would be less than that caused by the Standard Project Flood.
3. Loss of the dam would have little effect on operation of the project until repaired or replaced. Complete loss of the dam would have an effect on the operation of the fish facilities.

On the basis of the preceding analysis, the Department has determined that no additional seismic analysis is recommended for the Fish Barrier Dam.

Power and Pumping Plant Facilities

Edward Hyatt Powerplant

The Edward Hyatt Powerplant is an underground, hydroelectric, pumping-generating facility located on the Feather River approximately 5 miles northeast of the City of Oroville, Butte County.

The powerhouse chamber, located in the left abutment near the axis of Oroville

Dam (Figure 189), was excavated in a metavolcanic rock formation that is predominantly amphibolite. The rock was fresh and three prominent joint sets imparted a certain blockiness to it, but the individual joints were generally tight.

Since much of the powerhouse is placed against the rock, (Figure 194), it can be assumed that it will experience peak ground acceleration (PGA) with negligible magnification. The powerhouse substructure is a rigid, massive, reinforced concrete structure which should experience little or no distress from the designated load factor.

As a result of the DWR Earthquake Hazard Committee inspection of the facility, minor modifications consisting principally of installations of additional holddown bolt anchorages and bracing were made to increase earthquake resistance of unit control centers, emergency equipment, spare parts storage shelves, CO₂ cylinder racks, and numerous other items. Items in the power plant still to be investigated are the anchorages that fasten the precast wall panels to the columns; and the columns themselves, which rest on the generator floor, Elevation 252.0 (Figure 195). The panels will most likely experience a higher response acceleration factor since their mode of vibration will be considerably different from that of the main structure. A pseudostatic analysis using a peak ground acceleration of 0.25g will be used to investigate the powerhouse components. This work is scheduled to be completed during the 1978-79 fiscal year.

It was determined that the intake structure to the powerhouse (Figure 196) was structurally stable; however, additional anchorages were installed for a number of items, the most important of which are the crane trolleys on the shutter gantry crane. Holddowns are required for the trolleys when the crane is not in operation to keep them on the track during seismic events.



Figure 195. Generator Room, Plan - Elevation 252.0



Figure 196. Overall View of Edward Hyatt Powerplant Intake Structure

Conclusion

The powerhouse substructure has been reviewed using a comparative pseudo-static analysis of previously designed powerhouse substructures. Based on this comparison, it has been determined that this substructure would be capable of resisting the forces induced by a 0.25g peak ground acceleration, therefore no modifications are required.

Modifications will be made to improve the seismic resistance of powerhouse superstructure components as necessary.

Thermalito Powerplant

Thermalito Powerplant is a pumping-generating facility located approximately 4 miles west of the City of Oroville, Butte County (Figure 193). The power plant substructure (Figure 197) is keyed into a basalt formation, and its foundation lies on an interflow material consisting of basalt breccia in a matrix of amorphous material. The plant substructure is a rigid, massive, reinforced concrete structure which should move with the basaltic rock formation and thus experience peak ground acceleration (0.25g) with little or no magnification.

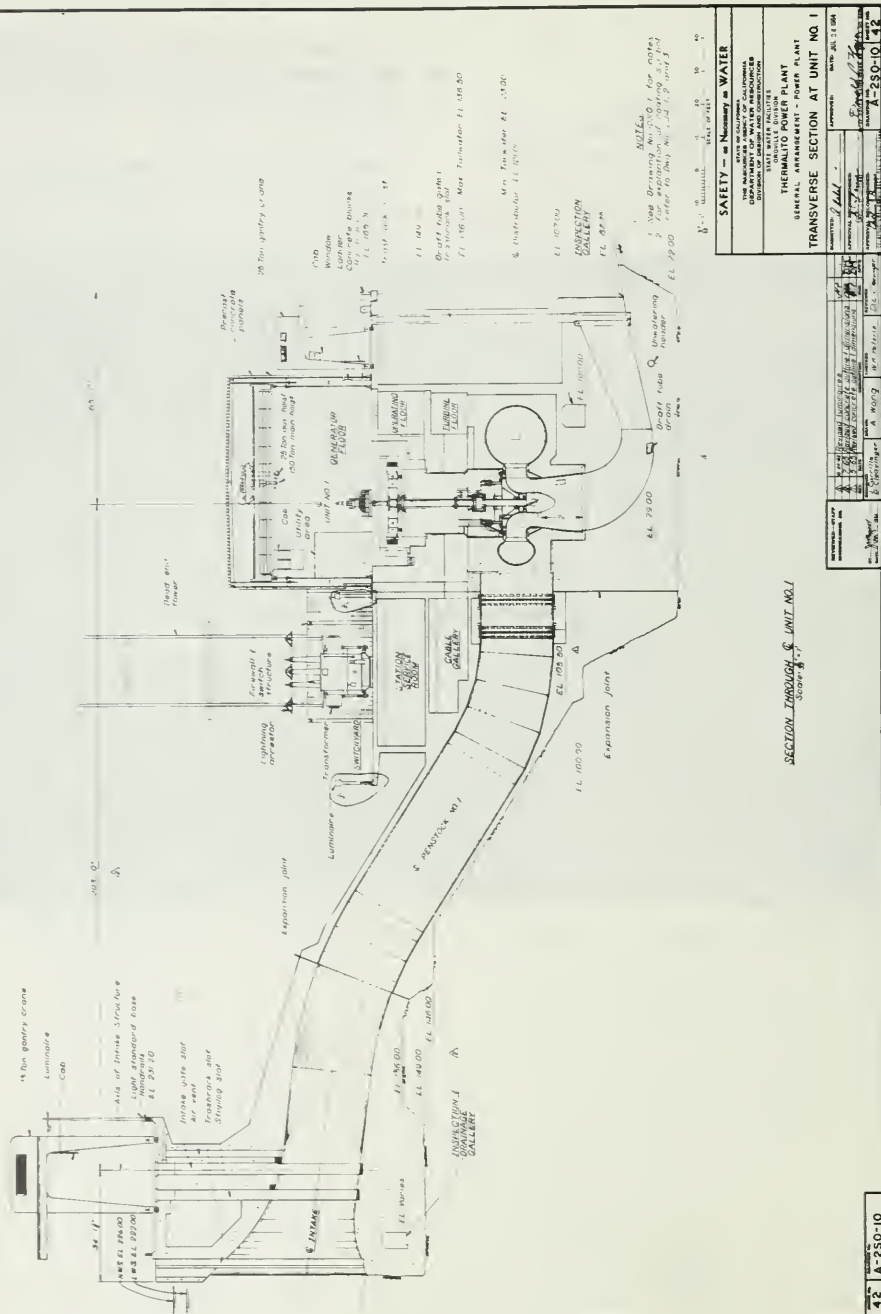
This facility was also inspected for earthquake hazards, and modifications similar to those at the Edward Hyatt Powerplant were made.

Items still to be investigated are the rigid steel frames that form the superstructure, and the precast concrete panels and the anchorages that fasten them to the superstructure (Figure 198). This work is scheduled to be completed during the 1978-79 fiscal year. Above elevation 165.0, the superstructure will vibrate in a lower mode of vibration than the substructure and therefore experience a somewhat higher response acceleration factor than the 0.25g assigned to the substructure.

Conclusion

The powerhouse substructure has been reviewed using a comparative pseudo-static analysis of previously designed powerhouse substructures. Based on this comparison, it has been determined that this substructure would be capable of resisting the forces induced by a 0.25g peak ground acceleration, therefore no modifications are required.

Modifications will be made to improve the seismic resistance of powerhouse superstructure components as necessary.



Miscellaneous Structures

The miscellaneous structures inspected by the DWR Earthquake Hazard Committee include those listed below:

Oroville Operations and Maintenance Center

Miscellaneous Structures

1. Administration and Maintenance Center
2. General Maintenance Headquarters Building
3. Plant Maintenance Shops
4. Mobile Equipment Repair Building
5. General Maintenance Warehouse
6. Vehicle Storage Building

Oroville Dam Miscellaneous Structures

1. Palermo Outlet Works Control House
2. Instrument Vault
3. Reservoir Gage Station

Thermalito Forebay and Afterbay Miscellaneous Structures

1. Heavy Equipment Building
2. Western Canal and Richvale Canal Outlet Control Building
3. PG&E Lateral Outlet Control Building
4. Sutter Buttes Canal Outlet Control Building
5. Feather River Outlet Control Building
6. Feather River Outlet Control Station

Feather River Fish Hatchery Miscellaneous Structure

1. Maintenance Office Building
2. Hatchery-Spawning Building
3. Ultraviolet Treatment Building

As a result of the earthquake hazard inspection, additional anchorages have been installed for much of the operational equipment in these facilities.

Conclusion

Damage that may occur to the miscellaneous structures is not considered to be a threat to public safety and property. For the purpose of the seismic reevaluation, these structures are classified as noncritical.

Bridges

Public bridges in the Oroville area were inspected by the Department of Transportation following the August 1, 1975, Oroville earthquake. Fourteen bridges in the general area showed evidence of movement, minor damage, or both.

If these bridges were to experience a peak ground acceleration of 0.25g, some of them may sustain greater damage. Therefore, all project-related bridges will be analyzed for such a loading during the 1978-79 fiscal year.

Conclusion

Bridge components that will not sustain the forces generated by a 0.25g peak ground acceleration will be modified to strengthen their seismic resistance.

Switchyard Structures and Apparatus

Switchyards play an important dual role in hydroelectric power systems. They collect and distribute generated or incoming power and protect power and pumping plants. Unlike many power plant features, switchyard electrical equipment exhibit only light damping characteristics, are fragile, and have very little ductility because much of the supporting systems are porcelain. In addition, many of the physical structures take on a "lollipop" type of mass distribution which is conducive to high amplification factors during severe earthquake-induced ground movements.

The two switchyards under investigation are at the Edward Hyatt and Thermalito Powerplants.

The Edward Hyatt Powerplant Switchyard is located at the downstream toe of the Oroville Dam on the south bank of the Feather River, approximately five miles northeast of the City of Oroville (Figure 189).

Thermalito Powerplant Switchyard "W" is located several hundred feet west of the power plant, approximately four miles west of Oroville (Figure 193).

Both switchyard facilities contain similar electrical apparatus; therefore, it will suffice to discuss weaknesses common to both of them.

The types of equipment in the switchyards are:

1. Current transformers
2. Potential transformers
3. Disconnect switches
4. Lightning arrestors
5. Line traps
6. Bus supports
7. 230 kV ATB-6 power circuit breakers

Since no loss of life is expected due to failure of equipment within the yard, the switchyards have been classified as noncritical facilities. Accordingly, a peak ground acceleration of 0.25g has been assigned for this seismic evaluation.

To determine dynamic characteristics of switchyard equipment, a testing program had previously been conducted at other Department switchyards containing similar power circuit breakers and structural support systems. Those tests had revealed critical frequencies and damping characteristics.

However, since a loss of certain switchyard equipment would create only

operational inconveniences and minor outages, investigation efforts were directed to the most earthquake prone and critical equipment in the switchyards; the 230 kV ATE-6 power circuit breakers (Figure 199).

The fundamental frequency for the circuit breakers ranged from 2.8 to 3.5 hertz, depending on the direction of excitation applied, and damping values ranged from 3.6 percent to 6.4 percent of critical. Dynamic magnification of about 7 was observed during the testing, which means at an acceleration input of 0.25g, the maximum response acceleration would be about 1.75g. Further studies indicated that the porcelain supports for the breaker heads cannot withstand loads of this magnitude without addi-

tional damping or isolation.

For the proposed study a newly developed seismic shock-isolation system will be tested under one of the power circuit breakers to determine its capability to protect the breakers during severe ground movements. The testing program is scheduled to be conducted during the 1978-79 fiscal year.

Conclusion

Based on the consideration that failure of electrical equipment in the Edward Hyatt or Thermalito Powerplant switchyards does not pose a threat to public safety or property, the switchyards are classified as noncritical elements of the Oroville Complex.

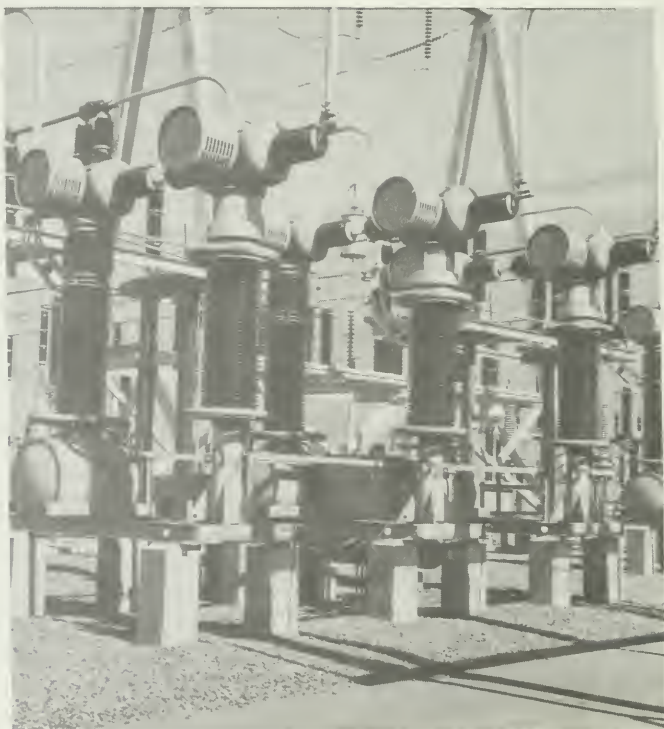


Figure 199. 230-KV Power Circuit Breakers

CHAPTER IX
CONTINGENCY PLAN FOR SEISMIC EMERGENCIES

The purpose of this chapter is to specify procedures to be followed by the Division of Operations and Maintenance in reacting to seismic events, and the process for returning equipment to pre-earthquake operating levels.

The discussion outlines (1) organization and responsibilities for both Headquarters and Field Division; (2) procedures for reacting to seismic events, including notification and response; and (3) procedures returning equipment and facilities to full operational status, which establishes the criteria for qualifying operational readiness.

Organization and Responsibilities

Division Policy

The policy of the Division of Operations and Maintenance during emergencies will be as follows:

1. Management and operation of the State Water Project during emergencies will be in accordance with the contingency plan.
2. The primary emphasis will be to provide all possible support to line activities.
3. The project facilities and control centers will continue to be operated in accordance with the Plan of Operation.
4. Operation will be on as nearly a normal basis as possible.
5. The Division Command Post in Sacramento, together with a Command Post in each of the five field divisions, if required, will be set up to coordinate activities.
6. A declaration of emergency will be made by the Director upon recommendation by the Division Engineer, if

required for the Division to expedite contracts, service agreements, and purchasing processes.

7. Instructions to cease operation of facilities, to operate additional facilities, or to change the plan of operation shall be made only by the Division Engineer or by the person in charge of the Division Command Post, after consultation with the Director, except in emergencies where immediate action is required.

Division Plan of Operation

Should an emergency occur, the Operations Control Branch will prepare, distribute, and implement a Plan of Operation appropriate to the situation. The Oroville power facilities will be kept in operation by all feasible means.

Where possible, the pumping and generating units will be operated on a continuous basis to minimize manpower requirements on start-up and shutdown, to lessen chances of shutdown.

Priority will be given to continuing the operation at the Hyatt Powerplant should circumstances require discontinuing operation of the Thermalito facilities.

Oroville Field Division Command Post

On determination of a seismic emergency, the Field Division Chief, upon direction or at this discretion, will establish a Command Post to be manned 24 hours per day to assure continuous communication with the Division Command Post.

The chain of command will not change because of emergency conditions. While the urgency of the moment may necessitate shortcuts in lines of communications and activities, every effort will be made, as time permits, to backtrack and reestablish that chain.

Every effort shall be made to maintain the normal channel of communication between the field and headquarters for the dissemination of operating orders, condition reports, and forecasts.

The Oroville Field Division has established two command posts; one is designated "Operational", which is the Master Command Post, and the other is designated as the "Security Command Post".

Operational Command Post. The Operational Command Post will be the responsibility of the Operations Superintendent under the authority of the Field Division Chief. He will have the responsibility to meet the Plan of Operation for water and power deliveries.

1. Operational Facilities. To the extent possible, the following facilities in the Oroville Field Division will remain operational for the duration of any emergency:

Area Control Center
Command Post - Operational
Edward Hyatt Powerplant
Thermalito Powerplant
All Hydraulic Structures

2. Operational Plan. The above facilities will be operated and maintained on as nearly a normal basis as possible and in accordance with existing power and water delivery schedules. The Operations Superintendent or his designee shall keep the Project Operations Control Center advised of all conditions relative to the operation of the Project.

If for any reason, communication links between the Oroville Operations Command Post and Project Operations Command Center are severed, the Operations Command Post shall maintain the same operating status that prevailed prior to the loss of communications. Any deviations from this procedure must be

authorized by the Operations Superintendent or his designee.

Security Command Post. The Security Command Post will be the responsibility of the Chief of the Civil Maintenance Section under the authority of the Field Division Chief.

1. The Security Plan. The Security Command Post Manager will:

- (a) direct and monitor Project facility inspections of civil features;
- (b) recommend to the Field Division Chief operational deviations when warranted due to detectable threats to the integrity of Project structures; and
- (c) maintain a log of damage and establish priorities for repair work.

The Security Plan involves two actions: Surveillance and Corrective Response.

Surveillance is defined as efforts expanded toward knowing what is happening project wide. Corrective response is defined as efforts expended toward maintaining integrity or restoration of facilities.

Procedures for Reacting To Seismic Events

Oroville Field Division

Detection

Seismic events are detected either by personal senses in the Field or by instrumentation response in the Earthquake Engineering Section in Sacramento.

Earthquake Magnitude and Epicenters

Accurate earthquake magnitude and hypocenter are determined and reported by

the Earthquake Engineering Section in Sacramento, normally well beyond the time required to help determine the need for Project inspections. Preliminary estimates of magnitudes above 4.0 are made by the Project Operations Control Center and generally reported to the ACC within 30 minutes after the event. This information is helpful but not complete enough to determine the need for inspection.

Criteria for Notification

When an earthquake exceeding an estimated magnitude of 3.0 Richter Scale is felt or reported with 25 kilometres (15.5 miles) of the Oroville Seismic Reporting Station, the Area Control Center shall notify the Surveillance Unit Chief, the State Police Mobile Unit on duty, and the Project Operations Control Center.

When an earthquake is felt or reported in excess of an estimated magnitude 4.0 Richter Scale, within 50 kilometres (31 miles) of the reporting station, the Area Control Center shall additionally notify the Civil Maintenance Section Chief.

Within the near future, peak acceleration values measured in the foundation and crest of Oroville Dam will be displayed in the Area Control Center on the Data Acquisition Panel. At that time, 0.10g recorded at the base of Oroville Dam will replace the 3.0 Richter Scale criteria for notification, and 0.15g will replace the 4.0 Richter Scale criteria.

Response

1. When an earthquake estimated in excess of magnitude 3.0 Richter Scale occurs, or the acceleration values are in excess of 0.10g:

- (a) Water and Power Operations shall continue to operate under routine constraints.

- (b) The Surveillance Unit Chief shall determine that seismic instrumentation is functioning and ready to record a subsequent event, and gather and record certain data in accordance with prescribed standing instructions.

- (c) The State Police mobile unit on duty will perform a general inspection of the Project in accordance with prescribed standing instructions.

2. When an earthquake exceeding an estimated magnitude 4.5 Richter Scale occurs, or with the determination that peak accelerations exceeding 0.15g have occurred at the base of Oroville Dam:

- (a) Water and Power Operations shall continue at the operating level resulting from a seismic event. For instance, if four units are on line when the event occurs and only two units remain on line, water and power operations shall remain in that configuration until either: (1) standard operating procedures dictate a change, or (2) an inspection reveals that it is safe to continue or to increase/decrease operations.

- (b) The Security Command Post shall be activated by the Civil Maintenance Section Chief at his discretion to an estimated magnitude 5.0, he may call the necessary personnel for an inspection. At an estimated magnitude 5.0, the complete Rapid Response inspection is mandatory. The ACC shall be advised when the Security Command Post is activated and when a Rapid Response Inspection has been initiated.

Inspection of Project Facilities Following an Earthquake

Significant seismic events are presumed to precede additional seismic events. Until enough time has elapsed to perceive a decay in the frequency and magnitude of shocks, inspection and investigations will continue in order to assure that structures have not been weakened to a point approaching failure.

Inspections are categorized two ways: Rapid Response and Follow-up or Final.

1. The Rapid Response Inspection Plan is a method to immediately determine that problems may or may not be developing projectwide. It is a means for the Field Division Chief to determine whether corrective action should be initiated and to what degree follow-up inspections are required.
 - (a) Operational Command Post. The Operations Section is obligated to comply with Operational Procedures (OP series of instructions) that specifically outline the inspection and safe operation of plant equipment. In addition, the Area Control Center has on its Status Display boards, indicators of water and power conditions of the overall Project Features. Rapid inspection and response therefore are well outlined.
 - (b) Security Command Post. The area of responsibility of the Security Command Post is divided geographically and assigned to three inspection teams. (See Schematic Diagram of Oroville Complex Figure 200).

- (1) Oroville Dam and vicinity
- (2) Thermalito Forebay and vicinity
- (3) Thermalito Afterbay and vicinity

Detailed instructions of routes to follow and items to inspect are provided for each team. In addition a training film has been prepared that defines the plan of inspection, shows the order of inspection, the types of damage to look for in each geographical area, and specifies the procedure to be used in reporting damage and conditions.

The surveillance crew, within all these geographical areas, attends seismic and performance instrumentation.

2. The follow-up Inspection Plan is developed as information becomes available. In some cases visual inspections may be adequate. Generally, when accelerations of less than 0.15g are experienced in Oroville Dam, follow-up inspections will not be required. Damage reports will be filled out for all abnormalities to civil features discovered during inspections. Damage reports will serve to identify large or small problems and to initiate Job Requests or Job Orders as may be determined by review and verification of the Security Command Post Manager.

Returning Facilities and Equipment To Full Operation Status

The following pages are lists of all operational facilities and features in the Oroville Complex, starting with Lake Oroville, moving downstream, and ending with the Thermalito Afterbay ground water pumping system.

The primary features of concern in the Lists of Operating Criteria are the four bodies of water that can be regulated in the Oroville Complex which are:

Lake Oroville (Page 414)	See Figure 201
Thermalito Diversion (Page 417)	See Figure 202
Thermalito Forebay Reservoir (Page 418)	See Figure 202
Thermalito Afterbay Reservoir (Page 420)	See Figure 203.

Regulating Feature

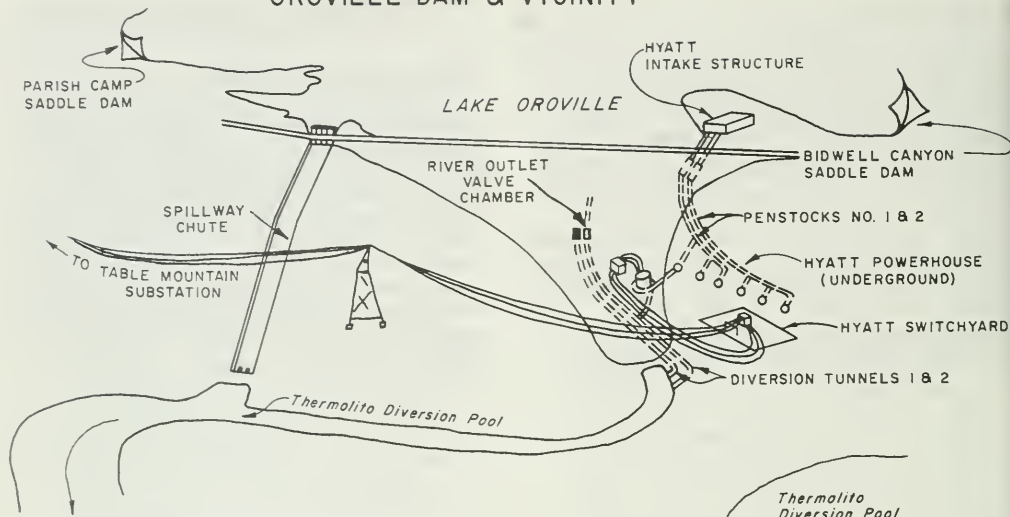
The features that can be regulated have a normal operating criteria, and an emergency operating condition. The emergency condition is dictated by the degree, or potential degree, of loss of structural integrity. The listed criteria is mandatory and must be met, either on an interim basis while investigations continue, or as assurances of integrity come in from either field or plant investigations. Many of the criteria conditions can be determined quickly, whereas others take time and

testing for full assurance that they are validly met.

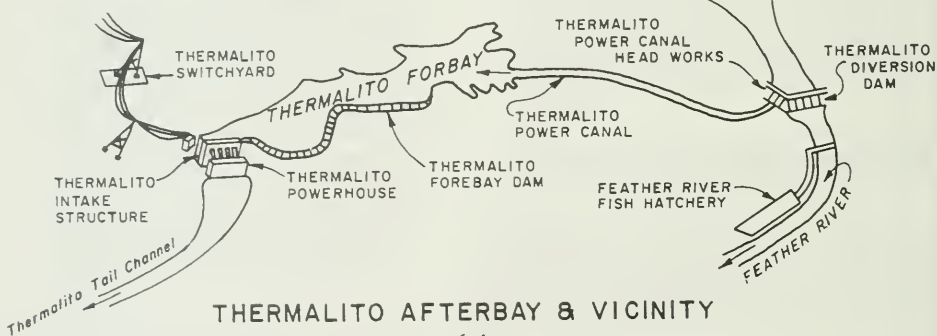
Nonregulating Features

Nonregulating features are those structures that cannot be operated, such as Oroville Dam or the Thermalito power canal. Certain conditions as are described after each nonregulating feature constitute a declaration of true emergency for that feature. Water and power operations or both then become secondary to whatever response is required to protect lives or reduce further damage.

OROVILLE DAM & VICINITY



THERMALITO FOREBAY & VICINITY



THERMALITO AFTERBAY & VICINITY

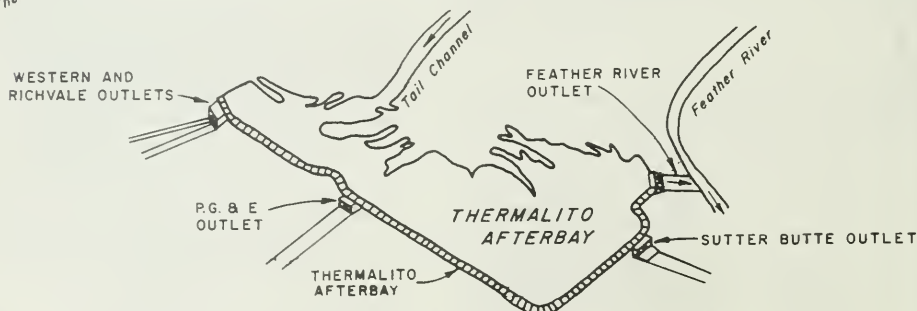


Figure 200. Schematic Diagram of Oroville Complex

OROVILLE DAM AND VICINITY

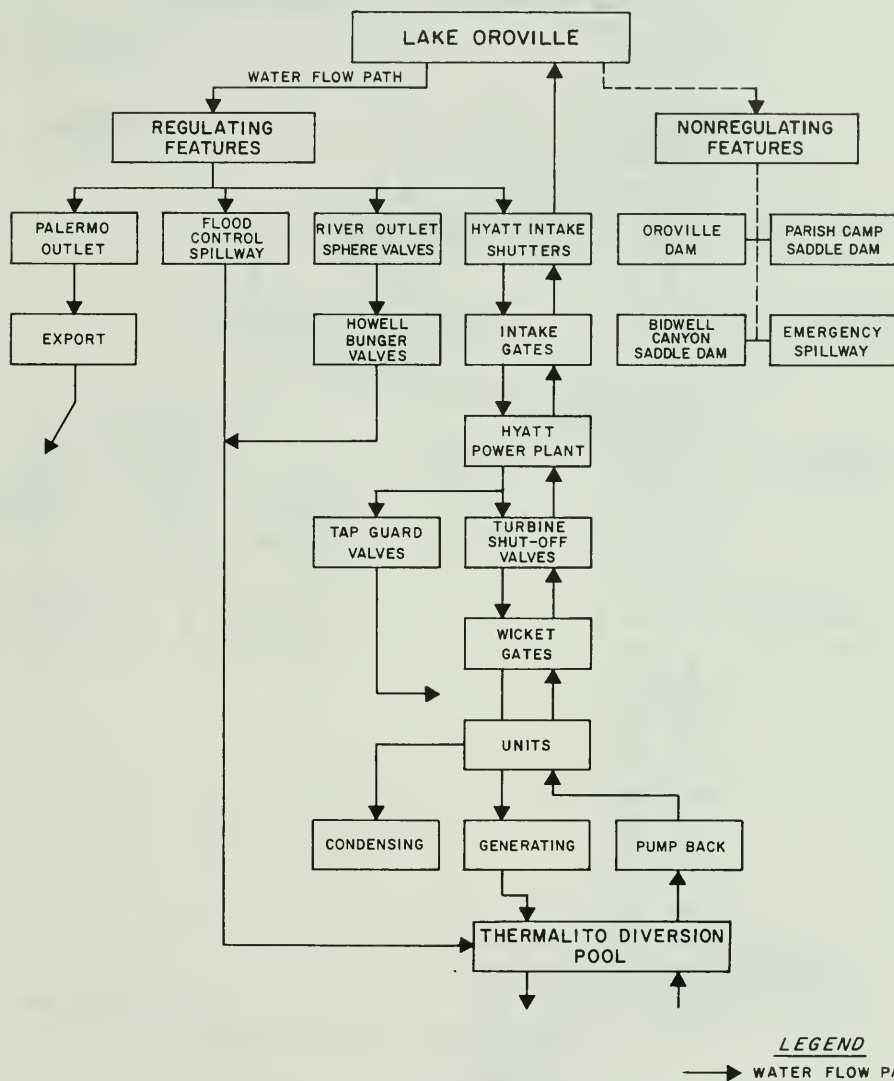


Figure 201. Schematic Diagram of Oroville Dam and Vicinity

THERMALITO FOREBAY AND VICINITY

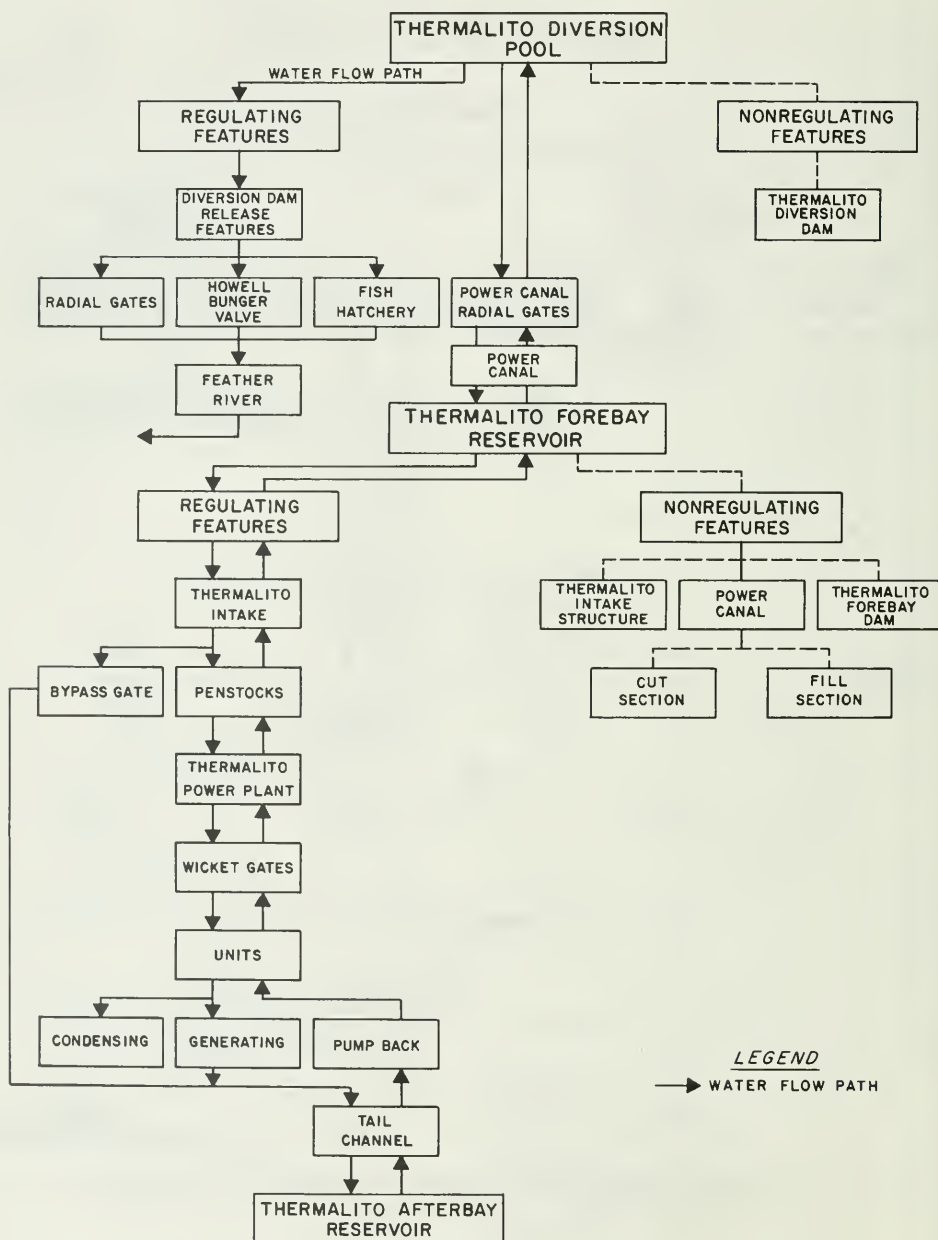
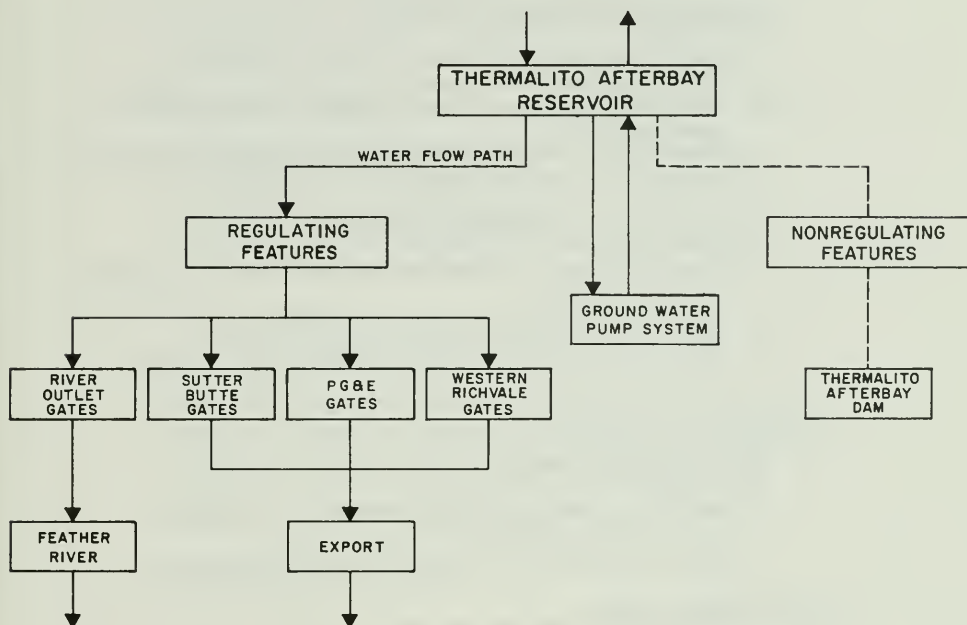


Figure 202. Schematic Diagram of Thermalito Forebay and Vicinity

THERMALITO AFTERBAY AND VICINITY



LEGEND
→ WATER FLOW PATH

Figure 203. Schematic Diagram of Thermalito Afterbay and Vicinity

LIST OF OPERATING CRITERIA FOR REGULATING LAKE OROVILLE

I. DECISION MAKING CRITERIA FOR OPERATING FEATURES WHICH CAN BE REGULATED

A. PALERMO OUTLET

1. 30-inch butterfly valve (1 valve)

- a. Must be closed when fixed dispersion cone valve integrity is questionable.
- b. Must be closed when Palermo intake works integrity is questionable.
- c. Must be open to meet water delivery demand by Oroville Wyandotte Irrigation District.

2. 12-inch fixed dispersion cone valve (1 valve)

- a. Must be closed when 30-inch butterfly valve integrity is questionable.
- b. Must be closed for Palermo Canal failure.
- c. Must be open to meet water delivery demand by Oroville Wyandotte Irrigation District.

B. OROVILLE DAM SPILLWAY

1. Radial gates (8 gates)

- a. Must be available for maintenance of the flood control reservation.
- b. Must be available for Lake Oroville regulation.

C. RIVER OUTLET VALVES

1. Spherical valves (2 valves)

- a. Must be closed when Howell Bunger valves integrity questionable.
- b. Must be closed when intake integrity is questionable.
- c. Must be open when Howell Bunger valves will be operated.
- d. Should be closed when Howell Bunger valves are not needed.

2. Howell Bunger valves (2 valves)

- a. Must be closed when diversion tunnel No. 2 has severe blockage.
- b. Must be closed when spherical valve integrity is questionable.
- c. Must be opened when water delivery is unavailable thru Hyatt Powerplant.

D. EDWARD HYATT INTAKE

1. Intake gates (2 gates)

- a. Must be closed during a powerhouse disaster.
- b. Must be closed for Penstock, turbine shutoff valve or tap guard valve damage.
- c. Must be open to meet Edward Hyatt Powerplant water demand.

2. Shutters (26 shutters)

- a. Enough must be removed in order to comply with Shutter Submergence Criteria.
- b. Enough must be in place in order to control the temperature of water releases.
- c. Enough should be in place to provide protection from debris at lower levels.

E. EDWARD HYATT POWERPLANT

1. Turbine shutoff valves (6 valves)

- a. Must be closed if powerplant is flooded.
- b. Must be closed if penstock integrity is questionable.
- c. Must be open for unit operational demand.
- d. Should be open to control auto oscillation.
- e. Should be closed if tailrace tunnel is blocked.
- f. May be open if intake gates are closed.

2. Tap guard valves (6 valves)

- a. Must be open for raw and cooling water supply to Edward Hyatt Powerplant units.
- b. Must be closed for failure of cooling water line below the valves.
- c. Should be closed in the event of powerplant flooding.

3. Wicket gates (6 gate sets)

- a. Must be open if units are generating or pumping.
- b. Must be closed for synchronous condensing.
- c. May be closed for unit shut down.
- d. May be closed for testing purposes of sediment bearing water appearing in the tailrace tunnel.

4. Unit operation-synchronous condensing (6 units)

- a. Cannot be done if units are generating or pumping.
- b. May be done for power system stability (as requested by the power company.)

5. Unit operation-generating (6 units)

- a. Cannot be done if intake gates are closed.
- b. Cannot be done if powerplant disaster exists.
- c. Must not be done if unit integrity is questionable.
- d. Must not be done if an incompatible stage differential exists between Lake Oroville and Thermalito Diversion Pool.
- e. Cannot be done if units are pumping or synchronous condensing.
- f. May be done to provide station service.(units 1 or 4).
- g. Must not be done if tailrace tunnels are blocked.
- h. Should not be done if switchyard or transmission line integrity are not OK.
- i. Should not be done if no power or water demands exist.
- j. Should be done if regulation of Lake Oroville is required.

6. Unit operation-pump back (3 units)

- a. Cannot be done if intake gates are closed.
- b. Cannot be done if powerplant disaster exists.
- c. Must not be done if unit integrity is questionable.
- d. Must not be done if an incompatible stage differential exists between the Thermalito Diversion Pool and Lake Oroville.
- e. Cannot be done if units are synchronous condensing or generating.
- f. Must not be done if switchyard or transmission lines are not OK.
- g. Should not be done if tailrace tunnel is blocked.
- h. Should be done at the power company request.
- i. Should be done for water conservation.
- j. May be done for Diversion Pool regulation.

II. CRITICAL CONDITIONS FOR FEATURES WHICH CANNOT BE REGULATED

A. OROVILLE DAM

1. Uncontrollable water born sediment passing thru embankment, groins, foundation, grout gallery or tailrace tunnel.
2. Significant slips or cracks in embankment.
3. Crest settlement which could lead to overtopping.
4. Significant vertical or horizontal displacement.
5. Excessive increases in pore pressure.

B. BIDWELL CANYON SADDLE DAM

1. Uncontrollable water born sediment thru embankment, groins or foundation.
2. Significant slips or cracks in embankment.
3. Crest settlement which could lead to overtopping.
4. Significant vertical or horizontal displacement.

C. PARISH CAMP SADDLE DAM

1. Uncontrollable water born sediment thru embankment, groins or foundation.
2. Significant slips or cracks in embankment.
3. Crest settlement which could lead to overtopping.
4. Significant vertical or horizontal displacement.

D. OROVILLE DAM SPILLWAY

1. Extraordinary damage to concrete monoliths or groins.
2. Inoperable radial gates limit ability to maintain flood control reservation.

E. EDWARD HYATT INTAKE AND PENSTOCK

1. Extraordinary damage to structure, trash racks, emergency gates, or penstocks.

F. PALERMO INTAKE AND OUTLET

1. Loss of control of water thru outlet.

G. RIVER OUTLET VALVE CHAMBER

1. Loss of control of water thru outlet.
2. Extraordinary damage to tunnel plugs.

LIST OF OPERATING CRITERIA FOR REGULATING
THERMALITO DIVERSION POOL

I. DECISION MAKING CRITERIA FOR OPERATING REGULATING FEATURES

A. THERMALITO DIVERSION DAM

1. Radial gates (14 gates)
 - a. Must be open to pass flood control waters to Feather River.
 - b. Should be operable to regulate waters in Thermalito Diversion Pool and Thermalito Forebay.
 - c. Should be closed for Thermalito Powerplant operations.
 - d. May be used to meet water delivery commitments in the Feather River.
2. Howell Bunger valve (1 valve)
 - a. Should be open to maintain minimum water release for stream flow maintenance in the Feather River.
3. Fish hatchery valve (1 valve)
 - a. Should be open to meet water demand from the Feather River Fish Hatchery.

4. Radial gates to power canal (3 gates)

- a. Must be closed to protect the Thermalito Power Canal and Thermalito Forebay during extreme flood control conditions in Thermalito Diversion Pool.
- b. Must be open to keep Thermalito Powerplant operational.
- c. May be closed if Thermalito Power Canal or Thermalito Forebay Dam integrity is questionable.

II. CRITICAL CONDITIONS FOR FEATURES WHICH CANNOT BE REGULATED

A. THERMALITO DIVERSION DAM

1. If uncontrollable water born sediments are passing thru the groins or foundation.

B. THERMALITO POWER CANAL HEADWORKS

1. Extraordinary damage to radial gates.

LIST OF OPERATING CRITERIA FOR REGULATING THERMALITO FOREBAY
RESERVOIR AND POWER CANAL

I. DECISION MAKING CRITERIA FOR OPERATING REGULATING FEATURES

A. THERMALITO INTAKE STRUCTURE

1. Bypass gate (1 gate)

- a. May be open when Thermalito Powerplant is not operational.
- b. May be used for Thermalito Afterbay regulation.
- c. May be used for Thermalito Forebay regulation.

2. Fixed wheel gates (2 gates)

- a. Must be used for uncontrollable water thru units.
- b. Should be used for penstock rupture.

B. THERMALITO POWERPLANT

1. Wicket gates (4 gate sets)

- a. Must be open if units are generating or pumping.
- b. Must be closed for synchronous condensing.
- c. May be closed for unit shut down.

2. Unit operation-synchronous condensing (4 units)

- a. Cannot be done if units are generating or pumping.
- b. May be done for power system stability (as requested by the power company).

3. Unit operation-generating (4 units)

- a. Cannot be done if fixed wheel gates are closed.
- b. Cannot be done if a powerplant disaster exists.
- c. Must not be done if unit integrity is questionable.
- d. Must not be done if an incompatible stage differential exists between the Thermalito Forebay and the Thermalito Tail Channel.
- e. Cannot be done if units are pumping or synchronous condensing.
- f. Must not be done if tail channel is blocked.
- g. Should not be done if switchyard or transmission line integrity are not OK.
- h. Should not be done if there are no power or water demands.
- i. May be done for regulation of Thermalito Forebay or Thermalito Afterbay.
- j. May be done to provide station service.

4. Unit operation-pumpback (3 units)

- a. Cannot be done if fixed wheel gates are closed.
- b. Cannot be done if powerplant disaster exists.
- c. Must not be done if unit integrity is questionable.
- d. Must not be done if an incompatible stage differential exists between the Thermalito Forebay and the Thermalito Tail Channel.
- e. Cannot be done if units are synchronous condensing or generating.
- f. Must not be done if switchyard or transmission lines are not OK.
- g. Should not be done if tail channel is blocked.
- h. Should be done at the power company request.
- i. Should be done for water conservation.
- j. May be done for Thermalito Afterbay or Thermalito Forebay regulation.

II. CRITICAL CONDITIONS FOR FEATURES WHICH CANNOT BE REGULATED

A. THERMALITO FOREBAY DAM

- 1. If uncontrollable water born sediments are passing thru the embankment, groins or foundation.
- 2. Significant slips or cracks in embankment.
- 3. Crest settlement which could lead to overtopping.
- 4. Significant vertical or horizontal displacement.

B. THERMALITO INTAKE STRUCTURE

- 1. Uncontrollable water passing thru or under intake structure.
- 2. Extraordinary damage to structure, trash racks or bypass gate.
- 3. Extraordinary damage to end wall gravity dam.

C. THERMALITO POWER CANAL (Cut Section)

1. Extraordinary damage to canal cut or lining.

D. THERMALITO POWER CANAL (Fill Section)

1. If uncontrollable water born sediments are passing thru the embankment, groins, or foundation
2. Significant slips or cracks in embankment.
3. Crest settlement which could lead to overtopping.
4. Significant vertical or horizontal displacement.

LIST OF OPERATING CRITERIA FOR REGULATING
THERMALITO AFTERBAY RESERVOIR

I. DECISION MAKING CRITERIA FOR OPERATING REGULATING FEATURES

A. THERMALITO AFTERBAY RIVER OUTLET

1. Radial gates (5 gates)
 - a. Should be open to meet Feather River stream flow maintenance commitments.
 - b. May be open to regulate Thermalito Afterbay Reservoir.

B. SUTTER-BUTTE OUTLET

1. Slide gates (4 gates)
 - a. Must be open to meet Sutter-Butte Irrigation District water demands.

C. PG&E OUTLET

1. Slide gates (1 gate)
 - a. Must be open to meet PG&E water demands.

D. WESTERN CANAL AND RICHVALE OUTLETS

1. Slide gates (8 gates)
 - a. Must be open to meet Western Canal (PG&E) or Richvale Irrigation District water demands.

E. THERMALITO AFTERBAY DAM GROUND WATER PUMPING SYSTEM

1. Ground water pumps (15 pumps)
 - a. Must be on to maintain ground water aquifer level.
 - b. Must be off to prevent overdraft of ground water aquifer.

II. CRITICAL CONDITIONS FOR FEATURES WHICH CANNOT BE REGULATED

A. THERMALITO AFTERBAY DAM

1. If uncontrollable water born sediments are passing thru the embankment, groins, or foundation.
2. Significant slips or cracks in embankment.
3. Crest settlement which could lead to overtopping.
4. Significant vertical or horizontal displacement.

B. THERMALITO POWERHOUSE STRUCTURE

1. Uncontrollable inflow into Thermalito Tail Channel.
2. Extraordinary damage to Thermalito Powerhouse.

C. THERMALITO AFTERBAY RIVER OUTLET

1. Extraordinary damage to structure or radial gates.

D. SUTTER-BUTTE OUTLET

1. Extraordinary damage to structure.

E. PG&E OUTLET

1. Extraordinary damage to structure.

F. WESTERN-RICHVALE OUTLETS

1. Extraordinary damage to structure.

Commentary

Seismic emergencies at the Oroville Field Division are addressed through the preceding contingency plan.

Priorities for inspection and work are established on the following basis:

1. Attention to those structures whose failure can lead to loss of life and significant property damage.
2. Attention to those facilities whose operation can lead to further damage or failure to Project structures.
3. Attention to those structures whose condition may lead to limiting the

ability to meet power and water delivery commitments.

4. Attention to those structures and facilities that are supportive to efficient operation but are not in themselves, critical to priorities 1, 2, and 3.

Conclusion

The contingency plan is attentive to established Division Policy; it provides for detection, notification, and response to seismic events. The plan also includes a list of operational facilities and features along with criteria that must be met before returning to pre-earthquake operating status.

APPENDIX A

REPORTS PREPARED BY THE SPECIAL CONSULTING BOARD AND RESPONSES BY THE DEPARTMENT OF WATER RESOURCES

1. Reports of the Consulting Board for Earthquake Analysis, 11 August 1975 424
2. Report of the Special Consulting Board for the Oroville Earthquake to Mr. R. B. Robie, 12 September 1975 429
3. Memorandum, "Proposed Department Activities in Response to Consulting Boards." from Robert W. James to Mr. Ronald B. Robie, October 30, 1975 436
4. Report of the Special Consulting Board for the August 1, 1975 Earthquake to Mr. R. B. Robie, 23 November 1976 444
5. Memorandum, "Proposed Department Activities in Response to the Special Consulting Board Meeting of November 22 and 23, 1976," from Robert B. James to Ronald B. Robie, March 4, 1977 . . 452

REPORT OF THE CONSULTING BOARD FOR
EARTHQUAKE ANALYSIS

Messrs: Robert Jansen
H. G. Dewey, Jr.

Gentlemen:

At a meeting on 8 August 1975 with the Consulting Board for Earthquake Analysis, staff members of the Department of Water Resources reviewed the instrumental and other data obtained in the vicinity of Oroville Dam as a result of the series of moderate earthquakes which have occurred in that region, and presented evaluations of the performance of the SWP facilities in response to the earthquake effects. At the conclusion of the briefing the Board was asked to respond to questions relating to the earthquakes and possible future events. Our responses are presented below.

Question 1

The designs of the SWP facilities in the Oroville area were predicated upon certain appraisals of probable future regional seismicity in the site vicinities. In view of the recent earthquake activity in the Oroville area are the original appraisals still valid? What adjustments, if any, should be made in those appraisals?

1a. Although the original appraisal by DWR staff that "the Oroville dam site is in an area of relatively light seismic activity" may have been justified by the data available at the time of design (1958), it should now be modified in the light of the recent earthquake activity in the Oroville area and of knowledge gained since 1958. In view of the developments, it is appropriate to consider that earthquakes ranging up to magnitude 6.5 may occur within a few miles of the dam site.

Question 2

What factors should be examined in determining if recent appearance of extended seismic activity is related to the 10-year existence of Oroville Reservoir in the area of activity?

2a. If studies along these lines in other parts of the world are any indication, investigations of this relationship are likely to be quite difficult, and even inconclusive. Nevertheless, a number of sets of observations may throw some light on the matter and it is essential that they be made soon and as precisely as possible.

a) The DWR should arrange to have repeat geodetic surveys made of past triangulation nets and, particularly, level lines in the region of the reservoir and recent earthquake activity. These surveys should be made as quickly as practicable and perhaps repeated after a few months.

b) DWR should undertake a timed chemical explosion in a borehole near the epicenter of the main shock (August 1) while the majority of field seismographs are still operating in the earthquake area. Such an explosion is a proven way of calibrating the location of earthquake foci in the region against a seismic source with known position. In addition, the calibration explosion will calibrate the polarity of the seismograph responses thereby enabling more reliable fault-plane solutions to be computed.

c) It is essential that surface fractures possibly associated with faulting at depth be carefully delineated and documented without delay. Low-altitude, low-sun-angle aerial photography may be of assistance in this effort. It is also critical that the local surficial geology be more completely mapped and better understood, if surface faulting has indeed occurred. Two critical questions are: (1) Have the earthquakes occurred along a pre-existing fault, particularly one with Quaternary displacement and (2) can the causative fault be traced

beyond the area of recent earthquakes into areas of future hazard? In all geological efforts, DWR personnel should coordinate their work with those of other groups studying the earthquake.

d) Another line of investigation of any connection between the reservoir and recent earthquake activity depends upon computation of stresses in crustal models loaded by appropriate surface forces. Theoretical work along these lines should be supported and evaluated against the Oroville data.

Question 3

What does the board recommend in the way of immediate and future seismic data collection? Seismic data evaluation?

a) All instrumental data recorded by DWR in connection with the Oroville earthquakes should promptly be put into usable form and published. The significance to the Department and to scientific and engineering communities cannot be overestimated, and care must be taken not only to adequately preserve the original records, but also to reproduce the data in suitably annotated graphic form; and when appropriate, records should also be digitized. As soon as the recorded data are in an easily understood form, it is requested that copies be provided to each Board member.

b) DWR should establish a permanent telemetered seismic station near the epicenter of the August 1st main shock, and temporary stations should continue to be operated in the area as long as significant aftershock activity lasts. The Department should continue to make sure that it has portable seismographic units available to move into critical areas of suspicious seismic activity in California, as it did several weeks prior to the main Oroville event.

c) DWR should install additional strong-motion accelerographs in the vicinity of Oroville Dam. There should be two permanent accelerographs on the crest of the dam and one permanent accelerograph

on each abutment; and three temporary accelerographs should be installed in a triangular array in the epicentral region of the August 1975 earthquakes, replacing the Caltech instruments. All these instruments should be equipped with radio time recording. The two AR 240 accelerographs presently located on the dam and abutment should be removed from their present locations, renovated and used elsewhere.

d) DWR should review its procedures for reacting to the occurrence of an earthquake near a dam or other major facility, i. e., to plan appropriate actions for getting additional strong-motion accelerographs, and other instruments, in the field, checking operability of instruments, etc.

e) The static and dynamic data from instruments in and about the dam should be processed and put into completely usable form, and then be used together with current, accepted analysis procedures to evaluate the dynamic properties of the dam and its materials.

f) The experience gained from the Oroville earthquakes in sensing and recording significant physical behavior should now be applied to all major DWR dams and facilities with a view to improving the collection of data. This should include installation of new instruments, improving existing instrumentation, and increasing the reliability of the instrument systems.

g) DWR should specially review the seismic instrumentation program at Oroville with experts in instrumentation, in recording and processing data, making use of the latest knowledge and expertise to improve the system.

h) A survey program of leveling and triangulation of the dam and adjacent area should be completed as soon as possible, consistent with accuracy control, etc. In addition, arrangements should be made in collaboration with other appropriate agencies to resurvey a more general area and to tie the surveys together. Comparisons should be made with prior data to determine if there have been any changes of a differential or of an absolute nature in the region or the dam. The survey data from the dam and adjacent points should also be correlated with the measurements from movement devices in the dam.

C. R. Allen

C.R. ALLEN by G.W.H.

John A. Blume

J.A. BLUME

Bruce A Bolt

B.A. BOLT

G.W. Housner

G.W. HOUSNER

H. Bolton Seed

H.B. SEED

Report of the Special Consulting Board for the Oroville Earthquake to:

Mr. R. B. Robie, Director
Department of Water Resources

At a meeting on September 11 and 12, 1975 with the Special Consulting Board for the Oroville Earthquake, staff members reviewed information relevant to the Oroville earthquake and the performance of Oroville dam and its facilities, and described the proposed seismic reevaluation of the dams, structures and equipment. At the conclusion of the meeting the Board was asked to respond to seven questions. Our responses are presented below.

Question 1

At its meeting on August 8, 1975, the Consulting Board for Earthquake Analysis advised that the appraisals of the regional seismicity in the Oroville area be modified and recommended several specific actions as a part of that reappraisal. What comments and further suggestions does the Special Consulting Board on the Oroville Earthquake have with regard to the progress of the Department's implementation of those recommendations?

The Department has responded commendably to the actions recommended on August 8, 1975. A few projects are not yet complete and these should be carried forward as quickly as feasible. These include particularly the calibration explosion and the detailed geological mapping.

As well as the additional strong-motion instrumentation to be installed at the dam and the improved recording capability there, the Department should establish water gage stations at several suitable positions around the reservoir. The purpose of the gages would be to determine if regional tilting of the crust under the reservoir, perhaps related to an impending earthquake, is occurring.

During the presentations it became apparent that some additional administrative attention needs to be given to the line of responsibility for continuous maintenance, for emergency operation during earthquakes and modernization of monitoring equipment. In particular, it would seem best if the earthquake engineering group had the responsibility for ensuring the satisfactory performance of all seismographic instrumentation and analysis.

Question 2

What comments does the Board have regarding the performance of the dams and other structures?

The Board was presented with extensive oral and written reports covering observations of various structures of the Oroville-Thermalito complex immediately following the Oroville earthquake, and for many of these structures during the interim since that earthquake. All data submitted indicate that the related structures performed satisfactorily without distress or damage, and as anticipated in the design.

The Board commends the Department for its prompt inspection of project structures following the earthquake.

Question 3

What are the Board's views on the identification of the causative fault? Is it possible to identify the fault beyond the recent epicentral area?

The Board feels that the causative fault zone has already been identified with reasonable confidence, although the zone does not necessarily comprise a single fracture surface. Both the seismological and geological studies strongly suggest failure by normal (extensional)

faulting on a zone trending roughly north, and dipping steeply west. In all likelihood, the causative fault zone extends farther to the north and south than the segment broken at depth during this series of earthquakes, but these extensions have not as yet been positively identified. It is important that further work to identify these extensions be vigorously pursued--by detailed geologic mapping, by continued seismic monitoring, by repeated geodetic surveys across the suspected area, and by further trenching of suspicious features. Particular attention should be given to understanding the lineaments identified from aerial imagery and to searching thoroughly for all possible exposures of faulted Quaternary strata.

Question 4

What are the Board's recommendations concerning the design earthquakes proposed for use in the seismic reanalyses of the Oroville-Thermalito structures?

The Board considers that an appropriate earthquake motion for re-evaluation of structures critical to public safety in the Oroville-Thermalito complex would be one producing a peak acceleration of 0.6 g and having characteristics similar to those developed near Pacoima dam during the San Fernando earthquake of February 9, 1971. The time-history of such a motion should be obtained from a modified form of the Pacoima dam record, as discussed in the Report of the Consulting Board for Earthquake Analysis dated May 22, 1973. The actual time-history could be the same as that forwarded to Mr. Jansen by Clarence R. Allen with his letter of January 16, 1974, except that the duration of shaking should be limited to the first 20 seconds of the record provided, and all ordinates of the record should be multiplied by a suitable scaling factor to give a peak acceleration of 0.6 g .

In addition the structures should be checked for the motions produced by the following earthquakes:

- (a) a Magnitude 8.5 earthquake occurring at a distance of 100 miles
- (b) a Magnitude 7.25 earthquake occurring at a distance of 35 miles

It is unlikely that these latter two earthquakes will produce conditions more critical than the motion discussed in detail above, but the check should be made to verify that this is so. Design earthquakes for non-critical structures can be less severe in intensity than those discussed above and the Board will defer this recommendation until the evaluation of critical structures is completed.

Question 5

What are the Board's comments concerning the proposed program for the seismic reanalyses of the Oroville-Thermalito structures?

The Board concurs with the Department's concept of establishing criteria for the relative priority of reassessing the seismic safety of the various Oroville-Thermalito structures. It also concurs that those structures most critical in terms of public safety should be analysed by the best available dynamic methods. Among these structures the Board includes both Oroville dam and its Spillway.

In regard to the Thermalito embankment dams, it is suggested that those two or three sections of the Forebay and Afterbay dams which appear to be least stable from foundation and/or dynamic response points of view be selected for detailed reevaluation using dynamic analyses procedures. When these studies have been completed other embankment dams in the Oroville-Thermalito complex might well be reassessed by judgment without detailed analysis.

In regard to the many reinforced concrete structures in the complex, only those that can be shown to be critical to public safety would seem to justify the use of sophisticated dynamic analysis procedures, but all structures evaluated in the original design of the project should be checked for adequacy either by judgment procedures or by testing their adequacy under increased assumed earthquake loading.

Question 6

The Board is requested to provide further explanation and guidance concerning the Earthquake Analysis Board's recommendation (2d) to evaluate stresses in crustal models.

The Board has no further recommendations at this time. Upon completion of the crustal stress analyses now being made by others, the Department may wish to review the question again.

Question 7

Does the Board have any other comments or recommendations?

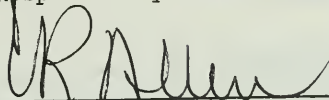
The Board offers the following suggestions, some of which constitute reinforcement of procedures discussed previously or in-process.

- (a) The Department should take full advantage of data collected or developed by all other agencies, both public and private, concerned with the Oroville area seismicity. Cooperation with such agencies and exchange of data would ensure that all reliable data are made available toward the solution of the problem.
- (b) The Department should develop a detailed procedure for the proposed seismic stability evaluation of Oroville dam embankment, with particular definition of the steps planned for

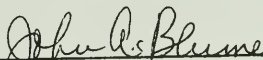
determining the dynamic strength properties of the various embankment materials under confining pressures of up to 500 psi.

- (c) The Department should review procedures and contingency plans at all dams and major installations for returning equipment and facilities to full service after a shutdown due to an earthquake. Directives for return of equipment to preearthquake operating levels should be based upon full knowledge of project conditions in order to avoid premature start-up and potential extension damage.
- (d) In view of recent press reports concerning the alleged likelihood of future large earthquakes near Oroville, the Special Board emphasizes that the hypothetical maximum earthquake of Magnitude 6.5 mentioned in the Earthquake Board's report of 11 August 1975 is considered to be a very unlikely event and is intended to be used for safety review. Furthermore, it is our judgment that any earthquake significantly stronger than the Magnitude ~~5.7~~ event of 1 August 1975 is improbable in the near future.

Respectfully Submitted,



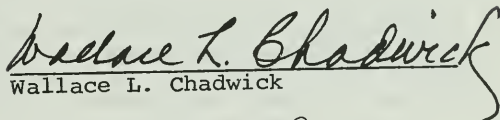
C. R. Allen



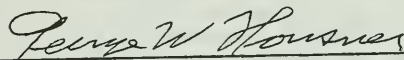
John A. Blume



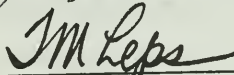
Bruce A. Bolt



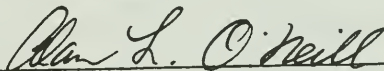
Wallace L. Chadwick



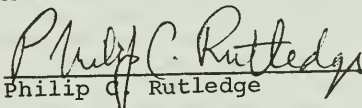
George W. Housner



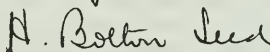
T. M. Leps



Alan L. O'Neill



Philip C. Rutledge



H. Bolton Seed

Memorandum

To : Mr. Ronald B. Robie

Date : OCT 30 1975

File No.:

Subject: Oroville Earthquake
of August 1975, Proposed
Department Activities in
Response to Consulting
BoardsFrom : Robert W. James
Department of Water Resources

As requested by your August 22, 1975 memorandum, presented below is a description of our program to implement the recommendations made by the Consulting Board for Earthquake Analysis in their August 8, 1975 report and by the Special Board for the Oroville Earthquake in their September 12, 1975 report. An estimate of cost for carrying out these activities is also included. This memorandum will also satisfy the requirements of Water Resources Engineering Memorandum No. 23 by accounting for the actions taken to the Boards' conclusions and recommendations.

The items below are listed by number as they appear in the Board reports. Copies of the reports are attached for easy reference.

Consulting Board for Earthquake Analysis

- 1a. The level of seismic activity in the Oroville area will be reappraised. Accelerograms will be developed for earthquakes that are considered to be credible. Included will be a local earthquake with Magnitude 6.5 as recommended by the Board and a Magnitude 8+ on the San Andreas fault. Finite element analyses will be conducted on Oroville Dam using one or more of the strongest accelerograms. These analyses will be carried out by personnel of the Division of Safety of Dams who presently have the expertise. Dr. H. B. Seed will be retained throughout the study to provide guidance. Additional soils testing, under the direction of Dr. Seed, will be conducted at the Richmond Laboratory. The Division of Design and Construction will fund the entire study and will have overall responsibility for its completion and final report. Dr. Seed has been contacted, and he generally agrees to this approach.

The accelerograms will be examined to determine if the seismic factors used for the design of other major structures in the Oroville-Thermalito Complex are still considered adequate. Structures will be reanalyzed as necessary. The manpower shown is tentative as it will depend upon early staff findings.

Staff time 2.5 man years
Laboratory soil testing

\$ 82,000
20,000
\$102,000

OCT 30 1975

- 2a. Five survey parties, two from the Division of Operations and Maintenance, two from the Division of Land and Right of Way, and one crew from the U. S. Geological Survey were involved in the work in the Oroville area. Coordination was provided by Division of O&M, Chief of Precise Surveys.

Principal objectives that have been achieved include: (a) vertical and horizontal surveys of Oroville Dam, (b) level runs over previously established lines to attempt to determine location of major faults, (c) a survey of the horizontal and vertical control network about Lake Oroville, (d) a survey of the epicentral area of the earthquake with a tie to established bench marks outside the affected area, (this work was done by U.S.G.S.), and (e) surveys of the smaller structures in the Oroville-Thermalito Complex.

The U.S.G.S. survey party operated at its own expense.

Department survey cost (including travel expenses)	\$ 55,000
--	-----------

- 2b. The calibration explosion is being coordinated with U.S.G.S. Because DWR equipment could be made available before U.S.G.S. equipment, the recommended shot was undertaken by this Department. The plan involves one drill hole with the explosion at a depth of about 300 feet. Drilling is now under way, and is expected to be completed before October 17. The hole will be loaded and shot as soon thereafter as possible.

Aside from the shot recommended by the Consulting Board, the U.S.G.S. has proposed to cooperate in staging two additional shots - one in the Yuba River near Marysville and another in one of the northern arms of Lake Oroville. These shots would supplement the Department shot and would more precisely define the crustal structure in the Oroville region.

Cost of DWR shot: drilling, materials	
staff time	\$ 40,000

- 2c. A search for the fault that caused the earthquake revealed a cracked zone along an old fault south of Wyandotte. It is believed this is the fault, or one of the faults, related to the recent seismic activity. Remote sensing imagery consisting of U-2 infrared color, ERTS satellite and side-looking airborne Radar (SLAR) imagery were obtained and used for a study of lineaments in the epicentral region.

Both vertical and low sun angle aerial photographs were obtained in the epicentral area and will be used both for geologic mapping of the epicentral region and for detection of features that might be faults.

Geologic mapping is now progressing northward from the zone of surface cracking toward project facilities. Discussions have been held with Division of Mines and Geology to have them do some of the geologic mapping in the epicentral area at their cost. Discussions also have been held with PG&E, Woodward-Clyde Associates and U.S. Corps of Engineers on the problem of obtaining a better understanding of the regional tectonic framework of the western Sierra Nevada. Objectives of all these activities are:

1. Identify the causative fault and determine its relation to project facilities.
2. Obtain better knowledge of geology in epicentral area in order to decide if Oroville Lake was a contributing factor to the earthquake.
3. Get a better understanding of the regional tectonics to better evaluate potential for future seismic activity.

Cost: Aerial photos, imagery, etc.	\$ 7,000
Trenching and other exploration	15,000
Staff time 1.5 man years	60,000
	<u>\$ 82,000</u>

- 2d. Further contact with Board members revealed that computation of stresses in crustal models had been undertaken at Cal Tech. and U. C. Berkeley. Only preliminary results were available. The Board members indicated they had no further recommendations pending completion of these analyses. Upon their completion your staff will review the results with the Board to determine whether or not additional work is desirable.

Cost: None at this time

- 3a. Graphical presentations of various recorded seismic data were developed. Noteworthy accelerograms are being digitized. Some of this digitized data was ready by the time of the Special Board meeting.

Cost of data preparation	\$ 3,000
--------------------------	----------

- 3b. A permanent seismic station near the epicenter of the August 1st shock will be established. A site has been selected and right of entry acquired.

Cost: Staff time, planning & design	\$ 4,000
Equipment, materials & construction	4,000
	<u>\$ 8,000</u>

Three DWR portable sensitive seismographic units are presently installed and operating near Oroville, including one about 3 miles from the main shock epicenter. Two portable visual recorders are needed for portable units to aid in fast and precise determination of epicenters for calibrating a particular area for accurate epicenter determination.

Equipment cost: \$ 8,000

- 3c. Five SMA-1 strong-motion accelerographs have been ordered to replace and augment Oroville Dam strong-motion instrumentation. The instruments will be installed one on each abutment, two on the crest and one in the core block.

Six SMA-1 strong-motion instruments have been ordered to provide for emergency situations, such as the Oroville earthquake, to augment existing instrumentation on SWP structures. Three of these will be installed temporarily in a triangular array around the Oroville epicentral area. In addition to the equipment cost below, there will be some additional cost associated with maintenance of the equipment.

Equipment cost: \$21,000

- 3d. The Division of Operations and Maintenance's procedure for responding to significant or unusual seismic activity affecting SWP structures entails augmentation of existing instrumentation where needed. A check list of possible additional courses of action will be compiled for use in future earthquakes including review of instrument maintenance practices.

Cost for augmentation of instrumentation
at Oroville is covered under Item 3c.

Cost for additional instruments for
the remainder of the project \$48,000

OCT 30 1975

- 3e. Processing of the dynamic data is covered under Item 3a. Nondynamic data are being plotted on expanded scales for clarity and increased functionality.

The properties of the materials in Oroville Dam that can be derived from acceleration and stress data recorded during the earthquakes will be evaluated. This work will be accomplished in similar manner to that covered under 1a. with funding by D&C, the work accomplished by Division of Safety of Dams' personnel, and Dr. Seed utilized in a consulting capacity.

Cost: Staff time, nondynamic data processing	\$ 8,000
Staff time, stress analyses	40,000
Contract work	10,000
	<u>\$58,000</u>

- 3f. Improving seismic data collection at other SWP facilities is now in progress. New insights gained as a result of the Oroville earthquakes will be incorporated in a total system reevaluation.

The costs involved with this item are included under Item 3d. or are presently otherwise budgeted for.

- 3g. Department personnel will review Oroville instrumentation program and modify to strengthen elements where deficiencies may exist. Of particular need is a real time base (WWVB) and a noninterruptable power supply. Replacement of the four existing recorders for the dam dynamic instrumentation is under review.

Estimated cost (including recorders)	\$25,000
--------------------------------------	----------

- 3h. Surveys discussed under this item are included with Item 2a.

Special Consulting Board for the Oroville Earthquake

1. The preceding comments on the report of the Consulting Board for Earthquake Analysis have generally outlined the program and progress on the calibration explosion, geologic mapping, and dynamic instrumentation supplementation.

Additional lake stage recorders in the upper arms are planned for other operational purposes. It is believed that these recorders will serve the Board's intended purposes; however, a thorough evaluation will be made.

OCT 30 1975

The Department will review its programs for both the maintenance of the instrumentation and for the processes for handling and evaluation of records. At the present, responsibility for these activities is vested in the Project Surveillance program with participation by both the Division of Design and Construction and the Division of Operations and Maintenance's Earthquake Engineering Section.

Estimated cost: Included under ongoing programs.

2. Your staff agrees with the Board's conclusion and thanks them for their commendation.
3. See response to Item 2c of the Consulting Board for Earthquake Analysis Report.
4. The design earthquake motion suggested by the Board, modified February 1971 Pacoima recording, will be used for analyzing structures in the Oroville-Thermalito Complex. In addition, safety of the structures will be evaluated for the other suggested events: Magnitude 8.5 at 100 miles and Magnitude 7.25 at 35 miles.

Due consideration will be given to the criticalness of each structure within the complex when evaluating the intensity of loading to be applied.

Cost:

(Included under other items)

5. As stated under Question 4, evaluation of the criticalness of each structure will be made and appropriate loading criteria applied in the reanalyses for seismic safety. Oroville Dam and the spillway will, of course, be given maximum treatment. Suggested analyses for Thermalito Forebay and Afterbay Dams will be accomplished.

Analyses of Oroville Dam	(previously listed)
Analyses of spillway & other structures	(previously listed)
Analyses of Thermalito Dams:	
Staff time	\$30,000
Soils testing	40,000
	<u>\$70,000</u>

6. This subject is commented upon under Item 2d of the report of Consulting Board for Earthquake Analysis.

- 7a. It is our intent to utilize all data developed by others in the evaluation of seismic safety of the Oroville-Thermalito Complex. Similarly all data developed by the Department will be shared with those cooperating in the studies, in preliminary form as the studies develop, and in report form upon their completion.
- 7b. Detailed procedures for analyses of Oroville Dam and the necessary soils testing are being developed.
- 7c. The emergency plans for dams and the procedures for continuing operations of plants, or for return to full operations in event of shutdowns due to earthquakes, will be thoroughly analyzed relative to completeness or adequacy of assessments of potential damages.
- 7d. Your staff agrees with the Board's conclusion. No other comments are necessary.

Estimated cost: Included under ongoing programs or
under other items above.

The total estimated cost, as listed above, for implementation of the Boards' recommendations is \$520,000. For clarity the costs are summarized in the table below.

<u>Item</u>	<u>Cost</u> <u>(\$1,000)</u>	<u>Budget in</u> <u>Organization</u>
<u>Earthquake Analysis Board</u>		
1a. Reevaluate seismicity & design criteria	102	D&C
2a. Surveys	55	O&M
2b. Calibration explosion	40	O&M
2c. Mapping	82	D&C
2d. Crustal models	-	D&C
3a. Seismic record processing	3	O&M
3b. Seismic station	8	O&M
Portable sensitive seismograph units	8	O&M
3c. Strong motion accelerographs	21	O&M
3d. Augmentation of instrumentation:		O&M
Oroville	-	
Remainder of project	48	O&M
3e. Evaluate properties of dam	58	D&C
3f. Improve data collection	-	-
3g. Review Oroville instrumentation program	25	O&M
3h. Surveys	-	O&M

OCT 30 1975

<u>Item</u>	<u>Cost</u> <u>(\$1,000)</u>	<u>Budgeting</u> <u>Organization</u>
<u>Special Board</u>		
1. Implementation of Earthquake Board recommendations	-	-
2. Structure performance	-	-
3. Fault identification	-	-
4. Design earthquake	-	D&C
5. Seismic reanalyses	70	D&C
6. Crustal models	-	-
7. Other recommendations	-	-
	<hr/>	
Cost: O&M Budget	\$208*	
Cost: D&C Budget	<u>312</u>	
Total Cost	\$520	

With your approval the program described above, responding to the recommendations of the Consulting Board for Earthquake Analysis and the Special Board for the Oroville Earthquake, will be implemented.

APPROVED:

Ronald B. Robie
Director

Date 11/13/75

Attachments

*Implementation of O&M related items will require a budget augmentation of \$187,000.

Report of the Special Consulting Board
for the August 1, 1975 Oroville Earthquake to:

Mr. R. B. Robie, Director
Department of Water Resources

At a meeting on November 22 and 23, 1976 with the Special Consulting Board for the Oroville Earthquake, DWR staff members reviewed the work being done by the Department on the seismic reevaluation of the Oroville and Thermalito dams, structures and equipment, as supported by the related geological, seismological and surveillance observations accumulated by DWR and associated agencies. At the conclusion of the meeting the Board was asked to respond to six questions. Our responses are presented below:

Question No. 1. A considerable amount of work has been done along the western Sierra Nevada by various groups since the last Board meeting. Much of this work has been directed at trying to evaluate future seismicity. Has anything developed that would make the Board want to change the recommended earthquake motion for reevaluation of Oroville structures (report on September 12, 1975 meeting)?

Response. Since the last meeting of the Board, substantial investigations of past and potential future seismic activity along the western Sierra Nevada have been made by the Department of Water Resources, by Woodward Clyde Consultants, and by the U. S. Army Corps of Engineers. We are not aware that these investigations have produced any information to date which would cause the Board to change the earthquake motion it recommended in its response to Question No. 4 in the report of

12 September, 1975 for seismic re-evaluation of the Oroville-Thermalito structures. However, a special supplementary motion, applicable only to high frequency structures and facilities, is discussed in answer to Question 2 below.

Question 2. Does the Board have any comments or recommendations concerning the results or methods used in the seismic re-analysis of the critical structures completed to date?

Response. The Board considers the methods being used thus far in seismic re-analysis of critical structures to be appropriate and, in general to represent the current state of the art. It is obvious that care is being taken to model the structures in a realistic manner and to consider the dynamic aspects of the problems at hand. In most cases, final results have not yet been obtained in the sense that calculated stresses and strains have not been compared with allowable values. This aspect of the work should be pursued with vigor.

The matter of allowable tension in concrete should be resolved to the extent practicable at this time, with specific quotations from authoritative reference material. The appropriate extent of dynamic water loading of the 3D models needs to be resolved for the spillway system.

The Board recommends that, for critical structures with high fundamental frequencies, the previously recommended time history of earthquake motion be supplemented by a time history meeting the high frequency (10 Hz or greater) requirements specified by the Nuclear Regulatory Commission in its Regulatory Guide No. 1.60, with the spectrum scaled to 0.4 g at zero period.

Care should be taken in analyses, and in evaluating the results of analyses, not to compound safety factors by using only the most critical results or conditions in a sequential fashion.

Question 3. Does the Board have any conclusions regarding the possible relation between Lake Oroville and the Oroville Earthquake sequence? If not, does the Board have any recommendations or comments concerning gathering of additional data or making further analytical studies to enable reaching a conclusion in the future?

Response. At its meeting on 11 August 1975, the Consulting Board for Earthquake Analysis indicated that conclusions regarding any causal relation between Lake Oroville and the 1975 Oroville earthquake sequence would be difficult to reach. It was suggested that certain observations be made that might throw light on the matter. Even with more definitive seismological and geological information related to the sequence now available, however, it still appears that it is not possible to draw any firm inference on whether the earthquakes were, or were not, triggered by the reservoir.

It should be noted that the problem of association between large reservoirs and nearby earthquakes is now receiving considerable attention worldwide, and much research on the problem is now underway in the United States and abroad. We recommend that the DWR take steps to keep informed of the results of this research, with a view to possible application to the Oroville situation and other DWR facilities.

Question 4. Does the Board have any recommendations or comments concerning the draft copy of Bulletin 203 before it is published?

Response. Bulletin 203 will be useful as a documentation of the performance of the dam and related facilities during the August 1, 1975 earthquake and aftershock sequence, and as a vehicle for distributing the wealth of seismological and geological data gathered before and after the earthquake. In this regard, the Board believes Bulletin 203 should be limited to include only data describing the seismic events, related geological studies, and performance of the structures.. Although there are numerous minor editorial comments which could be made, at this time the Board offers only the following specific recommendations:

- (a) A more appropriate title would be "Performance of the Oroville Dam and Related Facilities during the August 1, 1975 Earthquake."
- (b) The purpose should be clearly defined in the beginning of the report.
- (c) The final draft deserves further editing to achieve uniform presentation of the findings and conclusions.
- (d) In reporting the factual observations and events, care should be taken to avoid the inference that the Department has made a definite conclusion regarding the relationship or lack of relationship of the reservoir to the earthquakes.
- (e) It is requested that the listing of the Board members on an introductory page of Bulletin 203 be deleted, inasmuch as the Board has not participated in preparing the report. It is similarly recommended that the reports of the Board included in Appendix D be deleted.
- (f) The re-evaluation earthquake studies, recommended previously by the Board, apparently will not be completed before mid-1977. Hence, any conclusions and recommendations relating to such

studies would be premature at this time. It therefore would appear appropriate to issue a separate bulletin or report on this phase of the work in late 1977, as a follow-up to Bulletin 203.

If the foregoing concept is adopted, it would seem desirable that Bulletin 203 include a specific list of all damages to the Oroville complex resulting from the Oroville Earthquake, together with a notation of the type and cost of repair work completed.

Question 5. Does the Board have any recommendations for future geologic work?

Response. The Board emphasizes the value of determining and attempting to understand the growth of surface faulting following the Oroville Earthquake, and it urges that this work continue to be pursued vigorously. On a broader scale, it is important, to the long-term safety of the Oroville Project, that the geologic environment associated with the Oroville earthquake be understood as well as is realistically possible. Two important questions are (1) what is the relationship of the surface faulting associated with the 1975 earthquake to the mapped surface geology, and (2) what can be said about possible future northward extensions of the 1975 fault break? Answers to these questions will undoubtedly require additional trenching and additional detailed geologic mapping, including areas north of the lake. Continuing efforts should be made to relate local geology to geodetically observed deformation patterns. To do this effectively, the area must be re-surveyed for elevation changes at regular intervals, preferably semi-annually, for the next several years.

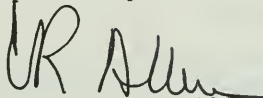
Question 6. Does the Board have any other comments or recommendations to make at this time?

Response. The Board offers the following comments and recommendations:

- (a) The Board would like to draw DWR's attention to the small but finite, likelihood of a future recurrence of an earthquake sequence similar to that of 1975 near to Oroville Dam and its associated facilities. Somewhat analogous seismological and geological conditions in other parts of the world make it not implausible that a possible repetition of the sequence may occur northward from the 1975 events. Indications, if any, of the above development should be sought in future seismological, geological and geodetic monitoring.
- (b) The Board believes that there is urgency to complete the re-analyses of all of the dam elements in the Oroville-Thermalito complex at an early date, in order to determine whether any reinforcement may be required to assure ability of those structures to resist the effects of a 6.5 magnitude local earthquake.
- (c) The surveillance attention being given to the project is commendable. The surveillance provides early detection of damage but time in which to mobilize effectively for major emergency repairs required by seismic damage to embankments would probably not be available. Therefore, inherent structural integrity must be the alternative. In particular, the most critical portions appear, at this time, to be some locations along the Thermalito Forebay and Afterbay Dams. Accordingly, it is recommended that locations of critical sections of these dams be determined on the basis of the existence of

low-density soils, particularly loose sands, in the foundations. Field sub-surface explorations, followed by analyses of these sections under the effects of the "re-evaluation earthquake," should be carried out on an urgent basis and, where potential instability may be indicated, corrective designs should be developed and the construction accomplished as soon as possible.

Respectfully Submitted,



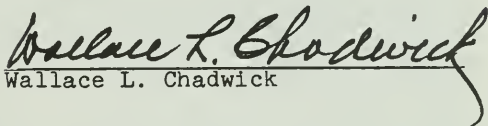
C. R. Allen



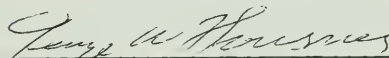
John A. Blume



Bruce A. Bolt



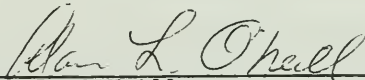
Wallace L. Chadwick



George W. Housner



T. M. Leps



Alan L. O'Neill



Philip C. Rutledge



H. Bolton Seed

Memorandum

To : Ronald B. Robie

Date : MAR 4 1977

File No.:

From : Robert W. James
Department of Water Resources

Subject: Oroville Earthquake of August 1975, Proposed Department Activities in Response to the Special Consulting Board Meeting November 22 and 23, 1976

Presented below is a description of our program to implement the recommendations made by the Special Board for the Oroville Earthquake of August 1975, in their report transmitted to us by letter dated December 15, 1976, for the meeting held November 22 and 23, 1976. The recommendations generally concern completing analyses and work initiated as a result of their recommendations in reports dated August 8, 1975 and September 12, 1975, and outlined in my memorandum to you dated October 30, 1975. Our response to each item in the Board's latest report is listed below by number as they appear in their report. A copy of their report is attached for reference:

1. No changes are required in the earthquake motions that are being used in our reevaluation of Oroville critical structures except for high frequency structures and facilities. Our action concerning these structures is covered under Question 2.
2. The staff agrees with the Board's comments that final results of the dynamic analysis be pursued with vigor and the final results be compared with allowable values. It is intended to proceed as rapidly as possible with the analysis. A funding augmentation of \$300,000 has been approved for the remainder of this fiscal year and it is now estimated that we will need \$166,000 for 1977-78 fiscal year. The additional funds were needed because the scope of the investigation was expanded.

The problem of allowable tension in concrete for dynamic or transient loads has been given considerable study in recent years as recent dynamic analyses of concrete dams have indicated larger tensile stresses than earlier design procedures. It is intended that we will determine what allowable tensile stresses can be used by a search of authoritative reference material to support our contention that dynamic tensile stresses indicated by the analysis are satisfactory. We will be investigating the extent of the dynamic water loading of the 3D models for the spillway system.

Both the diversion dam and the spillway have fairly high fundamental frequencies, therefore we will investigate the structures for the higher frequency ground motions as recommended by the Board.

We have attempted to evaluate the performance of the structures realistically and not compound safety factors. We have initially evaluated the structures conservatively and refined the analysis if the performance appeared to be questionable. We will continue to examine our results with this in mind.

3. We plan to keep informed of the results of research in the association between large reservoirs and nearby earthquakes by studying written material as it is published and by observing performance of structures in California. Of particular interest will be New Melones Dam on its initial filling. At the present time no additional funds are needed.
4. The report will be rewritten to include only data describing the seismic events, related geological studies, and performance of the structures. Conclusions from these studies will be in the final report after all studies are complete.
 - (a) The title has been changed as suggested to "Performance of the Oroville Dam and Related Facilities during the August 1, 1975 Earthquake."
 - (b) A statement on the purpose has been added to the foreword.
 - (c) The Report Administration Section in the Division of Planning has edited the bulletin to achieve uniform presentation of the findings and conclusions.
 - (d) The section discussing the relationship of the reservoir to the earthquake has been rewritten to avoid the inference. The conclusion on this subject will be in the final report.
 - (e) The listing of the Board members has been deleted from the introductory page. The Board members are still listed in the text where it is discussing that a Special Board had been established. The Board's reports have been deleted from Bulletin 203.
 - (f) The final report will be a "follow-up bulletin" and include the conclusions from the many studies now in progress, and the Board's reports.

A section is being prepared to list the damages to the Oroville Project Facilities including the type and cost of repair work.

5. We concur with the Board's recommendation that an understanding of the growth of surface faulting should be pursued vigorously and that it is important to the long-term safety of the Oroville project to understand the geologic environment associated with the Oroville earthquake. The Project Geology Section has developed the following program for geologic investigation to comply with the recommendations of the Special Consulting Board for the Oroville earthquake:
 - (a) Determine the extent of the fault thought to be responsible for the Oroville earthquake. It is particularly important to determine where the northern extension of the fault is in relation to the Oroville facilities.
 - (b) Verify the nature, age of last movement, and extent of the two faults previously mapped by others just west of Oroville Dam.
 - (c) Do geologic mapping in the Palermo and Bangor quadrangles. Also do geologic mapping north of Lake Oroville. Do geologic mapping of Tertiary formations in the vicinity of the O&M Headquarters.
 - (d) Investigate the Palermo Crack Zone-Prairie Creek lineament to see if it is a fault system that could pose a hazard to project facilities. Continue investigation of the Paynes Peak, Swain Ravine, and Prairie Creek lineaments, and other suspicious lineaments, both north and south of Lake Oroville. This will involve extensive field studies including both geologic mapping and trenching.
 - (e) Continue study of ground water levels in the epicentral area to determine interrelationship of local ground water systems with Lake Oroville.

Target date for completion of the above program is July, 1978. In order to meet that target date, we anticipate that four DWR geologists will work full time on the program. Additional temporary assistance may be required to do some geologic mapping. We anticipate the additional assistance required for geologic mapping possibly might be done by graduate students during the summer of 1977 and possibly the summer of 1978, but this kind of arrangement has not been explored yet with the universities.

Estimated cost of the geological program is \$143,000 for 1976-77 and \$334,000 for 1977-78 fiscal years. It will be necessary to hire two additional Junior Engineering Geologists to carry out the program.

The Division of Operations and Maintenance plans to resurvey this area again during the summer of 1977 with its precise survey crews plus a maps and survey crew if one is available to determine deformation patterns. Estimated cost for the resurvey is \$80,000.

6. (a) We concur that we should be prepared for additional seismic events in this area. Monitoring of seismic activity in the Oroville area will continue under the Division of Operations and Maintenance Earthquake Engineering Program. Our current plans for geological and geodetic monitoring are covered under our response to Question 5.
- (b) We plan to have the re-analyses of all the dam elements in the Oroville-Thermalito complex completed next fiscal year, 1977-78.
- (c) We concur that the structural integrity of Thermalito Forebay and Afterbay Dams under severe earthquake loading is uncertain. We are in the process of evaluating the stability under the recommended loading and expect to have these completed next fiscal year 1977-78.

Attachment

cc: H. H. Eastin
G. W. Dukleth
J. W. Marlette

APPENDIX B

ACCELERATION TIME HISTORIES AND RESPONSE

SPECTRA FOR THE AUGUST 1, 1975 AND

SEPTEMBER 27, 1975 RECORDED MOTIONS

ON DAM CREST AND BEDROCK, IN UPSTREAM-DOWNSTREAM DIRECTION

(FIGS. B-1 THROUGH B-8)

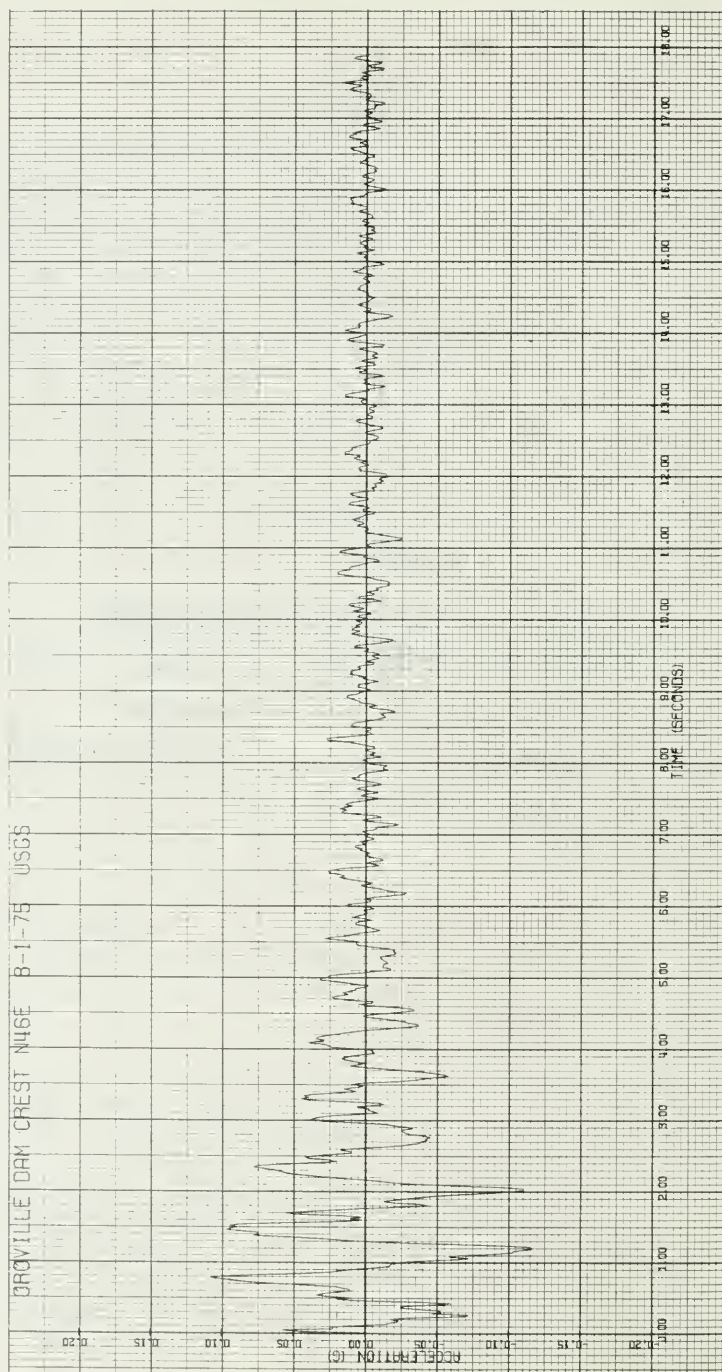


Figure B-1. USGS August 1, 1975 Recorded Crest Motion

PSU ACCELERATION RESP SPECTRA

OROVILLE DAM CREST N46E 8-1-75 USGS

DAMPING = 2%, 5%, 10%, 20%

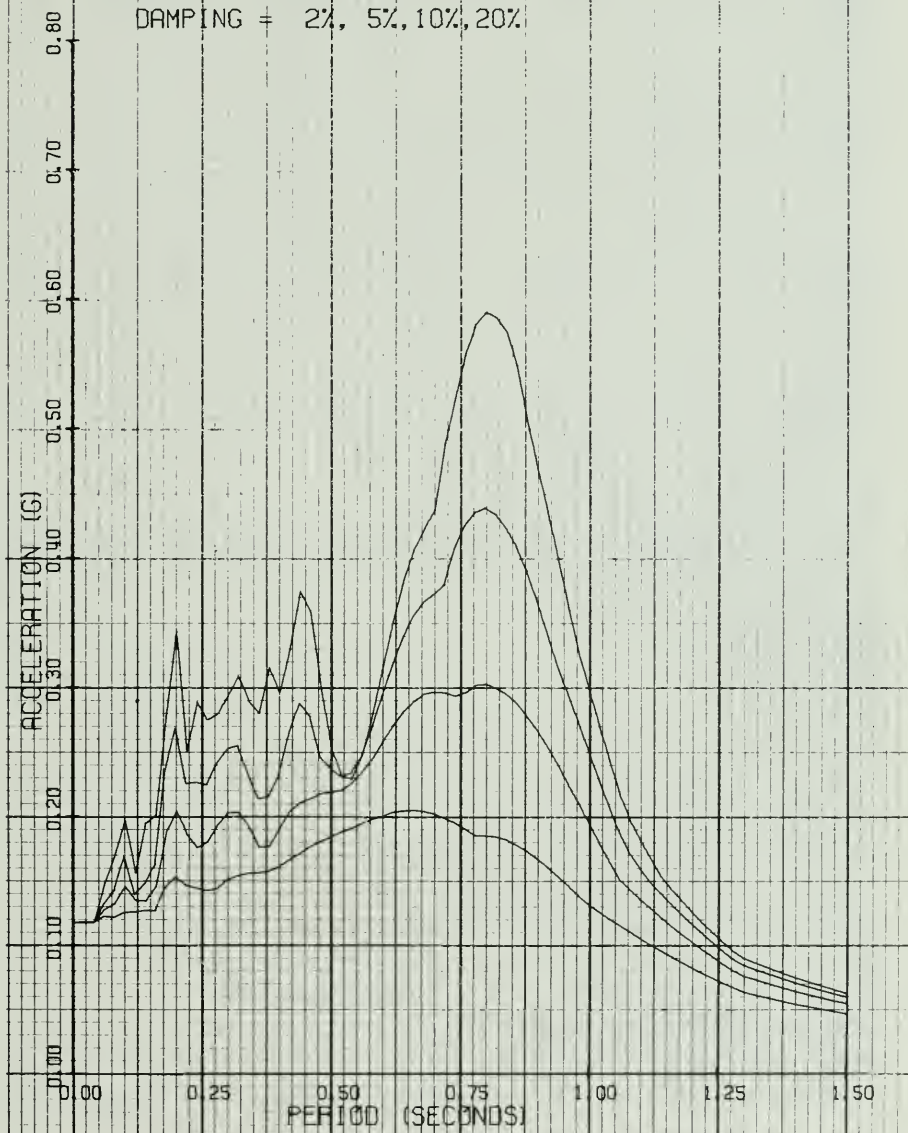


Figure B-2. Computed Acceleration Response Spectra for USGS August 1, 1975 Crest Motion

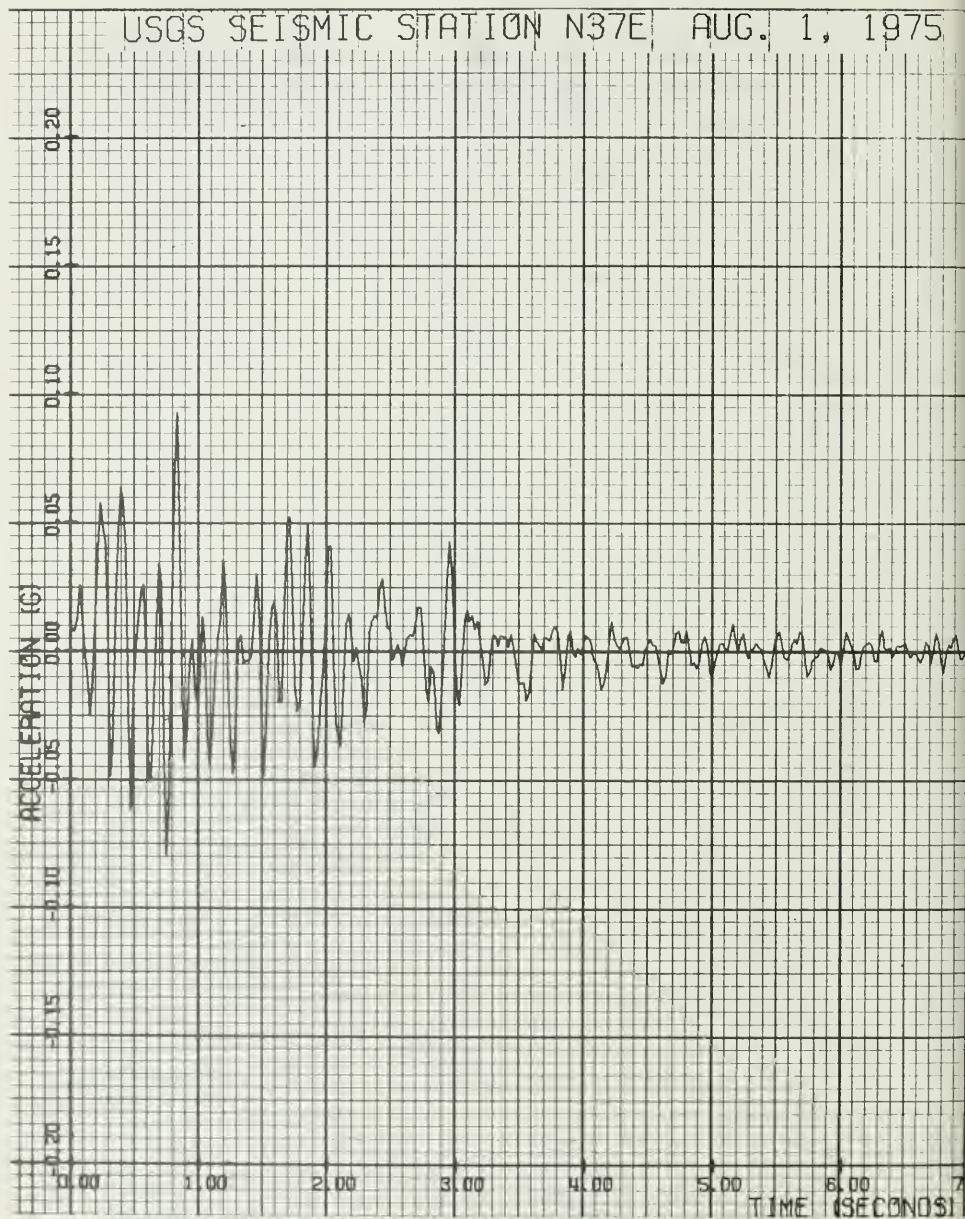


Figure B-3. USGS August 1, 1975 Recorded Rock Motion

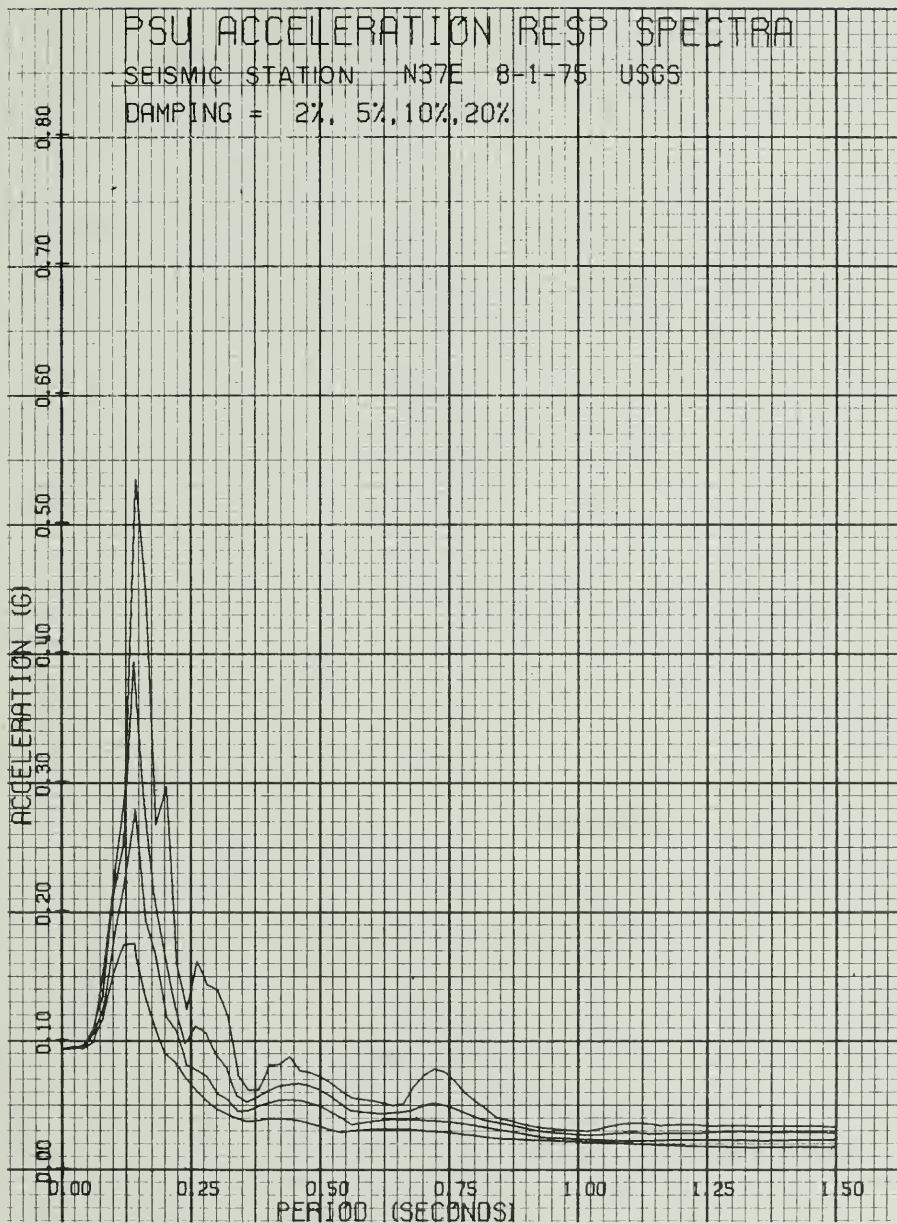


Figure B-4. Computed Acceleration Response Spectra for USGS August 1, 1975
Rock Motion

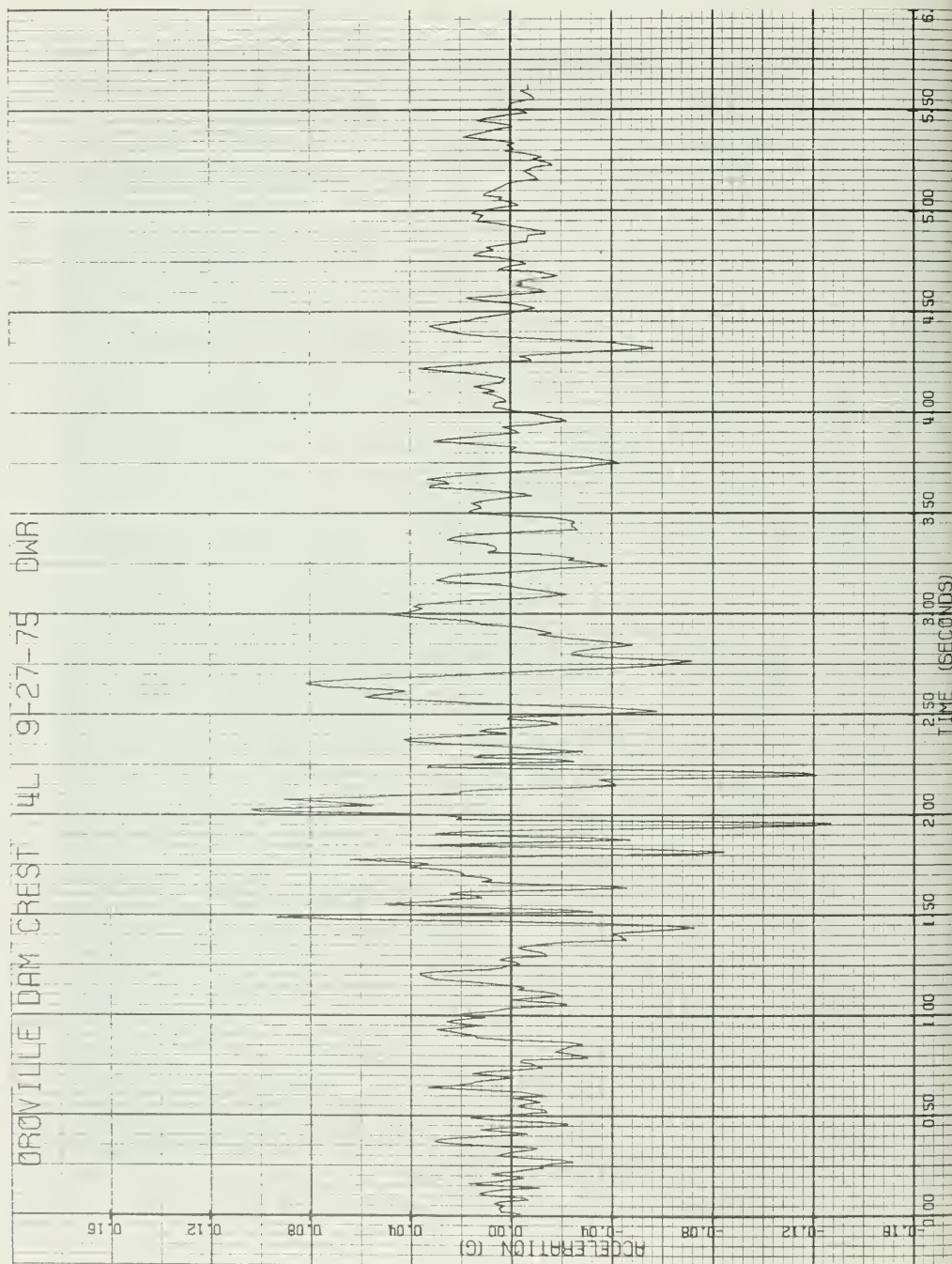


Figure B-5. DWR September 27 1975 Recorded Crest Motion

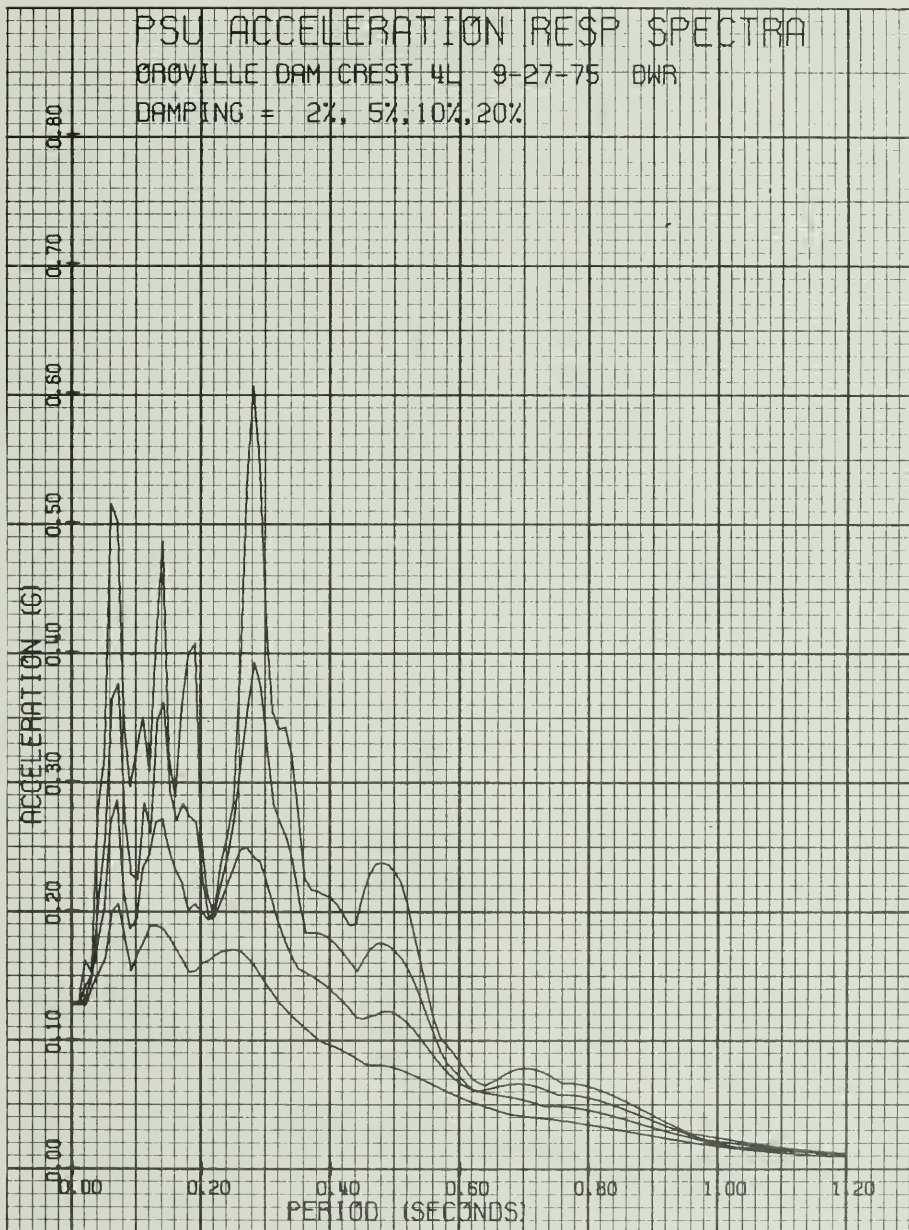
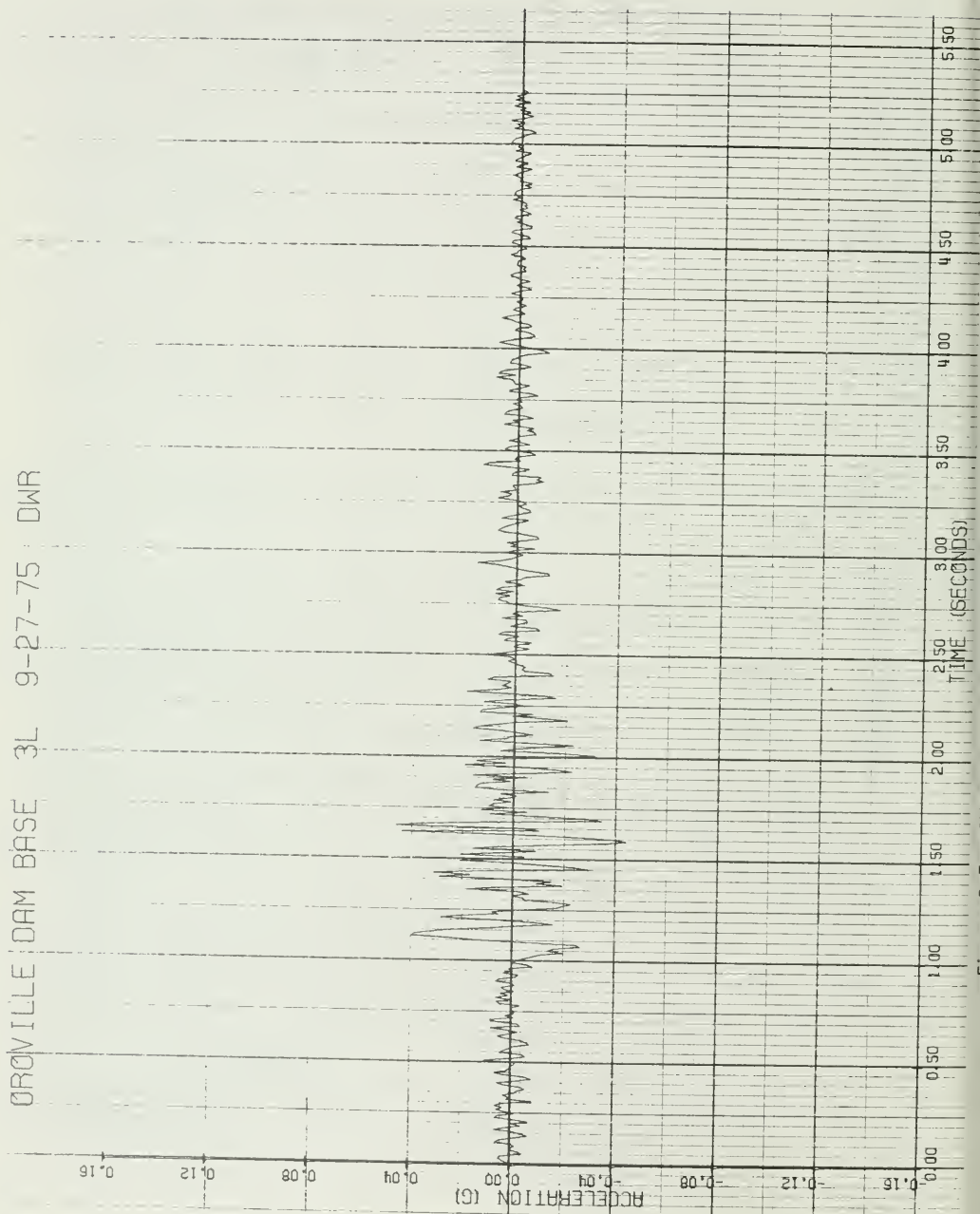


Figure B-6. Computed Acceleration Response Spectra for DWR September 27, 1975
Crest Motion

OROVILLE DAM BASE 3L 9-27-75 DWR



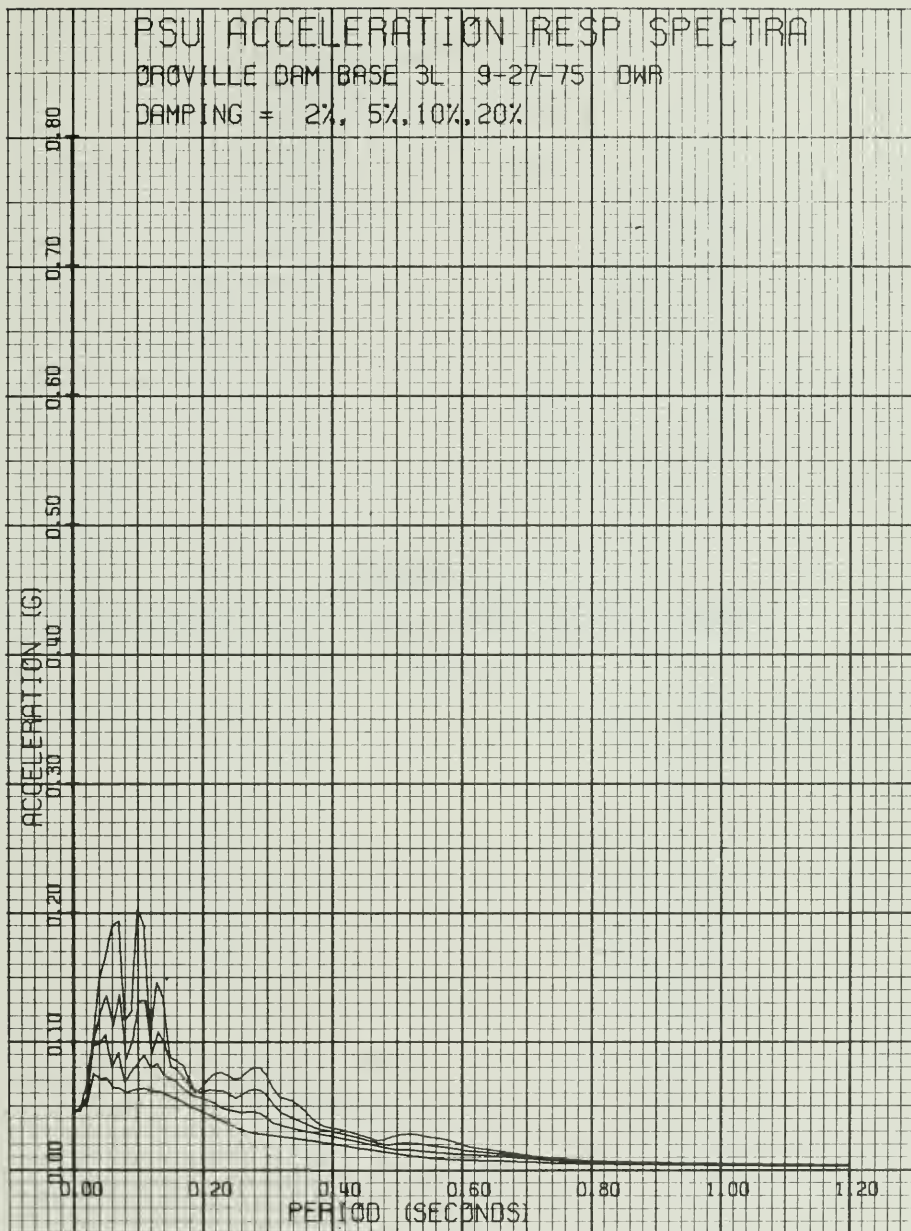


Figure B-8. Computed Acceleration Response Spectra for DWR September 27, 1975 Base Motion

APPENDIX C

STATIC STRESSES FROM STATIC FINITE ELEMENT ANALYSIS

(FIGS. C-1 THROUGH C-8)

OROVILLE DAM - MAXIMUM SECTION

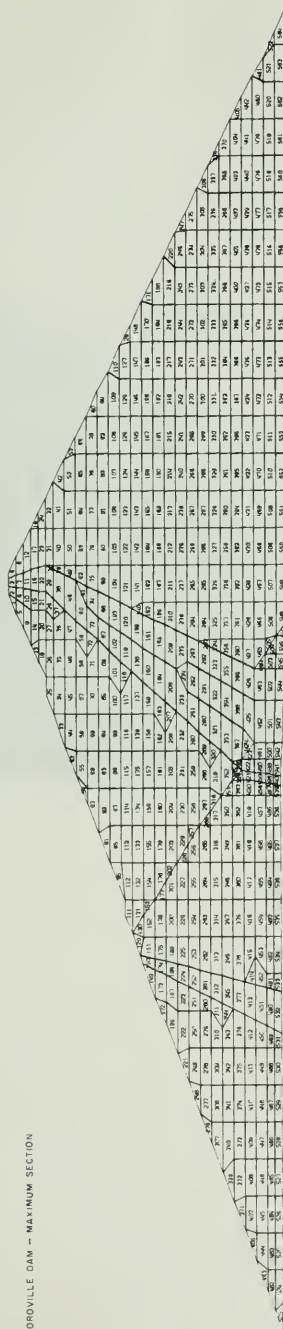


Figure C-1. Element Numbers

OROVILLE DAM - MAXIMUM SECTION

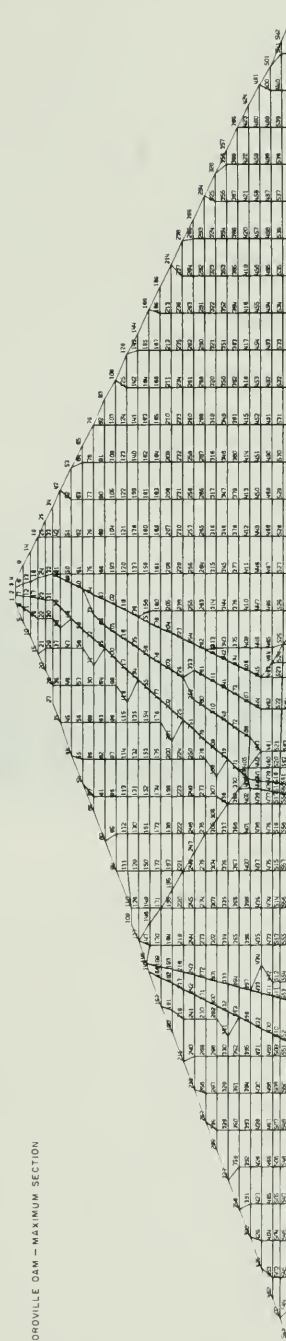
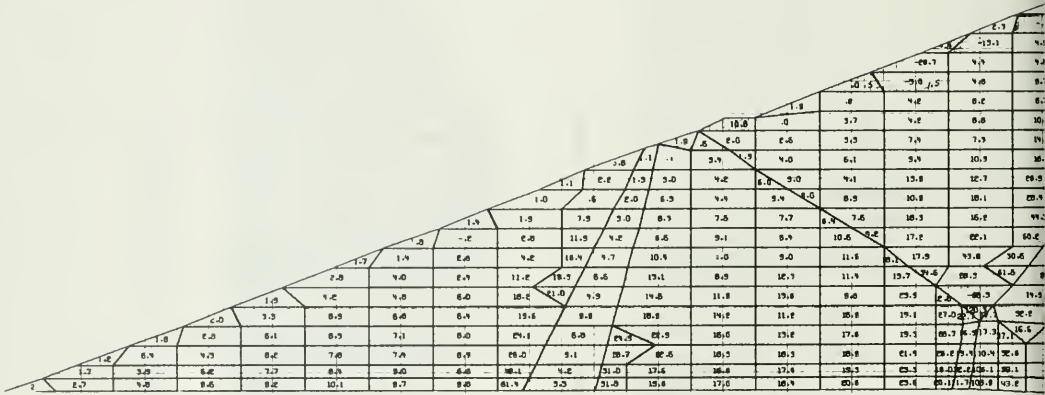


Figure C-2. Node Numbers

GROVILLE DAM - MAXIMUM SECTION



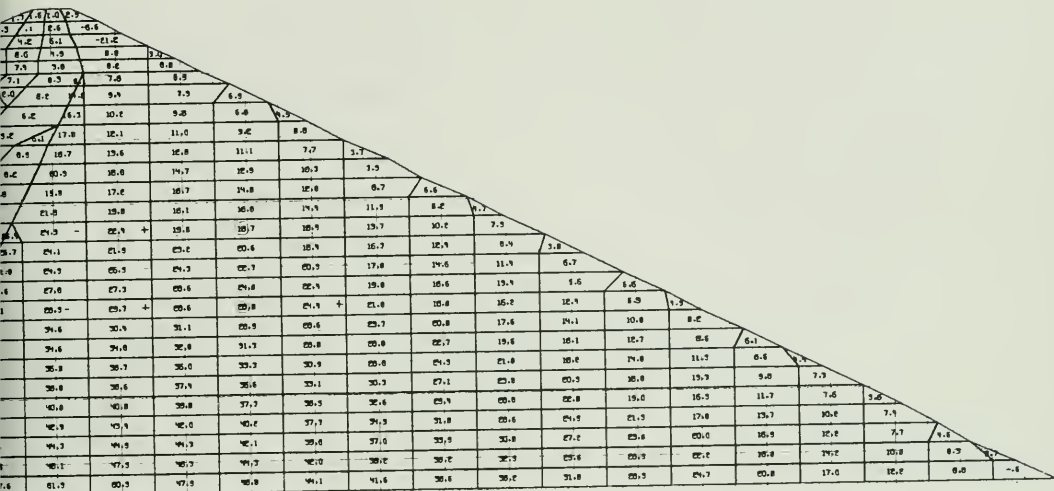


Figure C-3. Major Principal Stresses, σ_1 (tsf)

OROVILLE DAM - MAXIMUM SECTION

The diagram illustrates the maximum section of the Oroville Dam, showing a complex cross-section with various internal stresses or strains. The values are distributed across the section, with higher concentrations near the top and bottom edges. The values range from -1.1 to 1.1, indicating both compressive and tensile stresses. The diagram is oriented with the dam's upstream face on the left and the downstream face on the right. The top of the diagram is labeled 'OROVILLE DAM - MAXIMUM SECTION'.

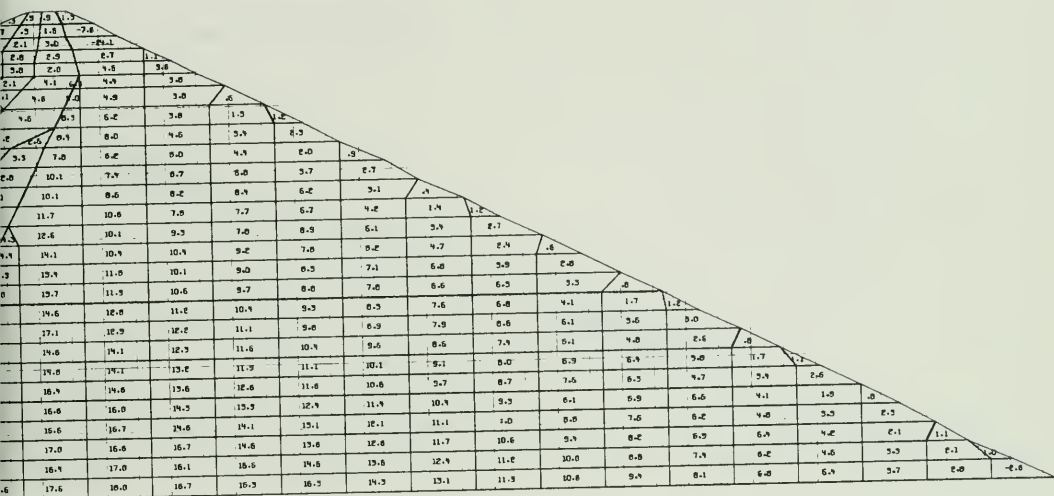


Figure C-4. Minor Principal Stresses, σ_3 (tsf)

OROVILLE DAM - MAXIMUM SECTION

For Shadow Elements
C. pond projects defined



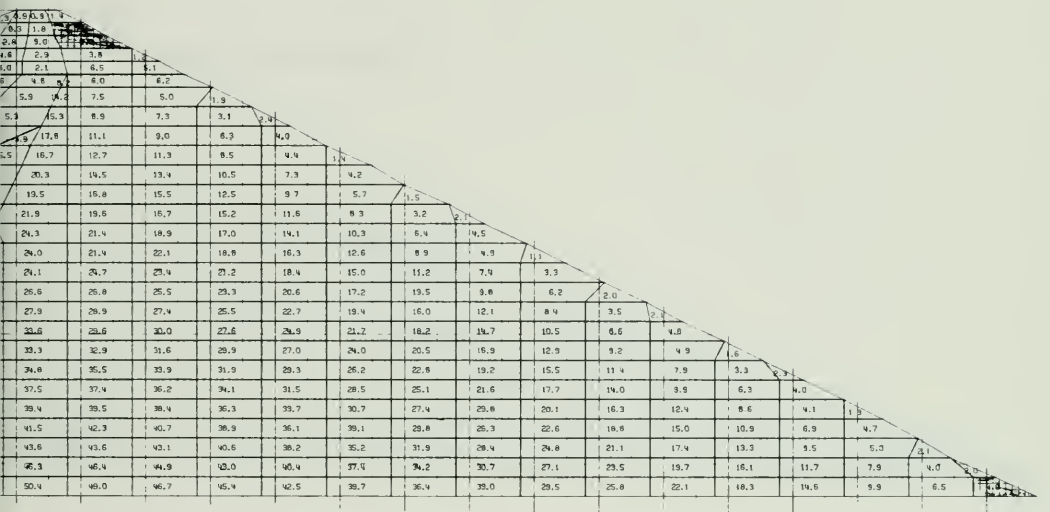
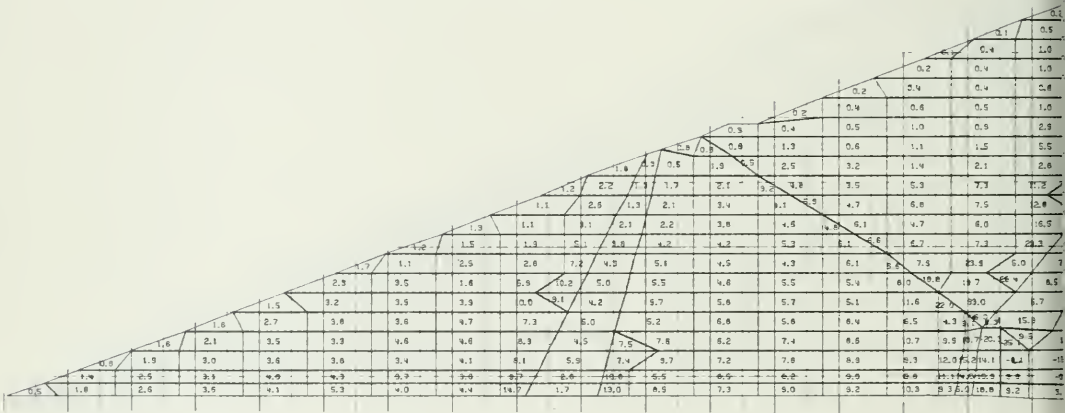


Figure C-5. Vertical Normal Stresses, σ_y (tsf)

OROVILLE DAM - MAXIMUM SECTION



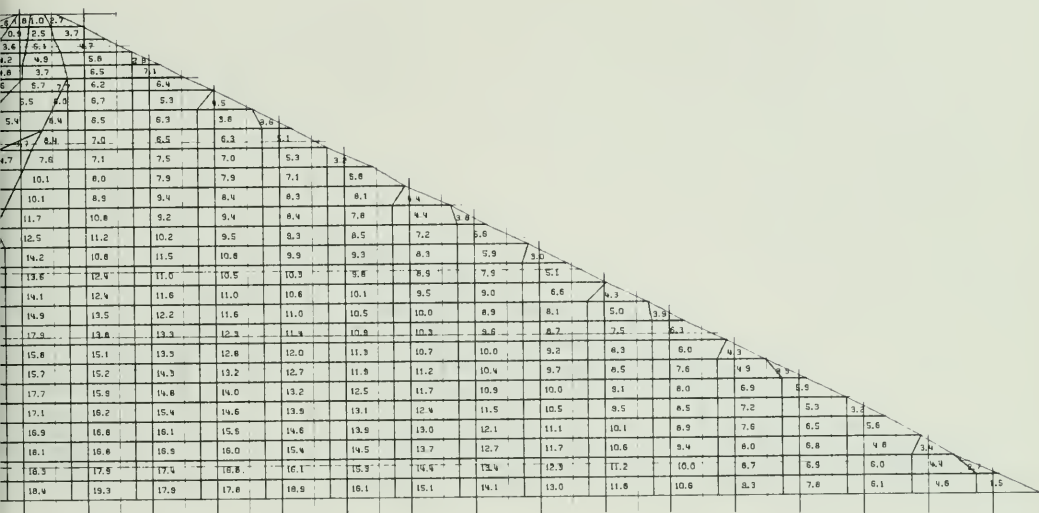
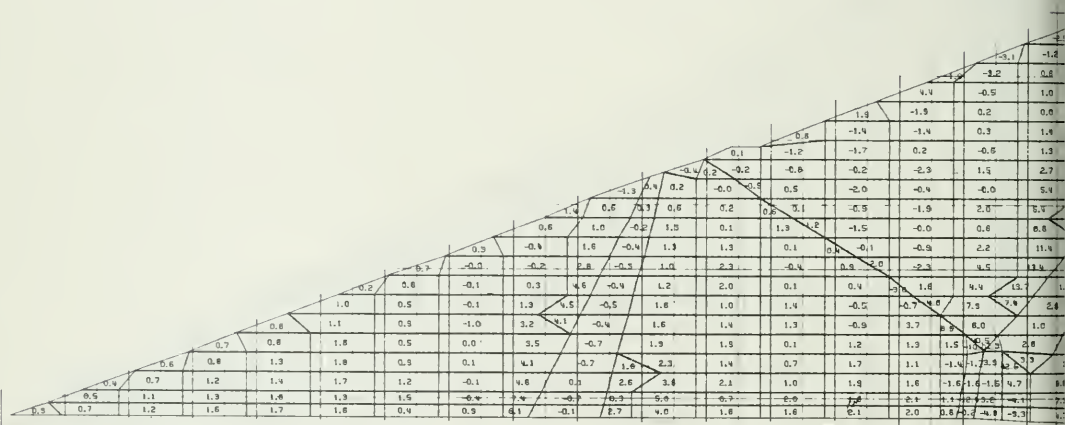
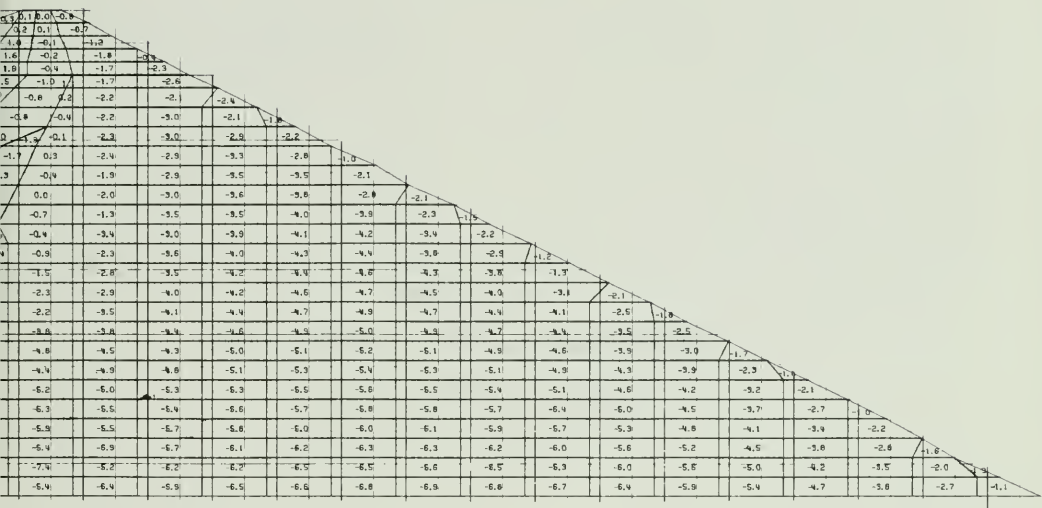


Figure C-6. Horizontal Normal Stresses, σ_x (tsf)

OROVILLE DAM — MAXIMUM SECTION





APPENDIX D
TIME HISTORIES AND RESPONSE SPECTRA
FOR REANALYSIS EARTHQUAKE
(FIGS. D-1 THROUGH D-6)

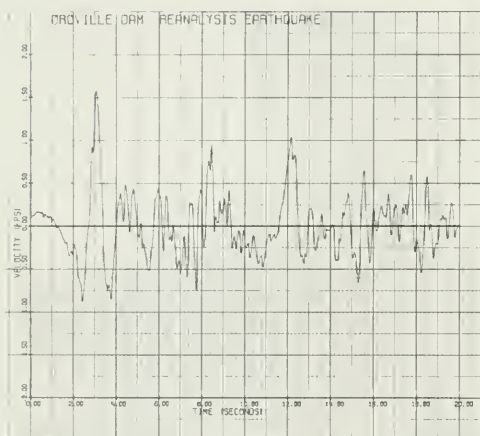


Figure D-1 Accelerogram
for Reanalysis Earthquake

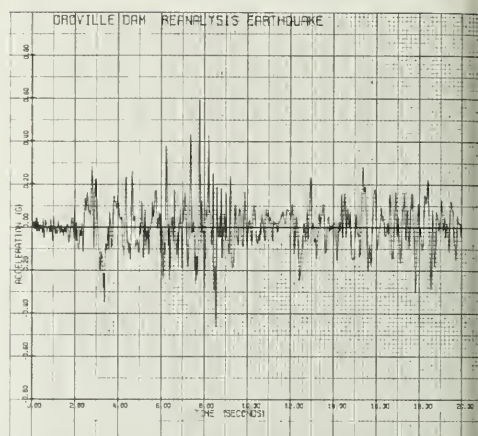


Figure D-2. Computed Velocity Time History
for Reanalysis Earthquake

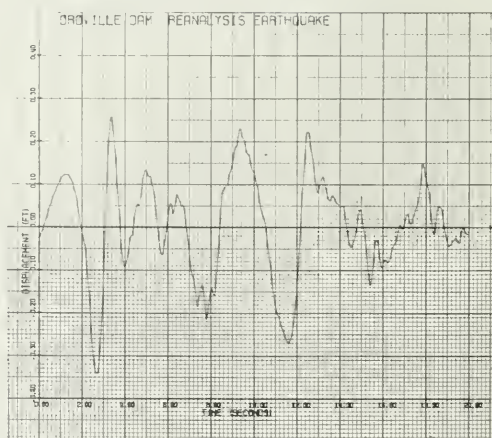


Figure D-3. Computed Displacement Time
History for Reanalysis Earthquake

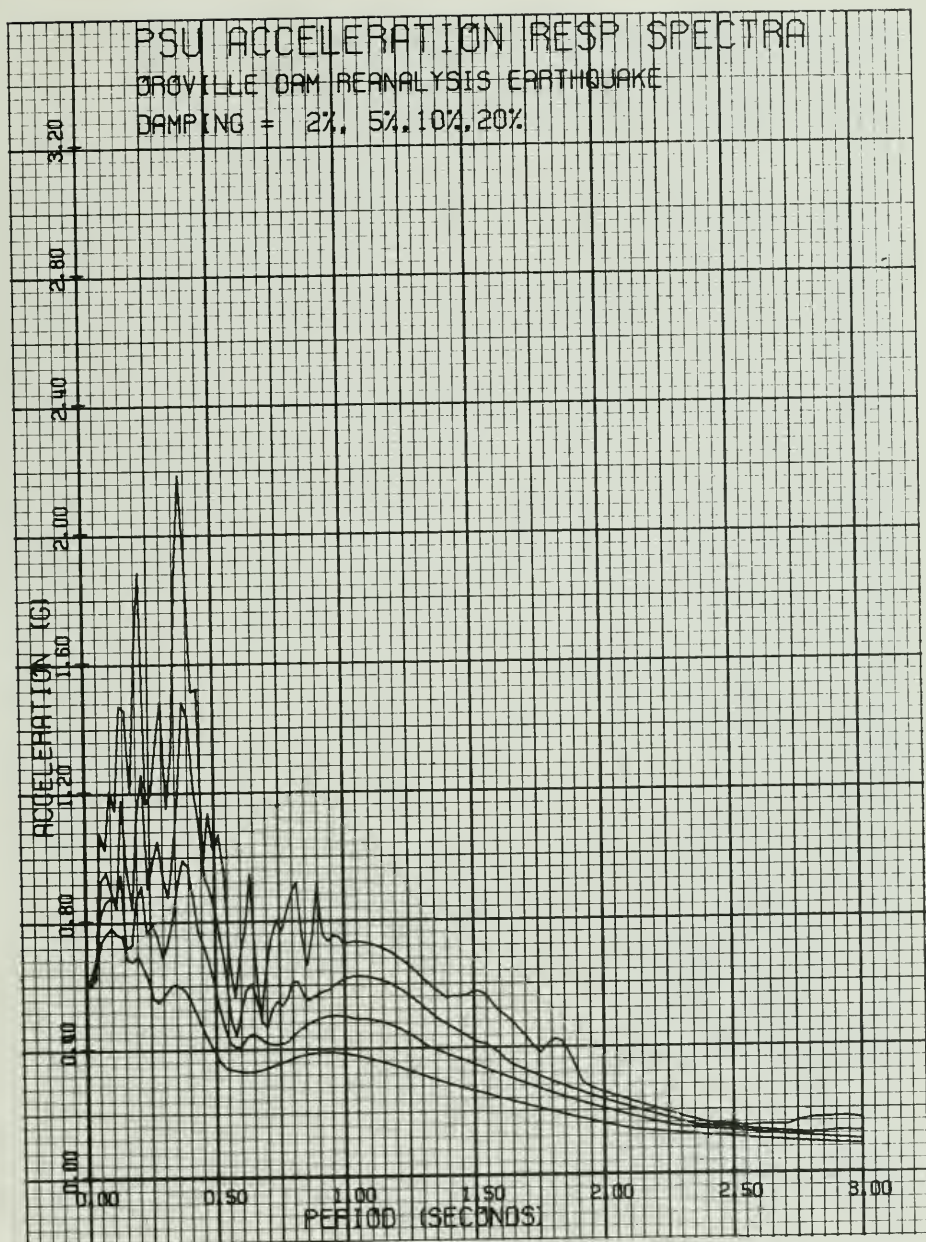


Figure D-4. Computed Acceleration Response Spectra for Reanalysis Earthquake

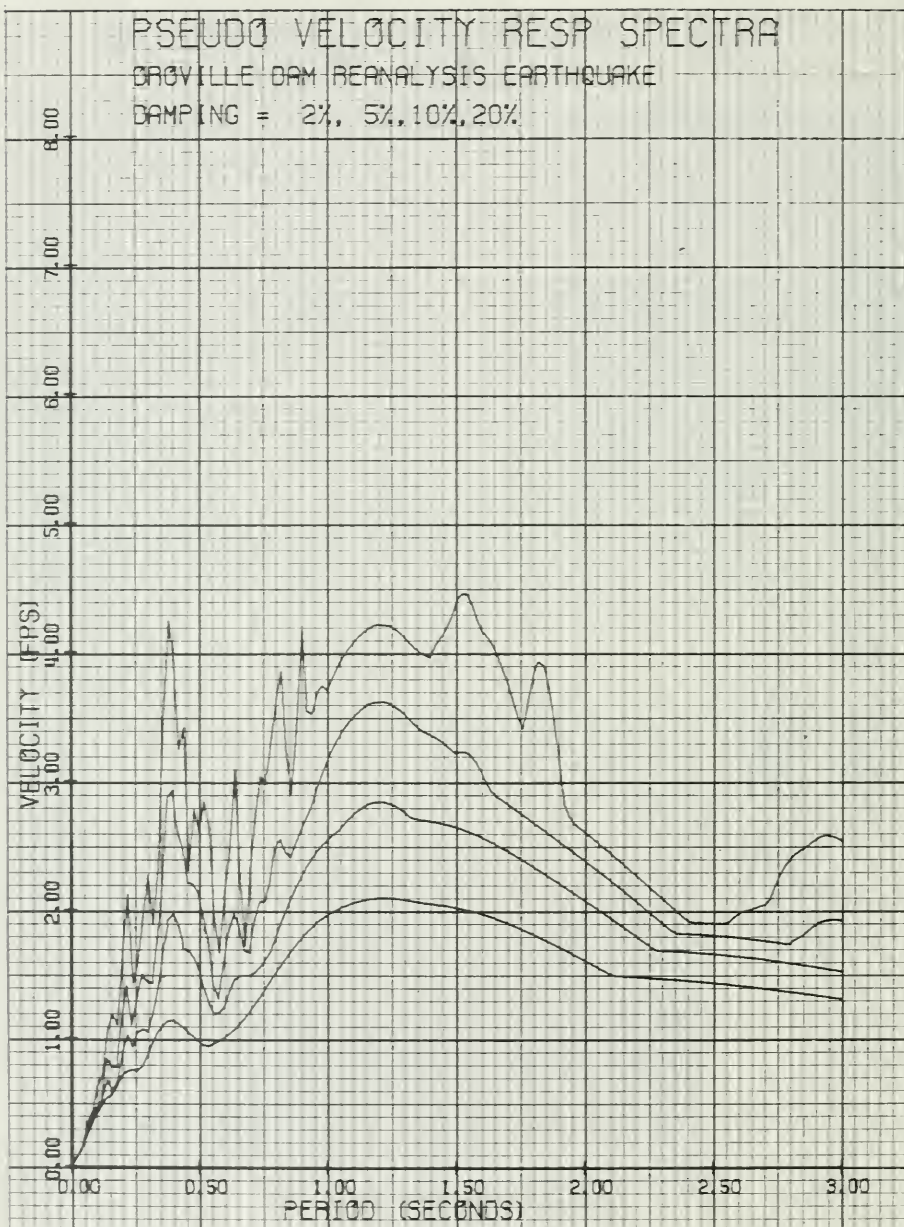


Figure D-5. Computed Velocity Response Spectra for Reanalysis Earthquake

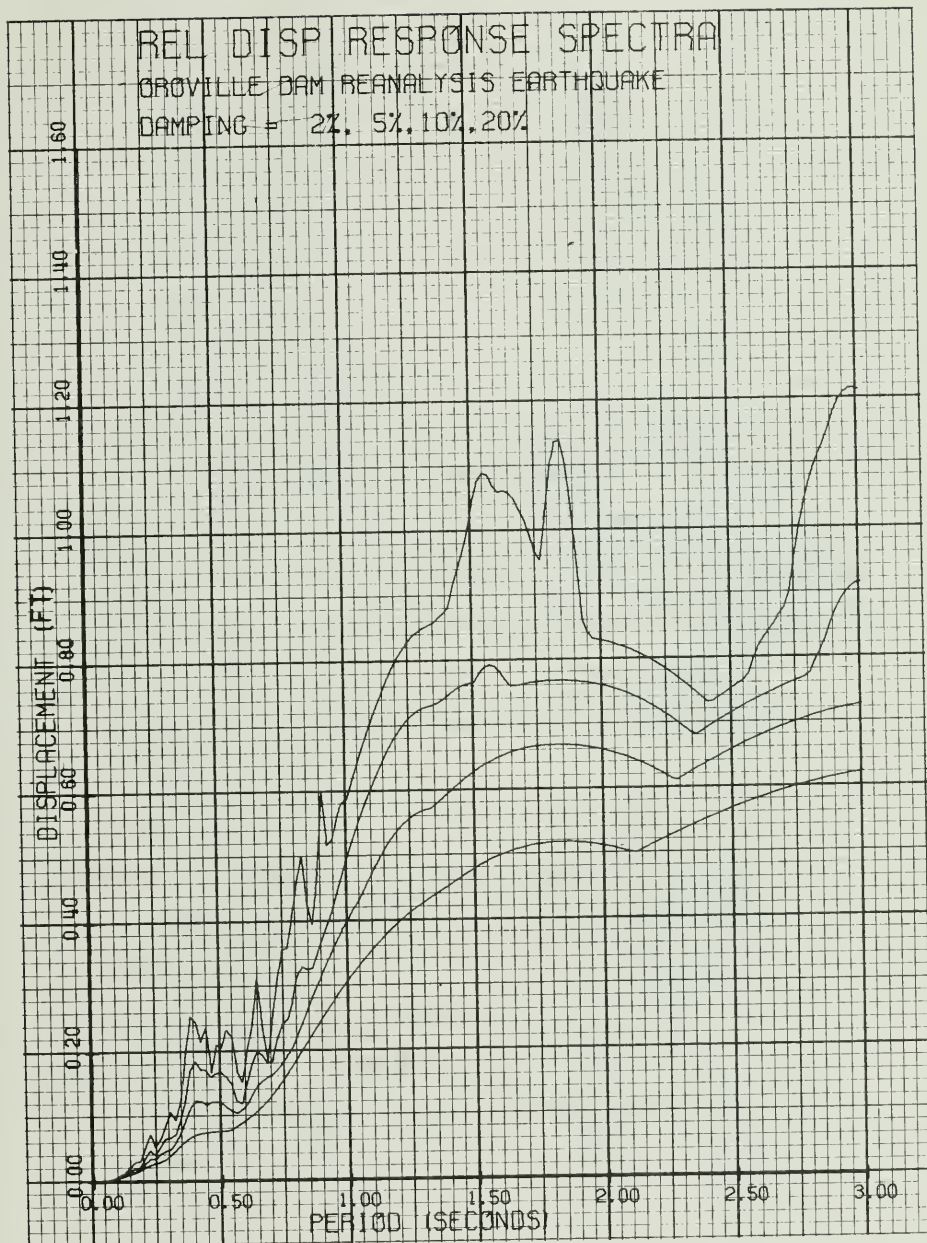


Figure D-6. Computed Displacement Response Spectra for Reanalysis Earthquake

APPENDIX E

RESULTS OF DYNAMIC FINITE ELEMENT ANALYSES

FOR REANALYSIS EARTHQUAKE

MAXIMUM SECTION -- SHELL $K_2 \text{ max} = 350, 200, 130$

ELEMENT STRESSES AND STRAINS (FIGS. E-1 THROUGH E-18)

SHEAR STRESS TIME HISTORIES (FIGS. E-19 THROUGH E-39)

SECTION 2 -- SHELL $K_2 \text{ max} = 130$ - LUSH AND QUAD-4

ELEMENT SHEAR STRESSES AND STRAINS (FIGS. E-40
THROUGH E-45)

ACCELERATION TIME HISTORIES (FIG. E-46)

SECTION 3 -- SHELL $K_2 \text{ max} = 130$ - LUSH AND QUAD-4

ELEMENT SHEAR STRESSES AND STRAINS (FIGS. E-47
THROUGH E-52)

ACCELERATION TIME HISTORIES (FIG. E-53)

MODEL EMBANKMENT -- SHELL $K_2 \text{ max} = 130$

EFFECT OF POISSON'S RATIO ON STRESSES (FIGS. E-54
THROUGH E-55)

ORVILLE DAM - MAXIMUM SECTION
 REANALYSIS EARTHQUAKE - MAXIMUM ACCELERATION : 0.6g
 LUSH DYNAMIC RESPONSE ANALYSIS
 SHELL #2 max. : 350
 G max. : 1750
 CORE S_u

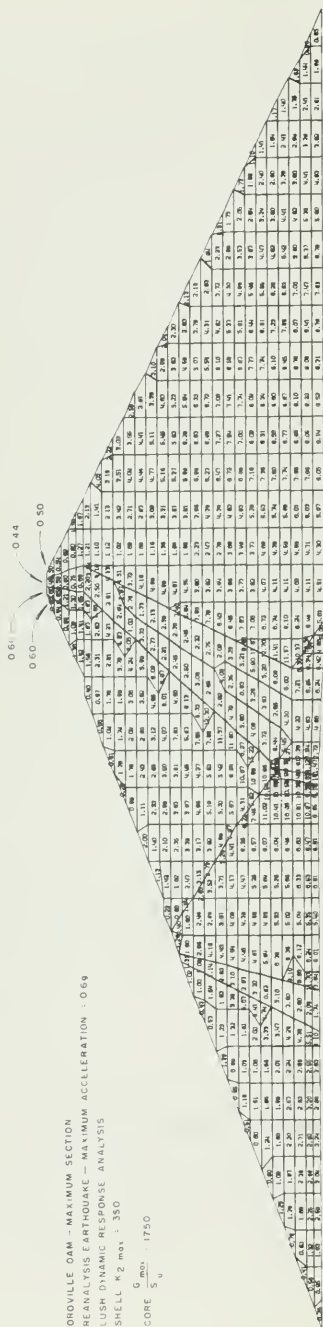


Figure E-1. Maximum Vertical Normal Stresses, σ_v , from LUSH Analysis of the Maximum Section (tsf)

ORVILLE DAM - MAXIMUM SECTION
 REANALYSIS EARTHQUAKE - MAXIMUM ACCELERATION : 0.6g
 LUSH DYNAMIC RESPONSE ANALYSIS
 SHELL #2 max. : 350
 G max. : 1750
 CORE S_u

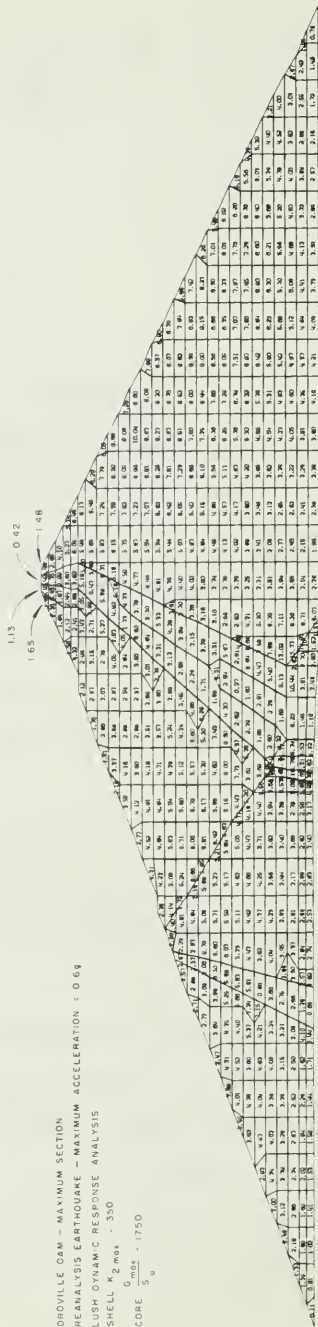


Figure E-2. Maximum Horizontal Normal Stresses, σ_x , from LUSH Analysis of the Maximum Section (tsf)

ORVILLE DAM - MAXIMUM SECTION
 REANALYSIS EARTHQUAKE - MAXIMUM ACCELERATION = 0.6g
 LUSH DYNAMIC RESPONSE ANALYSIS
 SHELL K₂ max = 350
 G max = 1750
 CORE S_u

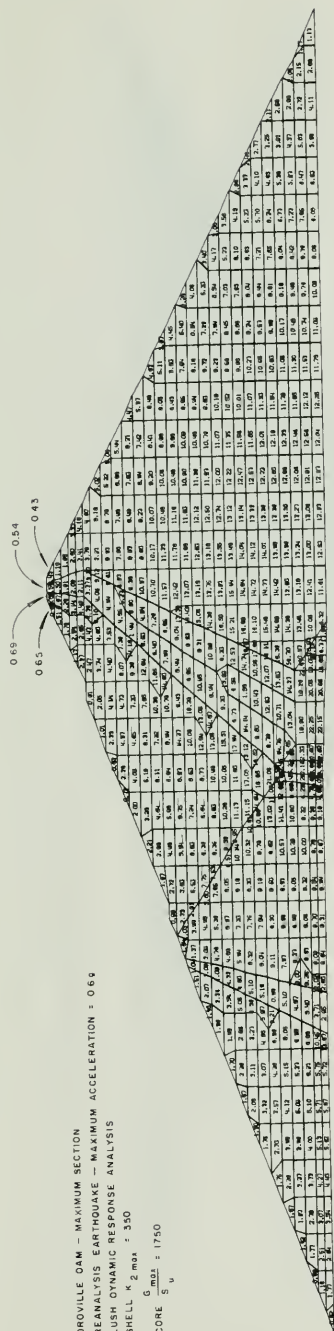


Figure E-3. Maximum Horizontal Shear Stresses, τ_{xy} , from LUSH Analysis of the Maximum Section (tsf)

ORVILLE DAM - MAXIMUM SECTION
 REANALYSIS EARTHQUAKE - MAXIMUM ACCELERATION = 0.6g
 LUSH DYNAMIC RESPONSE ANALYSIS
 SHELL K₂ max = 350
 G max = 1750
 CORE S_u

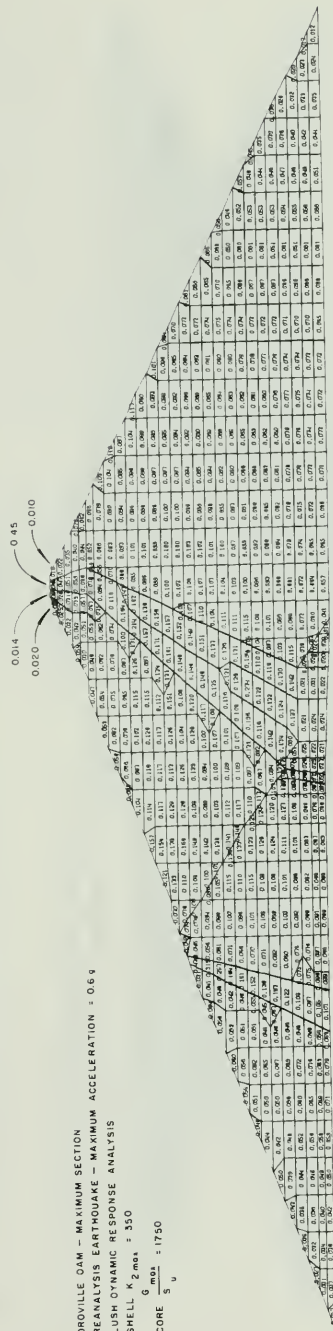


Figure E-4. Maximum Shear Strains, γ_{max} , from LUSH Analysis of the Maximum Section (percent)

ORVILLE DAM - MAXIMUM SECTION
 REANALYSIS EARTHQUAKE - MAXIMUM ACCELERATION : 0.6g
 LUSH DYNAMIC RESPONSE ANALYSIS
 SHELL # 2max : 205
 CORE # 1max : 1120

0.36
 0.29
 0.25
 0.28



Figure E-5. Maximum Vertical Normal Stresses, σ_y , from LUSH Analysis of the Maximum Section (tsf)

ORVILLE DAM - MAXIMUM SECTION
 REANALYSIS EARTHQUAKE - MAXIMUM ACCELERATION : 0.6g
 LUSH DYNAMIC RESPONSE ANALYSIS
 SHELL # 2max : 205
 CORE # 1max : 1120

0.37
 0.39
 0.40

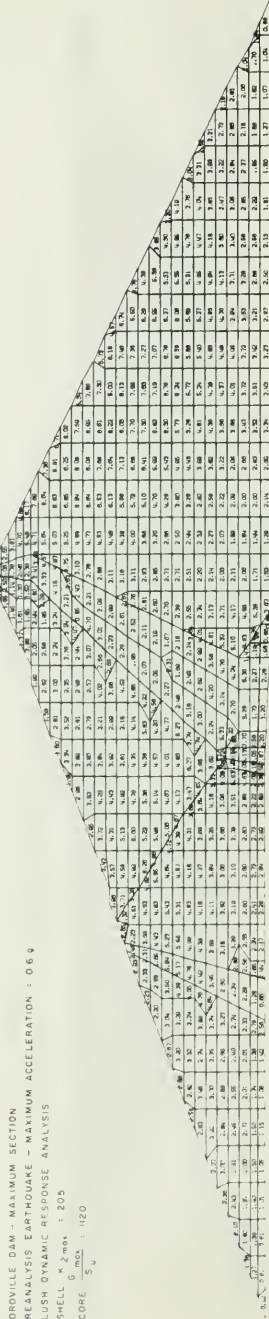


Figure E-6. Maximum Horizontal Normal Stresses, σ_x , from LUSH Analysis of the Maximum Section (tsf)

ORVILLE DAM — MAXIMUM SECTION
 REANALYSIS EARTHQUAKE — MAXIMUM
 LUSH DYNAMIC RESPONSE ANALYSIS
 SHELL K 2max : 205
 CORE K 2max : 1120
 ACCELERATION : 0.6g

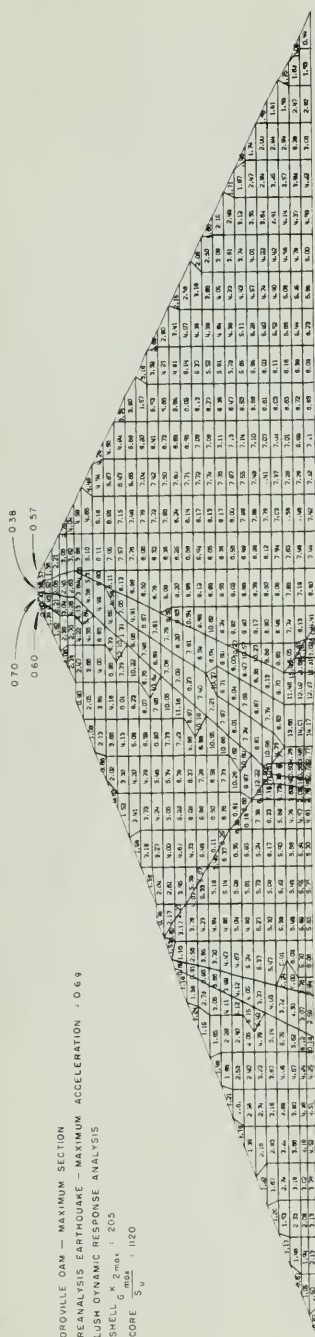


Figure E-7. Maximum Horizontal Shear Stresses, τ_{xy} , from LUSH Analysis of the Maximum Section (tsf)

ORVILLE DAM — MAXIMUM SECTION
 REANALYSIS EARTHQUAKE — MAXIMUM
 LUSH DYNAMIC RESPONSE ANALYSIS
 SHELL K 2max : 205
 CORE K 2max : 1120
 ACCELERATION : 0.6g

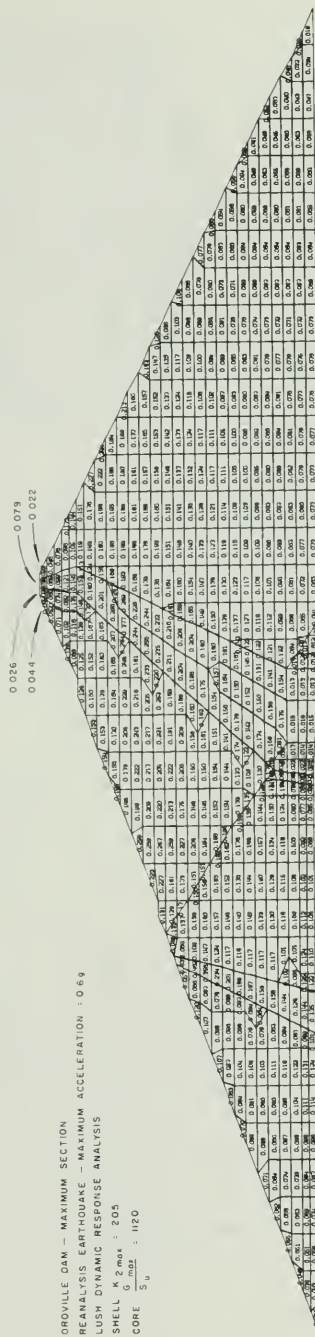


Figure E-8. Maximum Shear Strains, γ_{max} , from LUSH Analysis of the Maximum Section (percent)

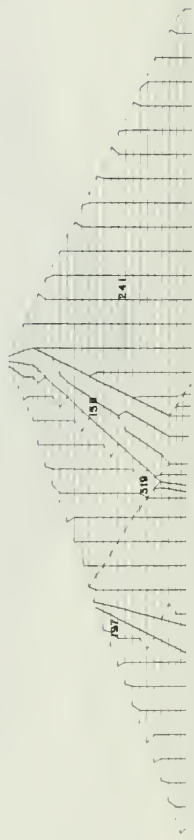
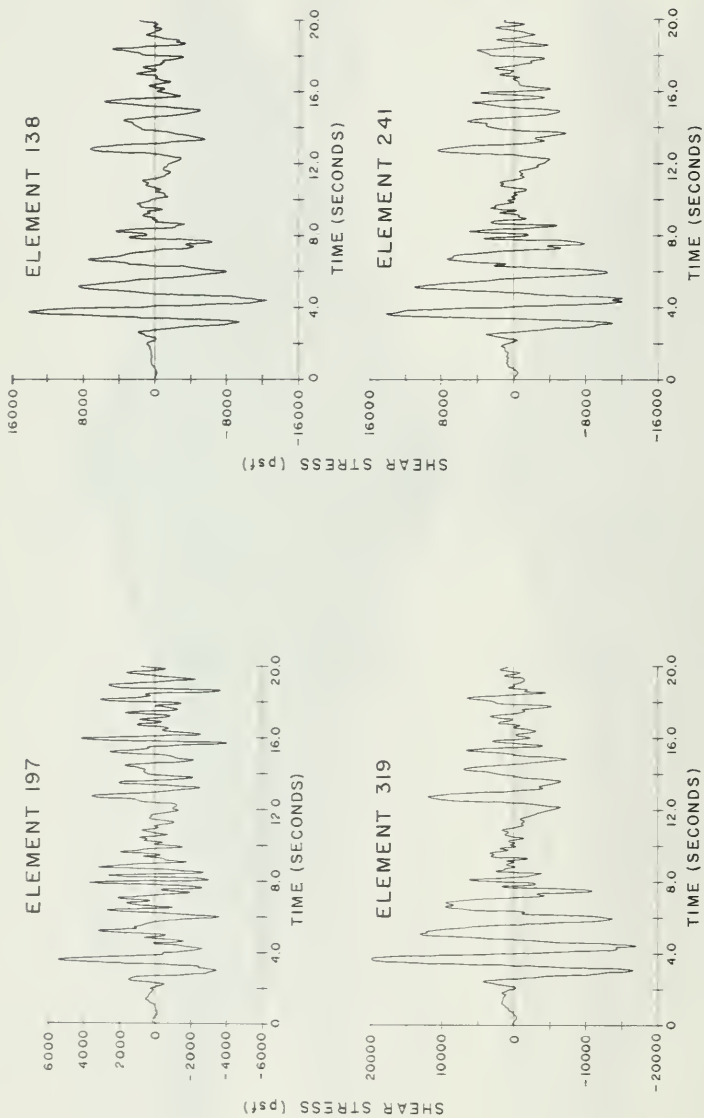


Figure E-9. Typical Shear Stress Time Histories from LUSH Analysis of the Maximum Section Using $K_{2max} = 205$

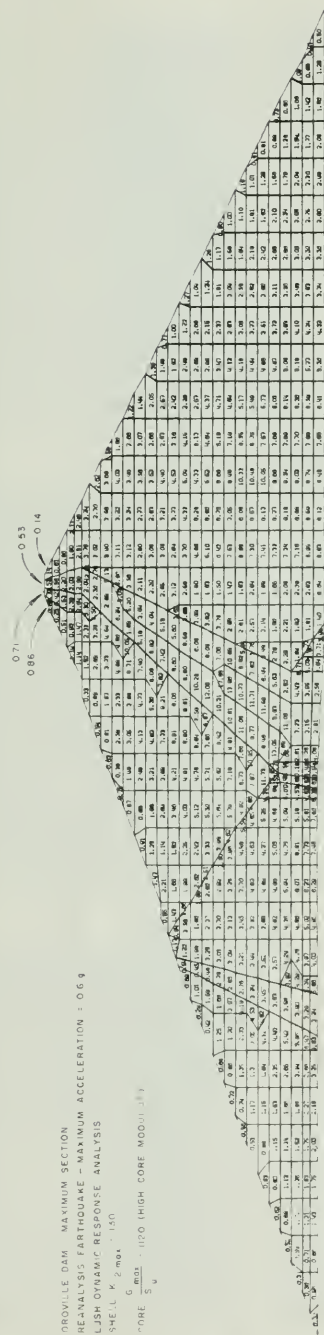


Figure E-10. Maximum Vertical Normal Stresses, σ_y , from LUSH Analysis of the Maximum Section (tsf)

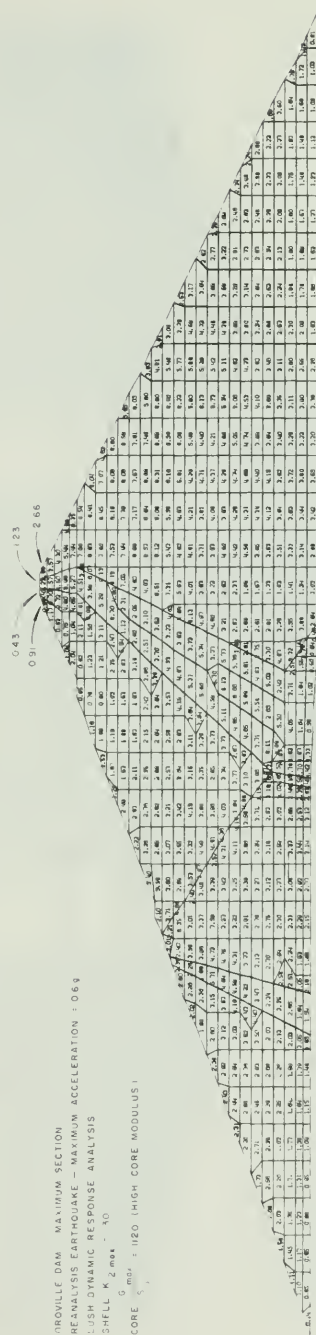


Figure E-11. Maximum Horizontal Normal Stresses, σ_x , from LUSH Analysis of the Maximum Section (tsf)

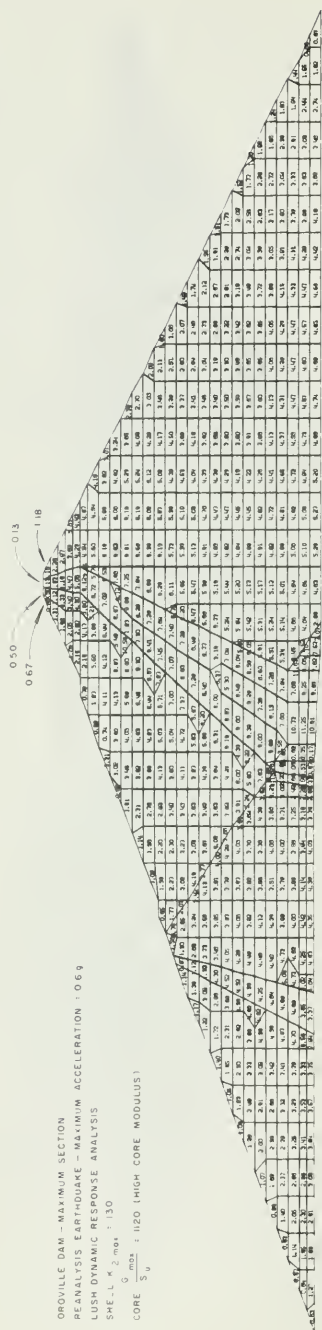


Figure E-12. Maximum Horizontal Shear Stresses, τ_{xy} , from LUSH Analysis of the Maximum Section (tsf)



Figure E-13. Maximum Shear Strains, γ_{max} , from LUSH Analysis of the Maximum Section (percent)

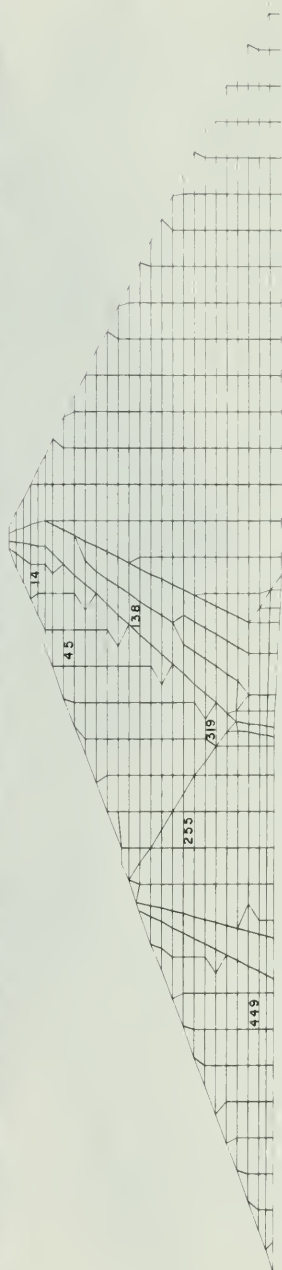
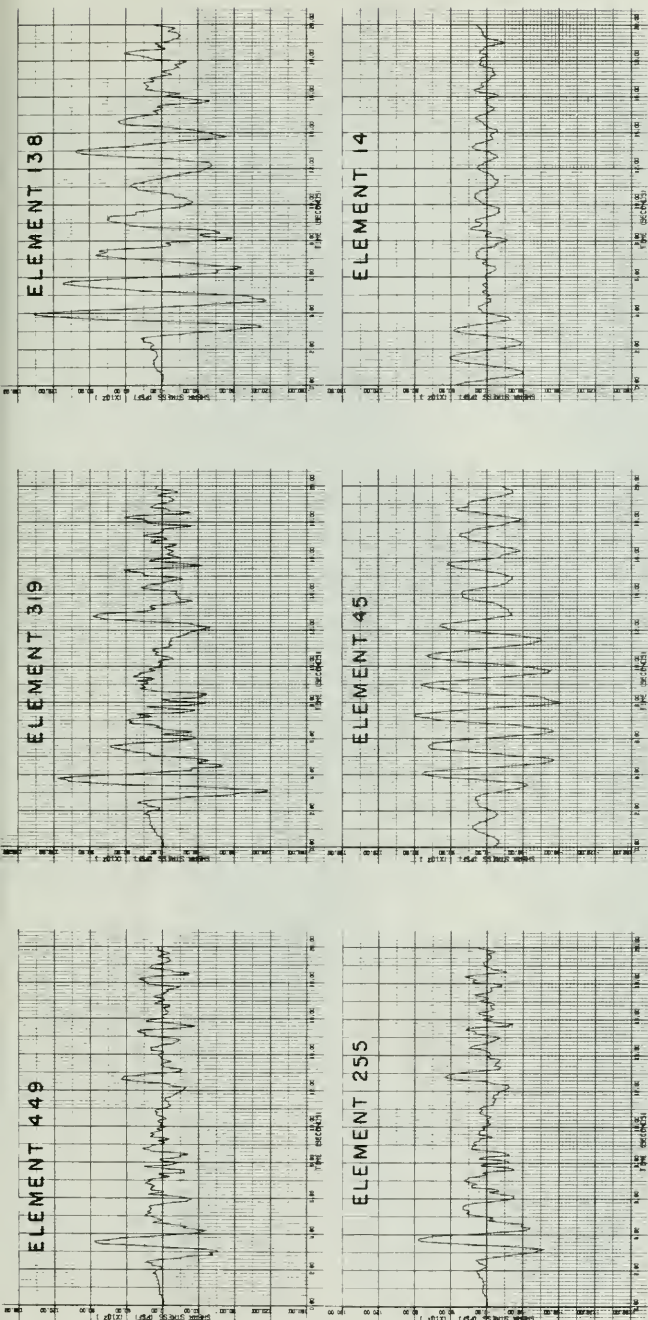


Figure E-14. Typical Shear Stress Time Histories from LUSH Analysis of the Maximum Section Using $K_{2\max} = 130$ and High Core Modulus

OROVILLE DAM - MAXIMUM SECTION
 REANALYSIS EARTHQUAKE - MAXIMUM ACCELERATION : 0.6g
 LUSH DYNAMIC RESPONSE ANALYSIS
 SHELL K 2 MOD : 130
 G MOD : 2200 (LOW CORE MODULUS)

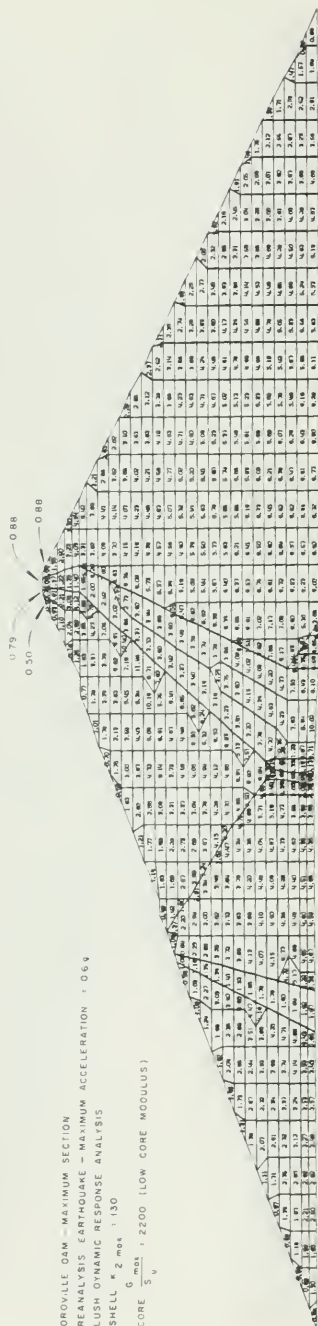


Figure E-15. Maximum Horizontal Shear Stresses, τ_{xy} , from LUSH Analysis of the Maximum Section (tsf)

OROVILLE DAM - MAXIMUM SECTION
 REANALYSIS EARTHQUAKE - MAXIMUM ACCELERATION : 0.6g
 LUSH DYNAMIC RESPONSE ANALYSIS
 SHELL K 2 MOD : 130
 G MOD : 2200 (LOW CORE MODULUS)

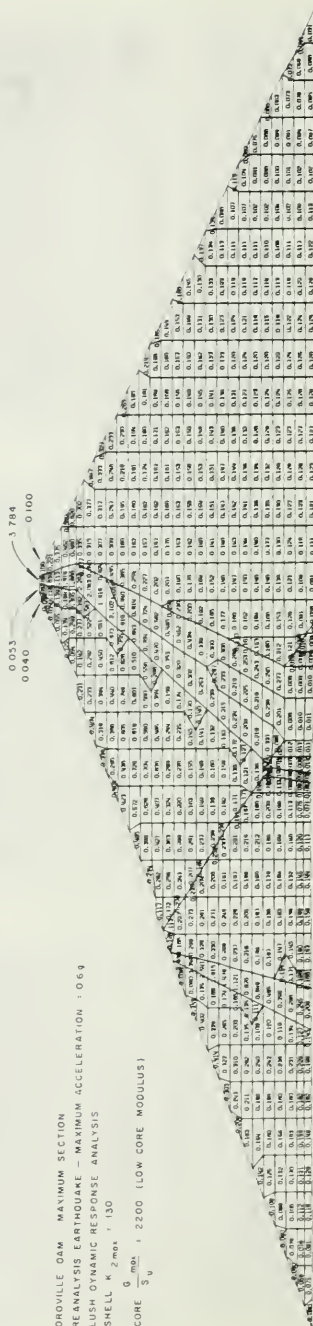


Figure E-16. Maximum Shear Strains, γ_{max} , from LUSH Analysis of the Maximum Section (percent)

OROVILLE DAM - MAXIMUM SECTION
 REANALYSIS EARTHQUAKE - MAXIMUM ACCELERATION = 0.6g
 QUAD 4 DYNAMIC RESPONSE ANALYSIS
 SHELL τ_2 max = 130
 CORE $\frac{G_{max}}{S_u}$ = 2200 (LOW CORE MODULUS)

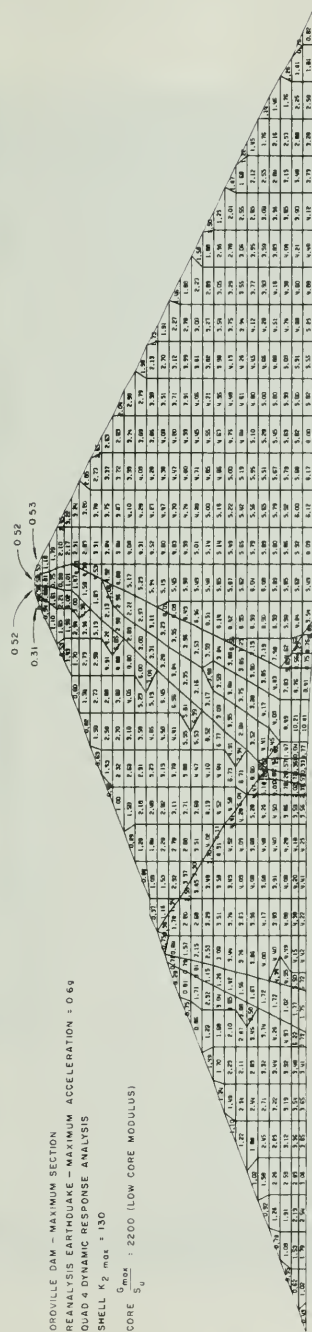


Figure E-17. Maximum Horizontal Shear Stresses, τ_{xy} , from QUAD4 Analysis of the Maximum Section (tsf)

OROVILLE DAM - MAXIMUM SECTION
 REANALYSIS EARTHQUAKE - MAXIMUM ACCELERATION = 0.6g
 QUAD 4 DYNAMIC RESPONSE ANALYSIS
 SHELL τ_2 max = 130
 CORE $\frac{G_{max}}{S_u}$ = 2200 (LOW CORE MODULUS)

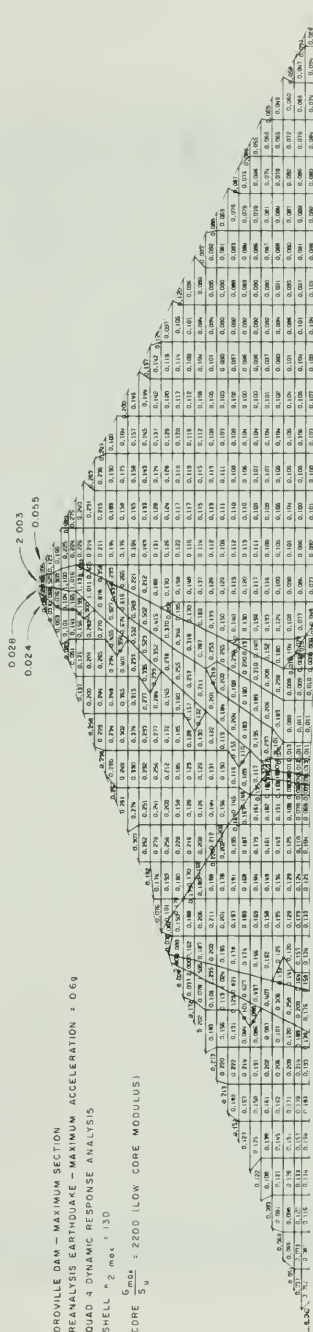


Figure E-18. Maximum Shear Strains, γ_{max} , from QUAD4 Analysis of the Maximum Section (percent)

OROVILLE DAM - MAXIMUM SECTION PROGRAM = QUAD 4
 K2MAX = 130 LOWER CORE MODULUS
 REANALYSIS EARTHQUAKE-MAXIMUM ACCELERATION = 0.6g
 ELEMENT NUMBER = 2

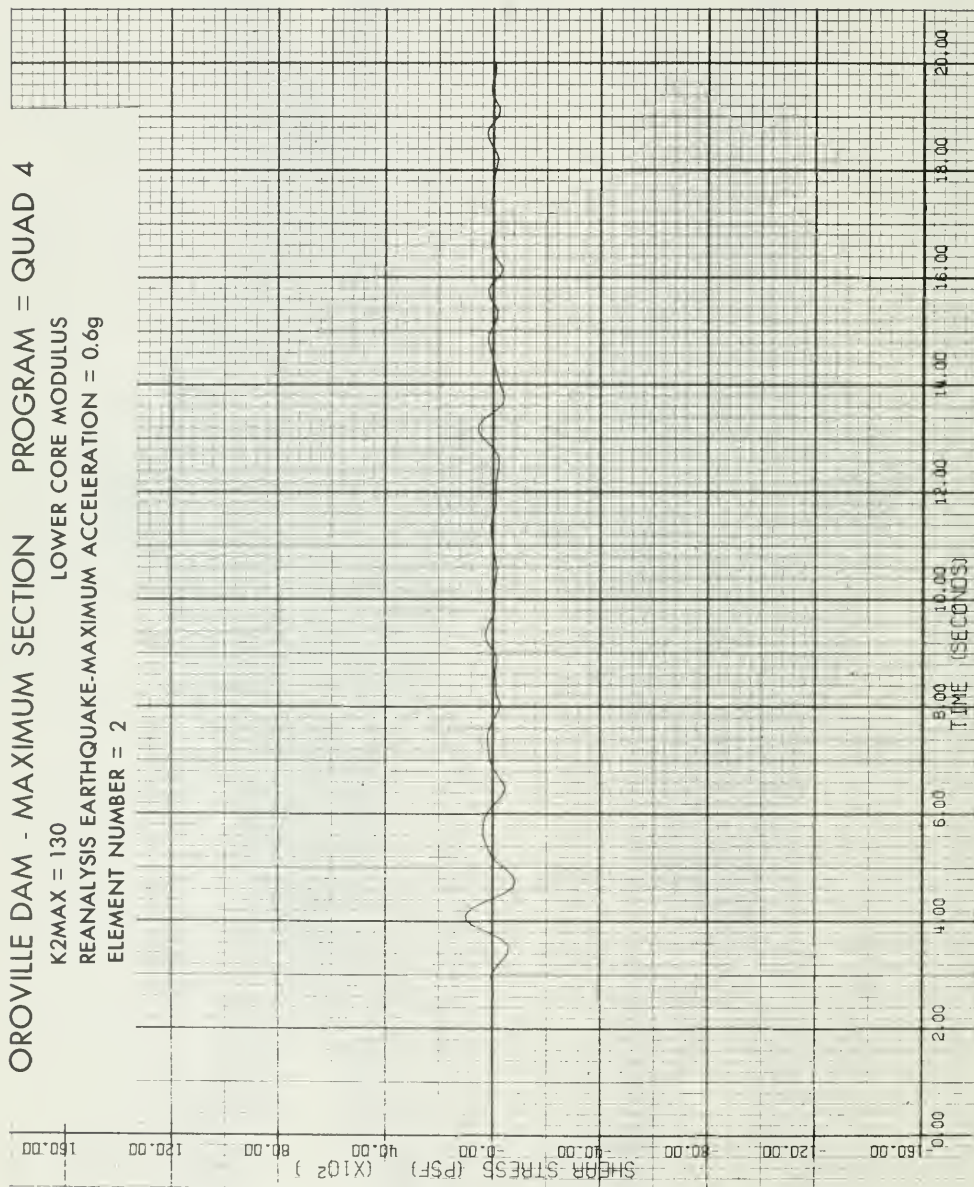


Figure E-19. Element Number 2

PROGRAM = QUAD 4

OROVILLE DAM - MAXIMUM SECTION

K2MAX = 130

LOWER CORE MODULUS

REANALYSIS EARTHQUAKE-MAXIMUM ACCELERATION = 0.6g

ELEMENT NUMBER = 10

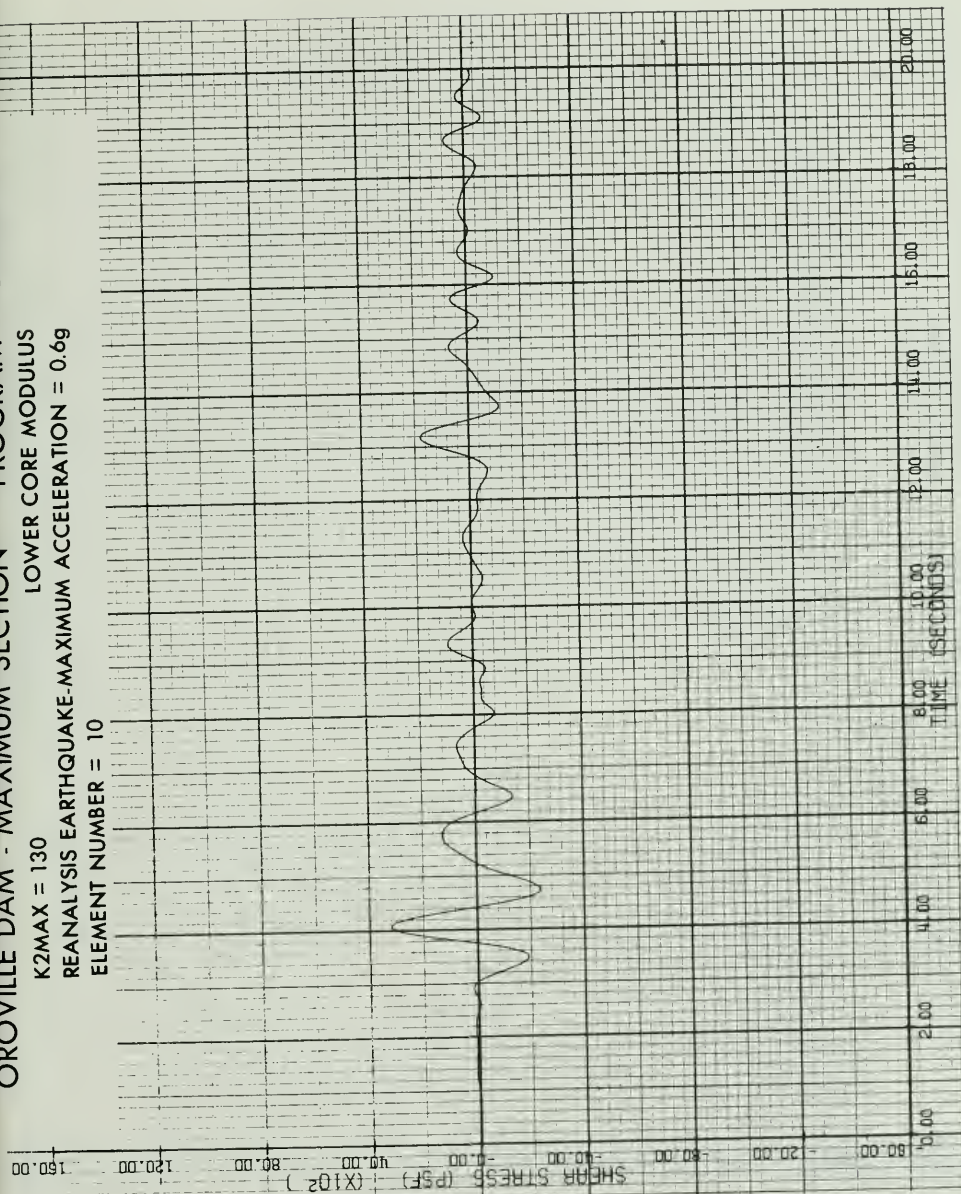


Figure E-20. Element Number 10

OROVILLE DAM - MAXIMUM SECTION PROGRAM = QUAD 4

K2MAX = 130 LOWER CORE MODULUS

REANALYSIS EARTHQUAKE-MAXIMUM ACCELERATION = 0.6g

ELEMENT NUMBER = 21

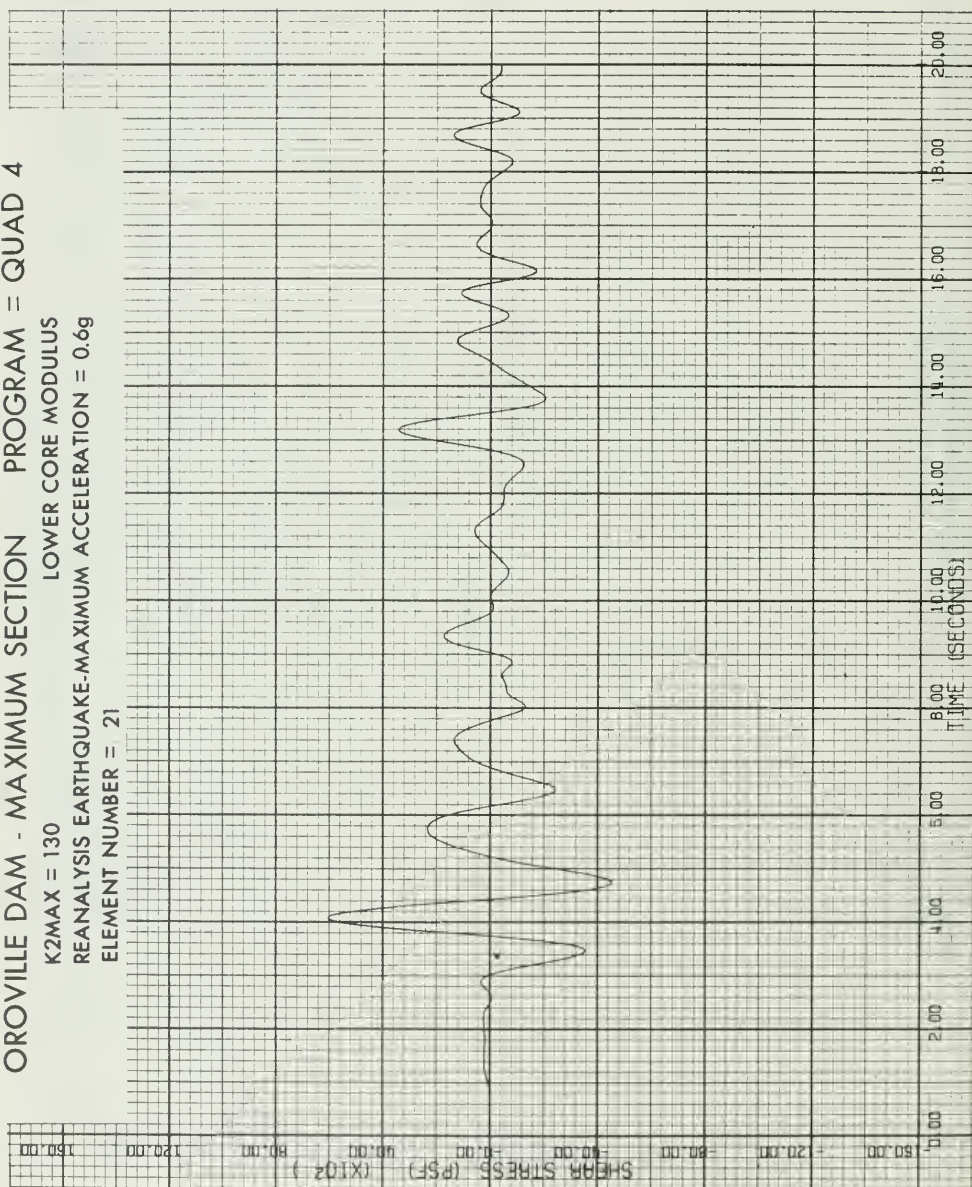


Figure E-21. Element Number 21

OROVILLE DAM - MAXIMUM SECTION PROGRAM = QUAD 4
 LOWER CORE MODULUS
 K2MAX = 130
 REANALYSIS EARTHQUAKE-MAXIMUM ACCELERATION = 0.6g
 ELEMENT NUMBER = 58

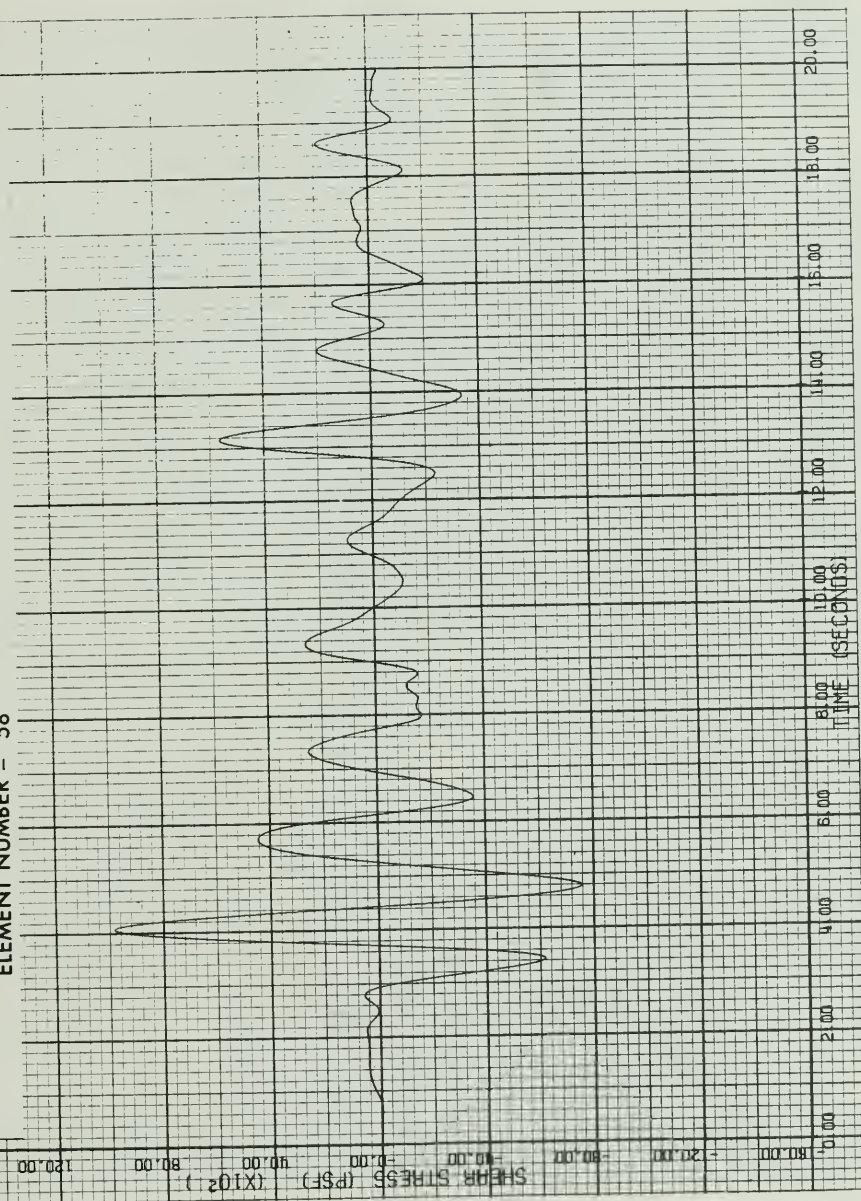


Figure E-22. Element Number 58

OROVILLE DAM - MAXIMUM SECTION PROGRAM = QUAD 4
 K2MAX = 130 LOWER CORE MODULUS
 REANALYSIS EARTHQUAKE-MAXIMUM ACCELERATION = 0.6g
 ELEMENT NUMBER = 64

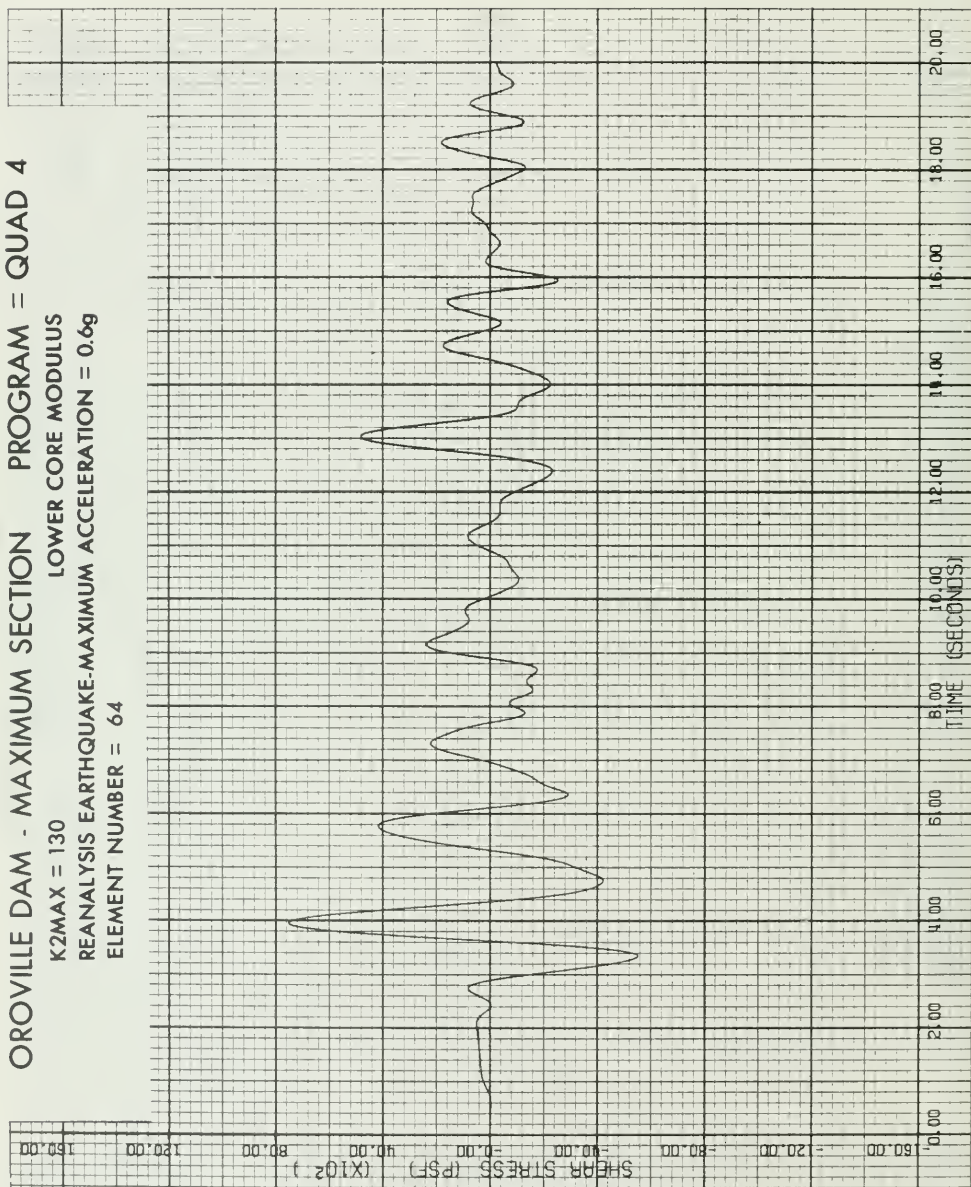


Figure E-23. Element Number 64

OKROVILLE DAM - MAXIMUM SECTION PROGRAM = QUAD 4
 K2MAX = 130 LOWER CORE MODULUS
 REANALYSIS EARTHQUAKE-MAXIMUM ACCELERATION = 0.6g
 ELEMENT NUMBER = 98

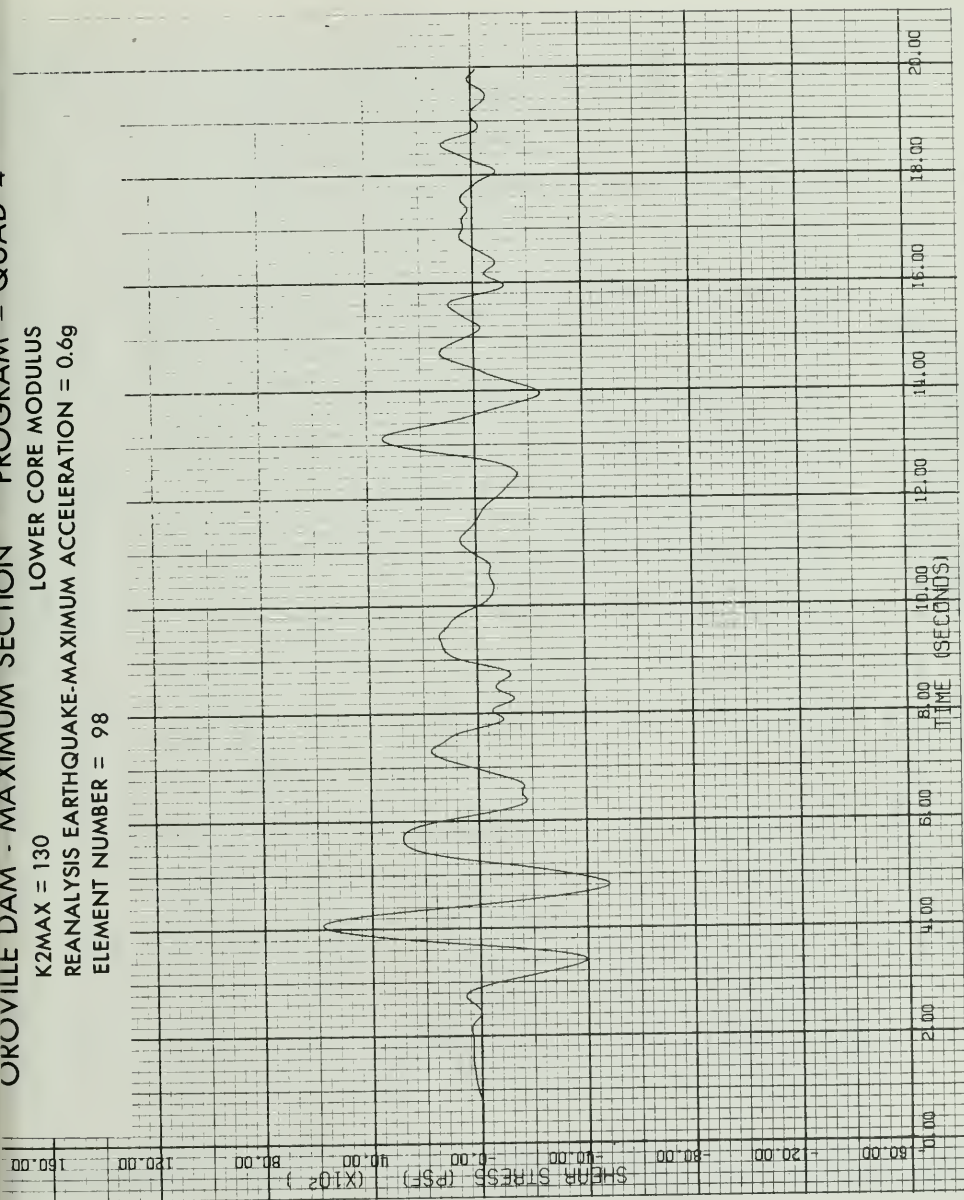


Figure E-24. Element Number 98

OROVILLE DAM - MAXIMUM SECTION PROGRAM = QUAD 4
 K2MAX = 130 LOWER CORE MODULUS
 REANALYSIS EARTHQUAKE-MAXIMUM ACCELERATION = 0.6g
 ELEMENT NUMBER = 106

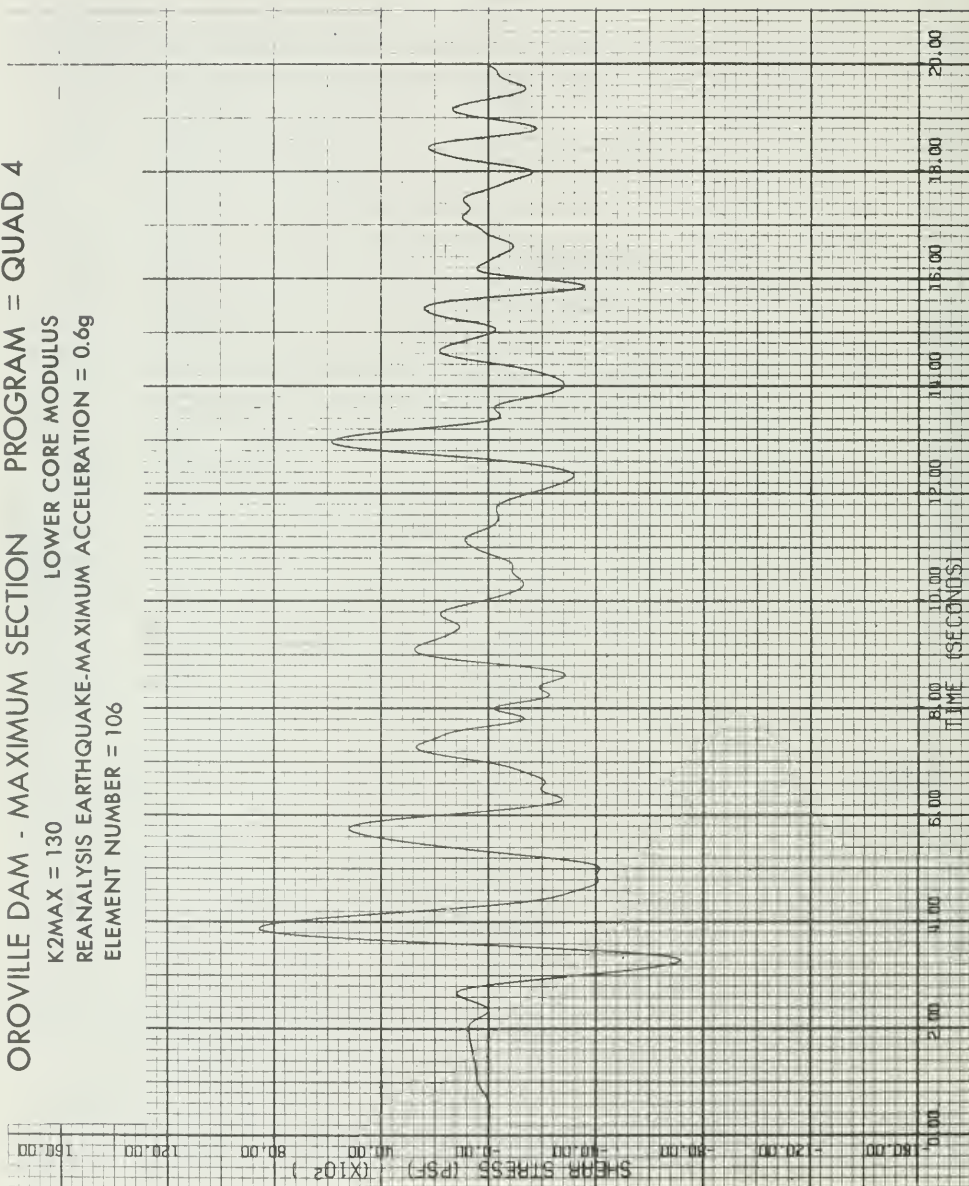


Figure E-25. Element Number 106

OROVILLE DAM - MAXIMUM SECTION PROGRAM = QUAD 4
 K2MAX = 130 LOWER CORE MODULUS
 REANALYSIS EARTHQUAKE-MAXIMUM ACCELERATION = 0.6g
 ELEMENT NUMBER = 137

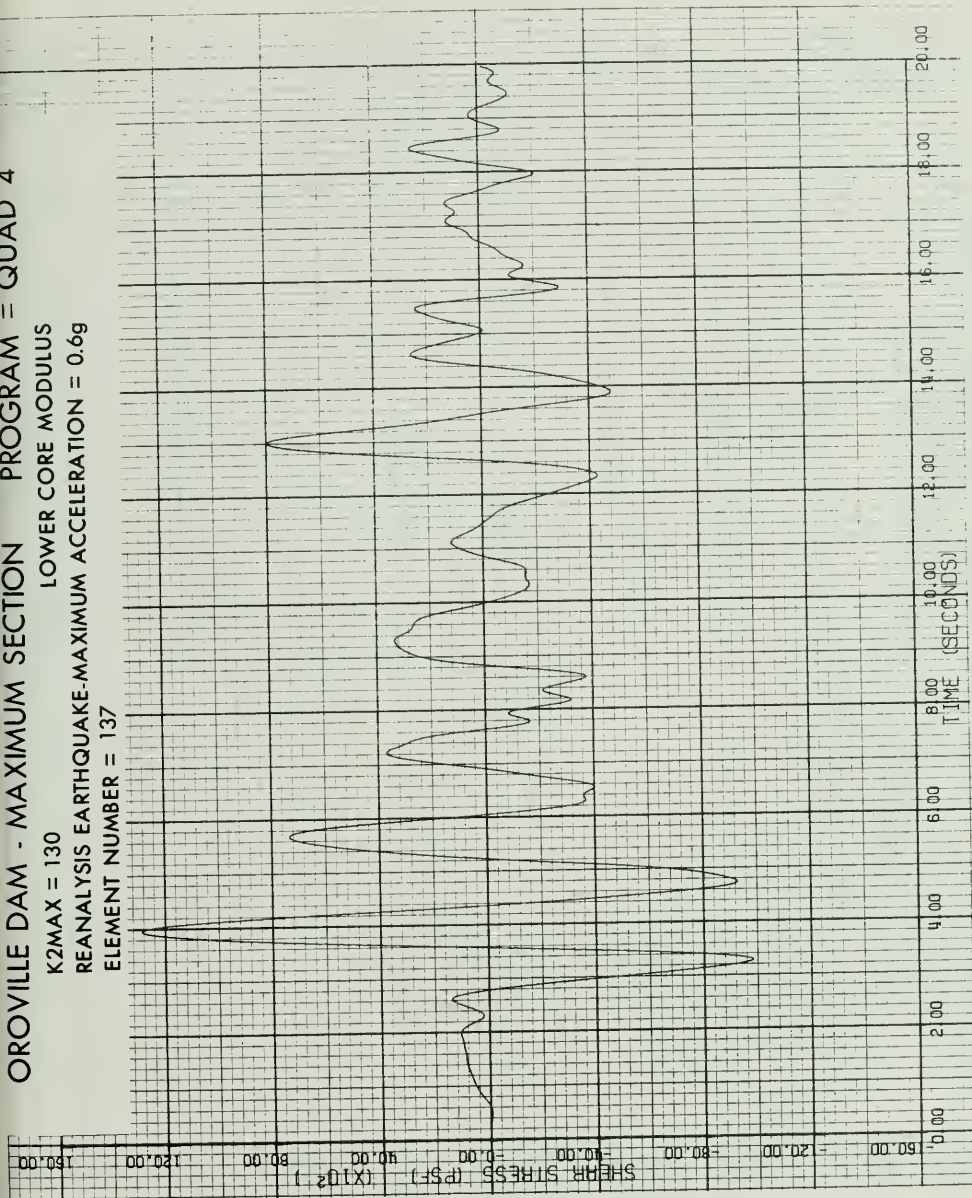


Figure E-26. Element Number 137

OROVILLE DAM - MAXIMUM SECTION PROGRAM = QUAD 4

K2MAX = 130
 LOWER CORE MODULUS
 REANALYSIS EARTHQUAKE-MAXIMUM ACCELERATION = 0.6g
 ELEMENT NUMBER = 175

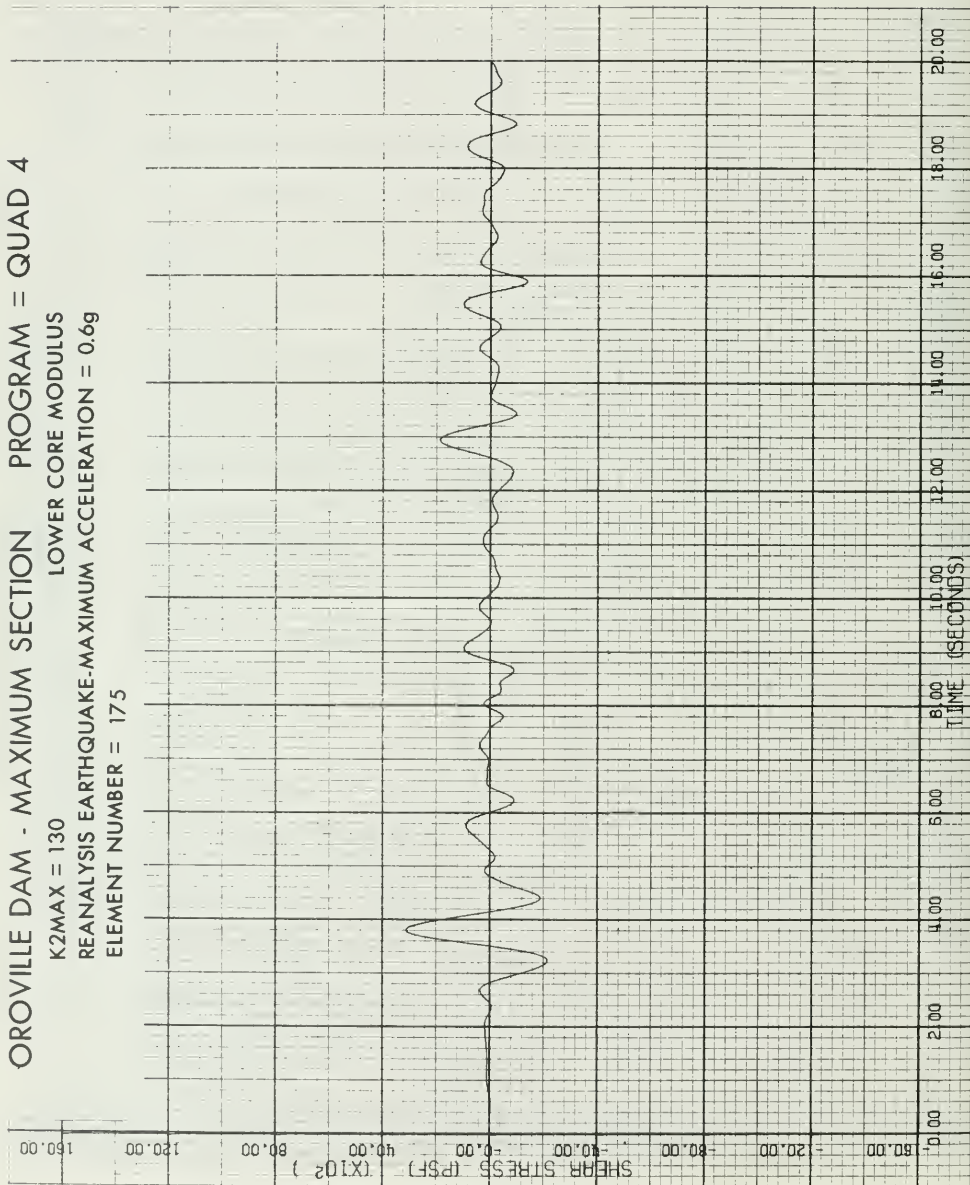


Figure E-27. Element Number 175

OROVILLE DAM - MAXIMUM SECTION PROGRAM = QUAD 4
 K2MAX = 130 LOWER CORE MODULUS
 REANALYSIS EARTHQUAKE-MAXIMUM ACCELERATION = 0.6g
 ELEMENT NUMBER = 181

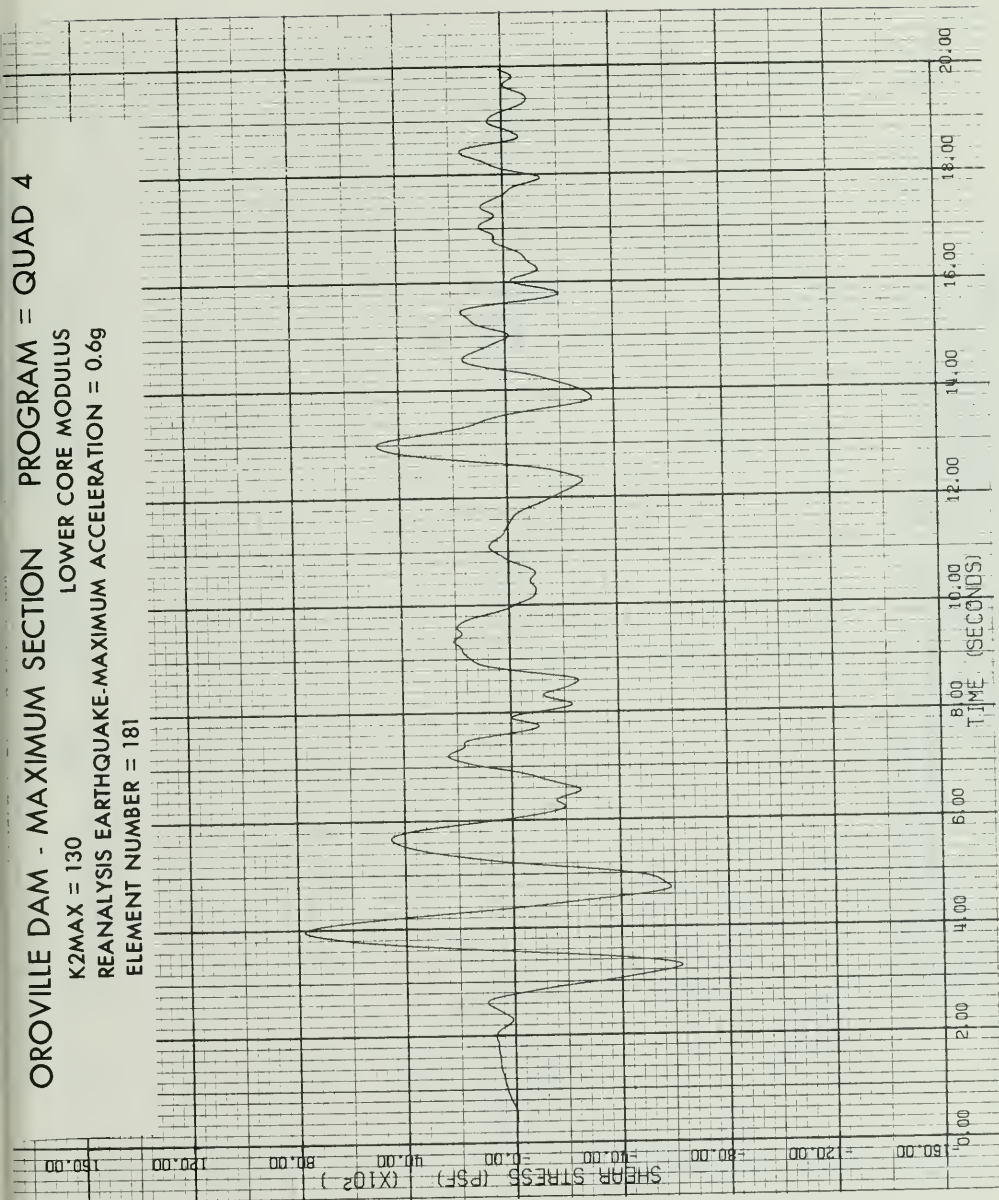


Figure E-28. Element Number 181

OROVILLE DAM - MAXIMUM SECTION PROGRAM = QUAD 4
 K2MAX = 130 LOWER CORE MODULUS
 REANALYSIS EARTHQUAKE-MAXIMUM ACCELERATION = 0.6g
 ELEMENT NUMBER = 189

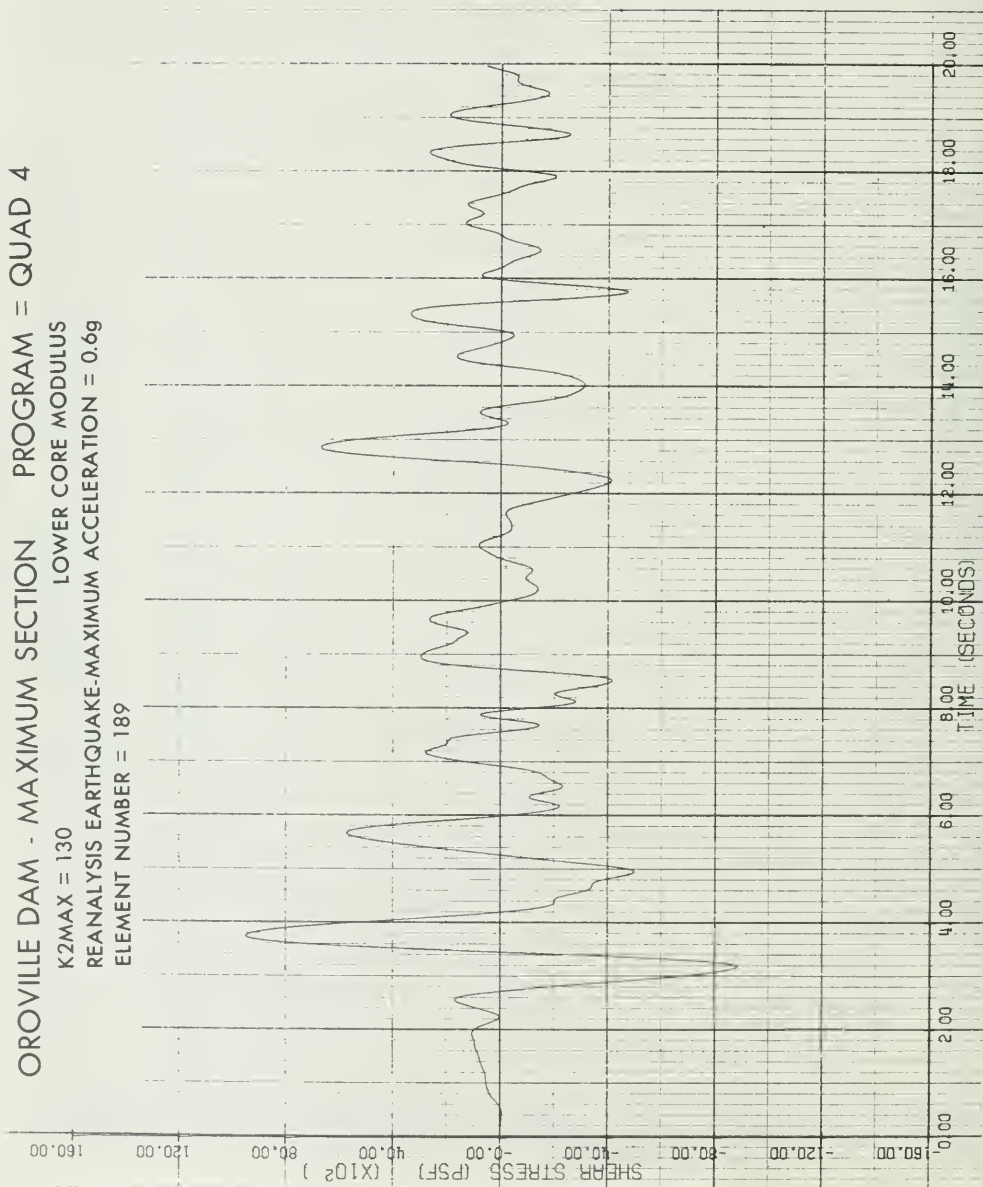


Figure E-29. Element Number 189

OROVILLE DAM - MAXIMUM SECTION PROGRAM = QUAD 4

K2MAX = 130 LOWER CORE MODULUS

REANALYSIS EARTHQUAKE-MAXIMUM ACCELERATION = 0.6g

ELEMENT NUMBER = 229

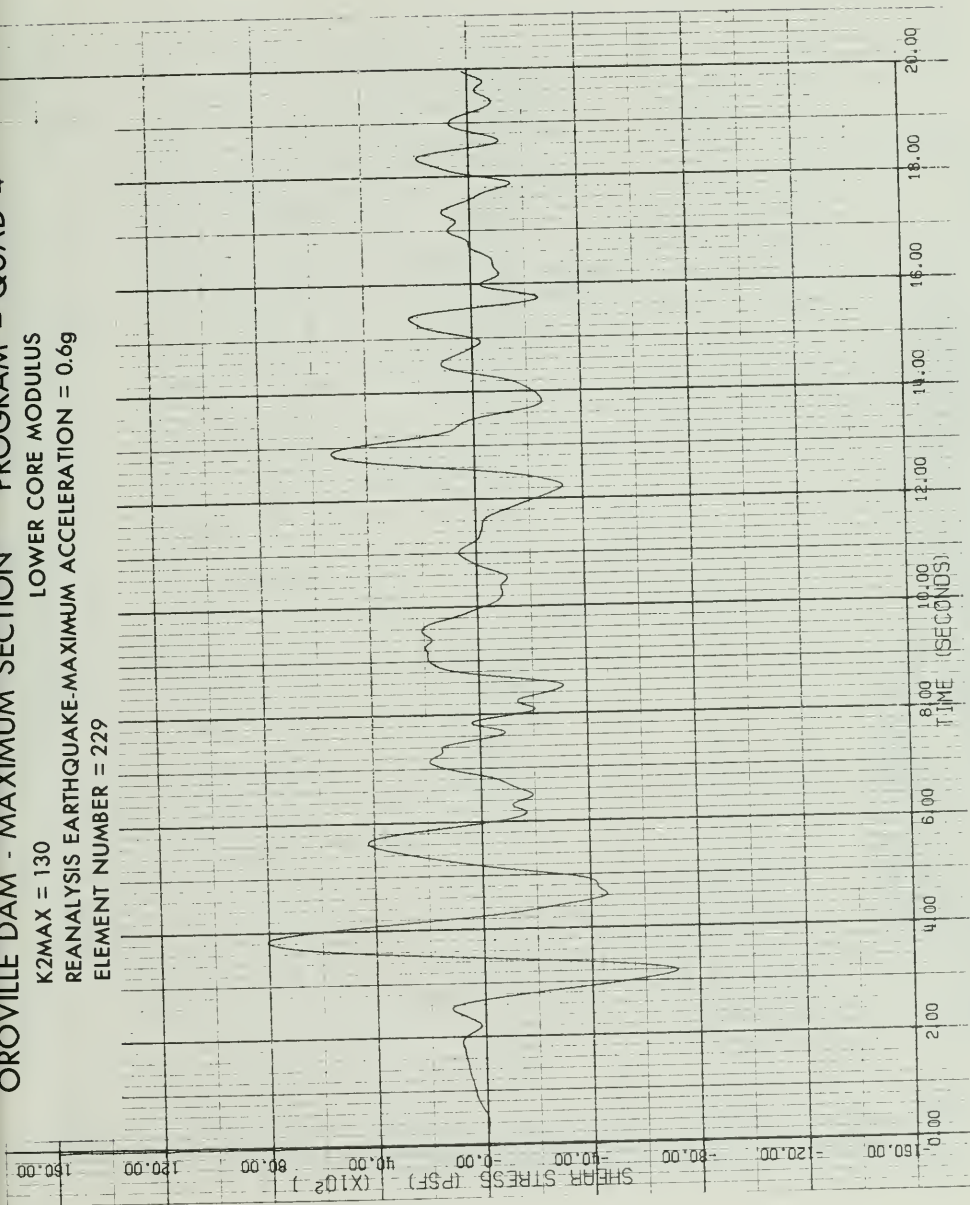


Figure E-30. Element Number 229

OROVILLE DAM - MAXIMUM SECTION PROGRAM = QUAD 4
 K2MAX = 130 LOWER CORE MODULUS
 REANALYSIS EARTHQUAKE-MAXIMUM ACCELERATION = 0.6g
 ELEMENT NUMBER = 239

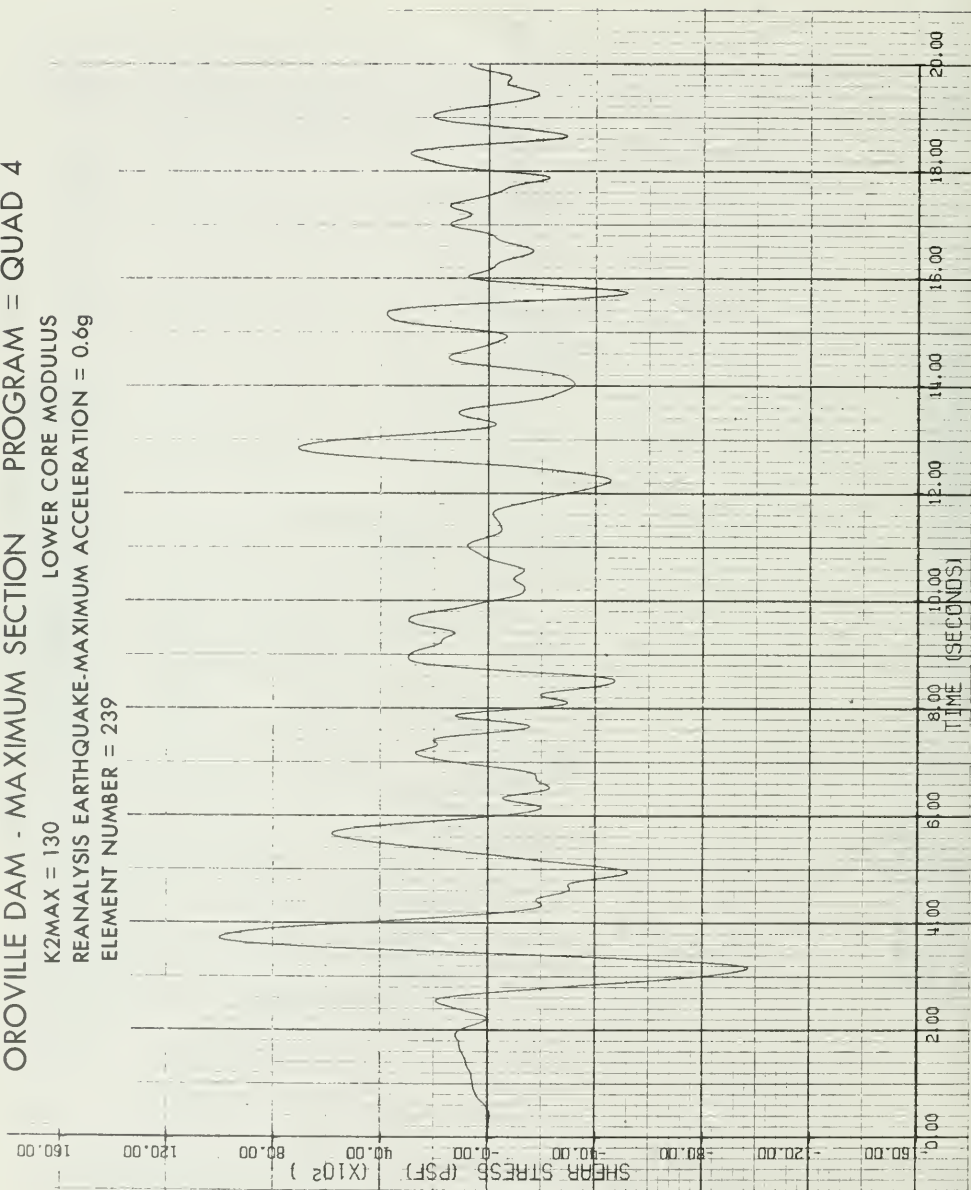


Figure E-31. Element Number 239

OROVILLE DAM - MAXIMUM SECTION PROGRAM = QUAD 4
 K2MAX = 130 LOWER CORE MODULUS
 REANALYSIS EARTHQUAKE-MAXIMUM ACCELERATION = 0.6g
 ELEMENT NUMBER = 251

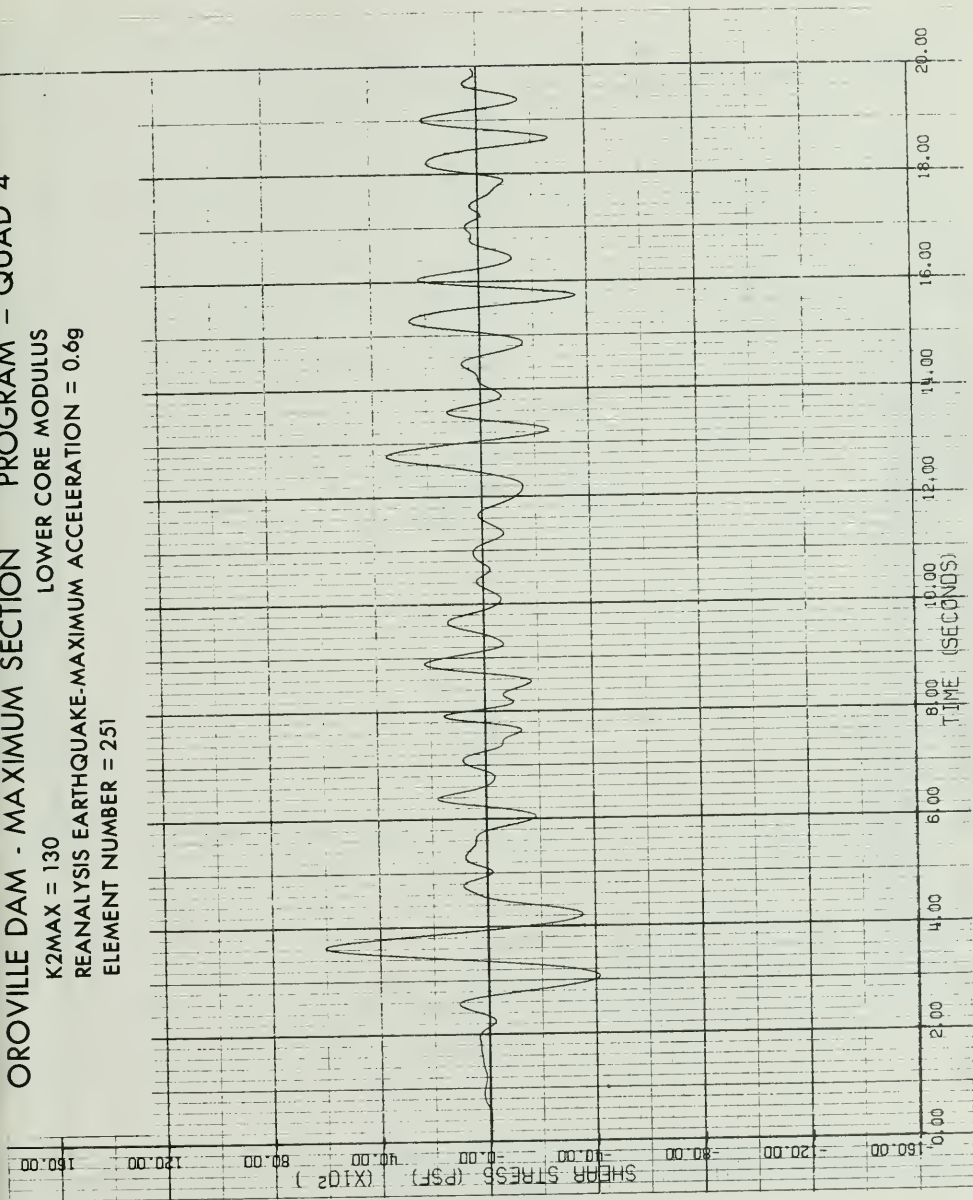


Figure E-32. Element Number 251

OROVILLE DAM - MAXIMUM SECTION PROGRAM = QUAD 4
 K2MAX = 130 LOWER CORE MODULUS
 REANALYSIS EARTHQUAKE-MAXIMUM ACCELERATION = 0.6g
 ELEMENT NUMBER = 282

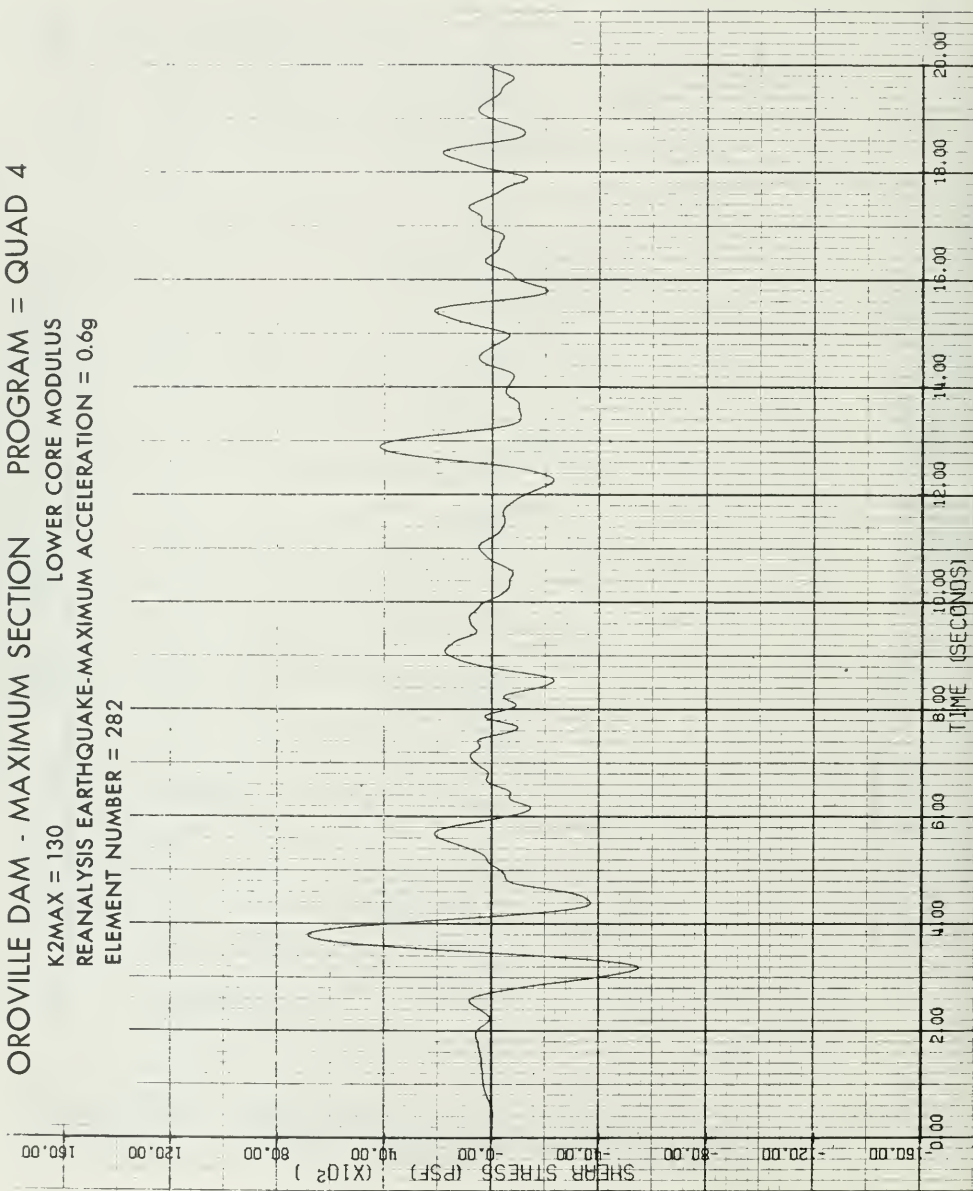


Figure E-33. Element Number 282

OROVILLE DAM - MAXIMUM SECTION PROGRAM = QUAD 4

K2MAX = 130
 LOWER CORE MODULUS
 REANALYSIS EARTHQUAKE-MAXIMUM ACCELERATION = 0.6g
 ELEMENT NUMBER = 375

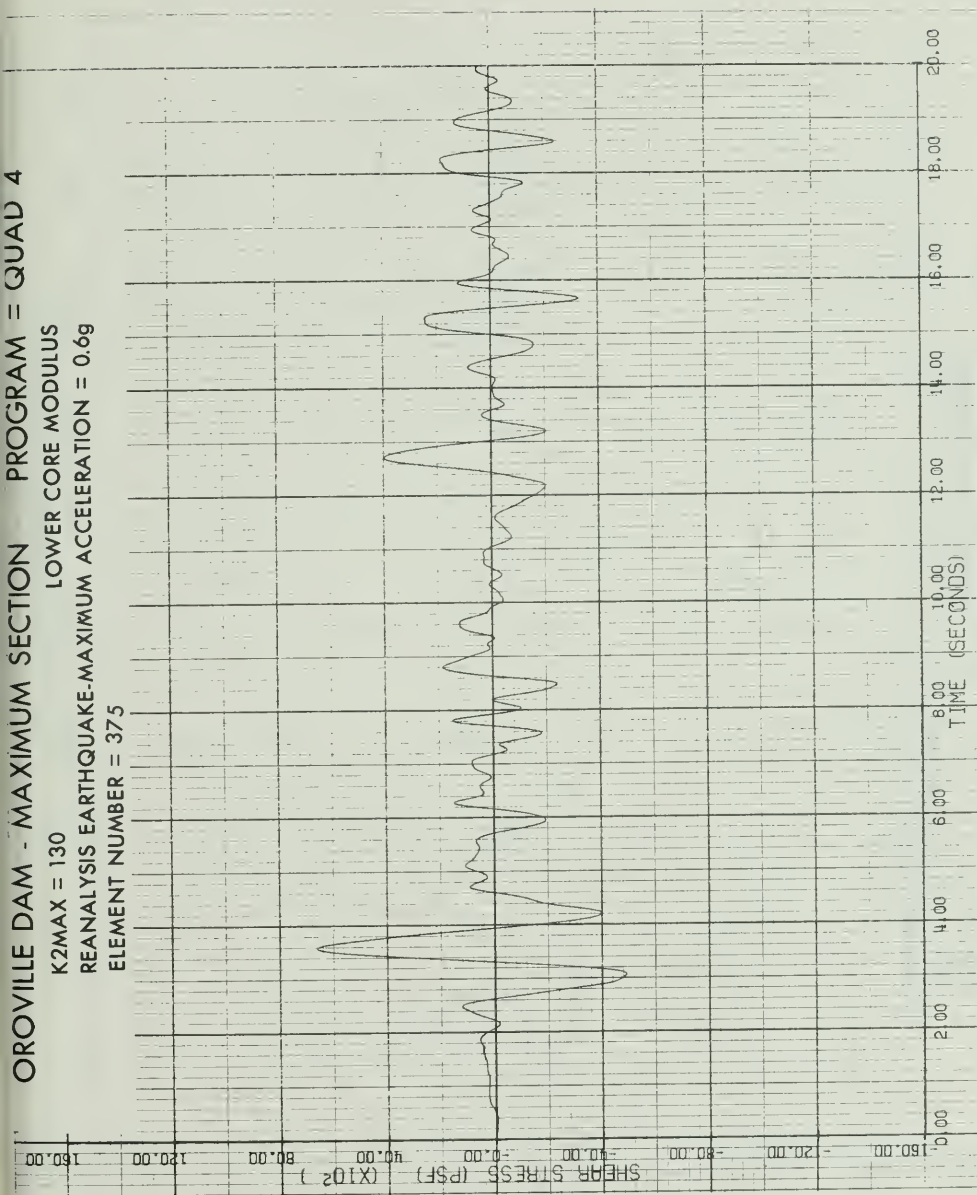


Figure E-34. Element Number 375

OROVILLE DAM - MAXIMUM SECTION PROGRAM = QUAD 4
 K2MAX = 130 LOWER CORE MODULUS
 REANALYSIS EARTHQUAKE-MAXIMUM ACCELERATION = 0.6g
 ELEMENT NUMBER = 381

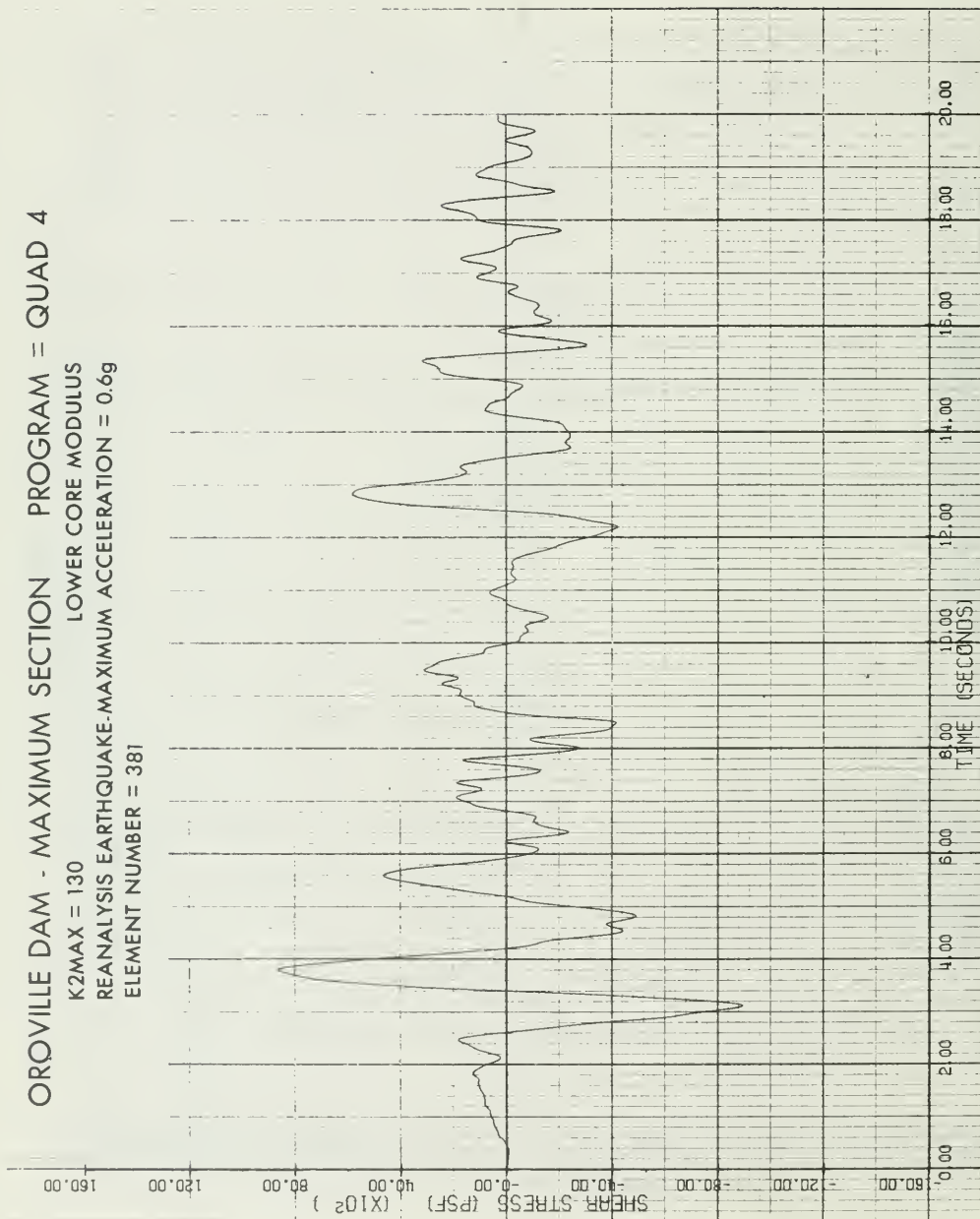


Figure E-35. Element Number 381

OKOVILLE DAM - MAXIMUM SECTION PROGRAM = QUAD 4
 LOWER CORE MODULUS
 K2MAX = 130
 REANALYSIS EARTHQUAKE-MAXIMUM ACCELERATION = 0.6g
 ELEMENT NUMBER = 409

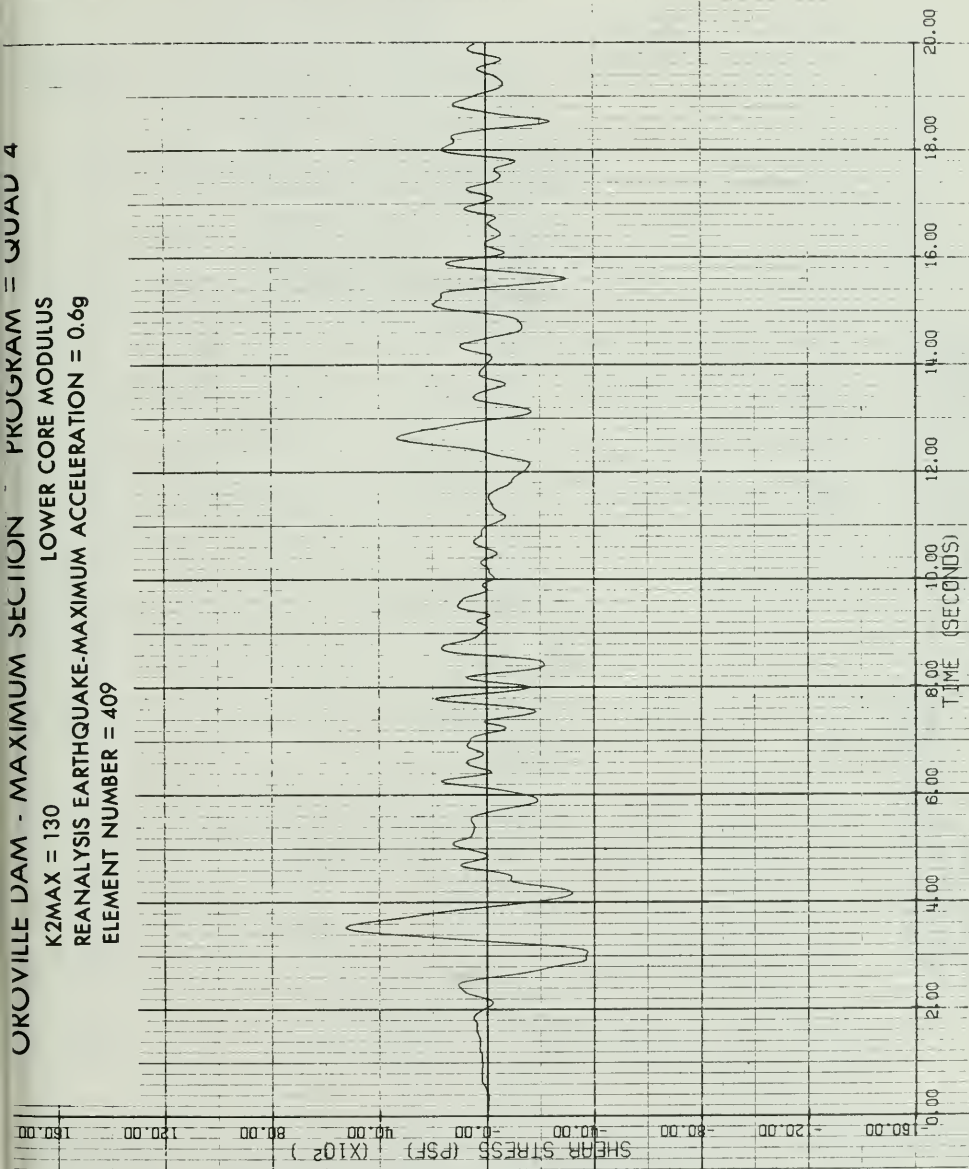


Figure E-36. Element Number 409

OROVILLE DAM - MAXIMUM SECTION PROGRAM = QUAD 4
 K2MAX = 130 LOWER CORE MODULUS
 REANALYSIS EARTHQUAKE-MAXIMUM ACCELERATION = 0.6g
 ELEMENT NUMBER = 496

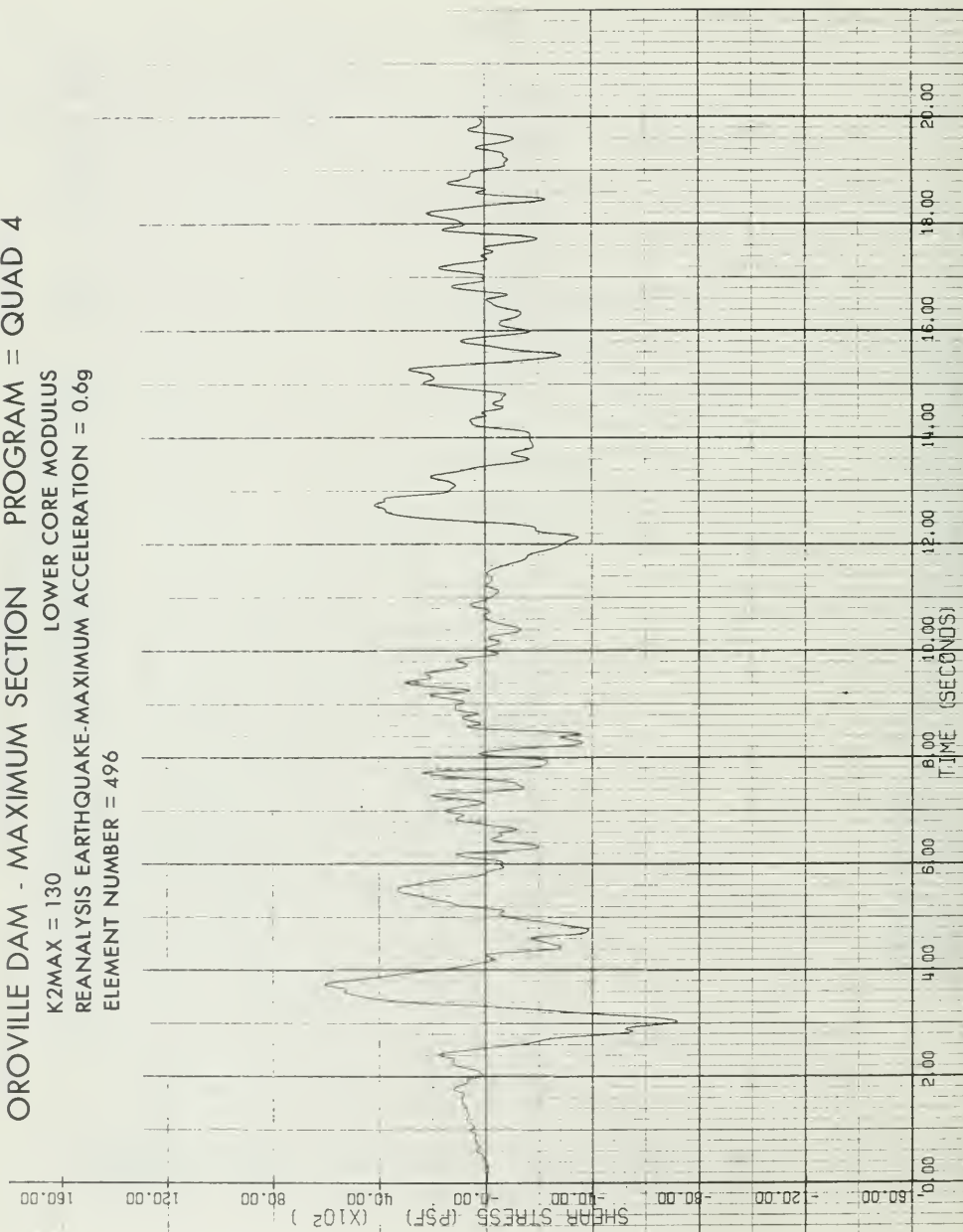


Figure E-37. Element Number 496

OROVILLE DAM - MAXIMUM SECTION PROGRAM - QUAD 4
 K2MAX = 130 LOWER CORE MODULUS
 REANALYSIS EARTHQUAKE-MAXIMUM ACCELERATION = 0.6g
 ELEMENT NUMBER = 526

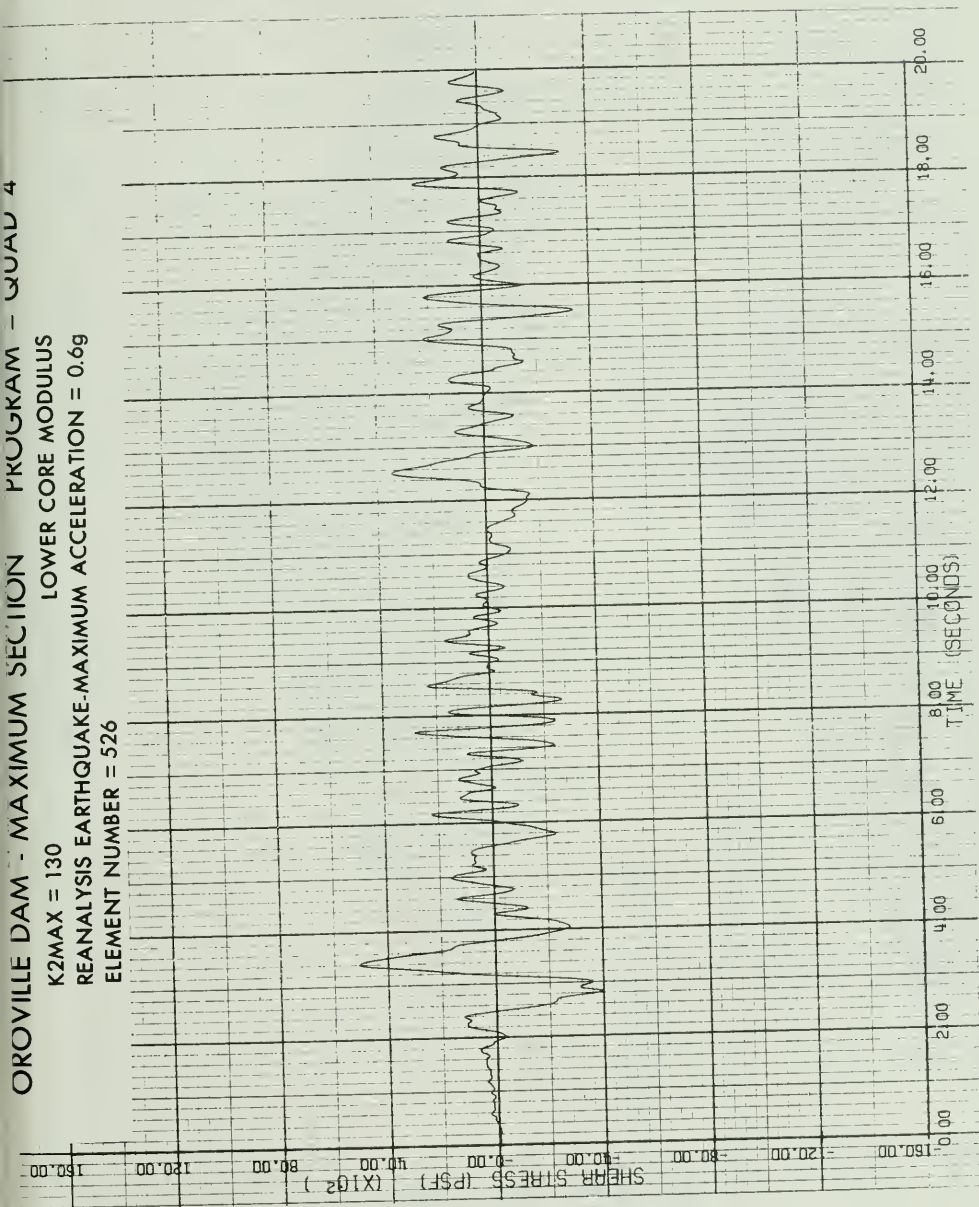


Figure E-38. Element Number 526

OROVILLE DAM - MAXIMUM SECTION PROGRAM = QUAD 4
 K2MAX = 130 LOWER CORE MODULUS
 REANALYSIS EARTHQUAKE-MAXIMUM ACCELERATION = 0.6g
 ELEMENT NUMBER = 535

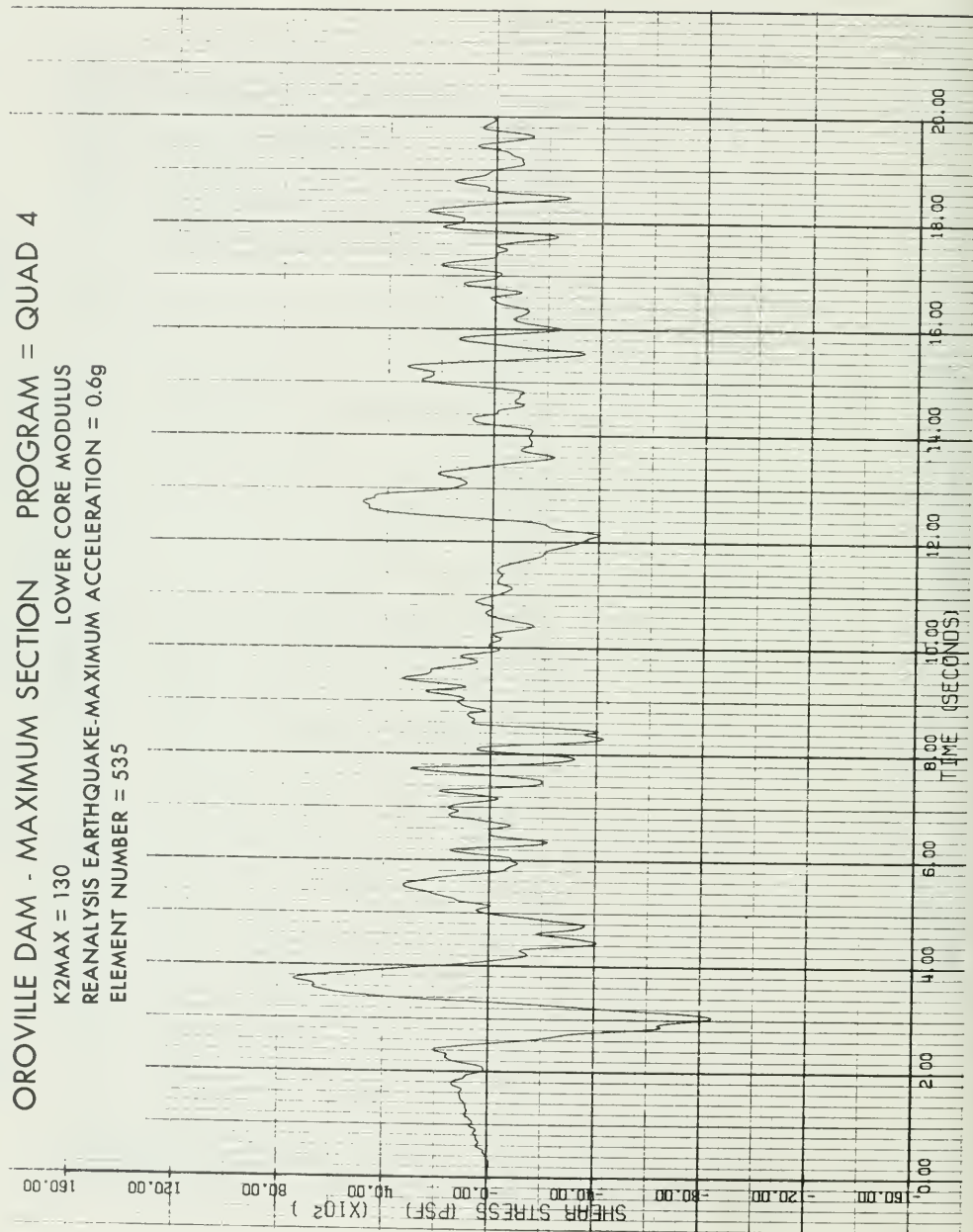
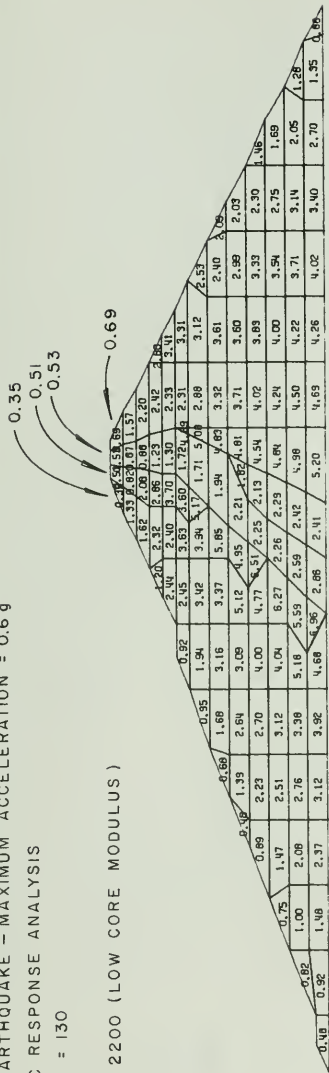


Figure E-39. Element Number 535

OROVILLE DAM - SECTION 2
 REANALYSIS EARTHQUAKE - MAXIMUM ACCELERATION = 0.6 g
 LUSH DYNAMIC RESPONSE ANALYSIS
 SHELL K₂max = 130

CORE $\frac{G_{max}}{S_u} = 2200$ (LOW CORE MODULUS)



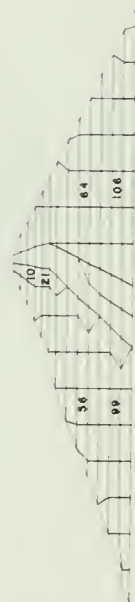
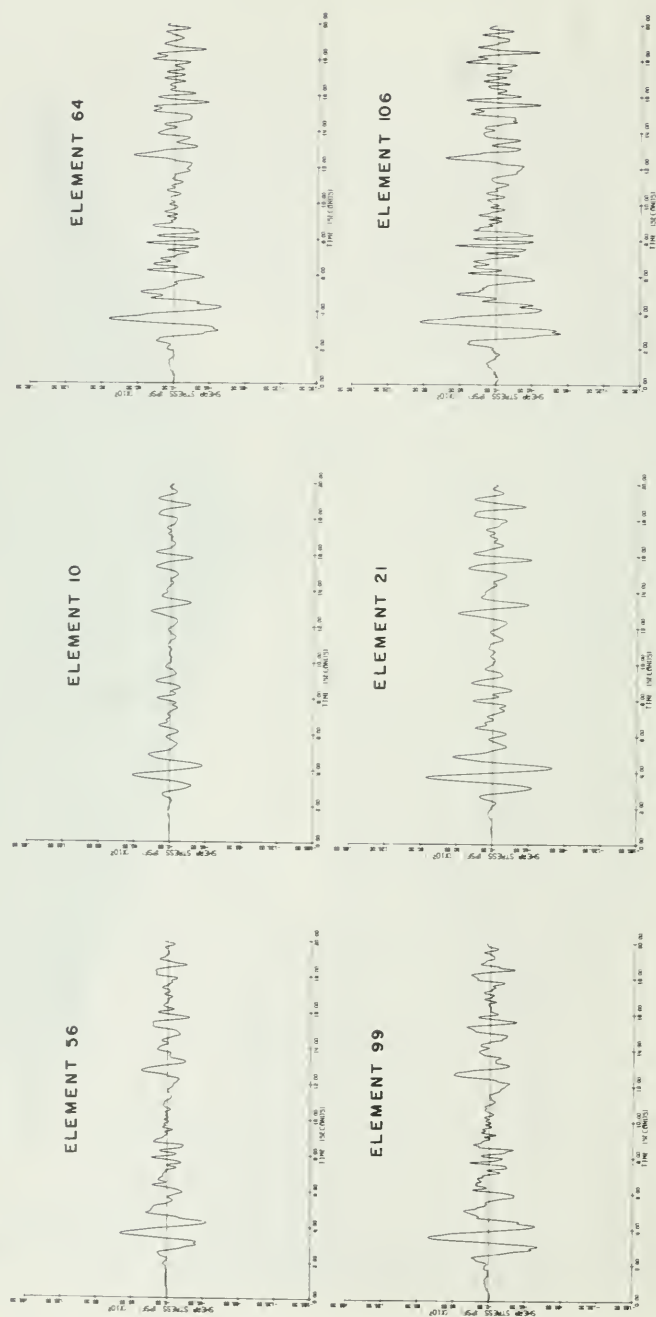


Figure E-42. Typical Shear Stress Time Histories from LUSH Analysis of Section 2 Using $K_2 = 130$ and Low Core Modulus

REANALYSIS EARTHQUAKE - MAXIMUM ACCELERATION = 0.6g
QUAD 4 DYNAMIC RESPONSE ANALYSIS
SHELL K2 max = 130

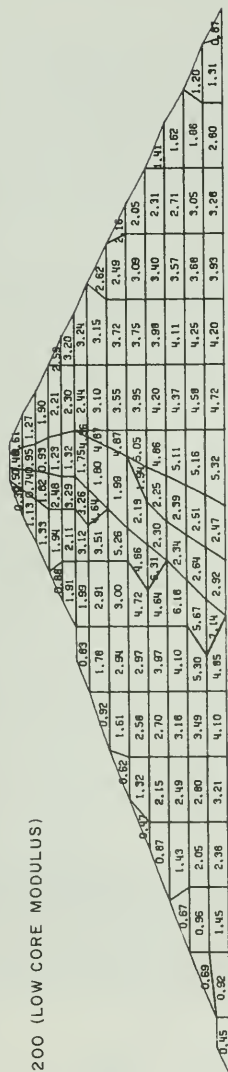
$$\text{CORE } \frac{G_{\max}}{S_u} = 2200 \text{ (LOW CORE MODULUS)}$$


Figure E-43. Maximum Horizontal Shear Stresses, τ_{xy} , from QUAD4 Analysis of Section 2 (tsf)

REANALYSIS EARTHQUAKE - MAXIMUM ACCELERATION = 0.6g
QUAD 4 DYNAMIC RESPONSE ANALYSIS
SHELL K2 max = 130

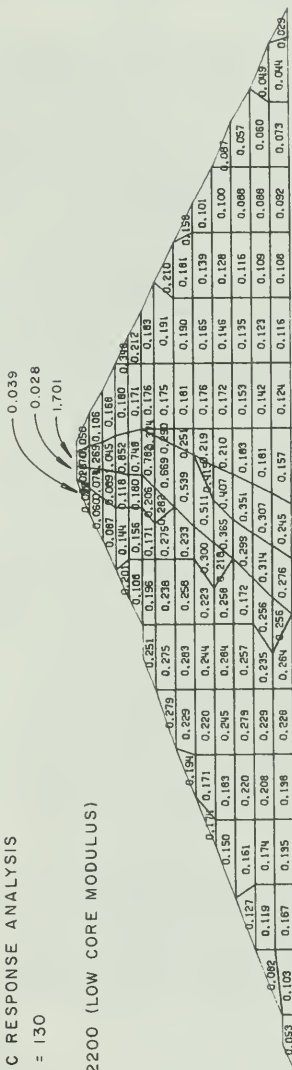
$$\frac{G_{\max}}{S_u} = 2200 \text{ (LOW CORE MODULUS)}$$


Figure E-44. Maximum Shear Strains, γ_{\max} , from QUAD4 Analysis of Section 2 (percent)

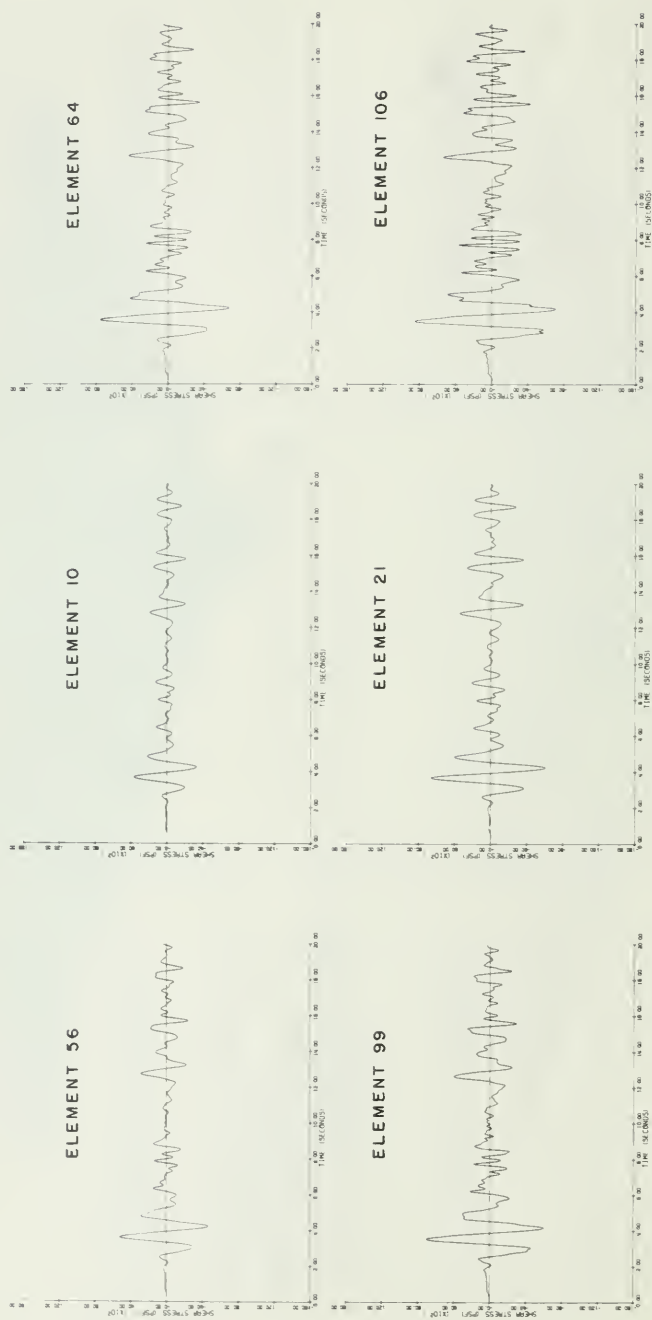


Figure E-45. Typical Shear Stress Time Histories from QUAD4 Analysis of Section 2 Using $K_{2max} = 130$ and Low Core Modulus

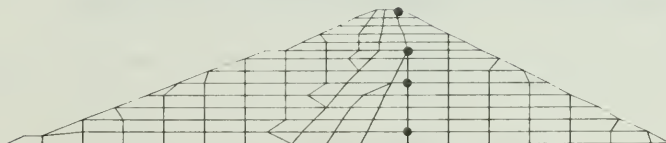
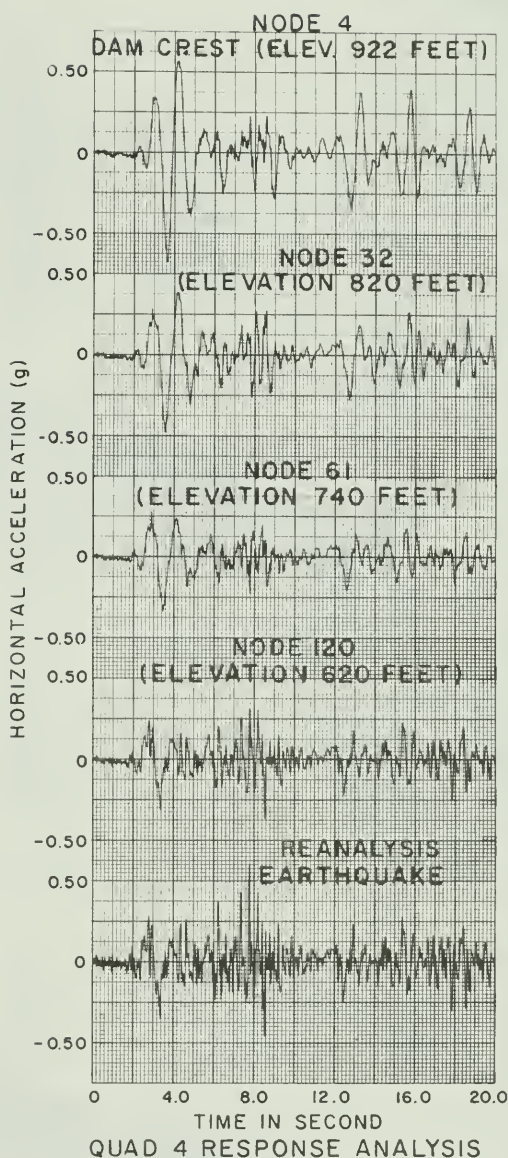
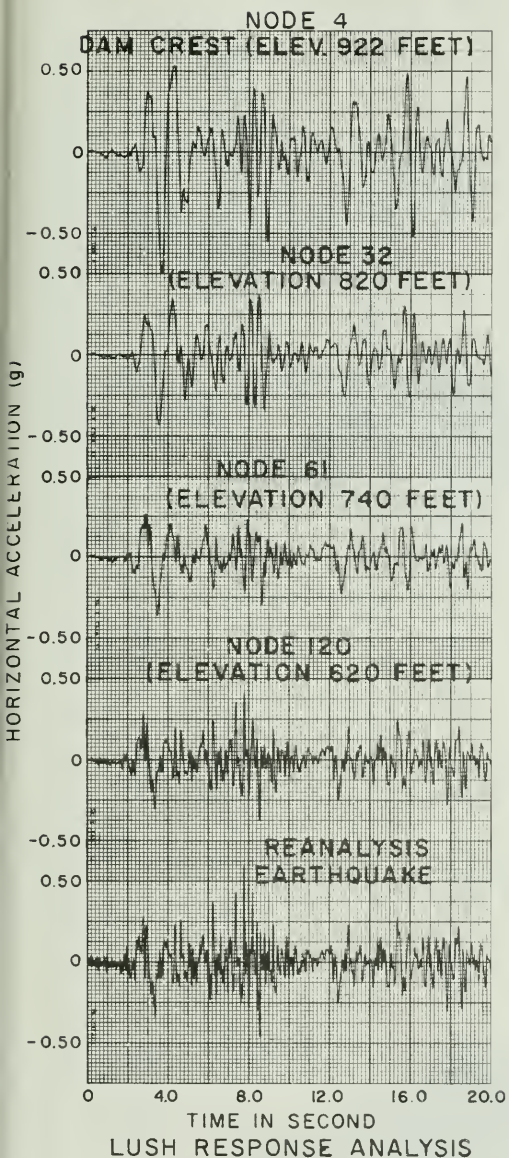


Figure E-46. Comparisons of Acceleration Responses between LUSH and QUAD4 Analyses of Section 2 Using $K_2 \text{ max} = 130$ and Low Core Modulus

OROVILLE DAM - SECTION 3
 REANALYSIS EARTHQUAKE - MAXIMUM ACCELERATION = 0.6 g
 LUSH DYNAMIC RESPONSE ANALYSIS
 SHELL $K_{2 \max} = 130$

CORE $\frac{G_{\max}}{S_u} = 2200$ (LOW CORE MODULUS)

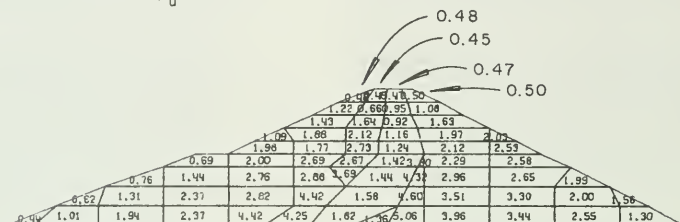


Figure E-47. Maximum Horizontal Shear Stresses, τ_{xy} , from LUSH Analysis of Section 3 (tsf)

OROVILLE DAM - SECTION 3
 REANALYSIS EARTHQUAKE - MAXIMUM ACCELERATION = 0.6 g
 LUSH DYNAMIC RESPONSE ANALYSIS
 SHELL $K_{2 \max} = 130$

CORE $\frac{G_{\max}}{S_u} = 2200$ (LOW CORE MODULUS)

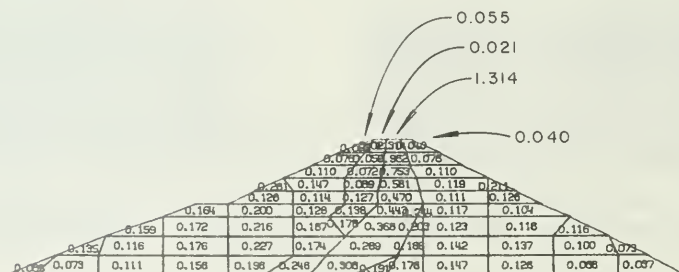


Figure E-48. Maximum Shear Strains, γ_{\max} , from LUSH Analysis of Section 3 Using $K_{2 \max} = 130$ and Low Core Modulus (percent)

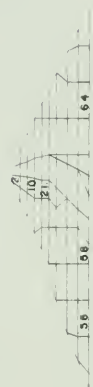
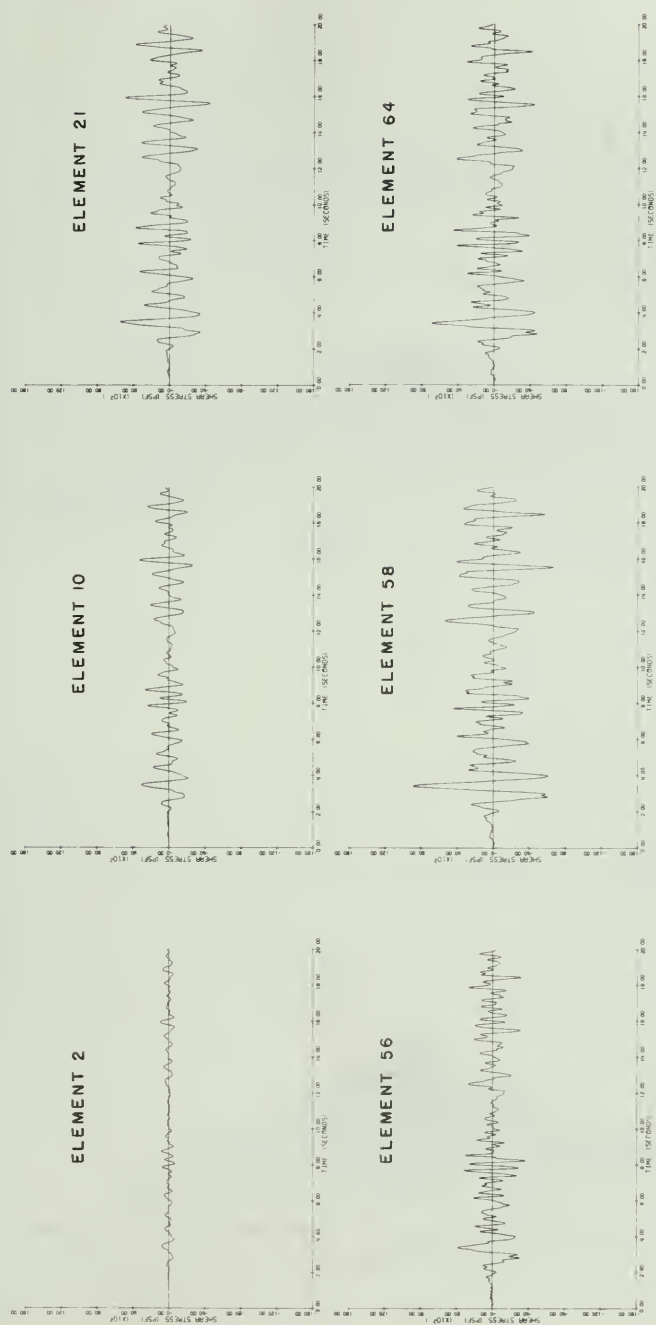


Figure E-49. Typical Shear Stress Time Histories from LUSH Analysis of Section 3 using $K_2 = 130$ and Low Core Modulus

OROVILLE DAM - SECTION 3

REANALYSIS EARTHQUAKE - MAXIMUM ACCELERATION = 0.6g

QUAD 4 DYNAMIC RESPONSE ANALYSIS

SHELL $K_{2 \max} = 130$

CORE $\frac{G_{\max}}{S_u} = 2200$ (LOW CORE MODULUS)

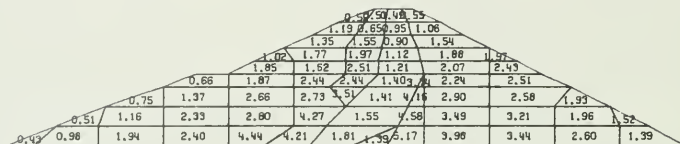


Figure E-50. Maximum Horizontal Shear Stresses, τ_{xy} , from QUAD4 Analysis of Section 3 Using $K_{2 \max} = 130$ and Low Core Modulus

OROVILLE DAM - SECTION 3

REANALYSIS EARTHQUAKE - MAXIMUM ACCELERATION = 0.6g

QUAD 4 DYNAMIC RESPONSE ANALYSIS

SHELL $K_{2 \max} = 130$

CORE $\frac{G_{\max}}{S_u} = 2200$ (LOW CORE MODULUS)

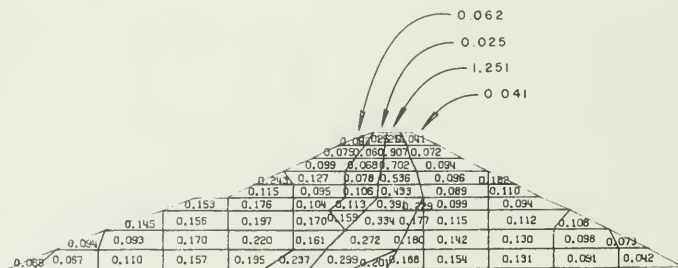


Figure E-51. Maximum Strains, γ_{\max} , from QUAD4 Analysis of Section 3 Using $K_{2 \max} = 130$ and Low Core Modulus

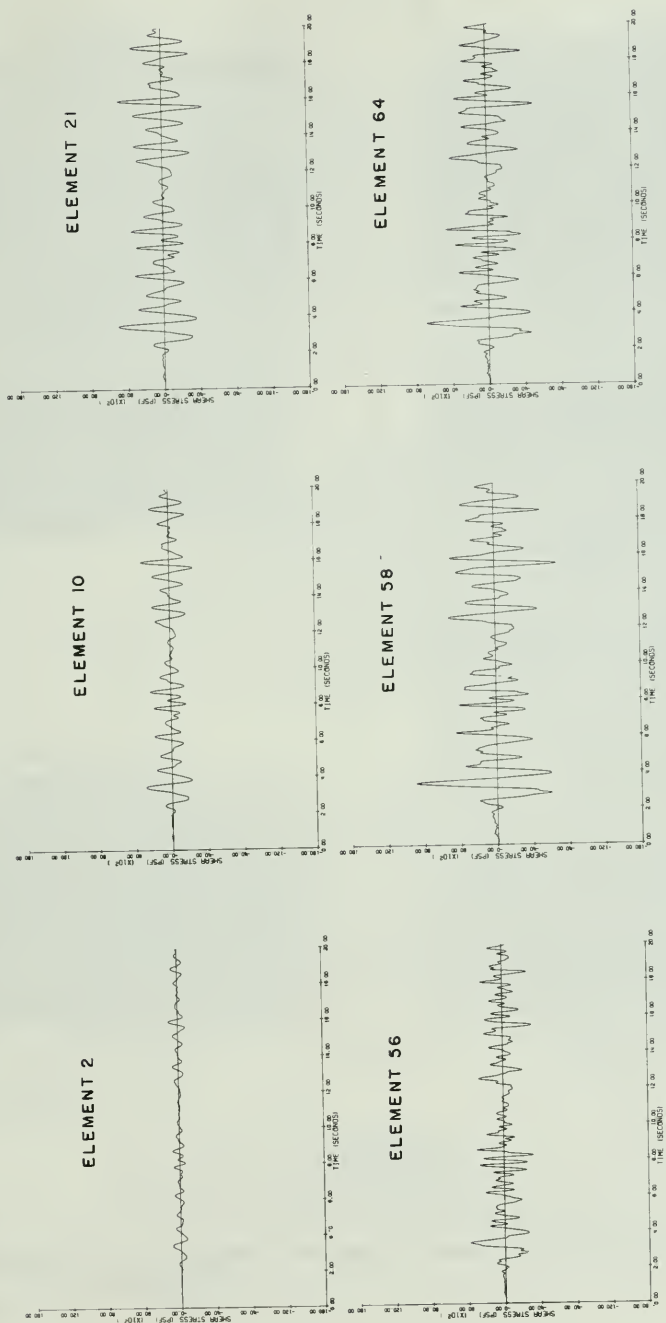


Figure E-52. Typical Shear Stress Time Histories from QUAD4 Analysis of Section 3 Using $K_{2max} = 130$ and Low Core Modulus

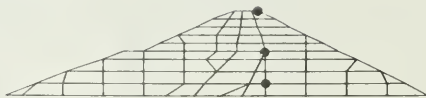
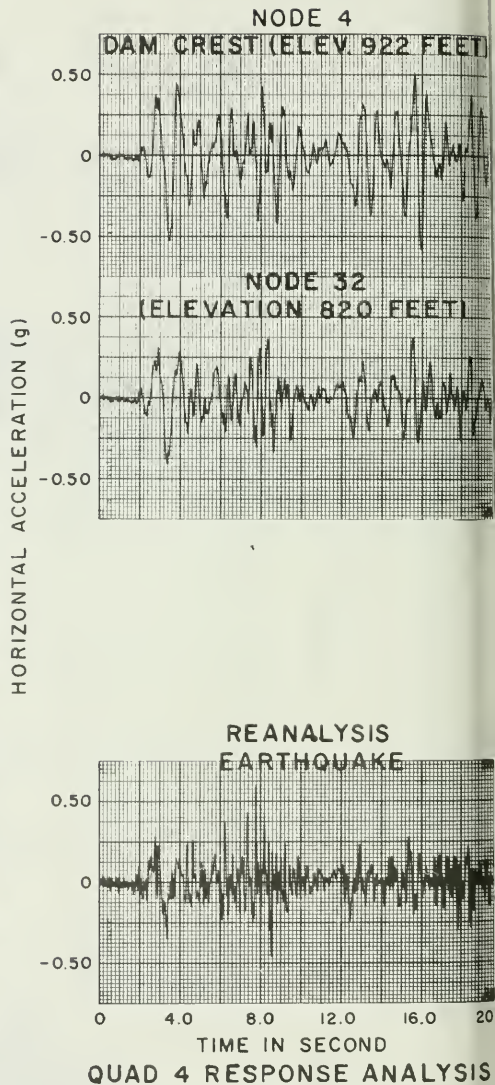
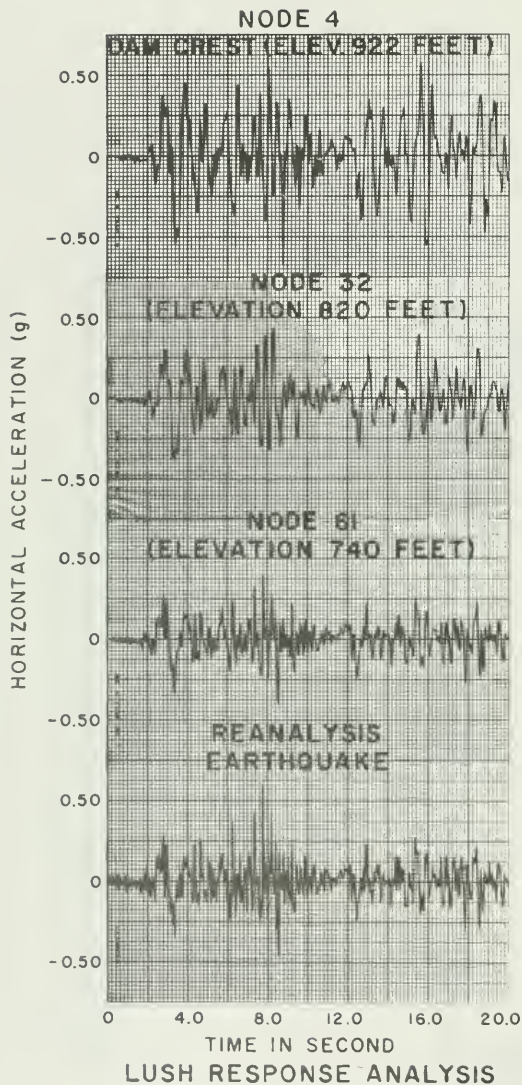
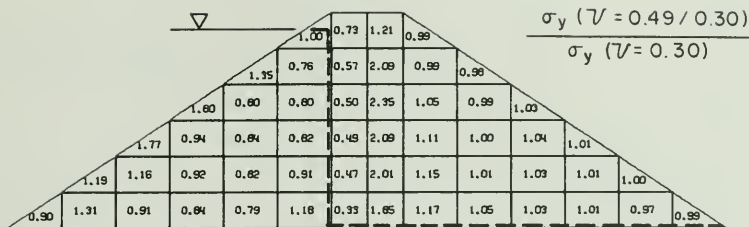
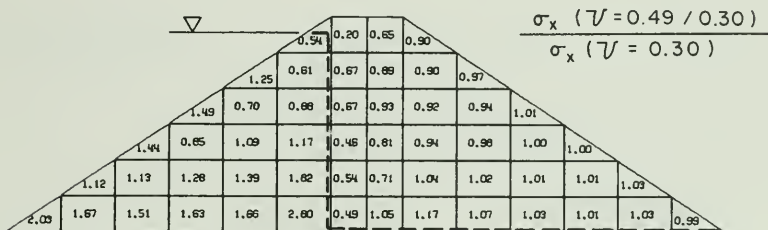


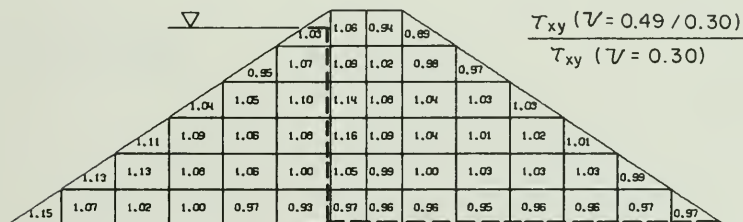
Figure E-53. Comparisons of Acceleration Responses Between LUSH and QUAD4 Analyses of Section 3 Using $K_{2 \max} = 130$ and Low Core Modulus



MAXIMUM VERTICAL NORMAL STRESS (σ_y)



MAXIMUM HORIZONTAL NORMAL STRESS (σ_x)



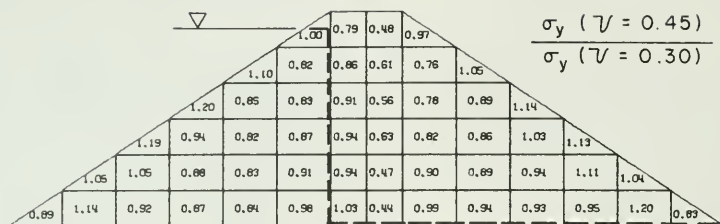
MAXIMUM HORIZONTAL SHEAR STRESS (τ_{xy})

LUSH DYNAMIC RESPONSE ANALYSIS

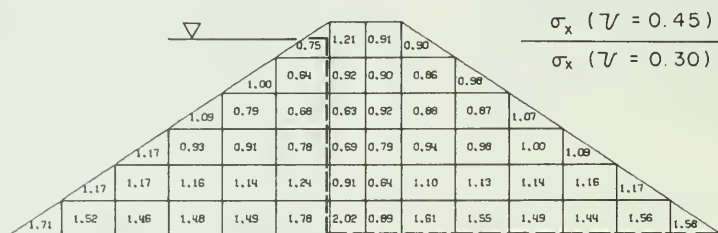
REANALYSIS EARTHQUAKE — MAXIMUM ACCELERATION = 0.6 g

EMBANKMENT $K_2 \text{ MAX} = 130$

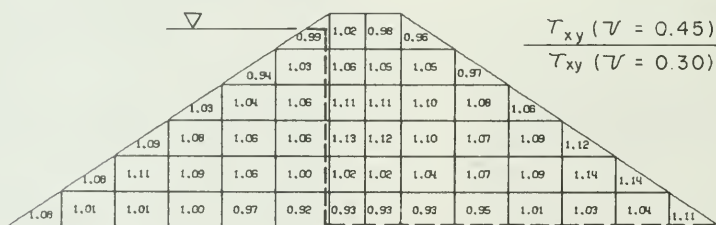
Figure E-54. Effect of Poisson's Ratio on the Induced Dynamic Stresses in the Model Embankment



MAXIMUM VERTICAL NORMAL STRESS (σ_y)



MAXIMUM HORIZONTAL NORMAL STRESS (σ_x)



MAXIMUM HORIZONTAL SHEAR STRESS (τ_{xy})

LUSH DYNAMIC RESPONSE ANALYSIS

REANALYSIS EARTHQUAKE — MAXIMUM ACCELERATION = 0.6g

EMBANKMENT $K_2 \text{ MAX} = 130$

Figure E-55. Effect of Poisson's Ratio on the Induced Dynamic Stresses in the Model Embankment.

APPENDIX F
EMBANKMENT RESPONSE MODEL

EMBANKMENT RESPONSE MODEL

As described previously in the main text, the Embankment Response Model is a two-dimensional plane strain analysis with a modified $K_{2 \text{ max}}$ (pseudo $K_{2 \text{ max}}$) value. This model was developed to account for the three-dimensional effect of the canyon on the dynamic response of the embankment.

Oroville Dam is located in a triangular-shaped canyon and has a variable cross-section (Figure F-1). In a two-dimensional plane strain analysis, the length of the dam (z-axis) is assumed to be infinite and all of the stresses induced to resist movement are in the x-y plane (Figure F-2). However, the abutments impart a restraining effect which gives additional stiffness to the embankment. This additional stiffness results from stresses in the y-z and x-z planes. Stresses in these two planes are not accounted for in a two-dimensional plane strain analysis.

In an attempt to simulate three-dimensional response, an artificially-high (pseudo) $K_{2 \text{ max}}$ was used to account for the stresses in the y-z and x-z planes. As detailed in Section 5, a value of 350 was developed for the pseudo $K_{2 \text{ max}}$ value. This value was determined from analyses of embankment response to the 1975 Oroville Earthquakes. In extending this model for use with the Reanalysis Earthquake, it is assumed that the model can simulate three-dimensional embankment response to earthquakes of varying magnitude and frequency content.



Figure F-1. Three-dimensional Problem

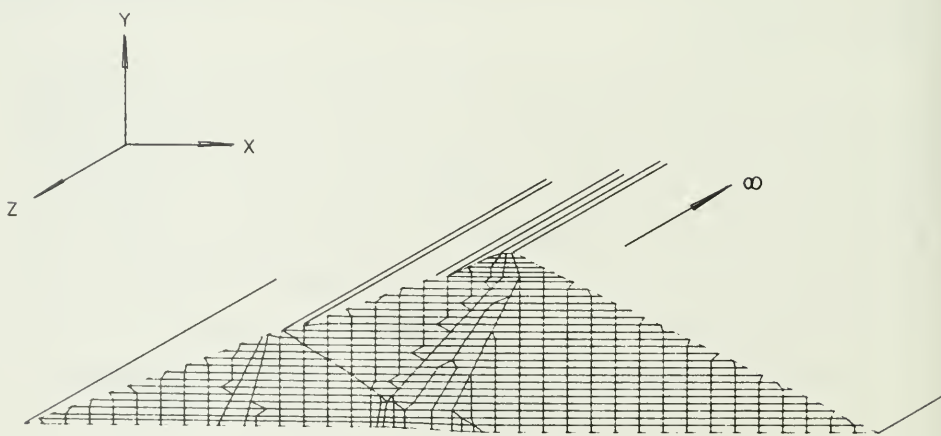


Figure F-2. Two-dimensional Plane Strain Representation

In applying the model, it is assumed that the model will simulate the three-dimensional response of the maximum section of the dam in the x-y plane. This means that the accelerations and displacements would be approximated. However, the shear stresses in the x-y plane would not be correct. This is due to the fact that all of the dynamic stresses have essentially been lumped together into the x-y plane by using the two-dimensional plane strain analysis with a pseudo $K_{2 \text{ max}}$ value of 350. Since the earthquake-induced shear stresses are of considerable importance in a dynamic analysis of an embankment, the stresses must be estimated in a different manner.

The method which was adopted to estimate the shear stresses in the x-y plane resulting from a three-dimensional embankment response assumed that the Embankment Response Model approximated the correct shear strains in the x-y plane. Using these shear strains, and the best estimate of the actual $K_{2 \text{ max}}$ value for the Oroville gravel, the horizontal shear stresses in the x-y plane were estimated.

The procedure is detailed in the following equations:

$$\tau = \gamma * G \quad (1)$$

where τ = Shear Stress

γ = Shear Strain

G = Shear Modulus

$$G = R_d * K_{2 \text{ max}} * (\sigma'_m)^{1/2} * 1000 \quad (2)$$

where R_d = Shear Modulus Reduction Factor, Dependent Upon Shear Strain

σ'_m = Effective Mean Normal Stress in psf

$$\tau = \gamma * R_d * K_{2 \text{ max}} * (\sigma'_m)^{1/2} * 1000 \quad (3)$$

Using the Embankment Response Model and the pseudo $K_{2 \text{ max}}$ value of 350:

$$\tau_{xy_{2D_{350}}} = \gamma_{xy_{2D_{350}}} * R_d * 350 * (\sigma'_m)^{1/2} * 1000 \quad (4)$$

The actual shear stress in the x-y plane induced in a three-dimensional response would be computed using the actual value of $K_{2 \text{ max}}$ for the gravel. As discussed previously, the best estimate of the actual $K_{2 \text{ max}}$ value is about 165. A comparison of the actual and pseudo K_2 values plotted against shear strain is presented in Figure F-3. The actual shear stress in the x-y plane would be defined by:

$$\tau_{xy_{3D}} = \gamma_{xy_{3D}} * R_d * 165 * (\sigma'_m)^{1/2} * 1000 \quad (5)$$

Assuming that the actual (3D) shear strains in the x-y plane are approximated by the strains produced in the Embankment Response Model,

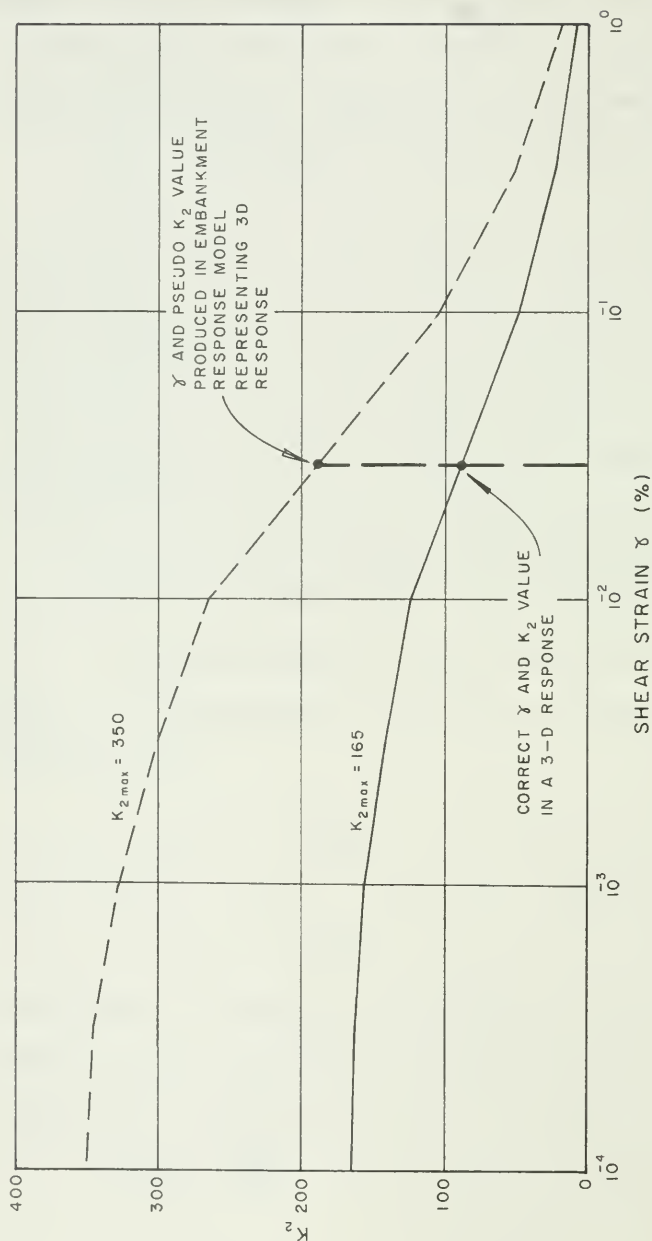
$$\gamma_{xy_{3D}} = \gamma_{xy_{2D_{350}}} \quad (6)$$

$$\tau_{xy_{3D}} = \gamma_{xy_{2D_{350}}} R_d * 165 * (\sigma'_m)^{1/2} * 1000 \quad (7)$$

Because the shear modulus reduction factor (R_d) and the initial effective mean normal stress (σ'_m) are the same, equations 4 and 7 may be combined to yield:

$$\tau_{xy_{3D}} = \frac{165}{350} * \tau_{xy_{2D_{350}}} \quad (8)$$

This approach employs many assumptions and has inherent limitations. However, it is considered to model the actual embankment response more accurately than the traditional plane strain analysis using actual material properties.



$$R_d = \frac{K_2}{K_{2max}} = \text{MODULUS REDUCTION FACTOR}$$

$$\tau_{xy_{30}} = \gamma_{xy_{30}} * G$$

$$\tau_{xy_{30}} \approx \frac{165}{350} * \tau_{xy_{20_{350}}}$$

Figure F-3. Modulus Reduction with Shear Strain

APPENDIX G

CYCLIC TRIAXIAL TEST SUMMARIES

OF MODELED OROVILLE GRAVEL TESTS

(FIGS. G-1 THROUGH G-68)

APPENDIX G

CYCLIC TEST SUMMARIES

In order to present the test behavior of the cyclic triaxial tests carried out for the modeled Oroville gravel, cyclic test summaries were prepared. These summaries show the peak values of cyclic deviator stress, pore water pressure increase, and axial strain, plotted against cyclic number.

The test summaries are derived from the cyclic test records and show uncorrected test behavior. Before utilizing this information, corrections for membrane compliance, calibration error, membrane strength, and consolidation conditions (C_r) should be applied.

Cyclic deviator stress peaks in the extension direction are considered negative and are labeled so. Cyclic deviator stress peaks in the compression direction are considered positive. The sign convention for axial strain is also defined as having compression being the positive direction. The strain peak envelopes, however, are labeled with either "extensive" or "compression" to identify the direction of the stress pulse when the strain peak occurred.

The peak values of pore pressure increase were plotted by using the back pressure value as a zero point. A value above the back pressure was denoted as positive and a value below the back pressure was denoted as negative. Also shown in the pore water pressure summaries as a horizontal dashed line is the initial effective confining pressure. Pore pressure envelopes

rising above this line show either incorrect calibration or a change in the triaxial cell pressure.

These summaries are only intended to illustrate the general behavior of the samples during testing. For a more detailed examination, the actual test records should be consulted.

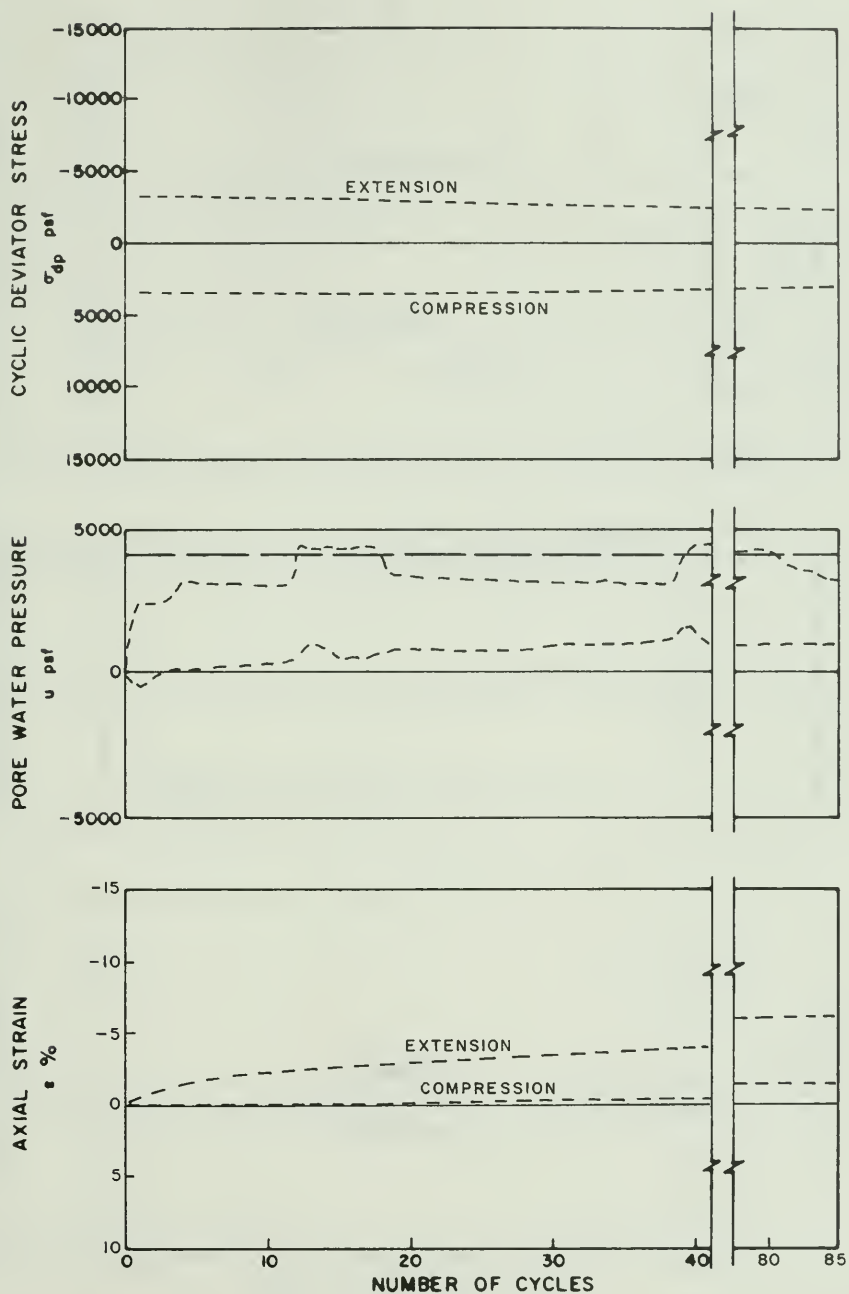


Figure G-1. Cyclic Test Envelopes for Test No. 6 ($\sigma'_{3c} = 4,100$ psf, $K_c = 1.0$)

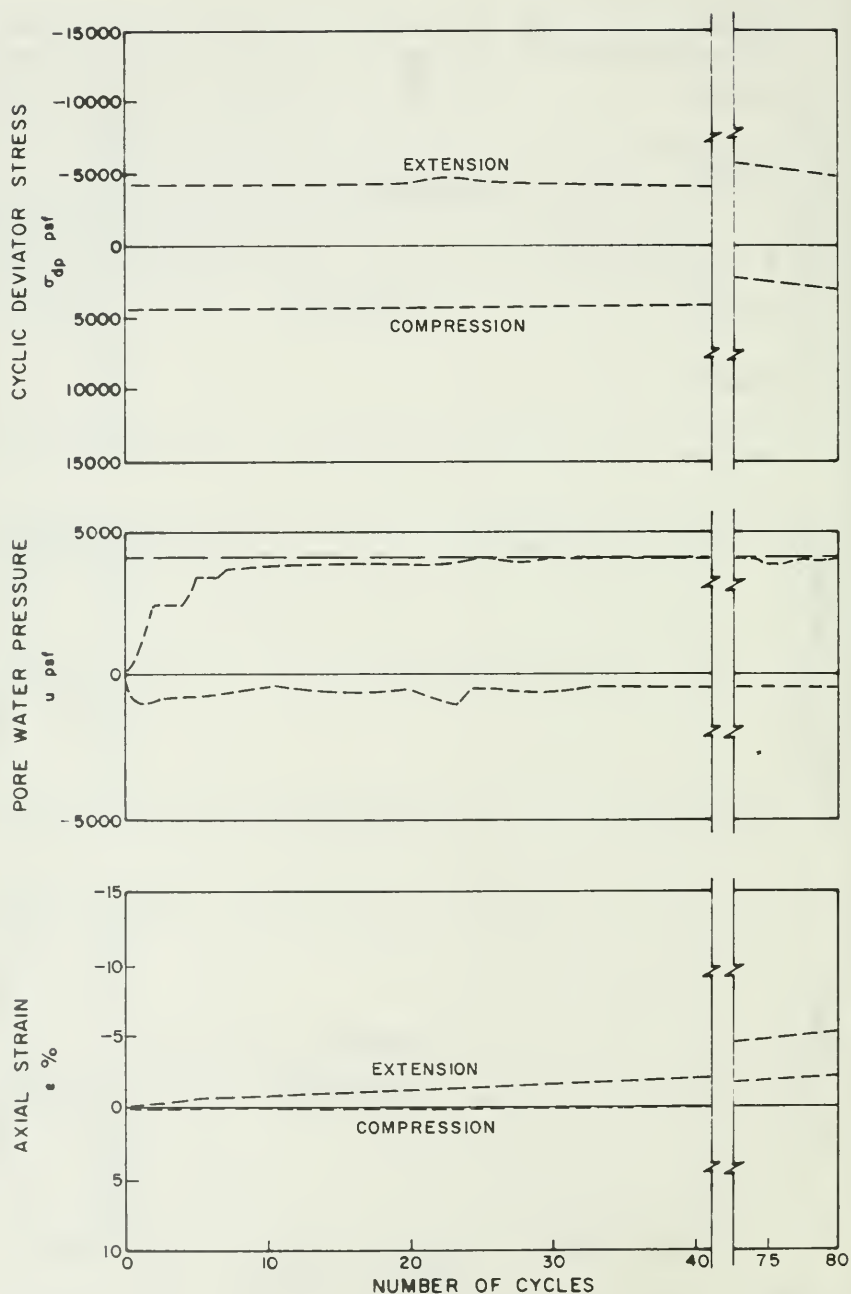


Figure G-2. Cyclic Test Envelopes for Test No. 7 ($\sigma'_{3c} = 4,100$ psf, $K_c = 1.0$)

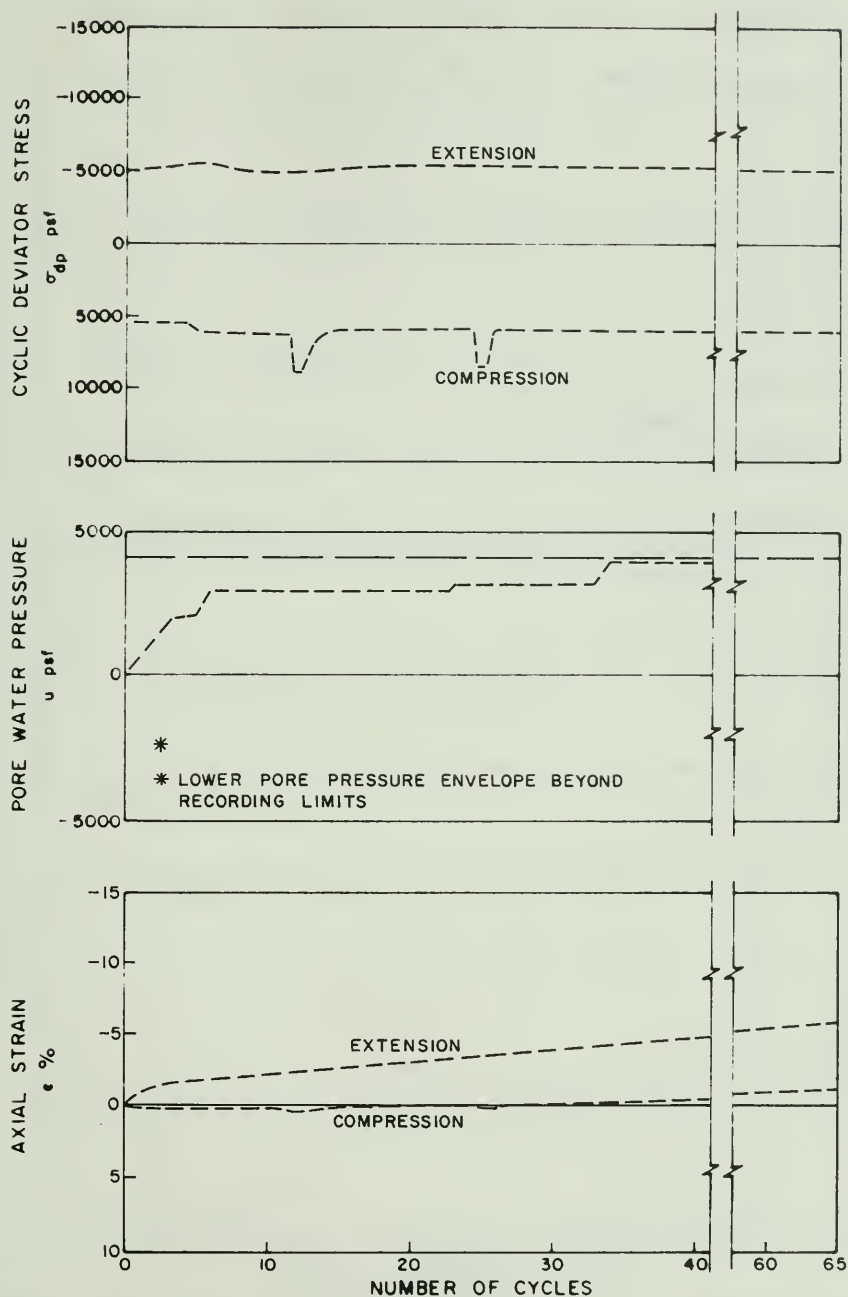


Figure G-3. Cyclic Test Envelopes for Test No. 10 ($\sigma'_{3c} = 4,100$ psf, $K_c = 1.0$)

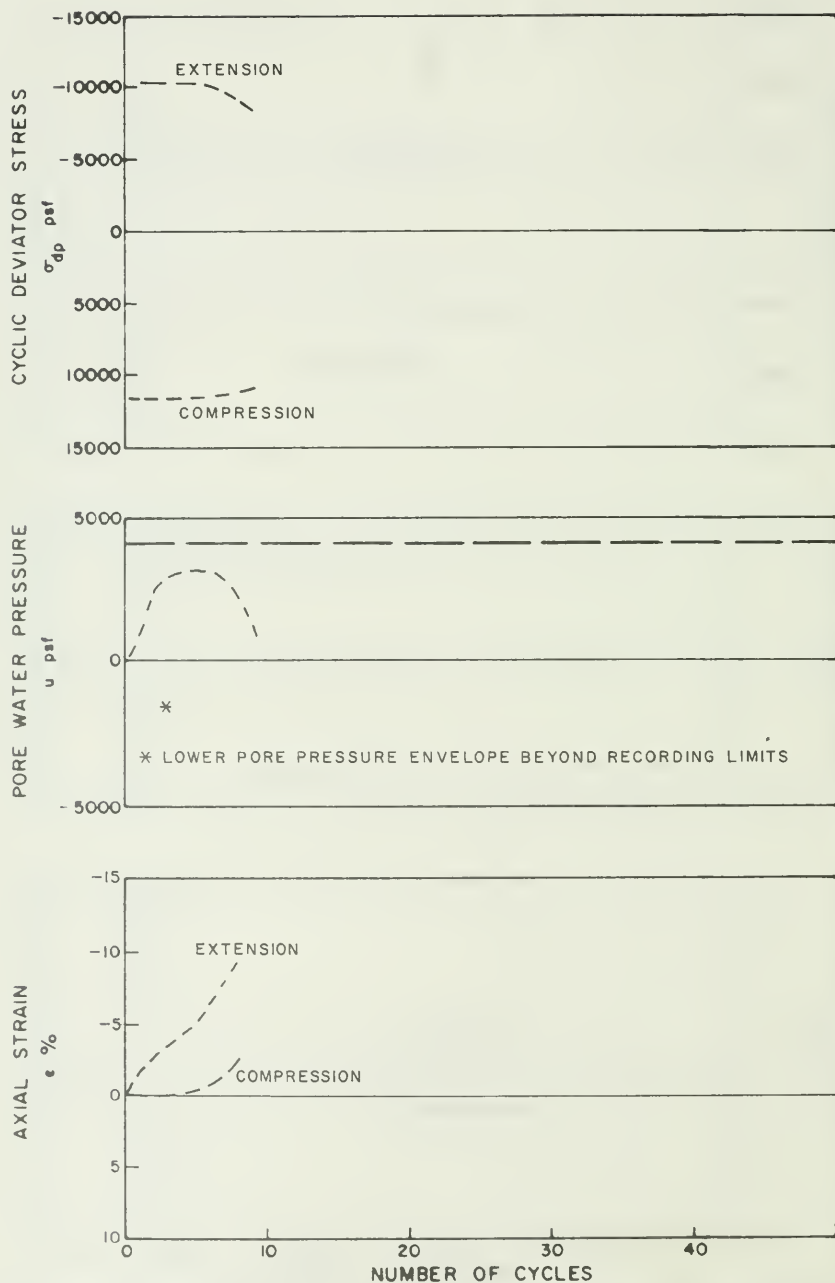


Figure G-4. Cyclic Test Envelopes for Test No. 11 ($\sigma'_{3c} = 4,100$ psf, $K_c = 1.0$)

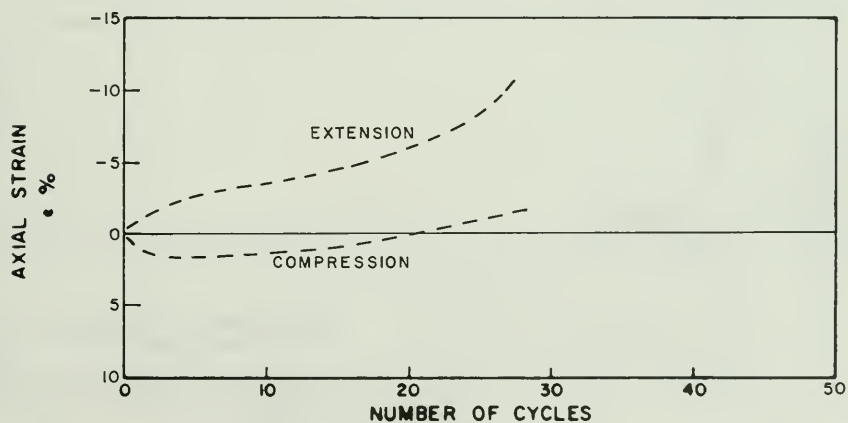
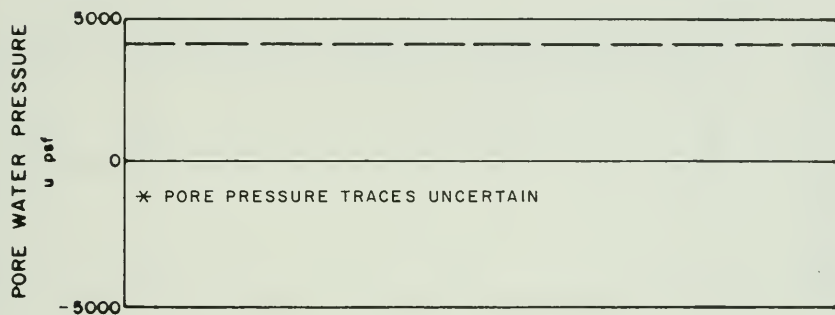
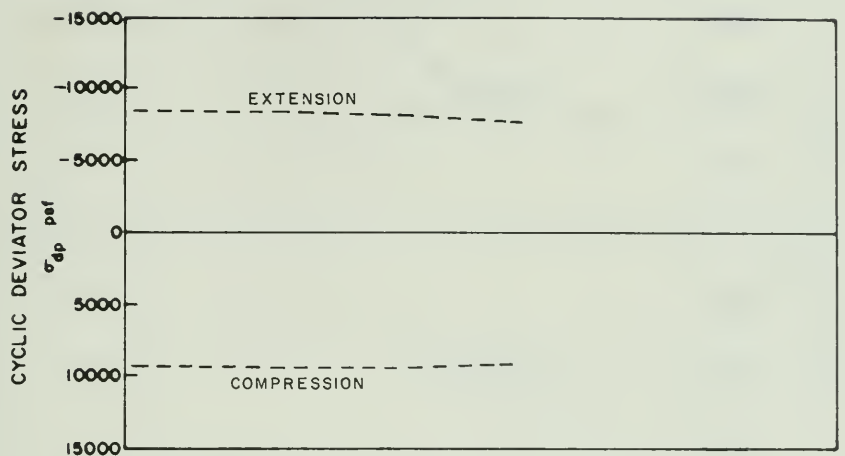


Figure G-5. Cyclic Test Envelopes for Test No. 12 ($\sigma'_{3c} = 4,100$ psf, $K_c = 1.0$)

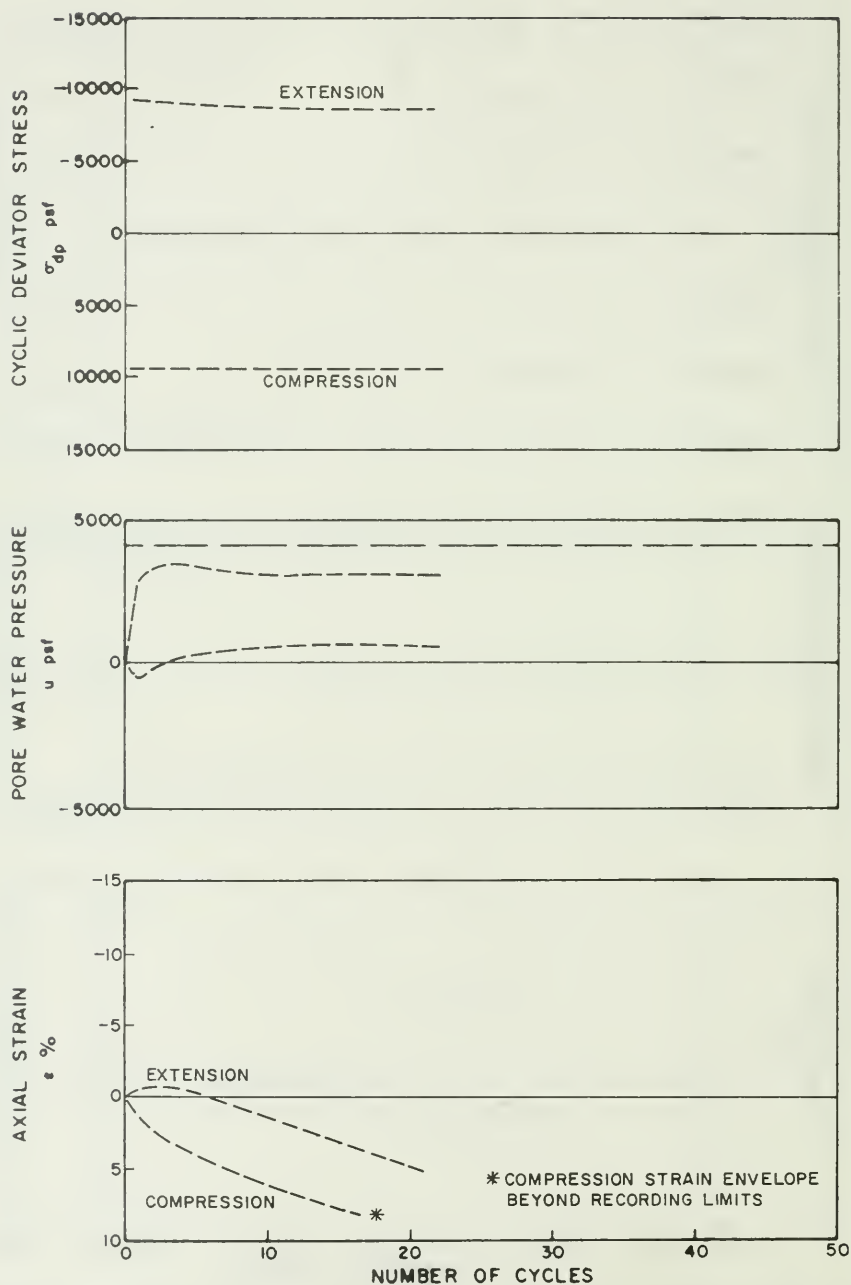


Figure G-6. Cyclic Test Envelopes for Test No. 13 ($\sigma'_{3c} = 4,100$ psf, $K_c = 1.5$)

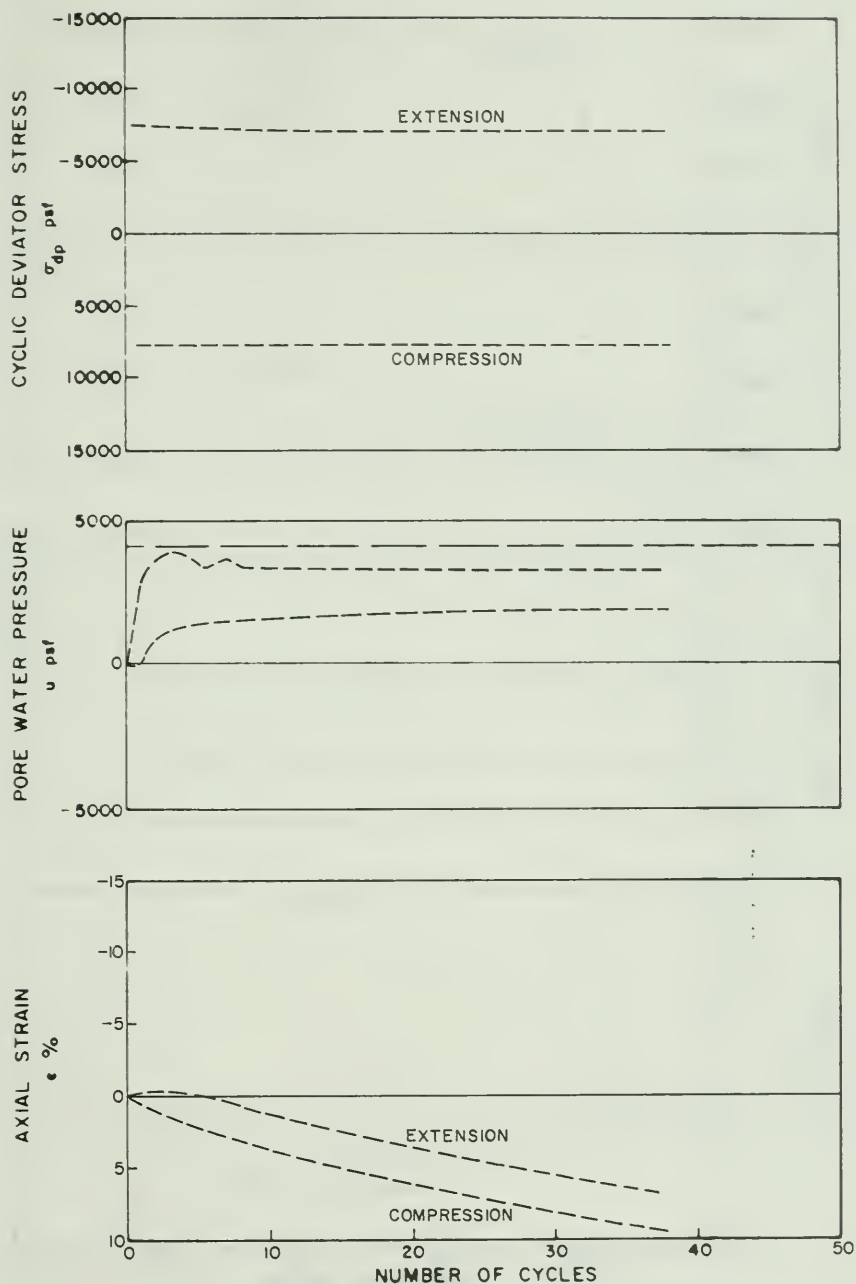


Figure G-7. Cyclic Test Envelopes for Test No. 14 ($\sigma'_{3c} = 4,100$ psf, $K_c = 1.5$)

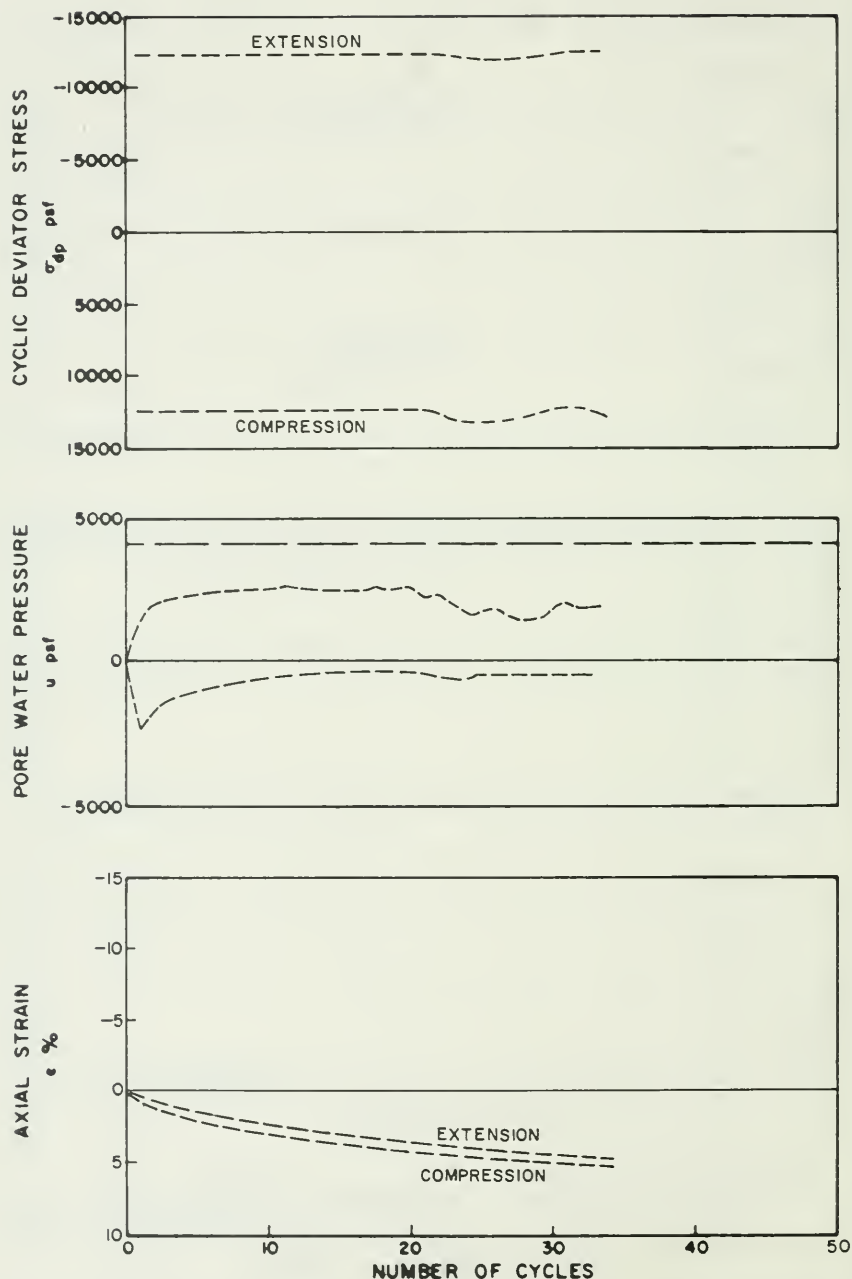


Figure G-8. Cyclic Test Envelopes for Test No. 15 ($\sigma'_{3c} = 4,100$ psf, $K_c = 2.0$)

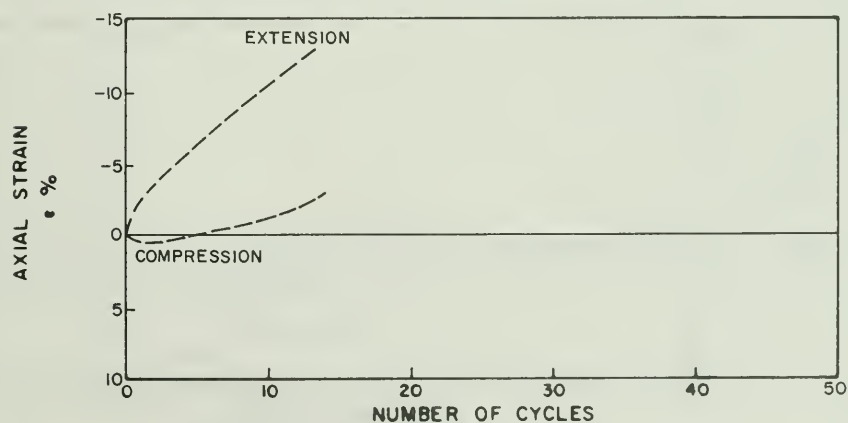
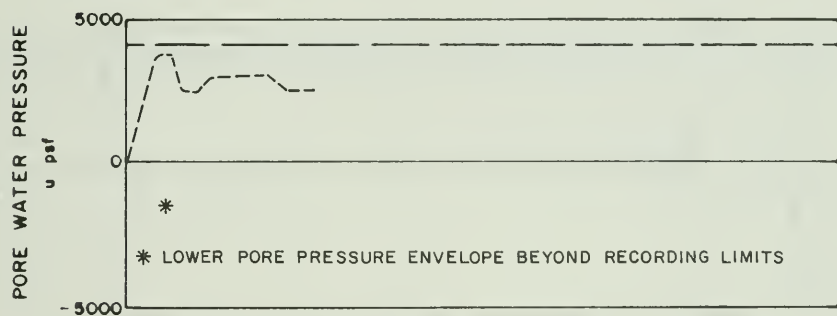
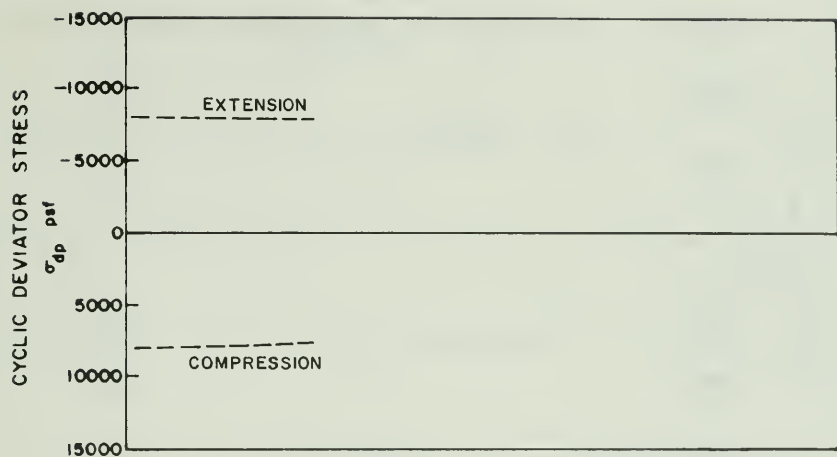


Figure G-9. Cyclic Test Envelopes for Test No. 16 ($\sigma'_{3c} = 4,100$ psf, $K_c = 1.0$)

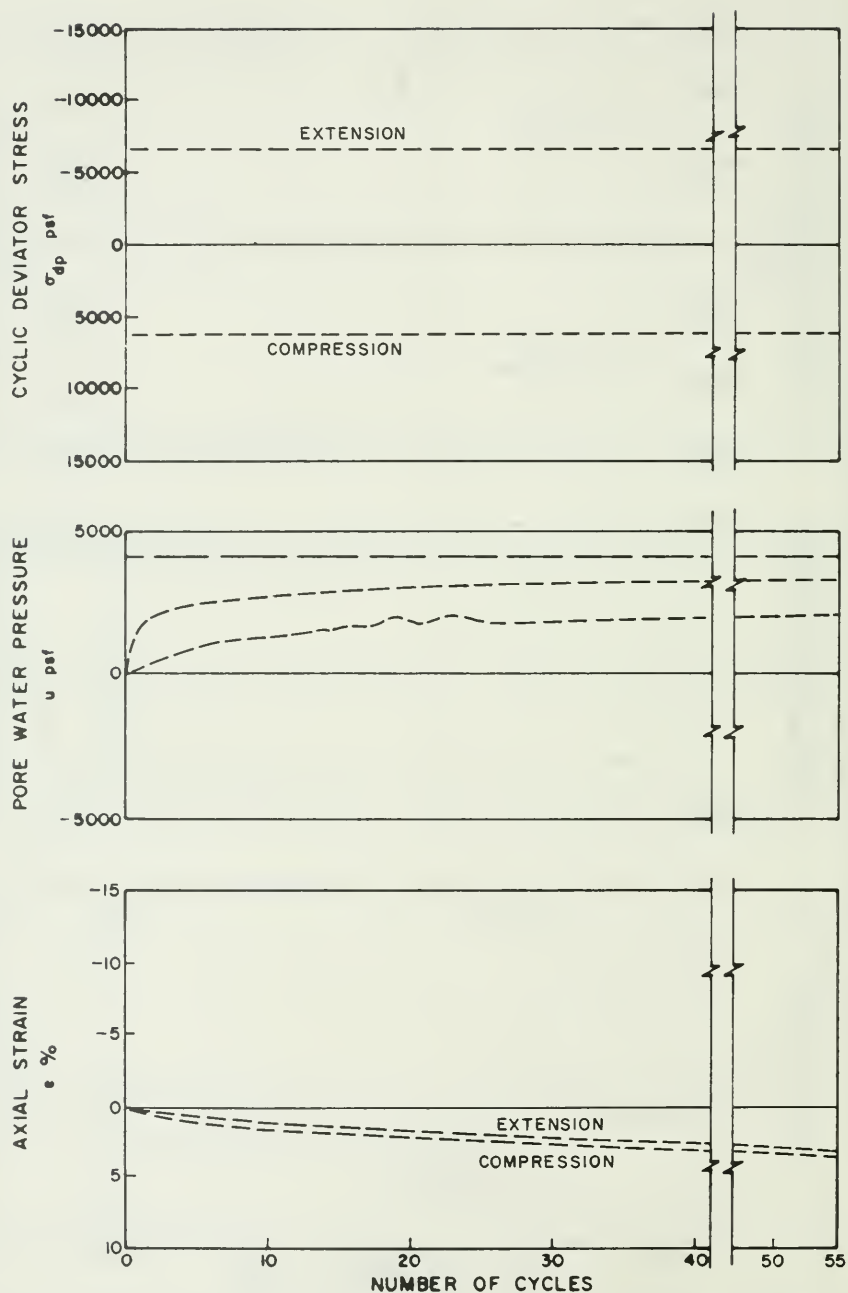


Figure G-10. Cyclic Test Envelopes for Test No. 17 ($\sigma_{3c} = 4,100$ psf, $K_c = 1.5$)

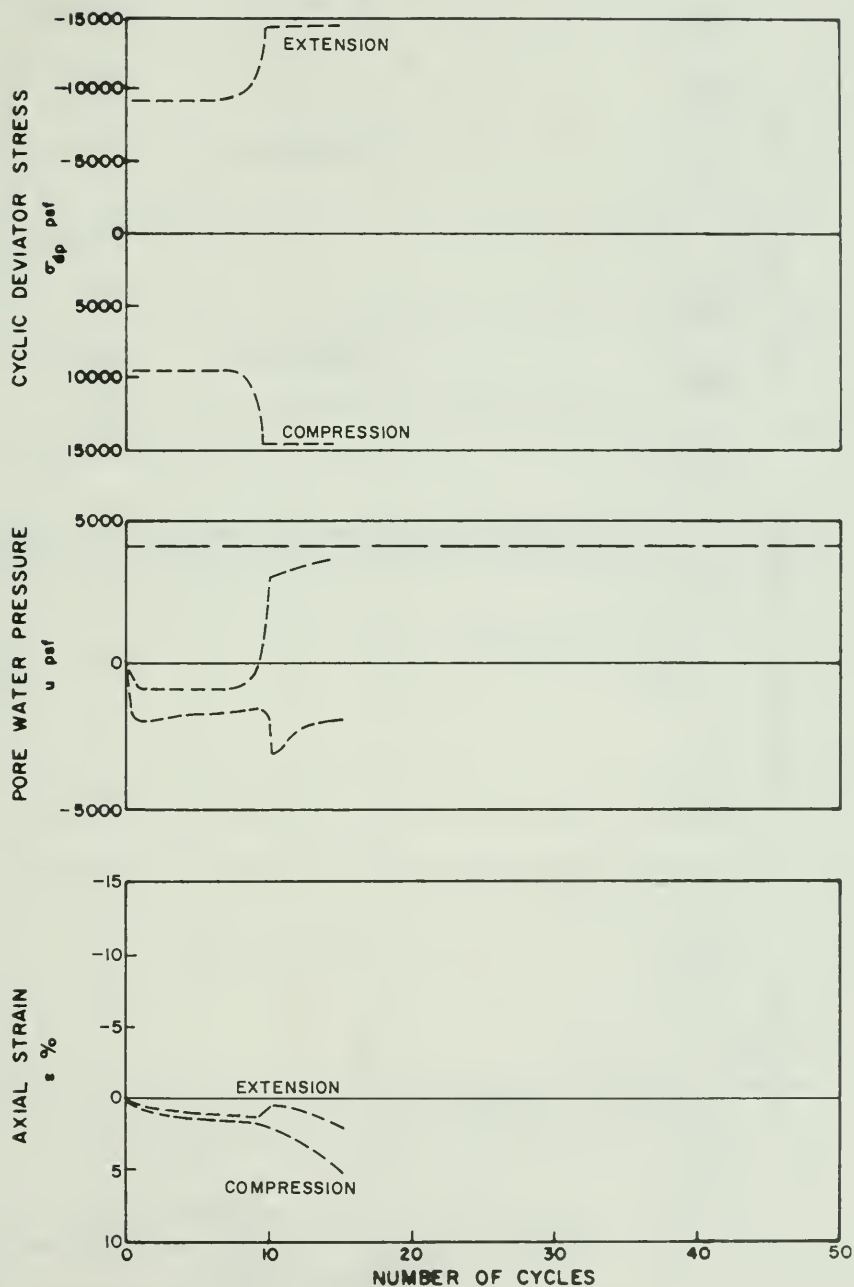


Figure G-11. Cyclic Test Envelopes for Test No. 18 ($\sigma'_{3c} = 4,100$ psf, $K_c = 2.0$)

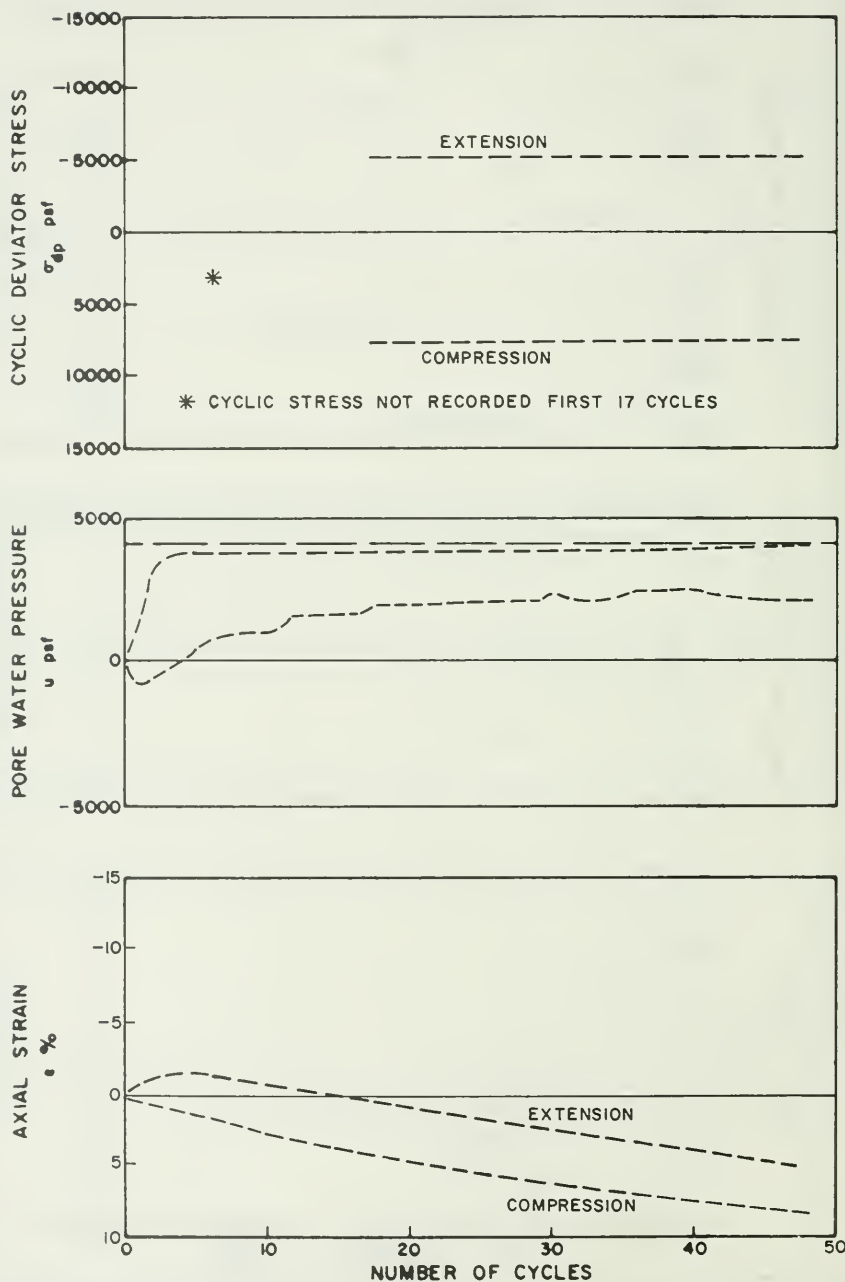


Figure G-12. Cyclic Test Envelopes for Test No. 19 ($\sigma'_{3c} = 4,100$ psf, $K_c = 2.0$)

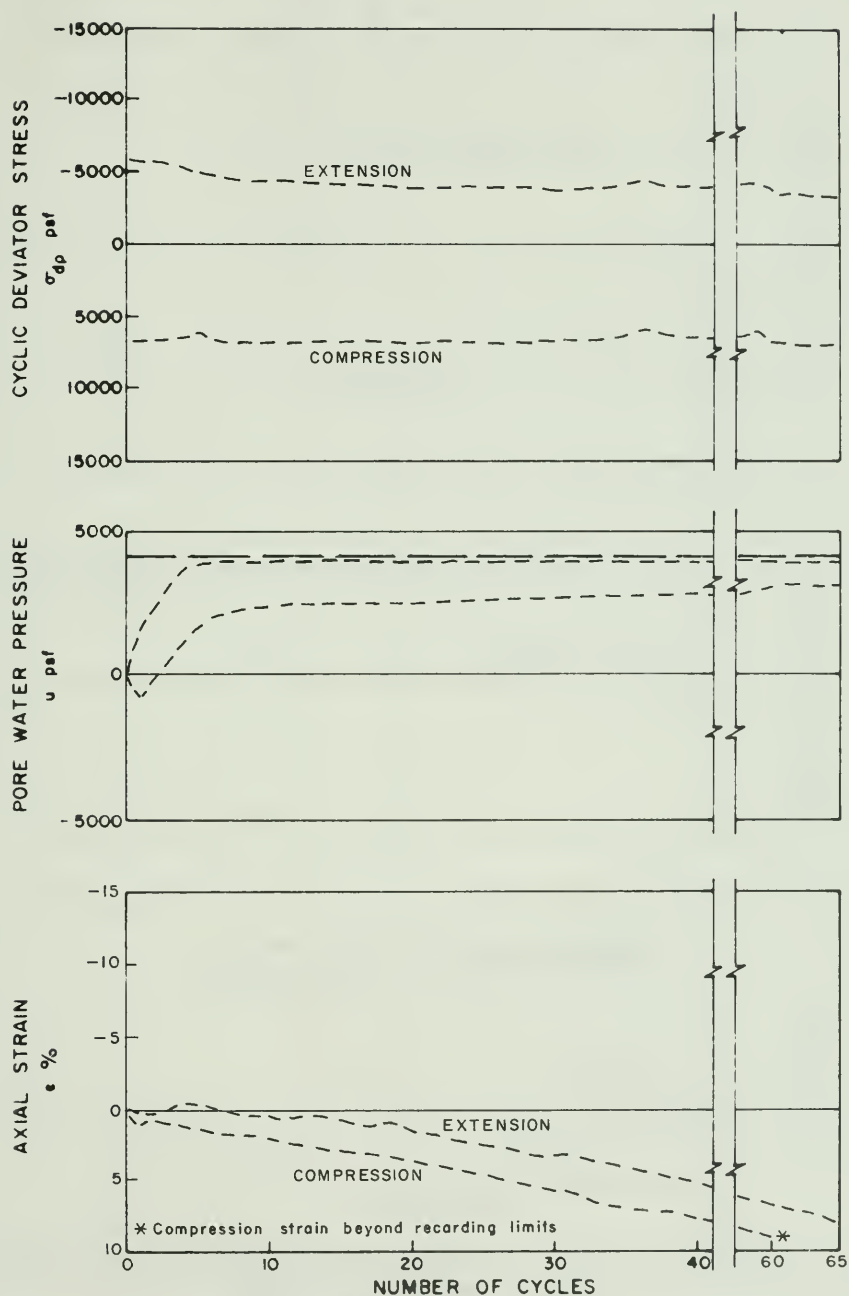


Figure G-13. Cyclic Test Envelopes for Test No. 20 ($\sigma'_{3c} = 4,100$ psf, $K_c = 2.0$)

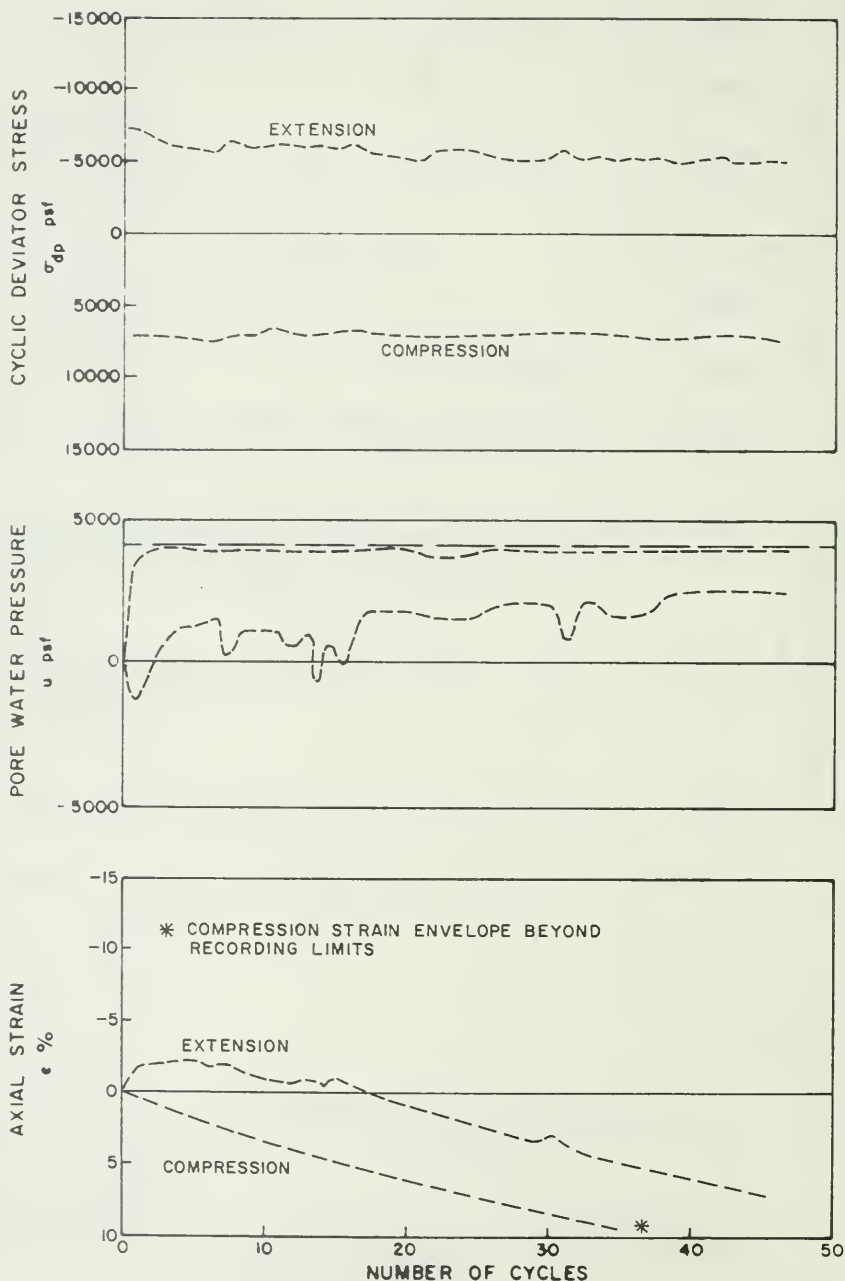


Figure G-14. Cyclic Test Envelopes for Test No. 22 ($\sigma'_{3c} = 4,100$ psf, $K_c = 2.0$)

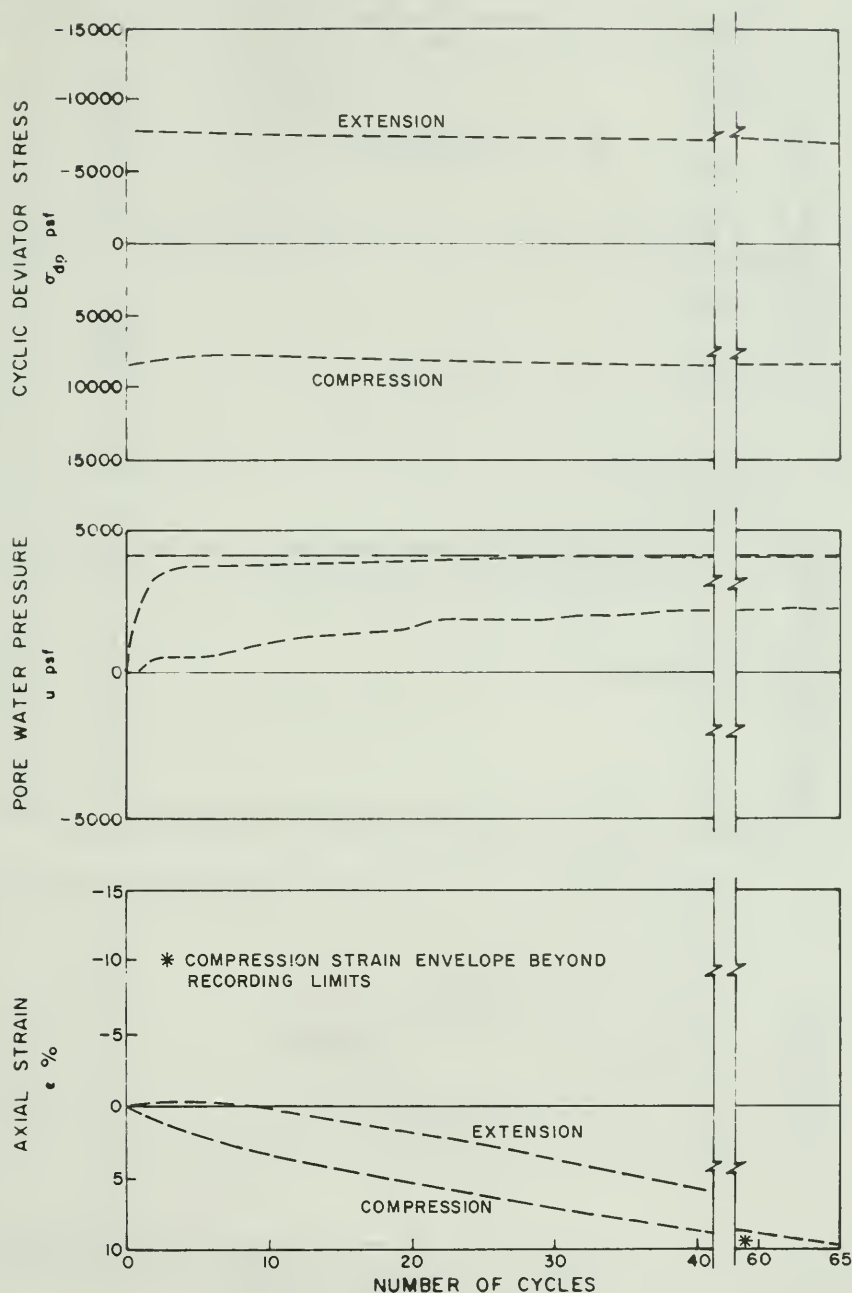


Figure G-15. Cyclic Test Envelopes for Test No. 23 ($\sigma'_{3c} = 4,100$ psf, $K_c = 2.0$)

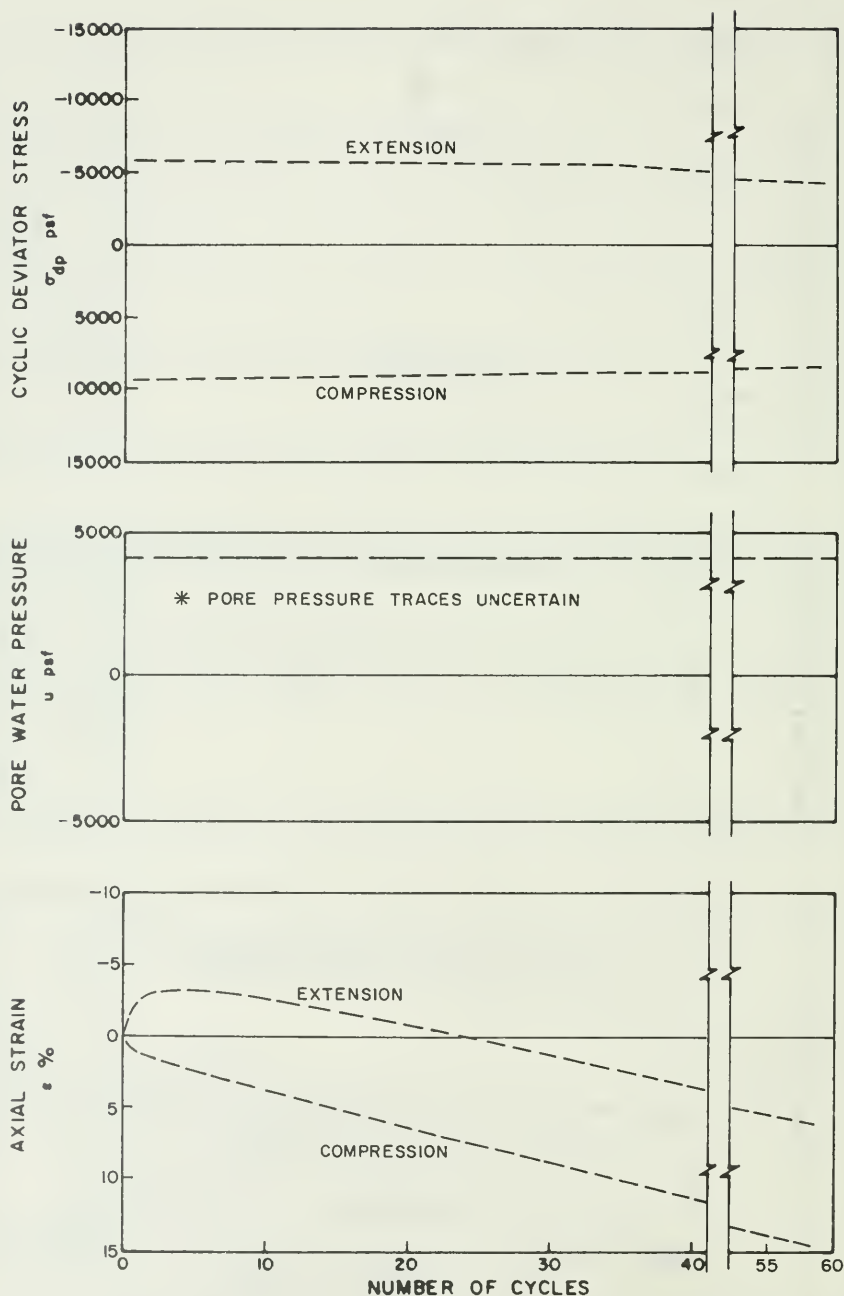


Figure G-16. Cyclic Test Envelopes for Test No. 24 ($\sigma'_{3c} = 4,100$ psf, $K_c = 2.0$)

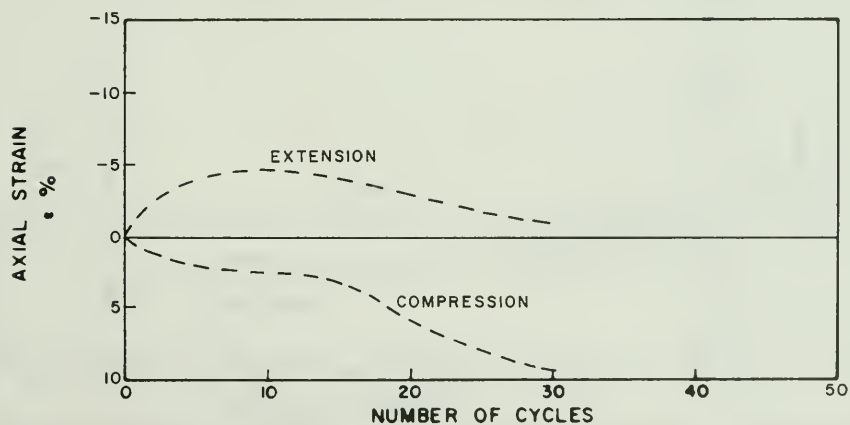
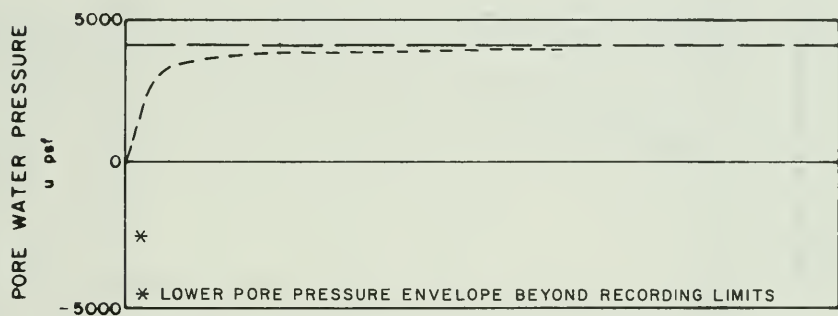
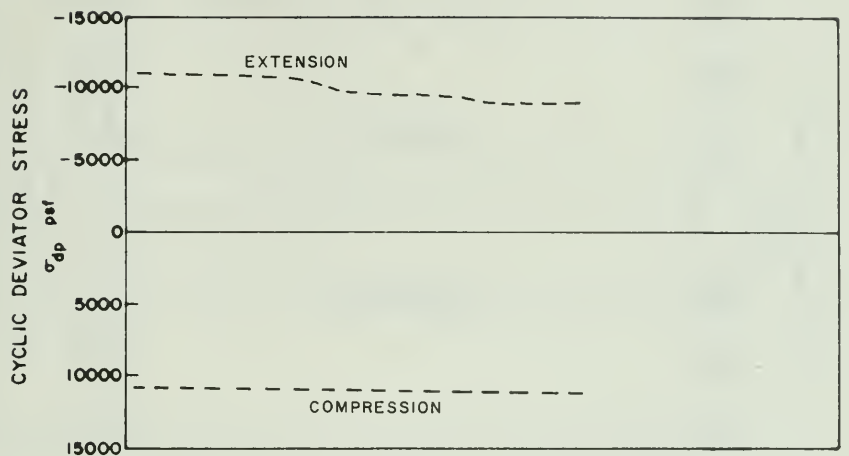


Figure G-17. Cyclic Test Envelopes for Test No. 25 ($\sigma'_{3c} = 4,100$ psf, $K_c = 2.0$)

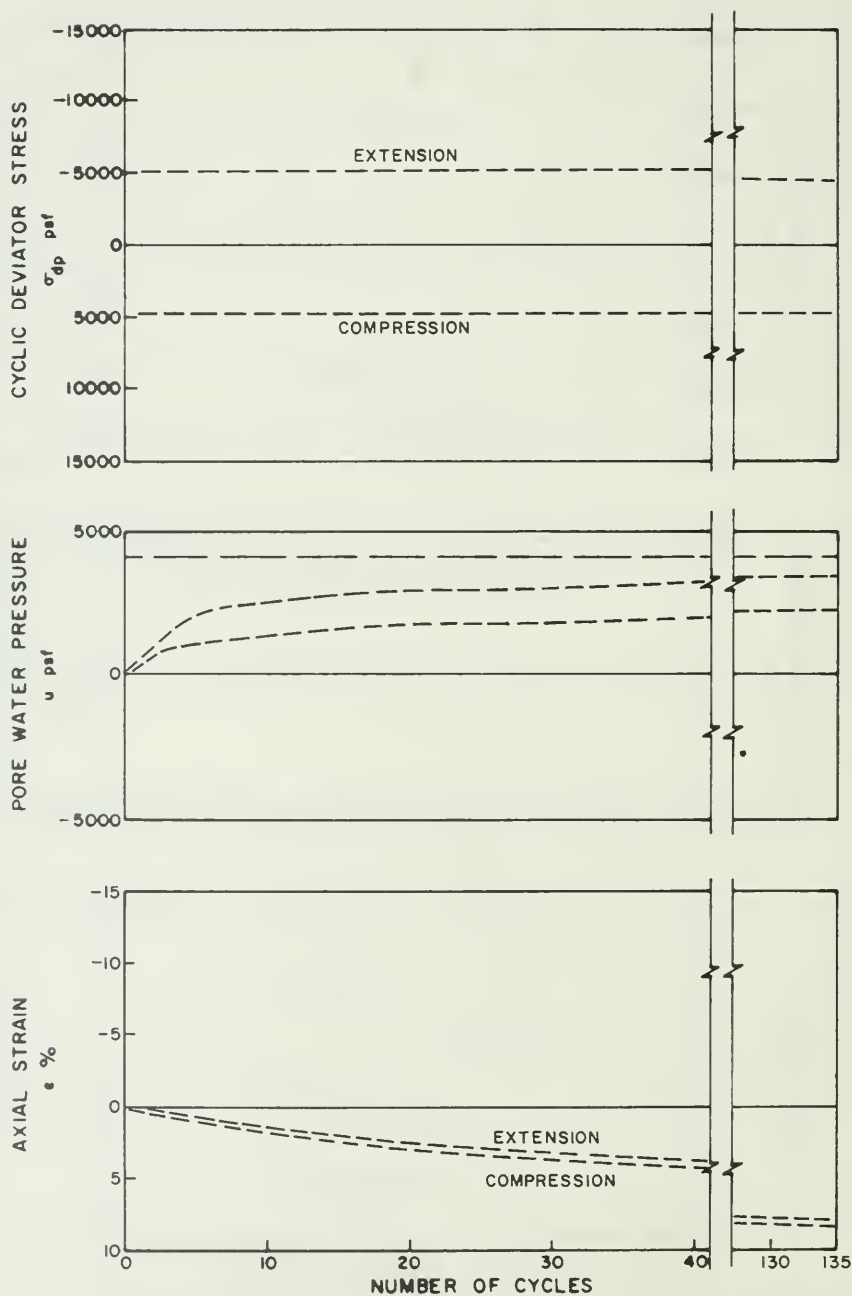


Figure G-18. Cyclic Test Envelopes for Test No. 28 ($\sigma'_{3c} = 4,100$ psf, $K_c = 2.0$)

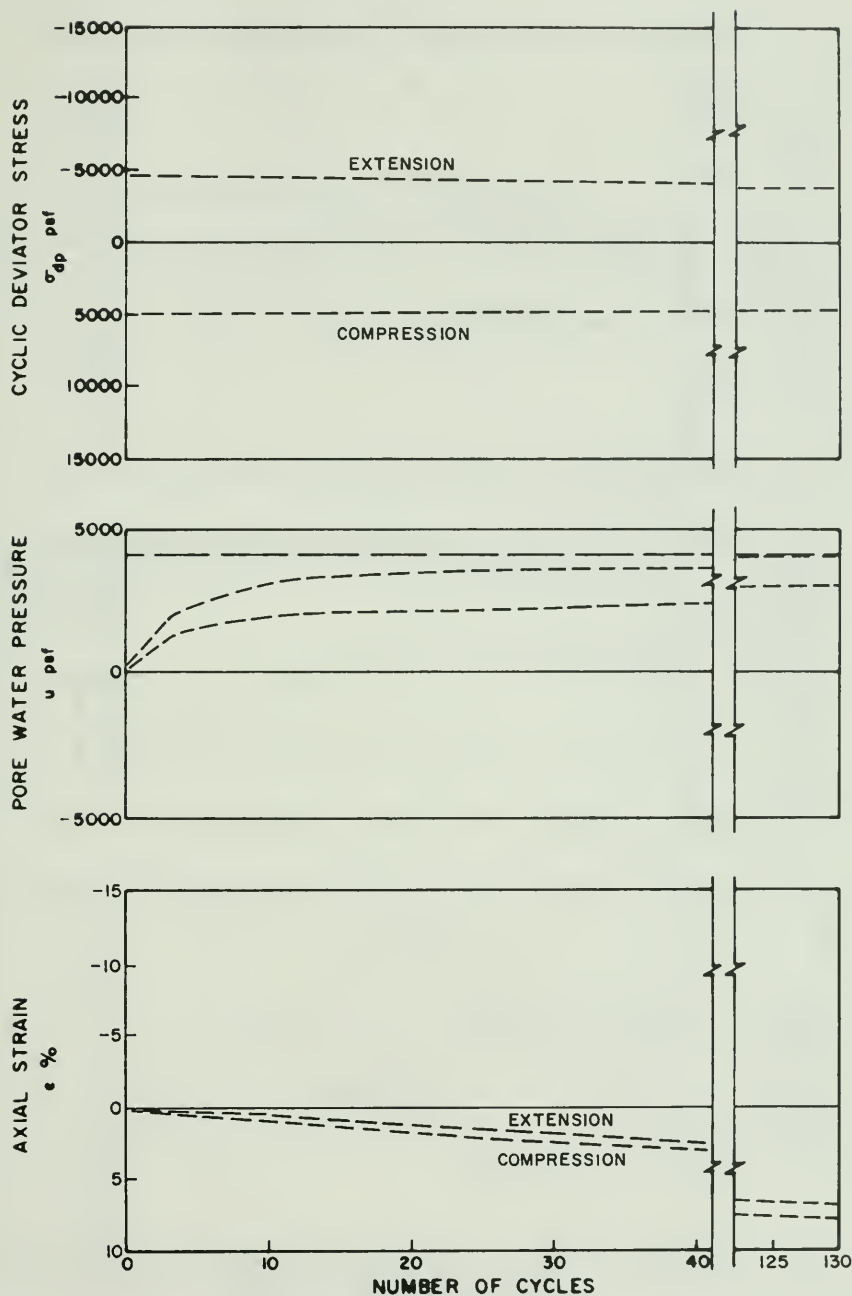


Figure G-19: Cyclic Test Envelopes for Test No. 29 ($\sigma'_{3c} = 4,100$ psf, $K_c = 1.5$)

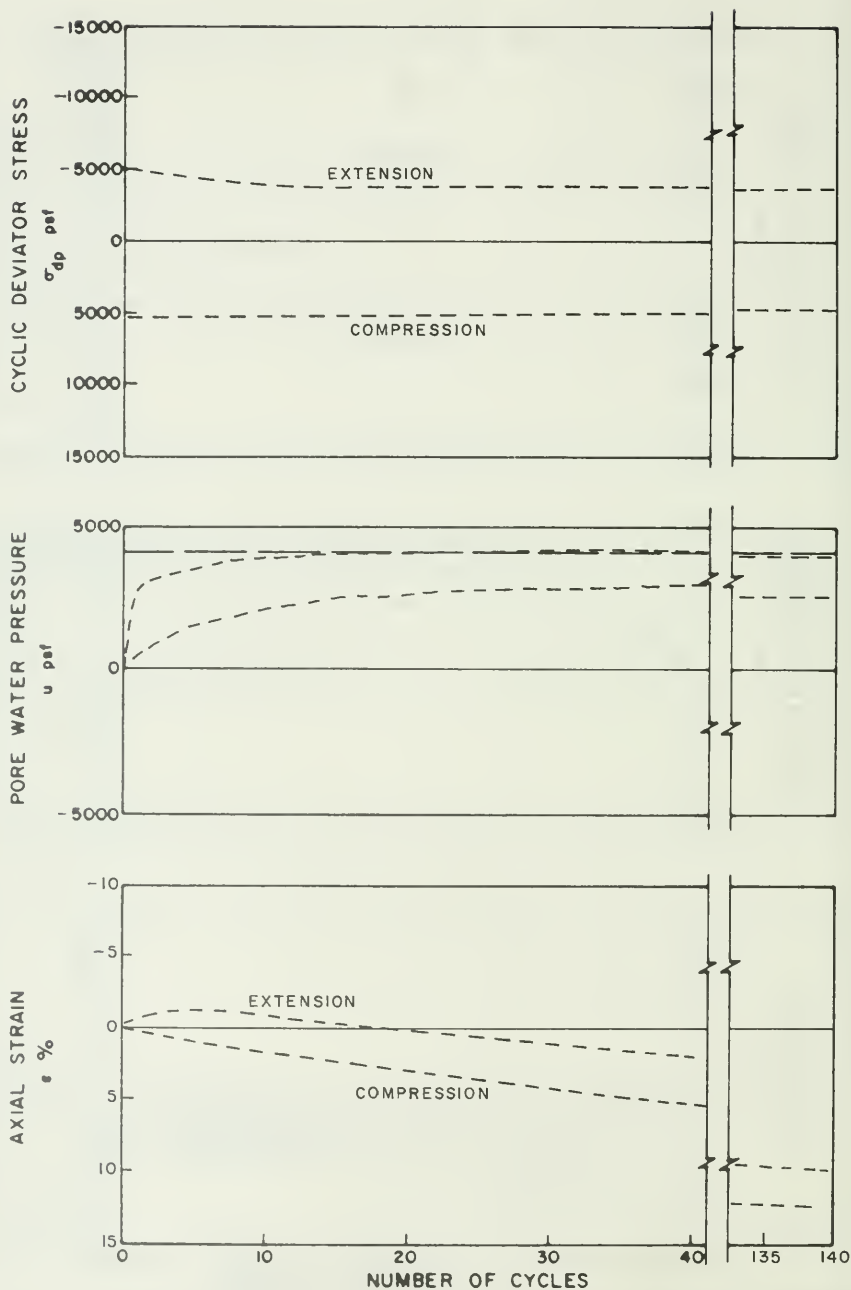


Figure G-20. Cyclic Test Envelopes for Test No. 30 ($\sigma'_{3c} = 4,100$ psf, $K_c = 2.0$)

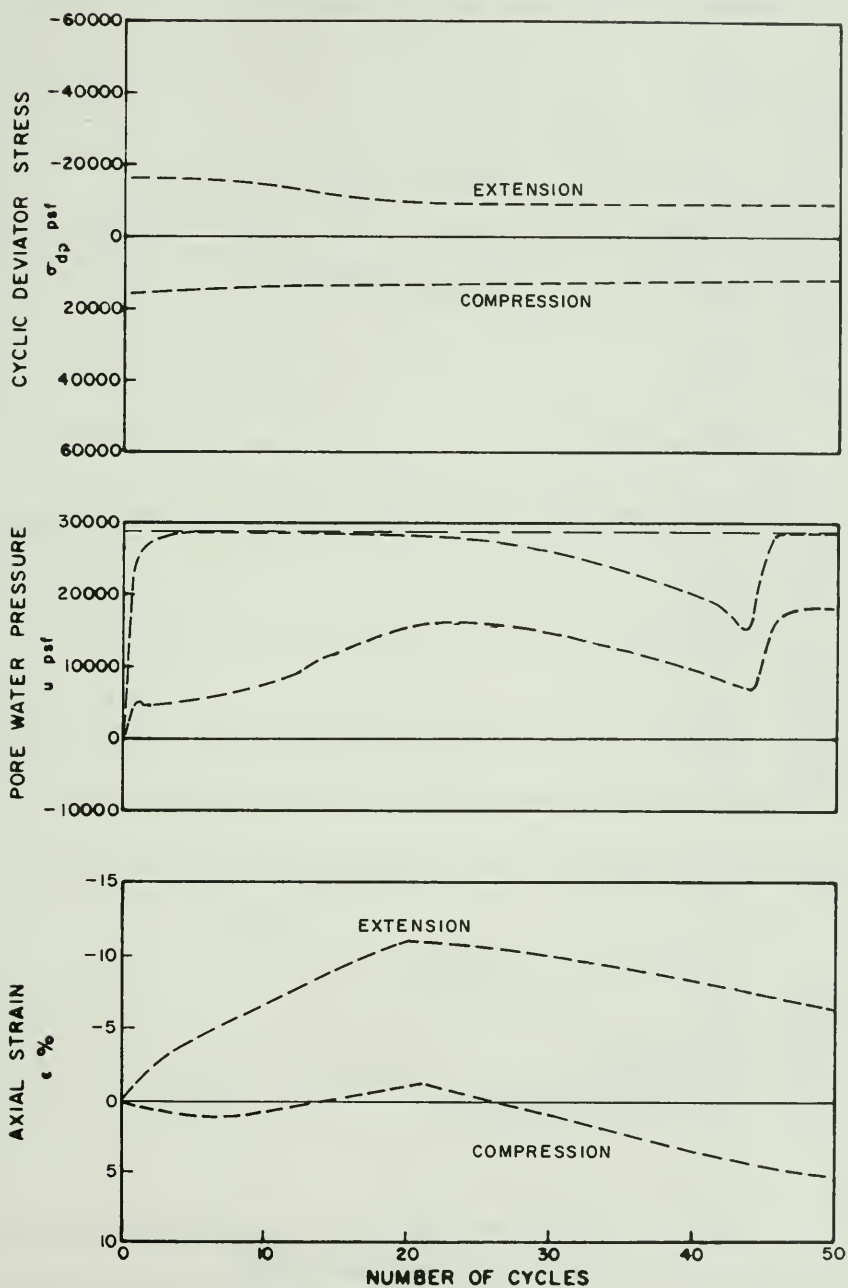


Figure G-21. Cyclic Test Envelopes for Test No. 33 ($\sigma'_{3c} = 28,700$ psf, $K_c = 1.0$)

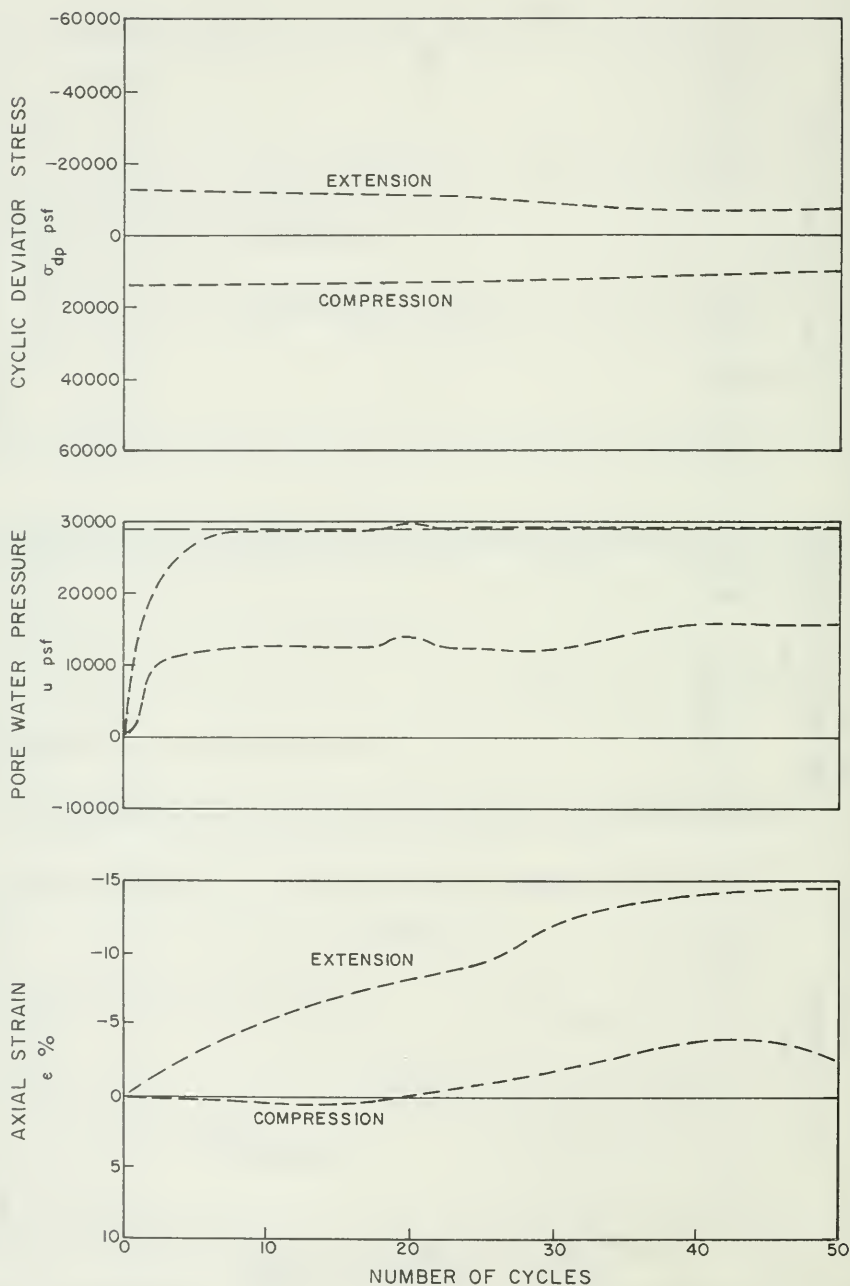


Figure G-22. Cyclic Test Envelopes for Test No. 34 ($\sigma'_{3c} = 28.700$ psf, $K_c = 1.0$)

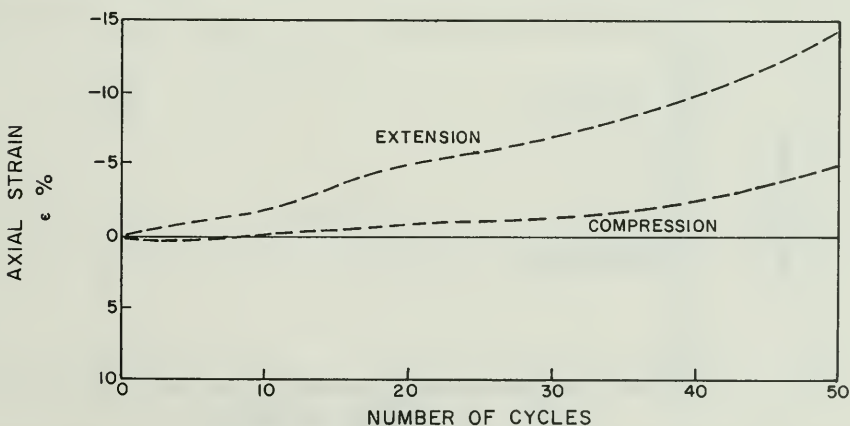
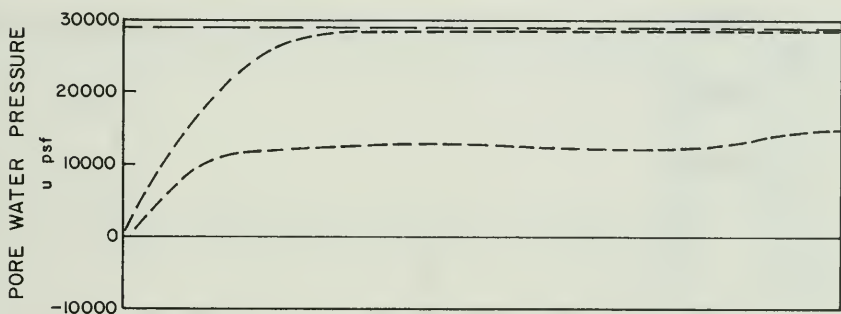
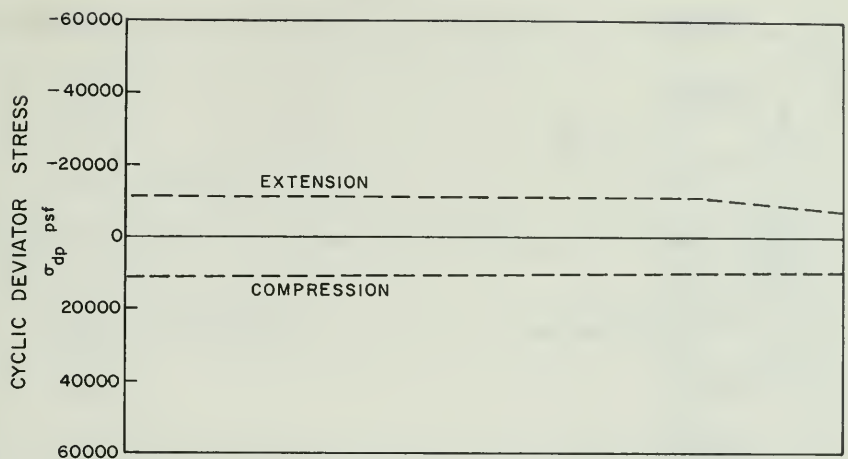


Figure G-23. Cyclic Test Envelopes for Test No. 35 ($\sigma'_{3c} = 28,700$ psf, $K_c = 1.0$)

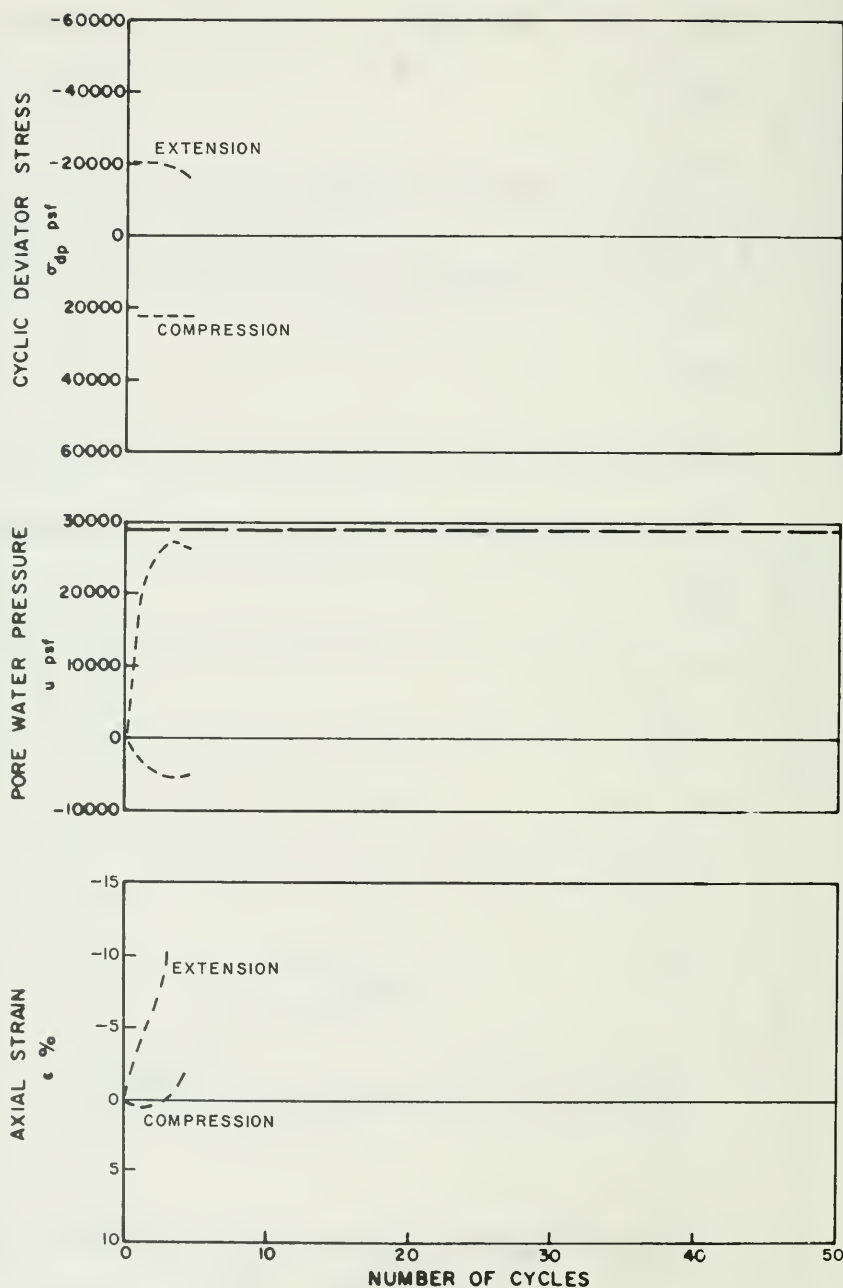


Figure G-24. Cyclic Test Envelopes for Test No. 36 ($\sigma'_{3c} = 28,700$ psf, $K_c = 1.0$)

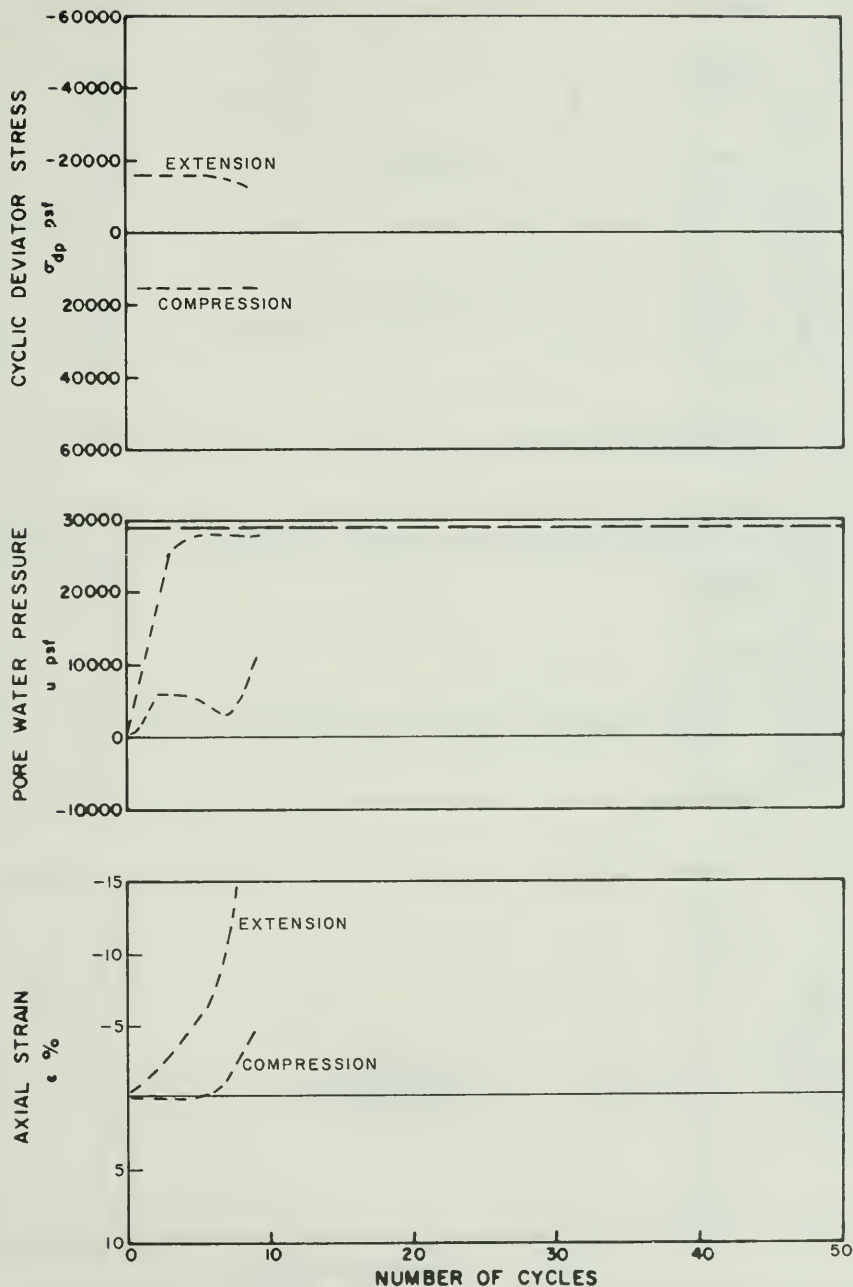


Figure G-25. Cyclic Test Envelopes for Test No. 37 ($\sigma'_{3c} = 28,700$ psf, $K_c = 1.0$)

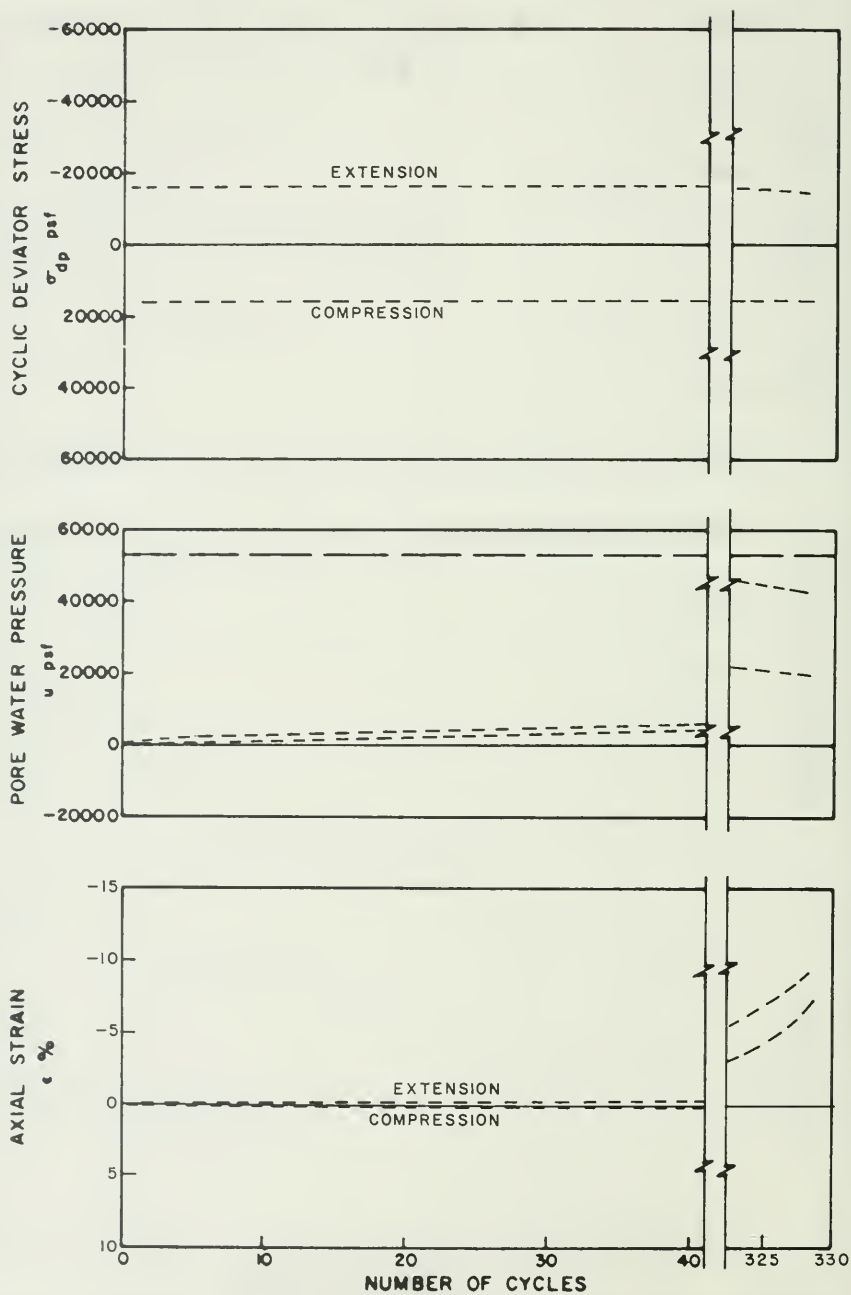


Figure G-26. Cyclic Test Envelopes for Test No. 38 ($\sigma'_{3c} = 53,300$ psf, $K_c = 1.0$)

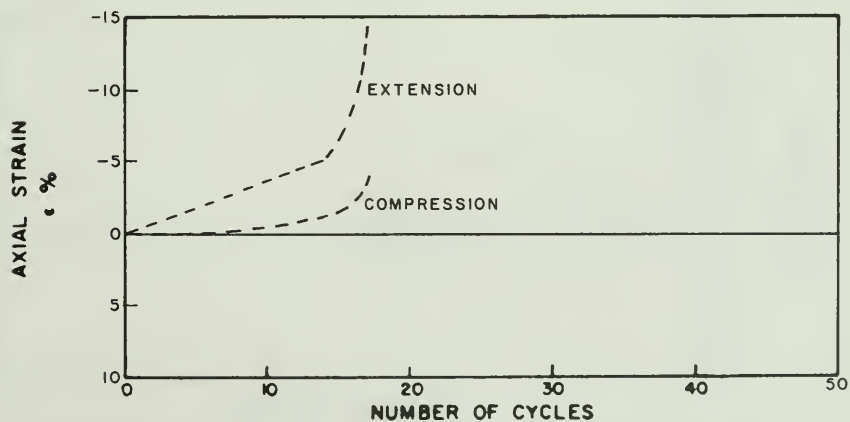
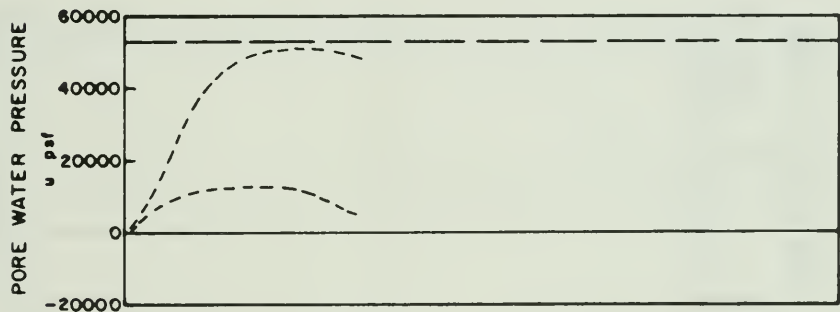
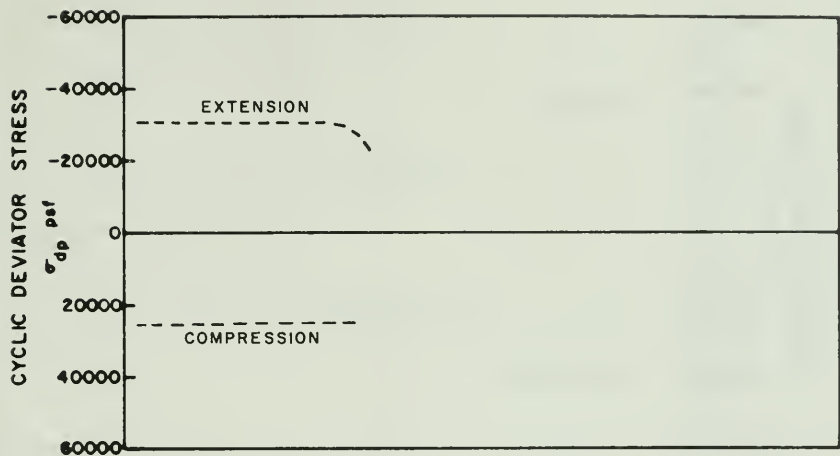


Figure G-27. Cyclic Test Envelopes for Test No. 39 ($\sigma'_{3c} = 53,300$ psf, $K_c = 1.0$)

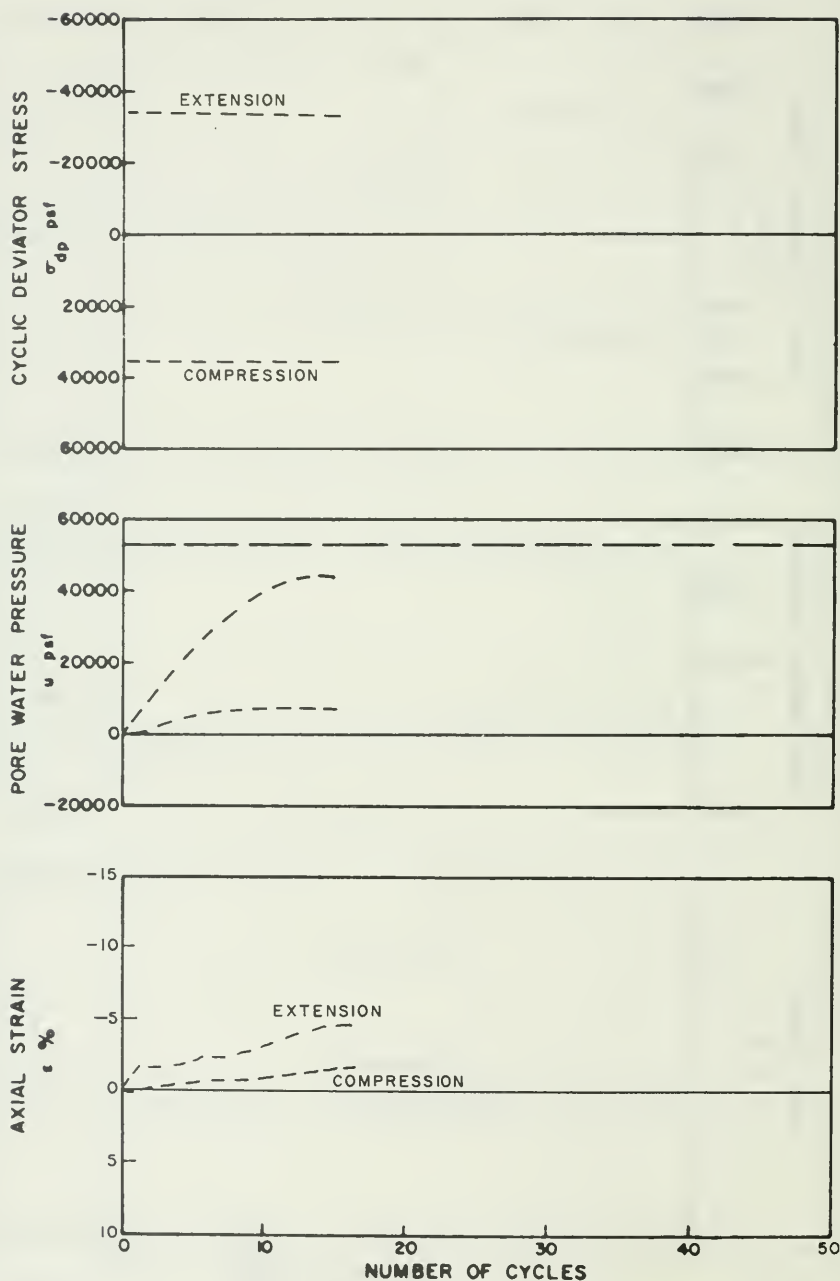


Figure G-28. Cyclic Test Envelopes for Test No. 40 ($\sigma'_{3c} = 53,300$ psf, $K_c = 1.0$)

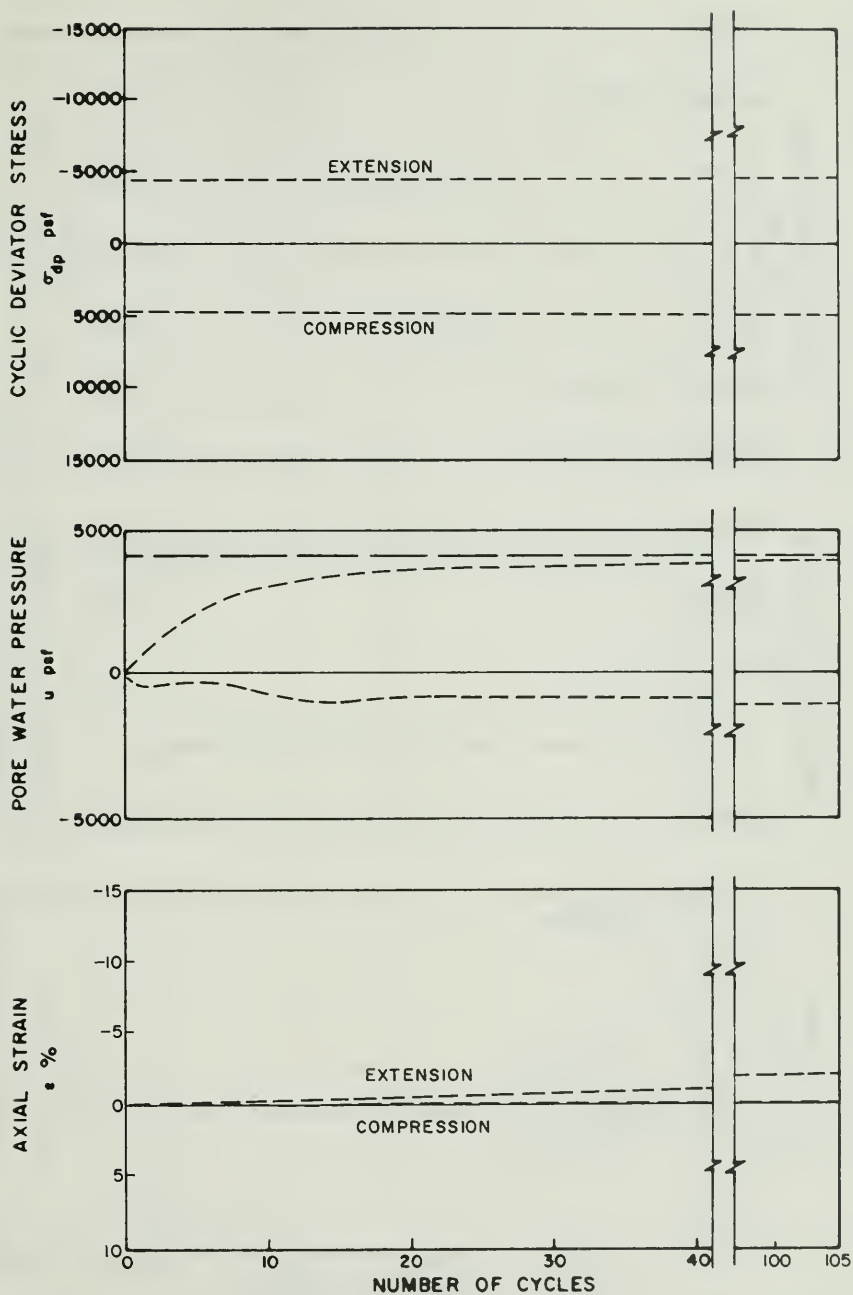


Figure G-29. Cyclic Test Envelopes for Test No. 41 ($\sigma'_{3c} = 4,100$ psf, $K_c = 1.0$)

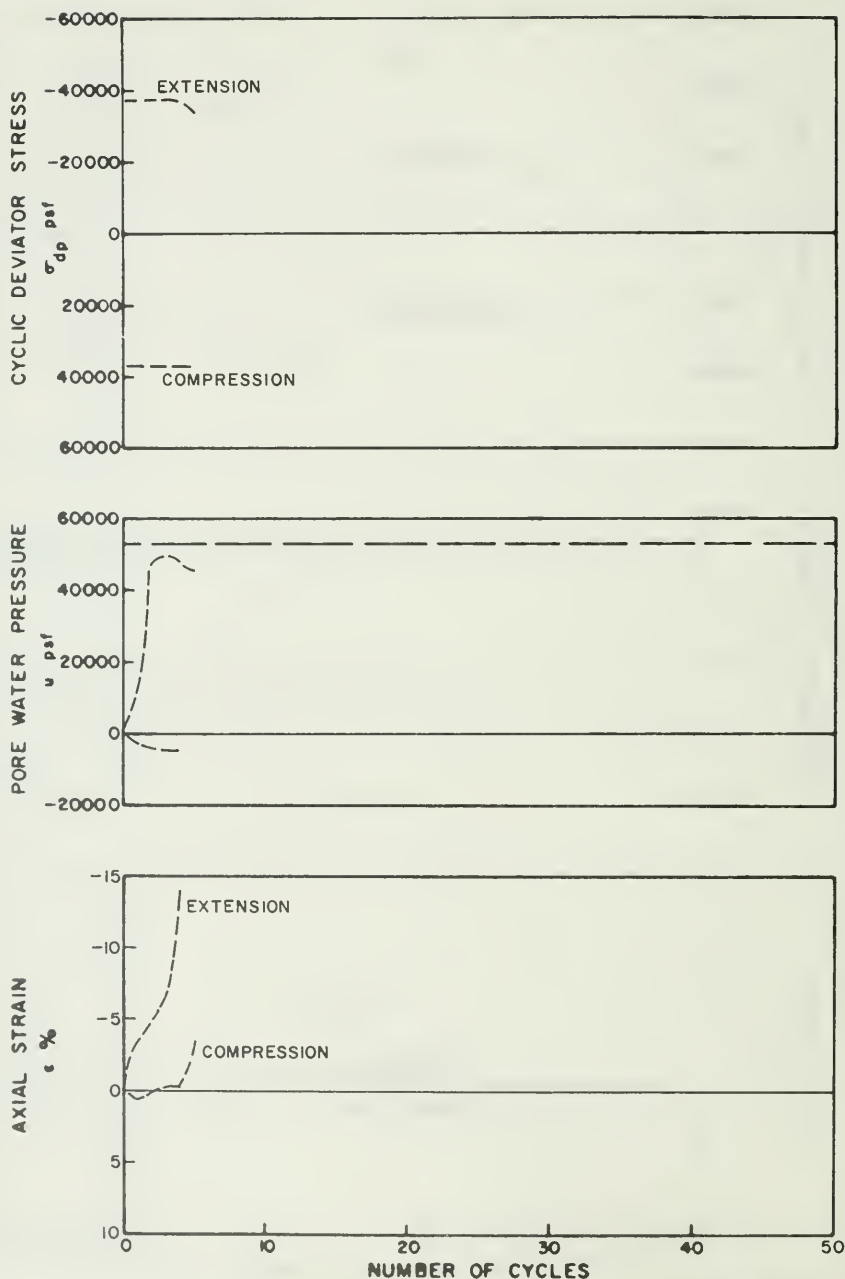


Figure G-30. Cyclic Test Envelopes for Test No. 42 ($\sigma'_{3c} = 53,300$ psf, $K_c = 1.0$)

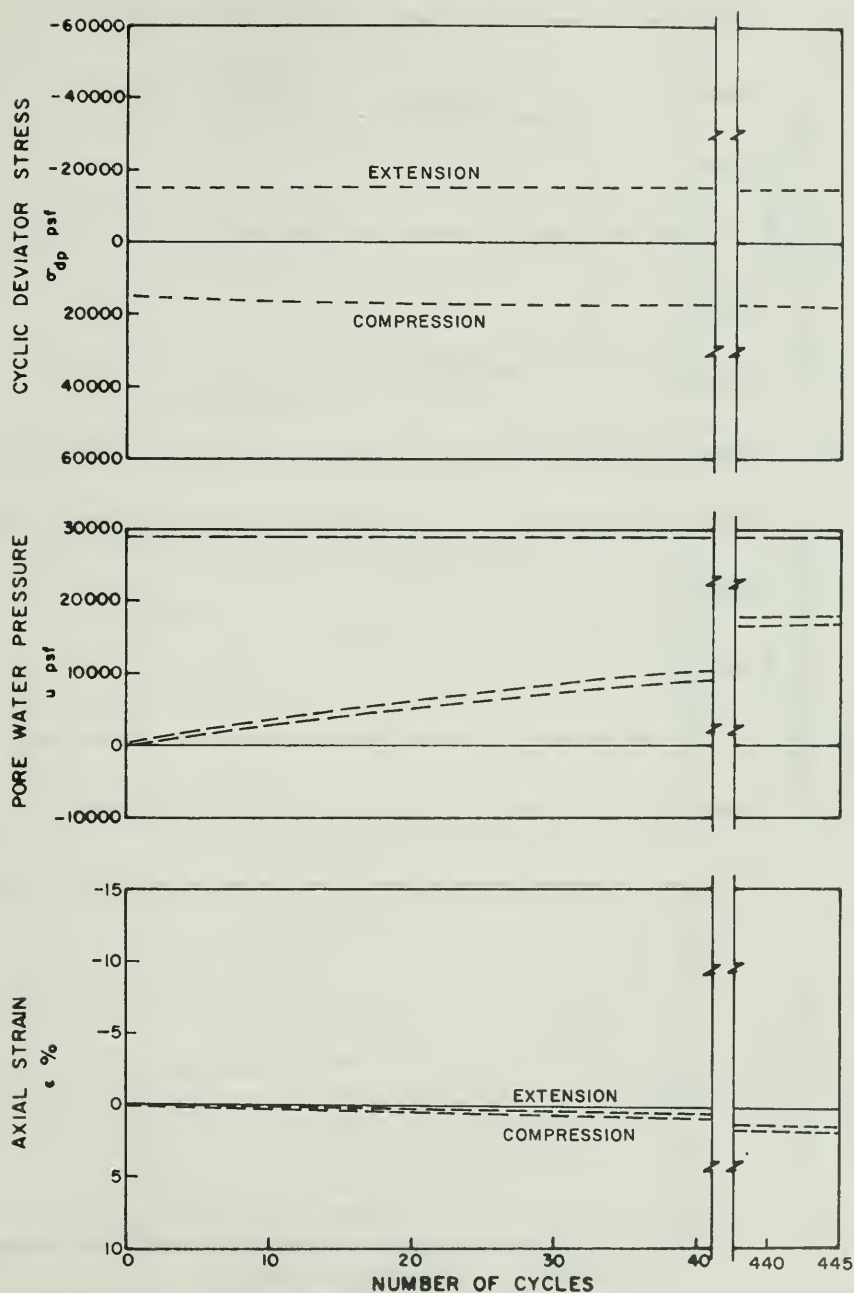


Figure G-31. Cyclic Test Envelopes for Test No. 43 ($\sigma'_{3c} = 28,700$ psf, $K_c = 2.0$)

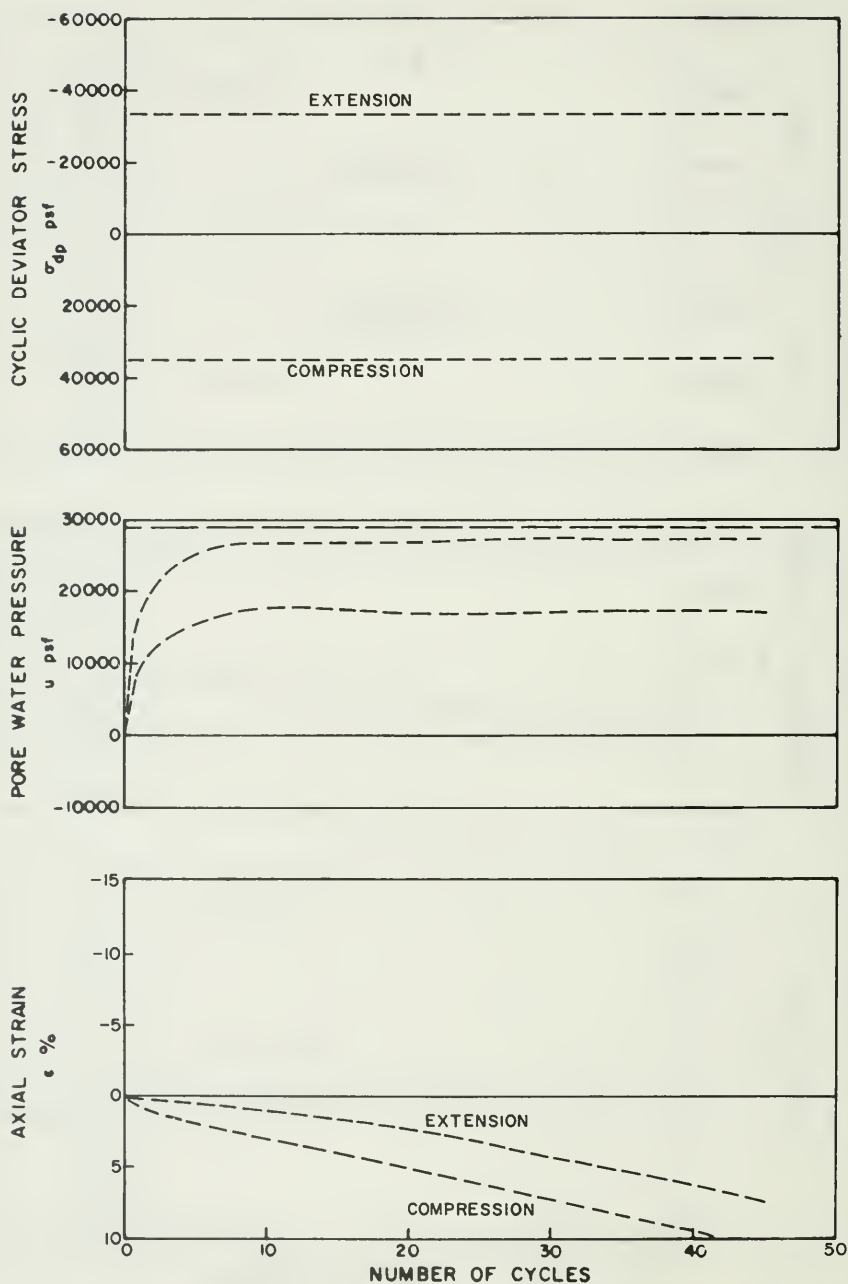


Figure G-32. Cyclic Test Envelopes for Test No. 44 ($\sigma'_{3c} = 28,700$ psf, $K_c = 2.0$)

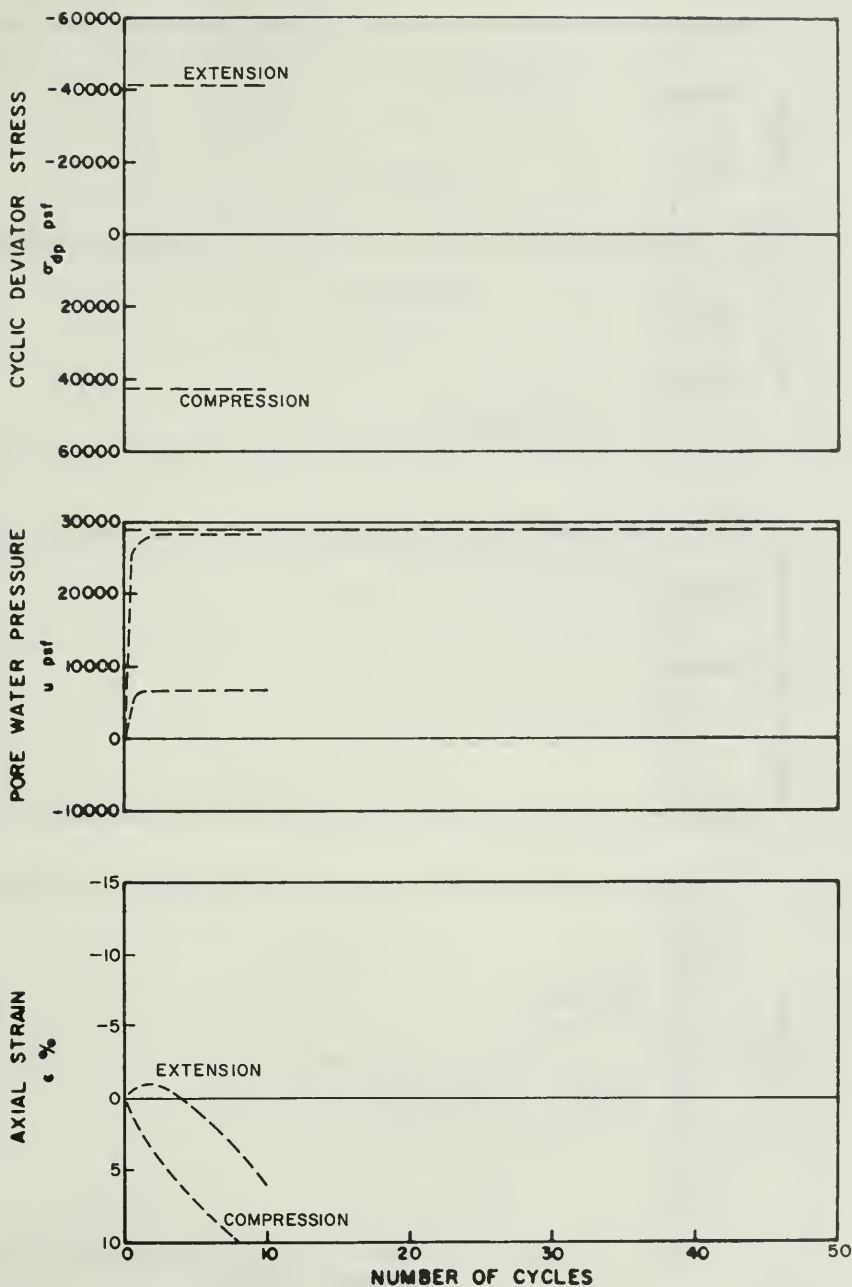


Figure G-33. Cyclic Test Envelopes for Test No. 45 ($\sigma'_{3c} = 28,700$ psf, $K_c = 2.0$)

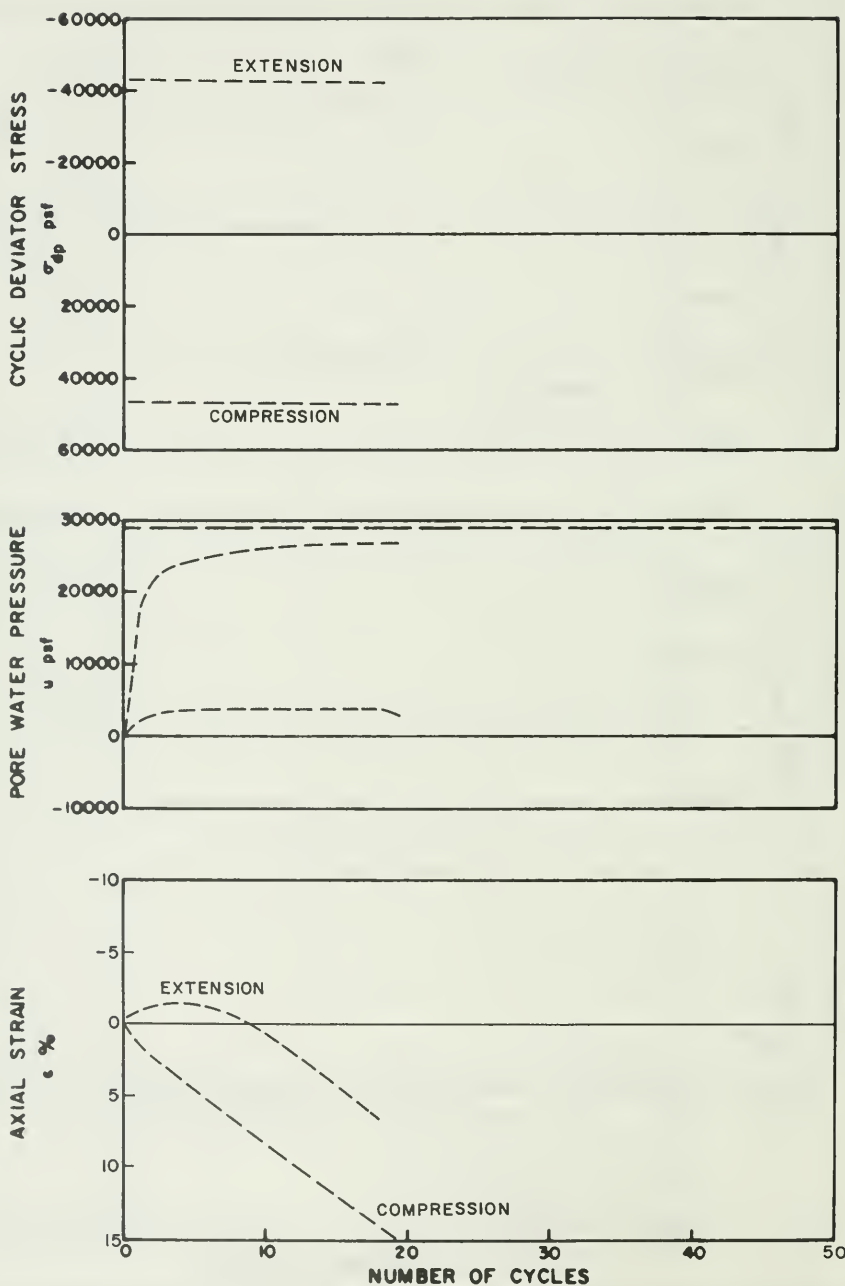


Figure G-34. Cyclic Test Envelopes for Test No. 46 ($\sigma'_{3c} = 28,700$ psf, $K_c = 2.0$)

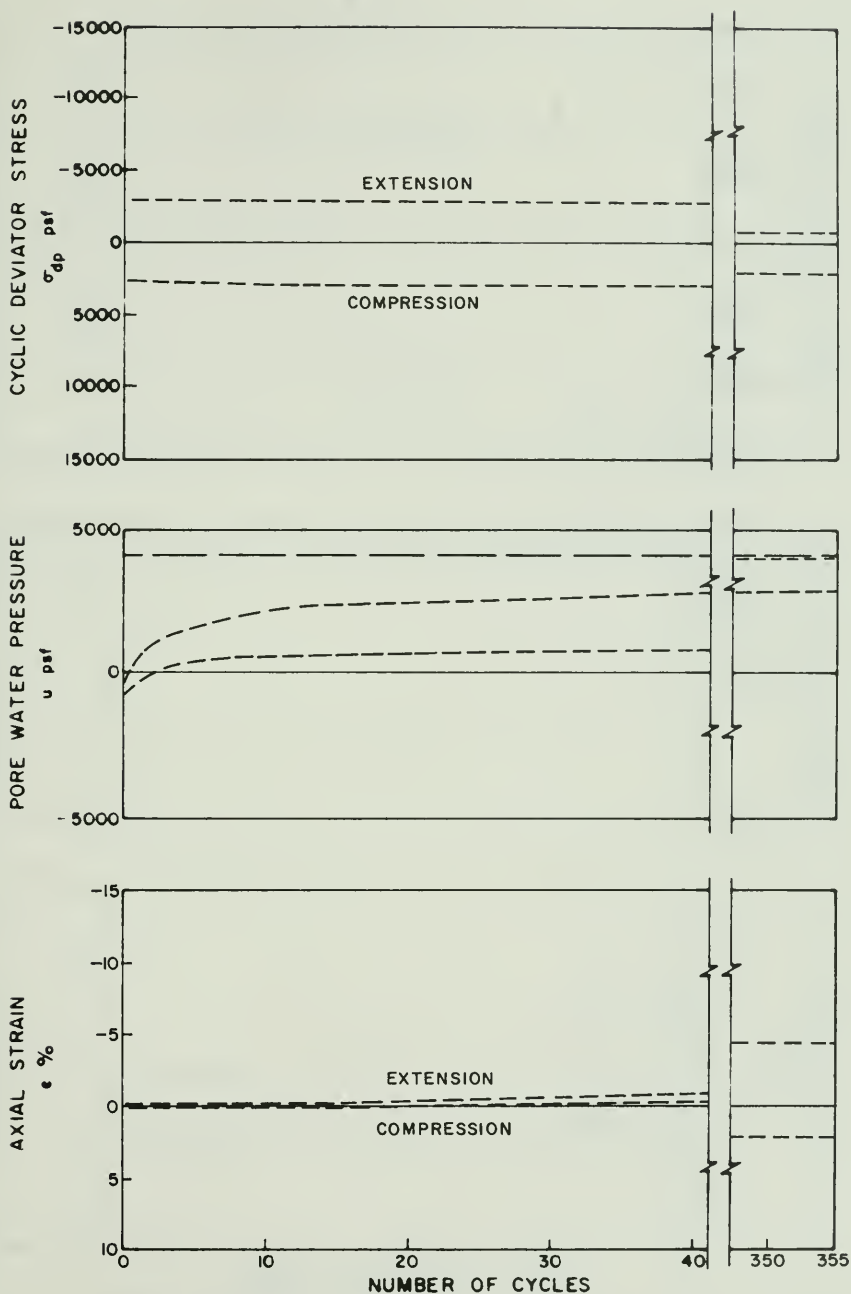


Figure G-35. Cyclic Test Envelopes for Test No. 47 ($\sigma'_{3c} = 4,100$ psf, $K_c = 1.0$)

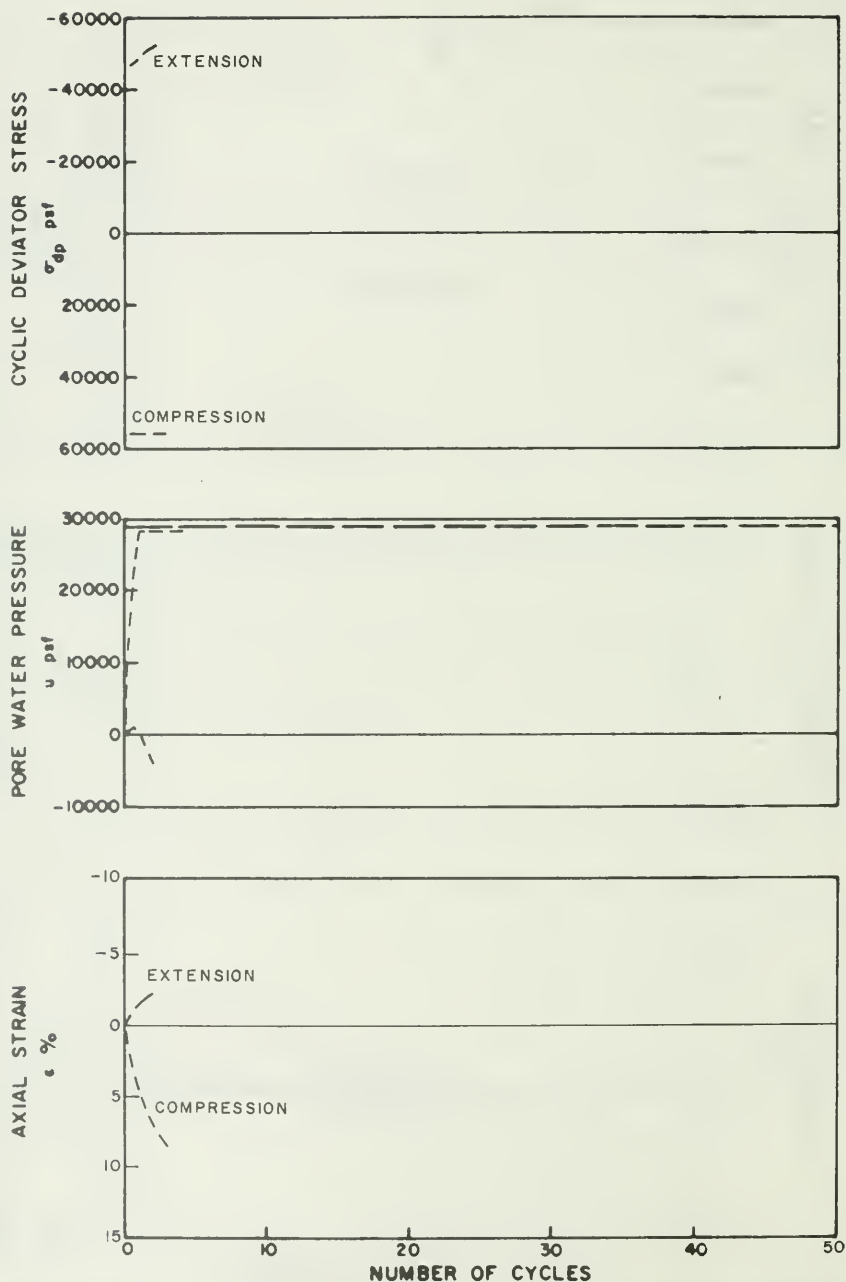


Figure G-36. Cyclic Test Envelopes for Test No. 48 ($\sigma'_{3c} = 28,700$ psf, $K_c = 2.0$)

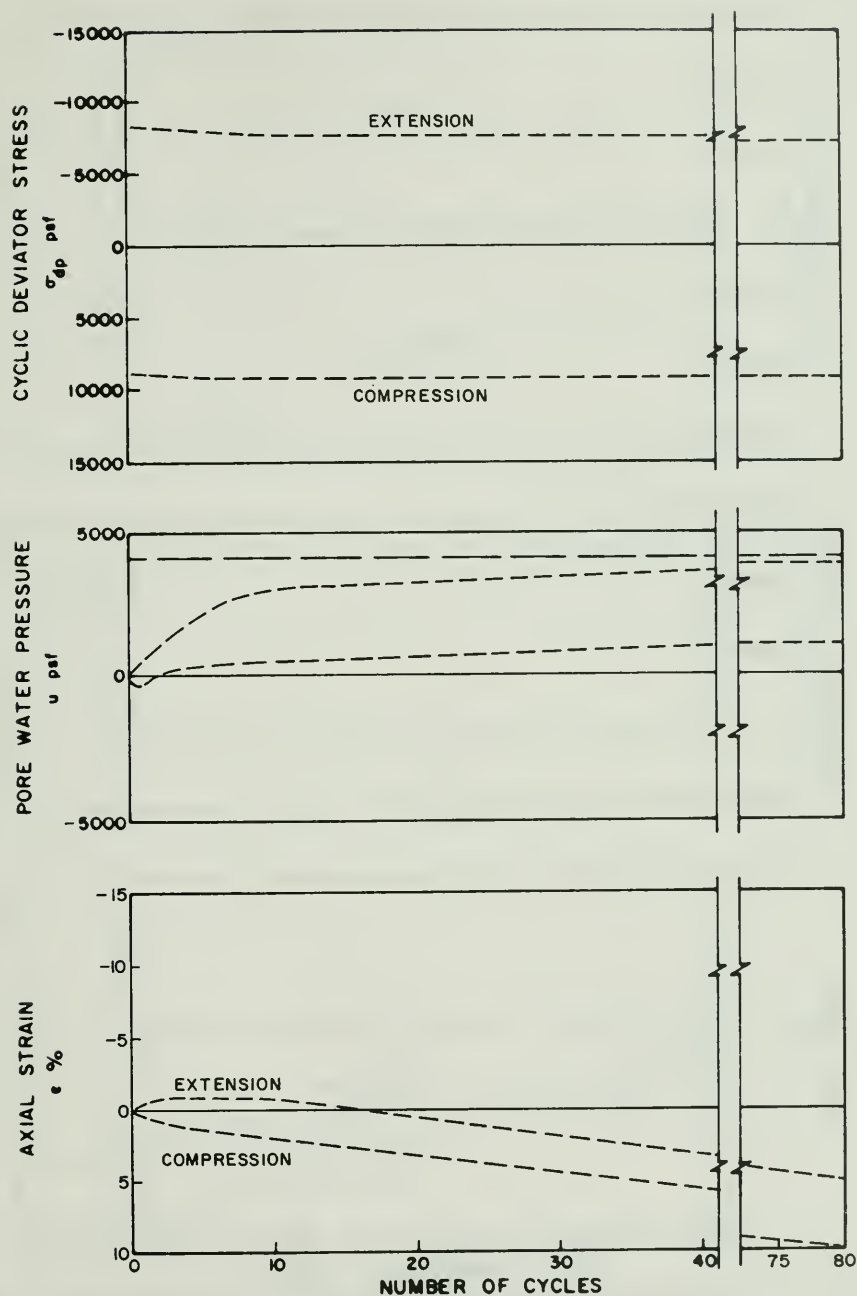


Figure G-37. Cyclic Test Envelopes for Test No. 49 ($\sigma'_{3c} = 4,100$ psf, $K_c = 2.0$)

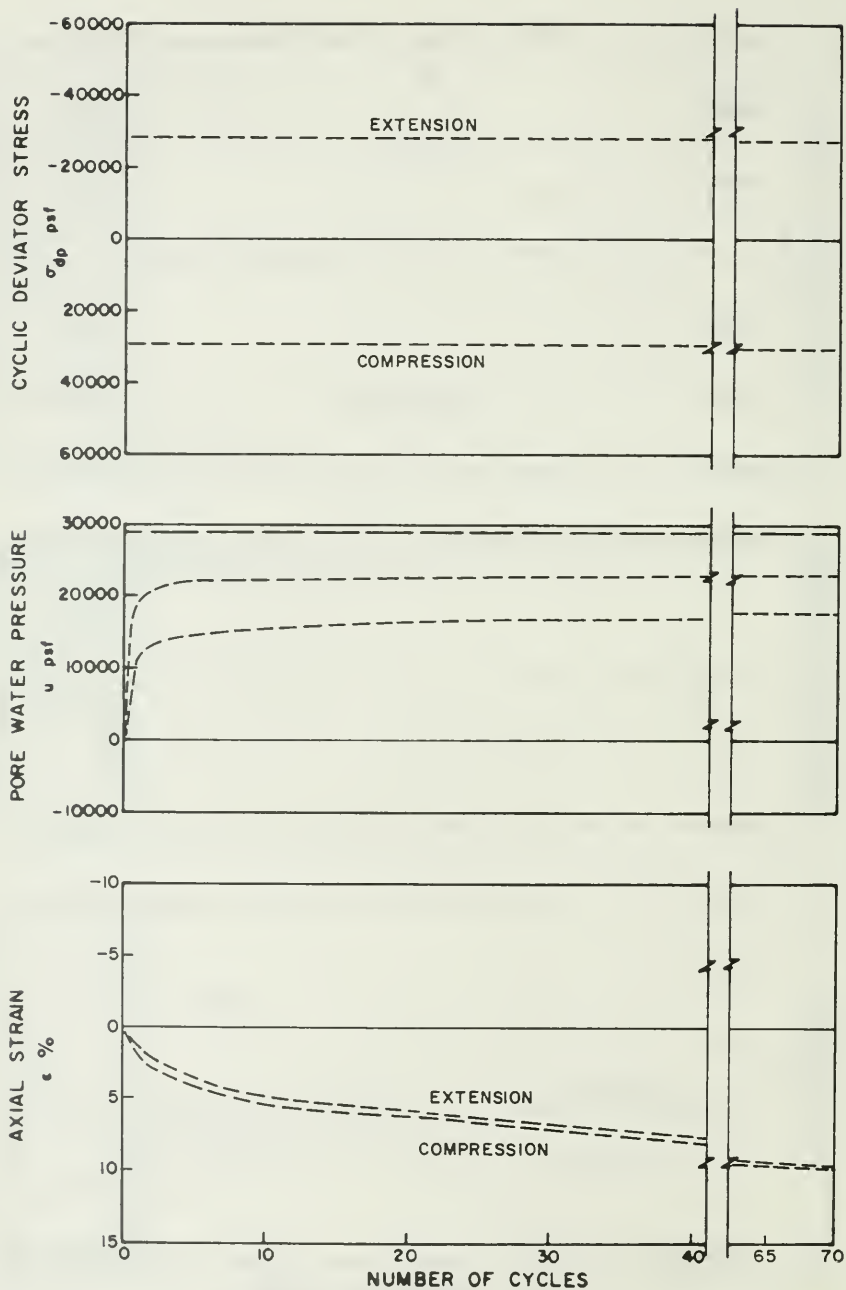


Figure G-38. Cyclic Test Envelopes for Test No. 50 ($\sigma'_{3c} = 28,700$ psf, $K_c = 2.0$)

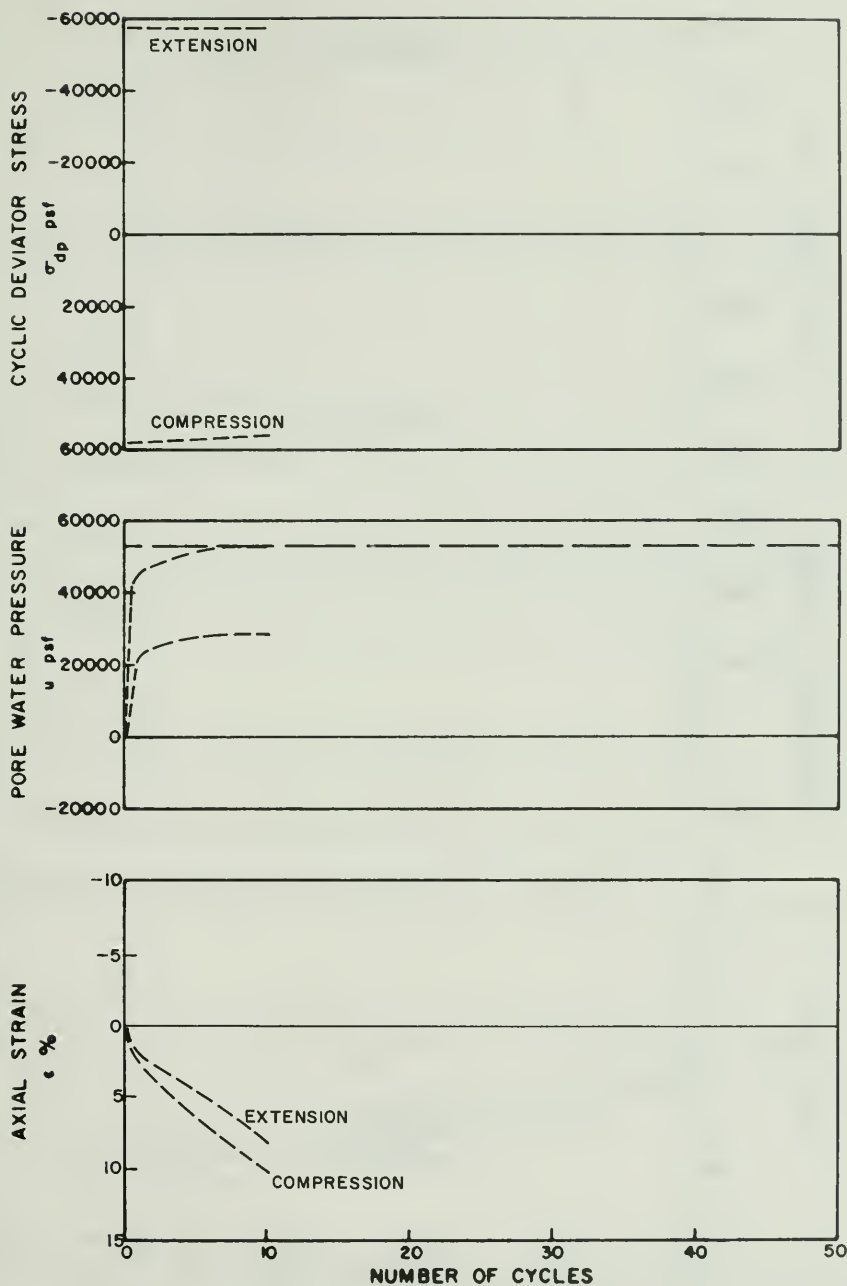


Figure G-39. Cyclic Test Envelopes for Test No. 51 ($\sigma'_{3c} = 53,300$ psf, $K_c = 2.0$)

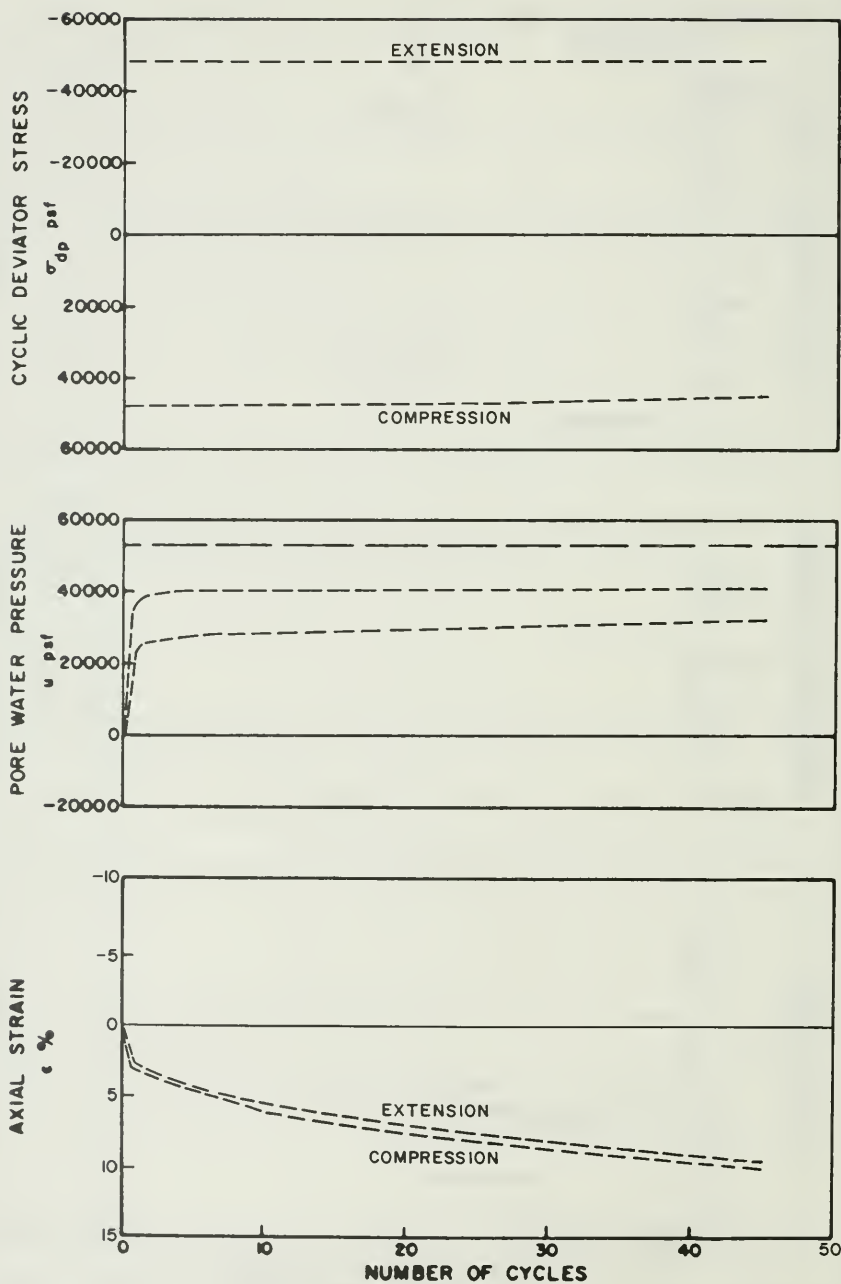


Figure G-40. Cyclic Test Envelopes for Test No. 52 ($\sigma'_{3c} = 53,300$ psf, $K_c = 2.0$)

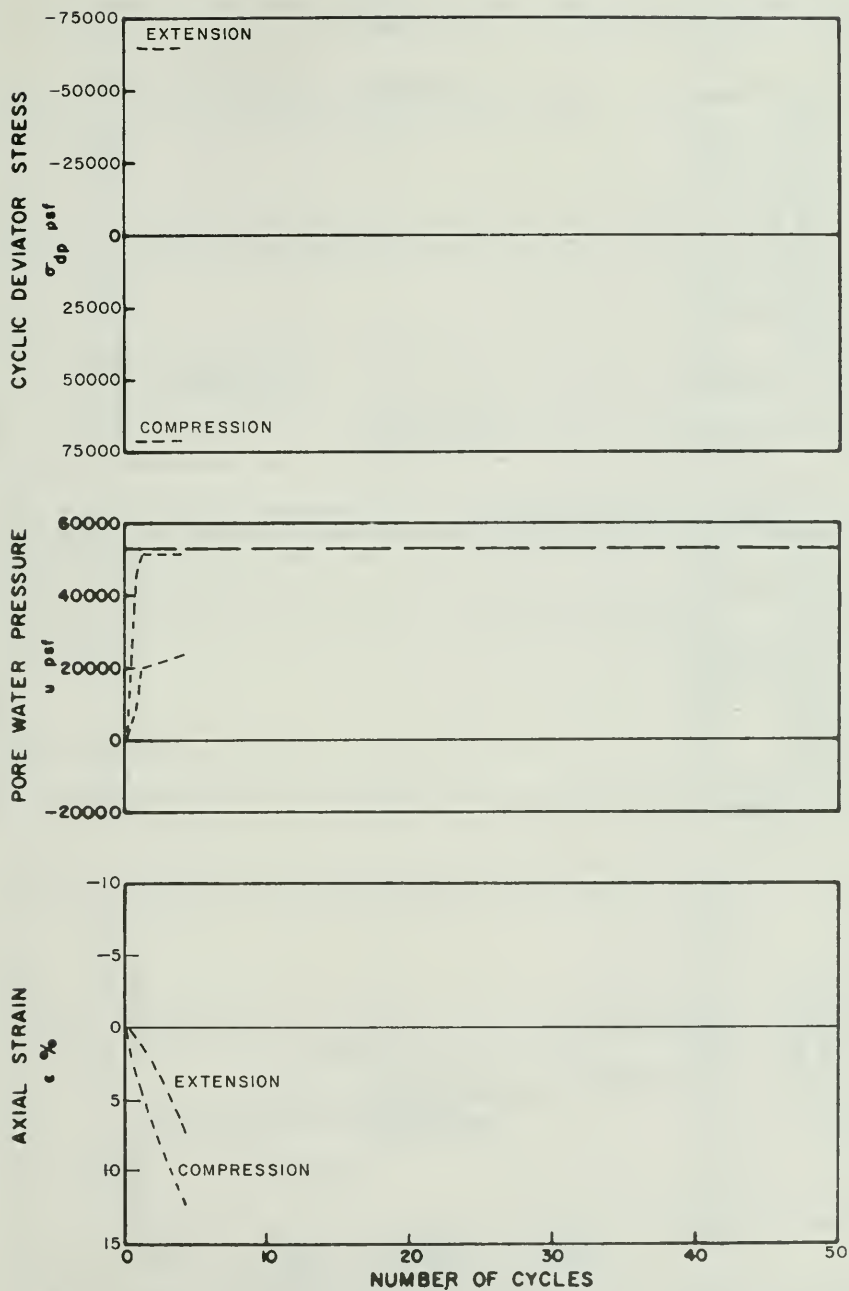


Figure G-41. Cyclic Test Envelopes for Test No. 53 ($\sigma'_{3c} = 53,300$ psf, $K_c = 2.0$)

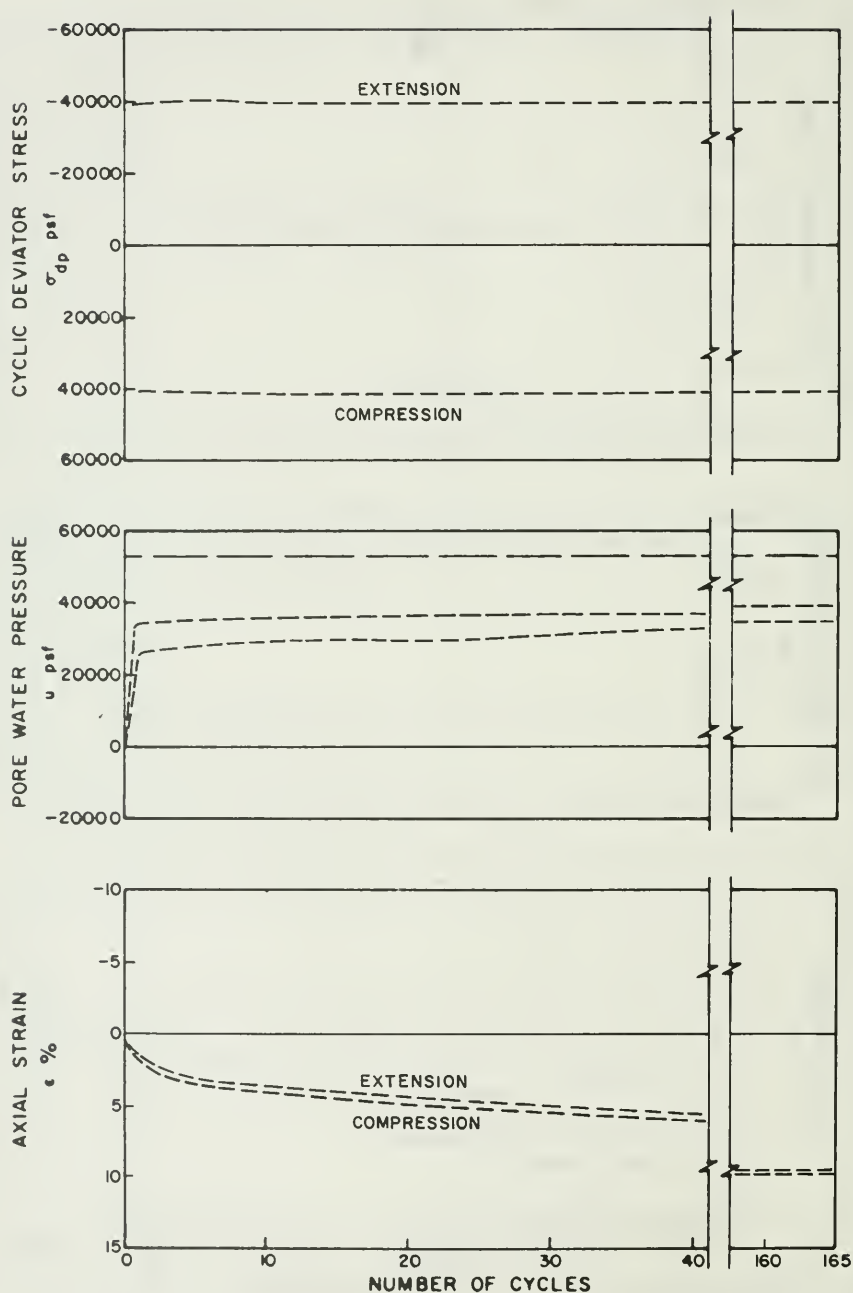


Figure G-42. Cyclic Test Envelopes for Test No. 55 ($\sigma'_{3c} = 53,300$ psf, $K_c = 2.0$)

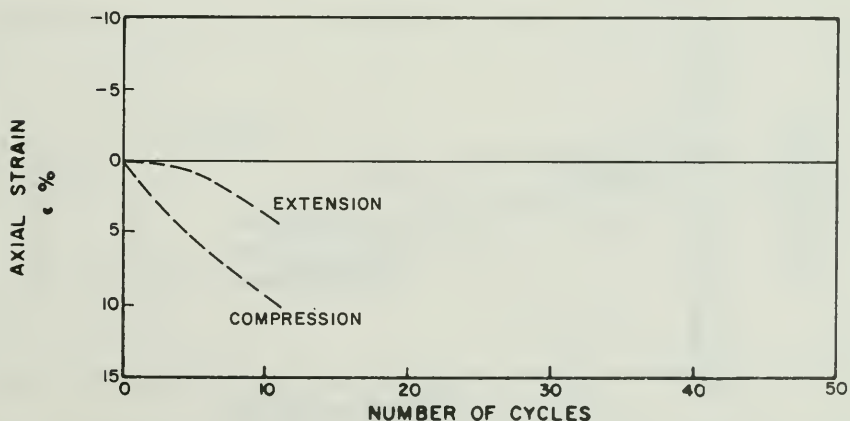
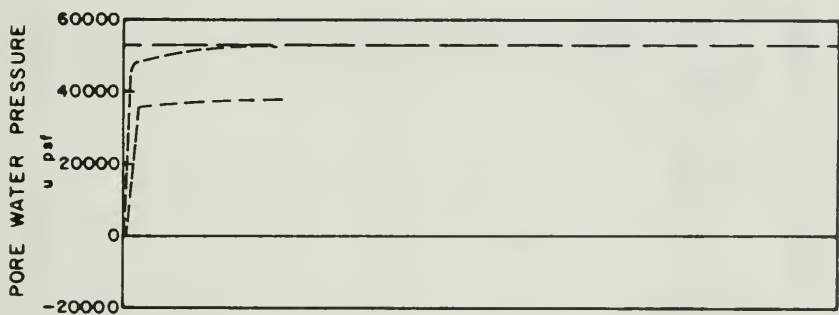
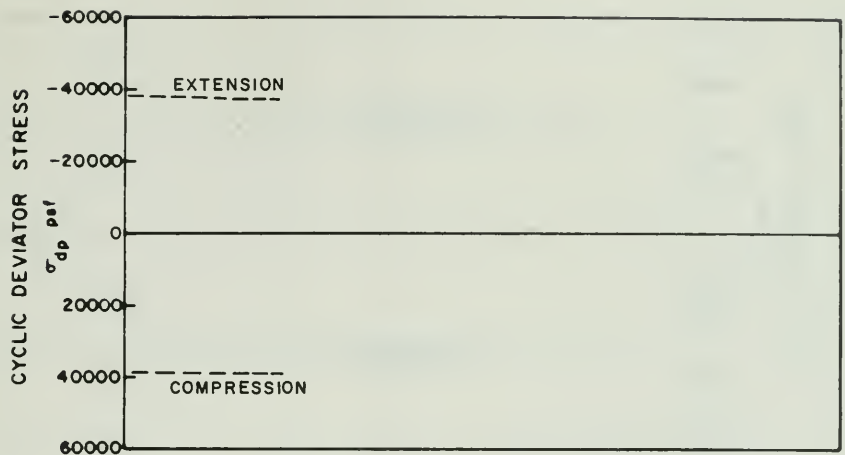


Figure G-43. Cyclic Test Envelopes for Test No. 56 ($\sigma'_{3c} = 53,300$ psf, $K_c = 1.5$)

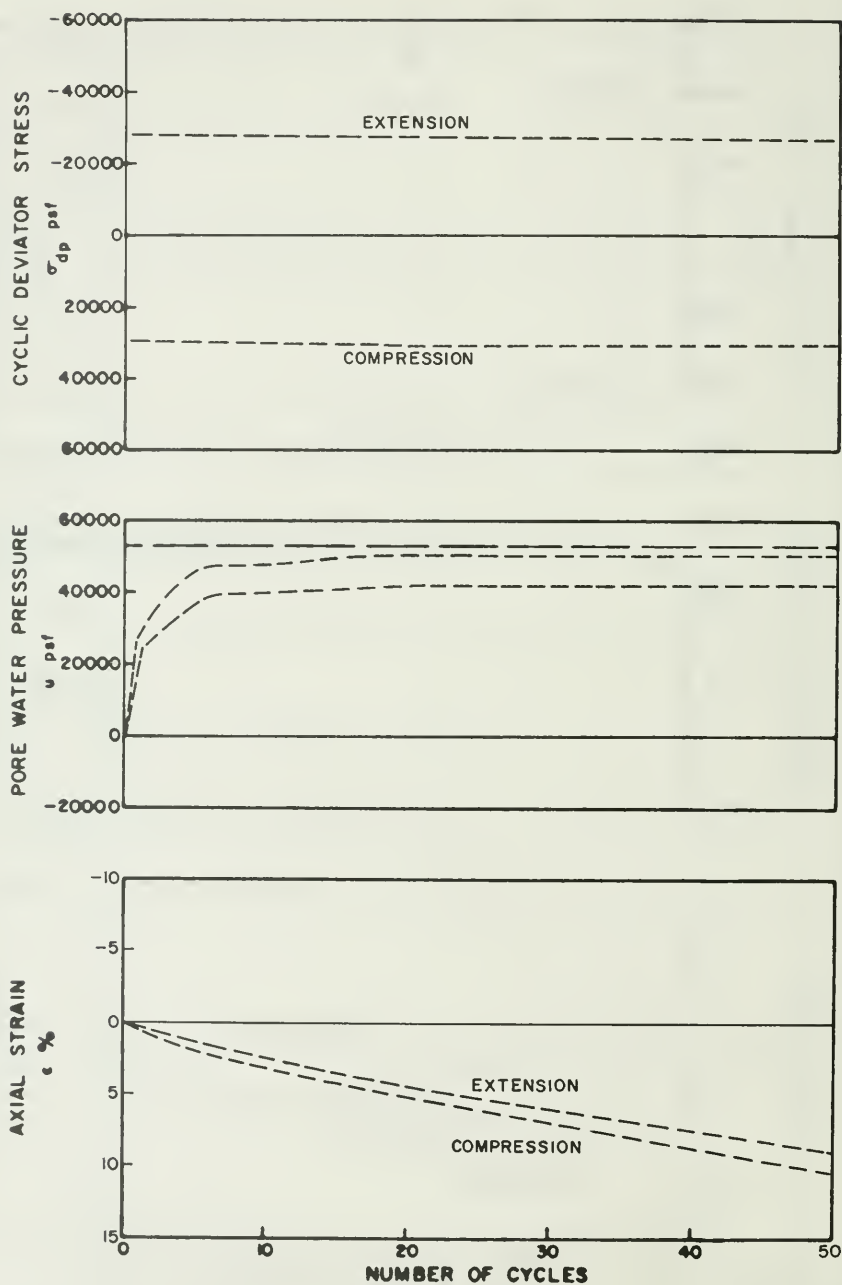


Figure G-44. Cyclic Test Envelopes for Test No. 57 ($\sigma'_{3c} = 53,300$ psf, $K_c = 1.5$)

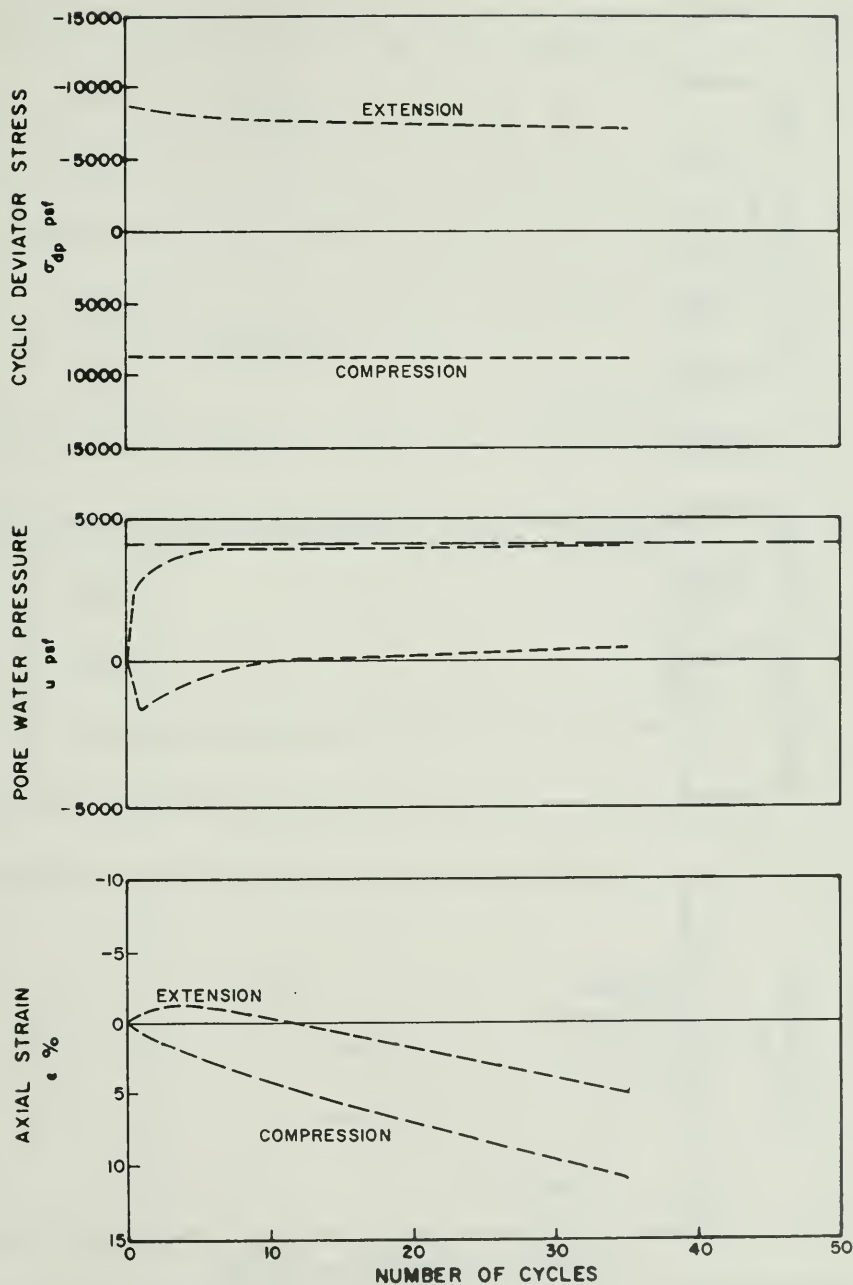


Figure G-45. Cyclic Test Envelopes for Test No. 58 ($\sigma'_{3c} = 4,100$ psf, $K_c = 2.0$)

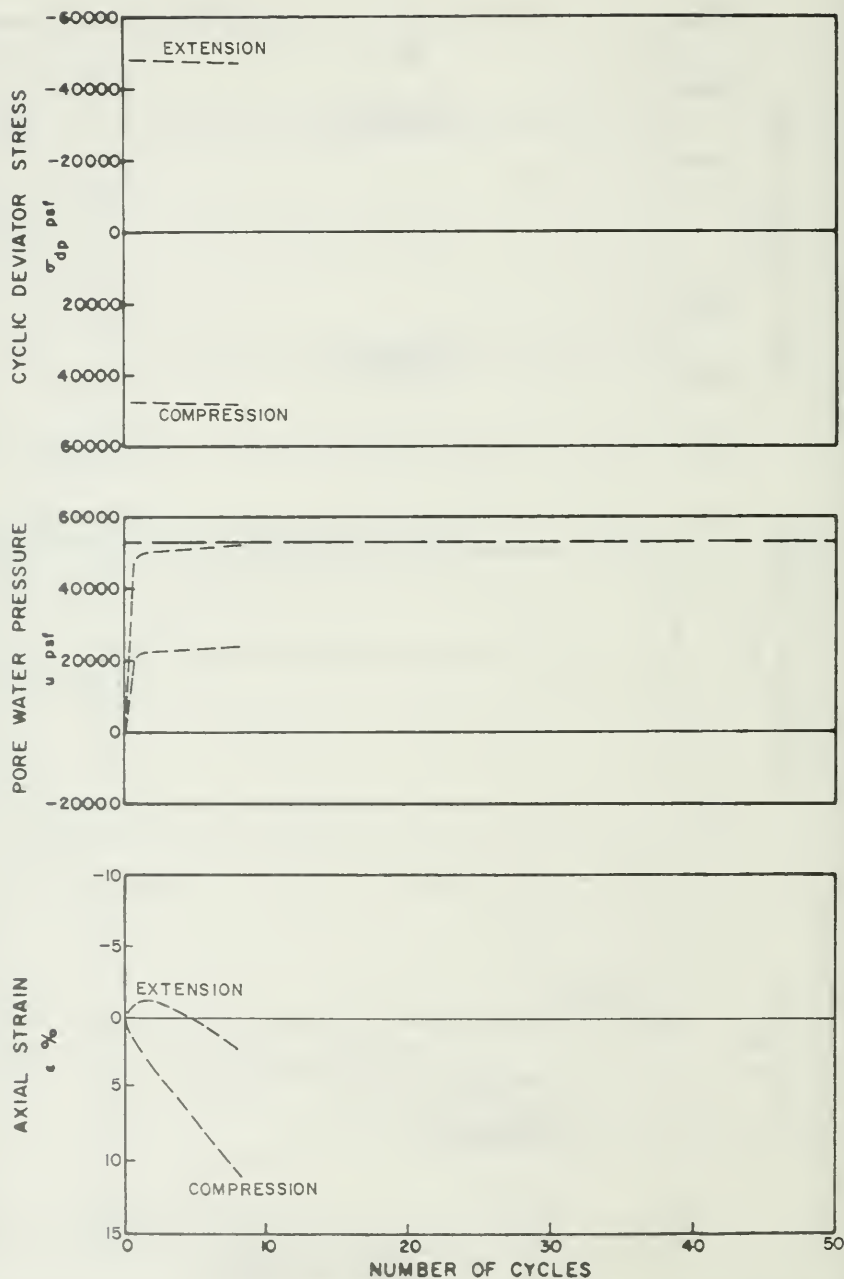


Figure G-46. Cyclic Test Envelopes for Test No. 59 ($\sigma'_{3c} = 53,300$ psf, $K_c = 1.5$)

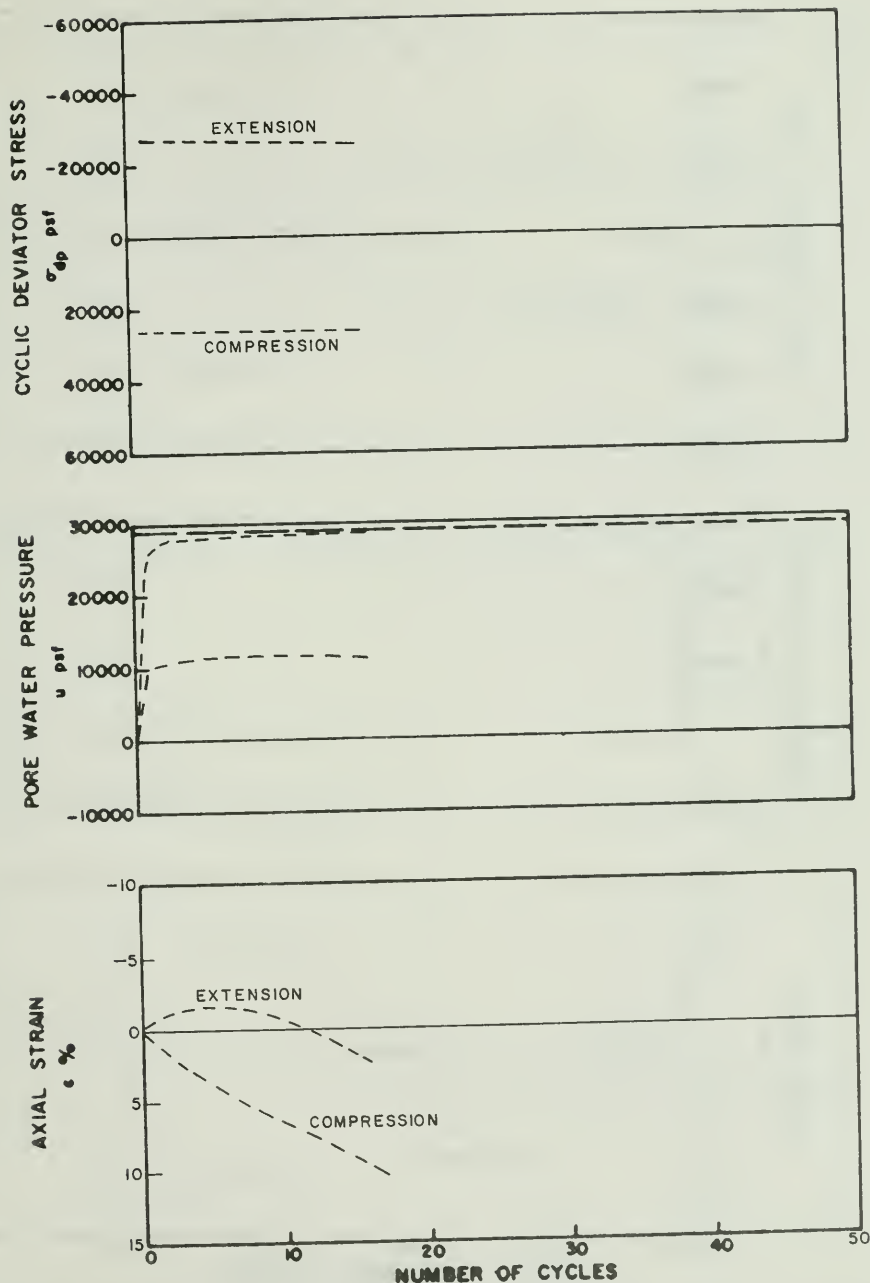


Figure G-47. Cyclic Test Envelopes for Test No. 60 ($\sigma'_{3c} = 28,700$ psf, $K_c = 1.5$)

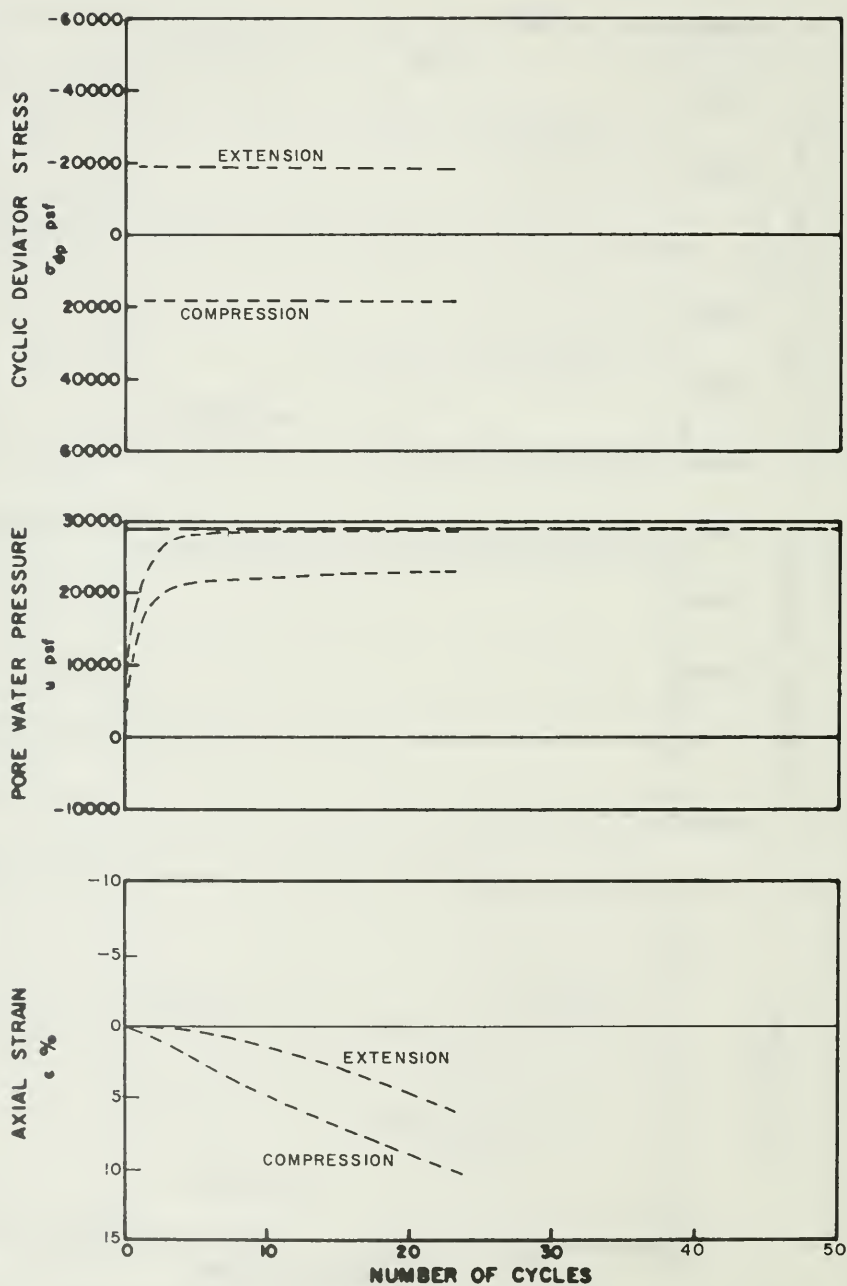


Figure G-48. Cyclic Test Envelopes for Test No. 61 ($\sigma'_{3c} = 28,700$ psf, $K_c = 1.5$)

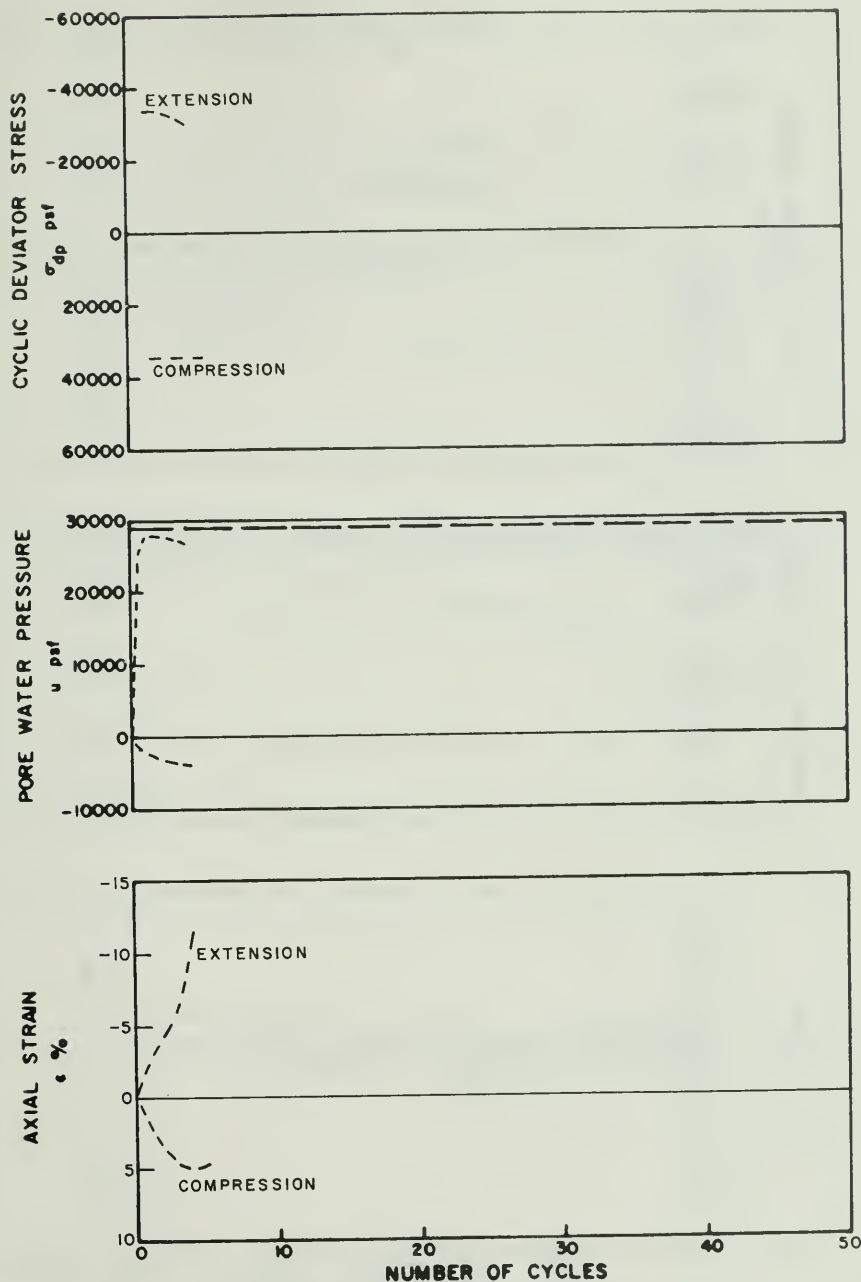


Figure G-49. Cyclic Test Envelopes for Test No. 62 ($\sigma'_{3c} = 28,700$ psf, $K_c = 1.5$)

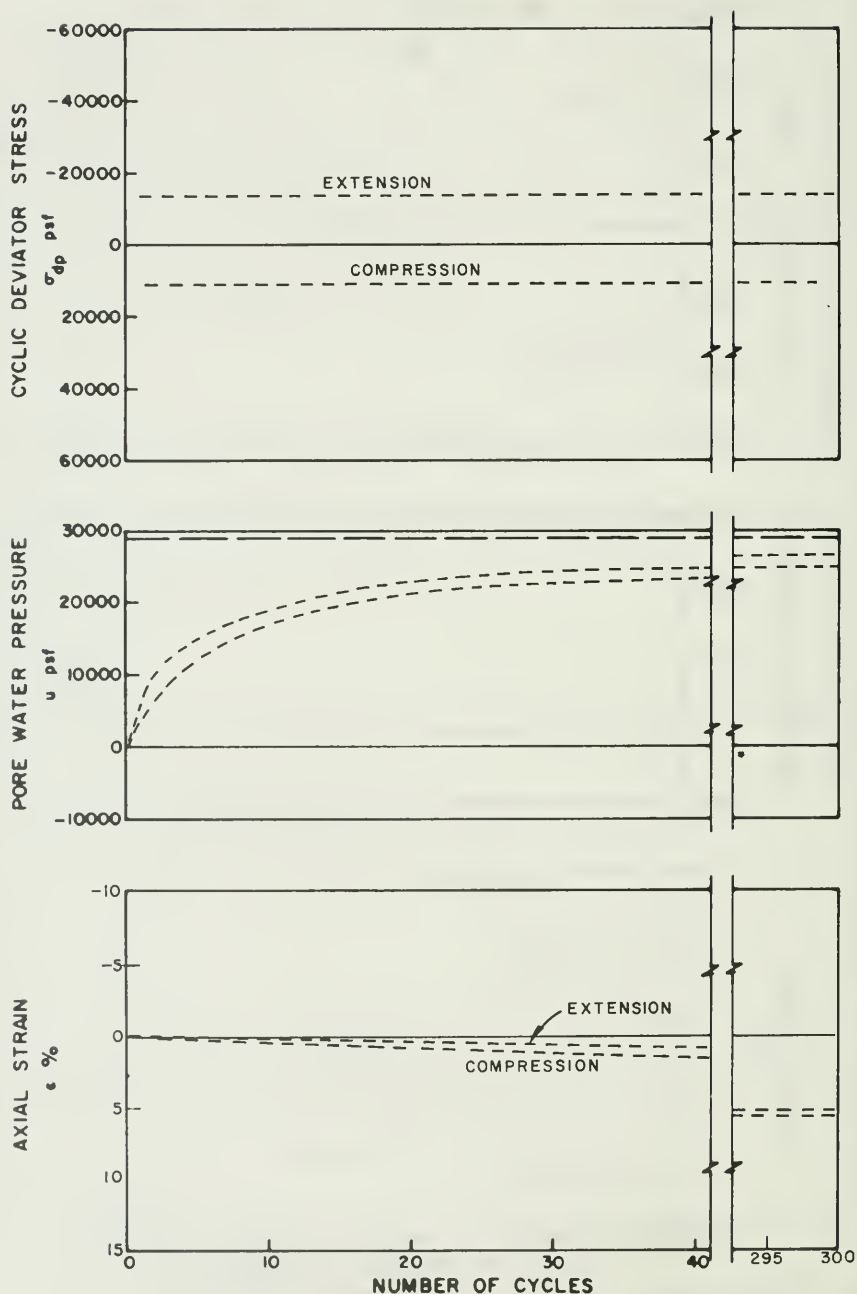


Figure G-50. Cyclic Test Envelopes for Test No. 63 ($\sigma'_{3c} = 28,700$ psf, $K_c = 1.5$)

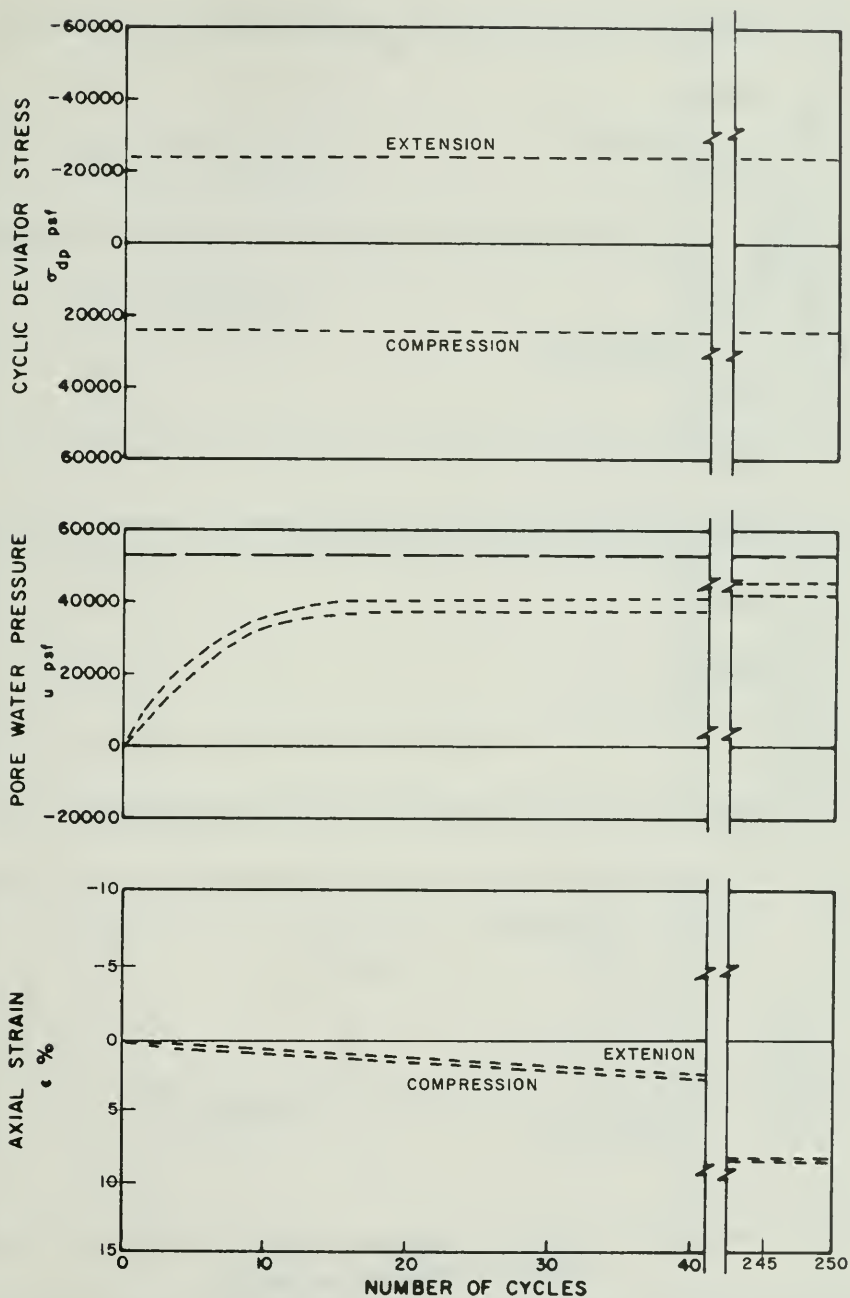


Figure G-51. Cyclic Test Envelopes for Test No. 64 ($\sigma'_{3c} = 53,300$ psf, $K_c = 1.5$)

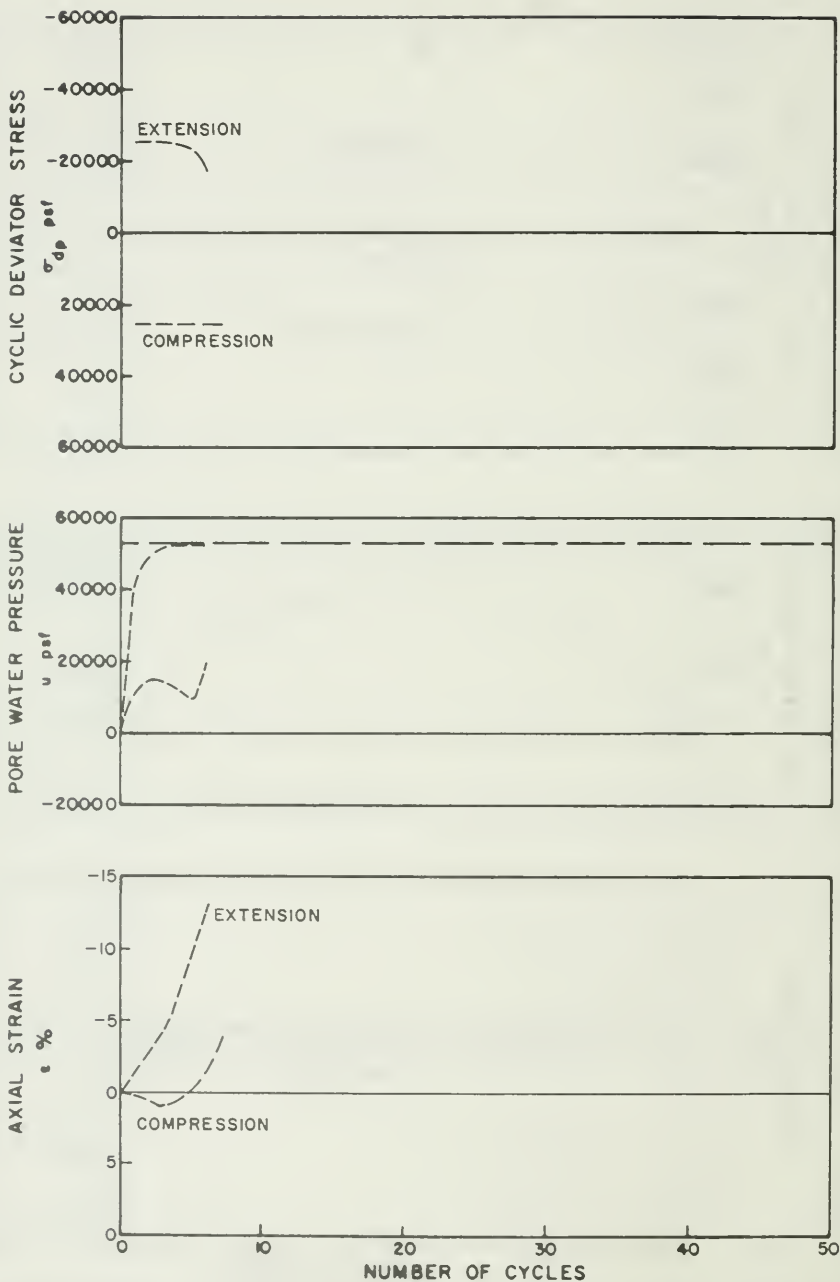


Figure G-52. Cyclic Test Envelopes for Test No. 65 ($\sigma'_{3c} = 53,300$ psf, $K_c = 1.0$)

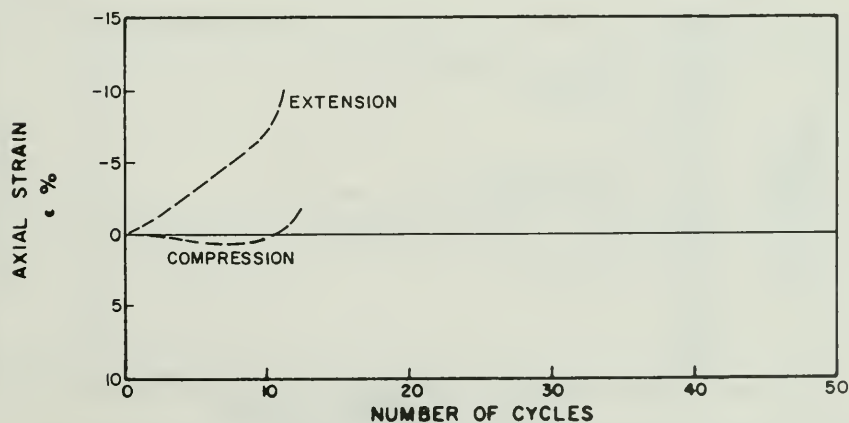
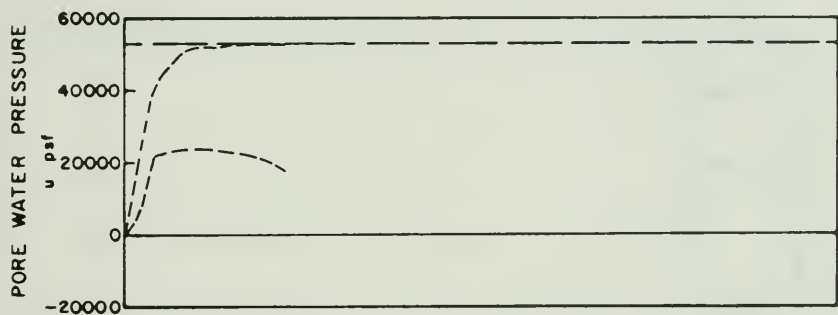
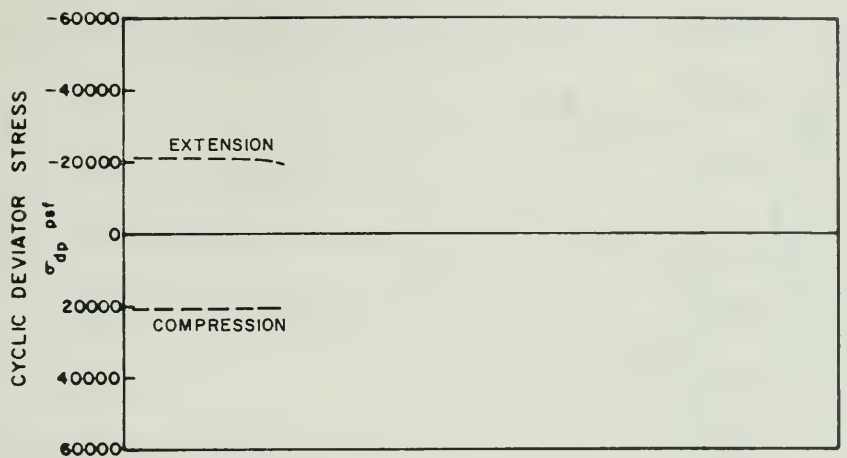


Figure G-53. Cyclic Test Envelopes for Test No. 66 ($\sigma'_{3c} = 53,300$ psf, $K_c = 1.0$)

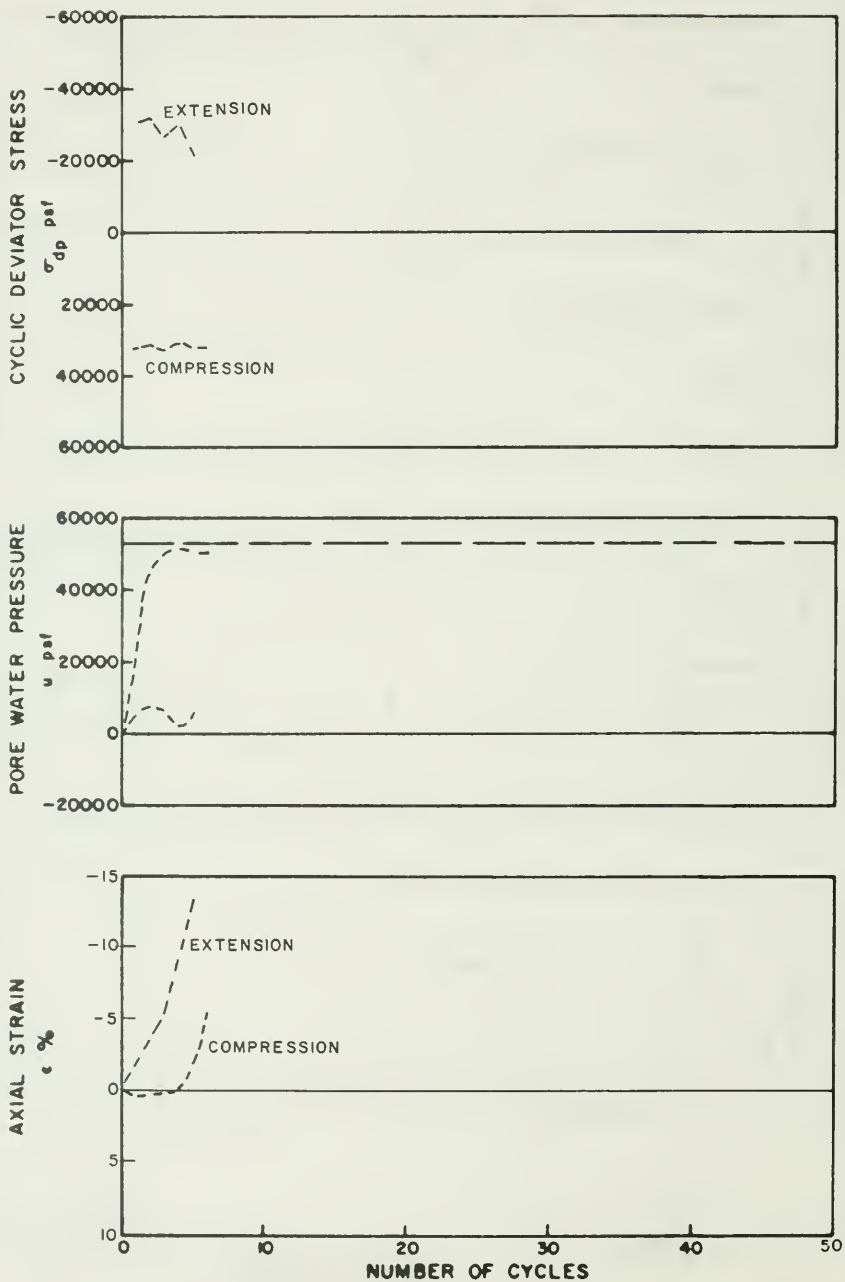


Figure G-54. Cyclic Test Envelopes for Test No. 67 ($\sigma'_{3c} = 53,300$ psf, $K_c = 1.0$)

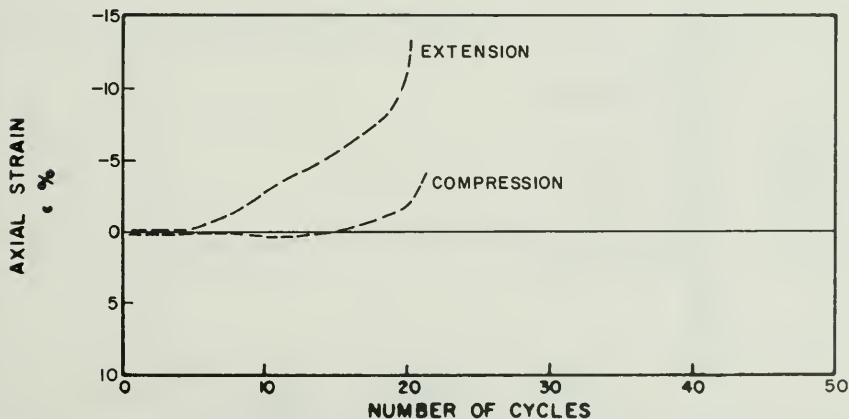
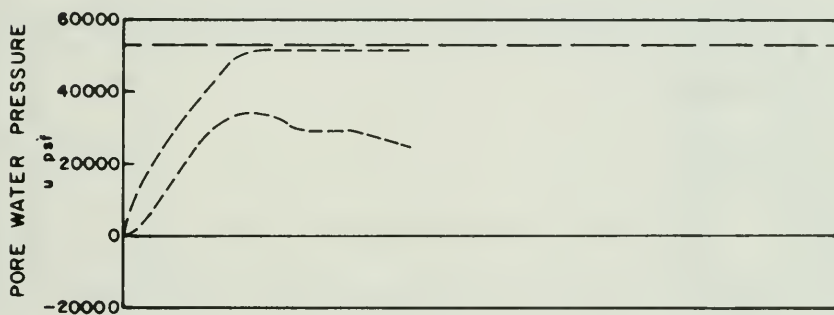
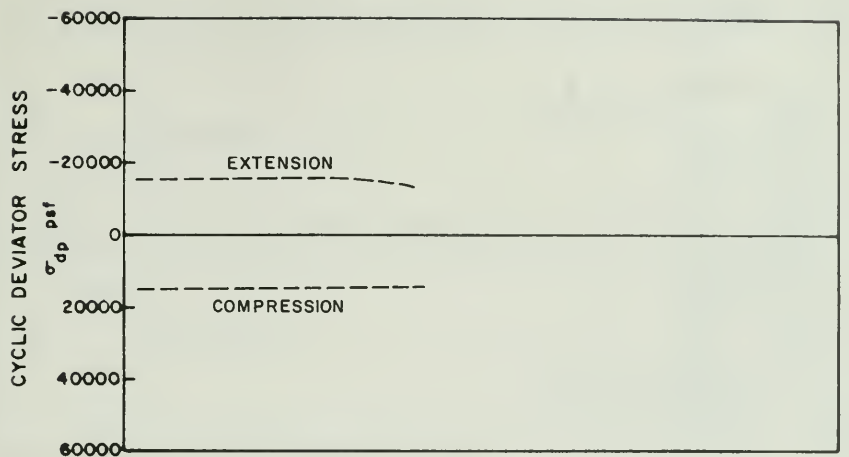


Figure G-55. Cyclic Test Envelopes for Test No. 68 ($\sigma'_{3c} = 53,300$ psf, $K_c = 1.0$)

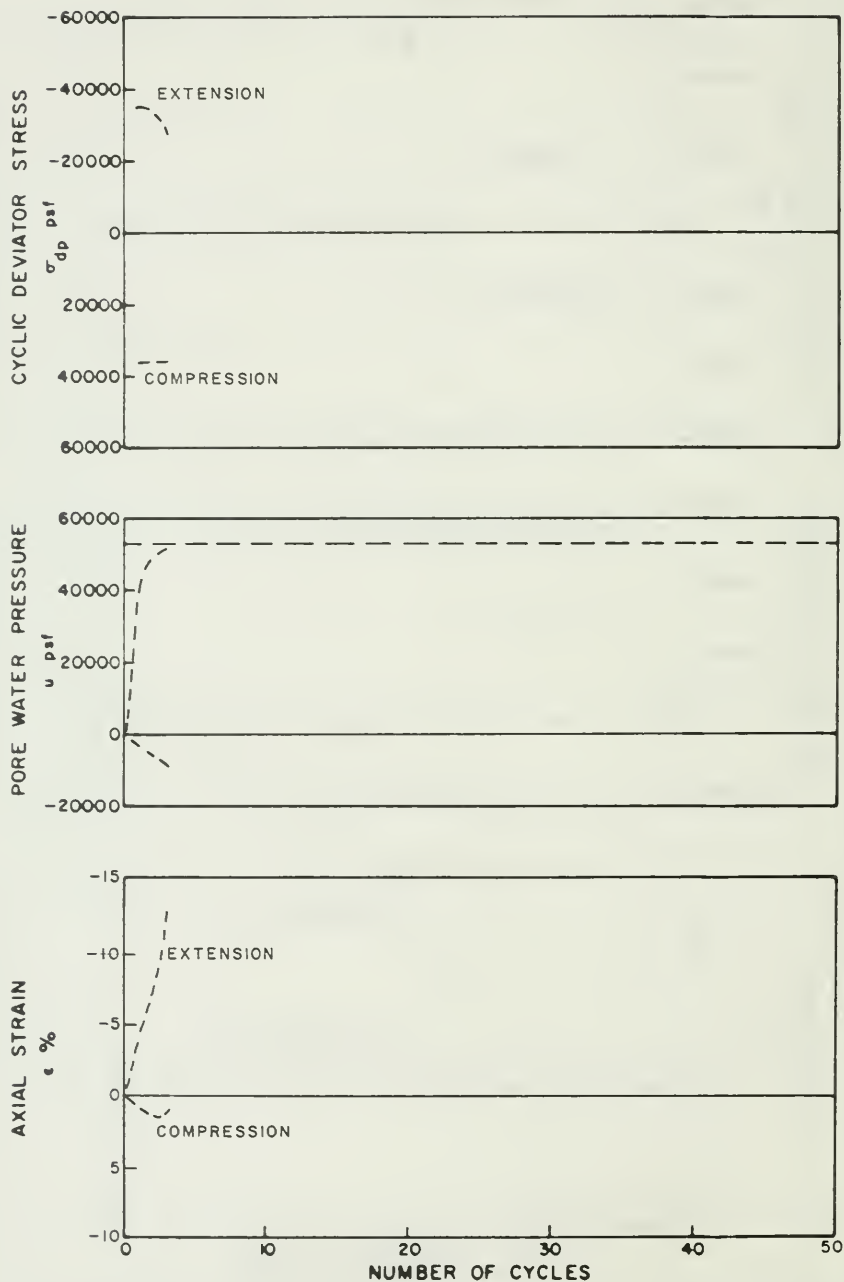


Figure G-56. Cyclic Test Envelopes for Test No. 69 ($\sigma'_{3c} = 53,300$ psf, $K_c = 1.0$)

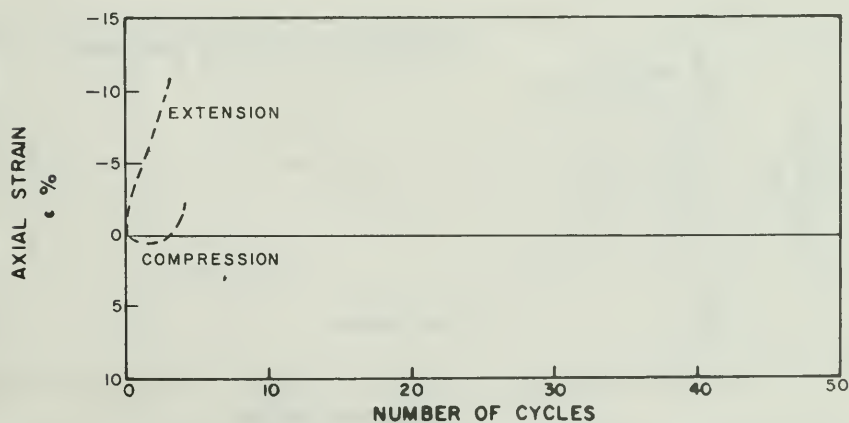
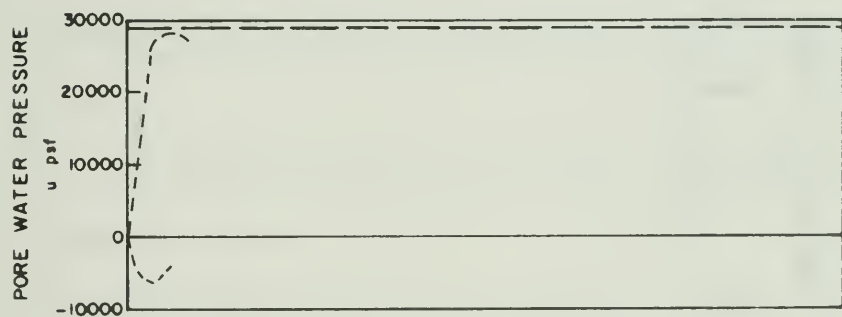
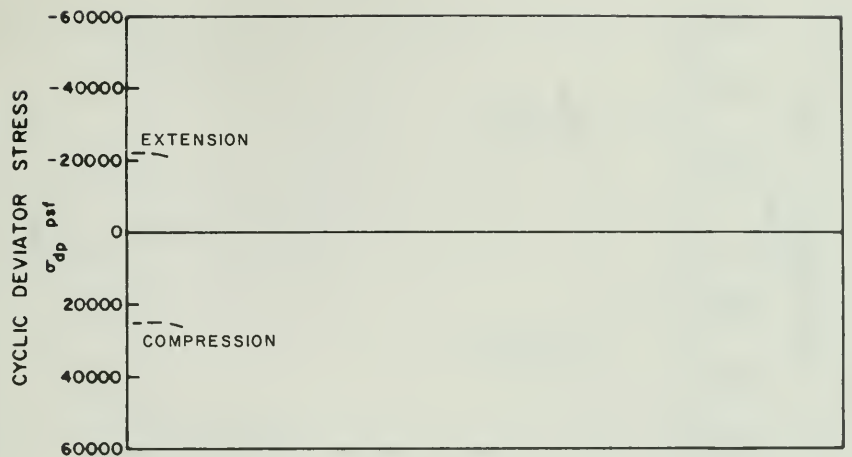


Figure G-57. Cyclic Test Envelopes for Test No. 70 ($\sigma'_{3c} = 28,700$ psf, $K_c = 1.0$)

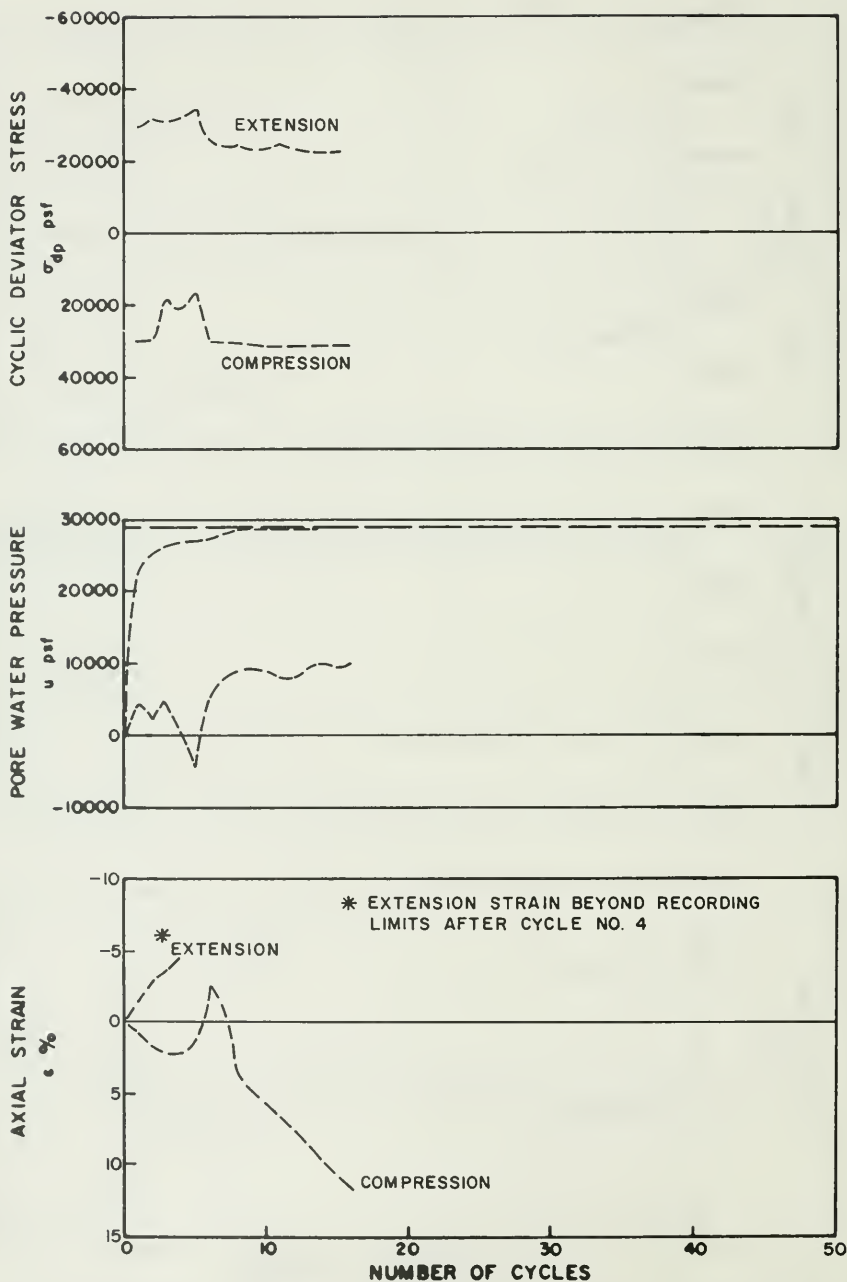


Figure G-58. Cyclic Test Envelopes for Test No. 71 ($\sigma'_{3c} = 28,700$ psf, $K_c = 1.5$)

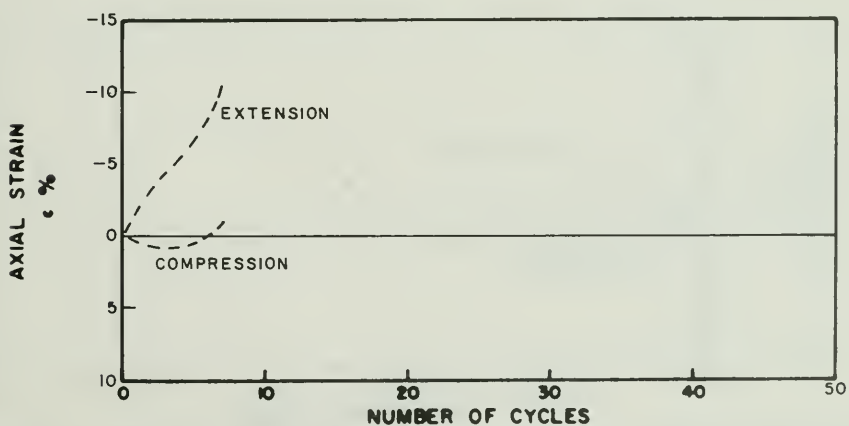
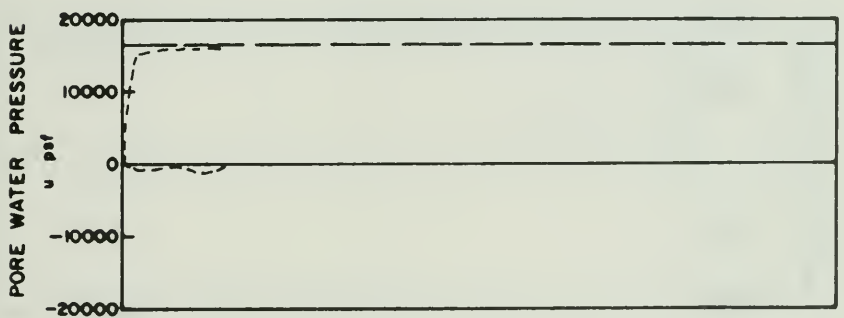
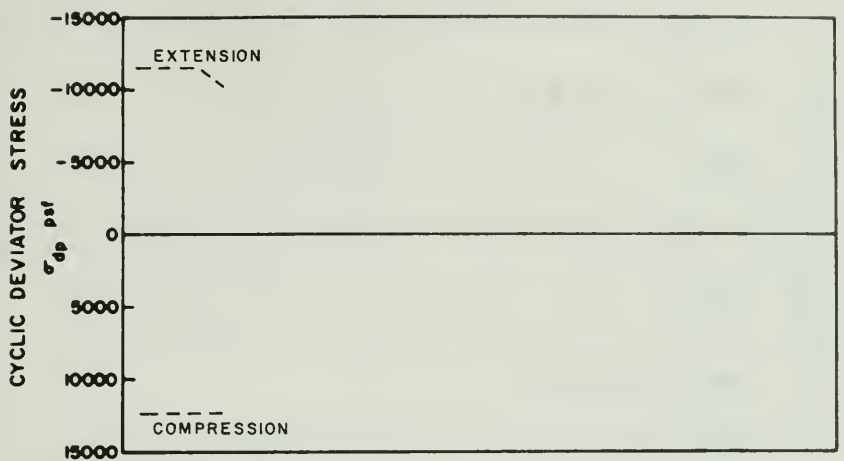


Figure G-59. Cyclic Test Envelopes for Test No. 72 ($\sigma'_{3c} = 16,400$ psf, $K_c = 1.0$)

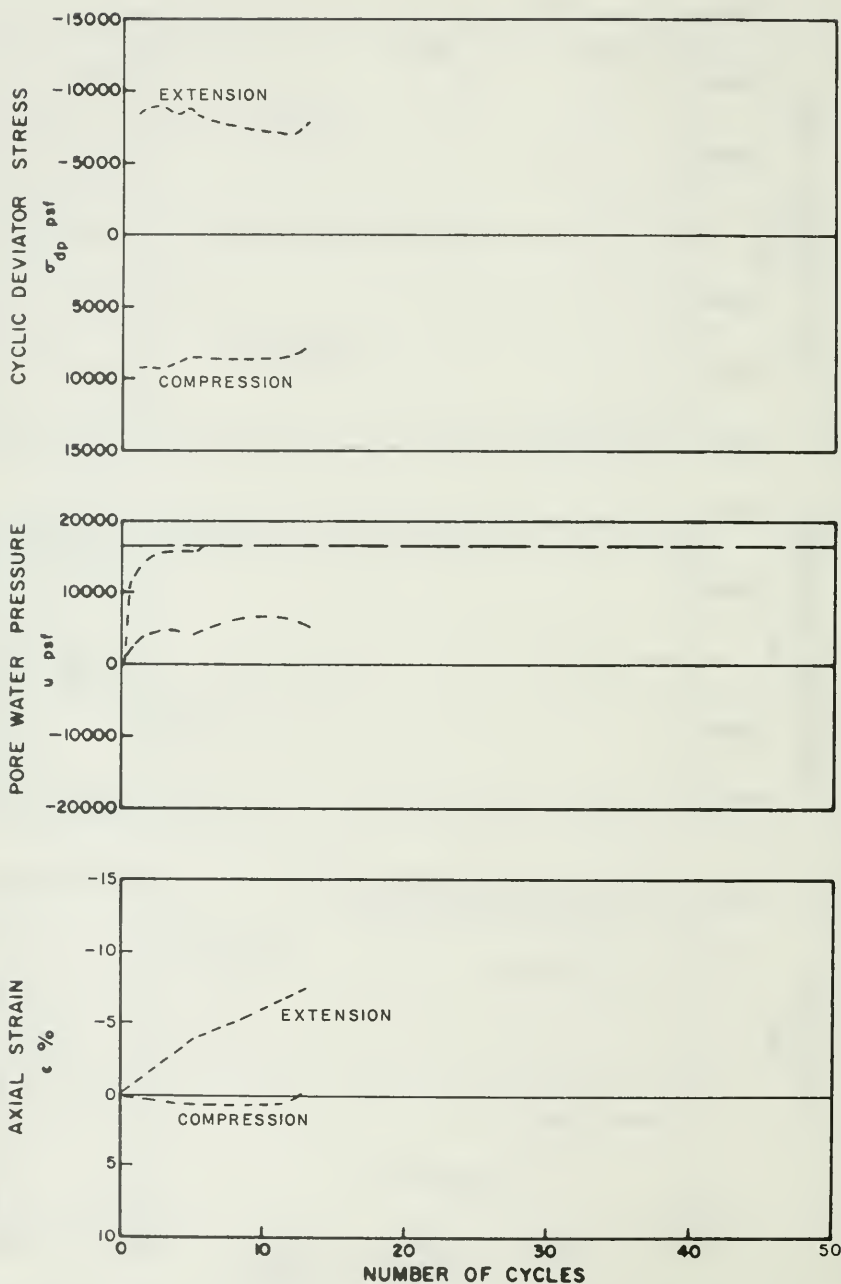


Figure G-60. Cyclic Test Envelopes for Test No. 73 ($\sigma'_{3c} = 16,400$ psf, $K_c = 1.0$)

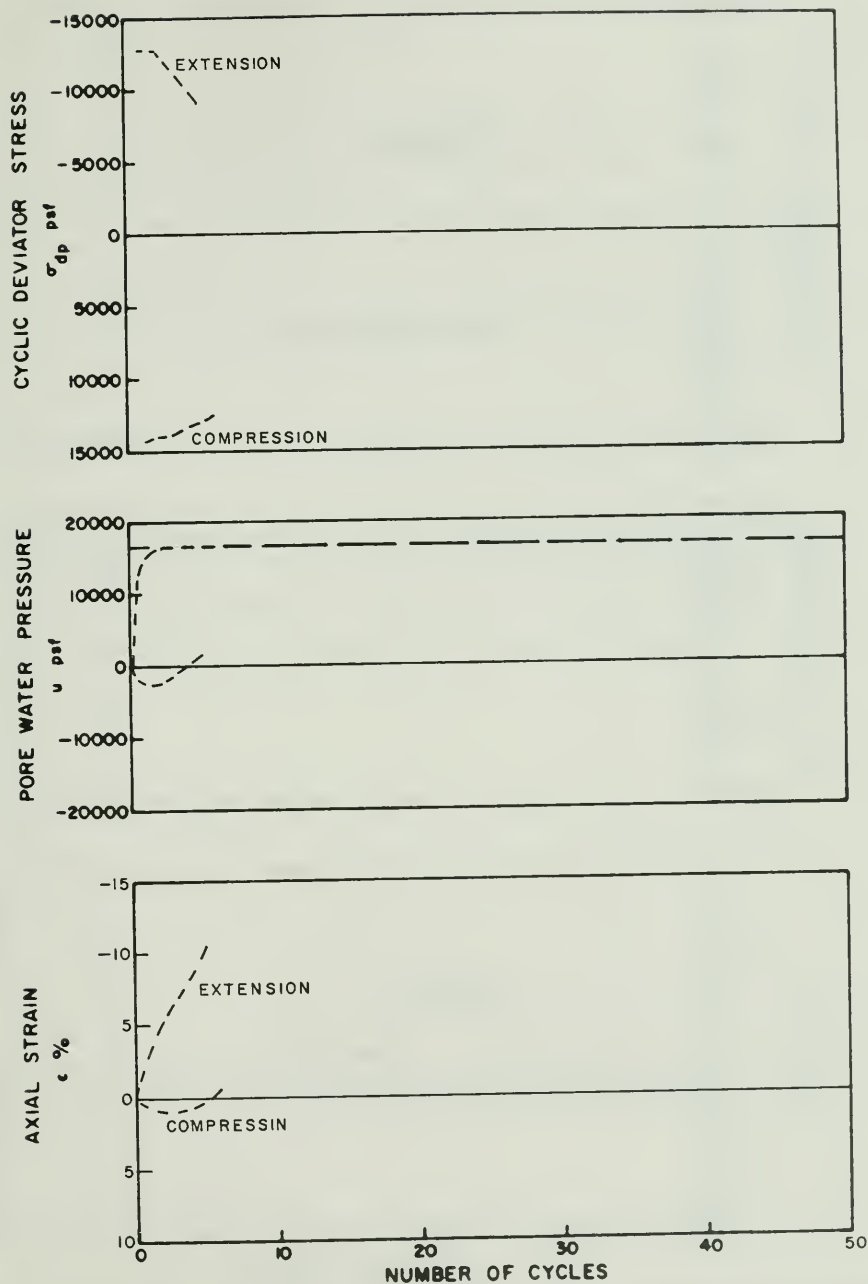


Figure G-61. Cyclic Test Envelopes for Test No. 74 ($\sigma'_{3c} = 16,400$ psf, $K_c = 1.0$)

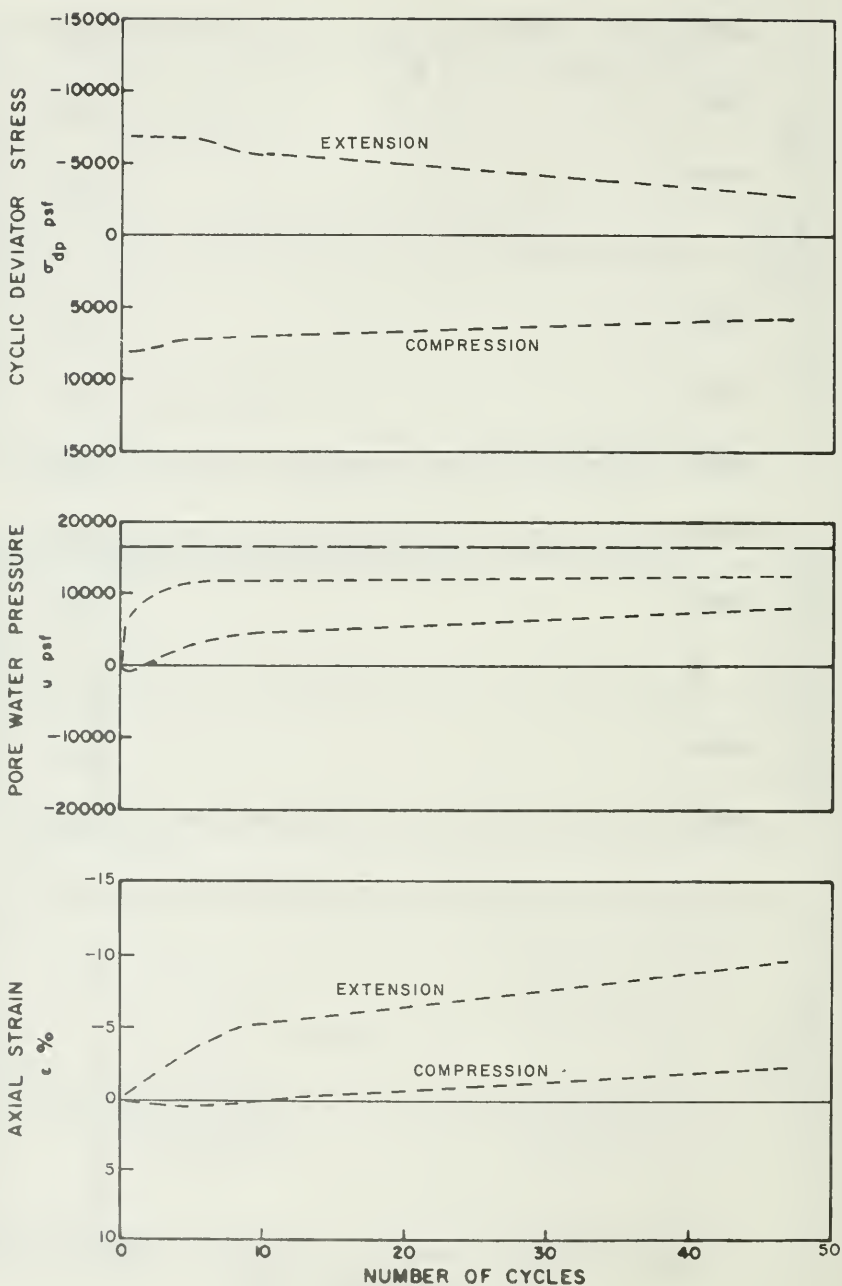


Figure G-62. Cyclic Test Envelopes for Test No. 75 ($\sigma'_{3c} = 16,400$ psf, $K_c = 1.0$)

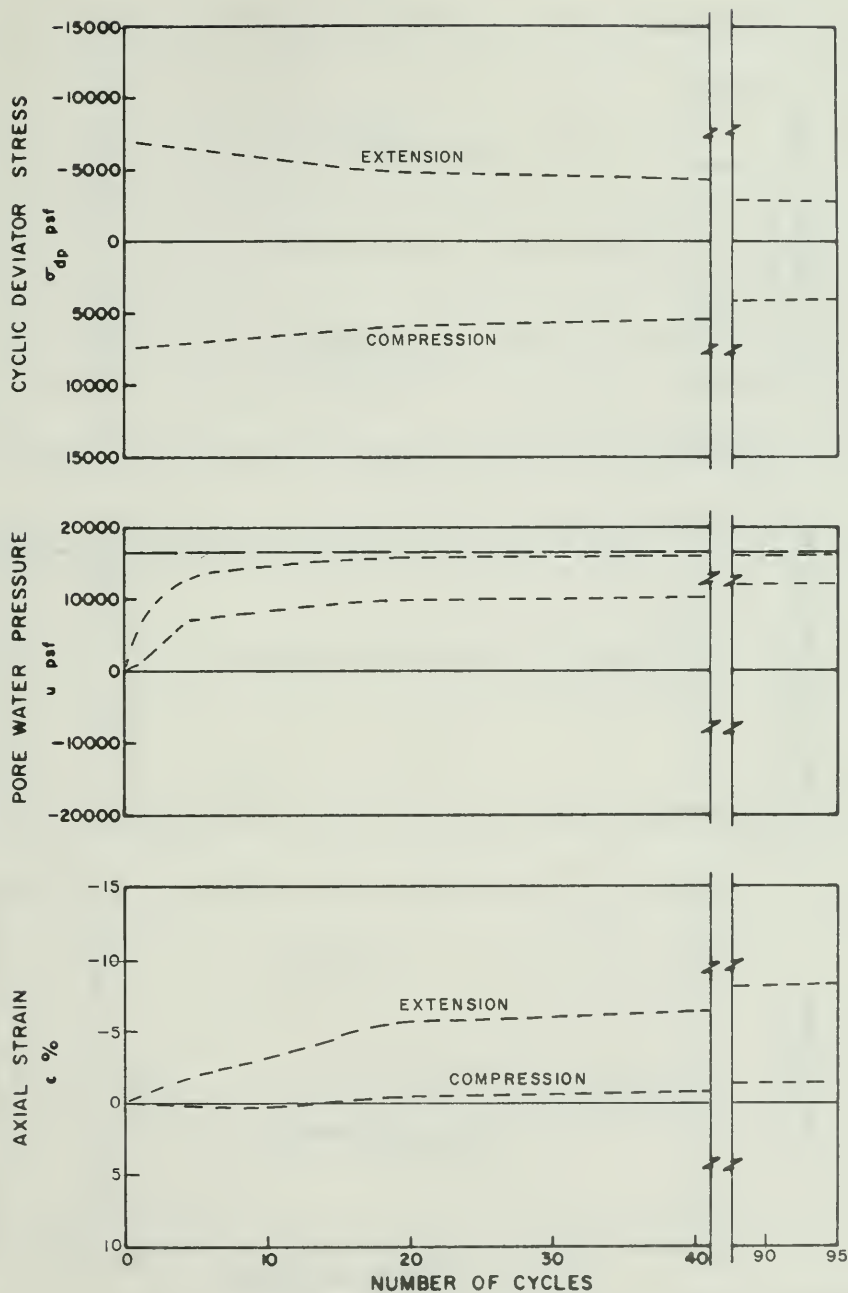


Figure G-63. Cyclic Test Envelopes for Test No. 76 ($\sigma'_{3c} = 16,400$ psf, $K_c = 1.0$)

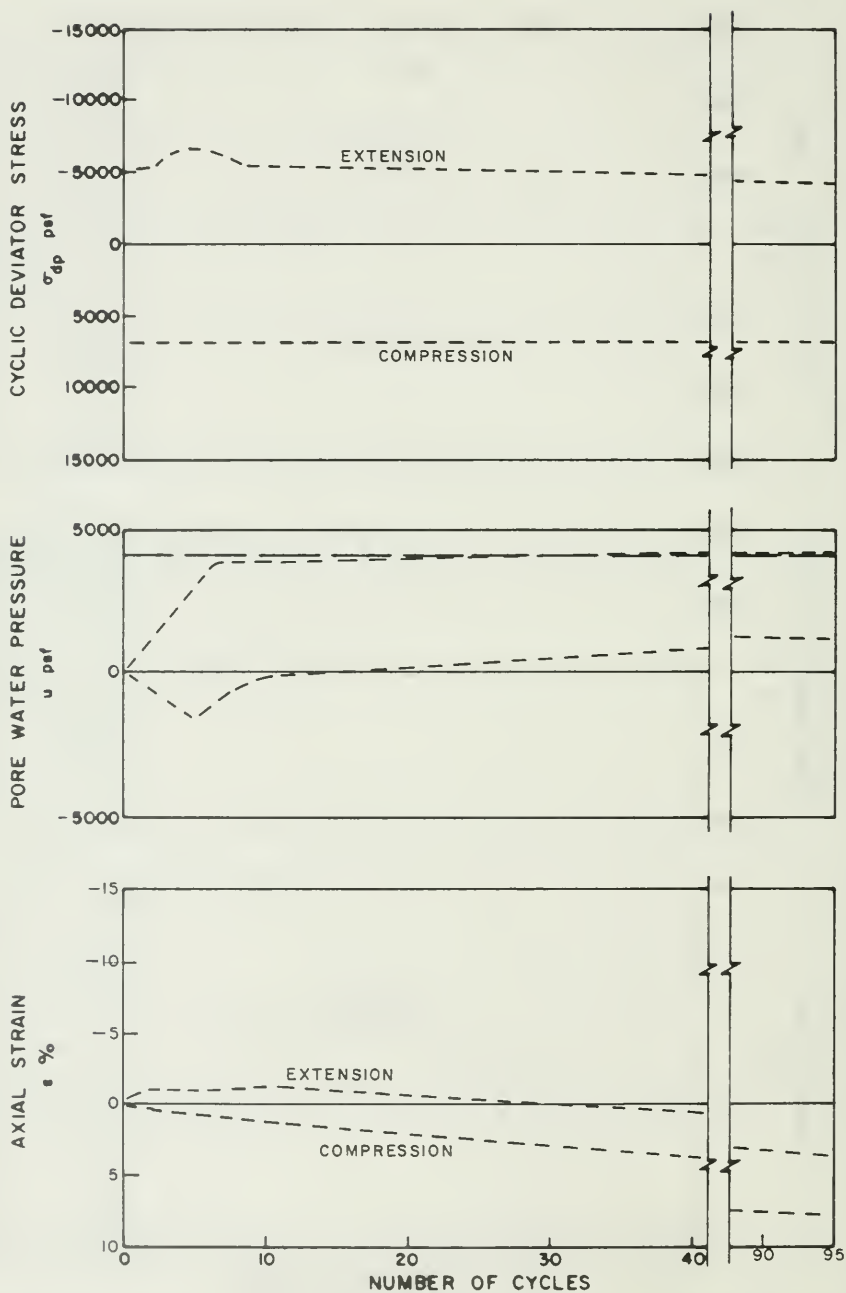


Figure G-64. Cyclic Test Envelopes for Test No. 77 ($\sigma'_{3c} = 4,100$ psf, $K_c = 1.5$)

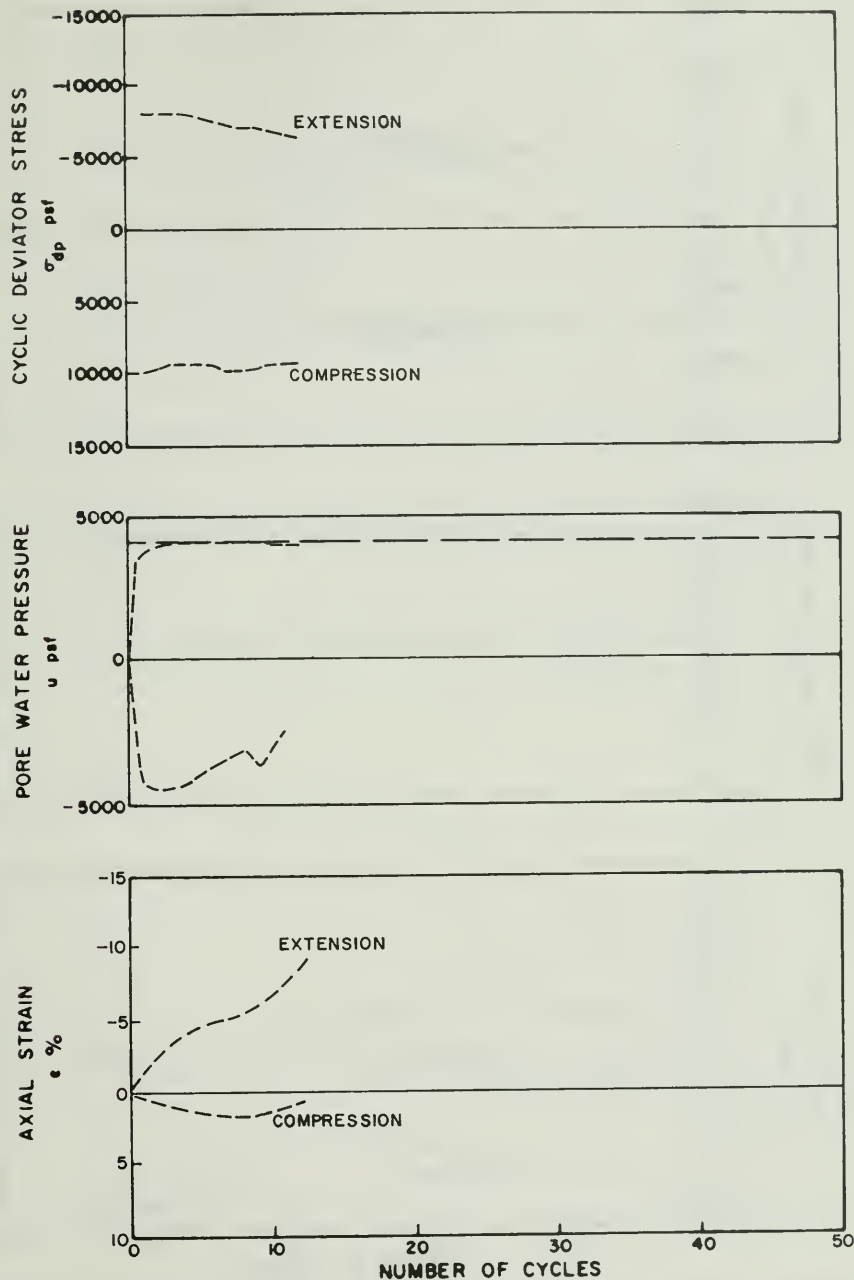


Figure G-65. Cyclic Test Envelopes for Test No. 78 ($\sigma'_{3c} = 4,100$ psf, $K_c = 1.5$)

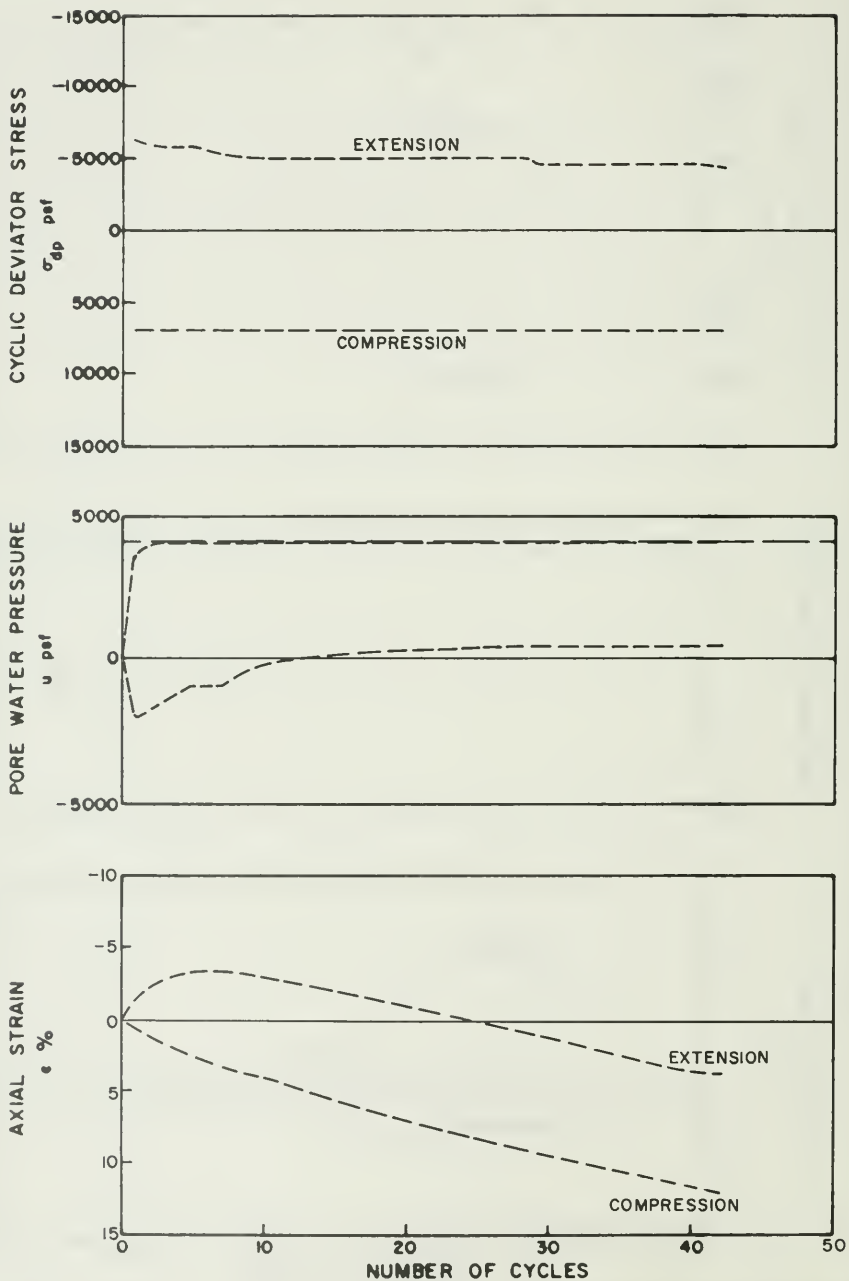


Figure G-66. Cyclic Test Envelopes for Test No. 79 ($\sigma'_{3c} = 4,100$ psf, $K_c = 1.5$)

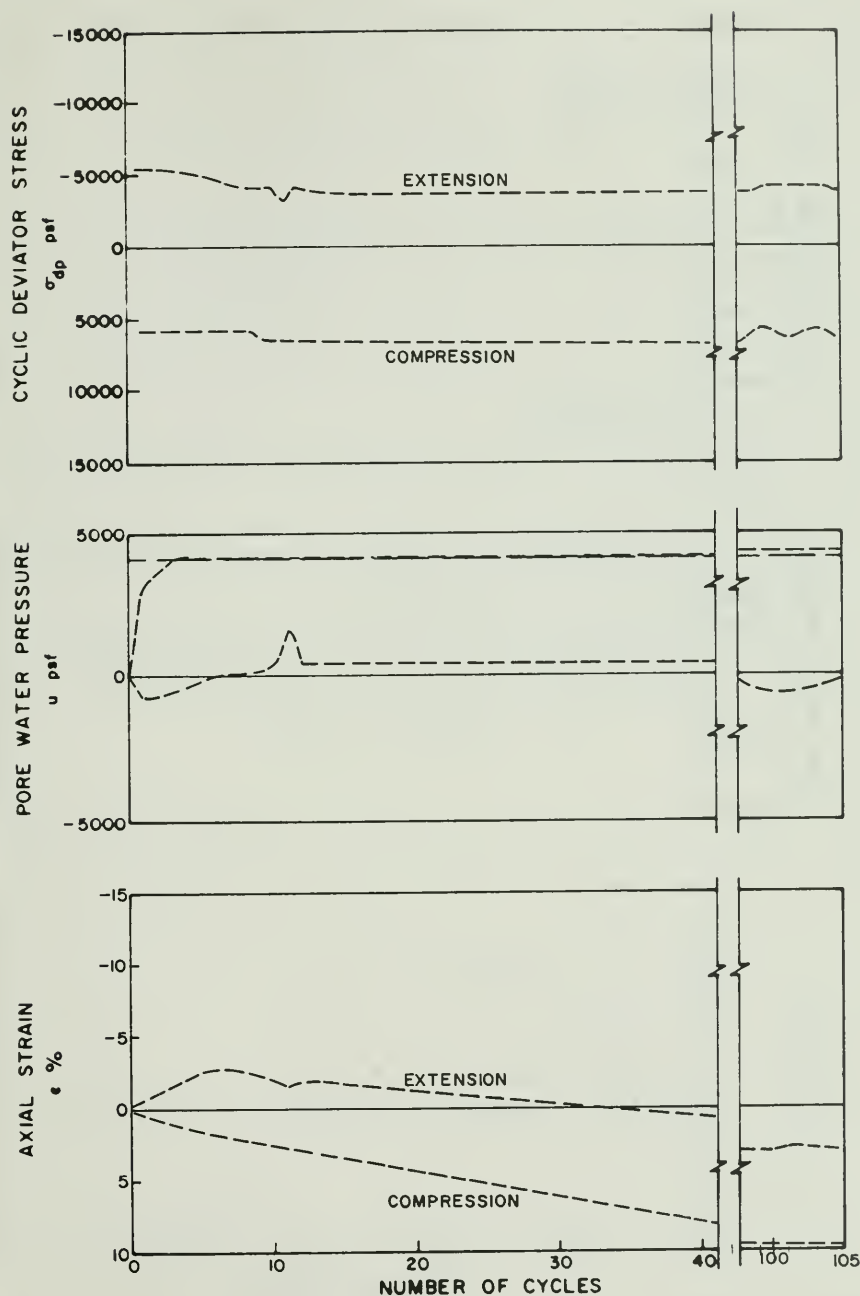


Figure G-67. Cyclic Test Envelopes for Test No. 80 ($\sigma'_{3c} = 4,100$ psf, $K_c = 1.5$)

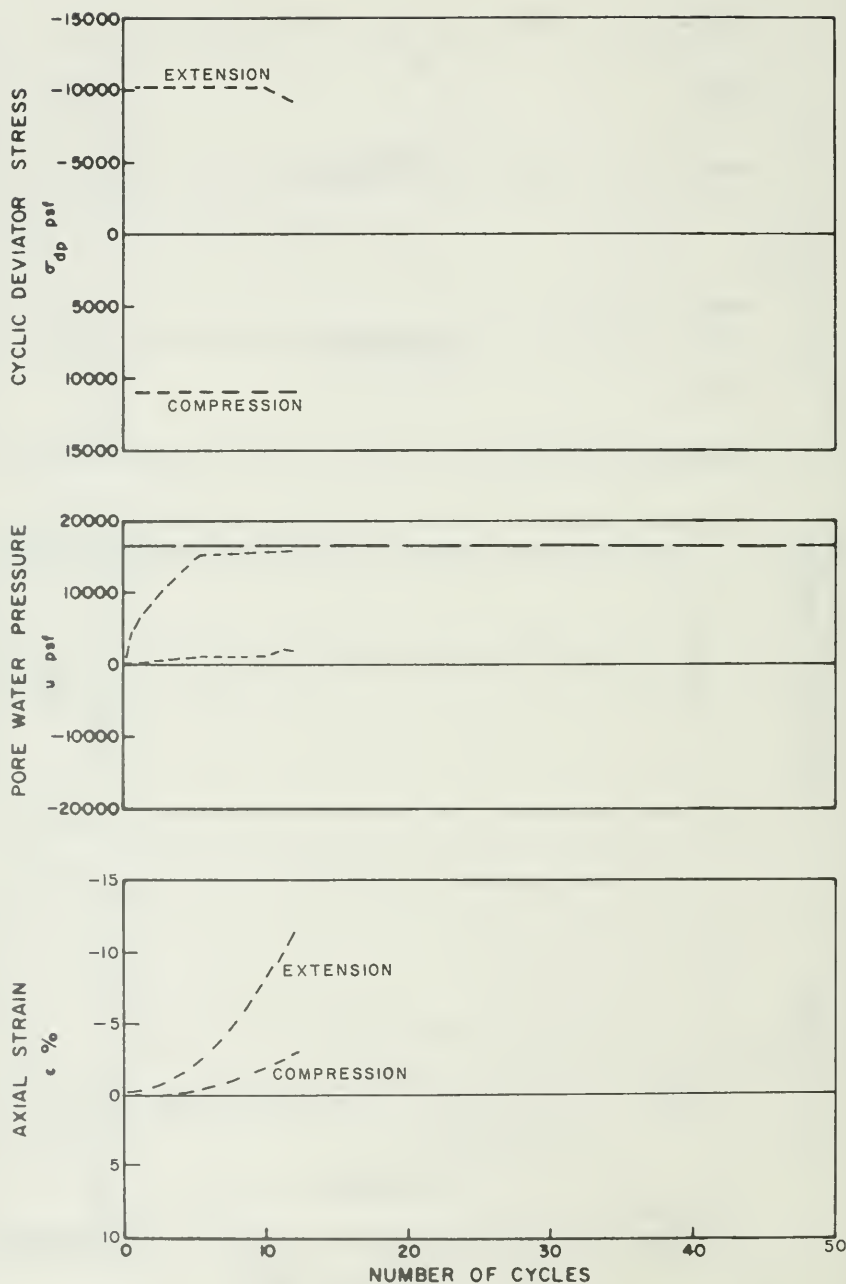


Figure G-68. Cyclic Test Envelopes for Test No. 81 ($\sigma'_{3c} = 16,400$ psf, $K_c = 1.0$)

APPENDIX H
EXTRAPOLATION OF ISOTROPICALLY-CONSOLIDATED CYCLIC
TRIAXIAL TESTS FOR STRENGTH INTERPRETATION II
(FIGS. H-1 THROUGH H-25)

APPENDIX H

EXTRAPOLATION OF ISOTROPICALLY-CONSOLIDATED CYCLIC TRIAXIAL TESTS FOR STRENGTH INTERPRETATION II

As described previously, the isotropically-consolidated test records were extrapolated to higher strain levels because of load attenuation and necking problems. These extrapolations were made conservative and are presented in the following figures. It should be noted that, although the extrapolations were intended to account for testing discrepancies, the straight line extrapolations were rather arbitrary and other extrapolations equally valid are possible. This strength interpretation is judged to be conservative because cyclic strain envelopes have a tendency to level off as cycling continues. A straight line extrapolation, therefore, can be considered relatively conservative.

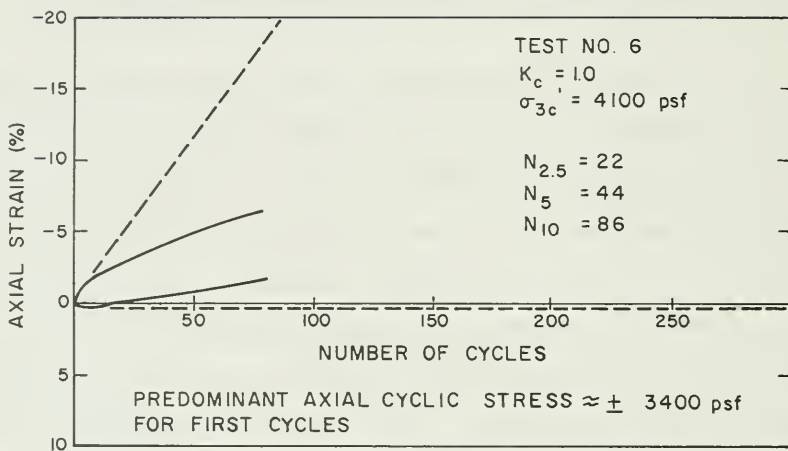


Figure H-1. Cyclic Triaxial Test No. 6

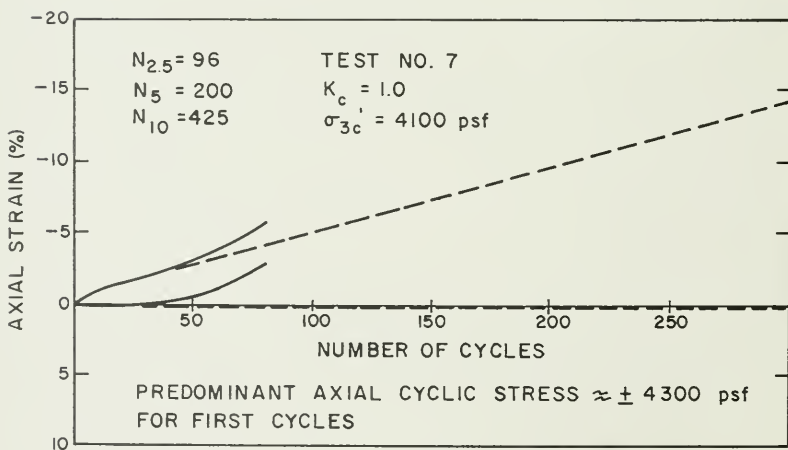


Figure H-2. Cyclic Triaxial Test No. 7

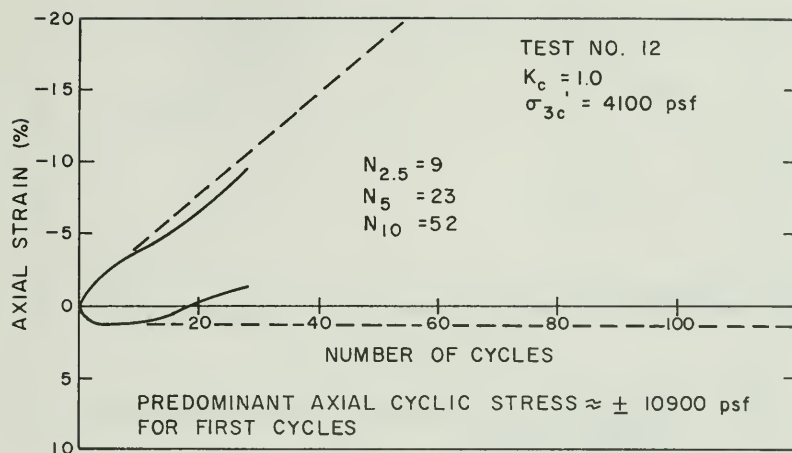


Figure H-3. Cyclic Triaxial Test No. 12

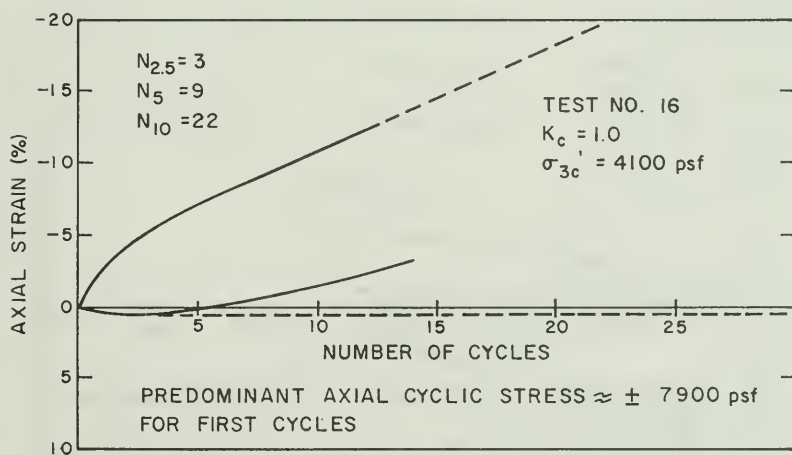


Figure H-4. Cyclic Triaxial Test No. 16

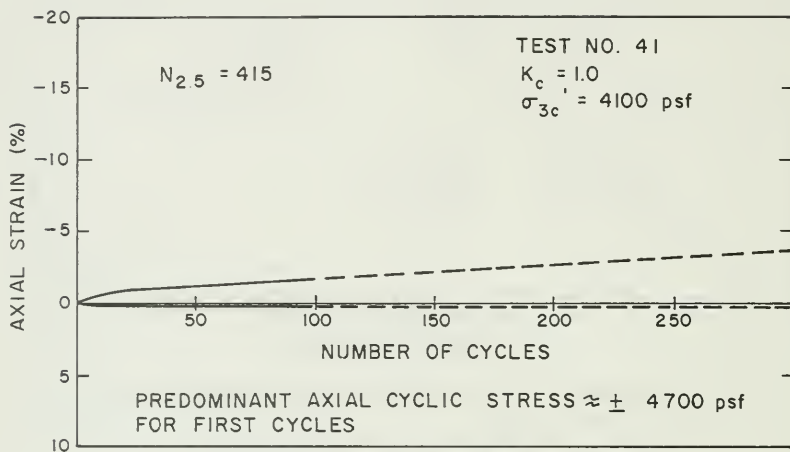


Figure H-5. Cyclic Triaxial Test No. 41

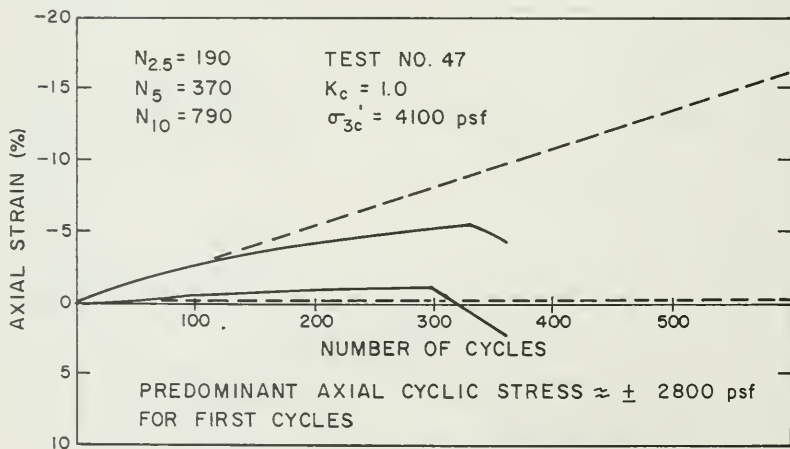


Figure H-6. Cyclic Triaxial Test No. 47

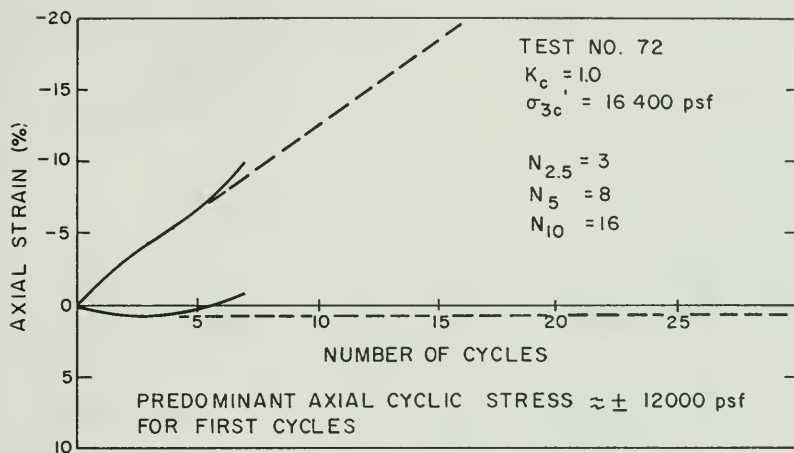


Figure H-7. Cyclic Triaxial Test No. 72

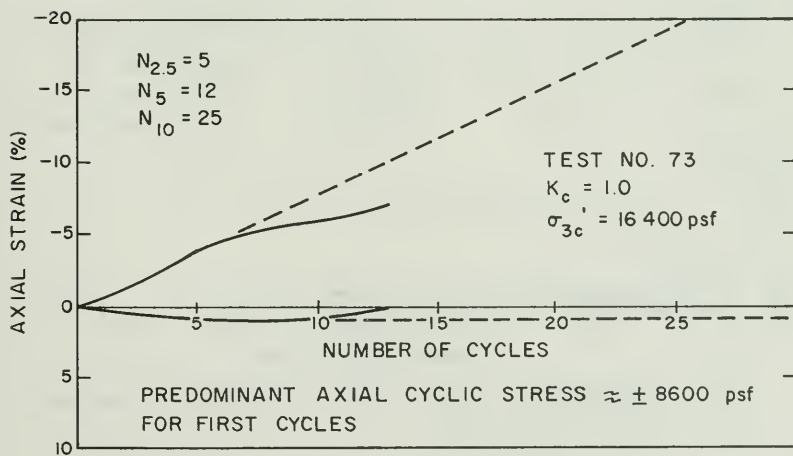


Figure H-8. Cyclic Triaxial Test No. 73

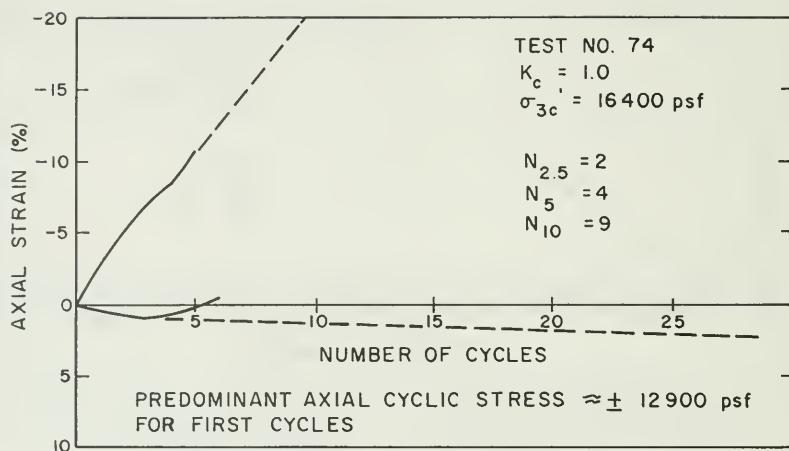


Figure H-9. Cyclic Triaxial Test No. 74

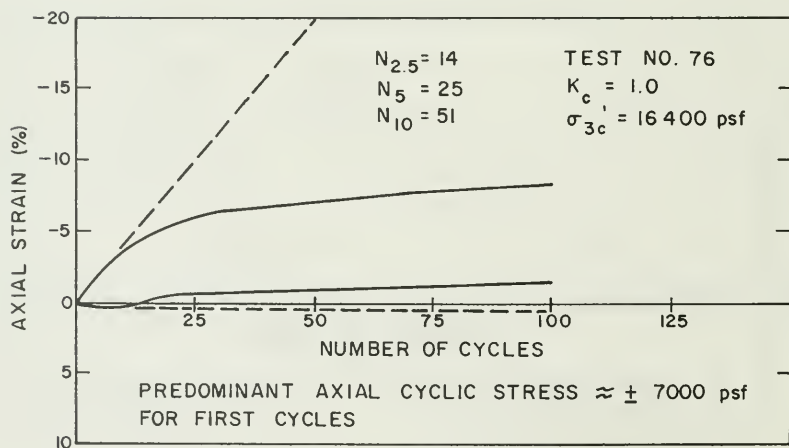


Figure H-10. Cyclic Triaxial Test No. 76

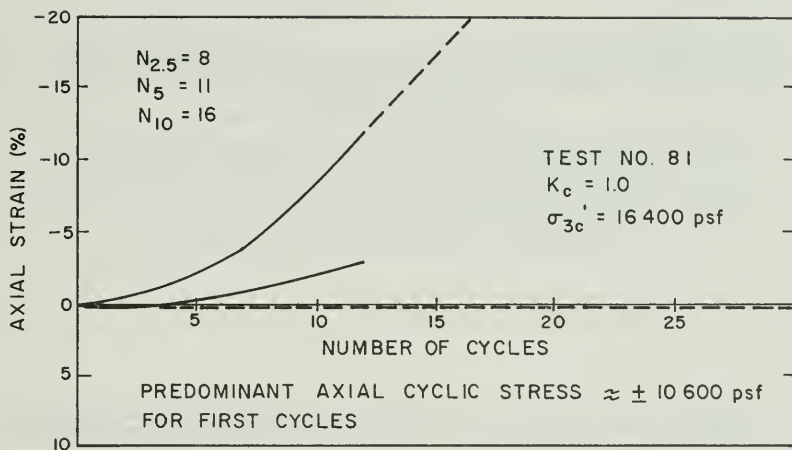


Figure H-11. Cyclic Triaxial Test No. 81

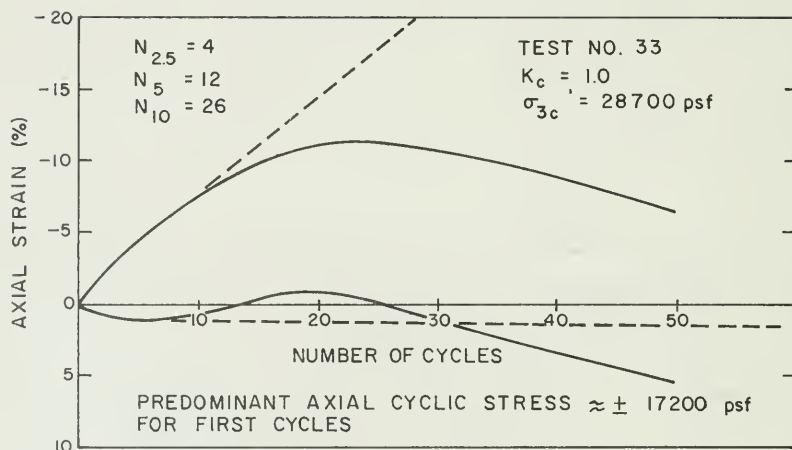


Figure H-12. Cyclic Triaxial Test No. 33

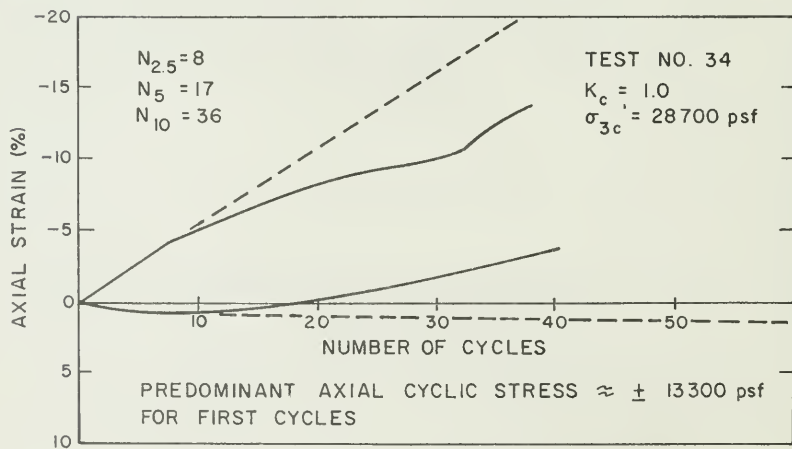


Figure H-13. Cyclic Triaxial Test No. 34

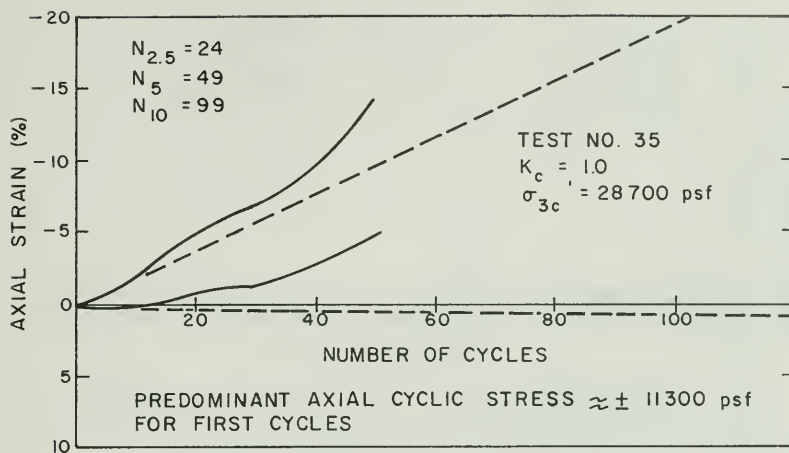


Figure H-14. Cyclic Triaxial Test No. 35

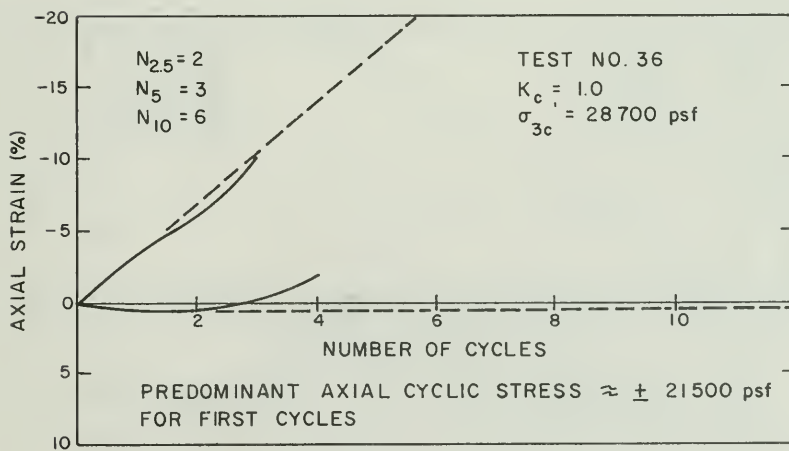


Figure H-15. Cyclic Triaxial Test No. 36

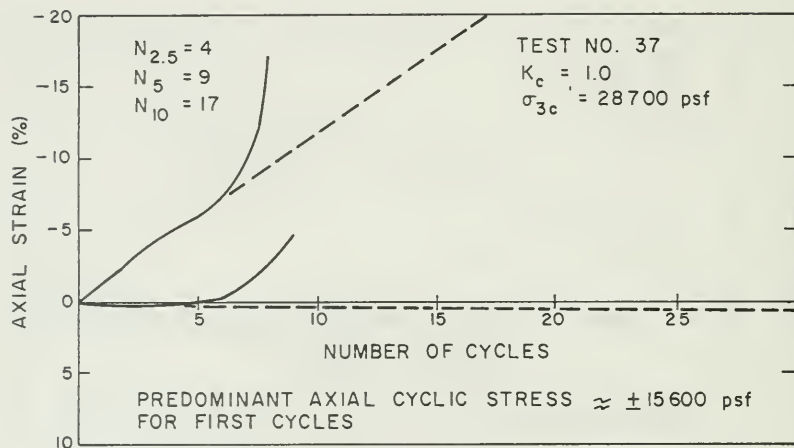


Figure H-16. Cyclic Triaxial Test No. 37

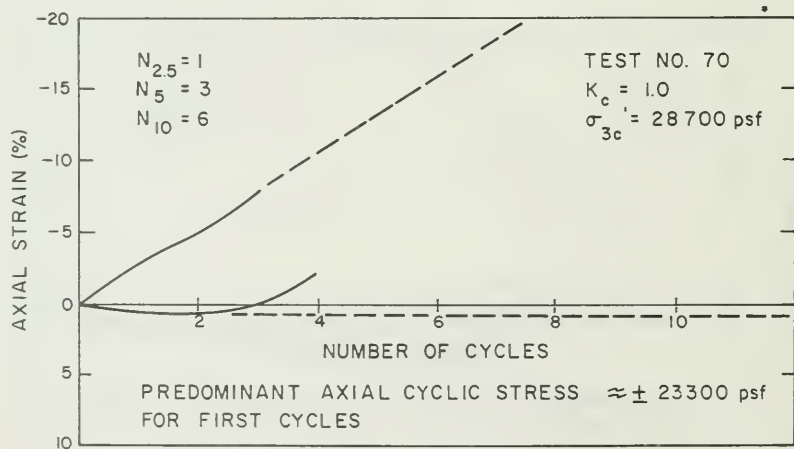


Figure H-17. Cyclic Triaxial Test No. 70

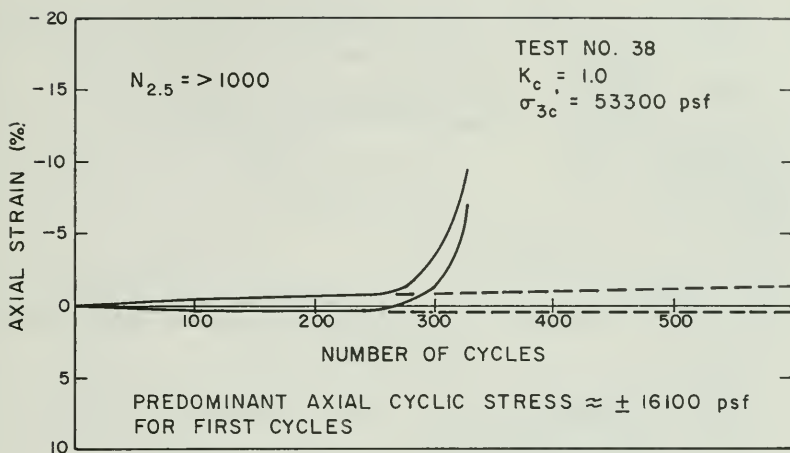


Figure H-18. Cyclic Triaxial Test No. 38

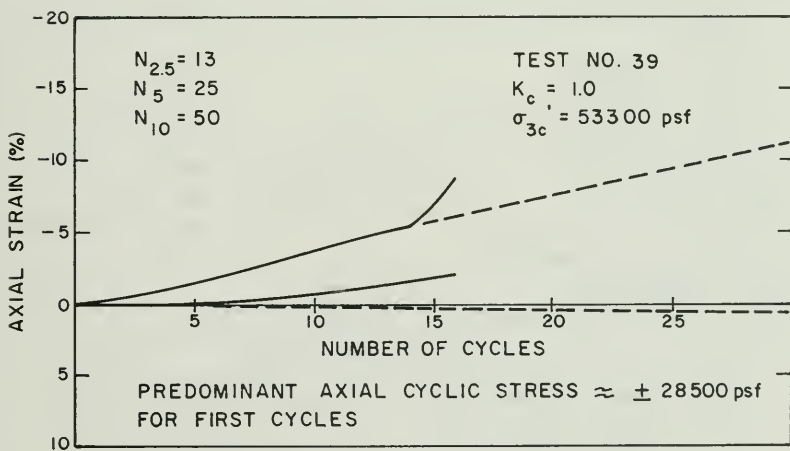


Figure H-19. Cyclic Triaxial Test No. 39

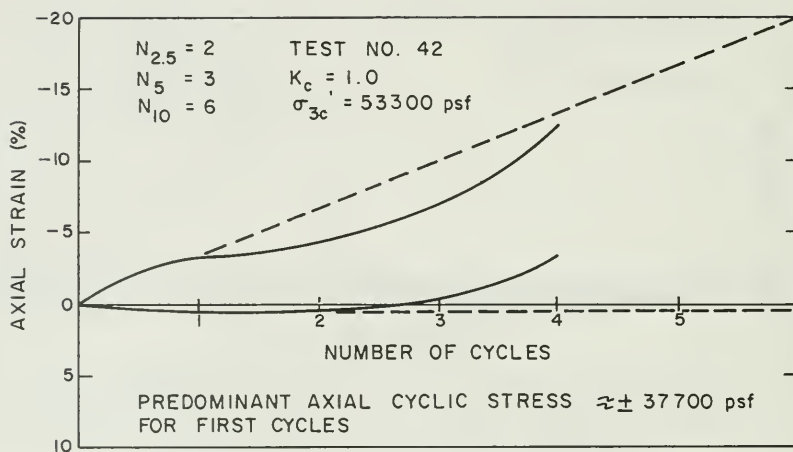


Figure H-20. Cyclic Triaxial Test No. 42

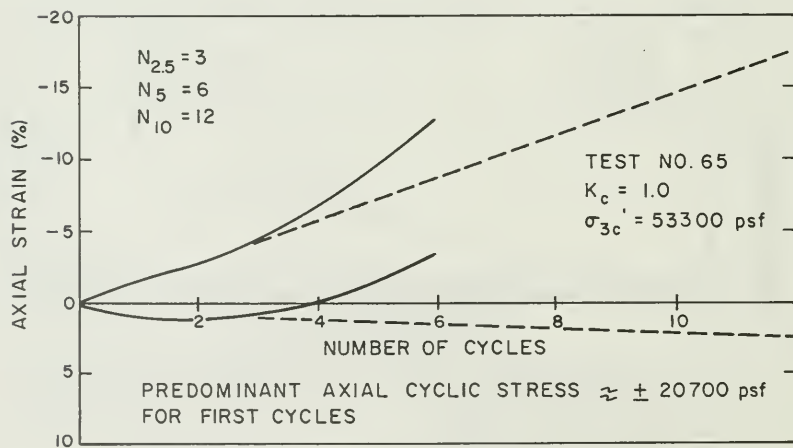


Figure H-21. Cyclic Triaxial Test No. 65

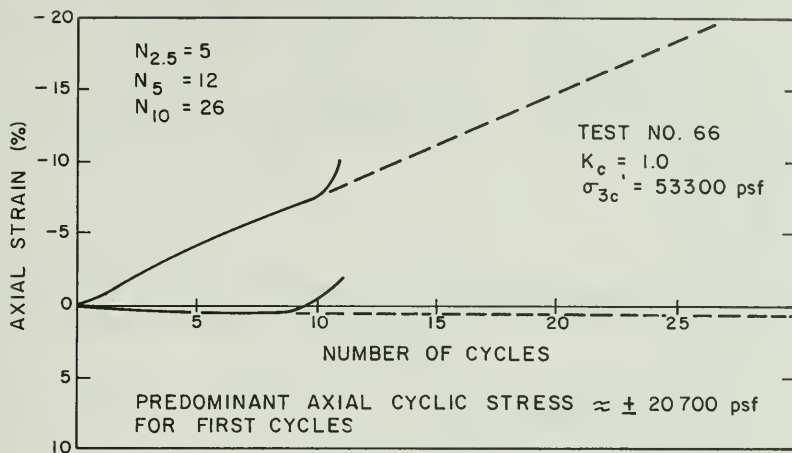


Figure H-22. Cyclic Triaxial Test No. 66

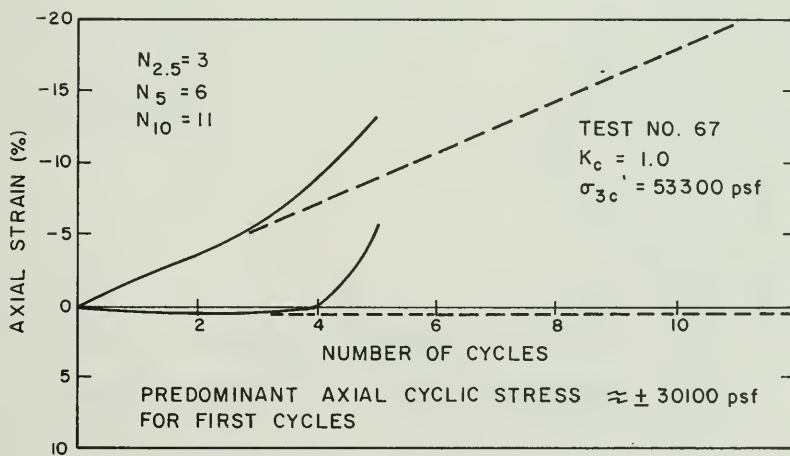


Figure H-23. Cyclic Triaxial Test No. 67

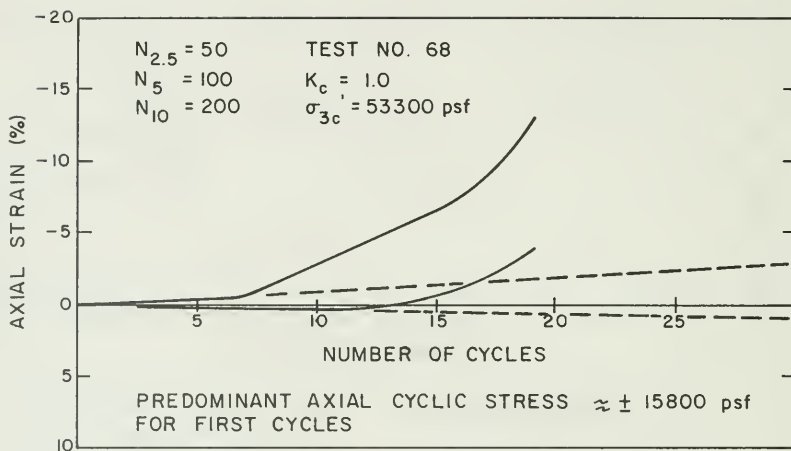


Figure H-24. Cyclic Triaxial Test No. 68

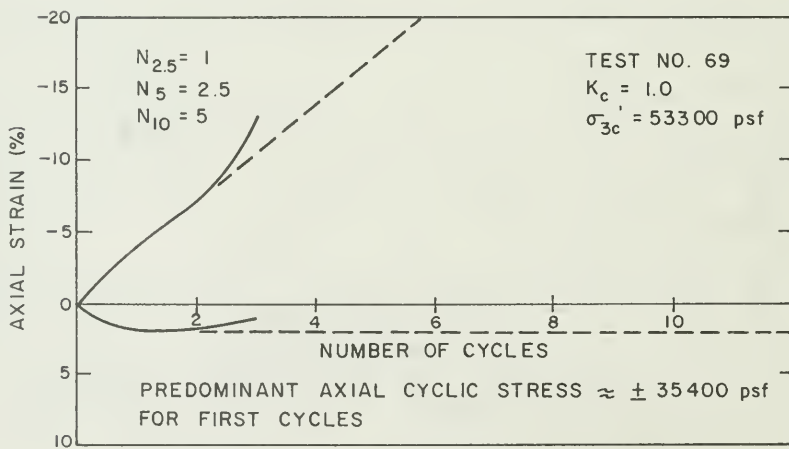


Figure H-25. Cyclic Triaxial Test No. 69

APPENDIX I

CYCLIC TRIAXIAL TEST RESULTS FOR MODELED OROVILLE GRAVEL USING STRENGTH INTERPRETATION II

Figures I-1 through I-10 are cyclic test results employing strength interpretation II.

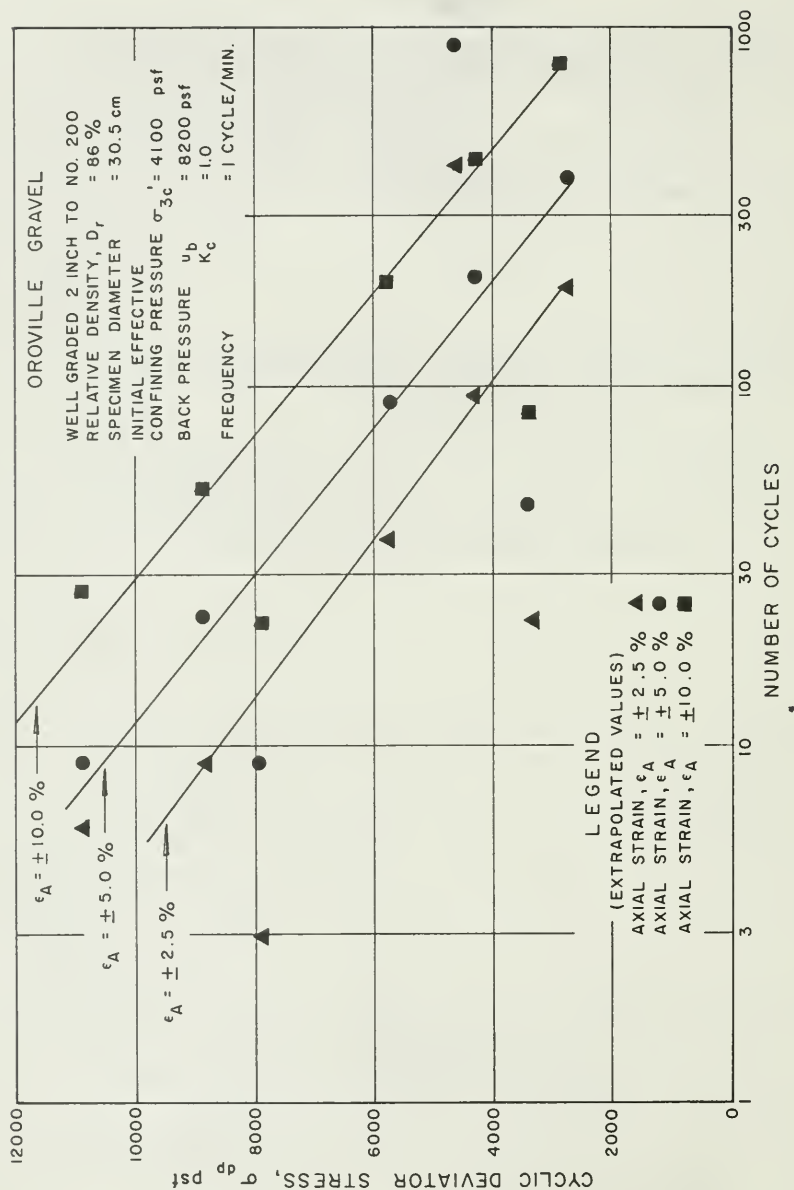


Figure I-1. Cyclic Triaxial Test Results (σ'_{3c} = 4,100 psf, K_c = 1.0)

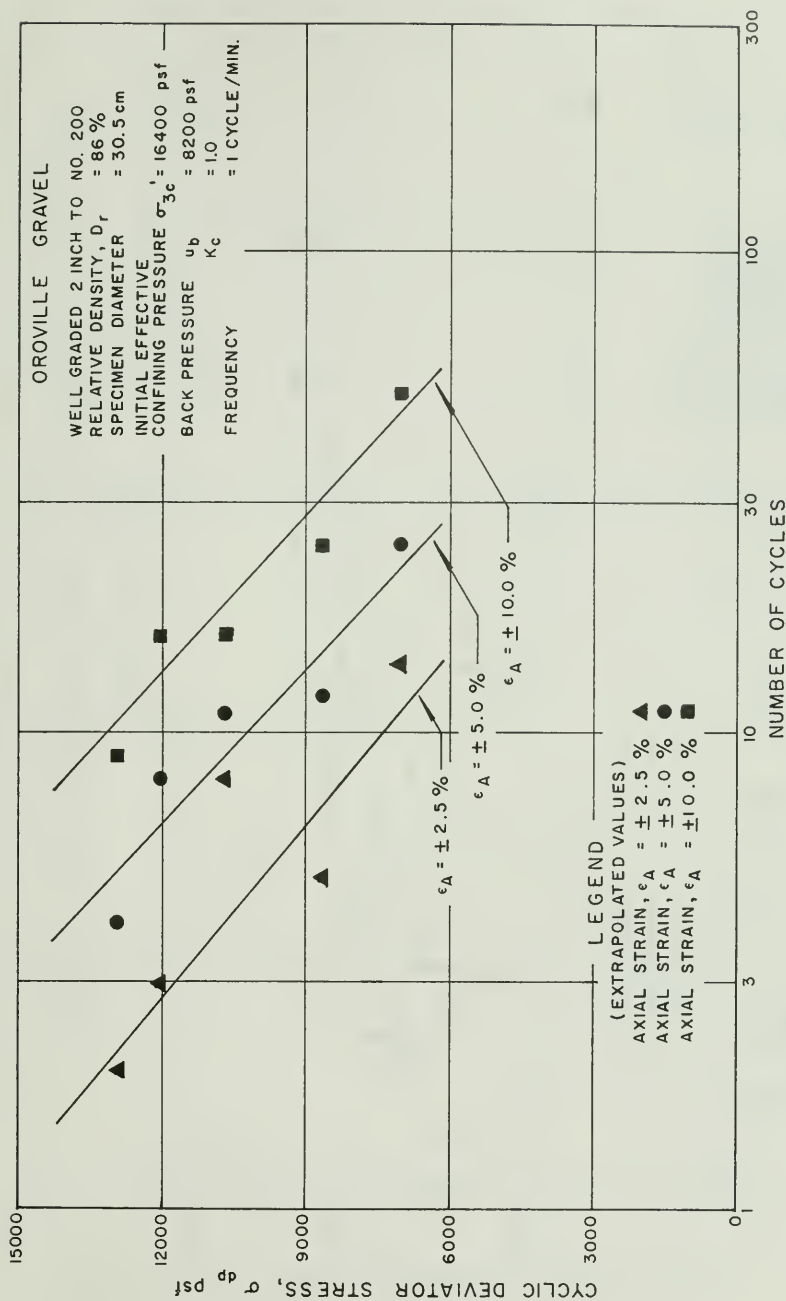


Figure I-2. Cyclic Triaxial Test Results (σ'_{3c} = 16,400 psf, K_c = 1.0)

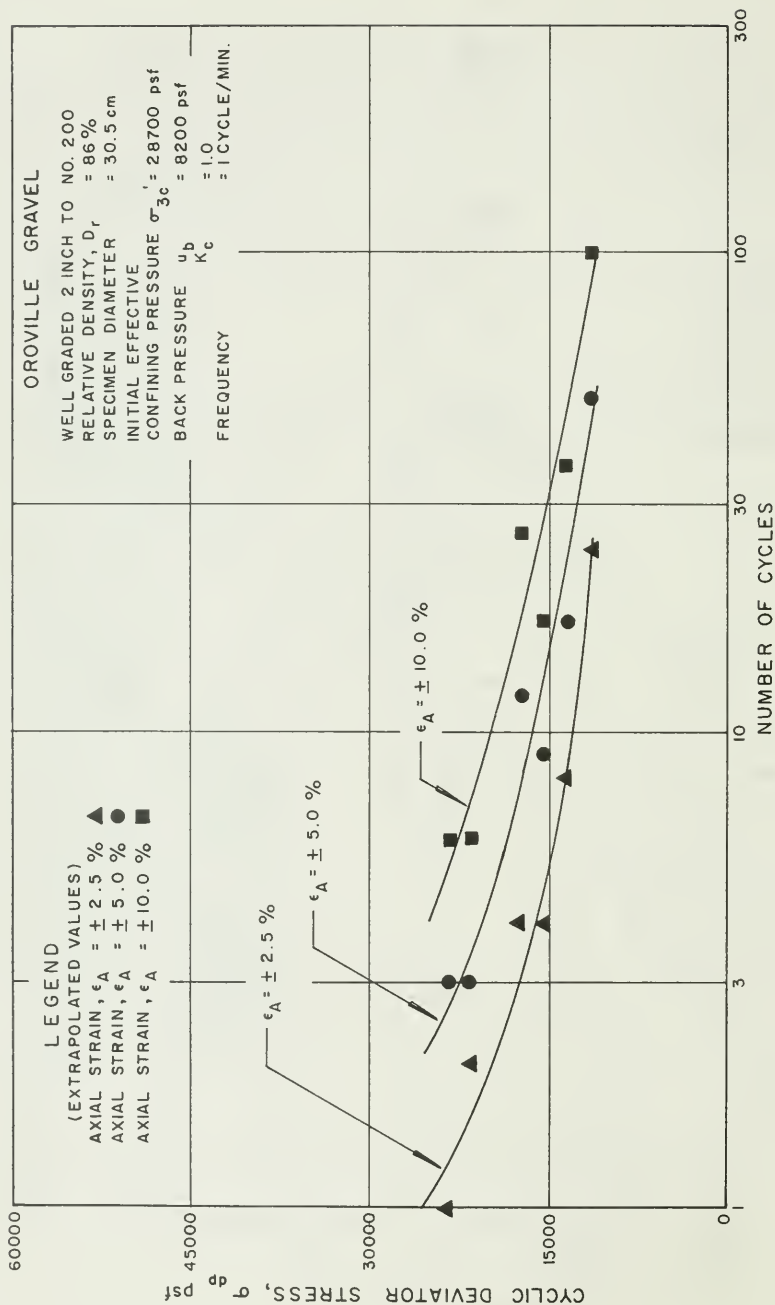


Figure 1-3. Cyclic Triaxial Test Results ($\sigma'_{3c} = 28,700$ psf, $K_c = 1.0$)

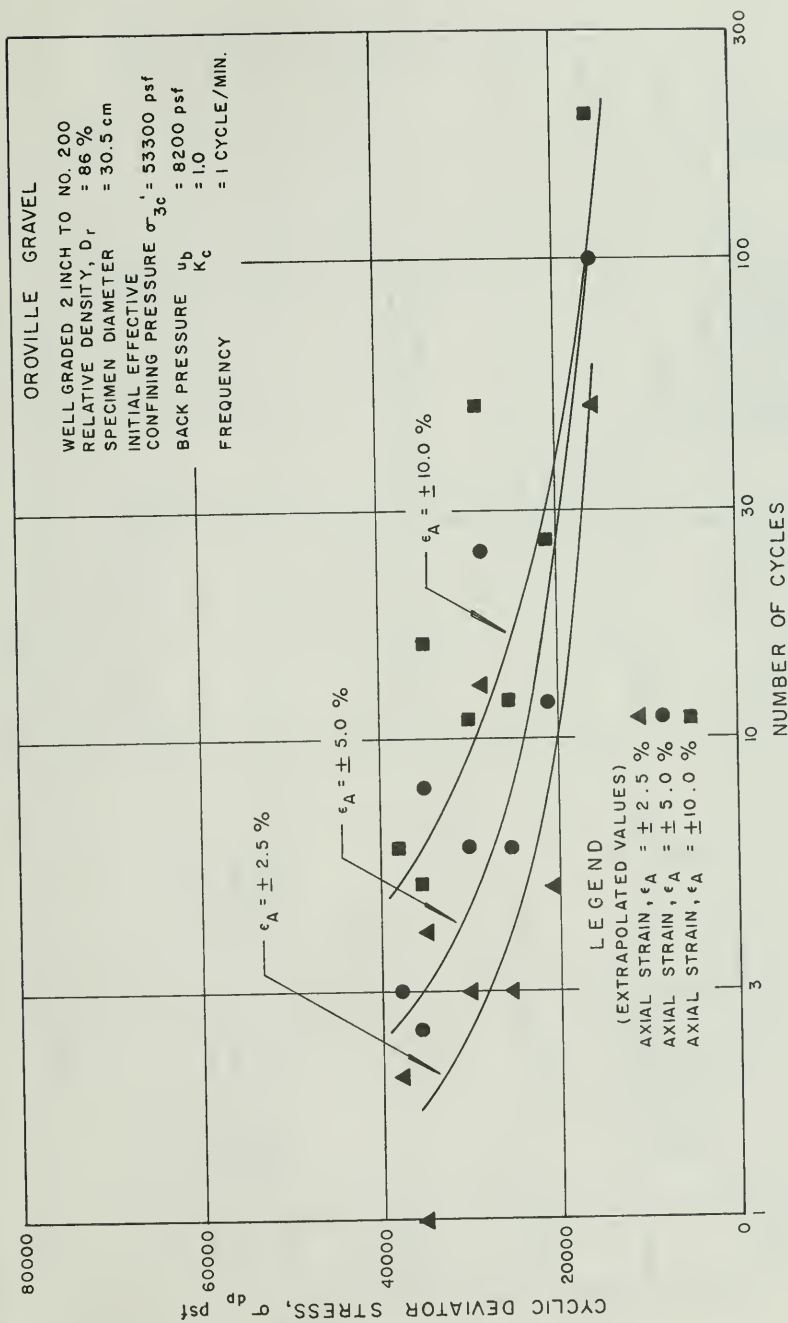


Figure I-4. Cyclic Triaxial Test Results (σ'_{3c} = 53,300 psf, K_c = 1.0)

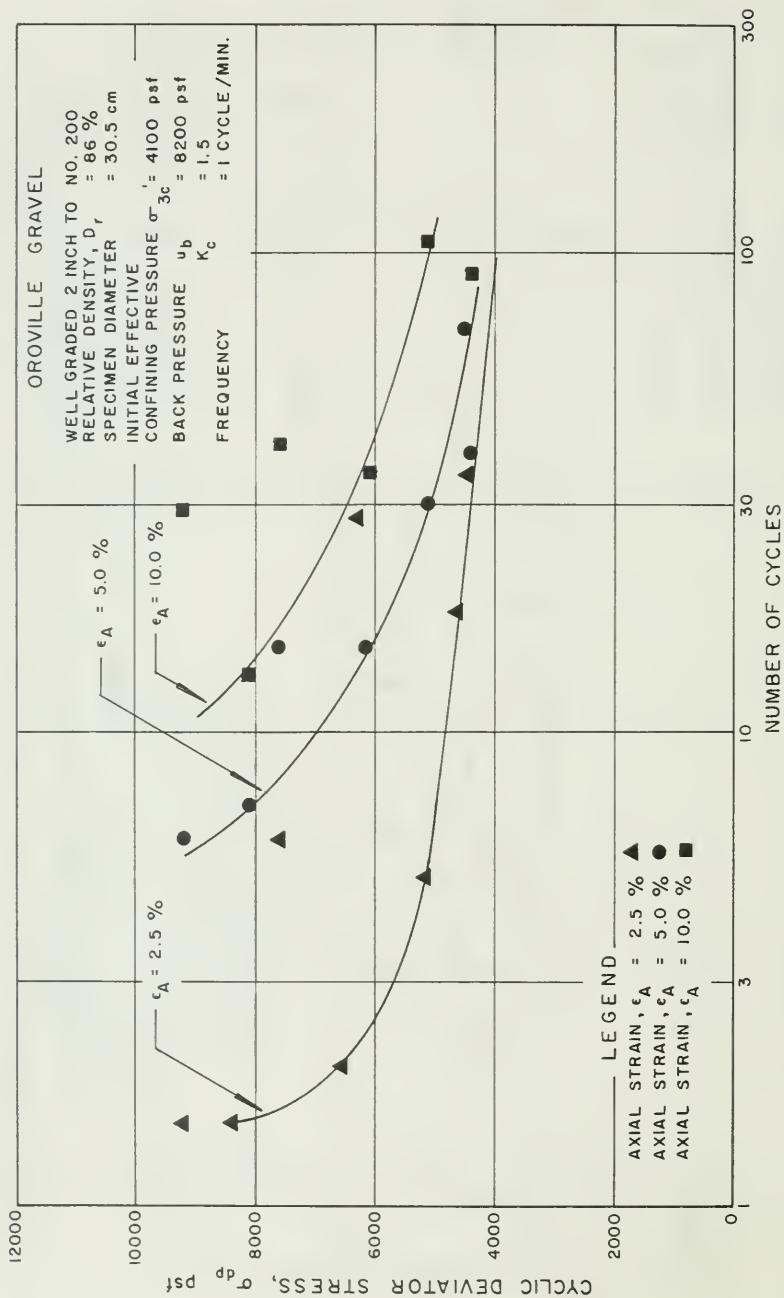


Figure I-5. Cyclic Triaxial Test Results ($\sigma'_{3c} = 4,100$ psf, $K_c = 1.5$)

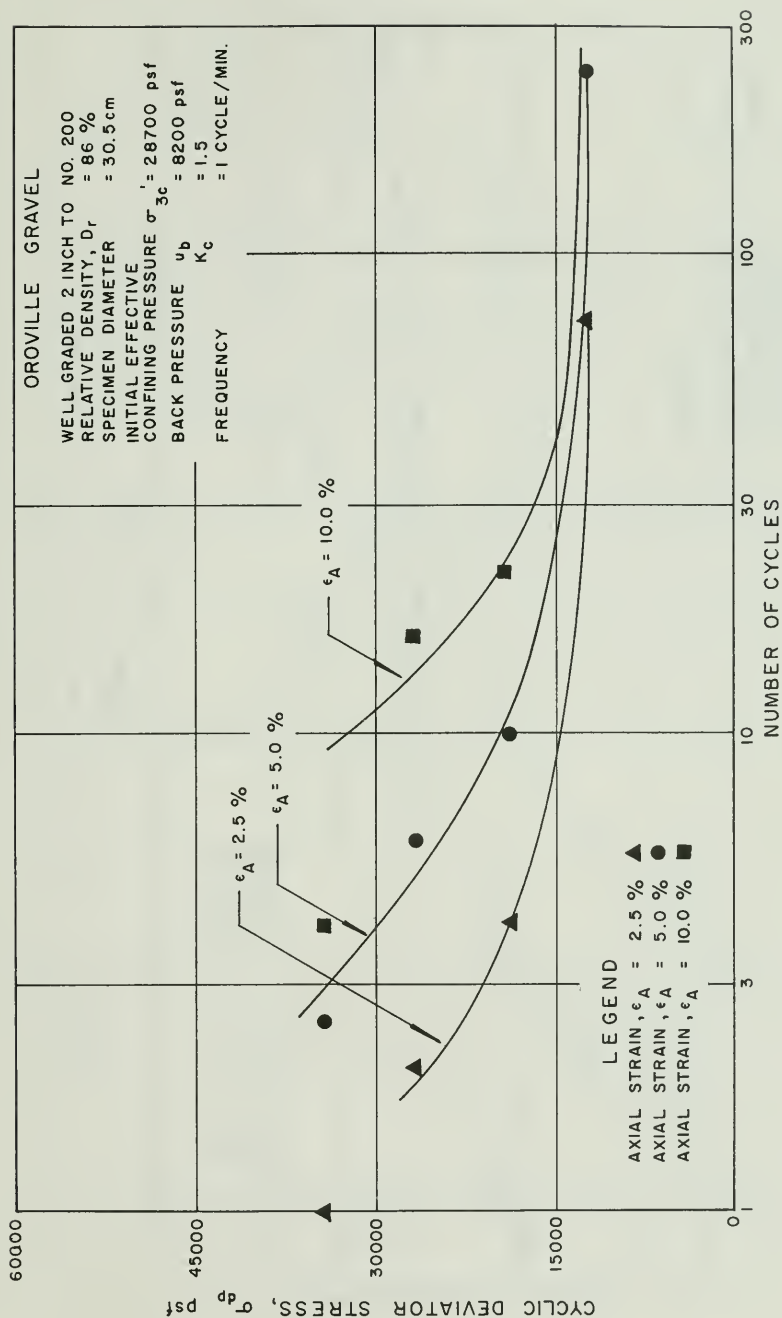


Figure I-6. Cyclic Triaxial Test Results (σ'_{3c} = 28,700 psf, K_c = 1.5)

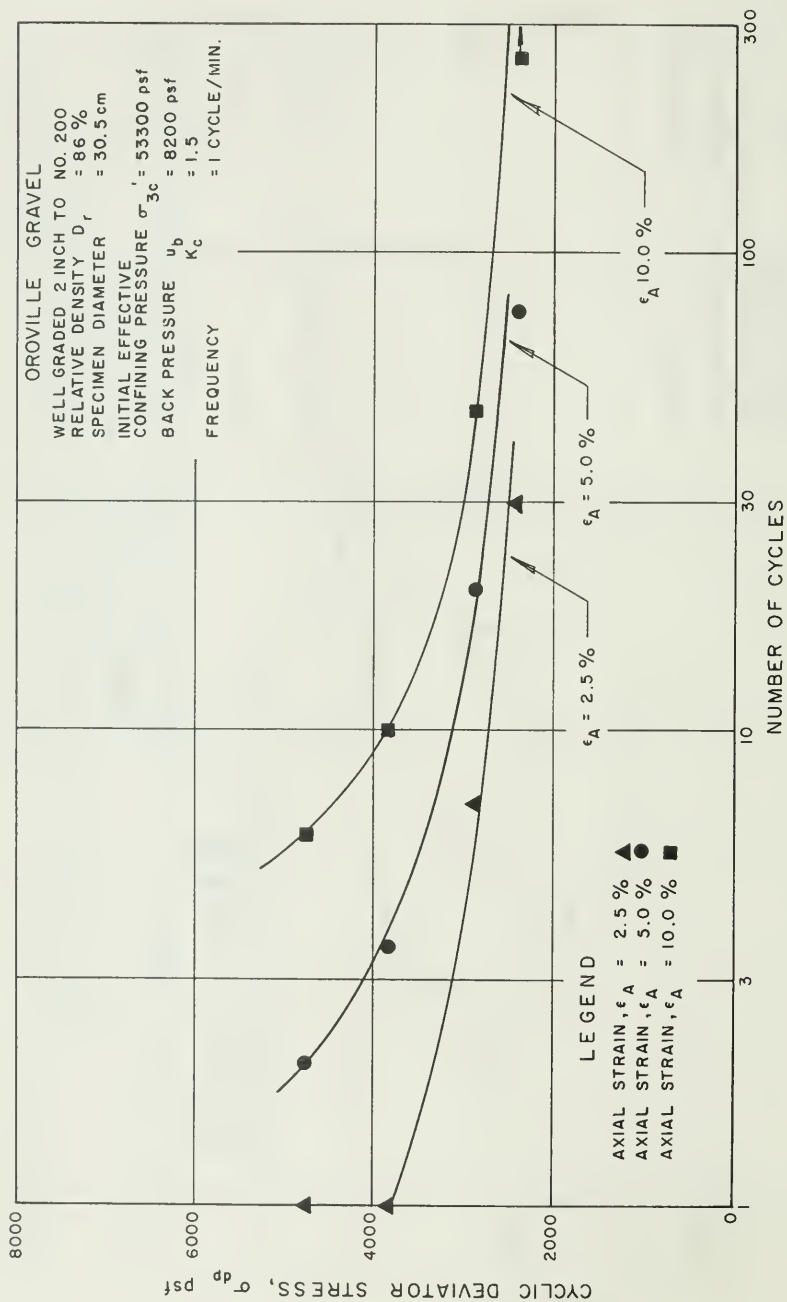


Figure I-7. Cyclic Triaxial Test Results ($\sigma'_{3c} = 53,300 \text{ psf}$, $K_c = 1.5$)

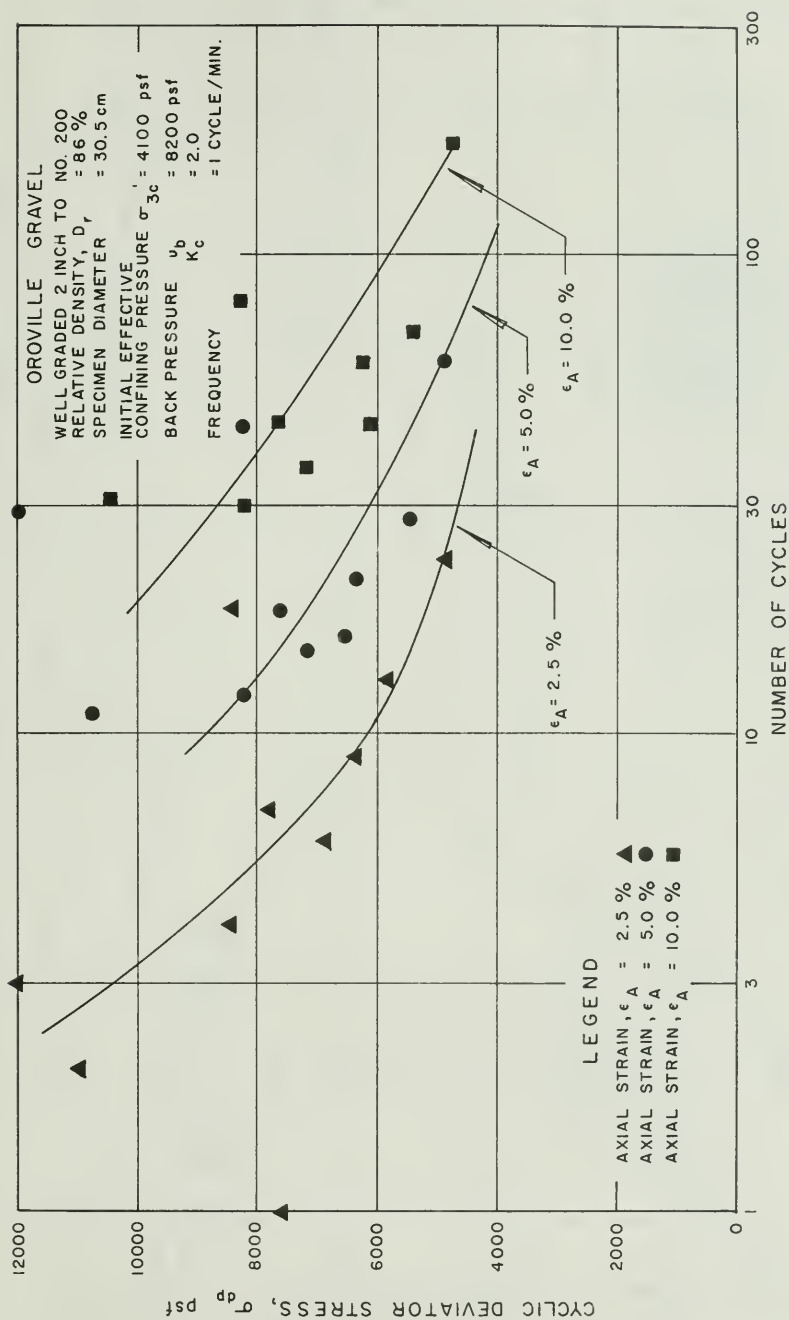


Figure I-8. Cyclic Triaxial Test Results (σ'_{3c} = 4,100 psf, K_c = 2.0)

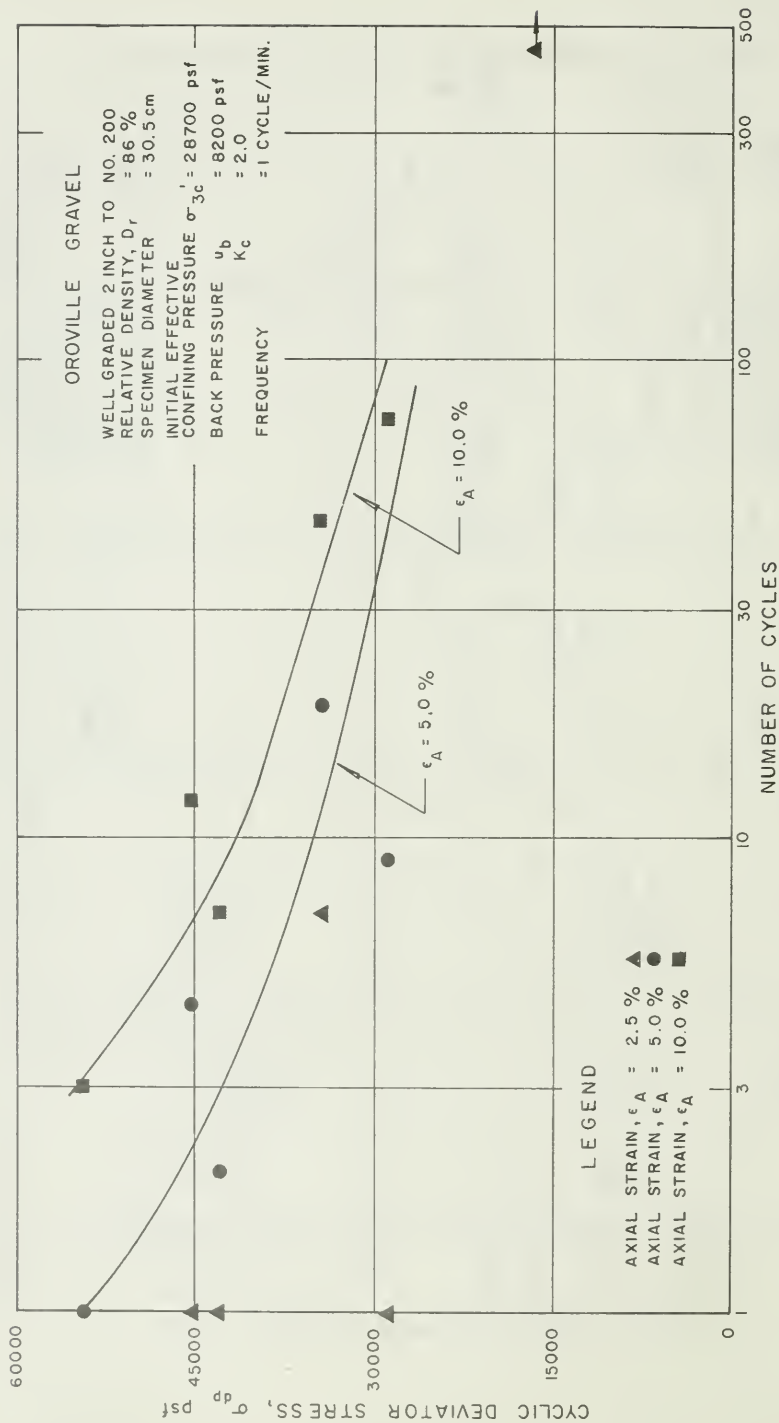


Figure I-9. Cyclic Triaxial Test Results (σ'_{3c} = 28,700 psf, K_c = 2.0)

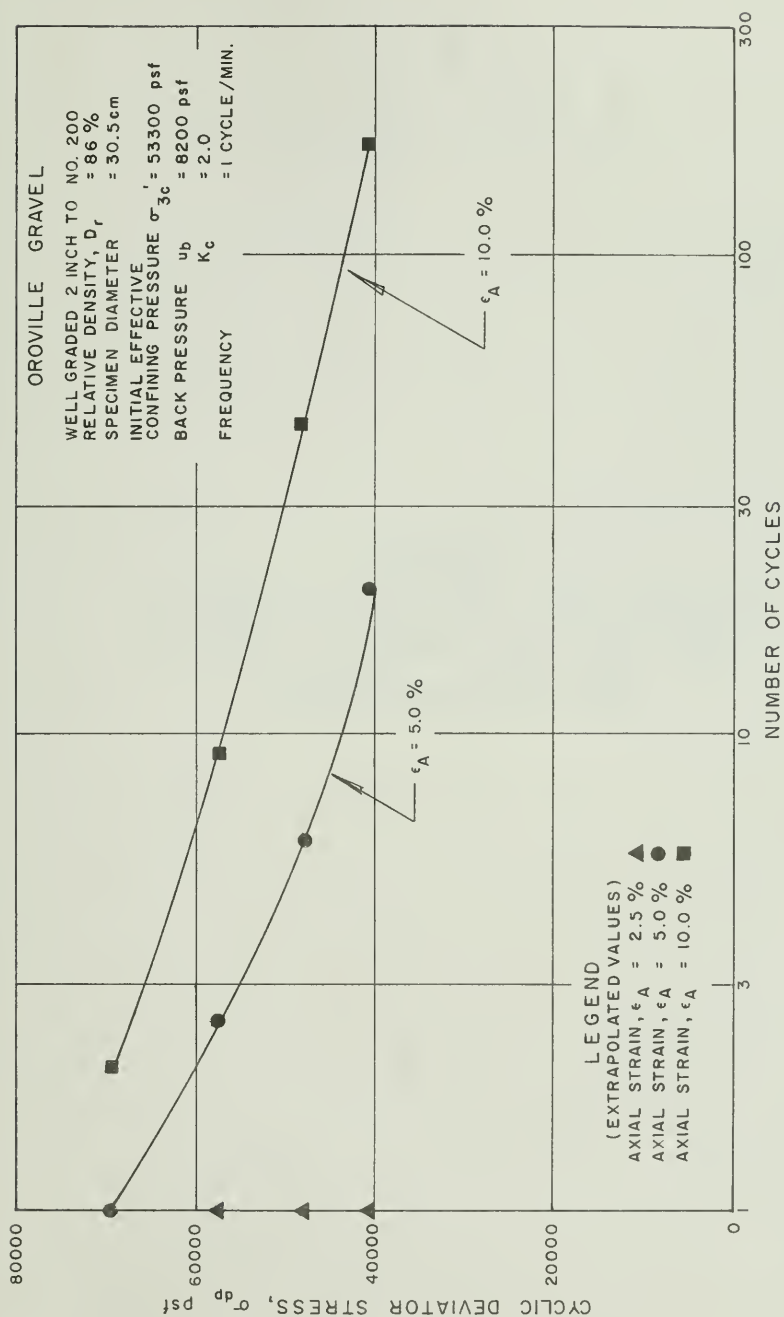


Figure I-10. Cyclic Triaxial Test Results ($\sigma'_{3c} = 53,300\text{ psf}$, $K_c = 2.0$)

APPENDIX J

PROCEDURE FOR INTERPRETING CYCLIC TRIAXIAL
TEST DATA TO DETERMINE CYCLIC SHEAR STRESS
ON POTENTIAL FAILURE PLANE

APPENDIX J

PROCEDURE FOR INTERPRETING CYCLIC TRIAXIAL TEST DATA TO DETERMINE CYCLIC SHEAR STRESS ON POTENTIAL FAILURE PLANE

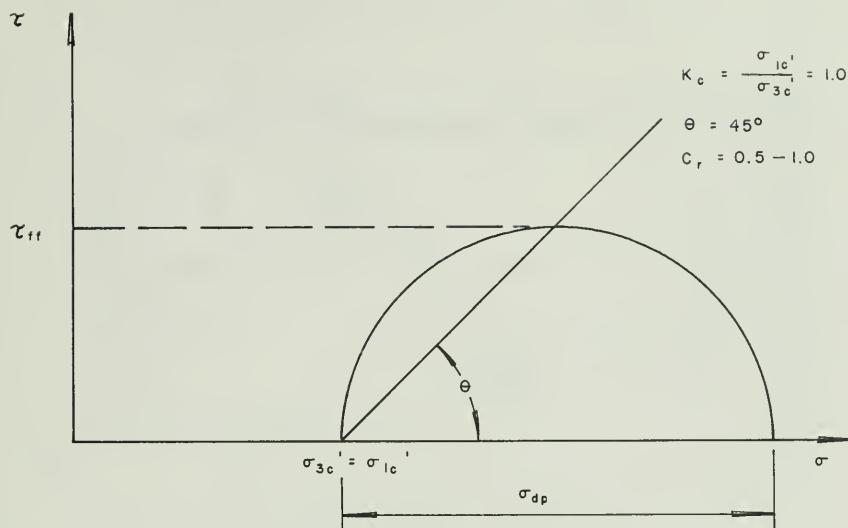
Current procedures in evaluating the dynamic strength of an embankment utilize cyclic strength test data to assess the strain potential of each individual soil element. The dynamic strength of the soil would be dependent upon the stress conditions existing on the potential failure plane prior to seismic loading. The dynamic strength of a soil element would be determined by the performance of a laboratory specimen which duplicated the static shear and normal stresses on the failure plane. A fundamental assumption is that the horizontal planes within an embankment are the most critical from a viewpoint of seismic stability. To represent the static stress conditions on the failure plane in the field, the static vertical normal stress (σ_y) and the alpha (α) value are used. The alpha value is defined as the ratio of the initial static shear stress, τ_{fc} , divided by the static normal stress, σ_{fc} , on the failure plane.

The potential failure planes in a triaxial sample are assumed to be dependent upon the consolidation stress ratio (K_c) of the sample. For isotropically-consolidated samples ($K_c = 1.0$) the failure planes are assumed to incline 45° from the horizontal. Failure planes for anisotropically-consolidated samples are assumed to incline $45^\circ + \phi'/2$ to the horizontal. To obtain the current stress conditions required to cause a specified amount of failure in a particular number of cycles,

Δp , Mohr's circle relationships must be employed. These relationships are used to determine both the initial static stresses and the superimposed cyclic stresses on the failure plane in the sample. The procedures for both isotropically-consolidated and anisotropically-consolidated triaxial samples are shown in Figures J-1 and J-2.

As discussed previously in the main text, the cyclic stresses in the cyclic triaxial test must be modified by the C_r correction. This correction is assumed to be unity for consolidation stress ratios (K_c) of 1.5 or greater. For isotropically-consolidated triaxial samples, C_r can range from 0.5 to 1.0 depending upon the field K_o value. For the isotropically-consolidated cyclic triaxial tests carried out for the modeled Oroville gravels, a C_r value of 0.6 was used.

A fairly large testing program was carried out for the modeled Oroville gravel. Because of this, sufficient data were generated to assess most static stress conditions within the embankment. The cyclic strength is plotted as the cyclic shear stress required to cause a particular failure criterion in a specified number of cycles for a range of consolidation stresses. The shear strength envelopes for five percent compressive strain in ten cycles is presented for illustration in Figure J-3.



$$\sigma_{fc} = \sigma_{3c'}$$

$$\tau_{fc} = 0.0$$

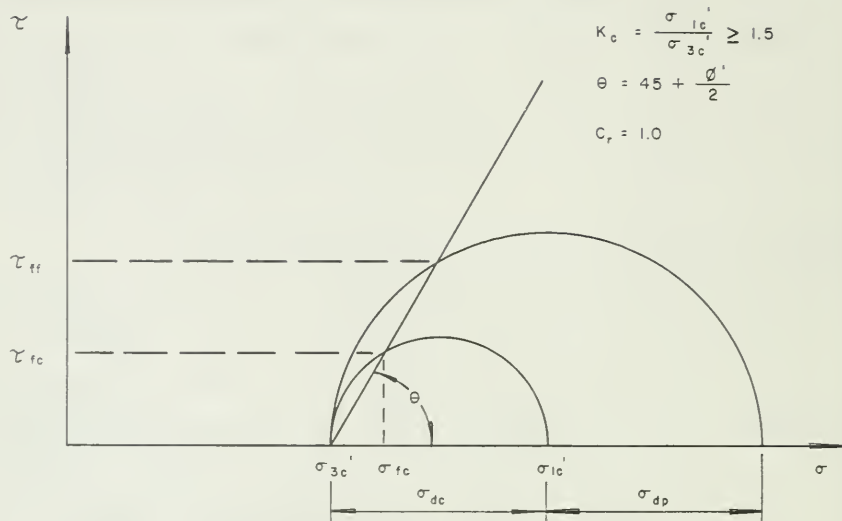
$$\Delta \tau_p = \tau_{ff} * C_r$$

$$\Delta \tau_p = C_r * \frac{\sigma_{dp}}{2}$$

$$\alpha = \frac{\tau_{fc}}{\sigma_{fc}} = 0.0$$

$$\tau_{ff} = \frac{\sigma_{dp}}{2}$$

Figure J-1. Procedure for Interpreting Cyclic Triaxial Test Data for Isotropically-Consolidated ($K_c=1.0$)



$$\sigma_{fc} = \frac{\sigma_{3c}'}{2} \left[(K_c + 1) - (K_c - 1) \cos (180 - 2\theta) \right]$$

$$\tau_{fc} = \frac{\sigma_{3c}'}{2} \left[(K_c - 1) \sin (180 - 2\theta) \right]$$

$$\alpha = \frac{\tau_{fc}}{\sigma_{fc}} = \frac{(K_c - 1) \sin (180 - 2\theta)}{\left[(K_c + 1) - (K_c - 1) \cos (180 - 2\theta) \right]}$$

$$\tau_{ff} = \left(\frac{1}{2} \right) \left[\sigma_{3c}' (K_c - 1) + \sigma_{dc} \right] \sin (180 - 2\theta)$$

$$\Delta \tau_p = \tau_{ff} - \tau_{fc}$$

$$\Delta \tau_p = \frac{\sigma_{dp}}{2} \sin (180 - 2\theta)$$

Figure J-2. Procedure for Interpreting Cyclic Triaxial Test Data for Anisotropically-Consolidated ($K_c=1.0$)

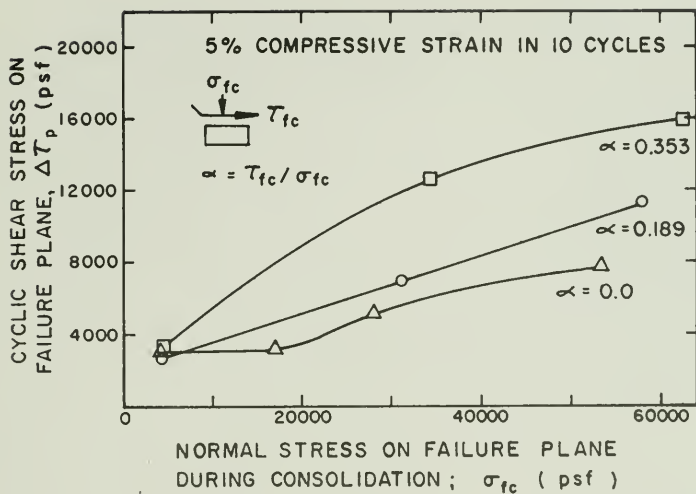


Figure J-3. Cyclic Strength Envelopes for Five Percent Compressive Strain in Ten Cycles

APPENDIX K

CYCLIC TRIAXIAL TEST RESULTS FOR MODELED OROVILLE GRAVEL USING STRENGTH INTERPRETATION I

Figures K-1 through K-10 are cyclic test results employing strength interpretation I.

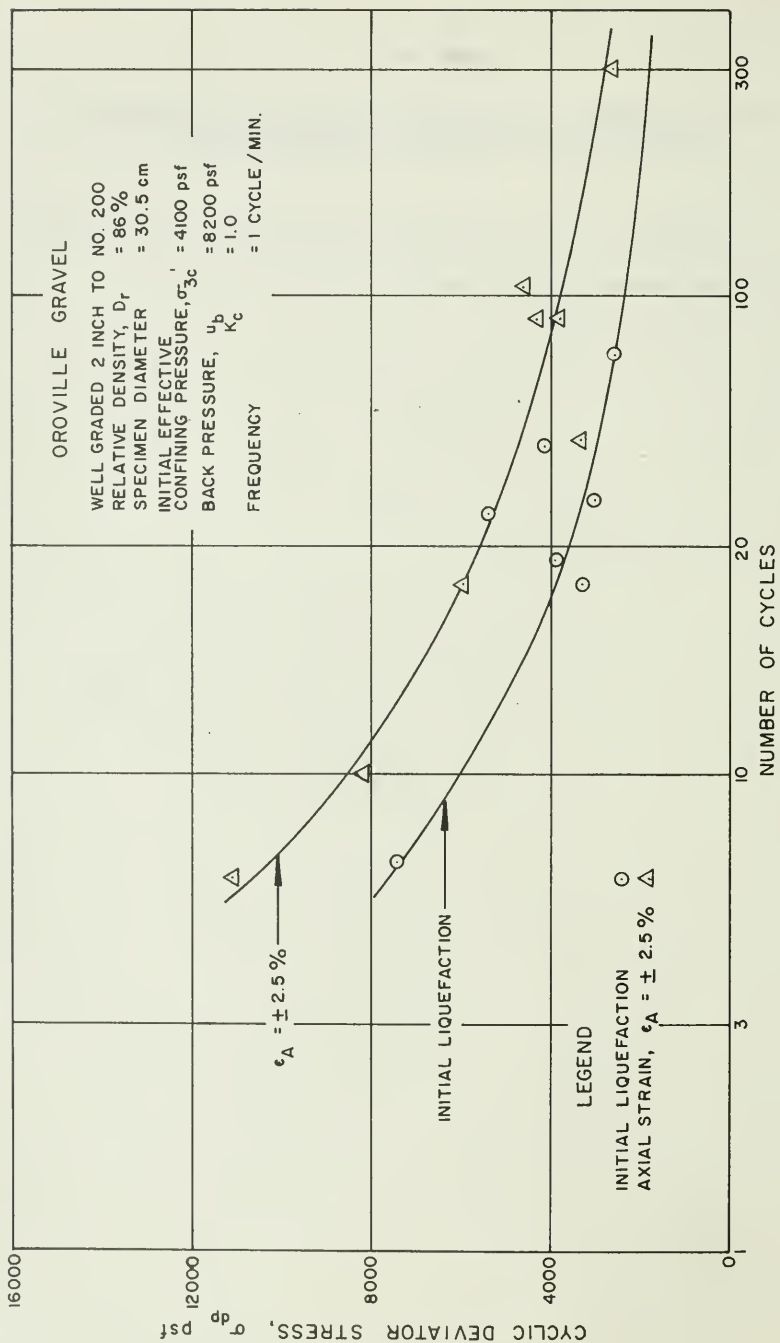


Figure k-1. Cyclic Triaxial Test Results ($\sigma'_{3c} = 4,100$ psf, $K_c = 1.0$)

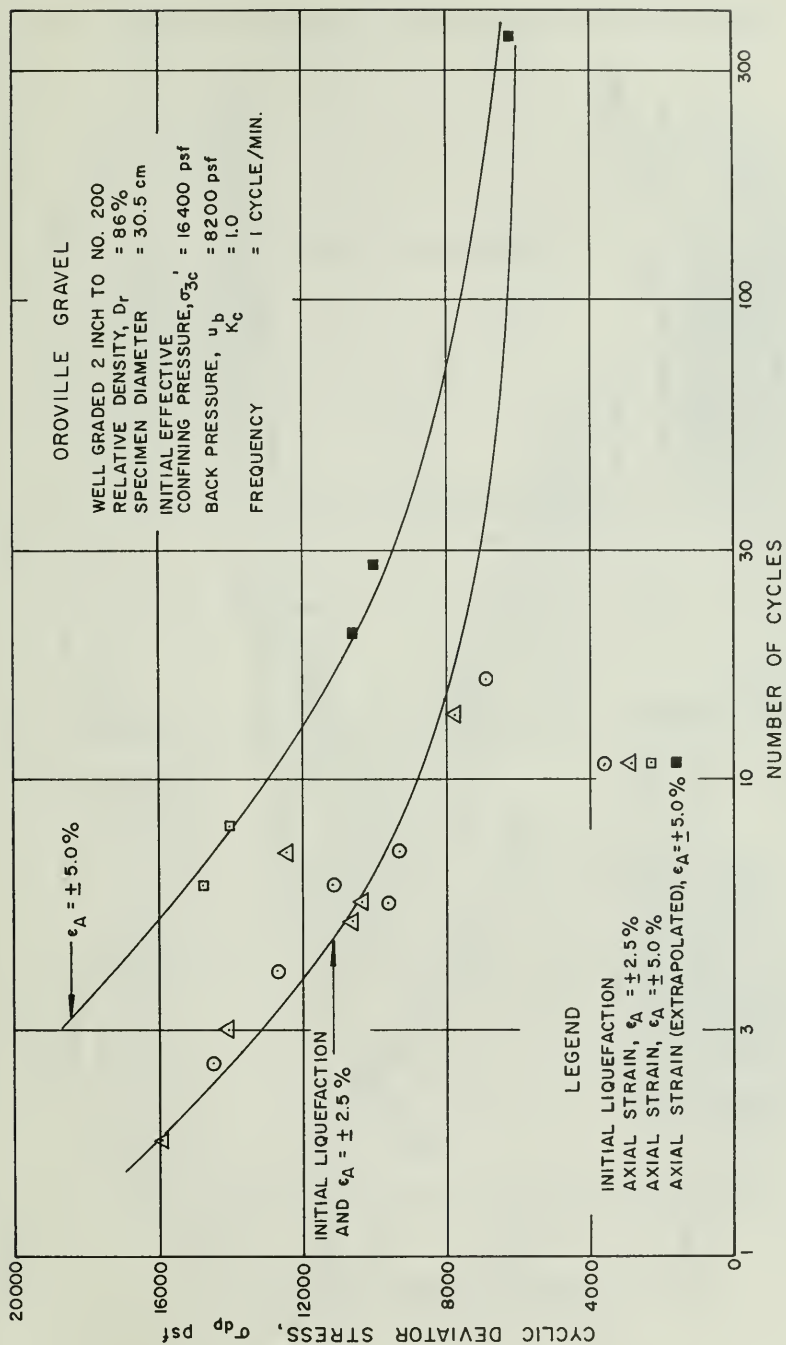


Figure K-2. Cyclic Triaxial Test Results (σ'_{3c} = 16,400 psf, K_c = 1.0)

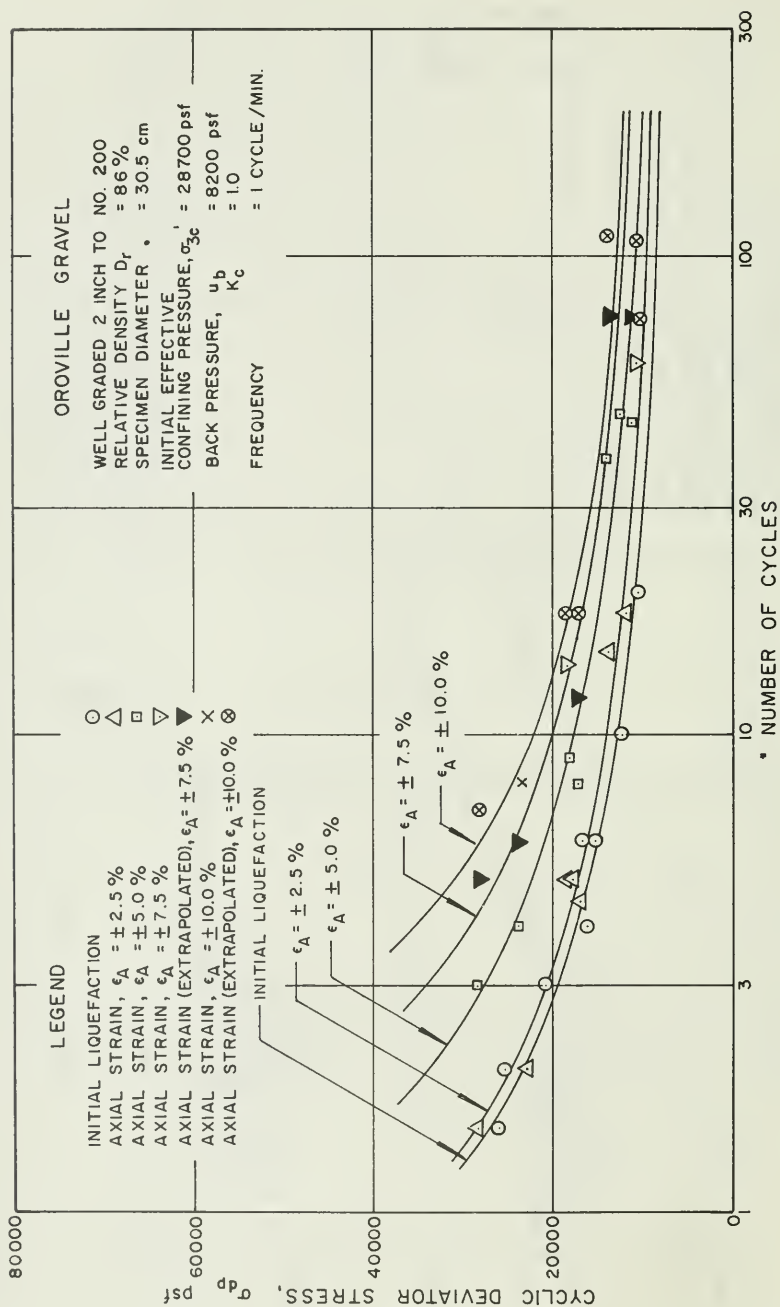


Figure K-3. Cyclic Triaxial Test Results ($\sigma'_{3c} = 28,700$ psf, $K_c = 1.0$)

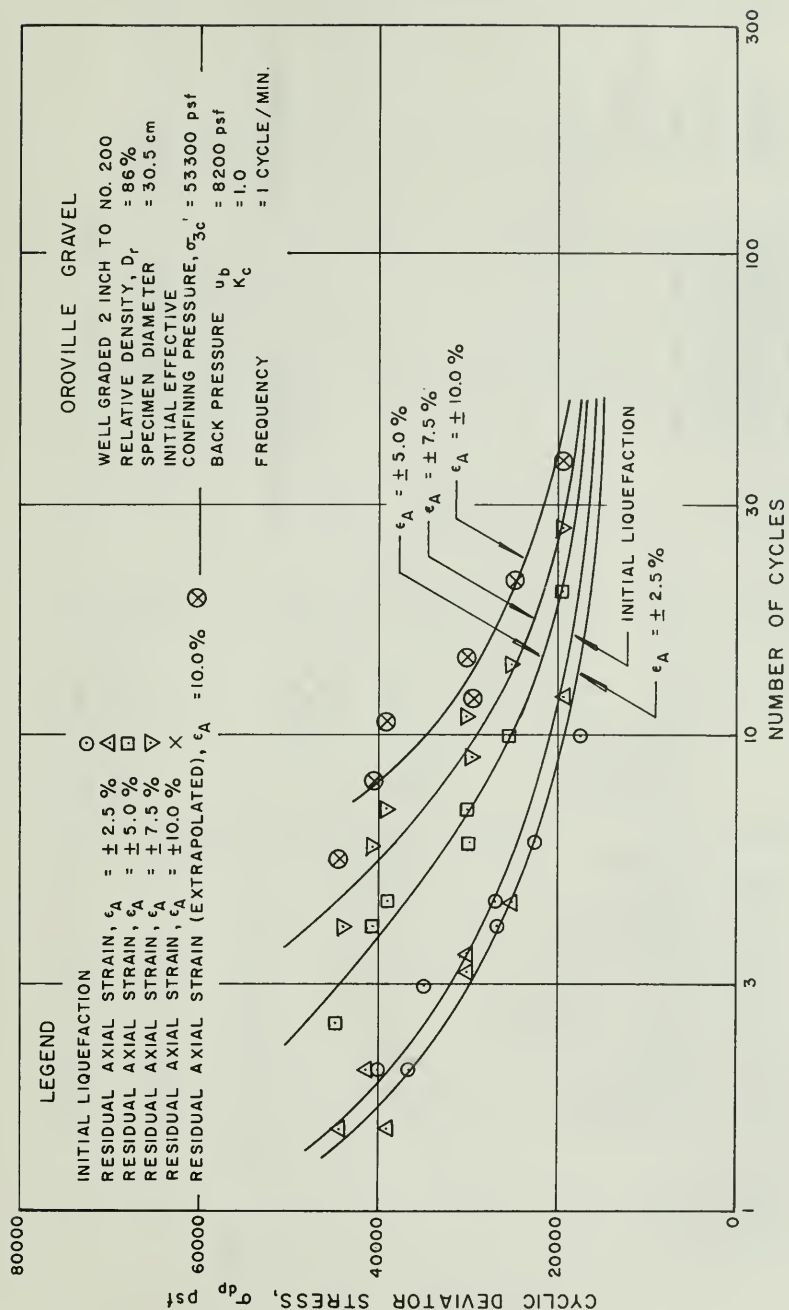


Figure K-4. Cyclic Triaxial Test Results ($\sigma'_{3c} = 53,300$ psf, $K_c = 1.0$)

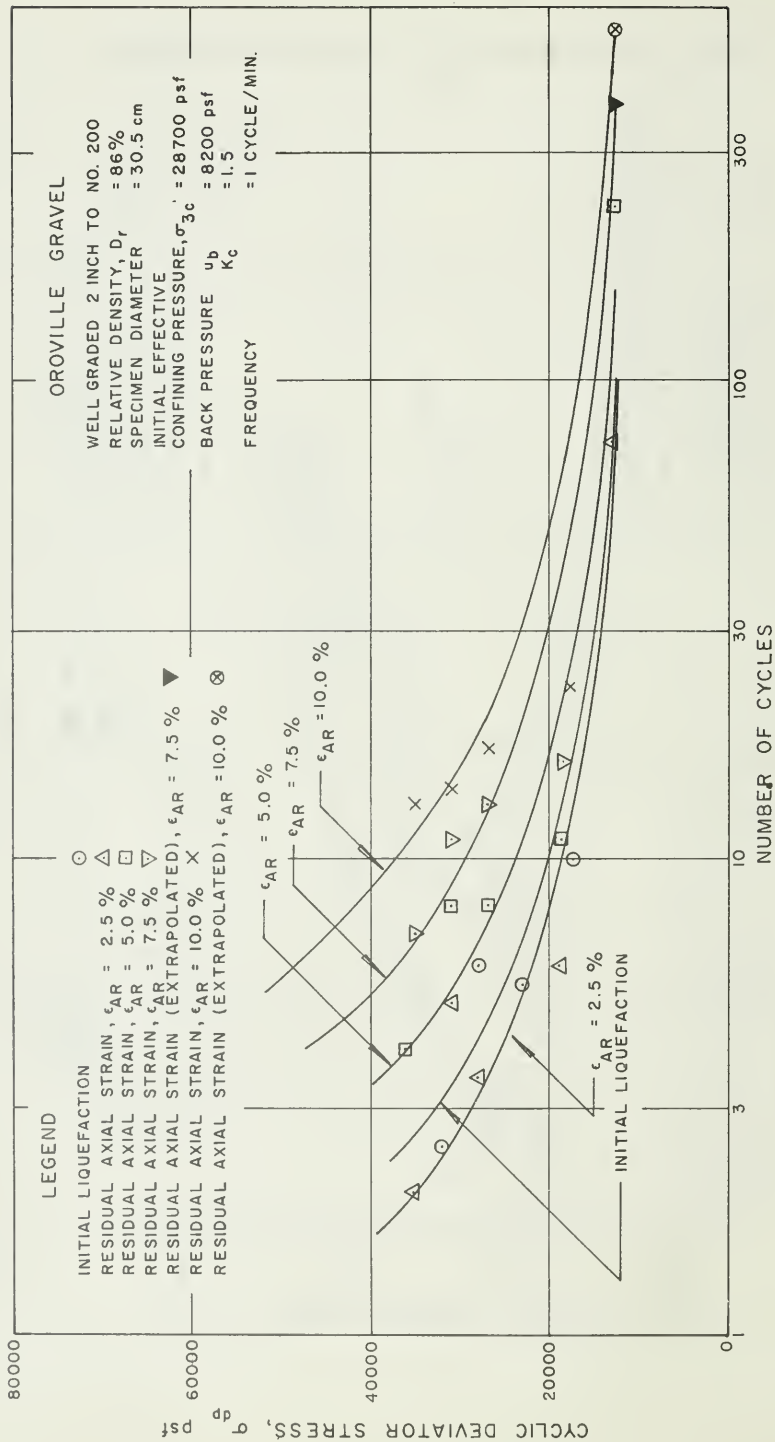


Figure K-5. Cyclic Triaxial Test Results (σ'_{3c} = 28,700 psf, K_c = 1.5)

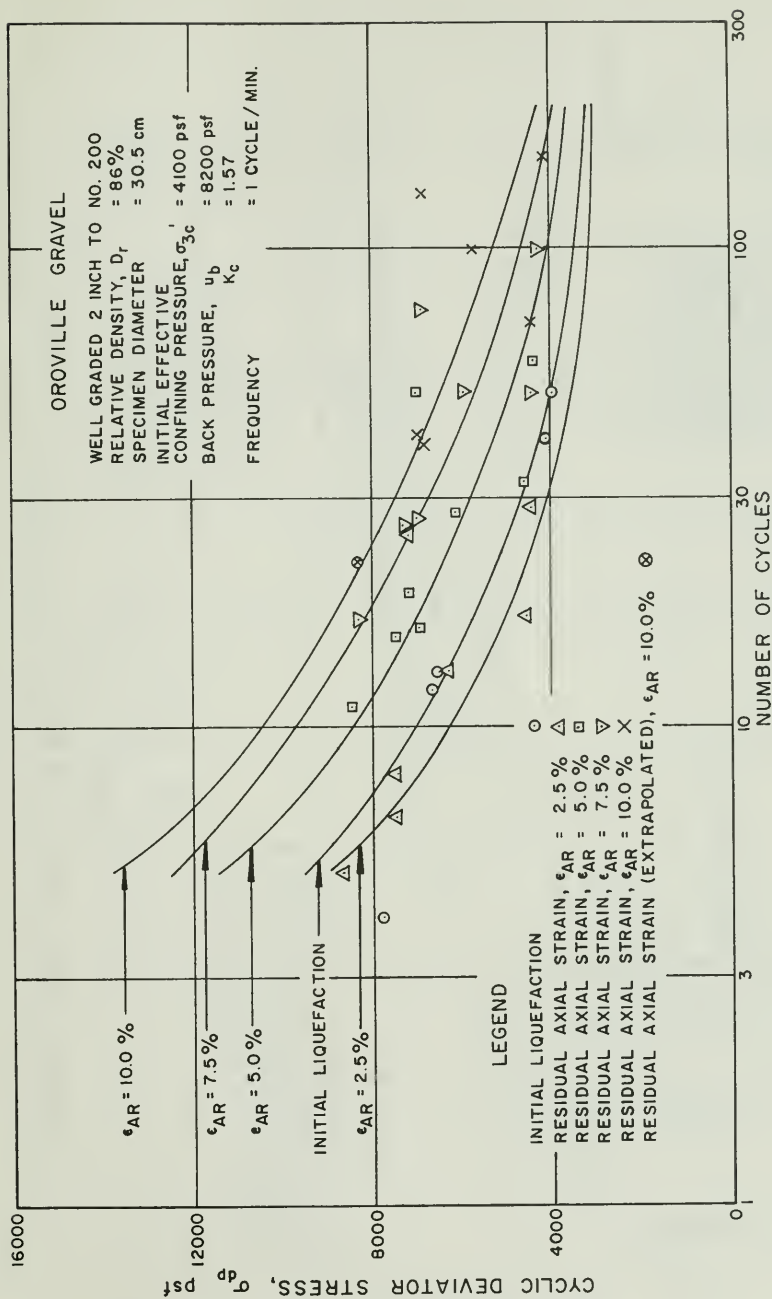


Figure K-6. Cyclic Triaxial Test Results (σ'_{3c} = 4,100 psf, K_c = 1.57)

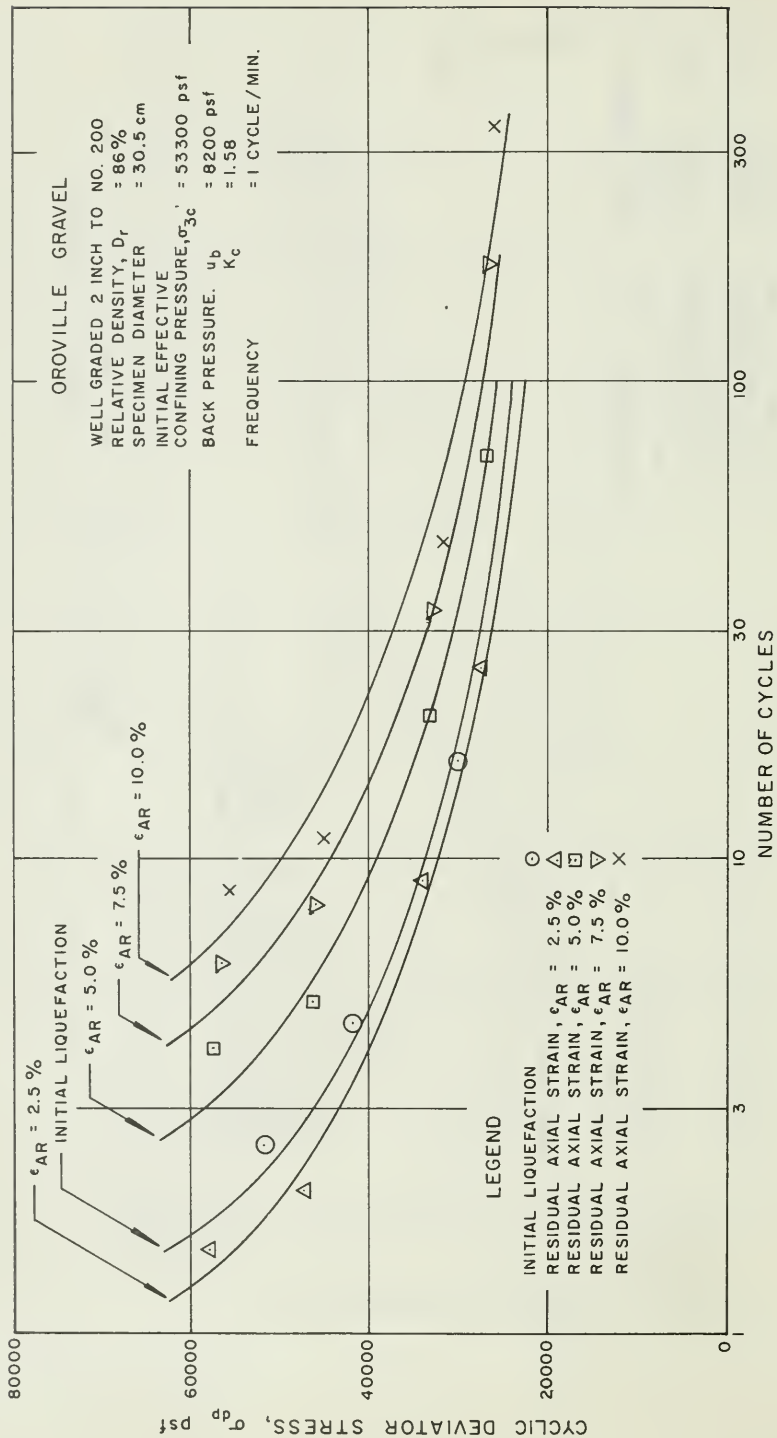


Figure K-7. Cyclic Triaxial Test Results (σ'_{3c} = 53,300 psf, K_c = 1.58)

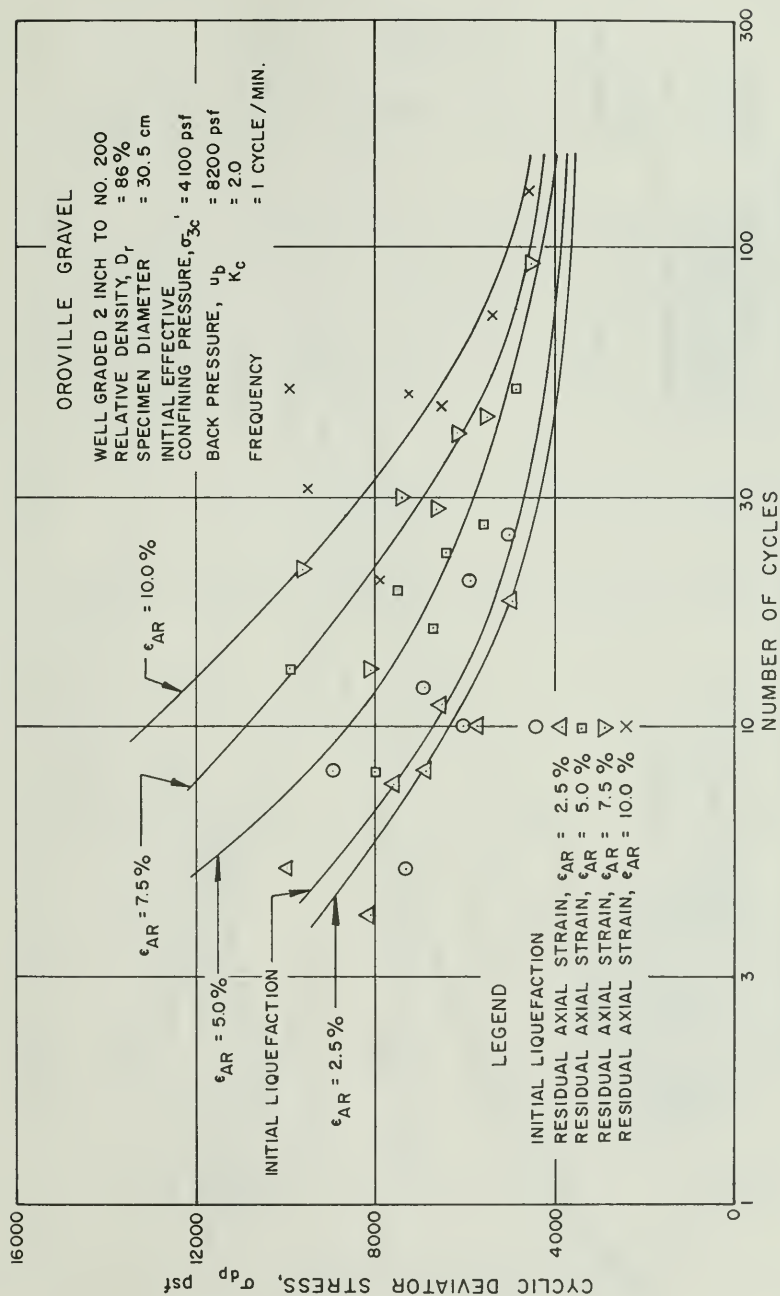


Figure K-8. Cyclic Triaxial Test Results ($\sigma'_{3c} = 4,100$ psf, $K_c = 2.0$)

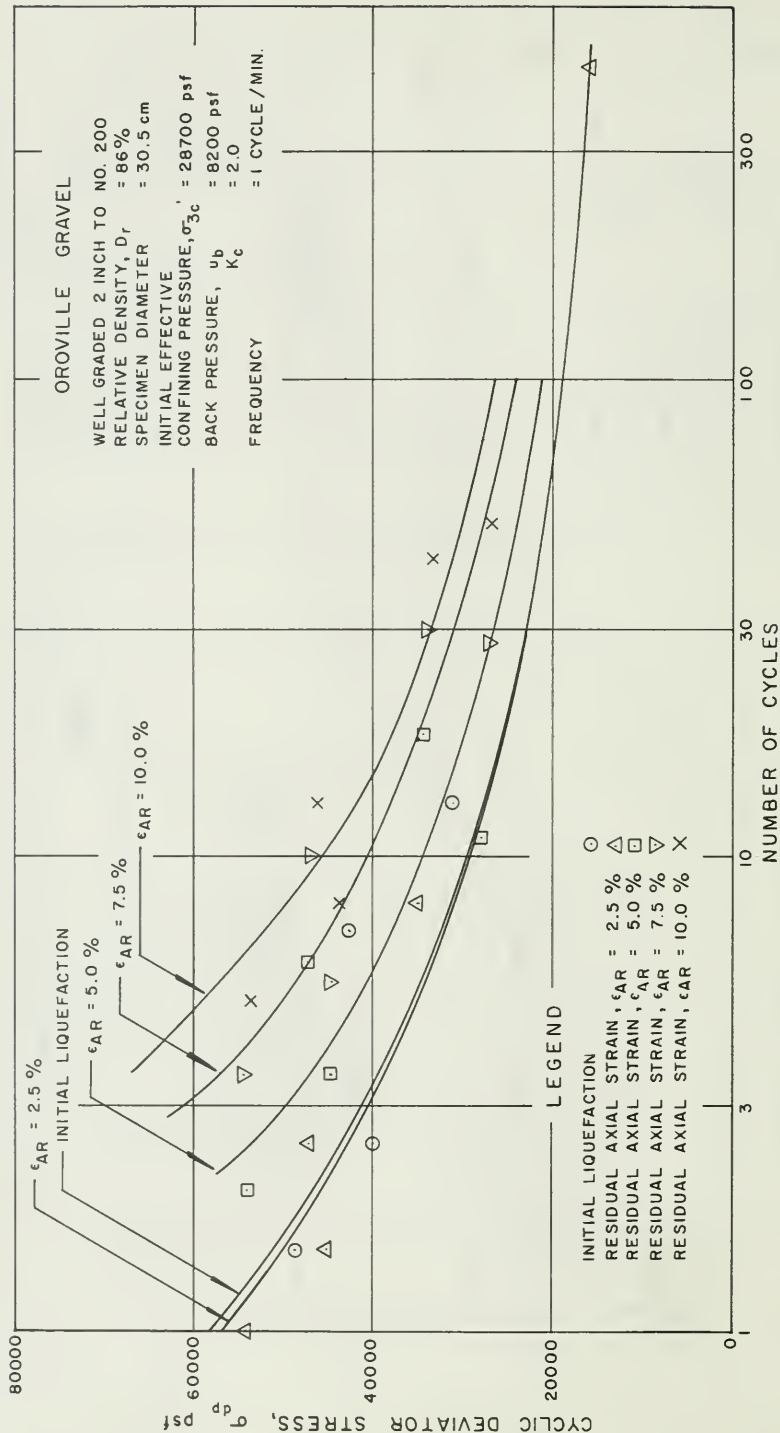


Figure K-9. Cyclic Triaxial Test Results ($\sigma'_{3c} = 28,700$ psf, $K_c = 2.0$)

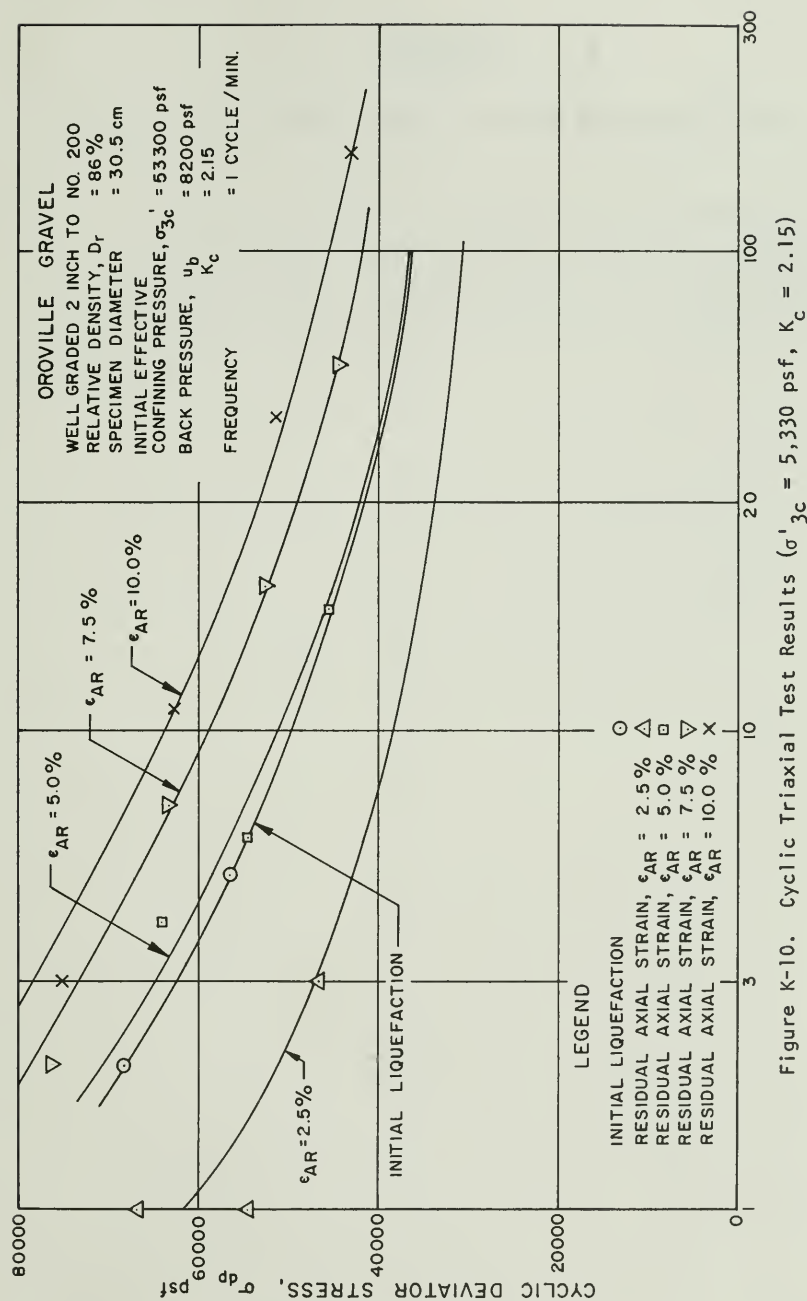


Figure K-10. Cyclic Triaxial Test Results (σ'_{3c} = 5,330 psf, K_c = 2.15)

APPENDIX L

CYCLIC TRIAXIAL TEST REPORT - TO BE AVAILABLE EARLY 1979

Appendix L is the cyclic triaxial testing report concerning tests made for modeled Oroville Gravel samples. It will be made available in 1979 and will be supplied on request.

APPENDIX M
EMBANKMENT STRAIN POTENTIALS
(FIGS. M-1 THROUGH M-4)

APPENDIX M

EMBANKMENT STRAIN POTENTIALS

Figures M-1 and M-2 show the computed compressive strain potentials in the upstream shell for the "best judgment case" and the "conservative case". Figures M-3 and M-4 show two other cases which will not be considered further because they are within the range defined by Figures M-1 and M-2.

A rigorous or well-tested procedure has not been developed for relating actual displacements of an embankment to computed strain potentials. However, two rough correlations between strain of laboratory test samples and embankment deformations have been made -- Otter Brook Dam for static loading, and Upper San Fernando Dam for earthquake shaking. In both cases, surface deformations of several feet were found for locations corresponding to axial strain of test samples greater than 10 percent. These deformations were considered "excessive".

On the basis of these correlations, the zones within the 10 percent compressive strain potential contours in Figures M-1 and M-2 could be expected to develop excessive deformations. This would be the three small zones for the "conservative case" and no zones for the "best judgment case".

The method used to calculate displacement of the Upper San Fernando Dam can be used as a rough indicator of the magnitude of displacements. The method is carried out by estimating deformation in critical zones of high strain potential. This

PSEUDO THREE DIMENSIONAL ANALYSIS

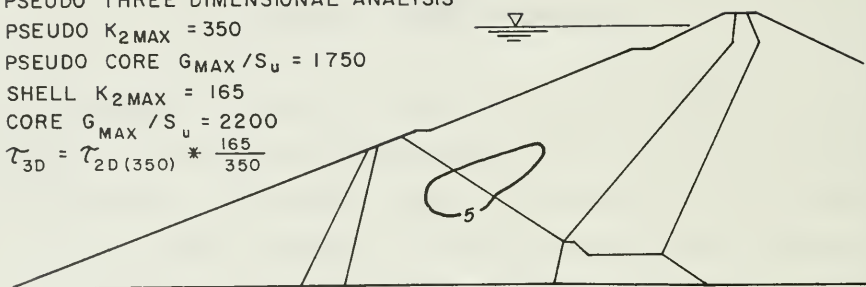
PSEUDO $K_{2MAX} = 350$

PSEUDO CORE $G_{MAX} / S_u = 1750$

SHELL $K_{2MAX} = 165$

CORE $G_{MAX} / S_u = 2200$

$\tau_{3D} = \tau_{2D(350)} * \frac{165}{350}$



CASE a: PREDICTED FOR BEST JUDGMENT CASE

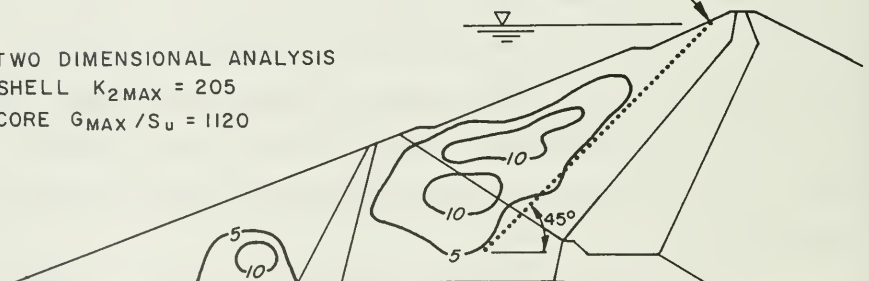
Figure M-1. Predicted for Best Judgement Case

ESTIMATED UPSLOPE LIMIT OF SLUMPING

TWO DIMENSIONAL ANALYSIS

SHELL $K_{2MAX} = 205$

CORE $G_{MAX} / S_u = 1120$



CASE b: POSSIBLE EXTREME FOR CONSERVATIVE CASE

Figure M-2. Possible Extreme for Conservative Case.

NOTES :

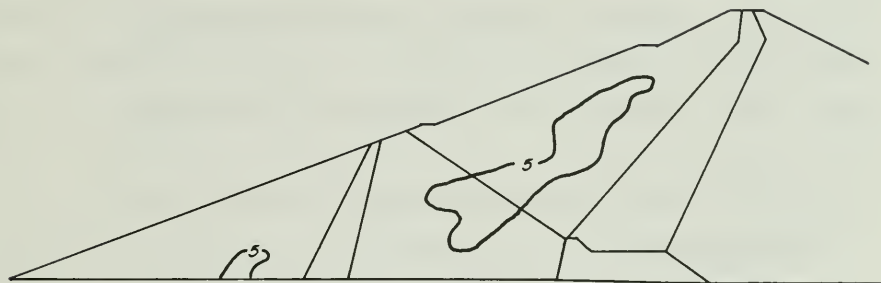
REANALYSIS EARTHQUAKE

COMPUTER PROGRAM LUSH

CYCLIC STRENGTH INTERPRETATION II - EXTRAPOLATED CYCLIC
TRIAxIAL TEST RESULTS

UNDRAINED CONDITIONS

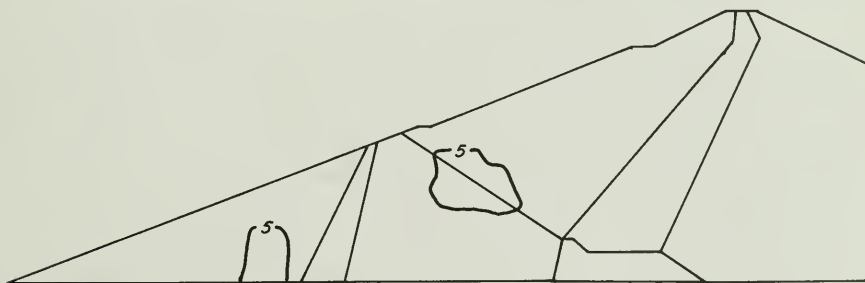
TWO DIMENSIONAL ANALYSIS - COMPUTER PROGRAM LUSH
 REANALYSIS EARTHQUAKE
 SHELL $K_{2MAX} = 205$
 CORE $G_{MAX} / S_u = 1120$
 CYCLIC STRENGTH INTERPRETATION I
 UNDRAINED CONDITIONS



CASE c

Figure M-3. First Strength Interpretation

TWO DIMENSIONAL ANALYSIS - COMPUTER PROGRAM QUAD 4
 REANALYSIS EARTHQUAKE
 SHELL $K_{2MAX} = 130$
 CORE $G_{MAX} / S_u = 2200$
 CYCLIC STRENGTH INTERPRETATION II
 UNDRAINED CONDITIONS



CASE d

Figure M-4. Second Strength Interpretation

procedure requires conversion of compression strain potential to shear strain potential. For saturated soils deforming at constant volume in plane strain conditions, the shear strain potential can be taken as 1.5 times the compressive strain potential. Since the elements developing lower strain potentials will tend to restrain the movement of elements of higher strain potentials, an appropriate estimate of the deformation in a zone would employ an average value of shear strain potential. By taking this average shear strain potential and multiplying it by the height of the critical zone, one obtains the relative horizontal displacement between the top and bottom of the zone.

For the "best judgment case", distribution of compressive strain potentials has not been defined except that they are less than 5 percent essentially throughout the upstream shell. For illustration purposes, an average of 2 percent is assumed for compressive strain potential over a height of 91 metres (300 ft.). Horizontal displacement would then be calculated as $0.02 \times 1.5 \times 91 = 2.7$ metres (9 ft.).

For the "conservative case", the average compressive strain potential within the 5 percent contours is about 8 percent, and the average height within this contour is 91 metres (300 ft.). Relative horizontal displacement between the surface of the slope and bottom of this contour would be calculated as $.08 \times 1.5 \times 91 = 11$ metres (36 ft.). Because this method is only a rough indicator, the displacement can best be described as a few tens of feet, or in round numbers, 10 metres.

Overall behavior associated with the illustrated strain potentials might reasonably be as follows:

- upstream displacement of the slope by a few tens of feet in the interval between the two berms.
- slumping of the shell material near the upper berm.
- bulging of the shell material near the lower berm.

Displacement and slumping would be limited to the upstream shell material as indicated by the strain potential pattern. Slumping would not be expected to extend upslope beyond the 45 degree line shown in Figure M-2 (judgment based on extent of slumping at Lower San Fernando Dam). The compacted gravel in the upstream shell would be as strong and perform as well after deformation as before.

COLLATE:

___ PIECE\$

THIS BOOK IS DUE ON THE LAST DATE

THIS BOOK IS DUE ON THE LAST DATE
STAMPED BELOW

BOOKS REQUESTED BY ANOTHER BORROWER
ARE SUBJECT TO IMMEDIATE RECALL

AUG 21 2008

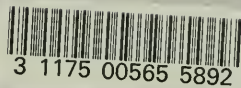
RECEIVED

AUG 22 2008

Physical Sciences Library

LIBRARY, UNIVERSITY OF CALIFORNIA, DAVIS

D4613-1 (5/02)M



3 1175 00565 5892

